LEVEL II

AGARD-AG-257

AGARD-AG-257

AD A089049

AGARD

ADVISORY GROUP FOR AEROSPACE RESEARCH & DEVELOPMENT

7 RUE ANCELLE 92200 NEUILLY SUR SEINE FRANCE

AGARDograph No. 257

Practical Applications of Fracture Mechanics

DTIC
ELECTE
SEP 1 2 1980
S D
E

NORTH ATLANTIC TREATY ORGANIZATION

FILE COPY

DISTRIBUTION AND AVAILABILITY
ON BACK COVER

AGARD-AG-257

NORTH ATLANTIC TREATY ORGANIZATION

ADVISORY GROUP FOR AEROSPACE RESEARCH AND DEVELOPMENT

(ORGANISATION DU TRAITE DE L'ATLANTIQUE NORD)

AGARDograph No.257

PRACTICAL APPLICATIONS OF FRACTURE MECHANICS

Edited by

Harold Liebowitz
Dean and Professor of Engineering and Applied Science
School of Engineering and Applied Science
George Washington University
Washington DC 20052
USA

This AGARDograph was sponsored by the Structures and Materials Panel of AGARD.

THE MISSION OF AGARD

The mission of AGARD is to bring together the leading personalities of the NATO nations in the fields of science and technology relating to aerospace for the following purposes:

- Exchanging of scientific and technical information;
- Continuously stimulating advances in the aerospace sciences relevant to strengthening the common defence posture;
- Improving the co-operation among member nations in aerospace research and development;
- Providing scientific and technical advice and assistance to the North Atlantic Military Committee in the field of aerospace research and development;
- Rendering scientific and technical assistance, as requested, to other NATO bodies and to member nations in connection with research and development problems in the aerospace field;
- Providing assistance to member nations for the purpose of increasing their scientific and technical potential;
- Recommending effective ways for the member nations to use their research and development capabilities for the common benefit of the NATO community.

The highest authority within AGARD is the National Delegates Board consisting of officially appointed senior representatives from each member nation. The mission of AGARD is carried out through the Panels which are composed of experts appointed by the National Delegates, the Consultant and Exchange Programme and the Aerospace Applications Studies Programme. The results of AGARD work are reported to the member nations and the NATO Authorities through the AGARD series of publications of which this is one.

Participation in AGARD activities is by invitation only and is normally limited to citizens of the NATO nations.

The content of this publication has been reproduced
directly from material supplied by AGARD or the authors.

Accession For
NTIS GRA&I
DDC TAB
Unannounced
Justification
By
Distribution/
Availability Codes
Dist. | Avail and/or special
A

Published May 1980

Copyright © AGARD 1980
All Rights Reserved

ISBN 92-835-1359-2

Printed by Technical Editing and Reproduction Ltd
Harford House, 7–9 Charlotte St, London, W1P 1HD

PREFACE

The Structures and Materials Panel of the NATO Advisory Group for Aerospace Research and Development (AGARD) consists of engineers, scientists and technical administrators from industry, government and universities throughout the NATO nations, and is concerned with the advancement of aerospace research and development and the application of the results to the design and construction of, and the solution of problems arising during the operation of NATO military vehicles, systems and equipment. The biannual Panel Meetings provide forums for specialist multi-national discussions of problems and research information and for initiating and monitoring cooperative studies and experimental programmes. The Panel also provides a mechanism for the planning, preparation and distribution of surveys and reports on the present state of knowledge in technical areas within the fields of Structures and Materials selected because of their importance and their relevance to current or future problems facing the NATO aerospace community.

In recent years, fracture mechanics became an important factor in aircraft design and development. Even though considerable progress has been made with the application of advanced calculation methods and computer programmes improving the accuracy of flight-load prediction and calculated stresses, it has to be envisaged that cracks in aircraft structures may occur, initiated during manufacture or in service. These initial cracks will propagate under service loading and finally could lead to a complete failure of the part, i.e. the structure. Therefore, adequate measures have to be taken by the designer to avoid catastrophic service failures.

With the aim of ensuring the required safety in aircraft operation, different design philosophies have been developed in the last twenty years. However, it was learned by service experience that the fail-safe and safe-life philosophies applied in the fifties and sixties were not satisfactory. The progressing development of fracture mechanics theory opened new possibilities to investigate the fracture behaviour of aircraft components and predicting crack propagation and residual strength characteristics. New testing techniques were developed to determine the required material data necessary for fracture mechanical calculation. The application of fracture mechanics concepts in aircraft design, the theoretical and experimental investigation of the fracture behaviour of complete aircraft structures are also reflected in MIL-STD-83444.

Realizing the different problems in the field of aerospace-structures experienced with new high-strength materials, e.g. flaw susceptibility, stress corrosion, crack detection, crack propagation and residual strength aspects, the Panel was of the opinion that the existing knowledge and the experience gained by the application of fracture mechanics concepts in aircraft design should be collected and made available to engineers and designers in a handbook on Practical Applications of Fracture Mechanics. The Panel set up a Fracture Mechanics Working Group to commission and monitor the preparation of a comprehensive survey of the pertinent information presently available on the application of fracture mechanics to the fracture of metals and actual structures. In addition, this work had to cover engine components, built-up structures, integral structures, joints, lugs and fasteners, forgings, effects of stress corrosion and problems of scatter including fundamentals of determining stress concentration factors, fatigue crack propagation and residual strength calculations.

It was recognized that fracture mechanics was an inter-disciplinary growth area of research of ever increasing importance to those people concerned with the design and operational management of aircraft, especially in the light of the modern airframe fail-safe design philosophy and aircraft safety. It was therefore decided that the resulting critical survey report should be given a wide circulation within the NATO nations.

The Panel was very fortunate from the outset in securing the services as Coordinator and Editor of Dean Harold Liebowitz, School of Engineering and Applied Science, The George Washington University, Washington, D.C., a world renowned expert on the fracture of materials.

An essential feature of AGARD activities is the pooling of relevant knowledge within the NATO nations and the bringing together of specialists for informed discussions and debate on the subject concerned. This occurred in full measure within the Fracture Mechanics Working Group and the Panel is indebted not only to Dean H.Liebowitz, the Coordinator and Editor for his outstanding efforts but especially to the many contributors to the monograph "Practical Applications of Fracture Mechanics" itself from the nations: Canada, Belgium, France, Germany, Italy, Netherlands, UK and USA.

H.J.ZOCHER
Chairman, Fracture Mechanics Working Group
AGARD Structures and Materials Panel
Munich, Germany
January 25, 1980

LIST OF CONTRIBUTORS

(Numbers in parentheses indicate the pages on which the authors contributions begin.)

R.F.M.Anstee (8-1)
Structures Department
Royal Aircraft Establishment
Farnborough, Hampshire
United Kingdom

Francis I.Baratta (10-1)
Department of the Army
Army Material and Mechanics Research Center
Watertown, Massachusetts 02172
USA

M.Bradley (3-77, 4-20, 4-24, 4-35)
British Aerospace
Manchester Division
United Kingdom

David Broek (3-62, 4-1)
Battelle's Columbus Laboratories
505 King Avenue
Columbus, Ohio 43201
USA

Clive S.Carter (9-1)
Boeing Commercial Airplane Company
Seattle, Washington 98195
USA

D.J.Cartwright (10-1)
University of Southampton
Southampton
United Kingdom

L.Casalegno (3-68, 4-42)
Aeritalia, Turin
Italy

T.A.Cruse (2-1)
Pratt and Whitney Aircraft Group
Commercial Products Division
East Hartford, Connecticut 06108
USA

T.P.Forte (4-49)
Battelle's Columbus Laboratories
505 King Avenue
Columbus, Ohio 43201
USA

W.Geier (4-44, 7-1)
Materials and Fatigue Department
MBB-GmBH
Unternehmensbereich Flugzeuge
Postfach 80 11 60, 8000 Munich 80
Federal Republic of Germany

N.D.Ghadiali (4-49)
Battelle's Columbus Laboratories
505 King Avenue
Columbus, Ohio 43201
USA

D.Grange (2-24, 2-26, 3-35, 3-62, 4-24, 4-26, 4-28)
British Aerospace
Manchester Division
United Kingdom

Alan Jefferson (5-1)
Department of Aeronautics and Astronautics
The University of Southampton
Southampton
United Kingdom

Harold Liebowitz (1-1)
School of Engineering and Applied Science
George Washington University
Washington, D.C. 20052
USA

H.J.Malik (4-49)
Battelle's Columbus Laboratories
505 King Avenue
Columbus, Ohio 43201
USA

C.I.P.Martin (5-1)
British Aerospace
Bristol
United Kingdom

V.G.Nanduri (3-47)
The DeHavilland Aircraft of Canada Ltd.
Downsview, Ontario M3K 1Y5
Canada

L.F.Nicholls (5-1)
British Aerospace
Bristol
United Kingdom

D.P.Rooke (10-1)
Royal Aircraft Establishment
Farnborough, Hampshire
United Kingdom

A.Salvetti (3-97)
Institute of Aeronautics
University of Pisa
Italy

L.Schwarmann (3-88, 3-93)
Vereinigte Flugtechnische Werke-Fokker Gmbh
Bremen
Federal Republic of Germany

Walter Schütz (6-1, 8-1)
Industieanlagen-Betriebsgesellschaft
Einsteinstrasse 20
8012 Ottobrunn, Munich
Federal Republic of Germany

F.A.Simonen (4-52)
Battelle's Columbus Laboratories
505 King Avenue
Columbus, Ohio 43201, USA

O.K.Sippel (4-44, 7-1)
Head-Materials and Fatigue Department
MBB-GmBH Unternehmensbereich Flugzeuge
Postfach 80 11 60, 8000 Munich 80
Federal Republic of Germany

S.H.Smith (4-49, 5-50)
Battelle's Columbus Laboratories
505 King Avenue
Columbus, Ohio 43201
USA

T.Swift (3-26, 3-33, 3-38)
McDonnell Douglas Corporation
Douglas Aircraft Company
Long Beach, California 90843
USA

J.N.Thomas (3-70)
S.N.I. Aerospatiale
Toulouse
France

H.Vlieger (3-1, 3-51, 3-53)
National Aerospace Laboratory NLR
Anthony Fokkerweg 2
Amsterdam 1017
The Netherlands

D.P.Wilhem (3-43)
Northrop Corporation
Aircraft Division
Hawthorne, California 90250
USA

FOREWORD

The Structures and Materials Panel's Fracture Mechanics Working Group has been working, since its inception in 1971, to make available a requisite body of knowledge to facilitate an understanding of fracture and its implications for, and applications to, aircraft.

In 1974, the Structures and Materials Panel published AGARDograph 176 *Fracture Mechanics of Aircraft Structures*, to encourage the dissemination of fracture mechanics work in aircraft design, materials selection, and nondestructive evaluation as well as provide a detailed survey of the principal tools, testing methods, and materials data.

Following this publication, the Panel decided to continue its activities with a focus on Fracture Mechanics Design Methodology to address the following areas: practical applications of fracture mechanics in the design of new aircraft; durability and damage tolerance assessment in aircraft in service; design methodology for built-up sheet structures; selection of aircraft with forgings, lugs, etc. A specialists' meeting was set up and the results of this meeting are contained in AGARD CP-221, *Fracture Mechanics Design Methodology*.

This volume on fracture mechanics has essentially been oriented to present practical applications of all aspects of aircraft design, manufacture, and testing. Although theoretical discussions and presentations have been included to afford the engineer, scientist, and aircraft designer an appreciation of the complexity of the problems involved, the main emphasis has been on practical examples of the application of fracture mechanics. It is important to emphasize that this undertaking was to be an international effort, rather than being confined to one country.

The Editor, Professor H.Liebowitz, wishes to thank the Chairman, Mr Horst Zocher (Germany), and members of the Working Group, Dr L.A.Harris (USA), Dr G.Incarbone (Italy), Mr J.B. de Jonge (Netherlands), Dr R Labourdette (France), Mr E.L.Ripley (UK) Mr J.A.Dunsby (Canada), Prof. A.Salvetti (Italy), Prof. F.A.Deruyttere (Belgium), Prof. J.W.Mar (USA), Mr G.P.Peterson (USA), Dr N.M.Tallan (USA), Mr F.Niordson (Denmark), and Mr W.G.Heath (UK) who also served as Chairman of the Editorial Committee, for their significant efforts and assistance in providing guidance and direction during the course of preparing this publication.

Appreciation is also given to the administrative and technical staff, especially to Mr John M.N.Willis and Ms. Alice Guerillot, of the Structures and Materials Panel, Paris, for the many helpful suggestions and assistance rendered. In addition, the Panel Coordinators from each NATO country participated in obtaining the information to make this a truly international cooperative project.

Special thanks are due to Dr T.Gaymann (Germany), and Dr R.S.Berrisford (USA) and the other members and participants of the Structures and Materials Panel for their interest and participation in helping to achieve the objectives of this study.

Special thanks are also due to the many contributors indicated in the List of Contributors for their unfailing co-operation and untiring assistance in providing the material for the comprehensive discussions and descriptions of Practical Applications of Fracture Mechanics to aircraft design, manufacture, and testing.

H.LIEBOWITZ
Coordinator and Editor
Washington, D.C.

November 1979

CONTENTS

	Page
PREFACE	iii
LIST OF CONTRIBUTORS	iv
FOREWORD	vi
1. INTRODUCTION (Liebowitz)	1-1
2. ENGINE COMPONENTS (Cruse)	2-1
3. BUILT-UP STRUCTURES (Vlieger)	3-1
3.3 Residual Strength	3-11
3.3.3 Example Problems	3-25
(1) Residual Strength of 7075-T73 Panels with 8 inch Stiffener (Swift)	3-26
(2) Residual Strength of 7075-T73 Panels with 20 inch Frame Spacing (Swift)	3-33
(3) The Effects of Rivet Yielding on Residual Strength of Stiffened Structure Containing Cracks (Swift)	3-38
(4) The Use of Resistance Curves in Residual Strength Prediction (Wilhem)	3-43
(5) Application of Fracture Mechanics in Designing Lower Surface of Transport Aircraft Wing (Nanduri)	3-47
(6) Residual Strength of Bonded Panels with 2024-T3 Skin and 7075-T73 or 2024-T3 Stiffeners (Vlieger)	3-51
(7) Residual Strength of Riveted Panels with 7075-T6 or 2024-T3 Skins and 7075-T6 Stiffeners (Vlieger)	3-58
3.4 Fatigue Crack Propagation (Broek)	3-62
3.4.2 Example Problems	3-67
(1) Stiffened Wing Panel at Spar-Panel Joint (Casalegno)	3-68
(2) Crack Propagation and Deceleration in Stiffened Panels (Thomas)	3-70
(3) Crack Propagation in Wing Stringer-Skin Panels (Bradley)	3-77
(4) Engine Pylon of Medium Transport (Grange)	3-82
(5) Damage Tolerance of a Pressure Bulkhead (Grange)	3-85
(6) Crack Propagation Analysis of Flat Stiffened Panels (Schwarmann)	3-88
(7) Crack Propagation Analysis of Pressurized Fuselage Structure (Schwarmann)	3-93
(8) Fatigue Crack Propagation in Structures with Riveted Stiffeners (Schwarmann)	3-97
4. FASTENED JOINTS (Broek)	4-1
4.6 Example Problems	4-20
(1) Crack Propagation in Lugs on Aft Flaps Links (Bradley)	4-20
(2) Corner Defects at Holes of Wing Spar Booms (Grange and Bradley)	4-24
(3) Residual Strength Predictions for Corner Defects at Holes in Spar Booms (Grange)	4-26
(4) Damage Tolerance Estimated for a Landing Gear Component (Grange)	4-28
(5) Crack Growth and Fracture of a Loaded Hole in an Aircraft Boom End (Bradley)	4-35
(6) Titanium Alloy Wing Lug (Casalegno)	4-42
(7) Flight-by-Flight Crack Propagation Investigation on MRCA Tornado Components (Geier, Sippel)	4-44
(8) Aircraft Horizonal Stabilizer Lug (Smith, Forte, Malik, Ghadiali)	4-49
(9) Damage Tolerance Analysis of an Aircraft Structural Joint (Smith, Simonen)	4-52
5. INTEGRAL STRUCTURES (Nicholls, Jefferson, Martin)	5-1
6. FORGINGS, INCLUDING LANDING GEARS (Schütz)	6-1
7. FATIGUE CRACK PROPAGATION UNDER VARIABLE LOADS (Geier, Sippel)	7-1

	Page
8. ACCOUNTING FOR VARIABILITY IN MATERIALS PERFORMANCE	8-1
8A Treatment of Scatter of Fracture Toughness Data for Design Purposes (Schütz)	8-3
8B Allowance for Variability in Crack Propagation Data (Anstee)	8-15
9. APPLICATION OF FRACTURE MECHANICS TO STRESS CORROSION CRACKING (Carter)	9-1
10. SIMPLE METHODS OF DETERMINING STRESS INTENSITY FACTORS (Rooke, Baratta, Cartwright)	10-1
SUBJECT INDEX	11-1
AUTHOR INDEX	12-1

1. INTRODUCTION

by

Harold Liebowitz
School of Engineering and Applied Science
George Washington University
Washington, D.C. 20052
U.S.A.

Fracture Mechanics principles and their application in the aircraft industry have made significant gains in the last decade. The main reasons for this advancement are the requirements for damage tolerant design of the aircraft and the availability of efficient computer methods to deal with complex crack configurations. Recognizing the importance of Fracture Mechanics in aircraft design, AGARD first published a monograph on Fracture Mechanics of Aircraft Structures (AG 176) (Jan. 1974) and subsequently published the proceedings of a conference on Fracture Mechanics Design Methodology (CP 221) (Feb. 1977). On the basis of the presentations of these publications and subsequent discussions, it was felt that a manual on Fracture Mechanics Design Of Aircraft Structures would be of great help to both the designer and the researcher. It is expected that the present design manual will be useful to aircraft designers with a background knowledge of Fracture Mechanics as discussed in the publications mentioned above and to researchers in this field.

Fracture Mechanics applications to aircraft structures can be seen in the design and operational phases, as well as in the maintenance and failure analysis phases. Since the damage tolerance calculations require the residual strength and crack growth characteristics to be evaluated during the design phase, important trade off studies on the choice of materials and the optimum type of construction of different components can be performed at an early stage. Fail-safe criteria used in damage tolerance analysis provide useful information regarding safe inspection periods and the required crack detection capabilities, based on the initial crack size and shape and the subsequent crack growth. These aspects are discussed in this manual with regard to various aircraft components.

Experience has shown that practically all the components of the aircraft are vulnerable to crack propagation. This manual considers fracture mechanics applications to the built up structures of the fuselage and wing with special attention being paid to various joints and holes; also the landing gear and other forged components are treated in detail because of their special fracture characteristics. An outline of fracture mechanics applications to the gas turbine disk and blades is provided to indicate the interaction between thermal and fatigue cycling on crack growth, although damage tolerant design concepts are not presently applied to aircraft engine components. Special chapters on variable amplitude loading, stress corrosion cracking and simple analytical techniques to obtain stress intensity factors provide valuable background information.

Broadly speaking, the various design examples presented in this manual supplemented by expert comments, indicate that care should be exercised in modeling the damage and in relating the fracture toughness and crack growth characteristics of actual components to those obtained for laboratory specimens. Where possible, the fracture toughness and crack growth characteristics corresponding to the cracked specimens from the critical component locations should be compared with the standard laboratory results. Also the validity of the plane strain fracture toughness values for a cracked component should be checked based on the component thickness and yielding in the uncracked ligament of that component.

Design examples presented in this manual can be broadly classified into two categories: damage tolerant design of a new component and damage tolerance study applied to an existing component. In the case of a new component many assumptions are made regarding critical crack locations, geometry and orientations and here a parametric study of the influence of crack geometry has been recommended. Also, crack growth rates based on laboratory tests may be often widely different from those applicable to the component. In the case of an existing component the critical locations, shape and size of the damage as well as the crack growth characteristic can be obtained from the actual component performance using the techniques of NDT and fractography.

An outline of the contents of this manual and some significant findings are discussed below:

Engine Components

Continuing demands for increased engine efficiency and fuel economy in aircraft can be satisfied only through improved turbine disk and blade durability. Fracture mechanics principles and crack growth simulation techniques are presently applied to turbine disk and blade airfoil failure analysis although considerable

research is needed to establish a mathematical model for micro-crack growth under extreme thermal environments. Buried intrinsic defects were often the cause of premature disk failures though such defects may not be noticed in the population of fatigue test specimens because of the smaller volume of material in the specimen. Presently, Monte Carlo simulation techniques are used to develop SN curves for the fracture mechanics application. The defect size and the applicable crack growth data are treated as statistical variables while the inspection limit and fracture toughness are treated as deterministic. It is noted that a nonlinear crack growth equation provides better simulation of near threshold crack growth. An important aspect of the problem is that the stress ratio and mean cyclic stress are both influenced by plasticity. Extensive modeling capabilities of the finite element technique are applicable to a number of gas turbine engine problems.

In the case of turbine disks, load history and a local model of the cooling air hole may provide sufficient information for a thermomechanical fatigue analysis based on fracture mechanics. Assuming an elliptical surface crack and the appropriate test data, crack growth profiles in a turbine disk are obtained at various load cycles. Substantiating test data are often difficult to acquire in the case of engine components because of the cost and lack of proper instrumentation. The complex nature of these engine components pose serious difficulties for the application of fail-safe design concepts in aircraft engines.

Built Up Structures in Aircraft Wing and Fuselage

In the case of aircraft wing and fuselage, the requirements of damage tolerant design in terms of residual strength and crack propagation enable a proper choice of the material and the structural elements to be made in an early stage of the design. Very efficient computer techniques are presently available which can account for rivet flexibility, yielding and friction as well as crack tip plasticity and debonding of adhesive bonded panels. Two different approaches are available which are based respectively on crack tip stress intensity and the global energy release rate. In the case of curved panels the effect of internal pressure and load biaxiality are accounted for in recent studies. Many practical examples are presented here which indicate the effectiveness of modern computer programs to analyze built up structures. Some important results are indicated below:

- o Crack arrest properties of panels with 2024T3 stiffeners are inferior to those with 7075-T73 stiffeners.
- o Stress intensity factor is history dependent since load transfer takes place to remote rivets during overload, causing an increase in the stress intensity factor.
- o Cracks running into rivet holes experience a sudden increase in damage size which offsets the advantages due to the required reinitiation period for the crack to grow beyond the hole.
- o Unconservative predictions often result when damage development assumptions are too simple.
- o Analytical results indicate that integral stiffeners are more effective in slowing down the crack than riveted stiffeners.

Fastened Joints in the Aircraft Structure

This is an important area where complex crack locations and geometry often pose difficulties in estimating the elastic stress intensity factor and the effect of its variation on the residual strength. A thorough survey of the analytical and empirical formulations and experimental studies is presented here. Many practical suggestions are provided for modeling the damage.

In general, through cracks, occurring in thin sheets at circular holes, grow to a considerable distance from the hole before the magnitude of the stress intensity factor approaches the plane stress fracture toughness for the material. Hence, through cracks, in thin sheets at circular holes, can be safely modeled using an effective crack length approach. However, in thick sheets and components, stress intensity factors of the cracks (quarter circular, elliptical etc.) at the hole attain the plane strain toughness value even when the cracks are small. This calls for accurate determination of the stress intensity factors for part through cracks at structural holes.

Important results on the effects of rivet interference and cold working on the crack growth at holes are discussed in this chapter. It is shown that experimental data can be used to characterize stress intensity factors for complex crack shapes and that the fractographic data of actual components are often useful to obtain their crack growth characteristics. Many of the practical examples presented here include expert comments on the approaches used. Examples discussed include corner defects at holes of wing spans, damage tolerance analysis of landing gear components, titanium alloy wing lugs, aircraft horizontal stabilizers, and engine pylons of a medium

transport aircraft. Crack growth characteristics and inspection life are indicated in most of these examples.

Integral Structures

In the wing structure integral construction is often used instead of sheets with riveted stiffeners. Here, the residual strength of integrally attached stiffeners in a plate is derived using Poe's results for riveted stiffeners. It is shown that for flat panels the predicted crack growth characteristics compare well with experimental results. However, wide differences were indicated betwsen experimental and theoretical results in the case of curved panels which are attributed to load biaxiality and panel curvature.

Forgings Including Landing Gear

Forgings are single load path structures and hence can cause catastrophic failures due to crack growth. Here the special fracture characteristics of forgings used in wing spans, root ribs, bulkheads, wing or empennage attachment fittings, etc., are presented. It is noted that the scatter of fracture toughness values of specimens cut from the forgings is often more than the scatter seen in laboratory specimens. Also the assumption that at equal ΔK and R, the crack propagation in the specimen and the component are equal, is not always true in the case of forgings.

Interesting examples of test results from actual forgings of discontinued aircraft components are presented. In the case of certain nose landing gear struts, different struts having cracks of similar sizes and shapes produced widely differing failure loads. Also, a scatter of 1:7 or 1:5 was noticed in the crack propagation period; forgings with a long fatigue life often had a very short crack propagation period and vice versa. In several load sequences the Willenborg retardation model gave unconservative results. Examples presented include forged wing attachment fittings, hinge rib forgings and full scale fatigue tests on a main landing gear.

Fatigue Crack Propagation Under Variable Amplitude Loads

After a brief review of the fatigue crack propagation under constant loads, the different aspects of variable amplitude load fatigue are discussed. Methods for calculating crack propagation under variable loads are given, including an assessment of the currently used calculation procedure. Test results are given for various components and it is concluded that Willenborg and Wheeler models may not always give conservative results; while the Forman equation is always on the safe side (when wide fluctuations in the mean stress of the load sequence are taken care of by providing additional load cycles).

Accounting For Variability in Materials Performance

Since the numerical values of material properties such as fracture toughness and fatigue crack growth rate exhibit considerable scatter, their appropriate design values have to be determined using statistical procedures. Statistical methods to account for variabilities in fracture toughness data and crack propagation data are discussed in both sections of this chapter.

The first section, "Treatment of Scatter of Fracture Toughness Data for Design Purposes" (Schütz) deals with the treatment of scatter in fracture toughness values and emphasizes that a successful statistical analysis depends on a proper choice of the input data. Coefficient of variation in fracture toughness and the statistical mean value for fracture toughness are evaluated for several alloys and plots are given which indicate the expected mean fracture toughness values for several heats of the same material.

The coefficient of variation in fracture toughness for a particular material does not depend on such factors as the type of alloy, type of product (plate, sheet, extrusions), specimen orientation, temperature and corrosion. All the statistical data given in this chapter correspond to laboratory specimens and the designer implicitly assumes that the scatter in specimen fracture toughness is identical to the scatter in component fracture toughness. This assumption is not always correct as pointed out in chapter 6. For designing a component using probabilistic fracture mechanics the necessary probability of survival must be selected according to engineering judgement.

The second section "Allowance for Variability in Crack Propagation Data" (Anstee) deals with the statistical determination of variabilities in crack growth data for constant amplitude and variable amplitude loading. The standard deviations in crack growth data (derived from several tests) are indicated to enable a comparison of variabilities under constant amplitude and FALSTAFF loading for different materials. These results indicate that the variabilities in crack propagation under random loading are often more than the corresponding variabilities under constant amplitude loading. Also the effect of environment on variabilities is provided for constant amplitude and random amplitude testing of different materials. There is no evidence of any systematic influence of environment on variability. Finally, results on crack propagation in actual structures like aircraft lugs and rotor blades are used to calculate the statistical variabilities due to the type of component. It is found that there is no significant difference in the range of standard deviations in actual components as compared to simple specimens. Develop-

transport aircraft. Crack growth characteristics and inspection life are indicated in most of these examples.

Integral Structures

In the wing structure integral construction is often used instead of sheets with riveted stiffeners. Here, the residual strength of integrally attached stiffeners in a plate is derived using Poe's results for riveted stiffeners. It is shown that for flat panels the predicted crack growth characteristics compare well with experimental results. However, wide differences were indicated between experimental and theoretical results in the case of curved panels which are attributed to load biaxiality and panel curvature.

Forgings Including Landing Gear

Forgings are single load path structures and hence can cause catastrophic failures due to crack growth. Here the special fracture characteristics of forgings used in wing spars, root ribs, bulkheads, wing or empennage attachment fittings, etc., are presented. It is noted that the scatter of fracture toughness values of specimens cut from the forgings is often more than the scatter seen in laboratory specimens. Also the assumption that at equal ΔK and R, the crack propagation in the specimen and the component are equal, is not always true in the case of forgings.

Interesting examples of test results from actual forgings of discontinued aircraft components are presented. In the case of certain nose landing gear struts, different struts having cracks of similar sizes and shapes produced widely differing failure loads. Also, a scatter of 1:7 or 1:5 was noticed in the crack propagation period; forgings with a long fatigue life often had a very short crack propagation period and vice versa. In several load sequences the Willenborg retardation model gave unconservative results. Examples presented include forged wing attachment fittings, hinge rib forgings and full scale fatigue tests on a main landing gear.

Fatigue Crack Propagation Under Variable Amplitude Loads

After a brief review of the fatigue crack propagation under constant loads, the different aspects of variable amplitude load fatigue are discussed. Methods for calculating crack propagation under variable loads are given, including an assessment of the currently used calculation procedure. Test results are given for various components and it is concluded that Willenborg and Wheeler models may not always give conservative results; while the Forman equation is always on the safe side (when wide fluctuations in the mean stress of the load sequence are taken care of by providing additional load cycles).

Accounting For Variability in Materials Performance

Since the numerical values of material properties such as fracture toughness and fatigue crack growth rate exhibit considerable scatter, their appropriate design values have to be determined using statistical procedures. Statistical methods to account for variabilities in fracture toughness data and crack propagation data are discussed in both sections of this chapter.

The first section, "Treatment of Scatter of Fracture Toughness Data for Design Purposes" (Schütz) deals with the treatment of scatter in fracture toughness values and emphasizes that a successful statistical analysis depends on a proper choice of the input data. Coefficient of variation in fracture toughness and the statistical mean value for fracture toughness are evaluated for several alloys and plots are given which indicate the expected mean fracture toughness values for several heats of the same material.

The coefficient of variation in fracture toughness for a particular material does not depend on such factors as the type of alloy, type of product (plate, sheet, extrusions), specimen orientation, temperature and corrosion. All the statistical data given in this chapter correspond to laboratory specimens and the designer implicitly assumes that the scatter in specimen fracture toughness is identical to the scatter in component fracture toughness. This assumption is not always correct as pointed out in chapter 6. For designing a component using probabilistic fracture mechanics the necessary probability of survival must be selected according to engineering judgement.

The second section "Allowance for Variability in Crack Propagation Data" (Anstee) deals with the statistical determination of variabilities in crack growth data for constant amplitude and variable amplitude loading. The standard deviations in crack growth data (derived from several tests) are indicated to enable a comparison of variabilities under constant amplitude and FALSTAFF loading for different materials. These results indicate that the variabilities in crack propagation under random loading are often more than the corresponding variabilities under constant amplitude loading. Also the effect of environment on variabilities is provided for constant amplitude and random amplitude testing of different materials. There is no evidence of any systematic influence of environment on variability. Finally, results on crack propagation in actual structures like aircraft lugs and rotor blades are used to calculate the statistical variabilities due to the type of component. It is found that there is no significant difference in the range of standard deviations in actual components as compared to simple specimens. Develop-

ment of crack growth curves for design purposes poses a particular problem due to the demonstrated greater variability in crack growth rate as compared to the variability in total life.

An Appendix on statistical terms and methods used in analyzing experimental data is also included.

Application of Fracture Mechanics to Stress Corrosion Cracking

It is indicated that a number of landing gear failure in aircraft were due to stress corrosion cracking, making this an important field of study. A method for predicting potential crack size under stress corrosion cracking is presented here which was originally applied to assess the structural integrity of a primary component of the Saturn 1B space vehicle. Also, methods are suggested to determine the required inspection period for stress corrosion cracking. Typical values of stress corrosion cracking parameters are given for commonly used airframe materials and incorporation of these data into damage tolerance analysis is discussed.

Simple Methods of Determining Stress Intensity Factors

Here various techniques to estimate the stress intensity factors of complex crack problems from simple cases are indicated which include a superposition principle, Green's function method, weight functions approach, stress concentration approach, and compounding techniques specially applicable to stiffened structures. These methods provide quick and accurate solutions for many practical crack configurations.

An overall view of the information in this AGARDOgraph strongly indicates that it is the product of close collaboration between the practitioners and researchers in Fracture Mechanics application to aircraft structures. The advantages of such close collaboration are evident in almost all the chapters in this AGARDOgraph. It is hoped that the publication of this manual will stimulate further cooperation and collaboration to advance the state of the art in the significantly vital area of fracture mechanics design methodology in aircraft structures.

2. ENGINE COMPONENTS

by

Thomas A. Cruse

Pratt & Whitney Aircraft Group
Commercial Products Division
East Hartford, Connecticut 06108 USA

CONTENTS

SUMMARY 2-2

SYMBOLS 2-2

2 INTRODUCTION 2-2

2.2 TURBINE DISK CRACK GROWTH SIMULATION 2-2

2.2.1 Crack Initiation and Crack Propagation 2-2
2.2.2 Residual Life for Disk Bores 2-2
2.2.3 Life Extension for Notches in Disks 2-3

2.2.3.1 Fracture Mechnics Analysis for Surface Cracks. 2-3

2.2.3.2 Weight Function Simulation for Surface Cracks. 2-4

2.2.3.3 Definition of Local Stress Ratio. 2-4

2.2.4 Surface Crack Initiation Simulation. 2-4
2.2.5 Cumulative Damage Problems 2-4

2.3 TURBINE BLADE AIRFOIL CRACK GROWTH SIMULATION. 2-4

2.3.1 Thermo-Mechanical Fatigue (TMF) Cycle Definition 2-4
2.3.2 Fracture Mechanics Analysis. 2-5

2.3.2.1 Convection Cooled Airfoils. 2-5
2.3.2.2 Film Cooled Airfoils. 2-5

2.3.3 Crack Growth Rate Data Generation. 2-6

2.4 APPLICATIONS TO REAL STRUCTURES. 2-6

2.4.1 Example: Turbine Disk Fracture Mechanics Design Problem 2-6

2.4.1.1 Step 1: Perform Mission Stress/ Thermal Analysis of Turbine Disk . 2-6

2.4.1.2 Step 2: Predict Crack Growth Rate and Total LCF Life 2-6

2.5 EVALUATION OF APPLIED PROCEDURES AND RECOMMENDATIONS 2-7

2.6 REFERENCES 2-7

2. ENGINE COMPONENTS

T. A. CRUSE

SUMMARY

The chapter describes some of the major areas of fracture mechanics applications to aircraft gas turbine engine component analysis. The rotating disk structure is treated first due to its primary structural importance. While crack initiation and crack propagation are important design concerns for disks, only the propagation portion is discussed in detail. Disk crack problems which are described include growth of internal cracks due to defects and growth of surface cracks following initiation. The turbine airfoil is the second most mature area of fracture mechanics analysis and is briefly described in this chapter. Finally, a brief summary of a turbine disk fracture mechanics problem is presented.

SYMBOLS

a,c	crack size parameters
C	Material constant
$\sigma, \Delta\sigma$	Applied, cyclic strain
K, ΔK	Stress intensity factor
R	Stress ratio (min. stress/max. stress)
$\sigma, \Delta\sigma$	Applied, cyclic stress

2.1 INTRODUCTION

Practical applications of fracture mechanics to engine components is not a widely developed topic. Generally, such applications have emphasized failure analysis rather than design activities. However, some engine component design models have been developed using fracture mechanics methods. The most fully developed is the critical engine disk structure. The second component is the turbine airfoil which impacts performance and maintenance costs. Additional components such as combustor liners and engine cases are beginning to receive attention.

The present chapter, therefore, emphasizes the disk low cycle fatigue life prediction problem in some detail. Following the disk problems is a description of some fracture mechanics methods for turbine blade airfoil life prediction. An example problem from Ref. (1) is then summarized.

2.2 TURBINE DISK CRACK GROWTH SIMULATION

2.2.1 Crack Initiation and Crack Propagation

Fatigue life prediction for gas turbine engine structures may be simplified for most purposes into two distinct problem classifications: initiation of macrocracks at highly stressed locations in defect free material; and propagation of macrocracks in large volume, moderately stressed locations containing a statistical distribution of inherent defects. The fracture mechanics design problem for inherent defects is discussed further on.

Crack initiation is generally taken to be the generation of a surface related crack of sufficient size to be reliably detected in service. In disks, this size is approximately 0.030 inch surface length; smaller initiation sizes may be required in locations such as certain disk rims where vibration stresses can cause rapid crack growth. Initiation of surface macrocracks is a complex problem which is not fully understood. Some portion of the initiation life is required to generate single or multiple microcracks by metallurgical dissipation processes. These microcracks generally grow intermittently before one crack dominates the others. The remaining, and often the greatest percentage of, initiation cycles propagate the small crack. It is not yet clearly established that this microcrack propagation phase follows the standard elastic fracture mechanics models of crack growth.

It has been established through experience that fracture mechanics modeling can be used effectively to predict the subsequent growth of surface macrocracks in disks after initiation. The equally important initiation problem is almost always treated on a strictly empirical basis (see Ref. 2). Considerable further research is required in order to establish a more mathematical modeling basis for microcrack growth. Major issues as to the applicability of fracture mechanics methodology, surface retardation due to machining effects on residual stresses and hardness, multiple initiation and crack interaction, and inspection capabilities need to be addressed. This paper focuses on the design analysis of crack growth in gas turbine engine structures, following the crack initiation phase.

2.2.2 Residual Life for Disk Bores

Fracture mechanics failures of disks for early commercial gas turbine engines were experienced in limited numbers and forced a change in the fatigue life prediction methodology and processing techniques for these disks. It had been assumed that the disk fatigue life could be characterized by the usual specimen-based fatigue (initiation) data associated with surface stress initiated cracks. However, examination of these early failures showed that fatigue crack growth associated with a buried intrinsic defect was the source of the premature disk fractures, as shown in Figure 1. Such inherent defects were not present in the population of fatigue test specimens due to the much smaller volume of sampled material.

It was soon determined that the nature of the internal defect was that,regardless of its initial shape and orientation, the defect initiated a circular, buried crack which grew transverse to the principal normal stress direction. Simple fatigue life calculations for growing circular cracks confirmed

that the cracks were growing progressively through the entire engine operating life. These earliest disk fractures, described briefly in Ref.(3),were associated with calcium aluminide inclusions in the air-melted AMS 6304 compressor disks.

As a result of these early disk fractures, Pratt & Whitney Aircraft (P&WA) initiated extensive studies to characterize the buried defects in currently used titanium and nickel-base engine disks. The problem of buried defect characterization is particularly difficult because of the small defect sizes associated with current alloys and processes, as well as the large quantities of material that must be sectioned to obtain sufficiently complete histograms of defect sizes for clean disk alloys. Nickel disks, for example, contain inherent, process dependent inclusions such as carbide precipitates (0.001 inch), melt formed carbides (0.003 inch), oxides formed from dissolved oxygen (0.007 inch), accidental inclusions such as mold fragments (0.10 inch), and processing voids (0.10 inch) as described in Figure 2. The population distribution of inherent defects is not unimodal; further, the role each of these defect types play in crack initiation is not unimodal due to such issues as whether a critical initial size exists for very small defects, defect orientation and shape, residual stresses around defects, and other microstructural questions.

The fracture mechanics fatigue life prediction for inherent cracks is based on three elements. The first two, described above, are the specification of the distribution of inherent defects, and the identification of the stress cycle based on a mission analysis. Major idealizations are required for both of these elements. Inherent defects are assumed to be equivalent to circular buried cracks of a relatable size. Also, it is assumed that the largest crack that can occur in the fleet of disks is just smaller than the detection limit of the NDI method used (e.g., ultrasonic inspection). The mission is assumed to result in a simple stress excursion ($\Delta\sigma$) at isothermal conditions with no rate effects; subcycle damage is taken to be linearly additive to the major cycle damage.

The third element is, of course, the fracture mechanics model. Given an ideal circular planform buried crack, it is possible to utilize linear elastic fracture mechanics results for the cyclic stress intensity factor

$$\Delta K = \frac{2}{\pi} \Delta\sigma\sqrt{\pi a} \qquad (1)$$

Further, the crack growth rate, da/dN, is assumed to be uniquely related to ΔK, as characterized by standard laboratory testing.

Crack growth prediction for a given level of stress cycling defines the number of cycles to grow an initial crack to its unstable size. The fatigue life analysis is then based on maintaining a disk stress level below that necessary to achieve an adequate number of flight cycles. However, if the largest undetectable crack is assumed to be present in each disk, the model will be excessively conservative. Thus fatigue design for inherent defects requires the use of statistical modeling.

Statistical variables in the disk fracture mechanics model include the defect size and material crack growth rate. Associated variables, such as crack truncation size (inspection limit) and fracture toughness, are taken to be deterministic variables, as is the cyclic stress range. Monte Carlo simulation techniques are used to develop S-N curves for the fracture mechanics problem, as shown in Figure 3, by selecting a design level of risk.

The baseline simulation in Figure 3 is accomplished using the indicated distribution coefficients. Inherent crack size and crack growth rate data are taken to be log normal for the Monte Carlo simulation. Assigned risk is taken to be a probability of fracture of one part in one thousand. The additional curves in Figure 3 have been generated to show the sensitivity of the design curve to some of the principal statistical uncertainities.

A nonlinear crack growth equation is used for the simulation in order to simulate the near-threshold crack growth rates more accurately. The accuracy of the fracture mechanics model for small cracks is more important than accuracy at higher values of stress intensity factor. As a result of the growth model used, the influence of K_{IC} on the fatigue life curves in Figure 3 is an exaggeration of reality. Even with this, it is seen that K_{IC} does not have a major influence on fatigue life, except for low values of K_{IC}.

Further, it can be seen that the effect of crack size truncation level on the fatigue life is limited to those sizes near the threshold level of a given stress cycle. Thus, the defect distribution and the crack growth rate distribution are the principal statistical variables for fracture mechanics life prediction of disks.

2.2.3 Life Extension for Notches in Disks

2.2.3.1 Fracture Mechanics Analysis for Surface Cracks

The elastic fracture mechanics analysis of surface cracks requires numerical analysis. Some of the analysis methods to be used include singularity finite elements (Ref. 4), alternating techniques (Ref. 5), and the boundary-integral equation (BIE) method (Ref. 6). It is not appropriate to describe the relative merits of each method; the BIE method has been successfully used for design purposes at Pratt & Whitney Aircraft.

For fatigue simulation purposes, it has been established that LCF surface cracks in turbine disks may be treated as semi- or quarter-ellipses. This has the benefit of reducing the numerical task by reference of the numerical results to the analytical solution for the buried elliptical crack given in Ref. 7. The BIE-generated numerical results for elliptical surface cracks are given in Ref. 8, and illustrated herein in Figure 4 , for the case of simple, uniform tensile stress normal to the crack plane.

2.2.3.2 Weight Function Simulation for Surface Cracks

Design simulation of surface crack growth in complex geometries requires an efficient means of accounting for local geometrically-induced stress (strain) variations. The weight function method for two dimensional cracks (Ref. 9) has been successfully extended to three dimensional, surface cracks (Ref. 10). An example problem concerns a corner crack at a hole, as shown in Figure 5 taken from Ref. 11. Experimental results for crack growth of this geometry were reported in Ref. 12 for Plexiglas; comparison of the experimental and weight function data is given in Figure 6. Application of this technique to turbine disks is shown in Ref. 13.

2.2.3.3 Definition of Local Stress Ratio

The local stresses at a turbine disk notch are generally loaded beyond the elastic limit. When this occurs the effect of plasticity is to cause a shift in the mean cyclic stress and the stress ratio, as shown in Figure 7. The gradient in local stress ratio is generally along the notch radial direction with no gradient normal to the transverse-notch plane. LCF crack growth simulation can account for this through the use of the resulting local stress ratio in a modified stress intensity factor given as

$$\Delta K_{eff} = \left\{C/(C + 0.1 - R)\right\} \quad \Delta K \qquad (2)$$

In (2), the constant C is determined by laboratory testing at appropriate, constant values of R, the stress ratio.

2.2.4 Surface Crack Initiation Simulation

Inherent defect crack growth is generally limited to regions of the disk where large volumes of material are subjected to moderately high stresses, such as the disk bore or thick web regions. Surface crack initiation and propagation is the important fatigue life problem at disk notches. A major unresolved research issue is the determination of the amount of fatigue life for a surface crack that is microcrack initiation and how much is propagation that can be modeled using standard fracture mechanics techniques. Physical evidence of microcrack initiation is generally difficult to document.

Figure 8 shows a notched fatigue specimen used to simulate a fan disk bolt hole, together with a photo micrograph showing the fatigue fracture surface. It is seen that multiple microcracks were initiated in a surface zone; one of these microcracks subsequently grew to critical size and caused net section fracture. Detailed examination of the crack origins supported the contention of natural metallurgical crack initiation from a size associated with the α-phase of the titanium alloy (0.0003 inch typical). Unfortunately, striation indications were very limited and could not be used to support the use of fracture mechanics modeling of crack growth during the microcrack phase.

Surface crack initiation and early growth was modeled for the bolt hole specimen shown in Figure 8 . The variable stress field for the K-factor determinations and the R-ratio data for the crack growth models were taken from the data in Figure 5. The initial flaw size was taken to be 0.0003 inch, the approximate size of the α-phase microstructure. Crack growth simulation results for various stress analysis models are shown in Figure 9; no attempt was made to adjust the initial crack size in order to correlate the actual specimen failure data. Use of the elastic stress field at the notch is the most conservative assumption for crack growth modeling. The most realistic model included the variable local R-ratio for the elasto-plastic stress distribution.

Microcrack initiation and growth are strongly influenced by surface residual stress and hardness. It was shown in the study reported in Ref. (2) that the plastic work hardening of the surface layer had to be accounted for in correlating crack initiation data. It was further shown in Ref. (14) that this surface effect was apparently a major problem in predicting the surface length and aspect ratio for small surface cracks. Further, the applicability of elastic fracture mechanics models to small surface cracks in elastic stress fields has not been established. Finally, the growth of surface macrocracks may often be the result of the initiation, interrupted propagation, linkup and growth of surface microcracks. Difficult experimental developments are required in order to resolve many of these remaining problems.

2.2.5 Cumulative Damage Problems

It is generally recognized that a maximum stress excursion may retard subsequent cyclic crack growth due to the large plastic zone created by the overload. Gas turbine engine structures generally operate at stress levels close to the maximum safe operating stress for tensile failure (burst). Thus, most complex cycle stress excursions involve stress cycles at a nearly fixed value of peak stress with different values of minimum stress (see Ref. 2). In such cases, crack growth follows the usual linear damage, superposition models.

However, for exceptional situations, the retardation effect of plasticity, or the acceleration effect of creep must be included. Generally, these effects are accounted for in the empirical crack growth model used, and are considered beyond the scope of this chapter. Recent publications by researchers within the gas turbine engine industry (Refs. 15, 16) address the empirical modeling problem.

2.3 TURBINE BLADE AIRFOIL CRACK GROWTH SIMULATION

2. Thermo-Mechanical Fatigue (TMF) Cycle Definition

Turbine airfoil durability is a complex, multifaceted problem due to the extremely aggressive thermal environment in modern, high-powered gas turbine engines. During a typical flight cycle, the turbine airfoil may be subjected to maximum temperatures in excess of 1800°F, high rotational inertia loads, high frequency vibration, corrosive and erosive products of combustion, and occasional impact due to

hard carbon particles. Continuing demands for increased engine efficiency and fuel economy will be satisfied through higher turbine inlet temperature and rotational speeds; these increases must be satisfied with improved turbine blade durability in order to reduce engine maintenance costs.

In order to achieve the necessary turbine airfoil durability in large engines, the high pressure turbine (HPT) blades are generally cooled by compressor air, as shown in Figure 10. In addition, advanced nickel-base superalloys are used for their creep and fatigue resistance; further, the turbine blades are generally coated for corrosive resistance. The two cooling schemes shown in Figure 10 are typical; detailed aspects of the cooling configuration result from the trade-off of minimum cooling air for the necessary turbine blade life.

Many of the turbine airfoil durability problems are not directly related to fracture mechanics modeling. Most design concern with structural life prediction is associated with creep/fatigue interaction crack initiation, as described in Ref. (17). However, coated airfoils are sometimes life limited by crack growth, as described in the following sections.

Structural life prediction for turbine airfoils requires a detailed definition of the local stress, strain, and temperature history within the airfoil for various times within the flight cycle. Mission analysis begins with detailed gas flow and heat transfer calculations. Turbine airfoil temperatures are computed from the external hot gas flow and the internal cooling gas flow using the appropriate boundary layer heat transfer models. The temperature and rotational speed flight cycle history data form the basis for the thermomechanical fatigue (TMF) cycle definition.

In those airfoil life prediction problems requiring greater accuracy, the airfoil is modeled with three-dimensional, elastic finite element tools. A series of stress and strain calculations for various time points in the flight cycle are performed using the temperature data and rotational speed for each time point. The airfoil temperatures are nonuniform, even if the highly local temperature distribution at film-cooling holes is neglected; the resulting thermoelastic strains are the major source of the airfoil life limiting loads.

Figure 11 shows the variation in local strain-temperature history for a turbine airfoil location, including the coating on the outside and inside of the airfoil. It is seen that this TMF cycle, generated during takeoff, cruise, and idle engine operation, can be characterized by a simultaneous cycling of strain (increasing or decreasing) with cycling of temperature. The complex TMF cycle is generally simplified to two cycle shapes characterized by the maximum and minimum cycle temperatures, cycle slope (increasing or decreasing strain with increasing temperature), mean strain and strain range. These cycles form the basis for specimen characterization of airfoil fatigue life.

2.3.2 Fracture Mechanics Analysis

2.3.2.1 Convection Cooled Airfoils

Fracture mechanics modeling for convection cooled airfoils is essentially two-dimensional. Early in the fracture mechanics life of the airfoil, surface cracks initiate in the coating transverse to the maximum cyclic strain direction. These cracks rapidly develop a large aspect ratio (length to depth) and then propagate into the base metal. The edge crack problem is the simple plane strain solution using local strains rather than stresses.

$$\Delta K_e = 1.12 \sqrt{\pi c} \left(\Delta \epsilon_t + \Delta \epsilon_b \right) \qquad (3)$$

In Eq. (3), the crack depth is denoted by 'c', and the local strain field is broken into the transverse tensile strain (ϵ_t) and the wall bending strain (ϵ_b). Finite thickness effects on (3) are easily obtained.

The crack growth rate data for computing the fatigue life for Eq. (3) is generated using TMF cycle crack growth testing, as discussed under Crack Growth Rate Data Generation. Initial crack size data can be taken to be the coating thickness for conservative design puposes. Figure 12 shows the general agreement between analysis and field data that can be achieved using this fracture mechanics model.

2.3.2.2 Film Cooled Airfoils

Unlike the convection cooled airfoil crack, the film cooling hole induces essentially three-dimensional cracks at the acute corner of the cooling hole. The difficult three-dimensional fracture mechanics problem is further compounded by the three-dimensional stress and strain field near the cooling hole, under complex TMF cycle loading.

These modeling difficulties preclude the development of a cost effective fracture mechanics analytical model of reasonable generality. Thus, a semiempirical approach has been developed and reported in Ref. (20). Extensive testing of representative cooling hole geometries in flat plates with material whose crack growth rate was known forms the basis of the empirically defined stress intensity factors. Analytical corrections were reported for the effects of hole spacing on local strain and crack interaction, biaxial and bending loads, surface curvature, and other geometrical terms.

The TMF crack growth rate data used for the life prediction calculation is discussed in the next section. Ref. (18) shows that cracks with initial depths given by the coating thickness can be analytically grown in TMF; the results show good correlation with results obtained on prototypical airfoil specimens.

2.3.3 Crack Growth Rate Data Generation

The results of flight cycle analysis of turbine airfoils clearly establishes the need to simulate the TMF cycle in crack growth testing. Tubular, strain controlled specimens are used in the test reported in Refs. (19, 20). The temperature and strain cycles are independently controlled using induction heating and a servohydraulic test machine. Cooling is achieved using compressed air passed through the interior of the specimen.

TMF testing of the precracked specimens is accomplished using the idealized cycles described above. The cycle variables include maximum and minimum values of strain and temperature, cycle slope, and mean strain. Test data reported in Ref. (18) for isotropic airfoil materials showed that the crack growth rate for fixed strain cycles was independent of the mean strain and mean stress levels. Thus, the crack growth modeling reported above is restricted to a strain intensity factor approach.

Since certain locations of the airfoil are subjected to nominal creep during the airfoil life, this effect was also investigated in Ref. (18). Creep was simulated by periodic incrementation of the mean strain to a level of about one to two percent during the life of the specimen. The effect of superimposed creep was to introduce multiple secondary cracks, parallel to the primary crack. Some increase in crack growth rate was noted but the results were not conclusive, as shown in Figure 13.

Advanced airfoil materials are anisotropic including directionally solidified (DS) and single crystal, nickel-base superalloys. Ref. (20) shows that the TMF crack growth rate is strongly influenced by grain orientation in DS alloys. The strain intensity factor level gave crack growth rate variations of nearly an order of magnitude according to grain orientation; further, the cracking mode was seen to depend on the level of K together with grain orientation. However, it has been possible to correlate the various crack growth rate data for the DS tests in Ref. (20) through the use of the anisotropic elastic modulus dependence and its implications for single crystal behavior is the subject of ongoing research.

2.4 APPLICATIONS TO REAL STRUCTURES

2.4.1 Example: Turbine Disk Fracture Mechanics Design Problem

2.4.1.1 Step 1: Perform Mission Stress/Thermal Analysis of Turbine Disk

Fracture mechanics models for fatigue life prediction correlate crack growth rate data for various geometries based on the cyclic range of the stress intensity factor (K), the cyclic stress ratio (R = minimum stress/maximum stress), and component temperature. Such a local definition of operating conditions results from the component mission simulation analysis. An example problem has been selected from Ref. 1 for the case of the JT8D-17 high pressure turbine disk shown in Figure 14.

The major operating concerns for the turbine disk in Figure 14 include centrifugal stresses due to rotation, thermal stresses due to exposure to compressor discharge cooling air, and local stress concentrations, such as the drilled cooling air supply hole. As a result of the combined loading conditions, the limiting low cycle fatigue (LCF) location is at the cooling air hole exit in the disk rim slot. The detailed disk geometry is shown in Figure 15.

Prediction of the local disk operating conditions requires a thermal and aerodynamic system analysis of the engine for a given flight profile and flight environment, as shown in Figure 16. Following mission thermal cycle analysis, the detailed disk temperature history may be computed based on standard heat transfer analysis, together with estimates of the appropriate boundary conditions. Figure 17 shows a map of the JT8D-17 disk cross-section that was used in a finite difference thermal analysis computer program. The results of the thermal analysis for the disk bore and rim locations are shown in Figure 18. Finally, by combining the mechanical loads and thermal loads, the nominal disk stress history for the selected mission can be computed, see Figure 19. This load history together with a local model of the cooling air hole provide sufficient information to undertake fracture mechanics life prediction.

2.4.1.2 Step 2: Predict Crack Growth Rate and Total LCF Life

Surface crack growth for the JT8D-17 cooling air hole problem has been taken as the application problem, from Ref. (1). The disk geometry and mission analyses were reviewed in Figures 15 through 19. Initiation of a surface crack was predicted for the location shown in Figure 20. The present discussion concerns the predicted subsequent LCF growth of this surface crack. All necessary material properties for the analysis are given in Ref. (1).

LCF growth of the surface crack was predicted using the 700°K (800°F) data based on the mission analysis results. A substantial subcycle in the hoop stress occurs in the rim, as shown in Figure 19. This subcycle was treated as being equivalent to a major load cycle as the subcycle is within 10 percent of the major cycle range, thus giving two load cycles per flight.

The surface flaw was assumed to be semi-elliptical in shape and the orientation of the flaw was such that the plane containing the crack was normal to the local stress field. The growth of the surface flaw was modeled as if the disk was an infinite width structure; this assumption is viewed to be valid for a surface flaw depth less than or equal to three-fourths of the finite structural width. The initial crack aspect ratio of a/c = 0.48 was obtained by analytically growing to the 0.079 cm (1/32 inch) surface length from an 0.01 cm (0.004 inch) surface length crack. Local stress gradients define this initial aspect ratio.

The local stress concentration factor was 3.45 with a peak nominal stress of 3.10×10^8 N/m^2 (44.9 ksi). Stress variations in the engine axial and rotor radial directions were estimated from finite element analysis. LCF crack growth simulation results for R = 0 are shown in Figure 20, based on the weight function design method in Ref. (9).

2.5 EVALUATION OF APPLIED PROCEDURES AND RECOMMENDATIONS

The extensive modeling capabilities of fracture mechanics have been shown to be applicable to a number of gas turbine engine design problems. Further examples include static structures in engines, which are just now being modeled with fracture mechanics methods. It must be recognized, however, that the complex environment within the engine not only makes the use of these models difficult for the designer, but also makes acquisition of substantiation data expensive and, in some cases, beyond instrumentation capability.

It must also be pointed out that the safe life of rotating engine structures is generally based on crack initiation modeling. Advanced material developments emphasize high strength materials with good LCF initiation properties, often to the detriment of the crack propagation properties. Use of fail safe design philosophy for these problems involves potential performance/cost risks that may mitigate against its application.

2.6 REFERENCES

1. Alver, A. S. and Wong, J. K., "Improved Turbine Disk Design to Increase Reliability of Aircraft Jet Engines", NASA CR-134985, (1975).

2. Cruse, T. A. and Meyer, T. G., "A Cumulative Fatigue Damage Model for Gas Turbine Engine Disks Subjected to Complex Mission Loading," Journal of Engineering for Power, ASME (to be published).

3. Sattar, S. A. and Sundt, C. V., "Gas Turbine Engine Disk Cyclic Life Prediction," Journal of Aircraft, 12, 4, 360-365 (1975).

4. Raju, I. S. and Newman Jr., J. C., "Improved Stress-Intensity Factors for Semi-Elliptical Surface Cracks in Finite-Thickness Plates," NASA TMX-72825 (1977).

5. Kobayashi, A. S., Polvanick, N., Emery, A. F. and Love, W. J., "Corner Crack at the Bore of a Rotating Disk," Journal of Engineering for Power, 98, 4, ASME, 465-472 (1976).

6. Cruse, T. A., "Numerical Evaluation of Elastic Stress Intensity Factors by the Boundary-Integral Equation Method," The Surface Crack: Physical Problems and Computational Solutions, American Society of Mechanical Engineers, New York, N.Y., 1972, pp. 53-170.

7. Green, A. E., and Sneddon, I. N., "The Stress Distribution in the Neighborhood of a Flat Elliptical Crack in an Elastic Solid," Proceedings of the Cambridge Philosophical Society, Vol. 46, 1950, pp. 59-163.

8. Cruse, T. A. and Meyers, G. J., "Three-Dimensional Fracture Mechanics Analysis," Journal of the Structural Division, Vol. 103, No. ST2, ASCE, 309-320 (1977).

9. Bueckner, H. F., "Weight Functions for the Notched Bar", General Electric Report No. 69-LS-45 (1969).

10. Besuner, P. M., "Residual Life Estimates for Structures with Partial Thickness Cracks," Mechanics of Crack Growth, ASTM STP 590, Philadelphia, 403-419 (1976).

11. Cruse, T. A., Meyers, G. J., and Wilson, R. B., "Fatigue Growth of Surface Cracks", Flaw Growth and Fracture, ASTM STP 631, American Soceity for Testing and Materials, 174-189 (1977).

12. Snow, J. R., "Stress Intensity Factor Calibration for Corner Flaws at an Open Hole", Technical Report AFML-TR-74-282, Air Force Materials Laboratory, Dayton, Ohio (1974).

13. Cruse, T. A. and Besuner, P. M., "Residual Life Prediction for Surface Cracks in Complex Structural Details," Journal of Aircraft, 12, 4, 369-375 (1975).

14. Cruse, T. A., Gemma, A. E., Lacroix, R. F. and Meyer, T. G., "Surface Crack Life Prediction: An Overview," Part-Through Crack Life Prediction, ASTM STP (to appear).

15. Gemma, A. E. and Snow, D. W., "Prediction of Fatigue Crack Growth Under Spectrum Loads", Eleventh National Symposium on Fracture Mechanics (1978).

16. Annis, C., Sims, D. and Wallace, R., "A New Model for High Temperature Crack Propagation", Air Force Materials Laboratory Report AFML-TR-76-176 (3 parts), (1977).

17. Loferski, M. T., "Turbine Airfoil Life Predicion by Mission Analysis," Journal of Aircraft, 12, 4, 400-402 (1975).

18. Gemma, A. E. and Phillips, J. S., "The Application of Fracture Mechanics to Life Prediction of Cooling Hole Configurations in Thermo-Mechanical Fatigue," Engineering Fracture Mechanics, 9, 25-36 (1977).

19. Rau, C. A., Gemma, A. E. and Leverant, G. R., "Thermal-Mechanical Fatigue Crack Propagation in Nickel- and Cobalt-Base Super-alloys Under Various Strain-Temperature Cycles", Fatigue and Elevated Temperatures, ASTM STP 520, American Society For Testing and Materials, 166-178 (1973).

20. Gemma, A. E., Langer, B. S. and Leverant, G. R., "Thermo-Mechanical Fatigue Crack Propagation in an Anisotropic (Directionally Solidified) Nickel-Base Superalloy," Thermal Fatigue of Materials and Components, ASTM STP 612, D. A. Spera and D. F. Mowbray, Eds., American Society for Testing and Materials, 199-213 (1976).

ACKNOWLEDGEMENTS

The author wishes to express his sincere appreciation to Messrs. J. T. Hill, P. M. Besuner, G. J. Meyers, T. G. Meyer, and A. E. Gemma for their contributions to this expanding area of technology.

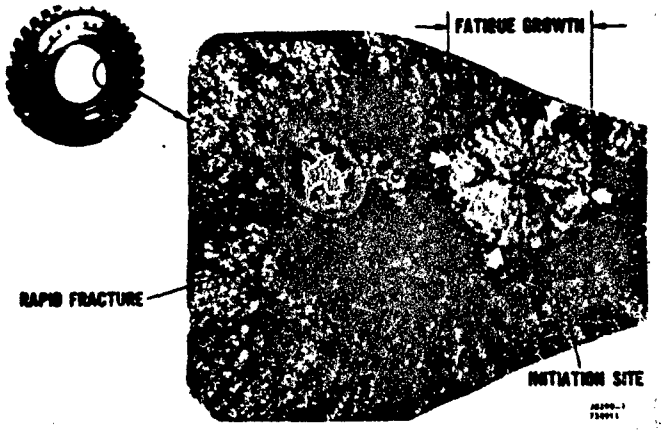

Figure 1 Failed Turbine Engine Disk

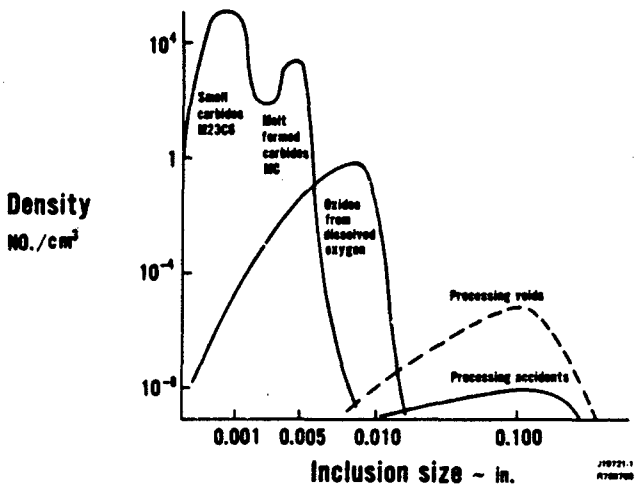

Figure 2 Hypothetical Disk Material Defect Distribution

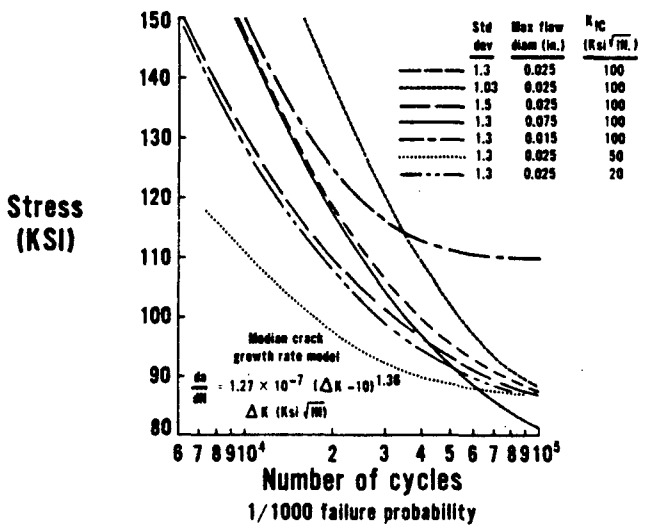

Figure 3 Monte Carlo Simulation Results for Disk Fatigue Life Prediction

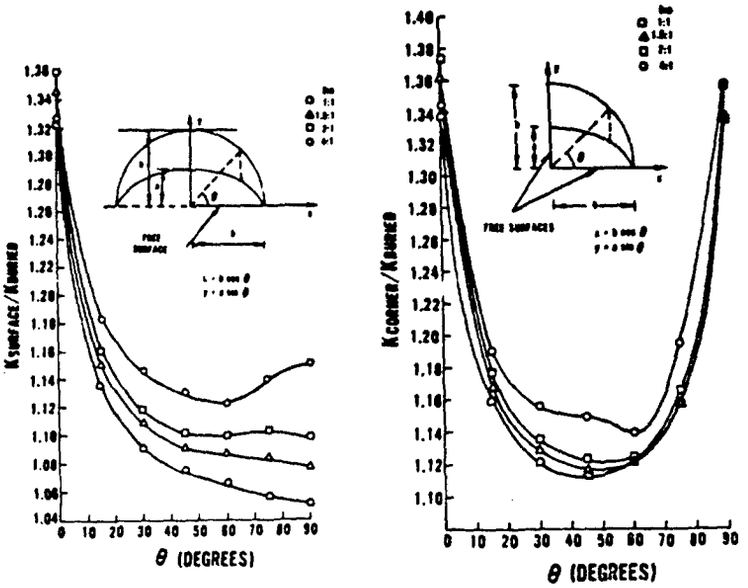

Figure 4 Effect of Free Surfaces for Elliptical: (a) Surface Cracks; (b) Corner Cracks

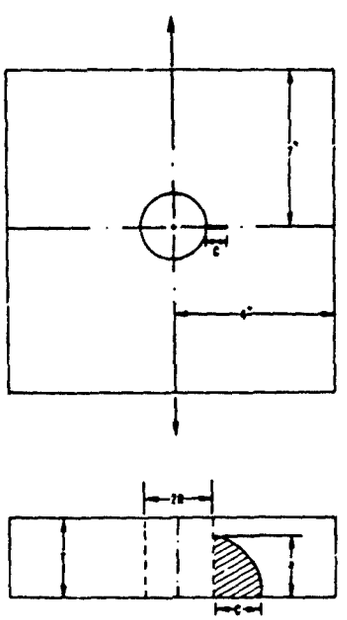

Figure 5 Test-Specimen Geometry for Corner-Crack Testing

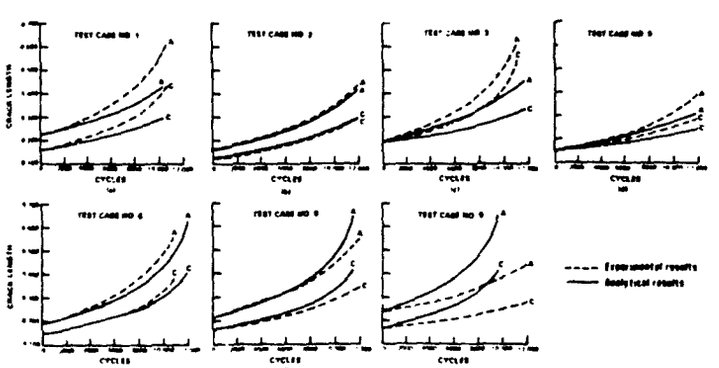

Figure 6 Comparison of Experimental Data for Corner Cracks to Weight Function Predictions for Various Initial Crack Sizes

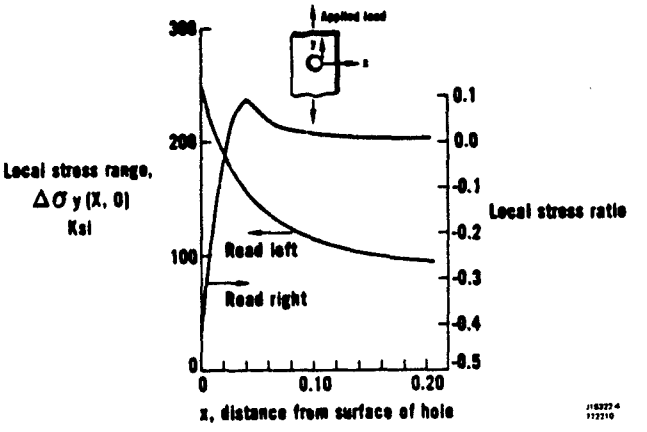

Figure 7 Stress Range and Stress Ratio Near the Bolt Hole

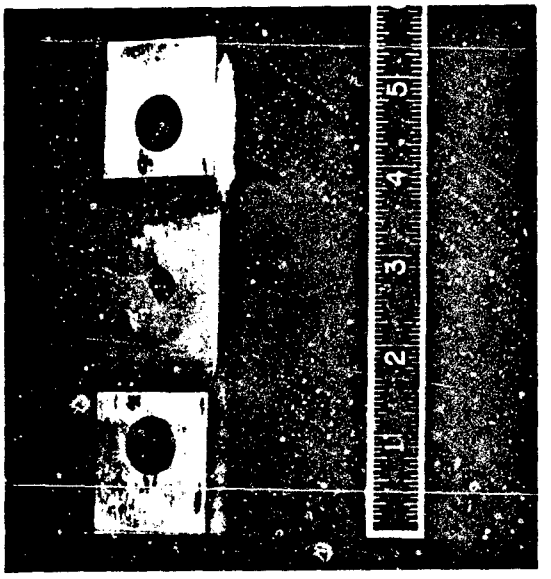

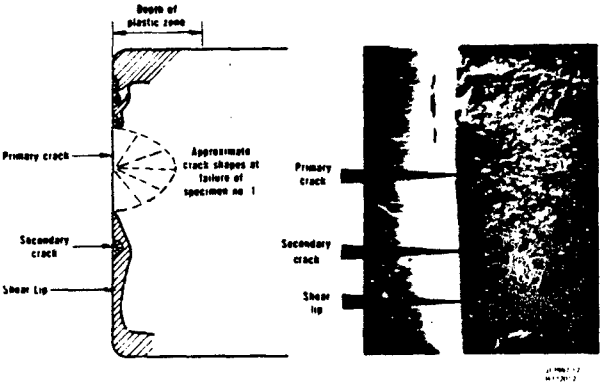

Figure 8 Bolt Hole Specimen

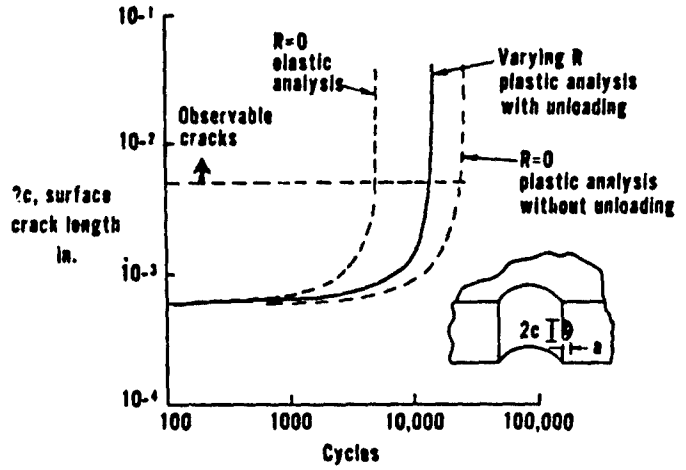

Figure 9 Crack Growth Simulation From Bolt Hole Surface

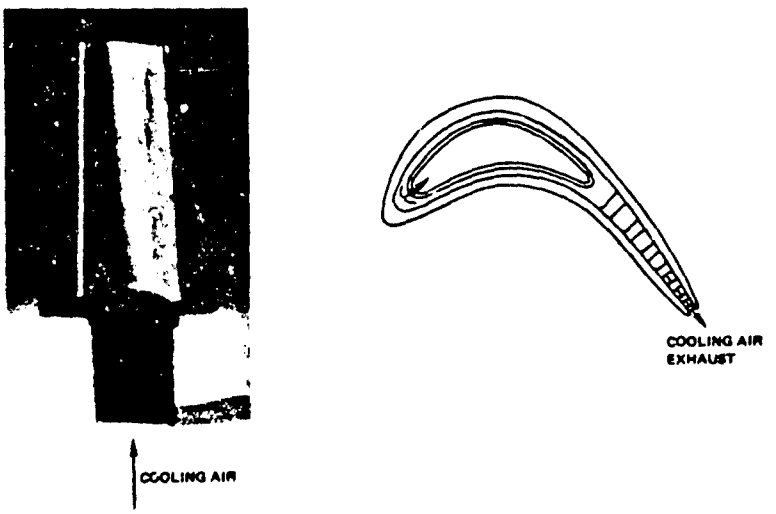

a) CONVECTION COOLED

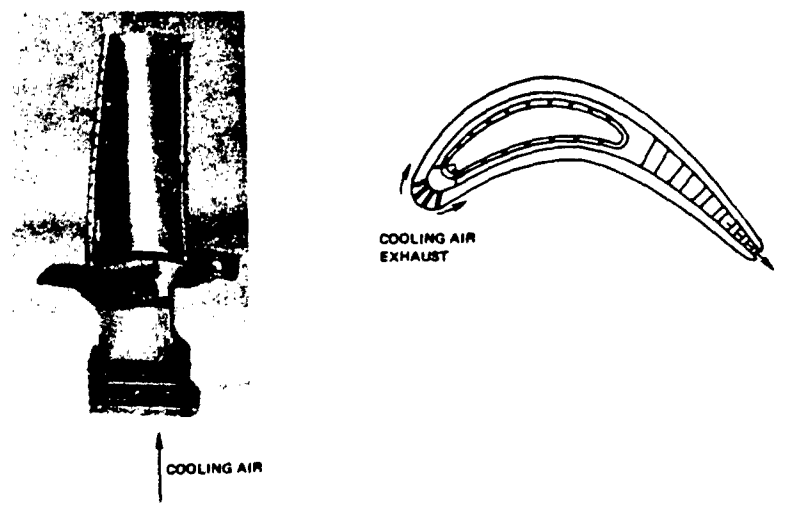

b) FILM COOLED

Figure 10 Air-Cooled Turbine Blades

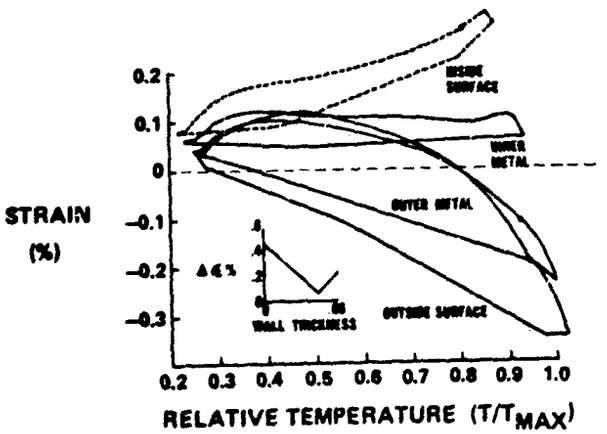

Figure 11 Typical Strain Temperature Relationships for Various Points Through Wall Thickness

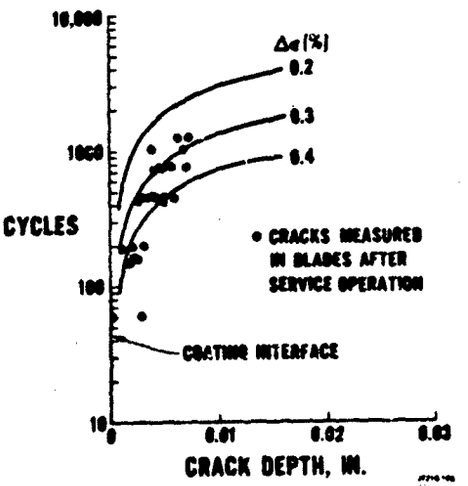

Figure 12 Turbine Blade Crack Growth - Suction Side

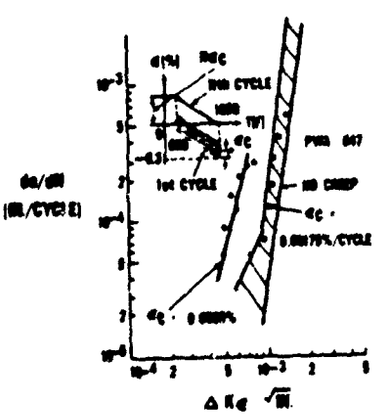

Figure 13 Creep-Fatigue Interaction Test Simulation

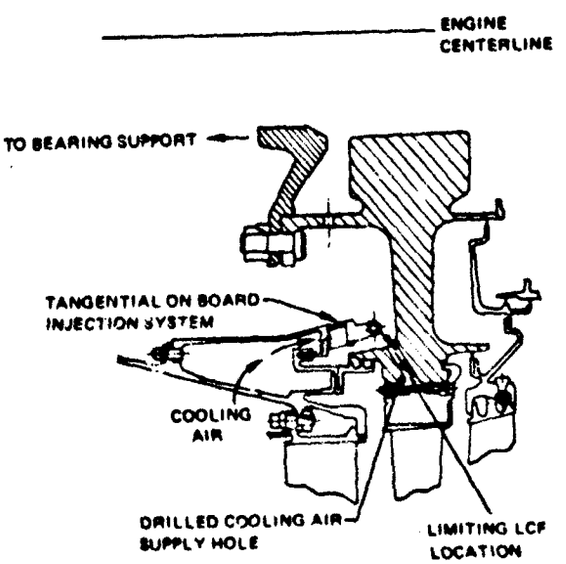

Figure 14 JT8D-17 High Pressure Turbine Disk Cross-Section

(FROM NASA CR-134985)

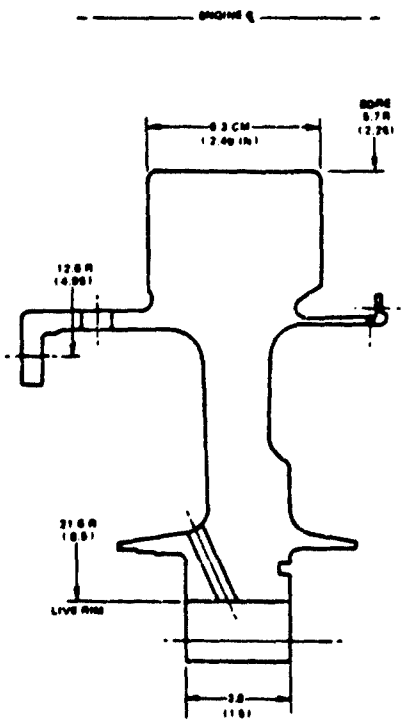

Figure 15 Schematic of Turbine Disk

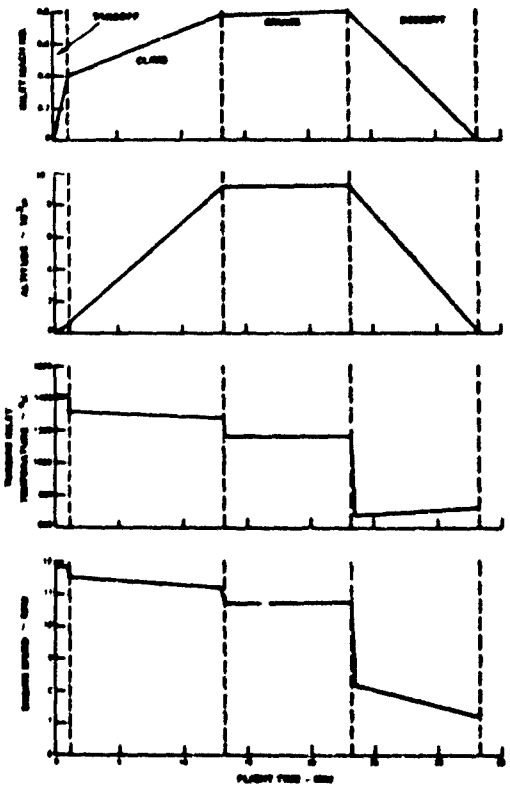

Figure 16 JT8D-17 Simplified Engine Flight Cycle

FIGURES FROM NASA CR-134985

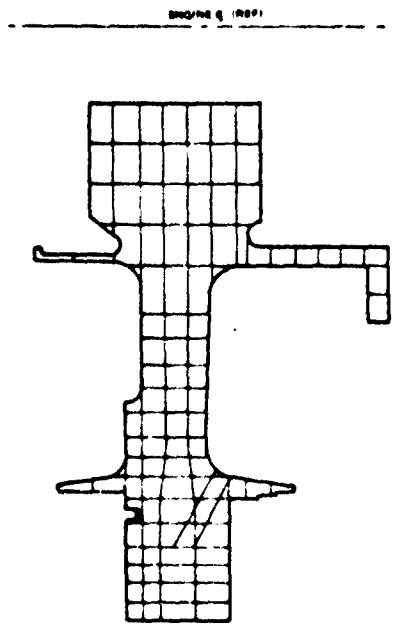

Figure 17 Finite Element Disk Thermal Models

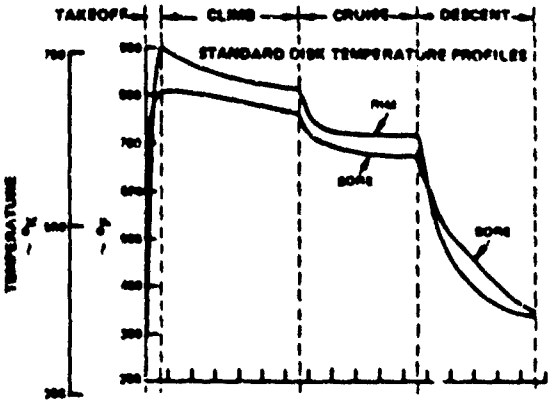

Figure 18 Disk Rim and Bore Averaged Surface Temperatures vs. Flight Time

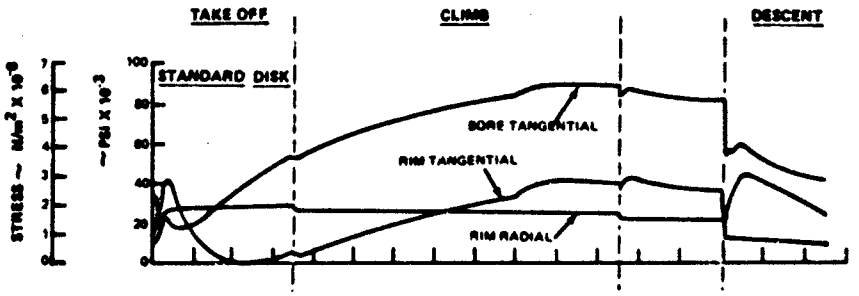

Figure 19 Nominal Disk Rim and Bore Stresses at Various Flight Conditions

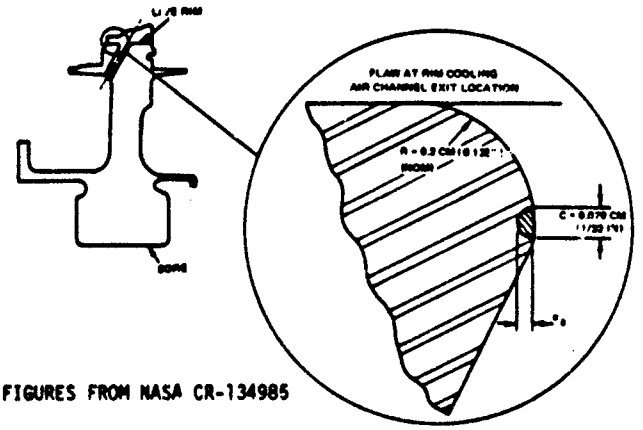

FIGURES FROM NASA CR-134985

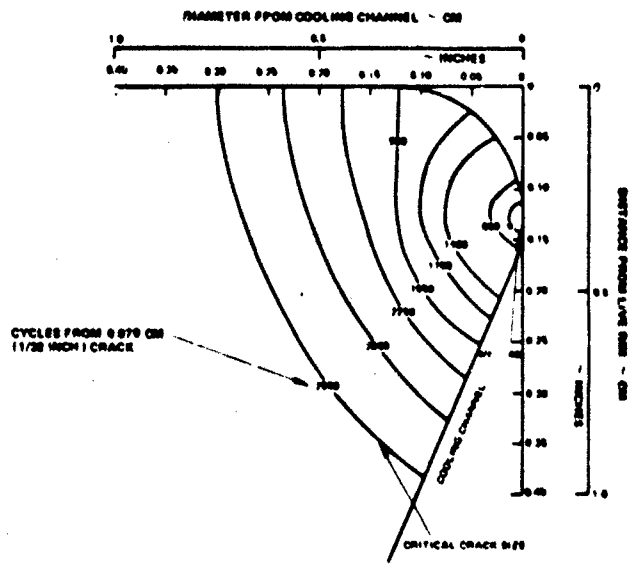

Figure 20 Crack Profiles for Disk Cooling Air Channel Exit Crack

CHAPTER 3 BUILT-UP STRUCTURES

H. VLIEGER

National Aerospace Laboratory NLR
Anthony Fokkerweg 2, 1059 CM Amsterdam
The Netherlands

3.1 INTRODUCTION 3-3
3.2 INTERACTION OF REINFORCING AND CRACKED ELEMENTS IN A BUILT-UP STRUCTURE 3-3
3.2.1 Application of fracture mechanics in general 3-3
3.2.2 First approaches to sheet-stiffener interaction problem 3-5
3.2.3 Reviews of first approaches and new solutions 3-7
3.2.4 Sheet-stiffener interaction computations related to fatigue crack growth 3-7
3.2.5 Modelling of the rivet connection 3-7
3.2.6 Double rows of rivets 3-7
3.2.7 Partial failure of stiffeners and debonding of adhesive bonded panels 3-7
3.2.8 Effect of crack tip plasticity 3-9
3.2.9 Laminated and sandwich panels 3-9
3.2.10 Available computer programmes 3-9
3.3 RESIDUAL STRENGTH 3-11
3.3.1 Residual strength of flat panels loaded in uniaxial tension 3-11
3.3.1.1 Stress intensity factor approach 3-11
(a) Unstiffened panels 3-11
(b) Stiffened panels with fully elastic stiffeners and fastening system and nominally elastic crack tip stresses 3-17
(c) Effect of yielding of stiffeners and fastening system 3-18
(d) Effect of crack tip plasticity 3-18
3.3.1.2 Energy balance concept 3-20
(a) Principles of the method 3-20
(b) Application to unstiffened panels 3-22
(c) Application to stiffened panels 3-22
(d) Use of the R-curve approach for structural applications 3-24
3.3.2 Residual strength of curved panels subjected to pressure cabin loads 3-24
3.3.2.1 Effect of internal pressure 3-24
3.3.2.2 Effect of biaxial loading 3-25
3.3.3 Application of fracture mechanics principles to real structures 3-25
(a) Information available from literature 3-25
(b) Practical examples 3-25
EXAMPLE PROBLEM 3.3.3.1 : Residual strength of 7075-T73 panels with 8 inch stiffener spacing (T.Swift) 3-26
" 3.3.3.2 : Residual strength of 7075-T73 panels with 20 inch frame spacing (T.Swift) 3-33
" 3.3.3.3 : The effects of rivet yielding on residual strength of stiffened structure containing cracks (T.Swift) 3-38
" 3.3.3.4 : The use of resistance curves in residual strength prediction (D.P.Wilhem) 3-43
" 3.3.3.5 : Application of fracture mechanics in designing lower surface of transport aircraft wing (V.G.Nanduri) 3-47
" 3.3.3.6 : Residual strength of bonded panels with 2024-T3 skin and 7075-T73 or 2024-T3 stiffeners (H.Vlieger) 3-51
" 3.3.3.7 : Residual strength of riveted panels with 7075-T6 or 2024-T3 skins and 7075-T6 stiffeners (H.Vlieger) 3-58
3.4 FATIGUE CRACK PROPAGATION (D. BROEK)
3.4.1 Fatigue crack propagation in built-up skin-stringer structures 3-62
3.4.1.1 Introduction 3-62
3.4.1.2 The crack propagation curve 3-62
3.4.1.3 Damage development assumptions 3-62
3.4.1.4 Integral panels 3-67
3.4.2 Application of fracture mechanics principles to real structures 3-67
(a) Information available from literature 3-67
(b) Practical examples 3-67
EXAMPLE PROBLEM 3.4.2.1 : Stiffened wing panel at spar-panel joint (L.Casalegno) 3-68
" 3.4.2.2 : Crack propagation and deceleration in stiffened panels (J.M.Thomas) 3-70
" 3.4.2.3 : Crack propagation in wing stringer-skin panels (M.Bradley) 3-77
" 3.4.2.4 : Engine pylon of medium transport (D.Grange) 3-82
" 3.4.2.5 : Damage tolerance of a pressure bulkhead (D.Grange) 3-85
" 3.4.2.6 : Crack propagation analysis of flat stiffened panels (L.Schwarmann) 3-88
" 3.4.2.7 : Crack propagation analysis of pressurised fuselage structure (L.Schwarmann) 3-93
" 3.4.2.8 : Fatigue crack propagation in structures with riveted stiffeners (A.Salvetti) 3-97
3.5 REFERENCES 3-108

LIST OF SYMBOLS

a	half crack length of through crack, crack depth of surface flaw
a_o, a_i	initial half crack length
a_c	half crack length at onset of unstable crack growth
a_{eff}	half crack length corrected for plastic zone size = $a+r_p$
A	cross sectional area
b	stiffener spacing
c	half crack length of surface flaw
C	stress intensity correction factor = $K_{STIFFENED}/K_{UNSTIFFENED}$
C_F	Forman constant
C_m	material constant in notch strength analysis
d	fastener diameter, debond length
E	Young's modulus
F	work performed by external force, stiffener load
F_{tu}	ultimate tensile strength
G	elastic energy release rate = $\partial U/\partial a$
G_i	G-value at initiation of stable crack growth
J	elastic-plastic energy release rate
K	stress intensity factor = $\sigma\sqrt{\pi a}$
K_c	plane stress fracture toughness related to critical stress and crack length = $\sigma_c\sqrt{\pi a_c}$
K_{c_F}	Forman constant
K_e	plane stress fracture toughness related to critical stress and initial crack length = $\sigma_c\sqrt{\pi a_o}$
K_i	plane stress fracture toughness related to initial stress and crack length = $\sigma_i\sqrt{\pi a_o}$
K_{I_c}	plane strain fracture toughness
K_P	stress intensity factor due to rivet loads P
K_u	static notch strength factor
K_σ	stress intensity factor due to end stress σ
L	stiffener load concentration factor = F_{MAX}/F_{REMOTE}
n, N	number of cycles
n_F	Forman constant
p	cabin pressure, stress distribution along x-axis (p(x)), rivet spacing
P_i	rivet force at point i
r_p	plastic zone correction factor, plastic zone radius
R	energy consumption during crack growth = $\partial W/\partial a$, stress ratio in fatigue cycle (= $\sigma_{min}/\sigma_{max}$)
R_C	radius of curvature
s	stiffener spacing
t	sheet thickness
U	elastic energy
v	displacement in sheet (components v_a, v_b, v_c)
W	energy required for crack growth, panel width
x, y	Cartesian coordinates
Y	stress intensity correction factor
β	bulging coefficient, ratio of crack tip stresses (σ_{yct}) in stiffened and unstiffened panel
δ	crack opening displacement, fastener displacement
μ	stiffening ratio
ν	Poisson's ratio
σ	stress (gross)
σ_c	stress at fracture of unstiffened sheet, stress at unstable crack growth initiation of stiffened panel
σ_i	stress at initiation of stable crack growth
σ_y, σ_{yield}	yield strength
τ	shear stress

Suffices

cs	critical value in stiffened panel
cu	critical value in unstiffened panel
g	gross
MAX,max	maximum
min	minimum
net,n	netto
PHY	physical
SH,sh	sheet
ST,st	stiffener
ult,u	ultimate

3.1 INTRODUCTION

The major part of an aircraft structure consists of built-up panels of sheets and stringers, e.g. wing and fuselage skin panels; spar webs; skin and stiffener doublers. Past experience has shown that despite all precautions cracks may arise in any of these structural elements. Cracks will reduce the stiffness and the load carrying capacity of the structure, and because in built-up structures any element is essential for the functioning of the structure as a whole, the possibility of cracking must be taken into account early in the design stage, i.e. the designer has to make his concept "damage tolerant". With a view to this the task of the designer is twofold. On the one hand he has to ensure that the chance of crack initiation will be minimized, and that if cracking occurs it will do so as late as possible in the service life and the cracks will grow very slowly so that repair will be minimized. This can be achieved by a well-considered detail design (avoidance of holes, cut-outs, sharp angles, sudden cross-sectional changes and eccentricities in components subjected to tension); by a good arrangement of structural elements; and by choosing material with good fatigue and crack propagation properties. On the other hand, the designer of a damage tolerant structure has to guarantee safe operation of the aircraft assuming a crack of a certain size to be present. To do this he has to be able to predict the fatigue life until final failure, starting with a certain minimum (= detectable) crack length. Further, he has to be able to demonstrate that a specified load (usually equal to limit load) can still be carried by the structure with a certain amount of damage being present (e.g. a two-bay skin crack with or without failure of the central stiffener). In other words, the crack propagation and residual strength capabilities of built-up structures have to be demonstrated to meet certain requirements early in the design stage of the aircraft. The foregoing implies that the designer is expected to have analytical and/or experimental tools available to demonstrate that his design meets these damage tolerant requirements. The present chapter deals with the latter part of the designer's task, i.e. prediction of residual strength and crack propagation properties. In the past, fracture mechanics has proved to be a valuable means to determine these properties. How designers applied fracture mechanics in recent projects and how it can be applied in future designs will be discussed here.

The reader of this chapter is assumed to have some knowledge of fracture mechanics. Background reading on fracture and the fundamentals of fracture mechanics can be obtained from textbooks published by Broek [1], Knott [2] or from a special issue of the Journal of Strain Analysis, written by different specialists in this field [3] .

When a crack occurs in any element of a built-up structure, it is characteristic of this type of structure that it has the ability to transfer load from the cracked to the intact elements, thus relieving the most critical part of the structure. Conceivably this interaction of intact and cracked elements will be essential for the residual strength and crack propagation behaviour of the built-up structure as a whole. In the literature a reasonable amount of information can be found dealing with this subject. A review of that literature will be given in section 3.2 of this chapter.

Following on from section 3.2, the residual strength and crack propagation behaviour of built-up structures are discussed in sections 3.3 and 3.4 respectively. At the end of each section a number of practical examples are compiled that illustrate residual strength and crack propagation analyses of skin-stringer combinations made available by various sources. In the heading of each example the source is mentioned. The examples are presented as much as possible in their original but edited form to give full credit to the contributors. It is emphasized that the way of presentation, the contents and conclusions are the responsibility of the contributors. Each example is followed by some concise editorial comments.

3.2 INTERACTION OF REINFORCING AND CRACKED ELEMENTS IN A BUILT-UP STRUCTURE

When a crack occurs in any element of a built-up structure one or more nearby intact elements will usually take over some load from the cracked component. Depending on the type of design, this load transfer will occur directly after initiation of the crack (e.g. a crack in one of the layers of a multi-ply laminate) or after some growth of the crack (e.g. a skin crack initiating at a stringer runout and propagating towards intact stiffeners). In other words, contrary to a monolithic structure, the built-up structure has the ability to transfer the load from the cracked element along an alternate load path, thus reducing the severity of the stress condition at the crack tip of the severed element. In general this load transfer will result in a higher failure stress of the built-up component as compared to that of a monolithic structure of the same dimensions and with the same crack size. However, owing to the local overload in the intact elements one of these elements may fail abruptly and completely (owing to its limited static strength) or become cracked as well and fail after some time. In such cases the effect of the additional load carrying elements on the stress condition at the crack tip will be detrimental, because of the pulling-open forces exerted by the failed component on the cracked part. These alternative possibilities imply that an accurate appraisal of the amount of interaction of the intact and cracked elements in a built-up structure is essential for prediction of the residual strength and crack propagation properties of the built-up structure as a whole.

Because most built-up structures in an aircraft consist of sheet (skin) reinforced by stiffening elements, and the skin usually commences to crack first, the configuration of a cracked skin provided with an intact stiffener is commonly used as a model for the interaction of built-up sheet structures. In some cases the effect of a partly or completely failed stiffener on the stress condition at the crack tip is considered (see literature review further on in this section).

3.2.1 Application of fracture mechanics in general

In elastic fracture mechanics it is usually assumed that the stress condition at the crack tip is governed by the stress intensity factor, K. For an unstiffened centrally cracked sheet K is defined by

$$K = f\,(a/W)\,.\,\sigma\sqrt{\pi a} \qquad (1)$$

where σ is the gross stress remote from the crack, a is the half crack length, W is the panel width and $f(a/W)$ is a factor accounting for limited panel size. Cracks in aircraft structures are generally limited to a small fraction of the panel width, and so the correction factor is close to unity. For this reason this factor will be ignored henceforth in the expressions for the stress intensity factor. More information concerning finite width correction factors can be found in textbooks on fracture mechanics (for example [1]).

TABLE 1 OVERVIEW OF FIRST APPROACHES TO SHEET-STIFFENER INTERACTION

CONFIGURATIONS STUDIED (ALL CONFIGURATIONS ARE LOADED BY UNIAXIAL TENSION)			AUTHORS AND SOURCES
INFINITE SHEET	RIVETED STIFFENERS	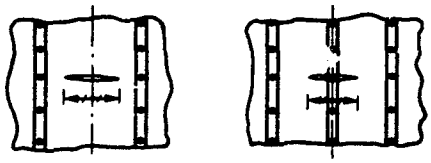 STIFFENERS INTACT	ROMUALDI, FRASIER, IRWIN, SANDERS, P.H., [4], [6-8]
	CONTINUOUSLY ATTACHED LINE STIFFENER	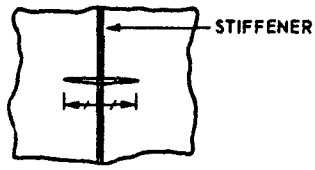 STIFFENER STIFFENER INTACT OR BROKEN	SANDERS, J.L., Jr., [9]
		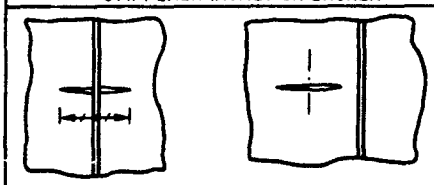 STIFFENER INTACT	GREIF, SANDERS, J.L., Jr., [10]
	RIVETED STIFFENER	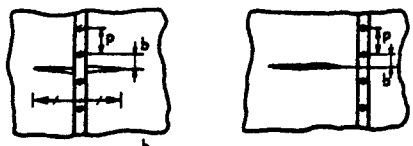 STIFFENER INTACT OR BROKEN	BLOOM, SANDERS, J.L., Jr., [11]
FINITE AND INFINITE SHEET	CONTINUOUSLY ATTACHED LINE STIFFENER WITH ARBITRARY BENDING STIFFNESS	CENTRALLY CRACKED STRIP WITH STIFFENED EDGES 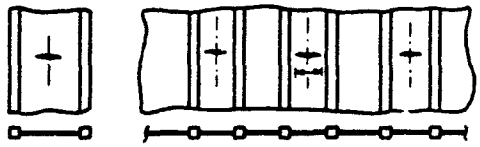 INFINITE CRACKED SHEET WITH ONE STIFFENER STIFFENED SHEET WITH PERIODIC ARRAY OF CRACKS PERIODIC ARRAY OF CRACKED STRIPS 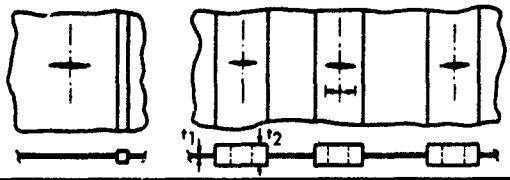	ISIDA, ITAGAKI, IIDA [14-19]
INFINITE SHEET	MULTIPLE RIVETED STIFFENERS	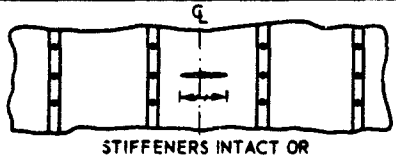 STIFFENERS INTACT OR ANY NUMBER OF STIFFENERS BROKEN 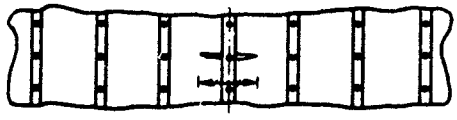	POE [20-22]

In the literature the effect of the stiffener(s) on the stress intensity at the crack tip is usually expressed by the value of the "stress intensity correction factor", C(a), defined as the ratio of the stress intensity factors of the stiffened ($K_{STIFFENED}$) and the unstiffened panel ($K_{UNSTIFFENED}$) at the same crack length, or

$$C(a) = \frac{K_{STIFFENED}}{K_{UNSTIFFENED}} \qquad (2)$$

The amount of overload in the stiffener(s) due to the presence of the crack is usually expressed by the value of the "stiffener load concentration factor", L(a), defined as the ratio of the stiffener loads occurring in the region of the crack (F_{max}) and remote from the crack (F_{REMOTE}), or

$$L(a) = \frac{F_{MAX}}{F_{REMOTE}} \qquad (3)$$

In the literature many publications dealing with sheet-stiffener interaction are available. Much less numerous are the publications dealing with the interaction in laminates and sandwiches. A review of the various publications on the crack-surroundings interaction in built-up sheet structures is given in the following sections. It is emphasized here that it is not the author's intention to present quantitative results published in the different references reviewed. The aim of the review is simply to let the designer know where and what is to be found in the literature available on this subject.

3.2.2 First approaches to sheet-stiffener interaction problem

In this sub-section a historical overview of the first approaches to sheet-stiffener interaction is given. Table 1 shows schematically the configurations studied by various investigators together with the assumptions made.

To the author's knowledge the first publication on this subject is from Romualdi, Frasier and Irwin [4]. Their work presents examples illustrative for the calculation of K in a cracked sheet with riveted stiffeners. Two crack locations are considered, viz. a crack symmetrically located at a stiffener, and between two stiffeners. The stress intensity factor is computed by considering the stress situation for a crack in a stiffened panel as that of an unstiffened sheet with superimposed fields of stress due to the rivet forces (see Figure 1). For that purpose the magnitude of the rivet forces has to be known. Romualdi computed the rivet forces from analytical equations expressing the consistency of displacements in sheet and stiffener at the rivet locations (see Figure 1). The stresses and displacements in the cracked sheet were found with the aid of a stress function suggested by Westergaard [5] . When the rivet forces are known, the total K-value is found by superimposing the K solutions for the different stress systems. The K-values found in [4] illustrate that the riveted stiffeners for both crack locations serve as effective crack stoppers. The calculations were checked experimentally by employing straingauge techniques for the measurement of the total stress intensity at the crack tip. Satisfactory correlation between analysis and tests was obtained. The principles of the work in [4] were further developed in later publications by Romualdi and Sanders [6,7,8] . It has to be noted here that the work of Romualdi et al. in fact has been the basis for most of the analytical procedures developed later by other investigators.

Independently of the work of Romualdi, reports and articles dealing with sheet-stiffener interaction were published by Sanders, Greif and Bloom [9,10,11] . Sanders [9] used in his analysis an analytical function of a complex variable to describe the stress-displacement relations, while Greif, Sanders and Bloom [10,11] applied the complex variable method of Muskhelishvili [12] . Sanders and Greif [9,10] presented a solution for the stress problem of an infinite cracked sheet stiffened by a continuously attached line stiffener of constant cross-sectional area. The crack extends perpendicularly to the stringer. Sanders [9] considered the case of a crack extending an equal distance on either side of the stiffener (symmetric crack) and treats the cases of a broken and an unbroken stiffener. Greif and Sanders [10] considered both symmetric and non-symmetric cracks (i.e. a crack located on one side of the stiffener) extending under or beside an intact stiffener. Bloom and Sanders [11] considered symmetric and non-symmetric cracks extending under or beside an intact or broken stiffener attached to the sheet by means of equally spaced rigid rivets of equal diameter. Sanders, Greif and Bloom [9-11] presented their results in the form of curves relating C and L (see equations (2) and (3)) to crack length and stiffness parameters. In their work C is the ratio of the stresses $\sigma_y(x)$ in the stiffened and unstiffened sheet for x approaching x_{tip} instead of the ratio of stress intensity factors. A brief review of the results obtained in [9-11] can be found in a report of Vlieger and Broek [13] .

While the work of Sanders, Greif and Bloom is related to infinite width sheet provided with only one stiffener, Isida and his co-workers [14-19] studied mainly the effect of continuously attached stiffeners on the stress intensity of centrally cracked sheets of finite widths. Their analysis is based on Laurent's expansions of the complex stress potentials, where the expansion coefficients are determined from the boundary conditions. The formulae for the crack tip stress intensity factors are presented in the form of power series of the ratio of crack length to sheet width for various combinations of the extensional and bending stiffness of the stringers. Numerical results for typical cases are summarized in diagrams.

The analyses performed by Sanders, Greif and Bloom [9-11] and Isida [14-19] were carried out on panels of simple configuration provided with only one or two stiffeners. Isida considered in some of his publications [15,17] panels with more than two stiffeners, but in those cases cracks were present in every other stiffener bay to account for finite panel width. Poe [20,21,22] published data relating to infinite wide panels of realistic design. He examined the effect of multiple stringers on the stresses in a cracked sheet with crack lengths up to six times the stiffener spacing. The stringers were assumed to be uniformly spaced and attached to the sheet by means of uniformly spaced rivets. Poe determined the unknown rivet forces in his analysis by requiring the displacements in the sheet and stringers to be equal at corresponding rivet locations (in fact the same approach as proposed by Romualdi et al.). The stress intensity factor for the cracked stiffened sheet was determined by superimposing the solutions of the stress intensity factor for the rivet forces and for the applied uniaxial stress. Two symmetrical cases of crack location were considered, viz. a crack extending equally on both sides of a stringer and a crack extending equally on both sides of a point midway between two stringers.

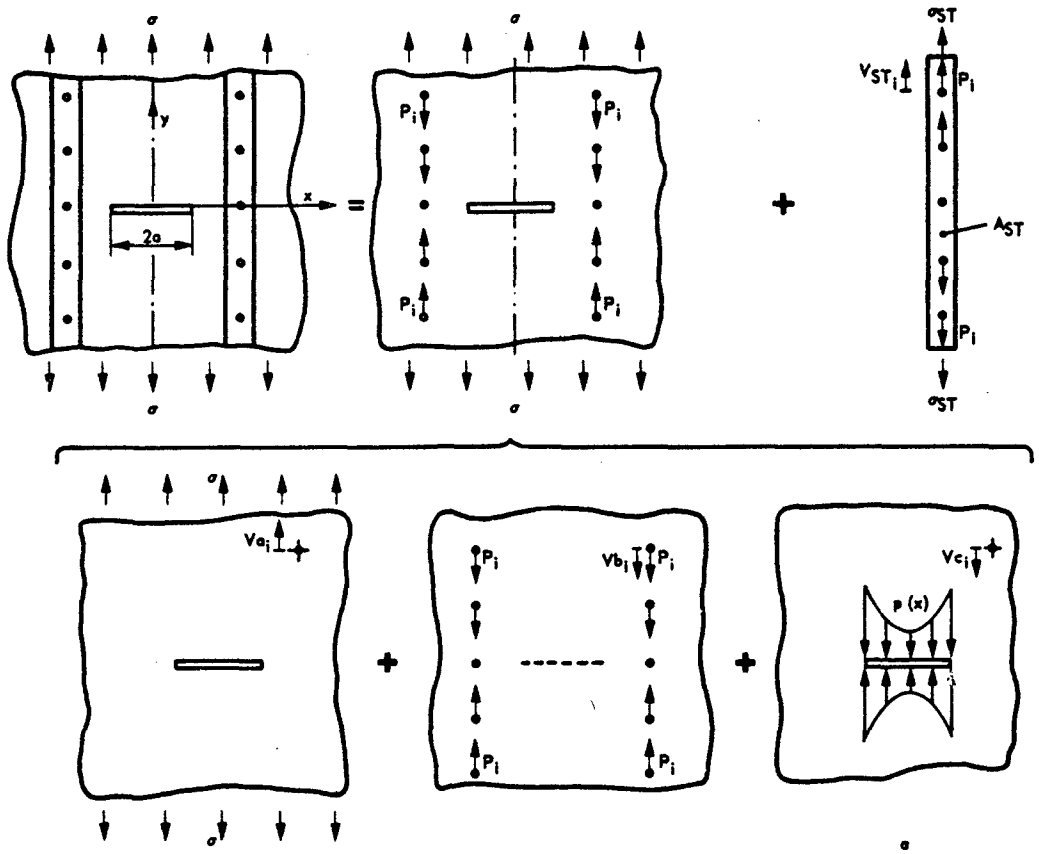

STRESS INTENSITY FACTORS: $K_\sigma = \sigma\sqrt{\pi a}$ $\qquad K = 0$ $\qquad K_p = -\frac{2}{\pi}\sqrt{\pi a}\int_0^a \frac{p(x)\,dx}{\sqrt{a^2 - x^2}}$

WHERE p (x) IS STRESS DISTRIBUTION ALONG x – AXIS DUE TO RIVET FORCES P_i

RIVET FORCES P_i FOLLOW FROM EQUAL DISPLACEMENTS IN CORRESPONDING POINTS OF SHEET AND STIFFENER:

$$V_{a_i} + V_{b_i} + V_{c_i} = V_{ST_i}$$

STRESS INTENSITY CORRECTION FACTOR:

$$C(a) = \frac{K_{STIFFENED}}{K_{UNSTIFFENED}} = \frac{K_\sigma + K_P}{K_\sigma}$$

STIFFENER LOAD CONCENTRATION FACTOR:

$$L(a) = \frac{F_{max}}{F_{REMOTE}} = \frac{\sigma_{ST} A_{ST} + \sum_{i=1}^{n} P_i}{\sigma_{ST} A_{ST}}$$

FIGURE 1 SHEET-STIFFENER INTERACTION FOR PANEL WITH RIVETED STIFFENERS

In [20,21] all stiffeners were assumed to be intact, whereas in [22] the effect of various numbers of broken stiffeners was investigated. Poe presented his results in the form of design graphs, giving stress intensity factors and forces in the most highly loaded rivet and stringer for a systematic variation of crack lengths, stringer stiffness, rivet spacing, and stringer spacing. These make Poe's results attractive for parametric studies in the design stage of new components, and his results have been frequently used for that purpose (see examples presented in section 3.4).

3.2.3 Reviews of first approaches and new solutions

In the early seventies a number of handbooks on available solutions to crack problems were published, namely those of Rooke and Cartwright [23] , Sih [24] , and Tada, Paris and Irwin [25] . These books also contain information about stiffened sheets. Rooke and Cartwright [23] devoted a whole chapter of their compendium to this structural configuration, in which they reviewed the results of Sanders, Greif and Bloom [9-11] , and some results of Isida [17,18] and Poe [21] . They presented these results in graphical form. Sih [24] reviewed in a section on stiffened sheets some results of Isida [19] and Poe [20] , while Tada, Paris and Irwin only considered the work of Isida [17] .
Apart from stress intensity solutions, [24] and [25] contain information concerning some methods commonly used in determining stress intensity factors. A review of the many methods available has been given by Cartwright and Rooke [26] . Based on this review they came to the conclusion that it will often be time consuming and costly to obtain stress intensity factors for complex configurations and that there was a need for simple methods of obtaining approximate solutions for new configurations. To meet this need they developed the so-called compounding method as a quick and versatile way of extending known stress intensity solutions to configurations for which stress intensity factors are not known. In applying the compounding method the (complex) configuration for which the stress intensity is desired is separated into a number of ancillary configurations which have known solutions. The solution of the original configuration is then obtained by superposition of the ancillary configurations and correcting the results for interaction of the separate solutions. The great advantage of the compounding method is that the importance of design parameters such as e.g. type of attachment, flexibility of attachment, and sheet curvature can be studied using a simple structure with a single stiffener. Results for a structure with multiple stiffeners can then be compounded from those for the simple structure.
The principles of the compounding method are discussed in [27] and [28] and a detailed description of this method is given in Chapter 10 of this handbook. Applications to stiffened panels are presented in [29-31]. In [29] and [30] the stress intensity factor is determined for a panel configuration with a crack which is located asymmetrically between two continuously attached stiffeners in a periodically stiffened sheet. The required ancillary configuration for this problem was provided already by Greif and Sanders [10] . The stress intensity solutions for both tips of the asymmetric crack are presented in [29] and [30] in graphical form. In [31] the panel configuration with riveted stiffeners and an array of collinear cracks (not necessarily of equal length) is considered. The practical significance of this problem is argued in [31] by the statement that multiple initiation of cracks at different stiffeners can result in such an array of cracks.

3.2.4 Sheet stiffener interaction computations related to fatigue crack growth

A vast amount of theoretical and experimental work, mainly related to the fatigue crack growth behaviour of stiffened structures, has been carried out by Salvetti and his co-workers [32-38] . They performed their work on cracked riveted panels of realistic design. The panel dimensions, stringer geometry and spacing were varied systematically in the construction of the panel. Apart from crack propagation data, References [32-35] and [38] present plots of C and L versus crack lengths for various stiffened panel configurations. References [36] and [37] are especially devoted to the evaluation of fatigue endurance of the stringers as a function of the crack length in the sheet and applied panel load.

3.2.5 Modelling of the rivet connection

It was shown in the foregoing that in the case of cracked riveted panels the magnitude of the rivet forces in the region of the crack has to be known to allow computation of the stress intensity factor of the stiffened panel (see Figure 1). The accuracy with which the value of the stress intensity can be determined will depend on the method of modelling of the rivet connection. In most references dealing with sheet-stiffener interaction mentioned so far [4-34] it is assumed that the attachments are infinitely rigid and so do not deflect under load. This assumption allows a rather easy determination of the rivet forces and thus of K. However, in practice the rivet and its surroundings will deform under bearing loads, thus making the sheet-stiffener interaction less effective. An additional complication in this context is that loads will also be transferred from sheet to stiffener by means of friction forces arising from sheet-stiffener contact due to riveting pressure. The effect of rivet attachment flexibility has been accounted for by Swift [39,40] , Cartwright and Dowrick [41] , Ratwani and Wilhem [42-44] and Salvetti [35-38] .
The effects of rivet attachment flexibility and friction forces have been discussed by Salvetti in a note especially prepared for this chapter (see example problem 3.4.2.8).

3.2.6 Double rows of rivets

Stiffeners are often attached to the sheet with a double row of rivets. In such a situation it may be unrealistic to assume that the stiffener is concentrated along a single line. The effects of a doubly riveted stiffener on the stress intensity factor as compared with the singly riveted stiffener are considered by Wang and Cartwright [45] .

3.2.7 Partial failure of stiffeners and debonding of adhesive bonded panels

In practice partial failure of the stiffener may occur. Such a situation has been observed by Poe [46] for the case of integral panels. Poe observed simultaneous crack growth in sheet and stiffener, at approximately the same rate, after the crack tip had reached the stiffener. Of course such a situation may also arise when the stiffeners are riveted or bonded to the sheet, although it is not expected then that initiation of the crack in the stiffener will occur at the instant the skin crack reaches the stiffener. An additional problem that may arise in the case of bonded stiffeners is debonding of the sheet-stiffener connection when the crack passes under a stiffener. This problem implies that there may be a region of

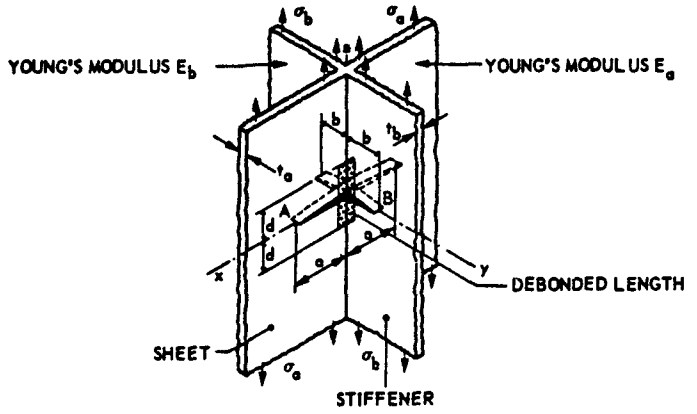

FIGURE 2 CONFIGURATION STUDIED BY CARTWRIGHT AND MILLER [48, 49]

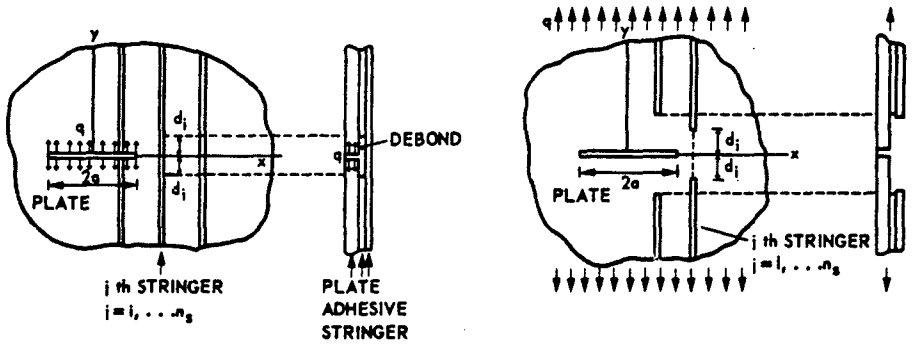

FIGURE 3 CONFIGURATIONS STUDIED BY ARIN [50-53]

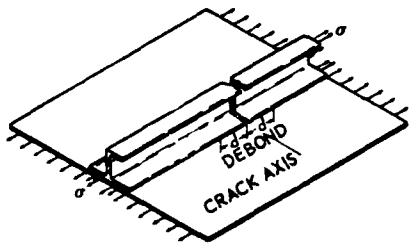

SHEET BONDED TO CRACKED STIFFENER

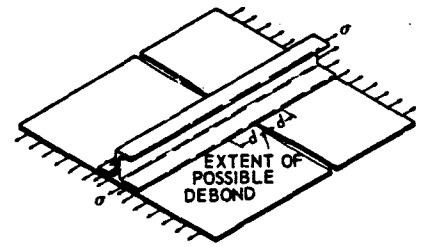

STIFFENER BONDED TO FULLY CRACKED SHEET

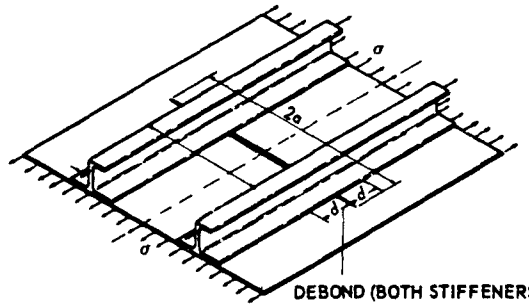

ONE-BAY SHEET CRACK RESTRAINED
BY BONDED STIFFENERS

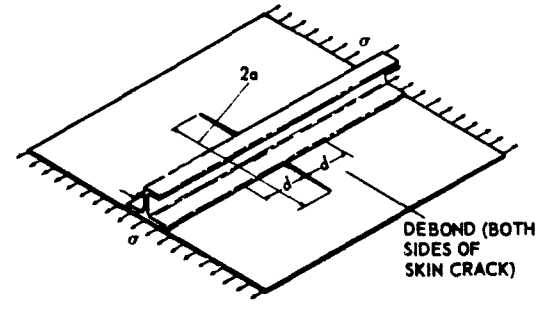

TWO-BAY SHEET CRACK RESTRAINED
BY BONDED CENTRAL STIFFENER

FIGURE 4 FOUR BASIC PROBLEMS FOR STIFFENED STRUCTURES STUDIED BY HART-SMITH [54]

crack growth in the skin that is affected by a stiffener which is either partially cracked or partially cracked and debonded or only debonded. The problem of partial stiffener failure has been studied by Kanazawa et al.[47] and Miller and Cartwright [48] for a panel in which the stiffener is continuously attached to the sheet (see Figure 2). A combination of partial stiffener failure and debonding of the skin-stiffener connection was considered by Cartwright and Miller [49] . Debonding of the skin-stiffener connection, with or without complete stringer failure, has been studied by Arin [50-53] (see Figure 3) and Hart-Smith [54] . In [50]Arin considered the effect of partially debonded, intact stringers on the stress intensity factor. The stiffeners were assumed to be adhesively bonded to an isotropic sheet, but the bending rigidity of the stiffeners in the plane of the sheet was neglected. In [51] Arin considered the same stiffener configuration but now accounting for the stringer bending rigidity. Due to high load levels in the stringers, failure of one or more of them may occur in addition to debonding. Therefore Arin also studied the same panel configuration as in [50] with the additional effect of one or more broken stringers [52] . In [53] the effect of orthotropy was investigated for the same panel configuration as studied in [52] . Hart-Smith [54] studied the effect of debonding, combined with a completely failed or intact stiffener, for panels of realistic design (see Figure 4).

3.2.8 Effect of crack tip plasticity

Assuming that the crack is located in a completely elastic stress field, then a stress singularity will exist at the tip of the crack. In practice, materials (especially metals) tend to exhibit a certain stress level above which they deform plastically. This means that there generally will be a region around the tip of a crack where plastic deformation occurs, and hence a stress singularity cannot exist. The plastic region is known as the crack tip plastic zone.
The effect of the stiffener on the amount of yielding around the crack tip and the reciprocal effect of the crack tip yielding on the load concentration in the stiffener were considered by Ratwani, Wilhem and Fitzgerald [42-44,55] and Cartwright and Rich [56] . The analyses in [42-44,55,56] are based on a Dugdale-type strip plastic zone [57] . Cartwright and Rich [56] presented computational results for the magnitude of the crack tip opening displacement, the stiffener load concentration and the maximum attachment force for a range of stiffness ratios and strip yield zone lengths for centrally cracked stiffened panel configurations with two or three riveted stiffeners.

3.2.9 Laminated and sandwich panels

In the foregoing the interaction between a cracked sheet and a discrete stiffener, attached to the sheet by means of riveting or adhesive bonding, was under discussion. Another type of built-up design is a sandwich plate or laminate, consisting of two or more layers of metallic or composite material connected to each other by means of an adhesive. When considering only those laminated structures in which one or more of the layers contain a through crack, with or without a partly debonded adhesive layer in the vicinity of the crack, there appear to be relatively few publications available dealing with the interaction aspects (in terms of stress intensity) of this type of structure.
The interaction of laminated structures has been studied by Erdogan and Arin [58] , Keer et al. [59] , Anderson et al. [60] and Ratwani [61-64] . Erdogan and Arin [58] and Keer [59] considered a structure of similar design, viz. a laminate consisting of two sheets bonded together by an adhesive of finite and constant thickness. In [58] one sheet was of isotropic (metallic), and the other of orthotropic (fibre reinforced composite) material, whereas in [59] both sheets were isotropic. In both cases only one sheet contained a through crack of finite length, namely the metallic sheet. A portion of the adhesive material surrounding the crack was assumed to be debonded in [58] . In [59] no loss of integrity of the adhesive layer was considered. In [58] and [59] a stress analysis was carried out, formulated by the utilization of integral transform methods, to calculate the crack tip stress intensity factor, and the boundary of the debonded area (in [58]). No comparison with experiments was given.
Anderson [60] treated the problem of two adhesively bonded metallic sheets of finite size both analytically and experimentally. Again one sheet contained an initial through crack while the other sheet was nominally free of defects. The finite element method was used to determine the stresses in the cracked sheet, the adhesive, and the uncracked sheet. Results of the analysis were used to predict the growth rate of the crack, debond zones in the adhesive and the number of cycles required to initiate a crack in the uncracked sheet. The experimental programme was directed to verification of the analytical results.
Much analytical and experimental data concerning laminated structures can be found in the work published by Ratwani [61-64] . He studied a two-ply (metallic) adhesively bonded structure, with a through crack in material 1, a debond or no debond in the adhesive around the crack in material 1, and no crack in material 2. Also studied was the case for which the width dimension of the uncracked ply was reduced to that of a stiffener. Ratwani used two different methods of analysis, namely the finite element method and the integral equation approach, to obtain the stress intensity factor in the cracked laminate. The analyses were carried out assuming no debond in the adhesive, and an elliptical debond with a minor-to-major axis ratio of 0.1, the end of the major axis of the debond coinciding with the leading edge of the crack. This debond shape and size was based on experimental observations. The presence of a crack in only one layer of a bonded structure will give rise to out-of-plane bending due to lack of symmetry caused by the presence of the crack. By comparison of computed and experimentally determined stress intensity factors, Ratwani found that neglecting this out-of-plane bending will yield unconservative results. A method to account for the influence of out-of-plane bending on the stress intensity factor was therefore developed [64] . A parametric study was conducted in [63] to evaluate the influences of debond size and adhesive and adherent properties on K.

3.2.10 Available computer programmes

In sub-sections 3.3.2 to 3.2.9 a review is given of publications available to the designer to evaluate the interaction of cracked and uncracked elements of a certain built-up structure. Data obtained from design graphs presented in these publications will usually be helpful during the predesign stage of an aircraft when the designer, on the basis of parametric studies, has to make a final choice from various alternative design configurations. However, when that choice has been made, he has to demonstrate that the design meets the residual strength and crack propagation requirements prescribed by the airworthiness regulations. In that stage of design the analyses discussed in the previous sub-sections will frequently be inadequate because of the assumptions made in them (e.g. rigid attachments, purely elastic behaviour

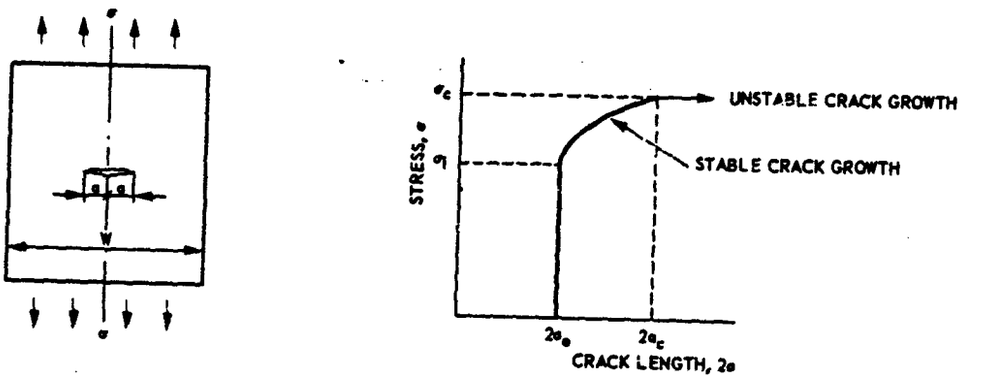

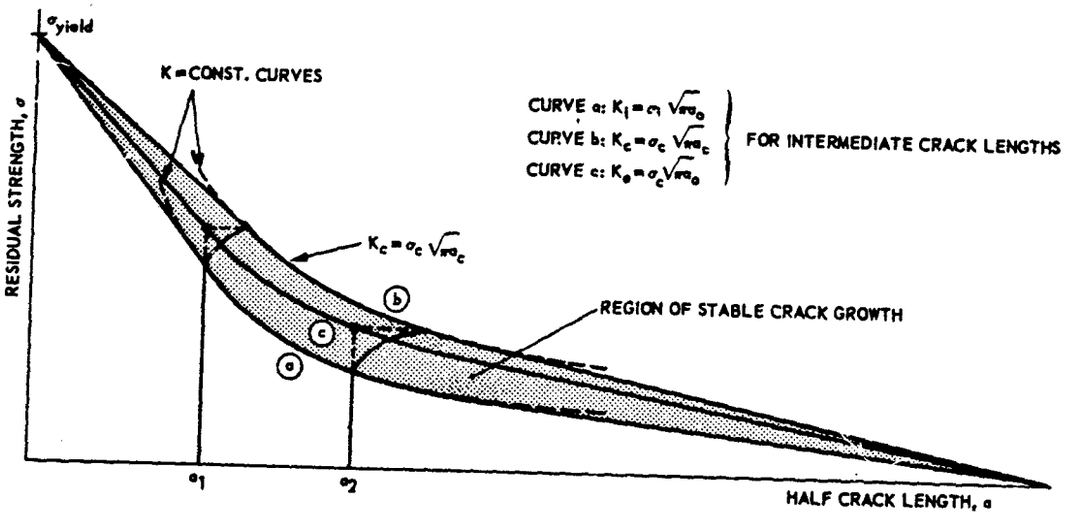

FIGURE 5 BEHAVIOUR OF UNSTIFFENED PANEL DURING RESIDUAL STRENGTH TESTS AND SHAPE OF RESIDUAL STRENGTH DIAGRAM (SCHEMATIC)

of attachments and stiffeners, neglect of stiffener eccentricity) or because of the fact that the actual design cannot be properly modelled to the available solution (e.g. due to its complex shape or construction). What the designer then needs is a computer programme that enables him to calculate the residual strength and crack propagation properties of a certain built-up structure. Such computer programmes, descriptions of which are available in the open literature, have been developed by Swift [39,40,65-71] , Vlieger [13, 72-79] , Lehrke, Huth et al.[80,81] and Schwarmann [82,83] . The programmes of Swift, Vlieger, Lehrke and Huth et al. are based on analytical solution of the displacement equations (see Fig.1), whereas Schwarmann used the finite element approach.
The advantage of the analytical method over the finite element method is that for the analysis of cracked stiffened panels solutions are either available in closed form or they can be obtained using numerical analysis. The numerical analysis techniques generally require small computer run times. This makes the analytical method excellently appropriate for parametric studies. However, a disadvantage of the analytical method is that there is a limitation on modelling of the structure. In those locations of built-up structures where many components are interconnected at one point (e.g. a skin-doubler-stiffener connection) the actual structure has to be reduced to a simple configuration and such an idealization may easily lead to inaccuracies in the computations. In this respect the finite element method is much more attractive, because structural complications can be easily accounted for and the results obtained have a high degree of accuracy. However, here the major disadvantages are the large computer run times and the fact that solutions are not closed form, and therefore cannot be easily generalized. If finite element techniques were to be used for parametric studies of any nature, the cost would probably be prohibitive. Hence this technique is unlikely to be suitable for parametric studies. In fact the latter point was the motive for Swift to change to analytical computation methods (see [40]).

3.3 RESIDUAL STRENGTH

3.3.1 Residual strength of flat panels loaded in uniaxial tension

In aircraft construction built-up structures usually consist of one or more sheet elements often reinforced by stiffening elements, e.g. stiffened sheet (lower and upper wing skins, spar webs, fuselage skin structure); sandwich structure; and laminated sheet (skin doublers). In each of these elements cracks may occur. When cracks occur there will be an interaction of cracked and uncracked elements. Predictions of residual strength of built-up structures will usually be based on the residual strength properties of the cracked element per se, taking into account the interaction of the cracked and intact elements. Because the greater part of built-up structures consists of sheet and sheet elements in which plane stress conditions prevail, knowledge of the behaviour of relatively thin cracked sheet under tension loads is essential.
In the literature many approaches to the residual strength problem of cracked unstiffened sheets can be found. A review of the literature on this subject was given by Broek [84] . For a more recent review article, dealing with the most current approaches to both residual strength and crack propagation analyses for aircraft structures, along with the assumptions and limitations of each method, the reader is referred to [85] . To the author's knowledge only two approaches have found ample practical application in predicting residual strength of built-up panels, viz. the stress intensity factor approach and the R-curve approach. In this section the principles of both methods and the application to built-up structures are discussed, starting with the application to unstiffened panels. For information about application of some other methods of analysis to stiffened panels the reader is referred to [74] .
Only cracks in plane panels and loaded in uniaxial tension are considered. The effects of curvature and combined loading conditions are discussed briefly in section 3.3.2.

3.3.1.1 Stress intensity factor approach

(a) Unstiffened panels

The behaviour of a sheet with a central transverse crack $2a_o$, subjected to an increasing tension stress σ, is illustrated in the upper half of Fig.5. The stress can be raised to a value σ_i at which the crack will start to extend slowly. This slow crack growth is stable; it stops immediately when the load is held constant, and increasing stress is required to maintain its propagation. Finally, at a certain critical stress σ_c a critical crack length $2a_c$ is reached where crack growth becomes unstable and sudden total fracture of the sheet results. Both slow stable crack growth and fast fracture instability occur at lower stress levels if the initial crack is longer. By testing panels with different initial crack sizes the curves labelled a and b in the lower half of Fig.5 are obtained. The shaded area between these curves is the region of stable crack growth. The curve labelled c can be derived from data points of curves a and b and relates the failure stress directly to the initial crack length. This curve is of special interest to the designer because he wants to know which peak load can still be carried by the damaged structure when a fatigue crack of certain size ($2a_i$) is detected during inspection. It is immaterial to him that the crack will show some stable growth (to a total length of $2a_c$) prior to final failure. Curve c is denoted as the residual strength curve.
Tests have shown that for brittle materials and for panels of a given thickness and size with an intermediate range of crack lengths the curves a, b and c of Fig.5 can be represented by constant values of the stress intensity factor, viz. by $K_i = \sigma_i\sqrt{\pi a_o}$, $K_c = \sigma_c\sqrt{\pi a_c}$ and $K_e = \sigma_c\sqrt{\pi a_o}$, respectively (see Fig.5, lower part). However, for the ranges of small and large crack lengths as compared to the panel dimensions the constant K-curves appear to overestimate the residual strength properties. This point is further elucidated in Fig.6a in which a curve for a constant $K = \sigma\sqrt{\pi a}$ is drawn (a curve of hyperbolic shape). Also shown in this figure is a straight line representing the line for net section yielding: at all points on this line the net stresses of the uncracked ligament of the specimen are just equal to the yield stress, σ_{yield}, of the material. The cross-hatched areas along the horizontal axis indicate the regions of crack sizes at which net section stresses above yield would be required to cause fracture at the given K. Since stresses above yield cannot occur in cracked components (except for very small crack lengths), fracture in these regions will occur at stresses lower than those predicted by the constant K-curve. Feddersen has shown [86] that the residual strength properties for these crack lengths can be obtained by drawing two linear tangents to the K-curve as shown in Fig.6b. One tangent is drawn from the point $\sigma = \sigma_{yield}$ on the vertical axis; the other tangent is drawn from the point $2a = W$ on the horizontal axis, where W denotes the specimen width. According to Ref. [86] the left-hand tangency point (point A in Fig.6b) is always at two-thirds of the yield stress, independent of the value of K, while the right-hand point of tangency

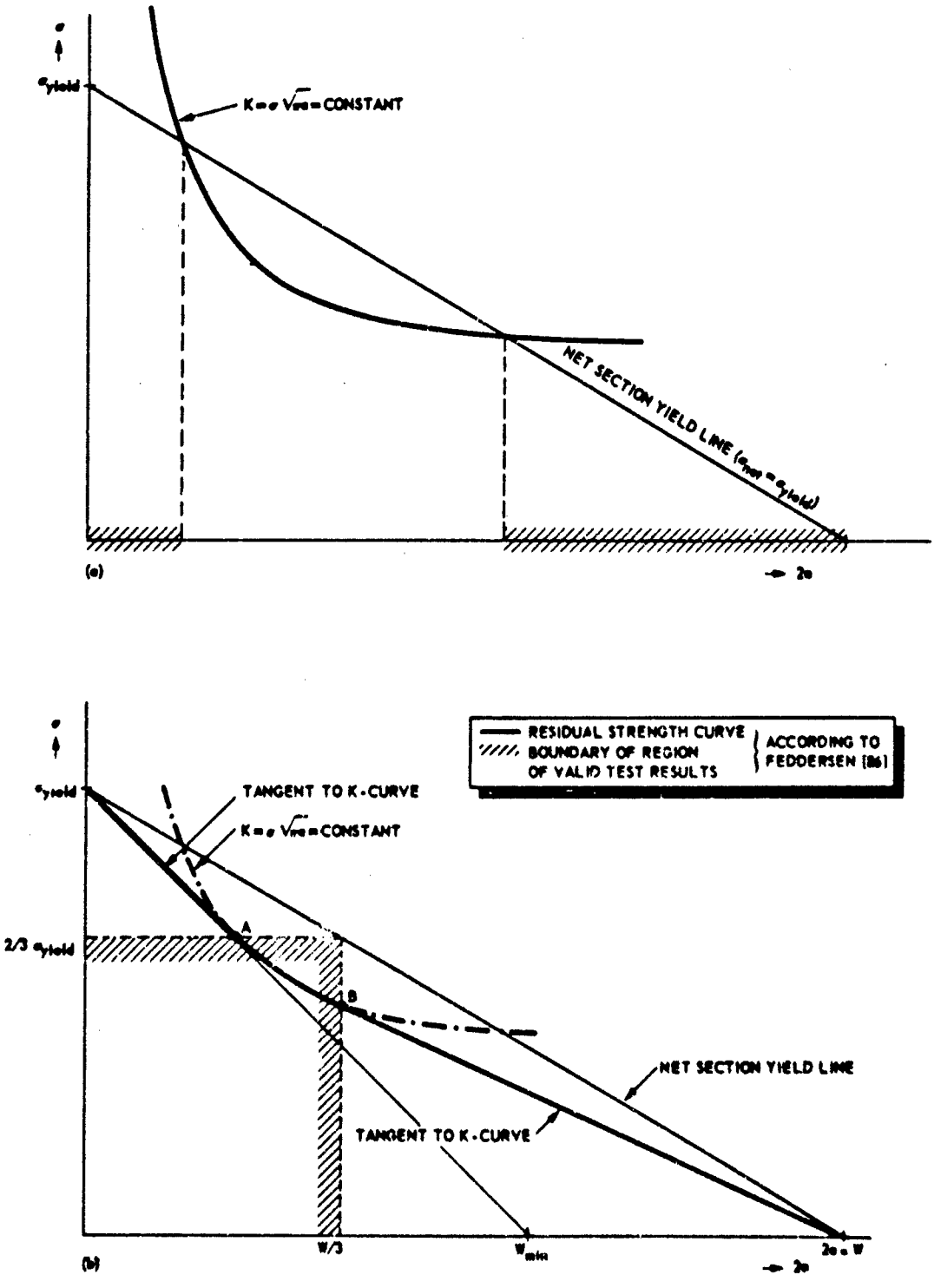

FIGURE 6 RESIDUAL STRENGTH DIAGRAM OF UNSTIFFENED PANEL (SCHEMATIC)

(point B in Fig.6b) is always at a total crack length of one-third of the specimen width.
When the approach proposed by Feddersen is assumed, the complete residual strength curve of a sheet of any width of a given material and thickness can be predicted from residual strength tests on panels having the same thickness but not necessarily the same width, provided the test data meet the following requirements (see Figure 6b):

$$\sigma_c < \frac{2}{3}\sigma_{yield} \quad \text{and} \quad 2a < W/3 \tag{4}$$

From data points meeting these requirements the K-value relevant to the material and thickness in question can be computed and the K-curve can be drawn in a σ versus 2a plot. Tangents drawn to this curve from σ_{yield} to $2/3\ \sigma_{yield}$ and from any panel width W to W/3 will complete the residual strength curve (see Fig.6b).
The foregoing implies that the validity requirements for the test data to yield useful K values are set by requirements (4). However, there is also a limitation as to the width of the panels used in the test. Panels should have a certain minimum size in order to provide valid (i.e. geometry independent) K values. As can be seen from Fig.6b this minimum panel size, W_{min}, is when the two points of tangency (points A and B) coincide. For panels having a width below W_{min} the residual strength for the whole range of crack lengths is determined by the net section yield criterion.
The minimum panel size for valid K data can be determined in the following way. Because points A and B in Fig.6b are points of tangency to the K-curve, using requirements (4) the crack lengths at these points are found to be equal to

$$2a_A = \frac{2}{2\pi}\left(\frac{K}{\sigma_{yield}}\right)^2 \tag{5}$$

$$2a_B = W/3$$

The condition for the two points to coincide yields

$$W_{min} = \frac{27}{2\pi}\left(\frac{K}{\sigma_{yield}}\right)^2 \tag{6}$$

Figure 7 illustrates the effect of panel width for residual strength tests on unstiffened panels of 2 mm thick clad 2024-T3 and 7075-T6. To investigate the effect of sheet width on residual strength and to be sure that the panels in all other respects were identical, the following test procedure was applied. First, residual strength tests were carried out on 540 mm wide panels. After these tests a number of specimen halves was used to prepare specimens of 300 mm and 120 mm wide by sawcutting lengthwise as indicated in the sketch of Fig.7. In plotting the results of the residual strength tests (failure values of stresses and crack lengths) the approach of Feddersen was used.
It can be observed from the results in Fig.7 that the test data of 2024-T3 panels having widths of 300 mm and smaller are on the net section yield line, whereas two data points for the 540 mm wide 2024-T3 panels appear to be points on the K_c-curve. Further, all 7075-T6 results are located on a single K_c-curve independent of panel widths. Using equation (6) together with the K_c values found in Fig.7, the minimum panel sizes for valid K_c-values appear to be equal to 74 mm and 508 mm for 7075-T6 and 2024-T3, respectively. Apparently, for relatively brittle materials like 7075 very small panel widths will yield valid K values, whereas for ductile materials like 2024 even the 540 mm width panels were hardly wide enough for this purpose.
One final remark has to be made regarding the minimum panel size found for the 2024 panels. In the foregoing it was stated that two data points for the 540 mm wide panels appeared to yield valid K_c-values for this material. On the basis of this assumption the minimum panel size for valid K data was found to be equal to 508 mm. However, although the two data points indeed meet the requirements set by equations (4), they are fairly close to the net section yield line so that the validity of the K_c values is questionable. In such doubtful cases it is preferable to test additional panels with larger width dimensions to check whether these panels indeed yield the same K_c value. Another possibility is to add to the validity requirements given by equations (4), the requirement

$$\sigma_{net} < 0.8\ \sigma_{yield} \tag{7}$$

In that case the boundary for valid test data will be modified as shown in Figure 7a.
So far it has been assumed that the residual strength curve is to be determined from test results. Of course the same procedure can be applied (and in the design stage often will be) on the basis of handbook values of K for nominally the same material and thickness. However, in such cases one should pay special attention to the point whether the stresses and crack lengths corresponding with the given K-value meet the requirements set by equations (4) and (7). In principle, availability of a valid K value allows the designer to establish the residual strength for any panel size, including panels smaller than W_{min} since the latter will fail at net section yield. This is the great attraction of the Feddersen method, and a compilation of K-values for various structural metal alloys of particular interest for aircraft and aerospace application can be found in [87].
Finally, the effects of sheet thickness and temperature on residual strength must be considered. However, these points will not be discussed comprehensively in this chapter, since detailed information as to their influence on fracture toughness can be found in textbooks on fracture mechanics (e.g. [1] and [2]). In general it can be said that the residual strength decreases with increasing thickness from a maximum value under pure plane stress conditions to a certain minimum value (the plane strain fracture toughness, K_{I_c}) at thicknesses where plane strain conditions prevail. In the transitional range of thickness the residual strength has intermediate values. Quantitative K_c values for aluminium alloy sheet materials (2024, 7075 and 7475) of various thicknesses can be found in Refs[84-91].
Regarding the effect of temperature, there is generally a decrease in residual strength with decreasing temperature. For aluminium alloy sheet materials (2024, 7075 and 7475) quantitative values of K_c as a function of temperature can be found in Refs[90-92].

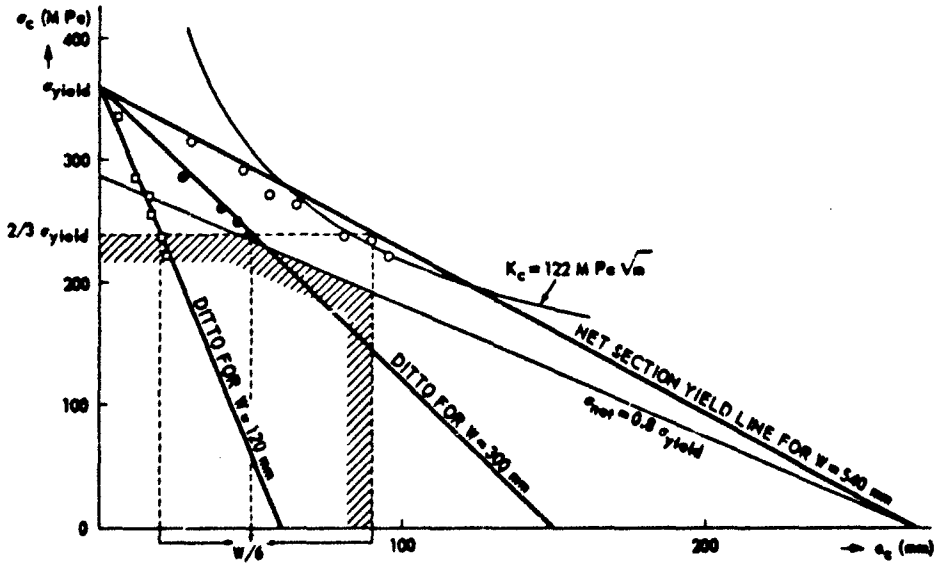

a 2024-T 3 SHEET OF 2 mm THICKNESS (σ_{yield} = 357 M Pa)

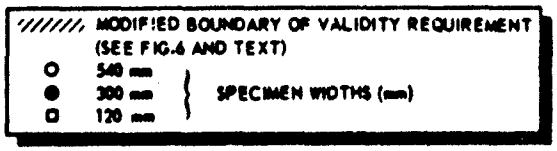

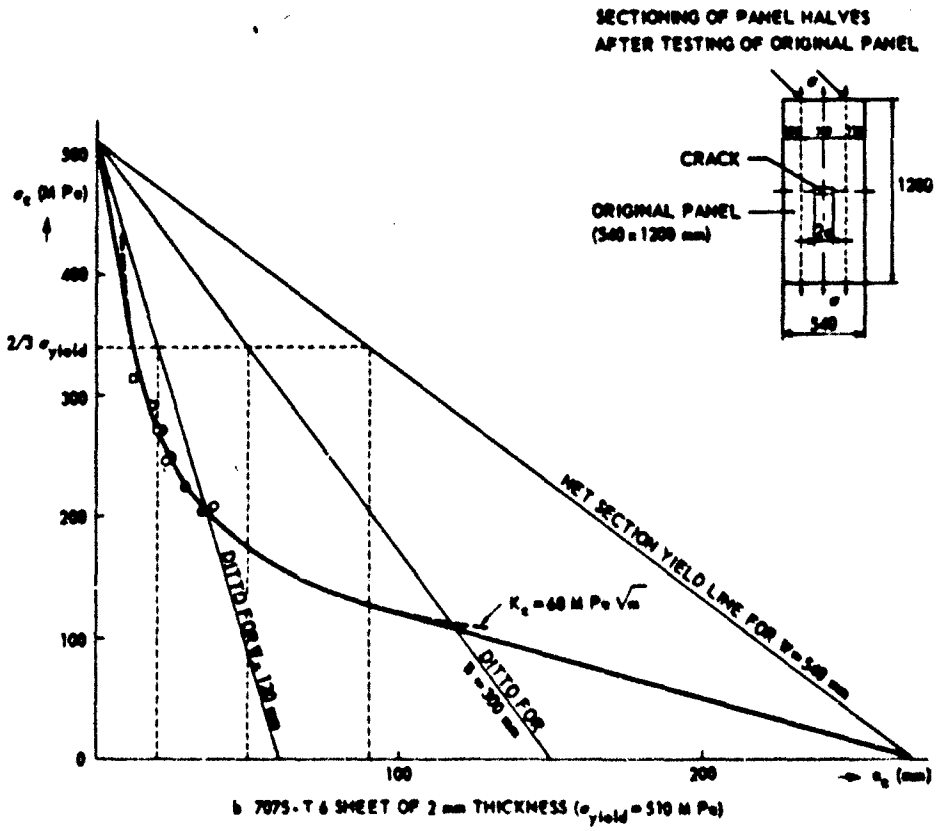

b 7075-T 6 SHEET OF 2 mm THICKNESS (σ_{yield} = 510 M Pa)

FIGURE 7 RESULTS OF RESIDUAL STRENGTH TESTS ON UNSTIFFENED PANELS OF DIFFERENT WIDTHS

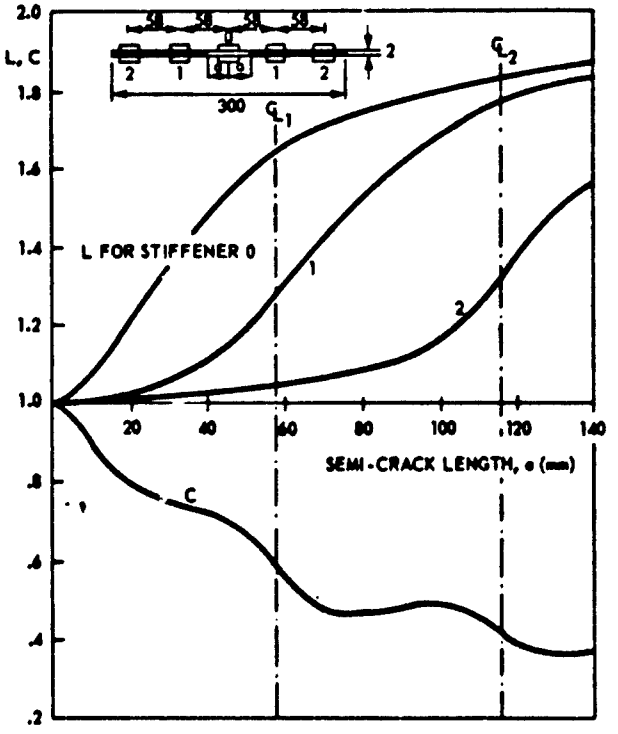

FIGURE 8a VALUES OF L AND C FOR A RIVETED PANEL WITH FIVE INTACT STRIP STIFFENERS. TOTAL STIFFENER CROSS-SECTIONAL AREA IS 50 PER CENT OF TOTAL GROSS AREA. CRACK PASSES THROUGH RIVET HOLES.

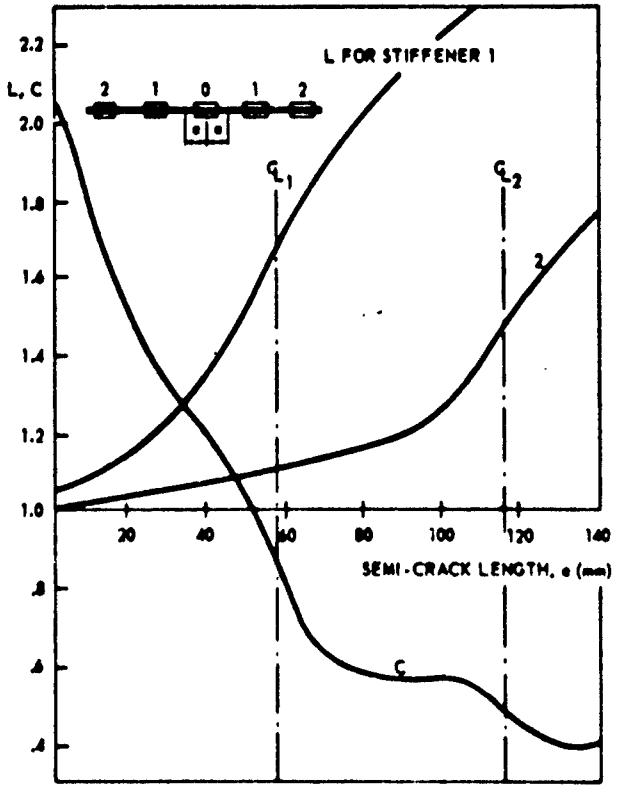

FIGURE 8b VALUES OF L AND C FOR THE PANEL CONFIGURATION OF FIGURE 8a BUT WITH A BROKEN CENTRAL STIFFENER.

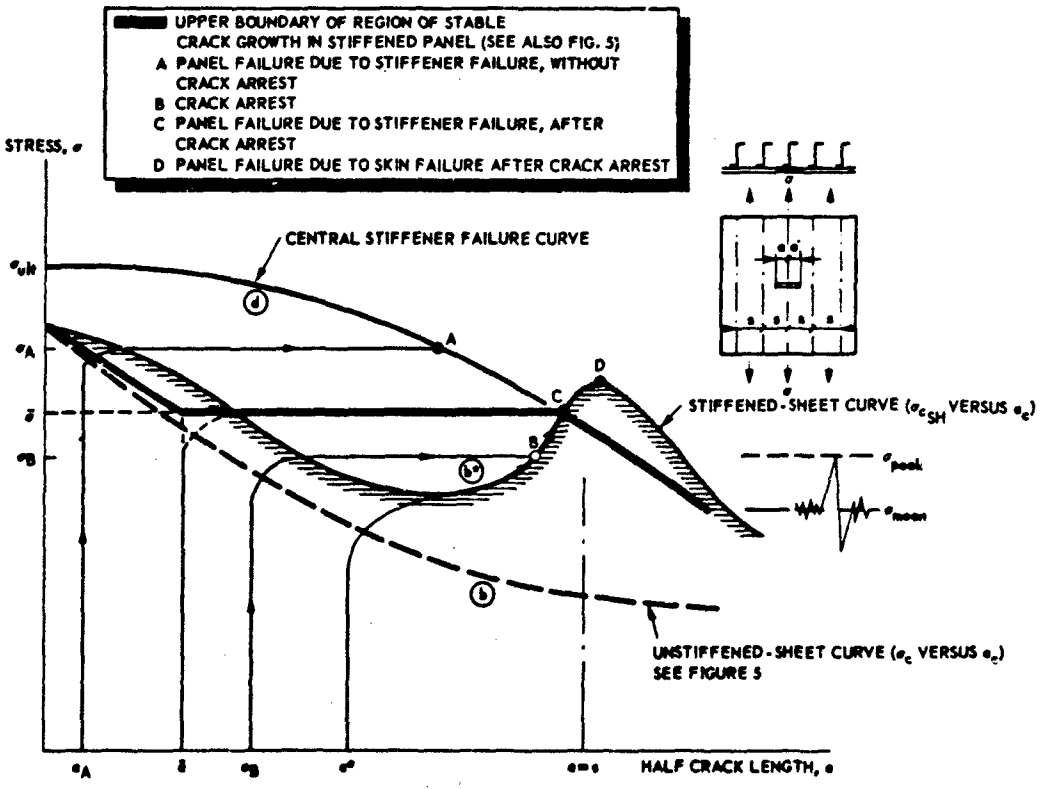

FIGURE 9 BEHAVIOUR OF STIFFENED PANEL DUE TO PEAK LOADS AND SHAPE OF RESIDUAL STRENGTH DIAGRAM (SCHEMATIC)

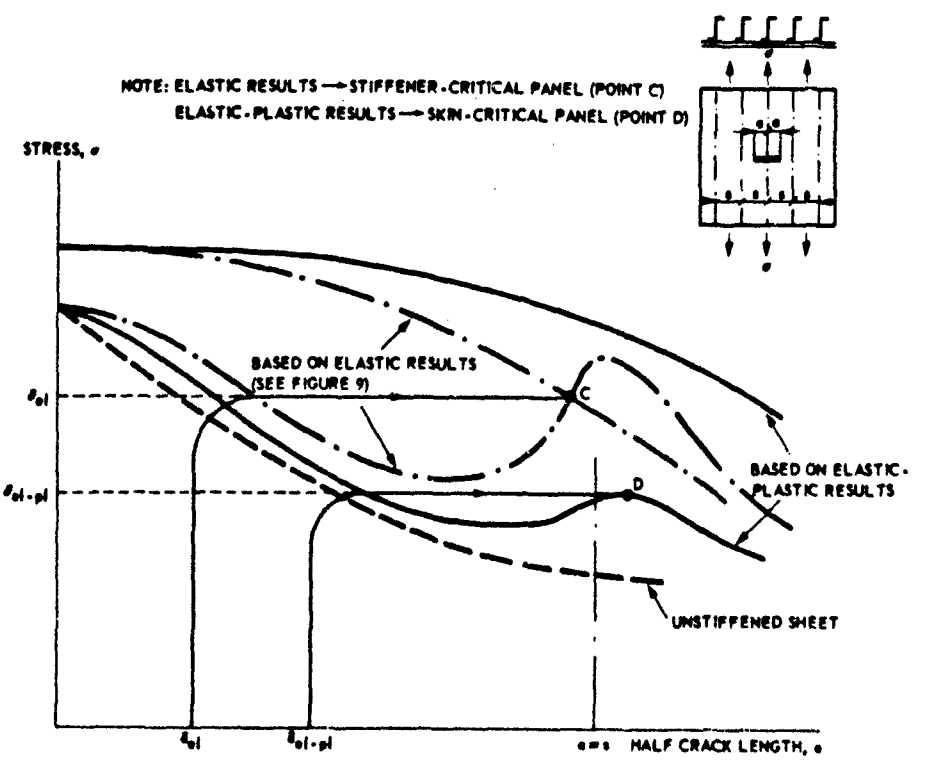

FIGURE 10 EFFECT OF YIELDING OF RIVETS AND STIFFENERS ON BEHAVIOUR OF STIFFENED PANEL (SCHEMATIC). COMPARE WITH FIGURE 9.

(b) Stiffened panels with fully elastic stiffeners and fastening system and nominally elastic crack tip stresses.

In the previous section the behaviour of an unstiffened, cracked panel with increasing external load was discussed (see Figure 5). Further, a prediction of the residual strength diagram for such a panel configuration was given on the basis of the stress intensity factor approach. This section deals with the change in behaviour of the panel, and thus the shape of the residual strength diagram, when the unstiffened cracked sheet is provided with stiffeners.

Comparing the stress distributions in the cracked regions of a stiffened and an unstiffened panel there will be a dissimilarity caused by the sheet-stiffener interaction in that region. In the case of a cracked sheet the stiffener provides extra stiffness that decreases the stress at the crack tip by load transfer from sheet to stiffener. In this connection two significant dimensionless parameters were introduced in section 3.2 of this chapter, viz. the "stress intensity correction factor", C(a) and the "stiffener load concentration factor", L(a). The factor C was defined as the ratio of the stress intensity factors of the stiffened and unstiffened panel at a certain crack length (see equation (2)). The factor L was defined as the ratio of the stiffener loads in the region of the crack and remote from the crack (see equation (3)).

It has already been shown in section 3.2 (see Fig.1) that quantitative values of C(a) and L(a) can be readily calculated when the fastener loads are known. The fastener loads can be computed for a certain panel configuration by assuming equal displacements of corresponding fastener points of sheet and stiffener. Values of C(a) and L(a), obtained in this manner using [76], are plotted in Figure 8 for a panel configuration with five riveted strip stiffeners containing a central crack; in making these computations yielding of rivets and stiffeners was not accounted for.

In Figure 8a the central stiffener is intact. The results show that the value of L for each stiffener increases with increasing crack length and that the curves level off when the crack tip has passed the rivet line of the adjacent stiffener. Further, C is smaller than unity over the whole range of crack lengths.

Alternatively, the load increase in the stiffeners during a peak load may become so large that fracture of a stiffener occurs. When this happens the load from the broken stiffener will be transmitted to the sheet and to the adjacent stiffeners. Thus stringer failure has an adverse effect on the stress intensity factor. This is illustrated in Figure 8b for the same panel configuration as in Figure 8a, but now the damage consists of a combination of a skin crack and a broken central stiffener. C is now larger than unity for cracks extending in the stiffener bays closest to the broken stiffener.

It will be clear that C and L are important parameters for determining the stiffener effectiveness with respect to crack growth and residual strength. The effect of these parameters on the shape of the residual strength diagram of the stiffened panel will now be discussed.

Combining equations (1) and (2) and ignoring the finite width correction, it follows that

$$K_{STIFFENED} = C(a).\sigma\sqrt{\pi a} \tag{8}$$

Assuming that unstable crack growth occurs when $K_{STIFFENED}$ attains a value equal to the plane stress fracture toughness of the unstiffened sheet material, $K_c (= \sigma_c\sqrt{\pi a_c})$, then the relation between the critical stress of the stiffened sheet, $\sigma_{c_{SH}}$, and a_c is given by the equation

$$\sigma_{c_{SH}} = \frac{K_c}{C(a)\sqrt{\pi a_c}} = \frac{\sigma_c}{C(a)} \tag{9}$$

where σ_c is the stress at which fracture instability in the unstiffened panel occurs. Equation (9) shows that the curve that gives the relation between the critical values of stress and crack length of the stiffened panel can be obtained by raising all points of the $\sigma_c - a_c$ curve of the unstiffened panel by a factor $\frac{1}{C(a)}$ pertinent to the particular length of crack. According to equation (3) the maximum load in the stiffener will be equal to (see also Fig.1)

$$P_{MAX} = L(a).P_{REMOTE} = L(a).\sigma_{ST}\,A_{ST} \tag{10}$$

where σ_{ST} and A_{ST} are the stiffener end stress and cross-sectional area, respectively. Ignoring load eccentricity and notch effects (i.e. the stress distribution over the stiffener cross-section is assumed to be uniform), failure of a stiffener will occur when the value P_{MAX} of that stiffener becomes equal to the ultimate strength of the stiffener material, $P_{ult} (= \sigma_{ult}.A_{ST})$. Thus the relation between the end-stress at which the stiffener fails, $\sigma_{c_{ST}}$, and the crack length is given by the equation

$$\sigma_{c_{ST}} = \frac{\sigma_{ult}}{L(a)} \tag{11}$$

The overall effect of the sheet-stiffener interaction on the shape of the residual strength diagram is illustrated in Figure 9.

The residual strength properties of the stiffened panel are determined by equations (9) and (11). From equation (9) and Fig.8a it can be concluded that in a stiffened panel with intact stiffeners unstable crack growth will occur at a higher stress level than in the unstiffened panel, the increase being dependent upon crack size. This means that curve b of the unstiffened panel (i.e. the upper curve of the region of stable crack growth in Figure 5) will be shifted upwards to curve b* in Figure 9. Curve b* shows a maximum for a crack length slightly larger than the stiffener spacing because the maximum reduction in tip stress will occur when the crack tip has just passed the stiffener centre line (see Figure 8a). However, in a stiffened panel the possibility of stiffener failure should also be considered. Based on equation (11) and the results in Figure 8a, curve d is drawn in Figure 9 as the locus for failure of the central stiffener (= stiffener that carries most load and thus can be assumed to fail first). At zero crack length the stiffener will fail at its ultimate tensile strength. With increasing crack size the increased load concentration in the stiffener causes it to fail at a lower panel end stress.

The diagram in Figure 9 illustrates four possible cases of panel behaviour, namely

(i) Panel failure due to central stiffener failure, without crack arrest (point A)
(ii) Unstable crack growth followed by crack arrest (point B)
(iii) Panel failure due to central stiffener failure, after crack arrest (point C)
(iv) Panel failure due to skin failure, after crack arrest (point D)

The different possibilities will be treated sequentially on the basis of the curves shown in Figure 9. Consider the behaviour under peak loads of a stiffened panel with two different crack lengths. When the panel contains a small crack of length a_A, after some stable growth the crack will propagate unstably at a stress level σ_A. During the propagation of this crack towards the next stiffener the load concentration in the central stiffener will become so high that this stiffener, and consequently the total panel, fails (point A). If the initial crack length is larger, of a length a_B, unstable crack growth due to a peak load will occur at a stress σ_B, but this crack growth will be stopped at the next stiffener (point B) owing to the reduction in crack tip stress. After crack arrest the load on the panel can be increased further, the tip stress is raised, and some additional stable crack growth occurs before the ultimate load of the central stiffener is reached, at point C. For any initial crack length between $\bar{a}$ and a^* the behaviour will be essentially the same as sketched for crack length a_B, i.e. fracture always occurs at the stress level indicated by $\bar{\sigma}$. This implies a predicted residual strength curve (σ_c versus a_o for the stiffened panel) of the shape drawn heavily in Figure 9. The curve contains a horizontal part determined by the stiffener strength (σ_{ult}), the sheet fracture toughness (K_c) and the sheet-stiffener interaction (which in turn is mainly determined by the relative stiffness of sheet and stiffeners and by the stiffness of the attachments). For initial crack lengths smaller than the stiffener spacing this flat part of the curve constitutes a lower bound of the residual strength of the stiffened panel and hence $\bar{\sigma}$ will be the fail-safe stress of the stiffened panel.

It must be pointed out here that the stiffener failure curve in Figure 9 intersects the stiffened sheet crack resistance curve (= curve that relates σ_c and a_c of the stiffened sheet). In that case, for crack lengths in the range from $\bar{a}$ to a^* panel failure due to peak loads will occur only after stiffener failure following crack arrest. However, the stiffener failure curve need not necessarily intersect the sheet crack resistance curve. If the curves do not intersect, failure of the panel will occur afte. crack arrest by sheet failure at point D in Figure 9.

In the foregoing the residual strength behaviour of the stiffened panel was discussed on the basis of the relative locations of the instability and failure curves of sheet and central stiffener. The relative location of these curves in the residual strength diagram was based on the fact that in the cracked region of a stiffened panel load will be transferred from the sheet to the stiffener by the fastening system (rivets or bonding connection). But in fact a third curve should have been incorporated in the philosophy, relating failure of the highest loaded fastener to crack length. This is because failure of a part of the fastening system (failure of one or more rivets or partial debonding close to the crack) will make the stiffener less effective in reducing the tip stress so that the sheet curve will shift downwards, resulting in a lower fail-safe stress (see Figure 9). However, in general the fastening system will yield prior to failure, so that load is shed from the highest loaded part of the fastening system, close to the crack, to parts farther away and the chance of fastener failure will be reduced. This brings us to a much more important aspect that has not been discussed so far, i.e. the effect of yielding of fasteners and stiffeners on the residual strength properties of the stiffened panel.

(c) Effect of yielding of stiffeners and fastening system.

The effect of yielding of stiffeners and/or fasteners is illustrated qualitatively in Figure 10. The dash-dot curves in this figure are based on elastic computations of C and L and are the same curves as drawn in figure 9. Due to the high loads to be transferred by the fastening system and the associated high load concentration in the stiffeners, yielding of fasteners and/or stiffeners may occur at relatively low external loads. This means that the stiffeners henceforth will behave less rigidly than was assumed, implying a less pronounced increase of the stiffened sheet curve and an upward shift of the stiffener failure curve. For the case shown in Figure 10 this signifies that the crack arrest and residual strength properties of the stiffened panel will be overestimated considerably when they are based on purely elastic computations of C and L. The effect of yielding on the residual strength properties is appraised here only on the basis of qualitative considerations. A quantitative evaluation of the effect of yielding, based on analytical computations of C and L, and a comparison of the calculation results with experimental data can be found in [77] and [78] . In conclusion it can be said that, in determining the residual strength properties of stiffened panels on the basis of the procedure discussed here, the effects of yielding of fasteners and stiffeners and the possibility of fastener failure (after yielding) has to be accounted for in the analysis.

(d) Effect of crack tip plasticity.

In the foregoing analysis it was assumed that the residual strength properties of the unstiffened panel over the whole range of crack lengths are given by a constant value of the stress intensity factor (the so-called plane stress fracture toughness, K_c). This assumption holds with good approximation for relatively brittle materials, like the aluminium alloy 7075, which show only a negligible amount of crack tip plasticity (apart from the extreme crack length regions where the tangents proposed by Feddersen apply, see Figure 7a). However, in practice the ductile aluminium alloy 2024 is frequently used as skin material and in this material failure usually is associated with a large amount of plasticity at the crack tip (see Fig.7b, where even panels of 540 mm wide failed by net section yielding). In principle, for this material the same method of residual strength prediction as discussed before can be applied as well by increasing the actual (visible) half crack length at failure by an amount r_p, which represents a measure of the crack tip plastic zone size. In other words, the actual stress in the elastic-plastic material, corresponding to a half crack length, a, is imagined to be equivalent to the stress that would arise from an "effective" half crack length

$$a_{eff} = a + r_p \qquad (12)$$

in a perfectly elastic material. Well-known plastic zone correction factors are those of Irwin [93] and Dugdale [57] . For plane stress conditions Irwin proposed a value

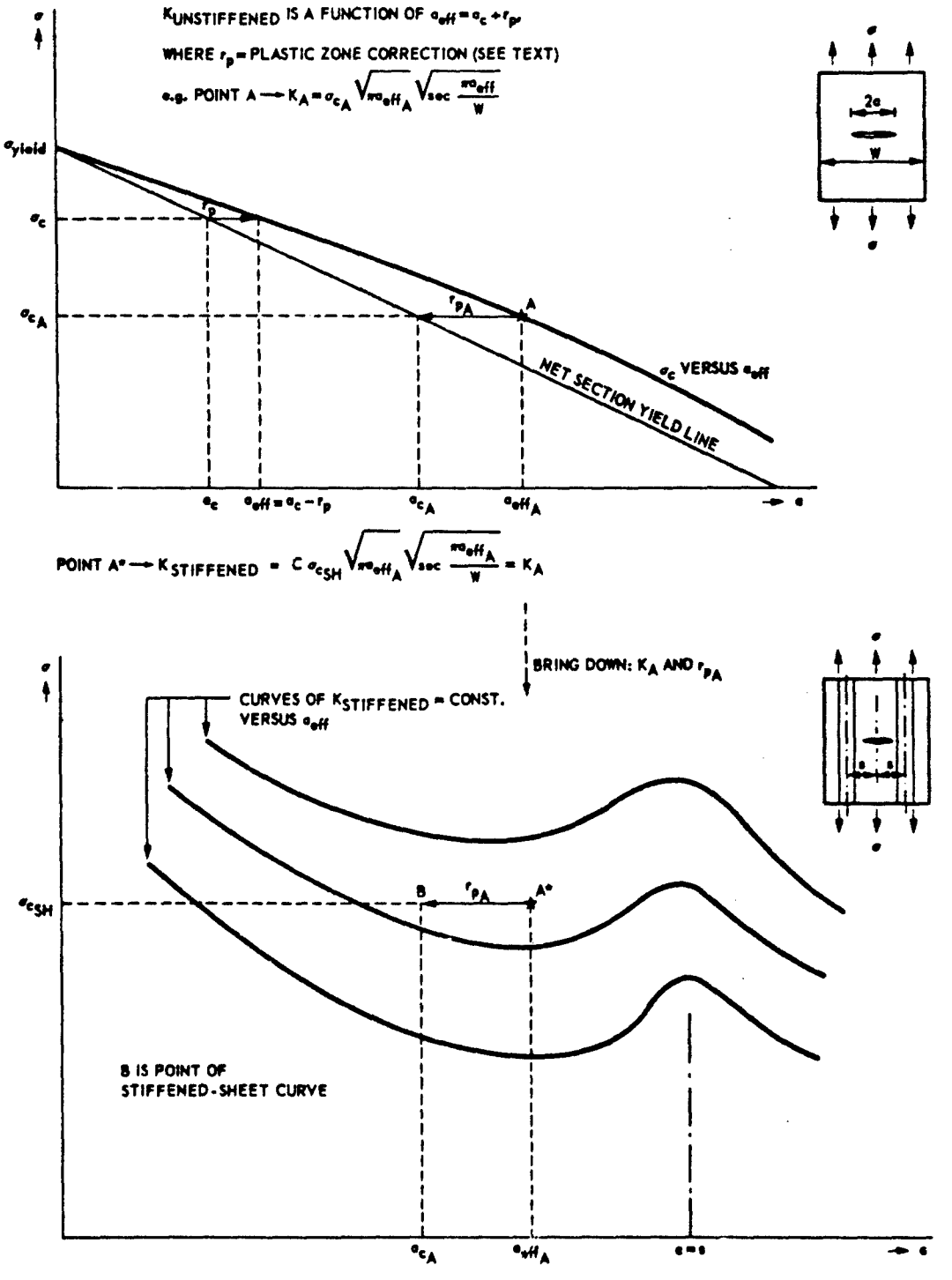

FIGURE 11 DETERMINATION OF SHEET CURVES FOR STIFFENED PANELS ($\sigma_{c_{SH}}$ VERSUS a_c) WITH DUCTILE SKIN MATERIAL

$$r_p = \frac{1}{2\pi}\left(\frac{K}{\sigma_{yield}}\right)^2 \qquad (13)$$

while Dugdale on the basis of a "strip-yield" model obtained the equation

$$r_p = \frac{\pi}{16}\left(\frac{K}{\sigma_{yield}}\right)^2 \qquad (14)$$

In equations (13) and (14) σ_{yield} represents the yield stress of the skin material. Using these equations the residual strength for stiffened panel configurations containing a skin of a ductile material can be predicted as illustrated in Figure 11. The upper half of this figure shows the residual strength diagram of the unstiffened panel. The net section yield line is assumed to be the locus of sheet failure (σ_c versus a_c). For points on this line the crack length is corrected for plasticity according to equations (13) or (14) and a curve is obtained relating σ_c to the effective crack length, a_{eff}. An iterative procedure has to be used because r_p is a function of the stress intensity factor, K, which has to be expressed in terms of a_{eff} to allow an elastic analysis. With this approach, for any combination of σ_c and actual (or visible) crack length, a_c, of the unstiffened panel, a value of the stress intensity factor will be obtained that determines fracture of the sheet. The value of this critical K will be a function of the crack length. The lower half of Figure 11 presents curves which relate constant values of the stress intensity factor of the stiffened panel to crack length and stress. Assuming that for a certain effective crack length in the stiffened panel fracture instability will occur at the same stress intensity value as found in the unstiffened panel, a fracture instability point of the stiffened panel will be obtained from the $K_{STIFFENED}$ = const. versus a_{eff} curves, as shown in Figure 11. This approach assumes that at a certain crack length the plastic zone sizes in the stiffened and the unstiffened panel are the same (see equation (13)).
In this section the prediction of the residual strength properties of stiffened panels is explained qualitatively. A quantitative determination of the residual strength, using the approach discussed here, is given in examples 3.3.3.6 and 3.3.3.7 for bonded and riveted panels, respectively.

3.3.1.2 Energy balance concept
(a) Principles of the method

The fracture behaviour of a cracked sheet under increasing tensile loads was illustrated earlier in Fig.5. When the load increases from a certain stress level, σ_i, slow stable crack growth takes place before final failure at the stress σ_c. According to the energy balance concept, during this slow stable crack growth there is a continuous balance between energy released from the system owing to crack extension and energy consumed for crack growth. This is because if there were no balance then either crack growth would stop (when the required energy exceeds the released energy) or become unstable (when the difference of both energy quantities yields an energy surplus).
The way by which energy is released from the system depends on the loading conditions during crack growth. The two extreme loading conditions are fixed grips and constant load. In practice the loading conditions will usually lie somewhere in between. In the case of fixed grips the external load cannot do work because the displacements of the plate ends remain constant. The energy required for crack growth is then delivered by a decrease of the elastic energy of the cracked sheet itself. If crack extension takes place at constant load the ends of the plate are free to move during crack growth and work will be done by the external load. The energy thus supplied will be used partly for an increase of the elastic energy of the cracked sheet and partly for crack growth.
The energy consumed by crack growth consists of work required for formation of a new plastic zone at the tip of the advancing crack plus the actual work of fracture. The latter amount of work is presumably small in comparison with the energy contained in the plastic zone and therefore the consumed energy is usually assumed to be equal to plastic work.
For a plate of unit thickness the energy balance concept yields the following condition for crack growth:

$$\frac{\partial}{\partial a}(U - F + W) = 0 \quad \text{or} \quad \frac{\partial}{\partial a}(F - U) = \frac{\partial W}{\partial a} \qquad (15)$$

where U is the elastic energy contained in the plate, F is the work performed by the external force and W is the energy required for crack growth.
Usually the energy release rate, $\frac{\partial}{\partial a}(F-U)$, is replaced by

$$G = \frac{\pi\sigma^2 a}{E} \left(= \frac{K^2}{E}\right) \qquad (16)$$

where σ is the panel end stress, 2a is the crack length and E is Young's modulus. Equation (16) comes from Griffith's criterion and applies to an infinite cracked plate of unit thickness with a completely elastic stress field. G is the so-called "elastic energy release rate" per crack tip. G is also called the "crack driving force", because its dimensions of energy per unit plate thickness and per unit crack extension are also the dimensions of force per unit crack extension.
The rate of energy consumption during crack propagation, $\frac{\partial W}{\partial a}$, is usually denoted by R, which is called the "crack resistance (force)". With these notations the energy condition for stable crack growth (15) can also be written as

$$G = R \qquad (17)$$

Using equations (16) and (17) the energy consumption, R, can in principle be found as a function of crack size. During crack growth the energy release rate, G, can be determined from recorded stress and crack length values. Because both σ and "a" increase during crack growth (see Figure 5) it follows from

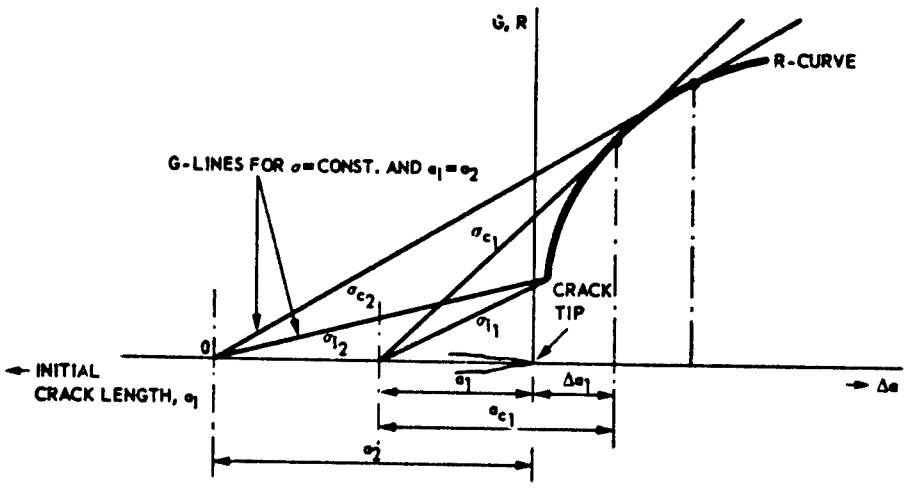

FIGURE 12 THE R-CURVE FOR PLANE STRESS

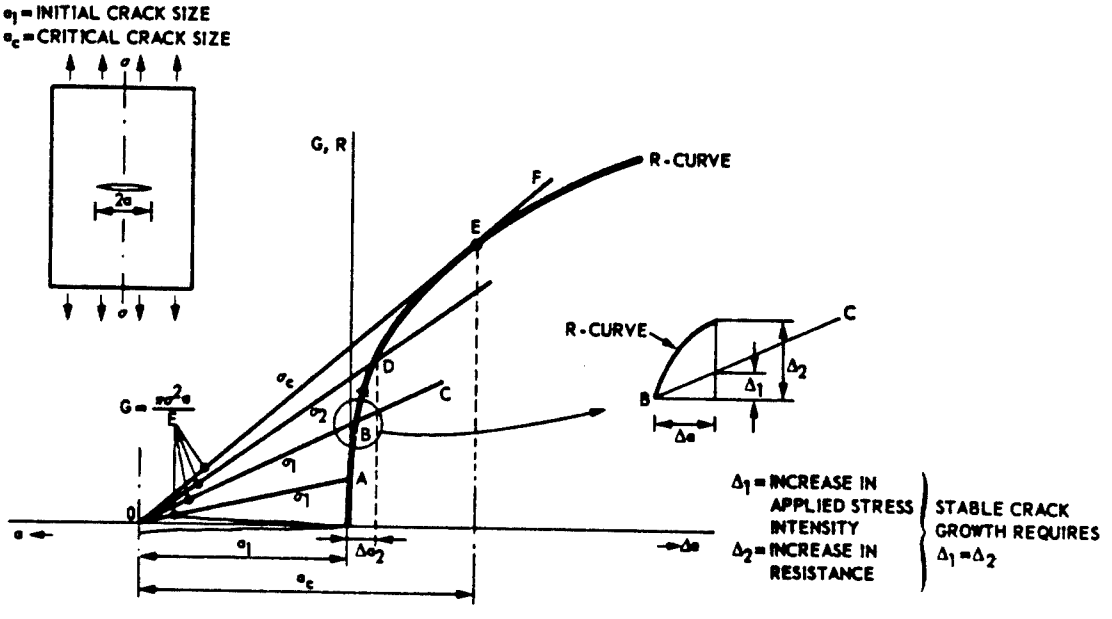

FIGURE 13 R-CURVE CONCEPT FOR UNSTIFFENED PANEL (SCHEMATIC)

equation (16) that G increases more than in proportion to "a", and thus R also increases as the crack proceeds. According to equation (17) the instantaneous values of G during crack growth will indicate how R depends upon crack size. R appears to increase during slow crack growth, as is depicted schematically in Figure 12. Also shown in this figure are lines indicating how G depends on crack size for constant stress values (the meaning of these lines will be explained in (b)). It is common practice to position the R-curve as in Figure 12, so that the origin of the co-ordinate axes coincides with the tip of the crack and R is plotted as a function of Δa. This is based on the suggestion proposed by Krafft et al. [94] that the R-curve is a function of Δa only and independent of a_i, i.e. the R-curve is invariant and is the same for any initial crack length. The G-lines in Figure 12 are drawn from the centre of the initial crack so that their location with regard to the R-curve depends on the value of the initial crack length. It was shown above that the R-curve can be determined experimentally from successive values of G during slow crack growth using the relation $R = G = \pi\sigma^2 a/E$. Typical R-curves as determined in this way for centre-cracked panels of aluminium alloys of different thicknesses can be found in [95] . The disadvantage of this method of R-curve determination is that in centre-cracked panels slow crack growth occurs only over a limited range of crack lengths, and so only a small part of the R-curve will be obtained. The results obtained by Heyer and McCabe [96,97] suggest that the use of a tapered cantilever beam specimen or a compact tension specimen (or, in general crack-line loaded specimens) has advantages. Since instability is postponed due to a different G versus "a" relation, it is possible to determine the R-curve over much greater lengths. This will give a better idea of its shape.
A review of R-curves for different materials as obtained from a variety of specimen types and test techniques is given in [98] . R-curves especially applying to aluminium alloys can be found in [99-101] . A standard test method for R-curve determination is given in [102] .

(b) Application to unstiffened panels

According to the diagram given in Figure 13, the behaviour with increasing load of a sheet containing a crack of length $2a_i$ will be as follows. Suppose the specimen is loaded to a stress σ_1. If the crack were to extend, the available energy release rate would be given by point A in the diagram. However, this value appears to be too low for crack growth to occur. The stress can be further increased to σ_i, where the available energy release rate is given by point B. Suppose this value is sufficient for crack growth. If the crack were to propagate under constant stress, G would increase according to line B-C. This line is lower than the R-curve and therefore crack growth under constant stress cannot occur. When the stress is further increased to σ_2, both G and R follow the R-curve from B to D according to equation (17) and crack extendion Δa_2 will occur. Finally, at σ_c the crack length has become a_c and both G and R are at point E in the diagram. Crack growth at constant stress σ_c gives an increase of G according to the line E-F. Because this line is above the R-curve, and the increase in stress intensity as the crack grows is greater than the increase in resistance, final fracture will occur at point E. That is, the fracture condition is the point of tangency (point E) or

$$G = R \quad \text{and} \quad \frac{\partial G}{\partial a} = \frac{\partial R}{\partial a} \tag{18}$$

Equation (18) is the energy criterion for fracture instability.

(c) Application to stiffened panels

The behaviour of a stiffened panel will be illustrated for two extreme cases of crack size, viz. a large crack that extends between two stringers, and a short crack with its tips remote from the stringers.
The first case is shown in Figure 14. As usual the R-curve is positioned at the crack tip. In a stiffened panel the stress intensity factor is reduced by a factor C (see equation (2)). Since $G = K^2/E$ the G-line for the stiffened panel will be given by $G = C^2.\pi\sigma^2 a/E$. This line is no longer straight, since C is a function of crack length (Figure 8). The deviation from straight line will be largest in the vicinity of the stringer. Slow crack growth will commence at a stress σ_i for which at point A there is an energy balance $G = R$. If the stringer were absent, failure would take place at the stress σ_{cu} (at point B). Owing to the curved G-line for the stiffened panel, however, the stress σ_{cu} will only cause slow crack growth to point C. The stress can be raised further to σ_{cs} (with simultaneous slow growth to D) before final failure takes place. At σ_{cs} the energy release rate for constant stress remains larger than R (line D-E).
The situation is more complicated for a short crack with its tips remote from the stringers. This case is depicted in Figure 15. It has to be noted that the same R-curve as in Fig.14 should be used, but it has to be displaced to the tip of the short crack. Slow stable crack growth will start at a stress σ_i. The part OA of the G_i-curve is still straight, since the stringer is remote. This means that slow crack growth commences at the same stress σ_i as in the unstiffened panel. At the stress σ_{cu} unstable crack growth occurs, since the line G_{cu} is tangent to the R-curve in point B. The part OB of the curve G_{cu} is also straight and hence unstable crack growth occurs at the same stress σ_{cu} as in the unstiffened panel. But in the stiffened panel crack arrest will occur at C, since the G-curve bends downwards in the vicinity of the stringer and dips under the R-curve. Further slow crack growth from C to D occurs if the stress is raised to σ_1 and eventually at σ_{cs} final fracture will occur, since the G-curve is tangent to the R-curve at E and G remains larger than R for constant stress.
The foregoing illustrates that when the R-curve of the skin material of a stiffened panel configuration is known the crack arrest properties and/or the stress and crack length at final failure can be predicted by drawing G-curves (for σ = constant) in an G,R versus "a" plot. The G-curves of a stiffened panel can be drawn when the C-values are known as a function of crack length (see Fig.8). However, in a stiffened panel final failure may be due to skin failure (skin-critical case) or stiffener failure (stiffener-critical case) and the possibility of stiffener failure has not been considered so far. Further, failure of the fastening system has not been allowed for. A problem in this respect is that to account for these effects the possibility of failure of stiffeners and fasteners has to be incorporated in the analysis as a function of crack length. This is because a small initial skin crack in a panel that originally is not stiffener-critical may show unstable growth followed by arrest. After crack arrest the stiffener will have to carry more load than initially (because the crack is larger) so that panel failure may now be induced by stiffener failure. Because the possibilities of stiffener failure and fastener failure

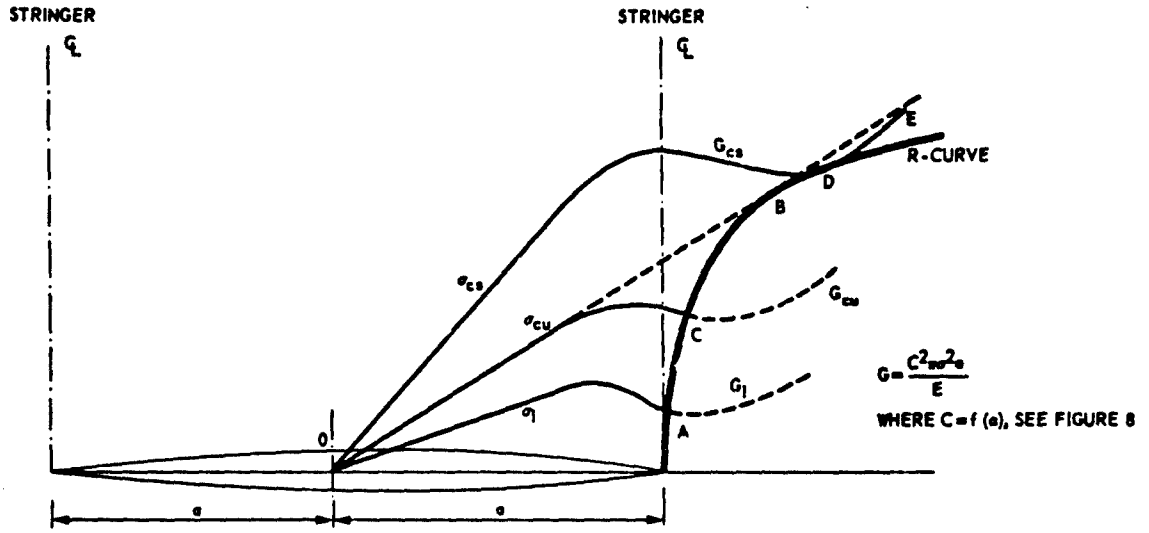

FIGURE 14 R-CURVE CONCEPT FOR STIFFENED PANEL, CRACK EXTENDING TO STIFFENERS

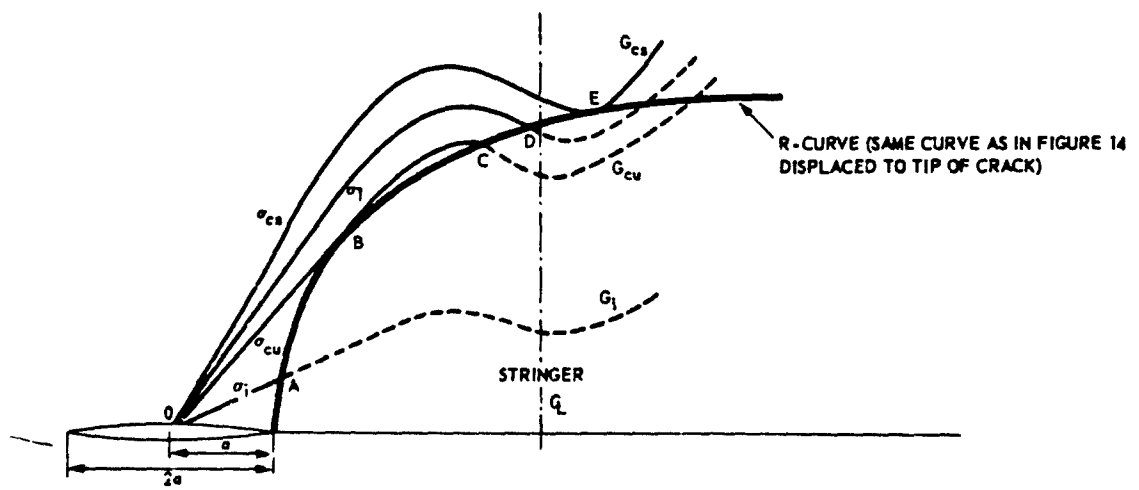

FIGURE 15 R-CURVE CONCEPT FOR STIFFENED PANEL, SHORT CRACK WITH CRACK ARREST

are not easily incorporated in a G,R versus "a" plot, for the time being the prediction of residual strength by means of the R-curve approach only holds for skin-critical configurations (it has to be emphasized that skin-critical refers here to the condition at final failure of the panel).

(d) Use of the R-curve approach for structural applications

The crack growth resistance curve (or R-curve) approach to fracture was originally introduced by Irwin [103] and later modified by Krafft, Sullivan and Boyle [94] . To obtain crack growth resistance data in terms of linear elastic fracture mechanics Heyer and McCabe [96,97] developed a new specimen type, viz. the crack-line loaded specimen. This specimen type enabled determination of the R-curve over a much greater range of crack lengths and allowed the use of much smaller specimens than the large centre-cracked tension specimens that were originally required to maintain net section stress below material yield. Recently, McCabe and Landes [104,105] modified the original test technique to accomodate R-curve determinations on structural materials showing large scale plasticity.
The first use of the resistance curve approach to structural applications was by Creager and Liu [106] to predict the residual strength of simple strap-reinforced sheet panels. However, the use of the resistance curve was restricted due to the lack of a suitable elastic-plastic analysis. The application of Rice's path independent J-integral [107] has proved to be a very suitable parameter in this respect. The application of the J-integral to structural problems, in combination with a $\sqrt{J_R}$ versus Δa curve was proposed by Verette and Wilhem [108] and Wilhem [109] . (Note: Due to the relationship between the J-integral and stress intensity factor (K) in the elastic case [107] , ($J = K^2/E$), it is better to speak of $\sqrt{J}$ rather than J. The suffix R is used to distinguish the resistance curve of the material from the stress intensity curve of the specimen). Verette and Wilhem [108,109] assumed in their analysis a Dugdale [57] plastic zone behaviour and employed the method of Hayes and Williams [110] to compute crack opening displacements using finite element techniques for a series of assumed plastic zone lengths at fixed physical crack lengths [110] . J-integral values could then be computed from the relationship $J = \sigma_{yield} \cdot \delta$ [111] , where δ is the crack opening at the physical crack tip and σ_{yield} is the material yield stress. Since the original publications in references [108] and [109] , much effort has been devoted by Wilhem and Ratwani [42,43,55, 112,113,44] to further develop this approach. In recent publications [114,115] they studied the early crack extension portion of the crack growth resistance curve in an attempt to apply the R-curve concept to fatigue crack growth.
By their studies and publications Wilhem and Ratwani have given an enormous impetus to a further development of the R-curve concept with regard to its application to residual strength predictions of stiffened panels. The designer who intends to use the R-curve concept for residual strength predictions is strongly recommended to acquire the large amount of information contained in the various publications of Wilhem and Ratwani on this subject [42,43,44,55,109,112-115] . To illustrate the application of resistance curves to residual strength prediction of a realistic structural configuration, an example problem was prepared by Wilhem as a contribution to this chapter (example problem 3.3.3.4).

3.3.2 Residual strength of curved panels subjected to pressure cabin loads

In the foregoing sections residual strength predictions for flat panels loaded by uniaxial tension were discussed. Such panels and loading conditions are present in e.g. a wing structure (apart from a slight curvature and a small amount of torsional shear loading). However, when considering a fuselage structure the conditions will be quite different. In that case the panels are curved and subjected mainly to biaxial tension loading due to cabin pressure. The effects of curvature and biaxial loading on residual strength will be discussed briefly in the following.

3.3.2.1 Effect of internal pressure

Consider a fuselage shell containing a skin crack, the tips of which are not close to a frame or stringer. Owing to the internal pressure the unsupported fuselage skin in the vicinities of the crack tips will bulge. This bulging, caused by loss of hoop tension reaction to the pressure loading, in turn causes local bending at the crack tips. This implies that there exist both bending and extensional stress singularities at the crack tips, or in other words the stress intensity factor in the pressurized shell will be larger than that in a flat panel subjected to the same extensional loads. Therefore residual strength properties of a fuselage structure cannot simply be derived from the flat panel data. In this respect one has to distinguish between circumferential and longitudinal cracks. The bulging at a circumferential crack will usually be smaller because (1) the spacing of the stringers is less than that of the frames, (2) the skin has additional bending stiffness due to curvature and (3) the hoop tension loads suppress the bulging.
The foregoing implies that to relate flat panel data to curved panels a bulging coefficient, β, has to be applied to the stress intensity factor of the flat panel carrying the same in-plane load as the curved shell, or

$$K_{CURVED} = \beta \cdot K_{FLAT} \qquad (19)$$

In the literature various proposals for the functional form of β can be found [116-129] , mostly applying to longitudinal cracks in unstiffened pressure vessels. The expressions in [116-118] are based on experiments, while the others are derived from theoretical analyses. A summary of expressions for β can be found in [127] , derived from publications before 1967, together with suggestions for improvements. Much effort has been devoted to this subject by Folias [121-123,126,128] . He analysed cracked spherical shells [121] and cylindrical shells with longitudinal [122] or circumferential cracks [123] . In [126] Folias gives a survey of existing solutions and discusses methods for estimating approximate stress intensity factors for other more complicated crack and shell geometries (e.g. an arbitrarily oriented crack in a cylindrical shell; a circular conical shell with a longitudinal or circumferential crack). References [121-123,126] treat elastic crack tip conditions, while in [128] the effect of crack tip plasticity is considered.
Almost all publications except [125,129] consider unstiffened pressure vessels. Of these latter, reference [129] uses an energy approach in conjunction with the finite element method to determine K.
It has to be noted that in a fuselage structure with frames and stringers the applied bulging coefficient must be a function of the distance of the crack tip to one of these elements: β will be a maximum when the crack tip is midway between two frames, and reduces to unity when the crack tip is at a frame. To account for this effect Swift suggested applying a cosine function in combination with β [71] .

3.3.2.2 Effect of biaxial loading

Most studies of biaxial loading have been limited to unstiffened panels [130-138] . Refs [130-134] are mainly experimental, while Refs [135-138] are analytical studies. It has been pointed out by Erdogan and Kibler [139] that analytically the effect of biaxial stress in unstiffened structures is of second order and is negligible if purely elastic analysis is considered. However, Hilton [136] showed by an elastic-plastic analysis that the stress intensity factors are reduced, and thus the residual strength increases, by applying a positive biaxial load (i.e. the load components in both directions are positive). The same study also indicated that the plastic zone size decreases with an increase in positive biaxial load ratios. Similar effects have been found by Smith [137] .
Less numerous are the publications dealing with the influence of biaxial loading on cracked stiffened panels. In Ref. [140] Beck investigated experimentally the effect of biaxial loading on crack growth in stiffened and unstiffened panels. Analytical studies of the effects of biaxial loading on the stress intensity factor were performed by Swift [40] and Ratwani and Wilhem [43,141] . Swift [40] found that the elastic stress intensity factor increased due to the application of positive biaxial loads and that the influence was not negligible. He explained this behaviour [39] by the fact that in pressurized shells, where the skin is biaxially loaded and the stiffeners are uniaxially loaded, the skin works at a higher stress than the stiffeners owing to strain compatibility. Ratwani and Wilhem [43,141] considered the influence of biaxial loading on stiffened sheets using both elastic and elastic-plastic analyses (in terms of $\sqrt{J}$) and compared their analytical results with experimental data. Both their elastic and elastic-plastic analyses showed trends similar to those observed by Swift [39,40] . Further, they found that the plastic zone size ahead of the crack tip decreases with an increase in positive biaxial load ratios. A similar reduction in plastic zone size was observed by Hilton [36] for unstiffened panels. Finally, Ratwani and Wilhem [141] obtained excellent agreement between analytical and experimental data.

3.3.3 Application of fracture mechanics principles to real structures

(a) Information available from literature (see section 3.5)

In the literature a large number of applications of fracture mechanics to the prediction of residual strength of real structures can be found. These applications either deal with actual designs or are more general in nature. In a number of cases the applications concern case studies. Without intending to give the impression of completeness, a list of relevant references is given here:

(a.1) Applications to actual designs or projects

Crichlow, Wells	[119]
Ekvall, Brussat, Liu, Creager	[143,145]
Heath, Nicholls, Kirkby	[147]
Nanduri, Radzins	[146]
Sanga	[144]
Stone, Swift	[68]
Swift	[39,66,67,69-71]
Swift, Wang	[65]
Thrall	[156]
Toor	[85]

(a.2) General studies

Creager, Liu	[106]
Crichlow	[149]
Eide	[151]
Hart Smith	[54]
Hunt, Denke, Eide	[150]
Schwarmann, Bauer	[154]
Smith, Porter, Engstrom	[153]
Sorensen	[148]
Ratwani, Wilhem	[42-44,113]
Verette, Wilhem	[108]
Vlieger	[13,72-79]
Wang	[152]
Wilhem	[109]
Wilhem, Fitzgerald	[55]

(a.3) Case studies and textbooks

Rich, Cartwright (Editors)	[155]
Broek	[1]
Rolfe and Barsom	[181]
Wilhem	[180]

(b) Practical examples

A number of investigators closely concerned with the application of fracture mechanics to actual designs were found willing to write up results of some of their recent residual strength computations as examples in this handbook. These examples are presented in this section. They were left as much as possible in their original but edited form, to give full credit to the contributors. The way of presentation, the contents and the conclusions are the responsibility of the contributors. Each example is followed by some editorial comments.

It has to be noted that the examples must be considered as self-contained texts, i.e. they have their own numbering system of figures and references.

EXAMPLE PROBLEM 3.3.3.1

RESIDUAL STRENGTH OF 7075-T73 PANELS WITH 8 INCH STIFFENER SPACING

T. Swift

McDonnell Douglas Corporation
Douglas Aircraft Company
Long Beach, Calif. 90846
(Literal)

1. STATEMENT OF THE PROBLEM

The fuselage of a modern jet transport aircraft is designed to sustain damage consisting of two bays of skin with a broken central stiffener in either a longitudinal or circumferential direction. During the development of just such a fuselage, several stiffened panels were designed and tested to determine their residual strength characteristics. The panels with circumferential cracks, measuring 60 inches wide by 120 inches long, were made from 7075-T73 sheet material 0.071 inches thick. They were stiffened by 7075-T6511 extruded stiffeners, placed at 8 inch centers to simulate fuselage longerons. Lateral stiffeners, representing circumferential frame members, were also included. The primary objective of the test program was to determine the effects of stiffener configuration and cross sectional area on residual strength. Four different stiffener configurations were included as shown in Figure 1. This example describes the analysis and testing of these panels and also shows analysis-test correlation.

2. ANALYSIS

The residual strength of a stiffened panel containing a skin crack, from a skin fracture standpoint, can be determined from

$$\sigma_c = K_c / [\beta \sqrt{\pi a} (\sec \tfrac{\pi a}{W})^{1/2}] \qquad (1)$$

where K_c = plane stress fracture toughness

a = half crack length

W = panel width

β = geometrical parameter (function of a)

In this case the geometrical term β was determined by "Lumped Parameter Finite Element Analysis" [1,2]. This method uses the Fortran Matrix Abstraction Technique, FORMAT [3] to solve the necessary matrix operations. The structural idealization used primarily for the aircraft is shown in Figure 2. The crack is simulated by successive disconnection of reactions from the centerline of the panel. The idealization shown in Figure 2 represents one quarter of the actual structure. The crack tip stress, σ_{yct}, is defined as the stress in the horizontal bar adjacent to the simulated crack tip. Analysis is performed on both unstiffened and stiffened panels having the same grid configuration. The term β is calculated as follows for each crack length considered:

$$\beta = \frac{\sigma_{yct}\ \text{Stiffened Panel}}{\sigma_{yct}\ \text{Unstiffened Panel}} \qquad (2)$$

where σ_{yct} is the simulated crack tip stress. The flexibility of the fastening system which attaches the stiffeners to the skins is an important consideration. An empirical equation, representing fastener displacement δ, was used for this analysis as follows:

$$\delta = \frac{P}{Ed} \left[5.0 + .8 \left(\frac{d}{t_1} + \frac{d}{t_2}\right)\right] \qquad (3)$$

where P = fastener load

E = sheet modulus

d = fastener diameter

t_1 and t_2 = thickness of joined sheets

This equation represents fastener displacement for aluminium rivets in aluminium sheet. The thickness of the shear panel representing the fasteners as indicated in Figure 2 is calculated to have the same flexibility as the rivets. The area of the idealized bars, representing skin in the simulated structure shown in Figure 2, is determined using skin width halfway between adjacent bars. The bars carry only axial load and the panels carry shear load. Stiffener idealizations for the four cases considered here are shown in Figure 2.

The strength of the stiffening elements plays an important role in the residual strength of stiffened panels. Stiffener stresses, as a function of crack length, are an output from the analysis. The outer cap of the stiffener is the most critical due to bending caused by transfer of load from the cracked sheet to the stiffener at the shear face of the fastening system, which is offset from the stiffener neutral axis. A unit stress of 1000 psi was applied to the top of the panels and reactions disconnected one at a time. The resulting values of β for the four cases considered are shown in Figure 3. It can be seen that β is higher than in the unstiffened panel case for total crack lengths up to about fourteen inches due to load input from the broken central stiffener. For crack lengths longer than fourteen inches the outer intact stiffeners start to pick up load and the stress intensity at the crack tip is reduced below that for an unstiffened panel. Stiffened stress concentration factors for the stiffener outer cap are shown plotted in Figure 4.

3. TEST RESULTS

The panels were mounted in a universal testing frame and uniaxial loads were applied at the bottom of the panel through a whiffletree system by six hydraulic jacks. Two tests were conducted on each panel. The damage created by the first test was repaired as indicated in Figure 1. The second test was conducted to failure. In each case, a half inch long saw cut was made in the skin over a cut stiffener. Uniaxial constant amplitude cyclic loading was applied to propagate a skin crack and then static load was applied in increments to cause fast fracture. The primary objective was to determine if a fast fracture could be arrested by adjacent stiffeners.

CASE 1 (See Figure 5)

In the case of the panel represented by case 1 of Figure 1, constant amplitude cyclic loading was applied to a maximum stress of 15.5 ksi ($R=\sigma_{min}/\sigma_{max}=0.05$). The crack was propagated to a total length of 1.95 inches and static load was then applied in increments up to a gross area stress of 28.15 ksi without fast fracture. Slow stable tear was observed starting at 20.73 ksi as indicated in Figure 5. Slow stable tearing took place from a total crack length of 1.95 to 2.17 inches during static loading. Cyclic loading was continued at a maximum gross stress of 18.0 ksi with R = 0.05 until the crack total length was 3.5 inches. Static load was again applied up to 28.62 ksi without fast fracture. Slow stable tear started to occur at 18.87 ksi and the crack grew to a total length of 4.14 inches. It has been the contention [4] that slow stable tear will not occur until at least the stress level has been reached, which was used to propagate the crack. These results confirm this contention. Cycling was continued at a maximum gross stress of 18.0 ksi with R = 0.05. Static load was applied and fast fracture occurred at a gross stress of 28.6 ksi. The crack was arrested in rivet holes at the inner attachment row. Cycling was continued until the crack had propagated out of second rivet row at a maximum gross area stress of 15.5 ksi with R = 0.05. Static load was again applied and the panel failed at a gross area stress of 29.61 ksi. The analytical fracture curve shown on Figure 5 was plotted from equation (1) using the value of K_c obtained from the fast fracture together with the β values plotted in Figure 3. Analysis-test correlation then was accomplished by predicting the correct residual strength for the full two bay crack. The stiffener strength curve in each case was determined using the analysis results shown in Figure 4 together with material properties obtained from the failed parts. It can be seen from Figure 5 then that failure stress was predicted with good accuracy. The crack arrested earlier than the analysis predicted due to its arrest in rivet holes.

CASE 2 (See Figure 6)

In the case of the panel represented by case 2 the skin crack was propagated to a total length of 2.0 inches at a maximum cyclic stress of 15.5 ksi with R = .05. Static load was applied and fast fracture occurred at 24.8 ksi after 1.21 inches of slow stable growth as shown in Figure 6. Slow stable tear in this case started at 16.3 ksi. The crack was arrested in rivet holes at the inboard row of rivets. During the previous test on this panel the crack had been arrested between rivets at the inboard row of rivets in each stiffener. Cycling was continued until the crack started out of one of the inboard rivet rows. Static load was applied up to 23.59 ksi and the crack jumped into a hole in the outboard rivet row. Cycling was continued at a maximum gross stress of 18.0 ksi, R = 0.05 until the crack had started out of the outboard rivet row. Static load was applied and fast fracture occurred at 27.8 ksi on one side and the crack was arrested between rivets in the inboard row of the adjacent stiffener forming a 3 bay crack. Loading was increased and fast fracture occurred again, and the crack was again arrested between rivets. The configuration at this point was a four bay crack, symmetrical about a saw cut central stiffener, with crack tips between rivets. Final failure occurred at a gross stress of 36.05 ksi which is higher than the predicted failure stress for two bays of skin shown by Figure 6. Figure 6 does however predict the fast fracture stress to the next stiffener very accurately. Analysis was not conducted for the 4 bay case.

CASE 3 (See Figure 7)

The panel for case 3 was subjected to uniaxial cyclic loading to a maximum stress of 22.0 ksi with R = 0.20. The skin crack was propagated to a total length of 4.98 inches. Static loading was then applied in increments up to a maximum gross stress of 26.0 ksi without fast fracture. During static loading the crack extended in total length by 0.23 inches. Slow stable growth in this case started at 22.0 ksi, the maximum stress at which the crack was propagated. This procedure was repeated four times as indicated by the test and analysis results shown on Figure 7. Fast fracture occurred on the fourth attempt at 26.54 ksi with a total crack length of 8.245 inches indicated by point E of Figure 7. The crack was arrested between rivets at the adjacent stiffeners at point F. Static loading was reapplied and further slow stable growth occurred to a total crack length of 16.31 inches when total failure occurred at a gross stress of 31.2 ksi. This value was higher than the intersection of the stiffener strength and skin fracture curves illustrated by point H in Figure 7.

CASE 4 (See Figure 8)

The panel representing case 4 was subjected to uniaxial cyclic loading up to a maximum gross stress of 22.0 ksi with R = 0.20. The skin crack was propagated to a total length of 4.10 inches when the cyclic maximum stress was reduced to 18.0 ksi. This stress was used to propagate the crack to a total length of 5.3 inches. Static load was applied and fast fracture occurred at a gross stress of 23.1 ksi after 1.95 inches of slow growth. Slow stable growth started at 18.0 ksi, the last peak value of cyclic stress. The crack was arrested between rivets at the adjacent stiffeners. Static load was reapplied and the panel failed at a gross stress of 29.6 ksi at a total crack length of 16.7 inches after 1.5 inches of slow stable growth as shown in Figure 8. It will be noticed from Figure 8 that slow stable growth started at 18.0 ksi, the stress at which the latter portion of crack growth had been propagated. The previously higher stress of 22.0 ksi did not influence this. An explanation of this is as follows [4]: when the stress level was reduced from 22.0 ksi to 18.0 ksi at a total crack length of 4.1 inches, the value of β at this point was 1.41 from Figure 3. The radius of the plastic zone at the crack tip can be calculated from the following classical equation for plane stress:

$$r_p = \frac{1}{2\pi}\left(\frac{K}{\sigma_y}\right)^2 \qquad (4)$$

Therefore at a total crack length, 2a, of 4.1 inches and a stress, σ, of 22.0 ksi, K is equal to 78.72 ksi$\sqrt{\text{in.}}$

The yield strength of the skin material was 61.844 ksi from coupon tests. The plastic zone radius at the crack tip was therefore 0.26 inches and the resulting value of $a + r_p$ was 2.31 inches. At the time of static load application the total crack length was 5.3 inches and β at this point was 1.35 from Figure 3. The plastic zone size using the lower cyclic stress of 18.0 ksi was therefore 0.2 inches and the resulting value of $a + r_p$ was 2.85 inches. Since this value is greater than the value of $a + r_p$ for the higher stress of 22.0 ksi it can be seen that the crack tip is out of the influence range of the higher stress and therefore slow stable growth would start to occur at the lower stress of 18.0 ksi. Further explanation of this phenomenon can be found in the literature [4] .

4. CONCLUSIONS

It has been shown that reasonable accuracy can be expected in the calculation of residual strength for stiffened panels using elastic finite element techniques. Because of non-linear fastener load displacement behaviour, this accuracy is not always possible, particularly when skin materials having higher fracture toughness are used. In this case, it may be necessary to resort to non-linear methods (See example 3.3.3.3).

5. REFERENCES

1. Denke, P.H., "A General Digital Computer Analysis of Statically Indeterminate Structures", Douglas Paper 834, September 1959.

2. Denke, P.H., "A Computerized Static and Dynamic Structural Analysis System; Part III, Engineering Aspects and Mathematical Formulation of the Problem", Douglas Paper 3213, presented to SAE International Automotive Congress and Exposition, January 1965.

3. Pickard, J., and Morris, R.C., "FORMAT II - Second Version of Fortran Matrix Abstraction Technique", AFFDL-TR-66-207, Volumes I and III.

4. Swift, T., "Application of Fracture Mechanics to the Design of Damage-Tolerant Stiffened Aircraft Structure". Published in "Fracture Prevention and Control", American Society for Metals, 1974.

6. COMMENTARY

This example is a good illustration of the application of the approach discussed in section 3.3.1.1 of this chapter. Contrary to what was proposed in that section, in this example the residual strength properties of the stiffened skin are determined from fast fracture data of the stiffened panel itself instead of from unstiffened panel data. However, this is not a fundamental point of difference. The behaviour of the panel after fast fracture, i.e. stresses and crack lengths at crack arrest after fracture instability and at final panel failure, agrees very well with the behaviour predicted by the calculated skin and stiffener curves.
This example clearly demonstrates that the applied method is to be recommended in the design stage. Because the method generates both the skin and stiffener curves, the effects of modifications in the design on the residual strength properties can easily be predicted on the basis of diagrams as shown in Figures 5-8.

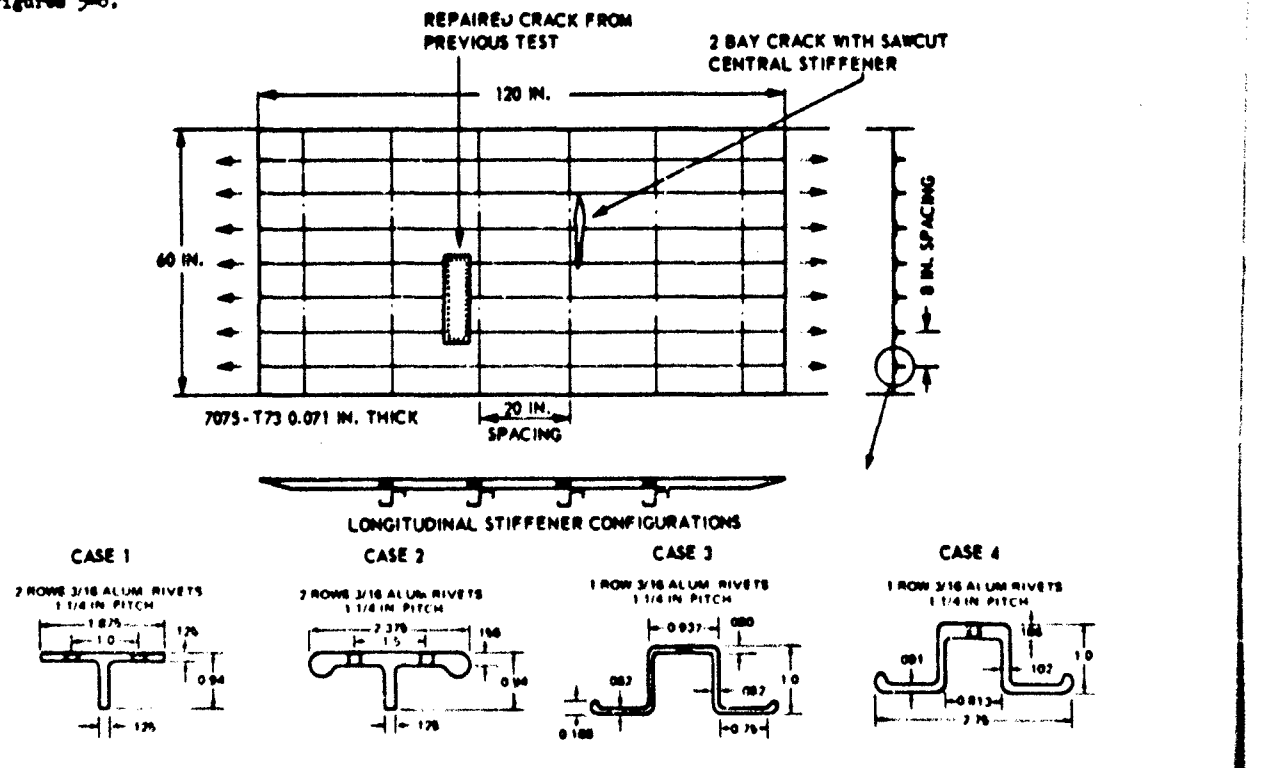

FIGURE 1 TEST PANEL DESCRIPTION

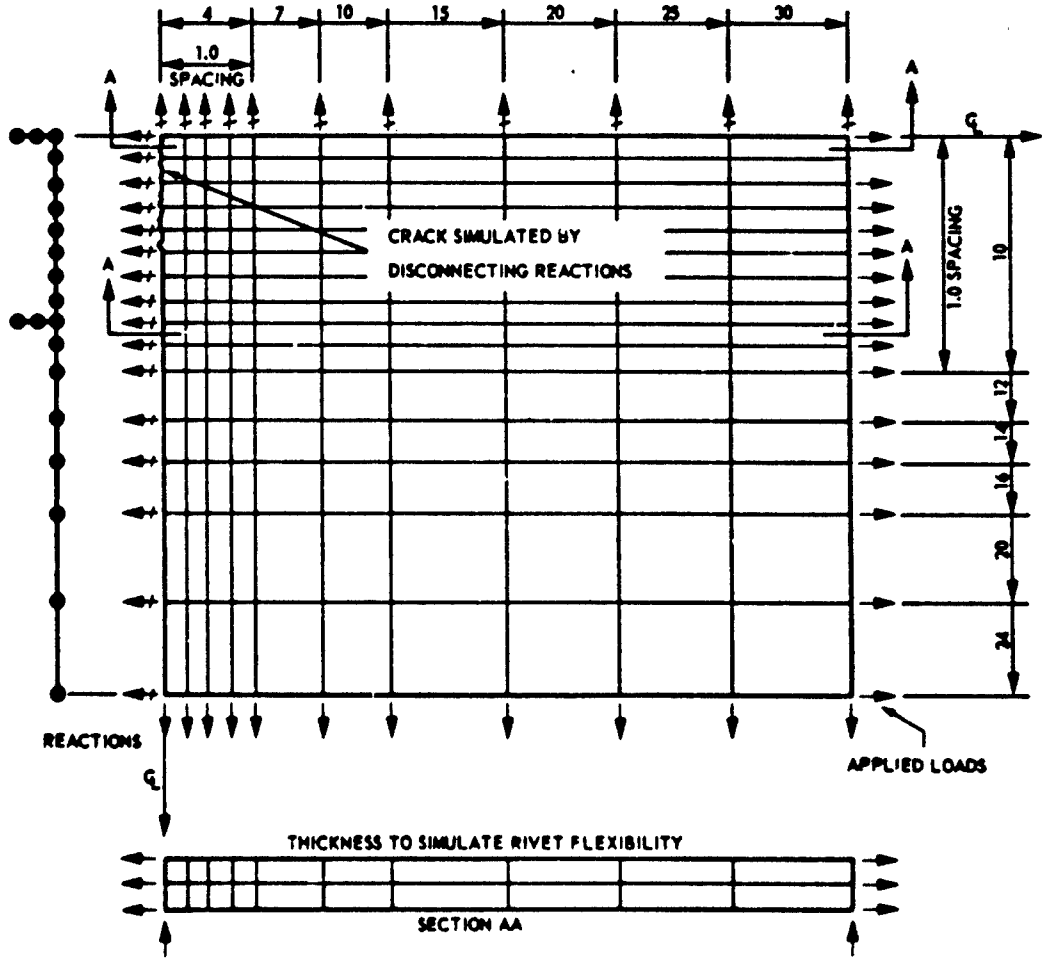

STIFFENER IDEALIZATIONS (SEE FIG. 1)

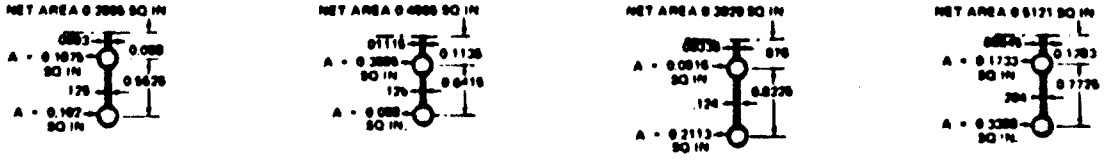

CASE 1 CASE 2 CASE 3 CASE 4

FIGURE 2 STRUCTURAL IDEALIZATION FOR CIRCUMFERENTIAL TWO BAY CRACK

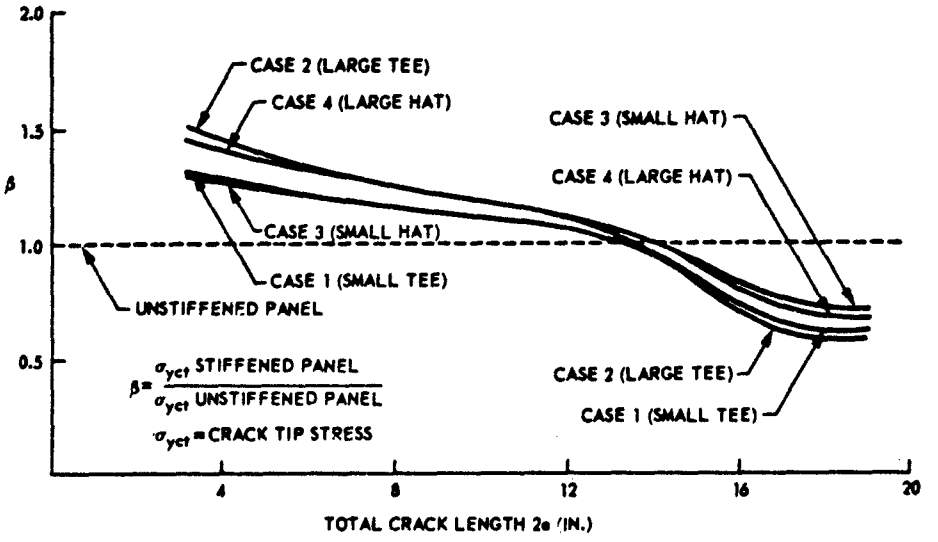

FIGURE 3 VALUES OF β AS A FUNCTION OF CRACK LENGTH

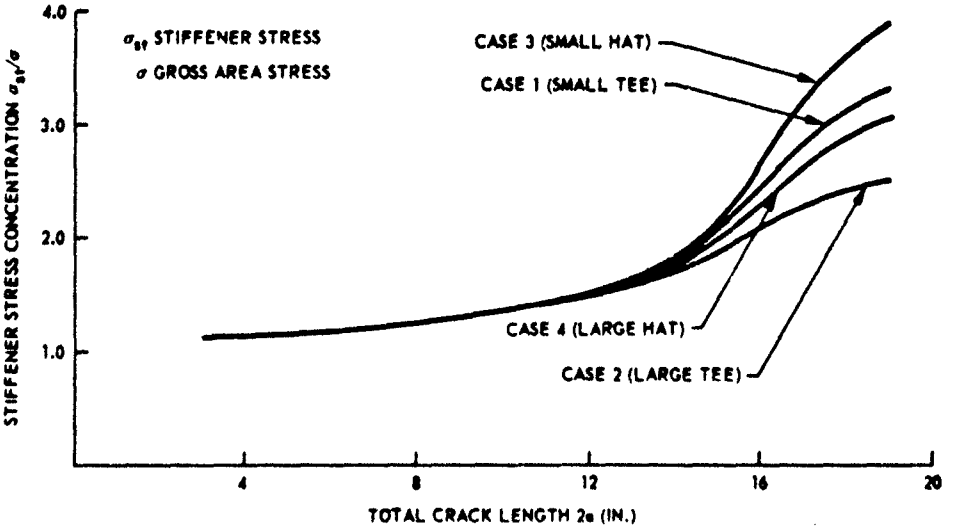

FIGURE 4 STIFFENER OUTER CAP STRESS CONCENTRATION FACTOR

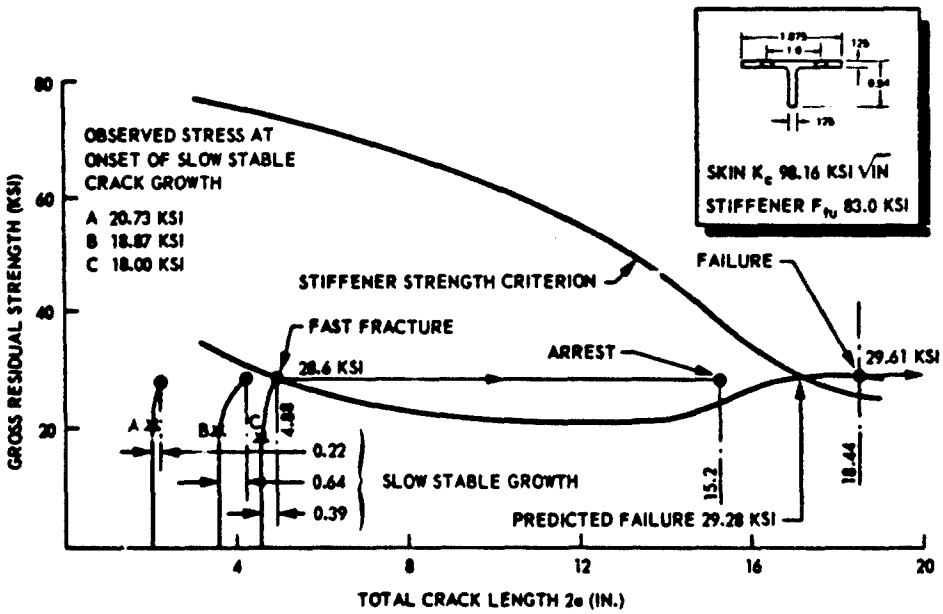

FIGURE 5 ANALYSIS AND TEST RESULTS FOR CASE 1

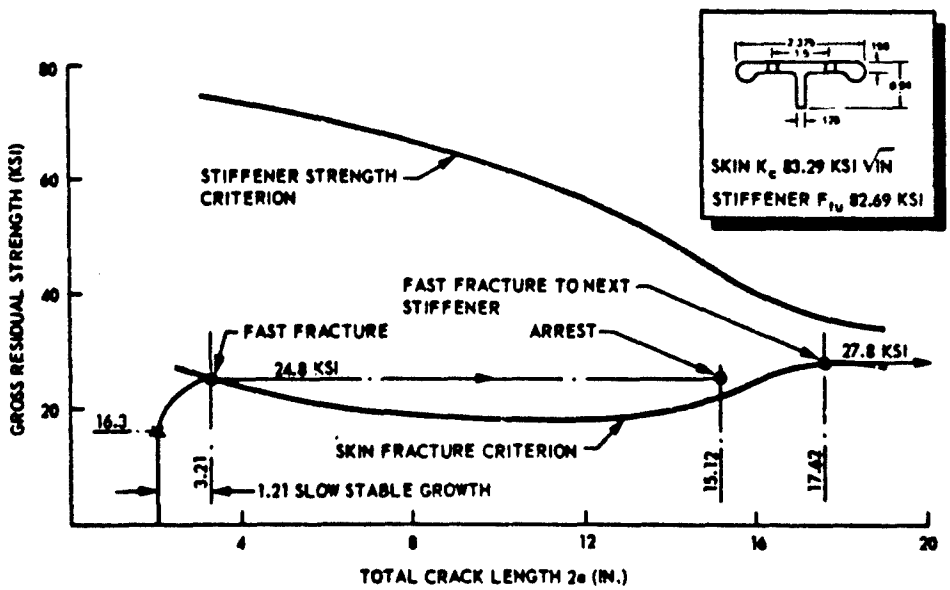

FIGURE 6 ANALYSIS AND TEST RESULTS FOR CASE 2

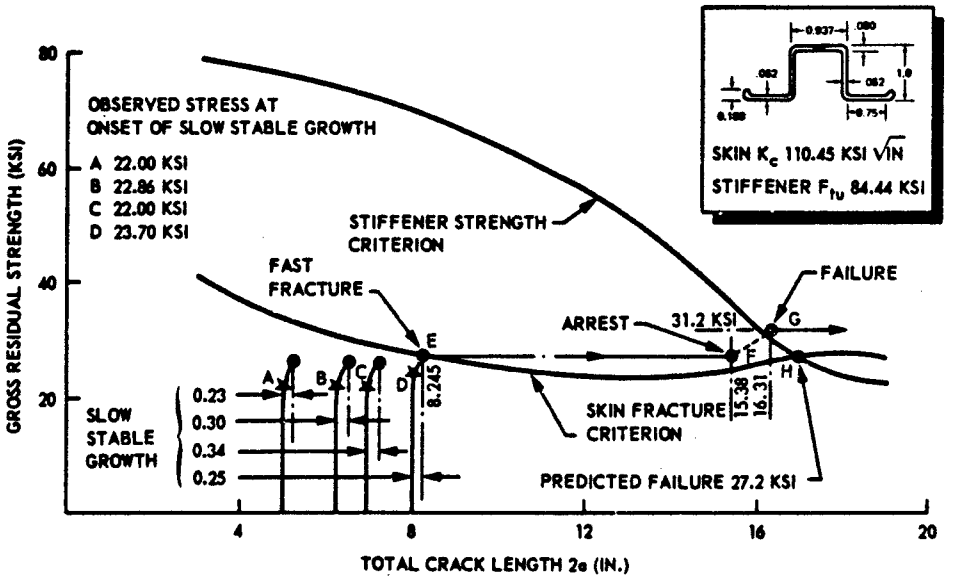

FIGURE 7 ANALYSIS AND TEST RESULTS FOR CASE 3

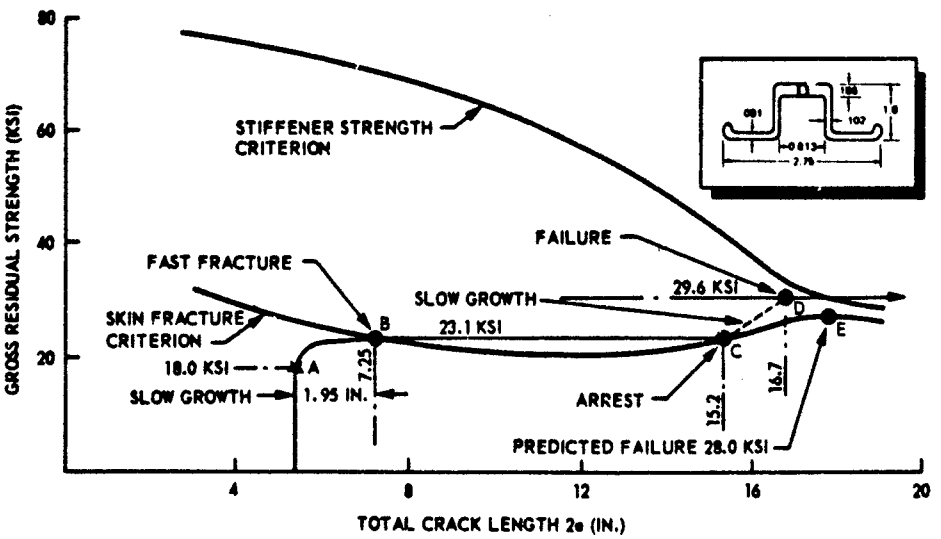

FIGURE 8 ANALYSIS AND TEST RESULTS FOR CASE 4

EXAMPLE PROBLEM 3.3.3.2

RESIDUAL STRENGTH OF STIFFENED 7075-T73 PANELS WITH 20 INCH FRAME SPACING

T. Swift

McDonnell Douglas Corporation
(Literal)

1. STATEMENT OF THE PROBLEM

During the early development phases of a large commercial transport aircraft, a study was undertaken to determine the residual strength of panels simulating typical fuselage construction. Panels with cracks in either a longitudinal or circumferential direction were designed and tested for that purpose. The panels were made from 7075-T73 sheet material having a thickness of 0.071 inches. The panels with longitudinal cracks measured 120 inches wide by 75 inches deep and were stiffened by frames at 20 inch spacing, parallel to the loading direction. Four different frame configurations were included as shown in Figure 1. Analysis and testing was performed on panels with and without titanium crack stopper straps. Lateral stiffening was provided by hat section longerons. The panels were intended to be used to gain information which would be useful in assessing the strength of a fuselage containing a two bay longitudinal crack. This example describes the analysis and testing for four of the panels and also shows analysis-test correlation. These four panels are described by Figure 1.

2. ANALYSIS

For the method of analysis the reader is referred to section 2 of example 3.3.3.1. Just as in that example, the geometrical term β, in the case of the four panels, was determined by finite element analysis of an idealized structure representing the panels. A typical idealization of the panels is shown in Figure 2. The idealizations for panels 1 and 3 were assumed to be the same even though the frame-to-skin shear clip was slightly different. Different idealizations were used for panels 2 and 4.
Stresses in the stiffening elements are an output of the finite element analysis. In the case of panels 1, 2 and 3, the most critical stiffeners are the frames at the center of the crack. The outer crack stopper is the most critical stiffening element for panel 4 since the center crack stopper is assumed failed. The stress concentration factor for the stiffeners is given by σ_{st}/σ, where σ_{st} is the stiffener stress and σ is the gross area stress applied to the top of the panel. The analysis results are shown in Figure 3.

3. TEST RESULTS

The panels were mounted in a test rig and uniaxial loads were applied through a set of whiffle trees attached to the top and bottom of the panels. Saw cuts were made in the skins over a central frame and cracks were propagated to pre-determined lengths under uniaxial loading. Loading was then increased statically in increments with a view to causing fast fracture in the skins. The objective was to cause fast fracture at the highest stress which could be arrested by the adjacent frames. One of the reasons for this was to assess the dynamic effects of crack arrest.

PANEL 1 (See Figure 4)
In the case of panel 1, constant amplitude cyclic loading was applied to a maximum stress of 14.04 ksi ($R = \sigma_{min}/\sigma_{max} = 0.05$). The skin crack was propagated to a total length of 27.05 inches. Static load was applied in increments up to a gross area stress of 17.0 ksi without fast fracture. The crack tips extended during static loading by a total of 0.45 inches. Cycling was continued until the total crack length was 29.0 inches. Static load was again applied without fast fracture. In this case, the slow stable crack growth was 0.40 inches. Slow stable growth in both cases did not start until the static stress was higher than the maximum cyclic stress. An explanation of this phenomenon has already been given [1]. Cycling was continued at a maximum stress of 17.0 ksi ($R = .05$). Fast fracture occurred at a total crack length of 35.0 inches and the crack was arrested in rivet holes at the adjacent frames. Cycling was continued to re-initiate cracks in the holes and static load was again applied. Failure took place at a gross area stress of 18.1 ksi with a total crack length of 41.93 inches. The results of this test are shown in Figure 4. The skin fracture toughness was calculated from the stress and crack length at fast fracture through the use of equation (1) given in example 3.3.3.1 and β values shown in Figure 3. The resulting value was 92.76 ksi $\sqrt{\text{in}}$. The skin fracture curve shown in Figure 4 was plotted using this value. It can be seen from Figure 4 that the peak of the skin fracture residual strength curve is predicted very closely by the finite element analysis when the actual fast fracture data is used.
The dynamic effects of crack arrest in this case can be no more than about 6 % since the static failure stress was only 1.1 ksi higher than the stress at crack arrest. If the dynamic effects had been any higher than this, the crack would not have been arrested.
Figure 4 illustrates the fact that the center frame strength criterion was almost the same as the skin fracture criterion with a 2 bay crack (40.0 inches). In view of this, the center frame of panel 2 was reinforced since the primary objective of the test was to fail the panel due to skin fracture.

PANEL 2 (See Figure 5)
The test procedure for panel 2 was essentially identical to that for panel 1. Again, the finite element analysis was able to predict the failure stress from a skin fracture standpoint very closely as indicated by the failure stress of 18.48 ksi being very close to the peak of the residual strength curve. The strength of the reinforced center frame is shown to be much higher than the unreinforced center frame of panel 1 and yet the failure stresses are almost the same. This illustrates that the skin fracture and stiffener strength criteria can be independent of each other as far as failure is concerned.
The dynamic effect for panel 2 can be no higher than 6.8 % for this case for the reasons previously described.

PANEL 3 (See Figure 6)
In this case, the analysis would predict failure due to center frame failure if MIL-HDBK-5 B values were used for frame strength, as used for panels 1 and 2. Tensile coupons cut from the frames of another panel for the same material batch used for the frames of panel 3 indicated a typical average ultimate strength value of 79.64 ksi for the 7075-T6 frame sheet material. If the frame strength is based on the typical value, Figure 6 indicates the failure criterion would be skin fracture.
In the case of panel 3, the dynamic effect would be no higher than 3 %.

PANEL 4 (See Figure 7)
This panel was fitted with titanium crack stopper straps. A 4 inch long saw cut was made in the skin over a crack stopper strap. Cyclic loading was applied to give a maximum gross area stress of 15.0 ksi with R = 0.05. After 13,125 cycles a 1.0 inch long crack was detected in the crack stopper and the 4 inch saw cut had extended to a total length of 6.6 inches. It was decided to increase the cyclic stress to a maximum of 16.4 ksi (R = .05) to compare crack growth with a previously tested panel. The skin crack was propagated to a length of 18.02 inches at which time the total number of cycles was 14,866. By this time the crack stopper was completely failed. The center frame was reinforced as in the case of panel 2, but the center crack stopper was left failed. Static load was applied to attempt to fast fracture the skin up to a gross area stress of 20.14 ksi. During this application of load, slow stable growth started to occur at about 16.2 ksi. The amount of growth was 0.32 inches. Fast fracture occurred on the second static load attempt and the crack was arrested at adjacent frames in rivet holes. Cycling was continued to re-initiate the cracks and static load was applied to 25.12 ksi when failure occurred. Sections of the outer crack stoppers were removed and tested in tension. The straps were tested as a whole, including the rivet holes. The average failure stress was 158.75 ksi for the Ti-8Al-1Mo-1V material. The residual strength curve using this value is shown in Figure 7. It can be seen that the finite element analysis would predict this failure very well.

The benefits of the titanium crack stopper straps can be seen when comparing the allowable stresses for the 2 bay crack case with the results of panels 1, 2 and 3.

4. CONCLUSIONS

It has been shown that the residual strength of stiffened panels containing large cracks can be predicted with reasonable accuracy using elastic finite element methods provided skin material K_c and stiffener material F_{tu} values are known. For the type of construction described herein the dynamic effects of crack arrest are small.

5. REFERENCES

1. Swift, T., "Application of Fracture Mechanics to the Design of Damage-Tolerant Stiffened Aircraft Structure".
Published in "Fracture Prevention and Control", American Society for Metals, 1974.

6. COMMENTARY

The same commentary as given in example 3.3.3.1 applies.

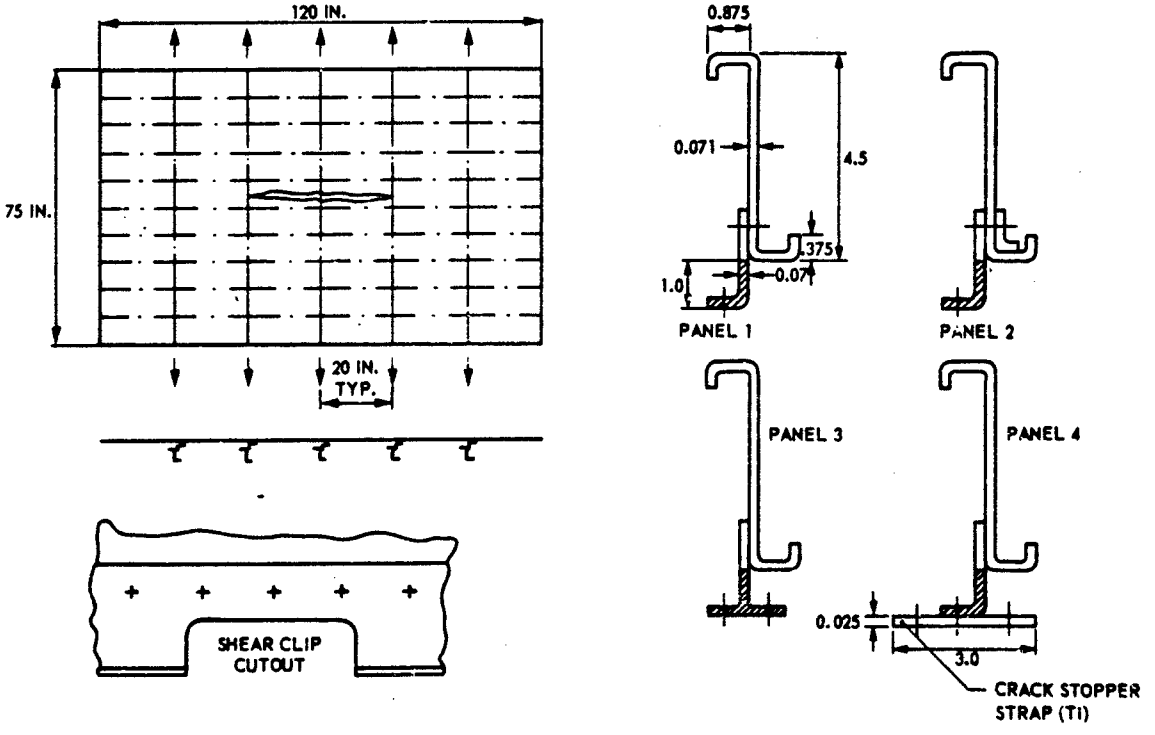

FIGURE 1 TEST PANEL DESCRIPTION

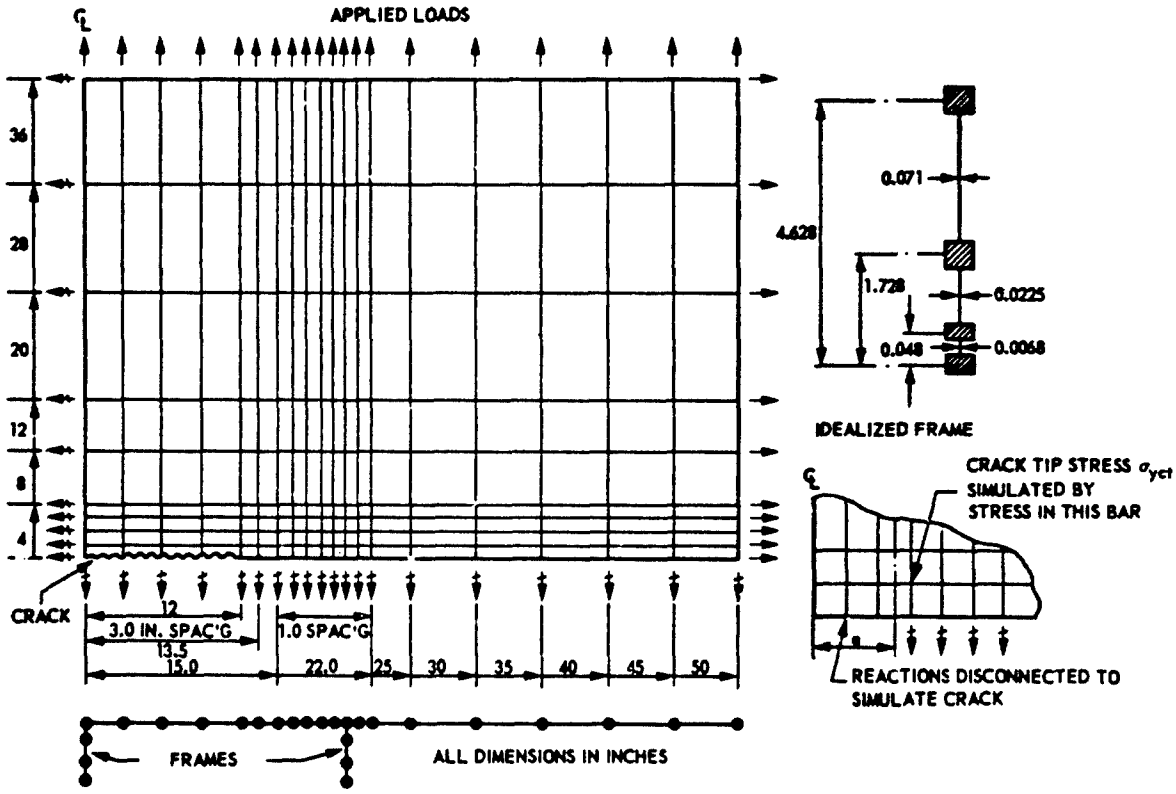

FIGURE 2 FINITE ELEMENT IDEALIZATION

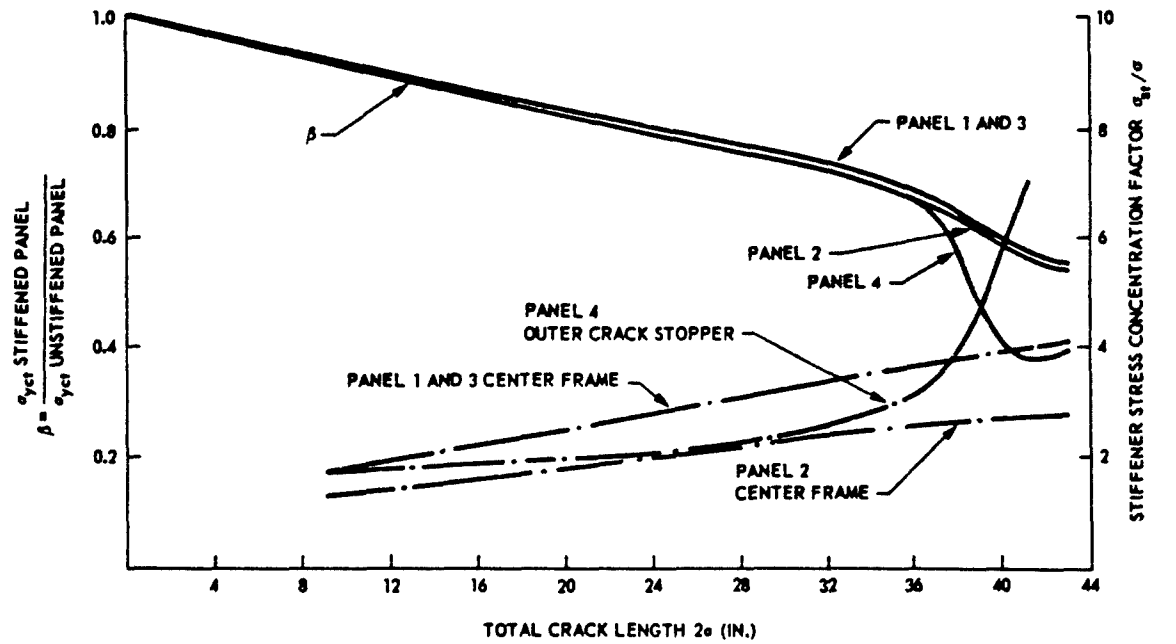

FIGURE 3 FINITE ELEMENT ANALYSIS RESULTS

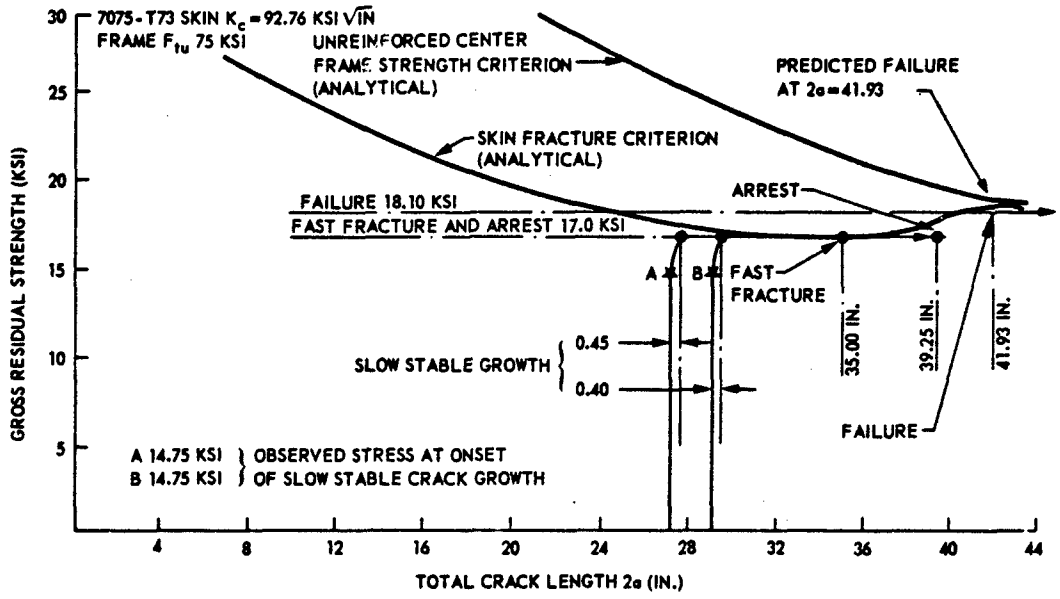

FIGURE 4 TEST AND ANALYSIS CORRELATION RESULTS FOR PANEL 1

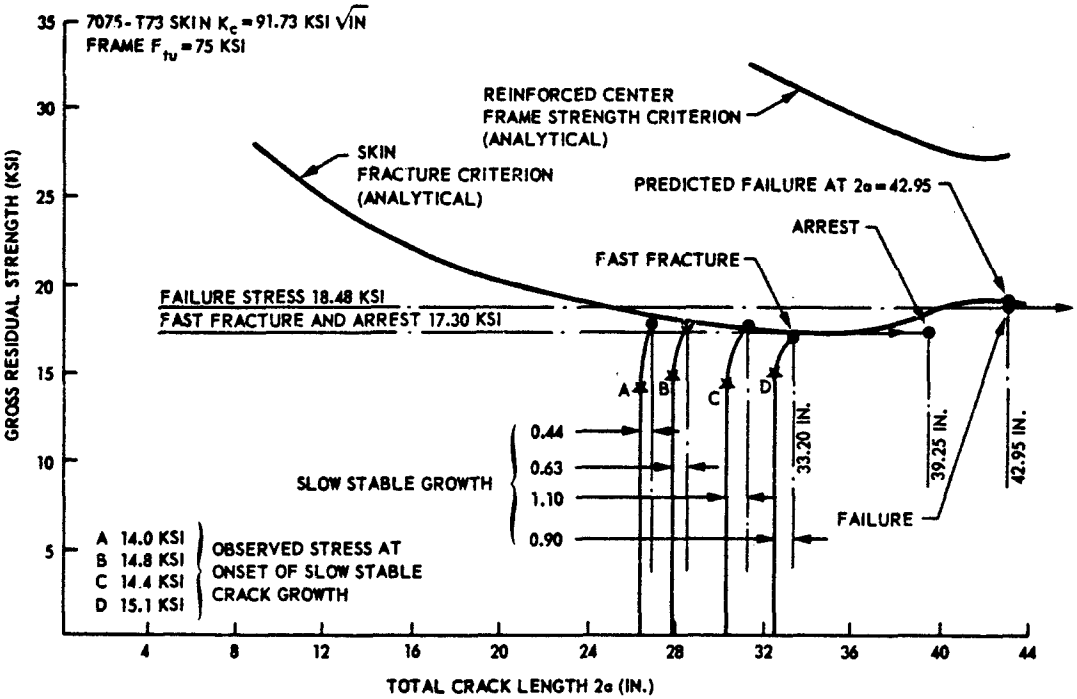

FIGURE 5 TEST AND ANALYSIS CORRELATION RESULTS FOR PANEL 2

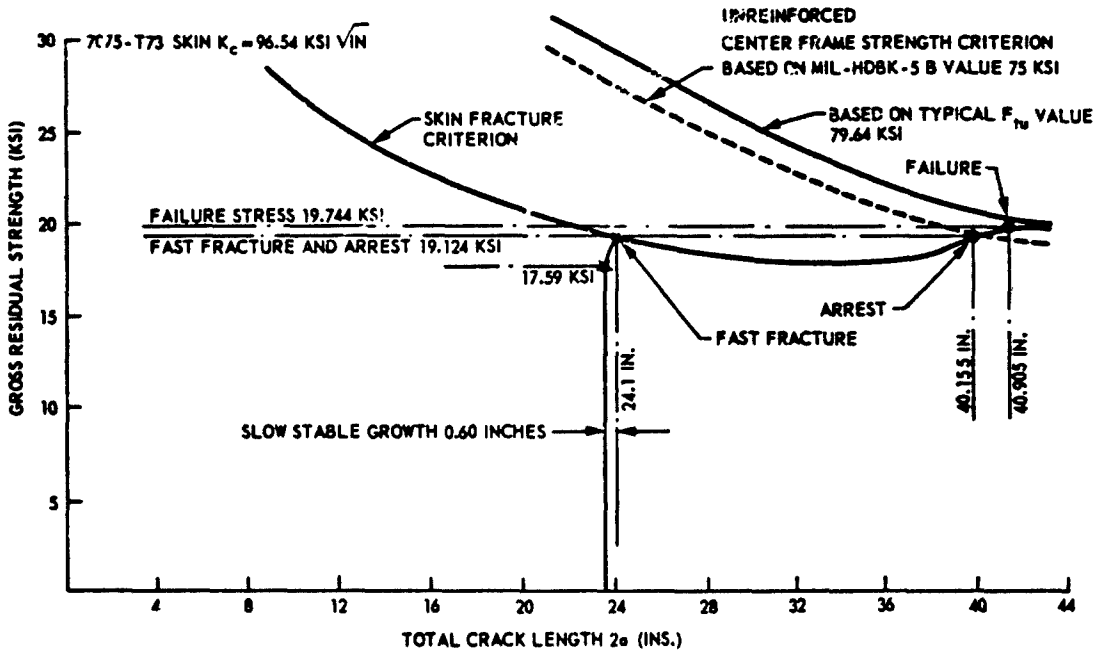

FIGURE 6 TEST AND ANALYSIS CORRELATION RESULTS FOR PANEL 3

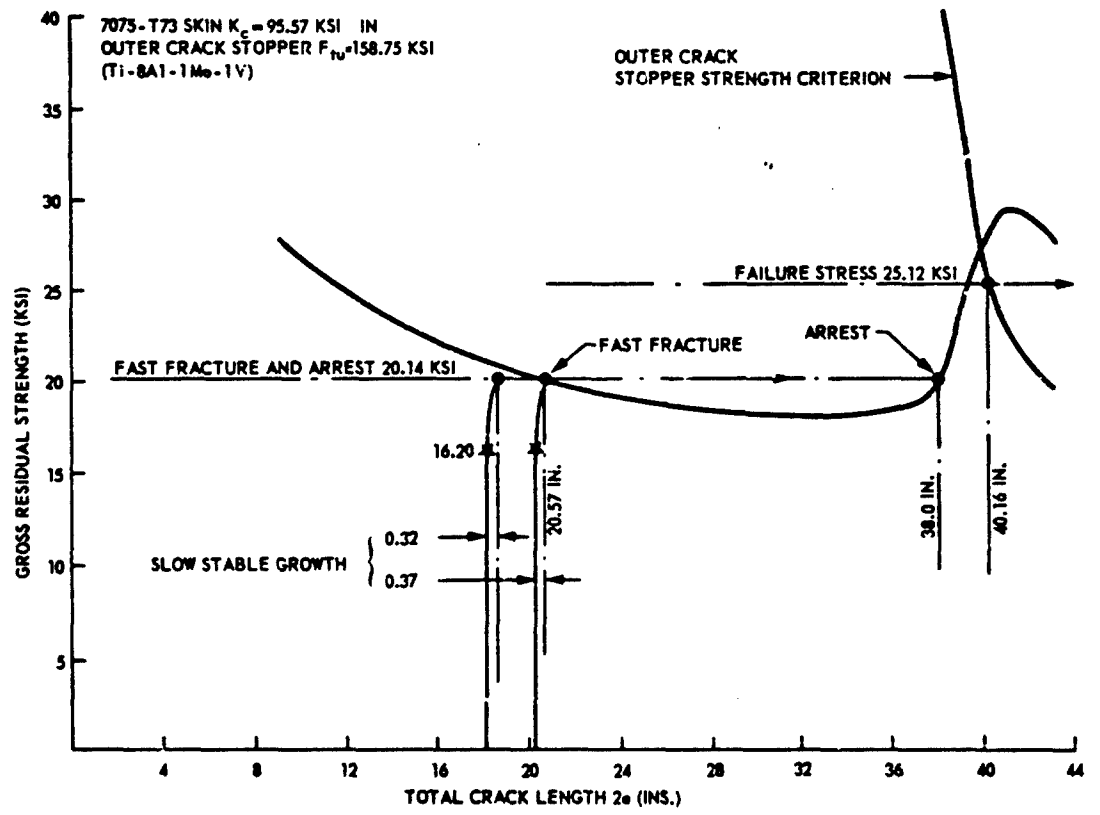

FIGURE 7 TEST AND ANALYSIS CORRELATION RESULTS FOR PANEL

EXAMPLE PROBLEM 3.3.3.3

THE EFFECTS OF RIVET YIELDING ON RESIDUAL STRENGTH OF STIFFENED STRUCTURE CONTAINING CRACKS

T. Swift

McDonnell Douglas Corporation
(Literal)

1. INTRODUCTION

The residual strength of a riveted structure containing cracks can be determined using elastic finite element methods. These methods have been shown to give reasonable results when the skin material fracture toughness is comparatively low [1]. In these methods, the simulation of rivet flexibility is essential to obtain reasonable analysis-test correlation. When material fracture toughness is high and when the crack tips extend beyond the crack arresting stiffeners, it is often necessary to consider nonlinear shear displacement characteristics of the rivets. If this is not considered, one can easily be misled by the elastic analysis results. Certain difficulties exist with non-linear finite element analyses. These difficulties are mainly associated with computer operational costs. Displacement compatibility methods offer considerable reductions in computer running time and the use of this approach together with non-linear fastener displacement characteristics becomes economically feasible. This example briefly describes just such an analysis which correlated with testing extremely well.

2. STATEMENT OF THE PROBLEM

During the development test phase of a large transport aircraft, a stiffened panel containing a 2 bay skin crack with a saw cut central stiffener, was tested for its residual strength. The panel, measuring 120 inches long by 60 inches wide, was made from 2024-T3 sheet 0.071 inches thick. Stiffeners, spaced at 8 inches, were made from "hat" section 7075-T6 extrusions, 0.5471 square inches in cross-sectional area. A skin crack was propagated into two skin bays, normal to the longitudinal stiffening and equally spaced about a central saw-cut stiffener. Static loading was applied to failure after the skin crack tips had propagated beyond the crack arresting adjacent stiffener.

Failure of the panel was precipitated by rivet failure over the entire length of the crack arresting stiffener at a gross area stress of 39.7 ksi with a half crack length of 9.88 inches. Elastic finite element analysis would predict the failure mode as being rivet critical but the allowable gross stress at failure would be too low by a factor of 3.5 to 1 . This analysis indicates that the load in the first rivet, adjacent to the crack in the crack arresting stiffener, is extremely high. In fact, considerable non-linear displacement of this rivet occurs causing adjacent rivets, progressively further away from the crack, to accept more load. When this occurs the stiffener becomes less effective in reducing the crack tip stress intensity factor and the panel gross allowable stress, from a skin fracture standpoint, is reduced. This effect, of course, cannot be assessed by elastic analysis.

3. ANALYSIS

The analysis used to correlate the results of the panel test was based on the displacement compatibility method. The details of this method are presented in the literature [2] . Figure 1 illustrates the method and as can be seen from the figure, either adhesively bonded or riveted structures can be considered. Correlation of an adhesively bonded test panel, using this approach, appears in the literature [3] . The approach is based on equating displacements in the cracked sheet with displacements in the stiffening elements after taking account of fastening system flexibility. Displacements in the cracked sheet are calculated at discrete points using the Westergaard Complex Stress Function approach. Fastening system flexibility and stiffener bending are both accounted for. The number of effective rivets on each side of the crack in each stiffener is usually 15. This was determined by obtaining solutions with different number of effective rivets assumed and then plotting crack tip stress intensity factor as a function of number of effective rivets. This plot becomes asymptotic at approximately 15 rivets for the 2 bay crack case with a broken central stiffener. A matrix of influence coefficients is inverted to obtain all the rivet loads. Crack tip stress intensity factor in the sheet is then determined from Muskhelishvili's methods [4] . The elastic-plastic load displacement characteristics, obtained from simple lap splice tests, was simulated by the tri-elastic model shown in Figure 2 for the test panel under consideration. The computer program, developed for this case, first generates an elastic solution based on the elastic slope of the rivet load displacement curve. All rivet loads are then compared to the tri-elastic model and the rivet flexibility matrix is then re-generated and a second solution produced. This procedure continues until the crack tip stress intensity factor difference between successive iterations is less than a specified value. The final stress intensity factor, for the specific applied gross area stress and crack size, is printed out together with all rivet loads and stiffener stresses.

4. ANALYSIS RESULTS

The analysis results for the first elastic iteration of the test panel configuration are shown in Figure 3. The skin fracture curve is plotted using β values (see analysis in example 3.3.3.1) obtained from the program together with a skin fracture toughness value K_c of 197.87 ksi $\sqrt{\text{in}}$, obtained from fast fracture of a previously tested stiffened panel of different configuration from the one considered here. At the failure half crack length of 9.88 inches, it can be seen from Figure 3 that the gross allowable stresses are 11.5 ksi, 32.5 ksi and 53.6 ksi from rivet failure, stiffener failure and skin fracture criteria respectively. Actual failure took place at 39.7 ksi. It can be seen therefore that one could be misled by the results of an elastic analysis. The elastic-plastic computer program has the ability to consider the effects of rivet failure and Figure 4 shows rivet displacement as a function of gross area stress for various number of rivets failed starting adjacent to the crack. As can be seen from the figure there is considerable difference between elastic and plastic solutions. With all the rivets intact the first rivet yields at a gross area stress of only 6.808 ksi. Yielding continues as the gross area stress is increased until point J is reached on line CD, when failure of the first rivet occurs.

Line CD represents the average failure displacement of the rivet. Lines AB and EF represent lower and upper bounds of rivet failure displacement respectively. The crack tip stress intensity factor as a function of gross area stress is shown in Figure 5. The upper curve considers that all rivets are intact and the other curves are for different number of rivets failed. When the first rivet fails at constant gross area stress the stress intensity factor increases as can be seen in Figure 5. The vertical line AB represents the critical stress intensity factor of 197.87 ksi $\sqrt{in.}$, obtained from a previous test. The vertical line CD represents a K_c value of 215 ksi $\sqrt{in.}$ used for illustration purposes later.

Figure 6 shows a cross plot of the intersection of vertical line CD of Figure 4 with the rivet displacement curves. This cross plot is titled Rivet Failure Curve. Similarly, vertical lines AB and CD of Figure 5 are cross plotted in Figure 6 and are titled Skin Fracture Curve K_c = 197.87 ksi $\sqrt{in.}$ and Skin Fracture Curve K_c = 215 ksi $\sqrt{in.}$ respectively. Figure 6 represents a residual strength diagram for a half crack length of 9.88 inches. To illustrate how this diagram works, assume for the time being that the skin fracture toughness K_c = 215 ksi $\sqrt{in.}$ Loading is applied slowly and the first rivet adjacent to the crack fails at point A of Figure 6 corresponding to gross area stress of 39.5 ksi. The panel allowable from a skin fracture standpoint immediately drops from point B to C. Total failure does not however take place because the panel allowable based on second rivet failure has increased to point D since this rivet is further away from the crack and therefore less critical. The load is still only at 39.5 ksi represented by point E and therefore lower than C or D. Total panel failure would now occur if the load is increased to point C due to skin fracture. In the case of the panel under discussion the fracture toughness K_c is only 197.87 ksi $\sqrt{in.}$ When the first rivet fails at 39.5 ksi gross stress, represented by point A of Figure 6, the entire panel fails due to fracture instability in the skin, since the panel allowable from a skin fracture standpoint drops from point F to point G, which is below the applied stress. This value is less than 1 % lower than the actual panel failure stress of 39.74 ksi. Variation in rivet failure displacement, represented by the lower bound line AB and the upper bound line EF of Figure 4, would give variation of panel failure between points G and F of Figure 6. The explanation here is that at the lower bound point G of Figure 4, failure of the first rivet would occur at 37.5 ksi. This is lower than point G of Figure 6 so the load could be increased to 39 ksi, represented by point G of Figure 6. Consider the upper bound point H of Figure 4, where the first rivet would fail at 42 ksi. In this case the panel failure stress would be limited to 41 ksi represented by point F of Figure 6. This then represents a spread in allowable between 39.0 and 41.0 ksi equivalent to minus 1.86 and plus 3.17 per cent of the actual failure stress.

5. CONCLUSIONS

It has been shown that when crack tips extend beyond the crack arresting stiffeners of a panel containing a two bay crack that elastic analysis will not predict the true gross stress at failure. For the configuration discussed, consideration of the elastic-plastic rivet load-displacement characteristics gave excellent correlation with test results. This elastic-plastic analysis was made economically feasible with the displacement compatibility method whereas non-linear finite element methods would have been extremely costly.

6. REFERENCES

1 . Swift, T. and Wang, D.Y., "Damage Tolerance Design-Analysis Methods and Test Verification of Fuselage Structure", AFFDL-TR-70-144, 1970.

2 . Swift, T., "The Effects of Fastener Flexibility and Stiffener Geometry on the Stress Intensity in Stiffened Cracked Sheet", published in "Prospects of Fracture Mechanics", Noordhoff International Publishing, Leyden, Netherlands.

3 . Swift, T., "Fracture Analysis of Adhesively Bonded Cracked Panels", TRANS. ASME Journal of Engineering Materials and Technology, Jan.1978.

4 . Paris, P.C., "Application of Muskhelishvili's Intensity Factors for Plane Problems, Part III, Lehigh University, 1960.

7. COMMENTARY

This is an excellent example of the application of fracture mechanics techniques to predict the behaviour of stiffened panels as a function of applied load. By performing analytical studies as described in this example, even during the design stage of an aircraft the designer can find out which structural elements will precipitate failure. If the results do not meet his requirements, on the basis of such an analysis he is able to modify his design.
Finally, this example clearly demonstrates that on the basis of purely elastic computations one may easily come to wrong conclusions when the prediction of residual strength behaviour of a structure is involved. In this respect analytical methods are preferable to finite element methods because yielding of one or more elements can easily be incorporated in the computation procedure.

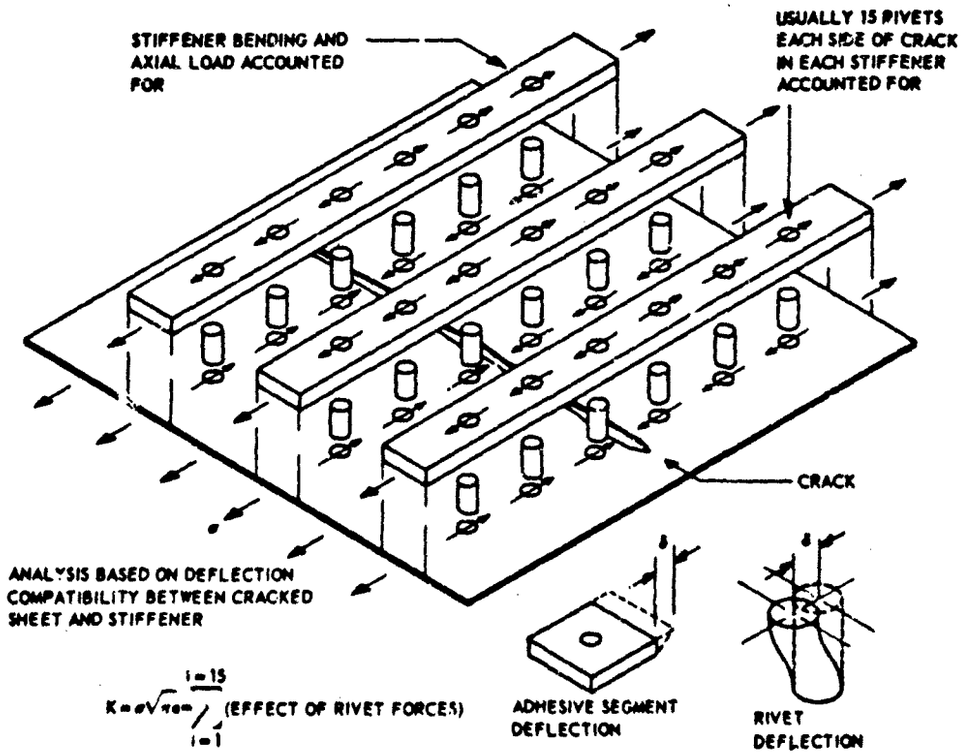

FIGURE 1 DISPLACEMENT COMPATIBILITY METHOD FOR FRACTURE ANALYSIS

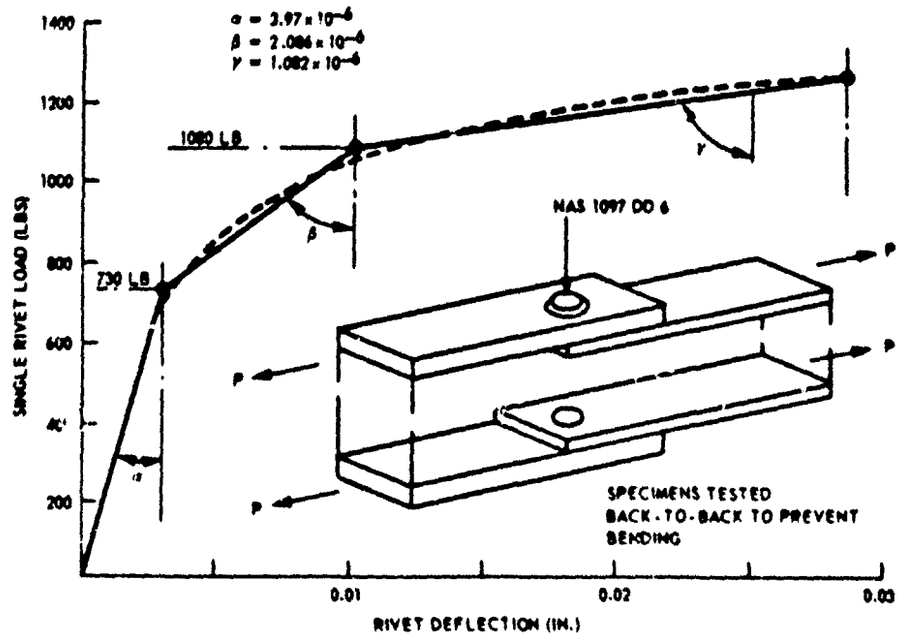

FIGURE 2 TRI-ELASTIC-PLASTIC MODEL FOR RIVET LOAD DISPLACEMENT

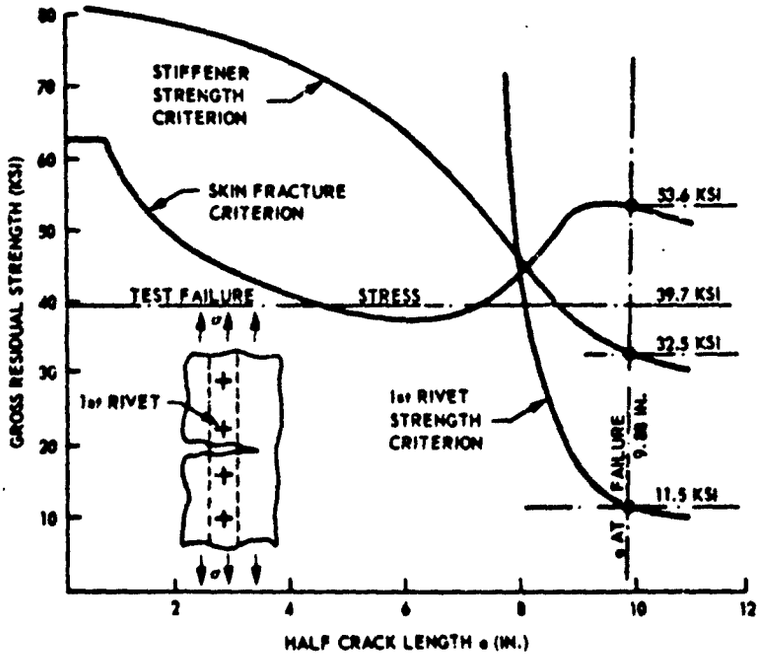

FIGURE 3 RESIDUAL STRENGTH DIAGRAM-ELASTIC ANALYSIS RESULTS

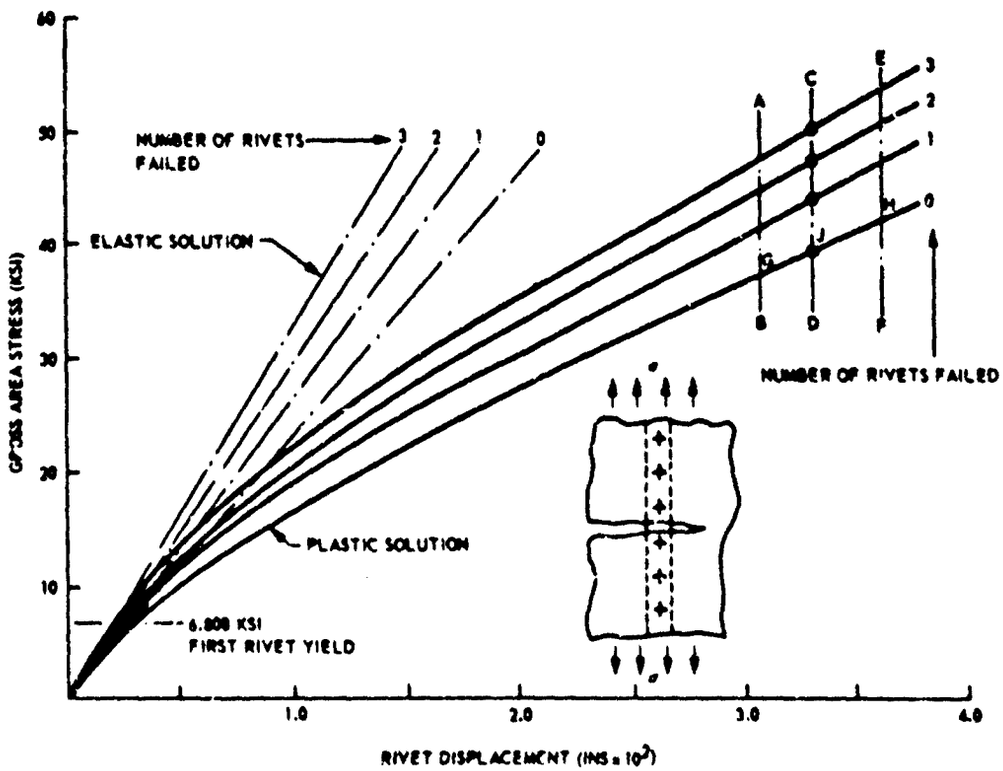

FIGURE 4 RIVET DISPLACEMENT AS A FUNCTION OF GROSS AREA STRESS (HALF CRACK LENGTH 9.88 INCHES)

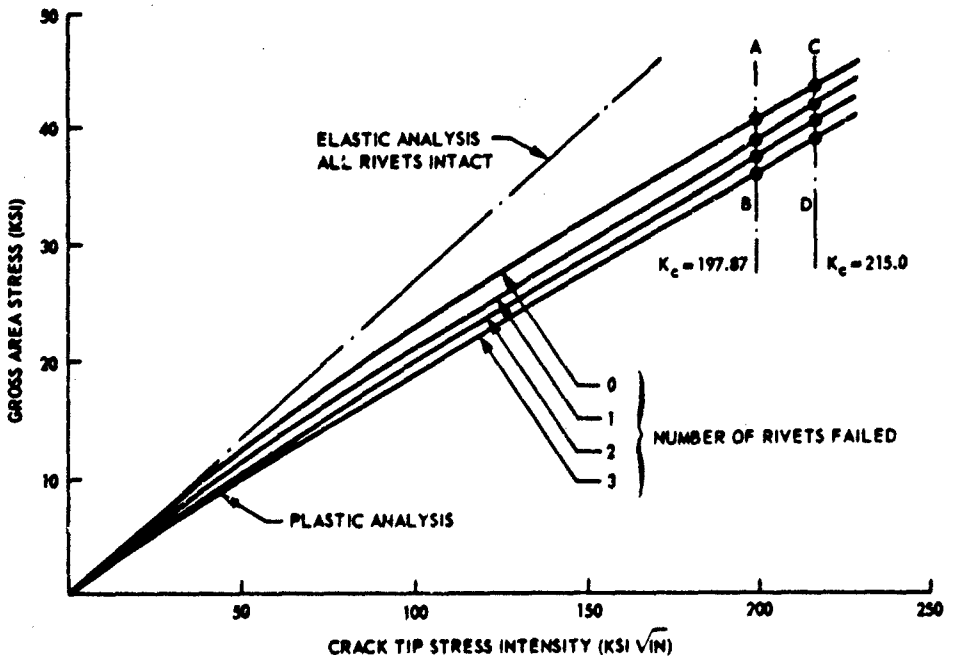

FIGURE 5 CRACK TIP STRESS INTENSITY FACTOR VERSUS GROSS AREA STRESS (HALF CRACK LENGTH 9.88 INCHES)

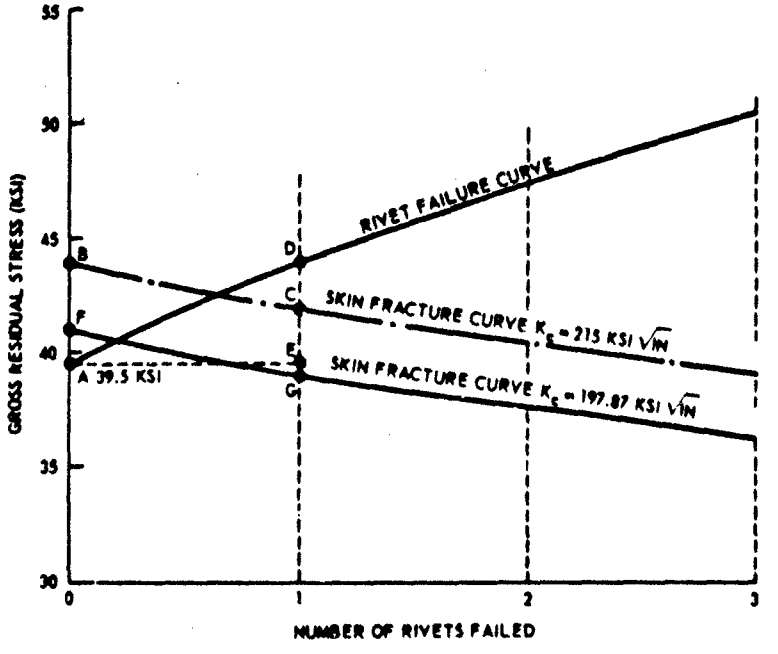

FIGURE 6 RESIDUAL STRENGTH DIAGRAM-HALF CRACK LENGTH 9.88 INCHES

EXAMPLE PROBLEM 3.3.3.4

THE USE OF RESISTANCE CURVES IN RESIDUAL STRENGTH PREDICTION

D.P. Wilhem

Northrop Corporation
Aircraft Division
Hawthorne, CA 90250
U.S.A.
(Literal)

1. STATEMENT OF THE PROBLEM

Since the last formal symposium on the development of crack growth resistance data [1] , several studies have been reported on materials' resistance to fracture [2,3] . The use of these data on real life, structural problems, however, has been limited. Ratwani and Wilhem [4] presented a summary of the predictive results of an extensive residual strength study given in [2] . These predictions were made using a J-integral based resistance curve which accounts for the materials' elastic-plastic behaviour. This example will describe the analysis, predictive techniques and fracture tests of a representative cracked aircraft structure, namely an angle stiffened wing panel. The geometry of these aluminum test panels is shown in Figure 1. These panels represented a 29 % stiffening ratio, typical of large transport aircraft lower wings. Two conditions were examined; a crack at an intact central stringer and at a broken central stringer.

2. METHOD OF ANALYSIS

Ten steps are involved in the analysis procedure. These are summarized below and have this typical pattern for all predictions. Details of each step are given in [2] .

Step 1 - Model the structure for finite element analysis or use existing finite element modeling. Special consideration must be given to fastener modelling to account for flexibility.

Step 2 - Select a crack length of interest and five other lengths based on the ratio of half crack length, a, to stiffener spacing, s, e.g. a/s up to 1.1.

Step 3 - From steps 1 and 2, perform non-linear calculations assuming Dugdale plastic zone behaviour.

Step 4 - From step 3, calculate stiffener stresses as a function of applied stress.

Step 5 - From the computed crack opening data of step 3, plot the $\sqrt{J}$ versus applied panel stress to yield stress ratio, σ/σ_{yield}, for various crack lengths.

Step 6 - Cross plot the data from step 5 as $\sqrt{J}$ versus crack length for specific applied stresses.

*Step 7 - Determine gross panel stress for a selected crack size at ultimate stiffener stress.

Step 8 - Obtain crack growth resistance data for the skin material in terms of $\sqrt{J_R}$ versus slow crack extension, Δa.

Step 9 - Plot the data from step 8.

Step 10- Overlay the $\sqrt{J}$ versus crack size curve of step 6 on the data of step 9 at the crack length of interest. Determine the amount of predicted slow tear. If greater than 0.25 inch, the structure will probably be skin critical. If less than 0.25 inch of slow tear is indicated, then a conservative estimate of residual strength will be made using step 7 data. The predicted instability, i.e. fracture stress will be the point of tangency between $\sqrt{J}$ curve and $\sqrt{J_R}$.

*If a skin critical fracture is anticipated, this step can be eliminated.

Using the above ten steps, the residual strength diagrams were developed as shown in Figure 2 for the intact stringer case. Predictions will be made of fracture and slow tear using this diagram. On the $\sqrt{J}$ versus crack size plot for the panel, the $\sqrt{J_R}$ versus Δa_{PHY} material resistance curve is overlayed at the initial physical crack length, a_{PHY} ,of interest. The applied stress at which $\sqrt{J_R}$ versus Δa_{PHY} and $\sqrt{J}$ versus a_{PHY} curves become tangential will determine the stress at which instability occurs and the crack propagates rapidly. After this point of instability, if the $\sqrt{J}$ curve for the panel dips below the $\sqrt{J_R}$ resistance curve of the material, the crack will be arrested, otherwise it will propagate catastrophically. The stresses in the stringer which are obtained from the elastic-plastic analysis and the ultimate strength of the stringer material are used initially to determine if a stringer critical case prevails. The ultimate strength of the stringer material (7075-T6 extrusions) was found to be 87.2 ksi from tensile test data. Using this ultimate stress value and the Dugdale type elastic-plastic analysis, the failure of the central stringer (angle) at a half crack length of 2.775 inches (initial half crack length in the tested panel) is predicted at $\sigma/\sigma_{yield} = 0.7$. Superimposed on the plot of Figure 2 is the $\sqrt{J_R}$ versus Δa_{PHY} resistance curve of the 7075-T73 skin material plotted at the same physical half crack length of 2.775 inches. It is seen from this figure that at the stringer critical stress $\sigma/\sigma_{yield} = 0.7$, there will be considerable slow tear in the skin. Therefore the computed failure stress of the central stringer for a half crack length of 2.775 inches will not be valid due to this extensive slow crack growth. Failure in a panel with this initial crack length will be skin critical. A failure of a skin critical type structure will be given by the point of tangency between $\sqrt{J}$ versus "a" curves for the panel and the $\sqrt{J_R}$ resistance curve of the material. From Figure 2 the resistance curve of the material plotted (dashed line) at a half crack length of 2.775 inches is tangential to the $\sqrt{J}$ versus crack length curve of the panel

at an applied stress of $\sigma/\sigma_{yield} = 0.545$ (point A in Figure 2). The first point of crack instability occurs (after a slow crack growth of Δa, see Figure 2) at this stress and the crack starts a rapid advance. However, from Figure 2, it is noted that at a half crack length of 4.45 inches, the $\sqrt{J}$ curve for the panel drops lower than the resistance curve of the material (point B), i.e. beyond this point the resistance of the material is higher than $\sqrt{J}$ developed in the stressed panel, and hence the running crack will become arrested. The crack was arrested at the rivet hole in the intact stringer panel where the stringer is connected to the skin. The resistance curve of the skin material is now replotted at a half crack length of 5.5 inches (distance from centerline of the stringer to panel centerline), where the crack became arrested. For this crack length the $\sqrt{J}$ curve of the panel becomes tangential to the resistance curve at an applied stress of $\sigma/\sigma_{yield} = 0.645$. Hence crack instability occurs at that stress and the crack starts running catastrophically. Beyond this point of instability the $\sqrt{J}$ values in the panel are higher than the resistance curve of the skin material and, therefore, no possibility exists for crack arrest. The $\sqrt{J}$ curve of the panel will continue to rise under increasing load until the influence of the next stringer on panel stress is felt (11 inches from the centerline of the panel), and the $\sqrt{J}$ value will once again have a decreasing trend and reach a second minimum at that point. From the trend of $\sqrt{J}$ curve in Figure 2 it is evident that at an applied stress of $\sigma/\sigma_{yield} = 0.645$ the $\sqrt{J}$ value of the panel will be higher beyond a half crack length of 7.5 inches. Therefore, no possibility of crack arrest is possible at the second stringer, i.e., 11 inches from the centerline of the crack, under increasing load conditions.

3. TEST RESULTS

The test panels were mounted in a 500 kip, electro-hydraulic load frame. Loading was accomplished through a slotted clevis attached directly to bolted-on-grip ends. Twenty strain gauges were placed at various locations on the angles and skin, and data recorded continuously to failure.
From the initial jeweler's saw slot, both panels were loaded to stress levels which would produce a maximum stress intensity level (for fatigue) of 15 ksi $\sqrt{\text{inch}}$ at a stress ratio (R) of 0.1. This fatigue cycling produced an overall crack length of 5.55 inches for the intact central stringer case and 5.46 for the broken stringer case.
The intact stringer panel was then tested to failure. Slow tear started at a load of 60 kips (σ/σ_{yield} of 0.32). At this applied load, slow tear at each crack tip was about 0.02 inch. The first point of instability (rapid crack extension) occurred after an applied load of 60 kips and before a load of 111.7 kips. At 111.7 kips the crack had already reached the angle stiffeners and was arrested. The analysis predicted the first point of instability at an applied stress of $0.545\ \sigma_{yield}$ (104 kips, see Figure 2). After the crack had advanced to the angle stiffeners, the panel was able to withstand a load of 111.7 kips ($\sigma/\sigma_{yield} = 0.58$) without any further slow tear. At this applied load, the slow tear analysis from Figure 2 is approximately 0.05 inches. This is less than the radius of the rivet hole. The measured residual strength of the panel was 116.1 kips compared to the predicted load of 123.4 kips ($\sigma/\sigma_{yield} = 0.645$), a 6 % difference in predicted load.
Since the broken stringer panel was identical in geometry to the previous panel, an elastic-plastic analysis was computed only for the tested crack length of approximately 5.5 inches. The elastic and elastic-plastic $\sqrt{J}$ values for the broken central stringer case are higher in both analyses. Hence, the $\sqrt{J}$ values will be higher at the same crack length and applied stress. Thus, in the case of the broken stringer, the first point of instability will be at some stress lower than $\sigma/\sigma_{yield} = 0.545$ and crack arrest will occur. Since the tested crack lengths for the broken and intact stringer panels were similar, the $\sqrt{J_R}$ values at failure for these two panels should also be expected to be similar. Using the predicted value $\sigma/\sigma_{yield} = 0.645$ and the elastic-plastic analysis for a half crack length of 2.75 inches (Figure 2, intact stringer) the $\sqrt{J}$ value at failure is 31.7 $(\text{in.} - \text{lbs./in.}^2)^{1/2}$. Using this $\sqrt{J}$ value and the elastic-plastic analysis for the broken stringer panel with a half crack length of 2.75 inches (Figure 2), the predicted failure stress is $\sigma/\sigma_{yield} = 0.553$ or 106.7 kips. The actual failure load was 107.2 kips. Thus, the predicted load was within 0.44 percent of the actual failure load.

4. CONCLUSIONS

The procedure outlined here and described in more detail in Reference [2] can be used to predict the residual strength of typical aircraft structure loaded in uniaxial tension. The slow tear, crack arrest, and elastic-plastic fracture can be predicted using a crack growth resistance approach and suitable Dugdale type plastic zone assumptions.

5. REFERENCES

1. Fracture Toughness Evaluation by R-Curve Methods, American Society for Testing and Materials, ASTM STP 527, 1973.

2. Ratwani, M.M. and Wilhem, D.P., "Development and Evaluation of Methods of Plane Stress Fracture Analysis, Part II, Volume I, A Technique for Predicting Residual Strength of Structure", Air Force Flight Dynamics Lab - TR-73-42, Part II, Volume I, April 1975.

3. Wilhem, D.P., Ratwani, M.M. and Zielsdorff, G.F., "A J-Integral Approach to Crack Resistance for Aluminum, Steel and Titanium Alloys", American Society of Mechanical Engineers, Journal of Engineering Materials and Technology, Volume 99, 1977, pp 97-104.

4. Ratwani, M.M. and Wilhem, D.P., "Application of Resistance Curves to Residual Strength Prediction", American Society of Mechanical Engineers, Journal of Engineering Materials and Technology, Volume 100, April 1978, pp 138-143.

6. COMMENTARY

The present example clearly illustrates the different steps that have to be carried out when applying the resistance curve approach for residual strength prediction of stiffened panels. Apparently, the criterion that determines whether in a panel with a certain initial crack length failure will be induced either by skin fracture (skin-critical case) or by stiffener failure (stiffener-critical case) is based on the amount of stable crack growth in the skin (from the initial crack size) at the stringer failure stress, the amount of 0.25 inch being the limit value (see step 10). If at that stress the amount of predicted slow tear is greater than 0.25 inch, then the structure will be skin critical, otherwise stringer critical. On the basis of this criterion a comparison of predicted and measured failure loads of various panel configurations [2,4] showed that the accuracy of prediction is usually much better than 10 percent.

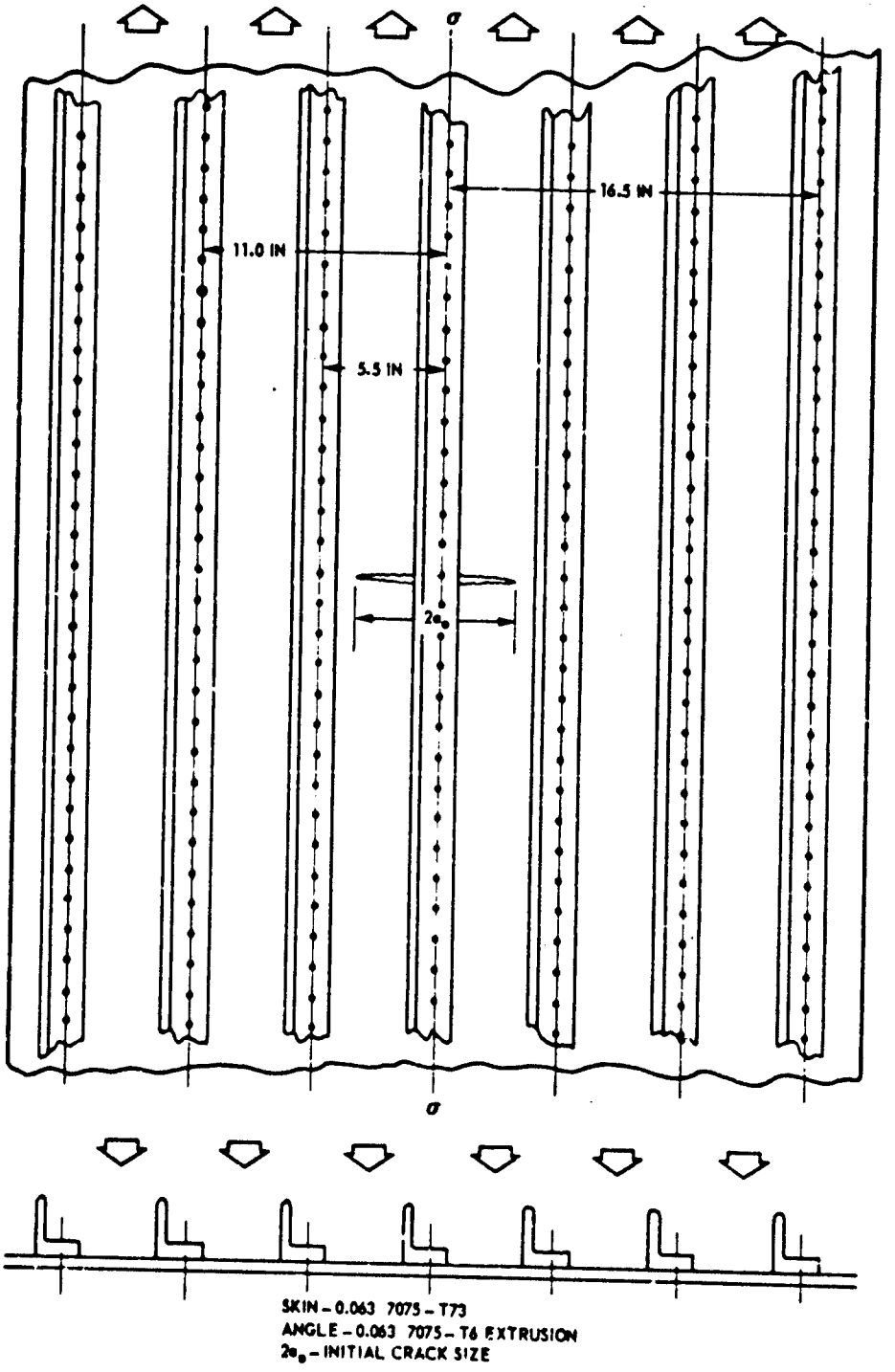

FIGURE 1 GEOMETRY OF TEST PANEL

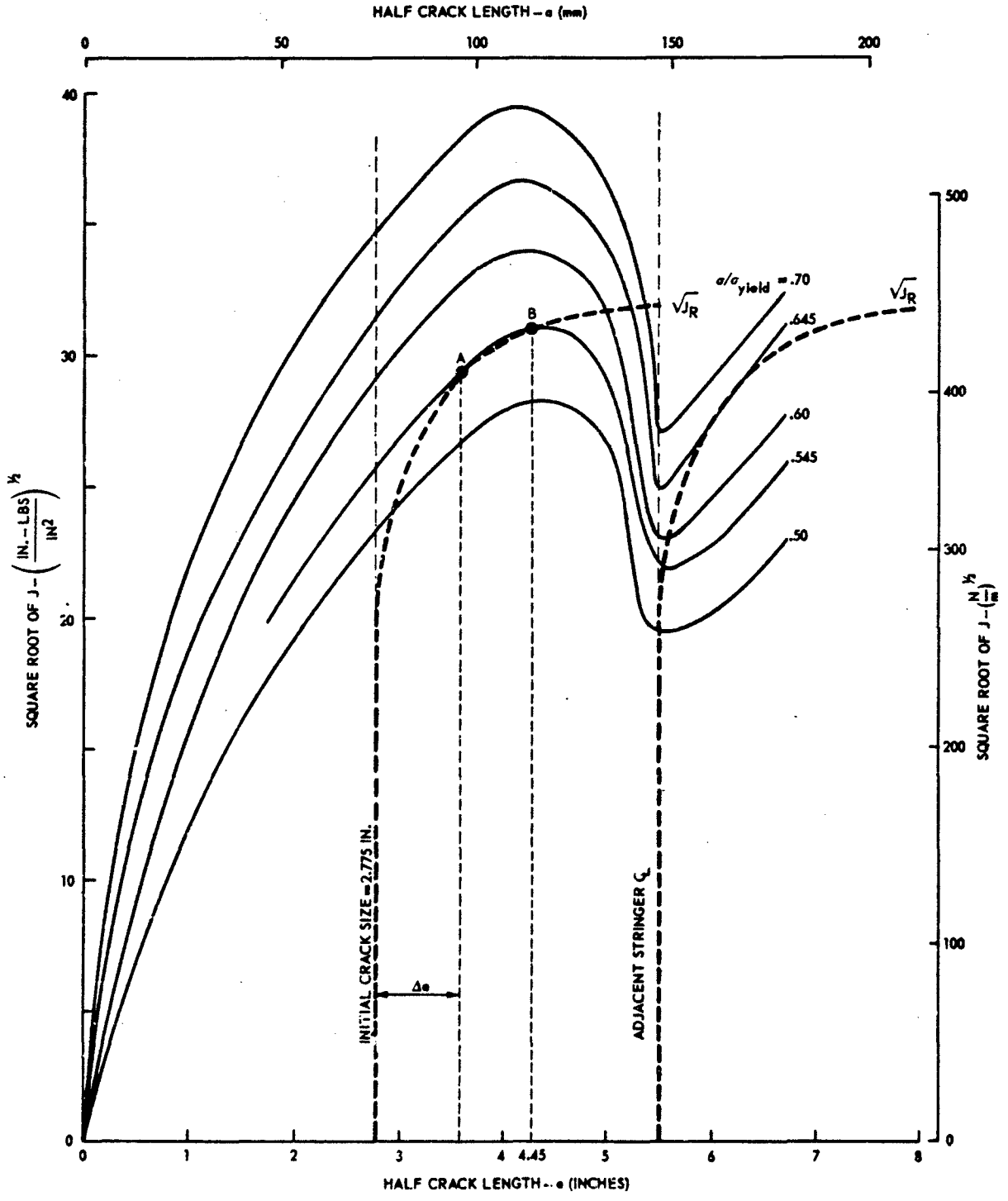

FIGURE 2 RESIDUAL STRENGTH – CRACK GROWTH RESISTANCE PLOT FOR INTACT STRUCTURE OF FIGURE 1

EXAMPLE PROBLEM 3.3.3.5

APPLICATION OF FRACTURE MECHANICS IN DESIGNING LOWER SURFACE OF TRANSPORT AIRCRAFT WING

V.G. Nanduri

The De Havilland Aircraft of Canada, Ltd.
Downsview, Ontario M3K 1Y5
CANADA
(Literal)

1. STATEMENT OF THE PROBLEM

The fail-safe integrity of aircraft primary structure is usually shown to be adequate by conducting Damage-Tolerance tests on stiffened panels and full scale airplane. Several methods of analysis, viz. Finite Element Method and Analytical Methods are used at various stages of the design. One of the methods that provided reasonable correlation with test data can be useful in the preliminary design stage. This simple method originally proposed by Figge [1] will be illustrated by considering narrow test panels similar to the lower surface of a transport aircraft wing. (Figures 1, 2, 3 and 4).

2. METHOD OF ANALYSIS

The cracked stiffened panel under consideration is assumed to be a composite material with the skin and stiffeners representing the matrix and fibers respectively. The application of the law of mixtures along with (1) the notch strength analysis of Kuhn [2] for sheet failure and (2) the proportional limit of the stress-strain curve as the limiting stress for the stiffeners, provides the net section stress for total panel failure as

$$S_n = \left(\frac{S_u}{K_u}\right)\left(\frac{A_{n-sh}}{A_n}\right) + P_L \cdot \left(\frac{A_{n-st}}{A_n}\right)$$

$$K_u = 1 + C_m (a_o)^{1/2} \left[\frac{1 - \left(\frac{2a_o}{W}\right)}{1 + \left(\frac{2a_o}{W}\right)}\right]^{-/2}$$

where

a_o = initial semi-crack length
A_{n-sh} = net section area of skin
A_{n-st} = total area of intact stiffeners
A_n = $A_{n-sh} + A_{n-st}$
C_m = material constant for the skin of specific thickness
K_u = static notch strength factor
P_L = proportional limit of the stiffener
S_n = net section failure stress
S_u = ultimate strength of skin material
W = panel width

The above equation expressed as gross failure stress of the panel is given by

$$S_g = \left[\frac{S_u(W-2a_o)t}{K_u(Wt+A_{g-st})}\right] + \left[\frac{P_L A_{n-st}}{Wt+A_{g-st}}\right]$$

where

t = skin thickness
A_{g-st} = total area of intact plus broken stiffeners

The choice of the parameter C_m is an important one. Analysis of data from reported unstiffened panel tests on 2024-T3 indicated that lower C_m values as obtained from tests with buckling guides may not be suitable in a design situation. For panels described here $C_m = 0.129(mm)^{-1/2}$ was assumed [1].

3. COMPARISON OF ANALYSIS AND TEST

The residual strength of panels 1, 2 and 3 (Figures 2, 3 and 4) calculated as per the above equation and the test results are given in Table 1. From the table it can be seen that the analysis and test results are in reasonable agreement for panels 1 and 2 (analysis is slightly unconservative). The failure mode for panel 3 is due to fastener failure as opposed to complete failure of panels 1 and 2 (Figures 5 and 6) and hence the lack of correlation between test and analysis. Configurations such as that of panel 3 will have to be analysed for fastener failure by the more rigorous methods such as that of Vlieger [3].

4. REFERENCES

1. Figge, I.E., "An Equation for Predicting the Residual Static Strength of Stiffened Panels", USAAVLABS, Report 70-17 (April 1970).

2. Kuhn, P., "Residual Strength in the Presence of Fatigue Cracks", AGARD Advisory Report 11 (1967).

3. Vlieger, H., "User's Manual of "ARREST", A Computer Routine for Prediction of Residual Strength of Cracked Stiffened Panel", NLR TR 75129 U (September 1976).

5. COMMENTARY

The method for the prediction of residual strength of stiffened panels as applied in this example and based on the notch-strength analysis of Kuhn and Figge [1,2] , is a very simple and approximate engineering method. In spite of its simplicity it provides a reasonable estimate of the panel failure load. This method can be useful in the preliminary design stage of an aircraft. In a later stage of design the approaches proposed by Swift and Vlieger (Stress intensity approach) and Wilhem (R-curve approach) are to be recommended, because these methods provide more information to the designer. Apart from the failure load, the latter methods predict the behaviour of a stiffened panel with increasing load, including the crack arrest capabilities, as a function of crack length.

Panel No.	C_m (mm-½)	S_u (MPa)	P_L (MPa)	Ag-st (mm^2)	An-st (mm^2)	W (mm)	t (mm)	$2a_o$ (mm)	Sg (Analysis) (MPa)	Sg (Test) (MPa)	% Difference
1 SEE FIG. 2	0.129	485.87	394.24	1855.16	1586.45	891.54	2.54	171.96	260.47	237.32	9.76
2 SEE FIG. 3	0.129	482.63	424.03	1565.80	1043.87	684.28	2.54	228.60	219.61	212.08	3.55
3 SEE FIG. 4	0.129	485.87	394.24	515.74	515.74	323.60	2.54	203.20	220.49	175.75	—

TABLE 1: CORRELATION OF ANALYSIS AND TEST FOR NARROW PANELS (1 ksi = 6.8947 MPa)

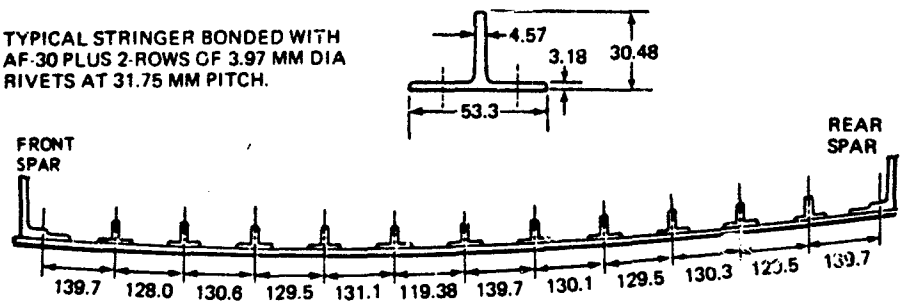

FIGURE 1: SCHEMATIC VIEW OF WING BOTTOM SURFACE (ALL DIMENSIONS IN MILLIMETERS)

PANEL 1

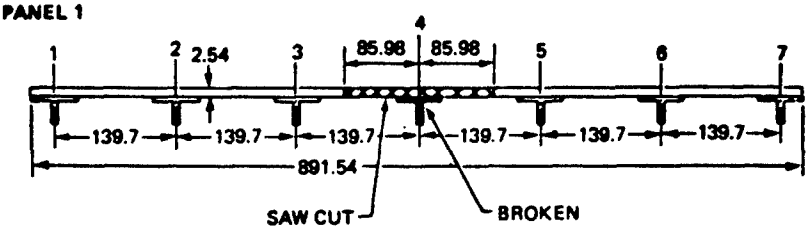

SKIN: 2024-T3 Aluminum Clad
S_U = 485.87 MPa (Coupon Test Results)
STRINGER: 2024-T4 Aluminum Extrusion
2-Rows of 4.76 mm Dia. Rivets at 31.75 mm for Stringers 3 and 4; All other stringers similar but 3.97 mm dia. Rivets
P_L = 394.24 MPa (Coupon Test Results)

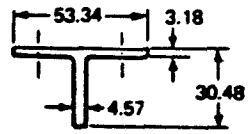

FIGURE 2: DETAILS OF THE NARROW 7-STRINGER PANEL (ALL DIMENSIONS IN MILLIMETERS)

PANEL 2

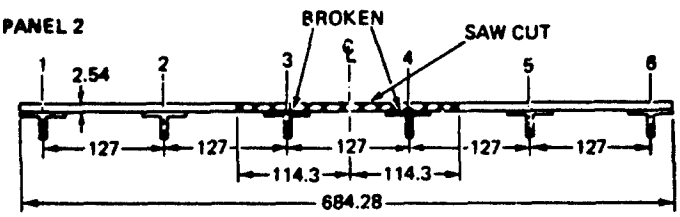

SKIN: 2024-T3 Aluminum clad
S_U = 482.63 MPa (Coupon Test Results)
STRINGER: 2024-T4 Aluminum Extrusion
Bonded with FM123-2 Glue; In addition 2 rows of 3.97 mm dia. rivets at 31.75 mm pitch
P_L = 424 MPa (Coupon Test Results)

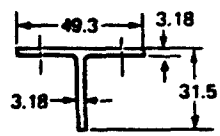

FIGURE 3: DETAILS OF THE NARROW 6-STRINGER PANEL (ALL DIMENSIONS IN MILLIMETERS)

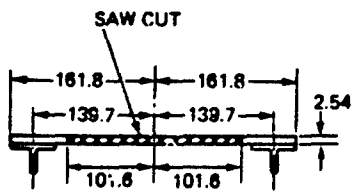

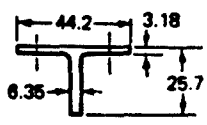

PANEL 3

SKIN: 2024-T3 Aluminum Clad
STRINGER: 2024-T4 Aluminum Extrusion
2 rows of 3.97 mm dia. rivets at 31.75 mm pitch
NOTE: Skin & stringer properties were assumed to be same as that of panel of Figure 2 for analysis.

FIGURE 4: DETAILS OF NARROW 2-STRINGER PANEL (ALL DIMENSIONS IN MILLIMETERS)

FIGURE 5 FAILURE OF 6-STRINGER PANEL DURING RESIDUAL STRENGTH TEST

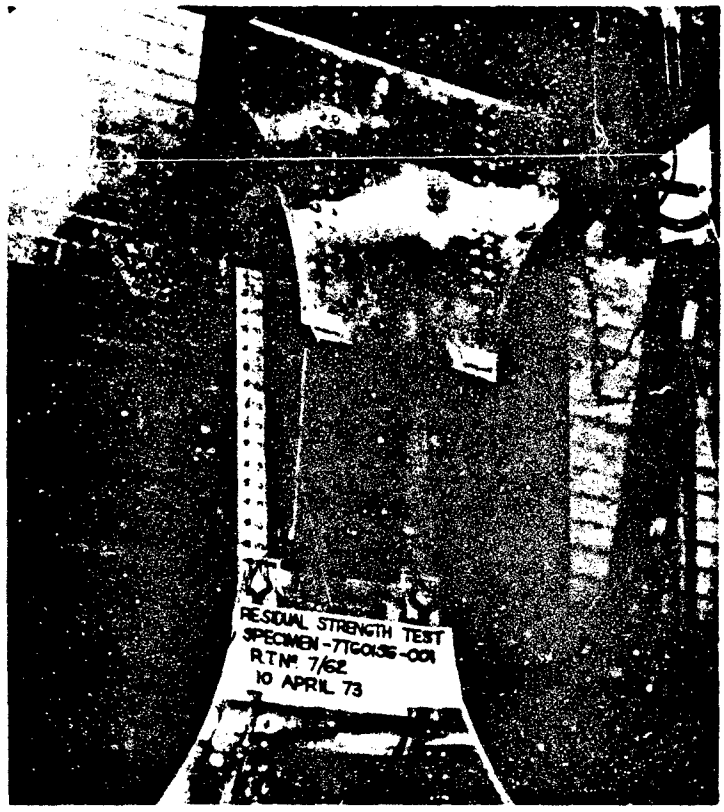

FIGURE 6 FAILURE OF 2-STRINGER PANEL DURING RESIDUAL STRENGTH TEST

EXAMPLE PROBLEM 3.3.3.6

RESIDUAL STRENGTH OF BONDED PANELS WITH 2024-T3 SKIN AND 7075-T73 OR 2024-T3 STIFFENERS

H. Vlieger

National Aerospace Laboratory NLR
Anthony Fokkerweg 2, 1059 CM Amsterdam
The Netherlands

1. STATEMENT OF THE PROBLEM

During the predesign stage of a new aircraft some residual strength tests were carried out on lower wing panels consisting of 2024-T3 skin and 7075-T73 stiffeners. The stiffeners were bonded to the skin. Two bonding materials were investigated, viz. Redux and FM 123/5. More details about the structural design are presented in Figure 1. To avoid an expensive clamping arrangement in connection with the prevention of initial bending, the actual configuration was idealized to a configuration with bonded strip stiffeners having approximately the same cross-sectional area. Owing to this investigation being performed primarily to study the behaviour of the bonding layer (and particularly the possible occurrence of debonding of such heavy-sized cracked panels) this idealization was considered to be allowable because such idealization is conservative with respect to the load transfer via the adhesive layer, i.e. the load transfer may be expected to be greater than that in the actual structure. The tests showed in a few cases that some small-scale debonding of the sheet-stiffener connection occurred in the region of the crack. Further, the panels proved to be skin-critical, i.e. fracture instability in the panels was induced by failure of the cracked skin.
Because the panels were skin-critical it was a point of interest to investigate whether and by how much the residual strength of this panel configuration would degrade if the stiffeners were made from 2024-T3 instead of 7075-T73 (in view of a possible improvement of the fatigue properties when using 2024-T3). This point has been studied analytically using a computer programme that allows determination of sheet-stiffener interaction in cracked panels with bonded stiffeners [1] . In doing so the following procedure was applied. Firstly, the residual strength was calculated for the panel configuration with 2024-T3 skin and 7075-T73 stiffeners. These computational results were compared with the test results to see whether the bonding connection was modelled properly. After that, using the same stiffener-bonding layer idealization computations were carried out for the panel configuration with 2024-T3 skin and stiffeners. The present example gives the results of the computations and the analysis-test correlation.

2. METHOD OF ANALYSIS

2.1 Prerequisites

The analysis is based on the stress intensity factor approach, as applied to ductile materials. The principles of this method are discussed in section 3.3.1.1 (d) of this chapter. It was found that a residual strength prediction for stiffened panels with a ductile skin material like 2024-T3 requires the following data:
(i) a relation between the critical stress, σ_c, and the effective crack length, $a_{eff} = a_c + r_p$, of the unstiffened panel.
(ii) curves of K = const. of the stiffened panel in a plot of stresses versus crack lengths.

(i) Residual strength data of the unstiffened panel (σ_c versus a_c) are shown in the upper half of Figure 3. The test data appear to obey the net section yield failure criterion (from coupon tests on the skin material σ_{yield} = 318 MPa was found, while the panel width equals 370 mm). From the net section yield line, labelled (a) in Figure 3, relations between σ_c and a_{eff} were determined (see curves labelled (b) and (c) in upper half of Figure 3) for two well-known plastic zone correction factors, r_p, viz. that of Irwin

$$r_{p1} = \frac{1}{2\pi}\left(\frac{K}{\sigma_{yield}}\right)^2 \qquad (1)$$

and Dugdale

$$r_{p2} = \frac{\pi}{16}\left(\frac{K}{\sigma_{yield}}\right)^2 \qquad (2)$$

In equations (1) and (2) the stress intensity factor, K, has also to be expressed in terms of a_{eff} to allow an elastic analysis (see section 3.3.1.1 (d) of this chapter). This implies that for a certain stress level the r_p-values have to be determined by an iterative procedure, starting with the σ_c and a_c values given by the net section yield line.

(ii) To determine the K = const. curves of the stiffened panel, the in-house developed analytical programme BOND was used [1] . This programme computes the sheet-stiffener interaction for cracked panels with bonded stiffeners as a function of the panel end stress, σ, and accounts for yielding of stiffeners and bonding material. The elastic and plastic extensional and shear stiffnesses of stiffener and adhesive are incorporated in the programme by using linearized versions of the σ-ε and τ-γ diagrams of stiffener and adhesive respectively.
To compute the sheet-stiffener interaction for the present panel configuration the stiffener and bonding layer were idealized as shown in Figure 2. Each stiffener was divided widthwise in three strips and each strip was imagined to be connected to the sheet at "n" points each side of the crack line. The number of elements and the length of each element was adjusted to the expected stress gradient in the stiffener. For the present problem "n" was chosen to be equal to 9. The element lengths are given in Figure 2. The load transferred by each element was assumed to be uniformly distributed over the element (see Figure 2).
The computation procedure operates broadly as follows. The programme starts for a certain crack length and a panel end stress σ equal to unity with the computation of the interacting forces on each element based on sheet-stiffener compatibility at the element ends. Using the calculated element loads the stress intensity

factor and the maximum load are determined. At the termination of this first step the panel stress level is determined at which yielding of a stiffener or bonding element will start anywhere in the structure. That stress level is used as the σ-value for the second step. After the second step the panel stress is increased with predetermined stress increments after having modified the stiffness of the stiffener or bonding element that started to yield. After each increment the stress intensity factor and the maximum stiffener load are determined. The procedure of increasing stress, checking whether other elements start to yield and if so, modification of the relevant stiffness, is continued until a predetermined stress level is reached.
By applying this calculation procedure for a number of crack lengths the stress intensity factor (corrected for yielding of stiffener and bonding layer) can be found as a function of panel stress and crack length. In this manner the K = const. curves, plotted in the lower half of Figure 3, were found for the panel configuration with a 2024-T3 skin and 7075-T73 stiffeners. In this case all the stiffeners were intact.

2.2 Computation of stiffened-skin curve

The computation of the stiffened-skin curve (σ_c versus a_c) is illustrated in Figure 3 for a panel configuration with five intact stiffeners containing an effective crack length a_{eff} = 75 mm. The failure stress levels of the unstiffened sheet corresponding with this crack length are given in the upper half of Figure 3 by points A and B for the Irwin and Dugdale plastic zone corrections, respectively. Using the K and the r_p-values belonging to these points (see Table 1), and plotting those in the lower half of Figure 3, a point on the stiffened skin curve (σ_c versus a_c) will be found. By applying this procedure for a number of a_{eff} values (see Table 1) the stiffened-skin curves labelled ⑧ and ⑨ in Figure 3 will be obtained.
In the same way the stiffened-skin curve of the same panel configuration but with a broken central stiffener was obtained. The results are shown in Figure 4.

3. TEST-ANALYSIS CORRELATION

A comparison of the computational results with residual strength test data is shown in Figures 5 and 6. Concerning the tests it has to be remarked that the plotted crack lengths at panel failure are rather doubtful. During the final part of the test, just before panel failure, the panels showed a large amount of stable crack growth at approximately the same stress level.
Comparing the analytical results with the test data it can be concluded that the predictions according to both the Irwin and Dugdale approaches agree fairly well with the test results. The predicted residual strength values as given by the top of the respective curves are within 10 % accuracy. Apparently the behaviour during stable crack growth of the panels with a broken central stiffener is best predicted by the Dugdale corrected curve (see panel 3 in Figure 6).

4. PREDICTION OF RESIDUAL STRENGTH FOR 2024-T3 PANEL

Applying the same procedure as described in section 2 the stiffened-sheet curves were determined for the same panel configuration but now provided with 2024-T3 stiffeners instead of 7075-T73. In doing so, only the Irwin plastic zone correction was considered. The computational results are shown in Figures 7 and 8 for panels with intact and broken central stiffeners together with the results of the panels with 7075-T73 stiffeners. The residual strength appears to be reduced by approximately 17 % when changing from 7075-T73 to 2024-T3 stiffeners. Further, it can be noted that in considering the shape of the stiffened-sheet curves for half-crack lengths of the order of the stiffener pitch the panels with 2024-T3 stiffeners show a less pronounced rise in the curve than those with 7075-T73 stiffeners. In fact, for the 2024-T3 panels with intact stiffeners (see Figure 7) there is only a horizontal part in the stiffened-sheet curves instead of a rise. This implies that these panels will not show crack arrest properties (see section 3.3.1.1 (b) of this chapter).

5. CONCLUSIONS

(i) The residual strength properties of panels with ductile skin materials like 2024 can be predicted with sufficient accuracy using the stress intensity factor approach (see section 3.3.1.1 of this chapter).
(ii) For the present panel configuration the residual strength was reduced by approximately 17 % when using 2024-T3 stiffeners instead of 7075-T73 stiffeners. This reduction was independent of the condition of the central stiffener (intact or broken).
(iii) The crack arrest properties of panels with 2024-T3 stiffeners are inferior compared to those of panels with 7075-T73 stiffeners.

6. REFERENCES

1. Vlieger, H., "BOND, a computer programme for the prediction of residual strength of cracked panels with bonded stiffeners", NLR report to be published shortly.

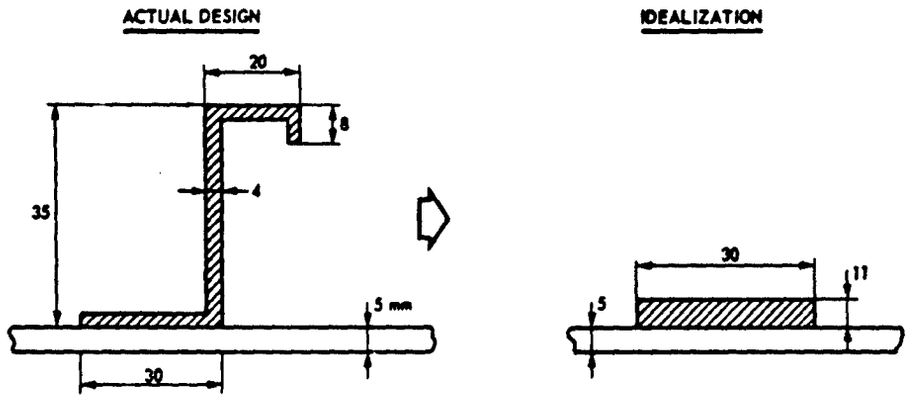

STIFFENER MATERIAL: 7075-T 73
SKIN MATERIAL: 2024-T 3
STIFFENER SPACING: 70 mm
BONDING MATERIAL: REDUX AND FM 123/5

FIGURE 1 STIFFENED PANEL CONFIGURATION. DIMENSIONS IN mm

SHEET THICKNESS: 5 mm
SHEET MATERIAL: 2024-T 3
STIFFENER MATERIAL: 7075-T 73 OR 2024-T 3
STIFFENING RATIO: 0.5
STIFFENER SPACING: 70 mm

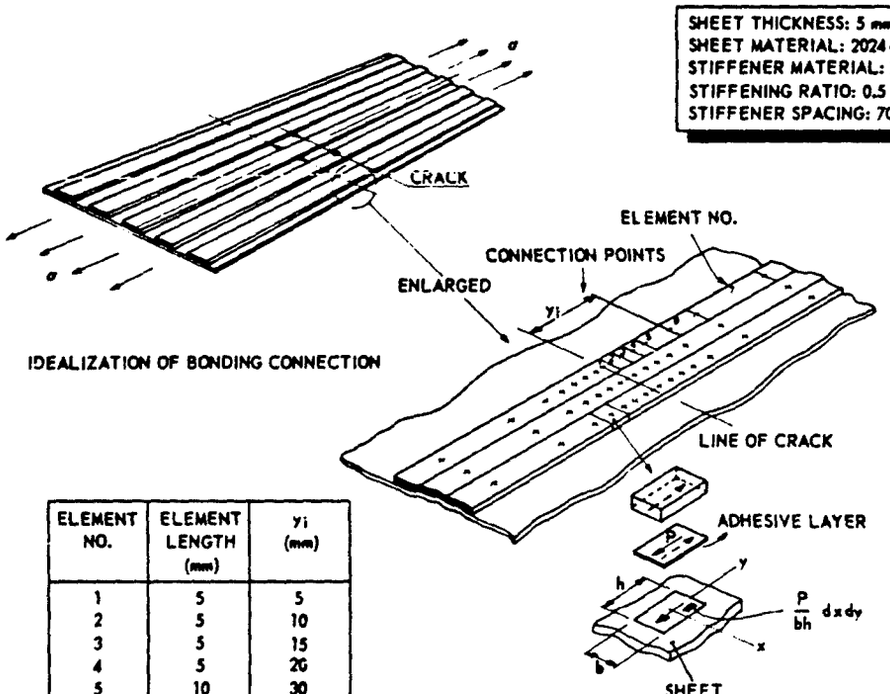

ELEMENT NO.	ELEMENT LENGTH (mm)	yi (mm)
1	5	5
2	5	10
3	5	15
4	5	20
5	10	30
6	10	40
7	20	60
8	40	100
9	85	185

FIGURE 2 STIFFENER AND BONDING LAYER IDEALIZATION

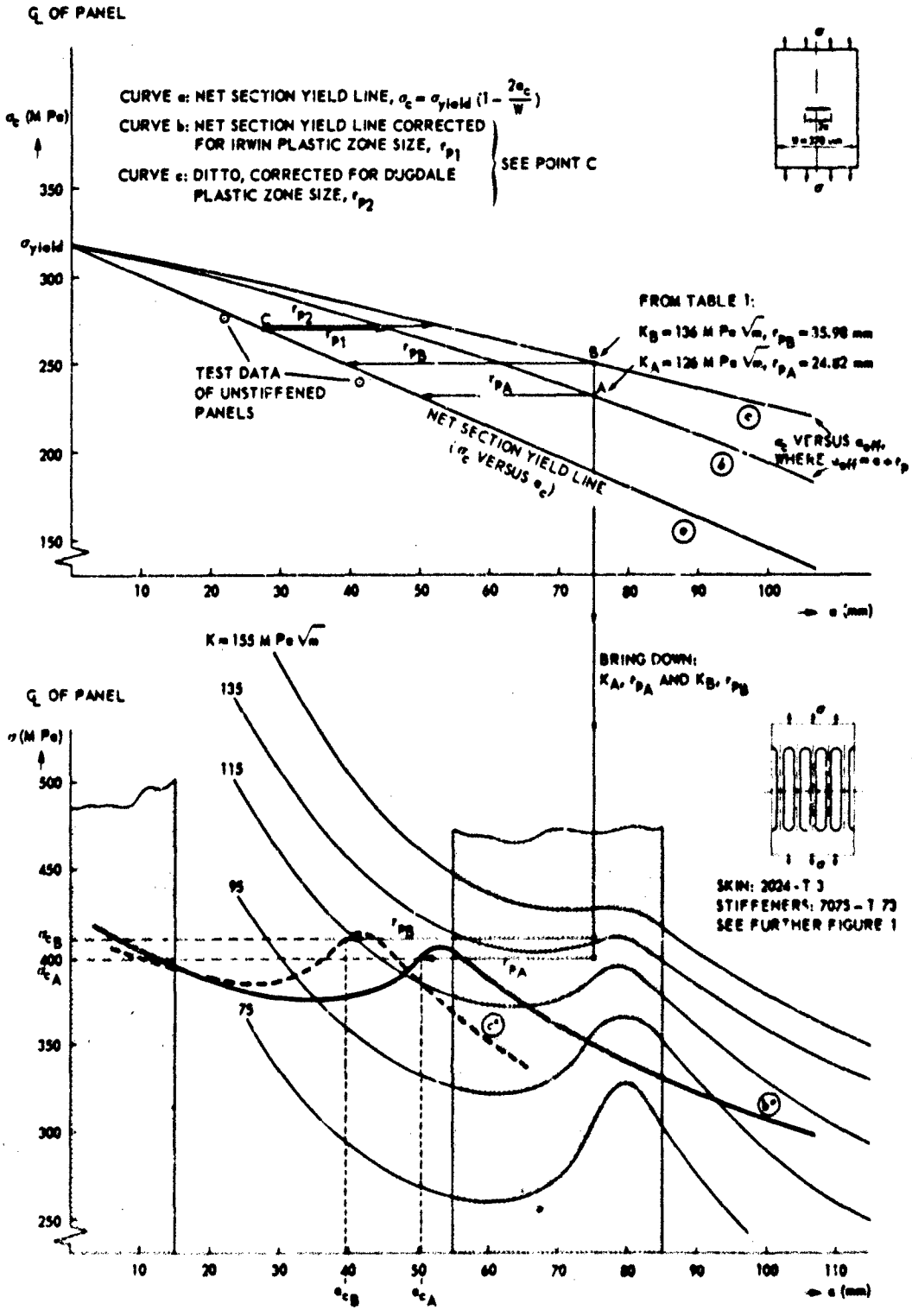

FIGURE 5 CALCULATION PROCEDURE OF STIFFENED-SHEET CURVES (CURVES b* AND c*) FROM UNSTIFFENED PANEL DATA (SEE ALSO TABLE 1) FOR A PANEL WITH 5 INTACT STRIP STIFFENERS

	Irwin plastic zone correction				Dugdale plastic zone correction			
a_{eff} (mm)	from upper half of Fig.3 σ_c (MPa)	$K=\sigma_c\sqrt{\pi a_{eff}}\cdot\sqrt{\sec\frac{\pi a_{eff}}{W}}$ (MPa$\sqrt{m}$)	$r_p=\frac{1}{2\pi}\left(\frac{K}{\sigma_{yield}}\right)^2$ (mm)	$a_c=a_{eff}-r_p$ (mm)	from upper half of Fig.3 σ_c (MPa)	$K=\sigma_c\sqrt{\pi a_{eff}}\cdot\sqrt{\sec\frac{\pi a_{eff}}{W}}$ (MPa$\sqrt{m}$)	$r_p=\frac{\pi}{8}\left(\frac{K}{\sigma_{yield}}\right)^2$ (mm)	$a_c=a_{eff}-r_p$ (mm)
30	288	90	12.71	17.29	295	92	16.45	13.55
55	258	114	20.27	34.73	271	119	27.59	27.41
65	246	120	22.83	42.17	261	128	31.59	33.41
75	232	126	24.82	50.18	252	136	35.98	39.02
85	218	130	26.60	58.40	242	144	40.27	44.73
95	203	133	27.97	67.03	233	153	45.26	49.74
110	177	135	28.65	81.35	218	166	53.61	56.39

NOTE: σ_{yield} = 318 MPa (2024-T3)

W = 370 mm

TABLE 1 CALCULATED VALUES OF K AND r_p FOR TWO PLASTIC ZONE CORRECTIONS

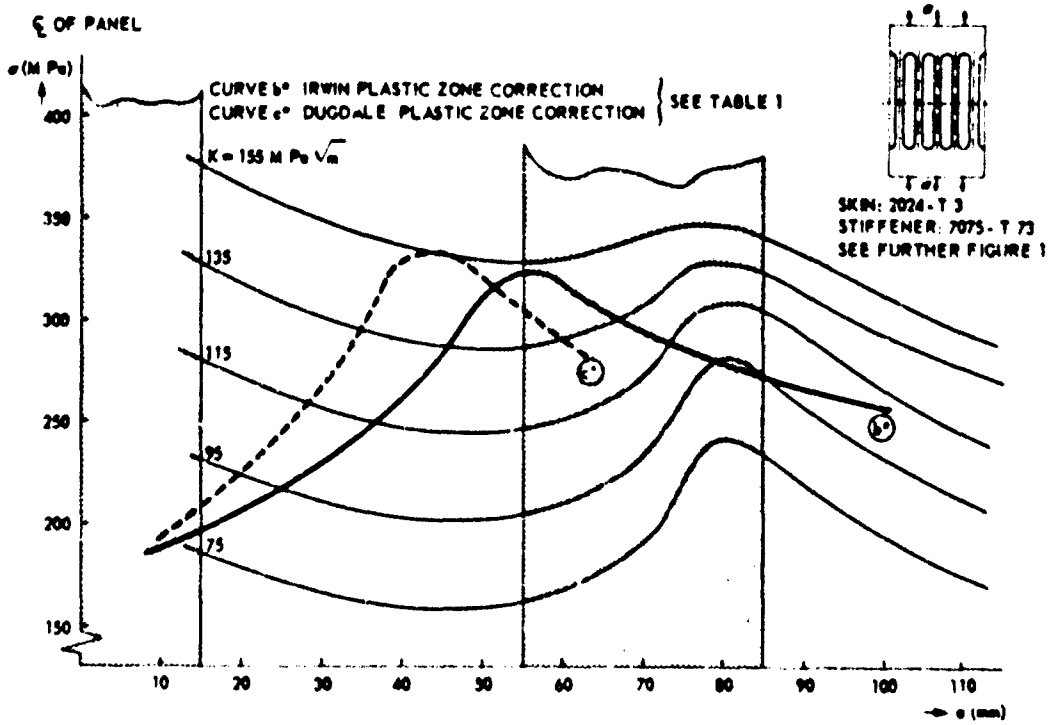

FIGURE 4 CALCULATION OF STIFFENED-SHEET CURVES (CURVES b° AND c°) FOR THE PANEL CONFIGURATION OF FIGURE 3 BUT NOW WITH A BROKEN CENTRAL STIFFENER (SEE ALSO TABLE 1)

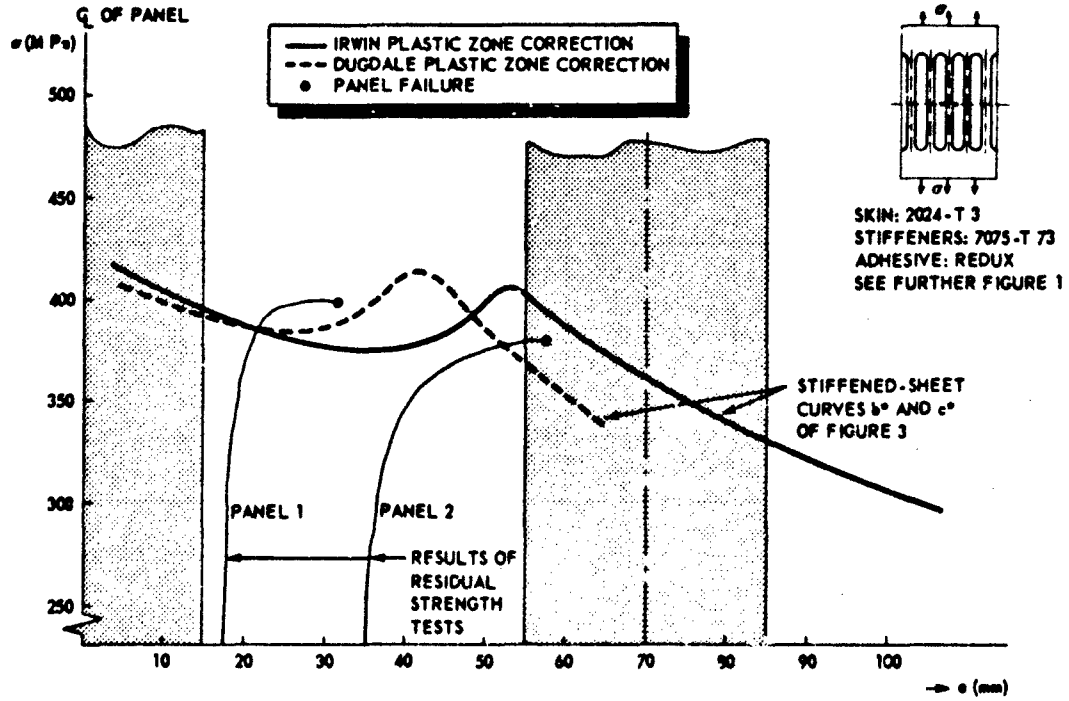

FIGURE 5 TEST-ANALYSIS CORRELATION FOR PANEL WITH INTACT STIFFENERS

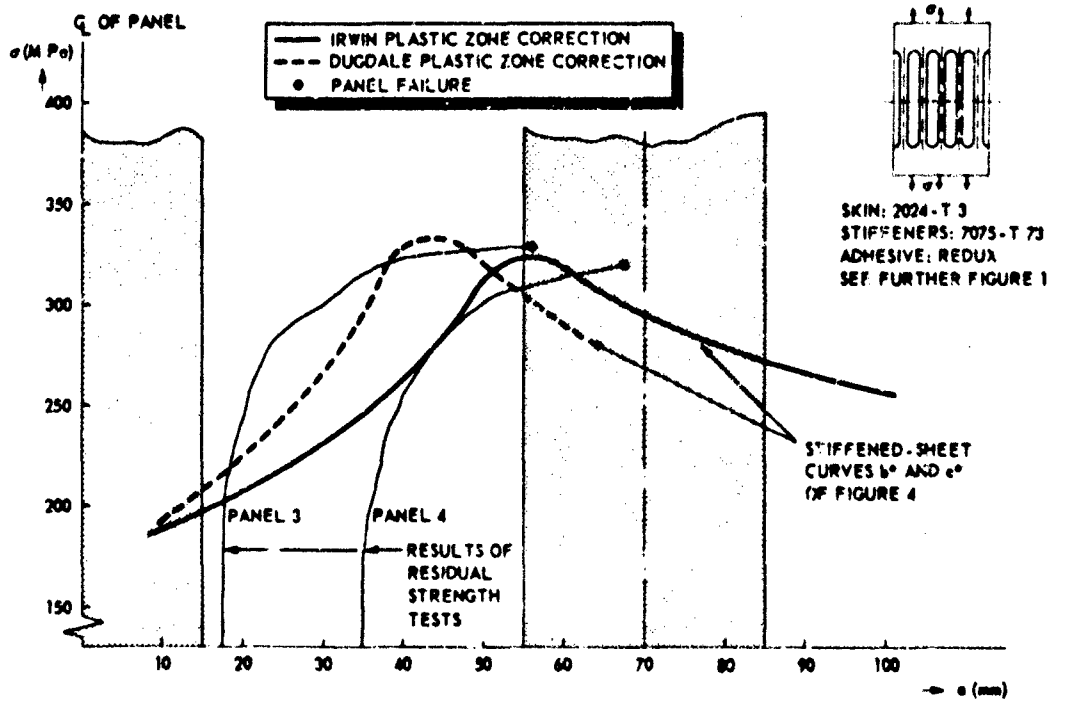

FIGURE 6 TEST-ANALYSIS CORRELATION FOR PANEL WITH BROKEN CENTRAL STIFFENER

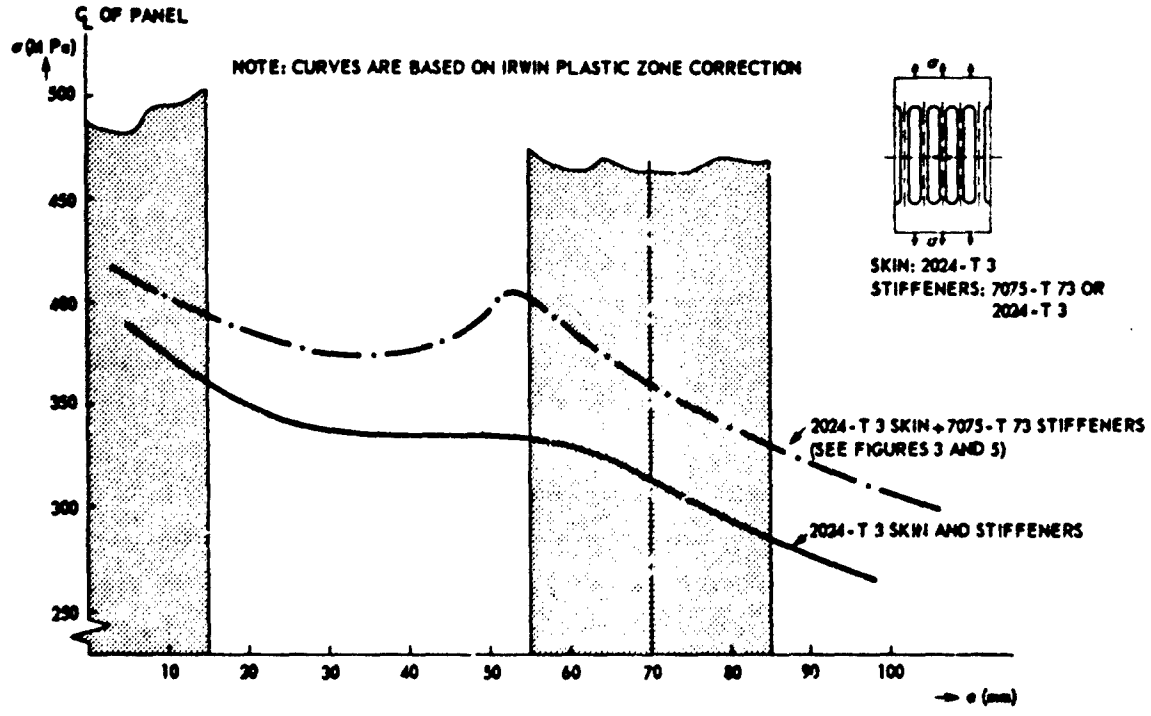

FIGURE 7 COMPARISON OF RESIDUAL STRENGTH OF PANELS WITH 2024-T 3 SKIN AND 2024-T 3 OR 7075-T 73 STIFFENERS. ALL STIFFENERS ARE INTACT

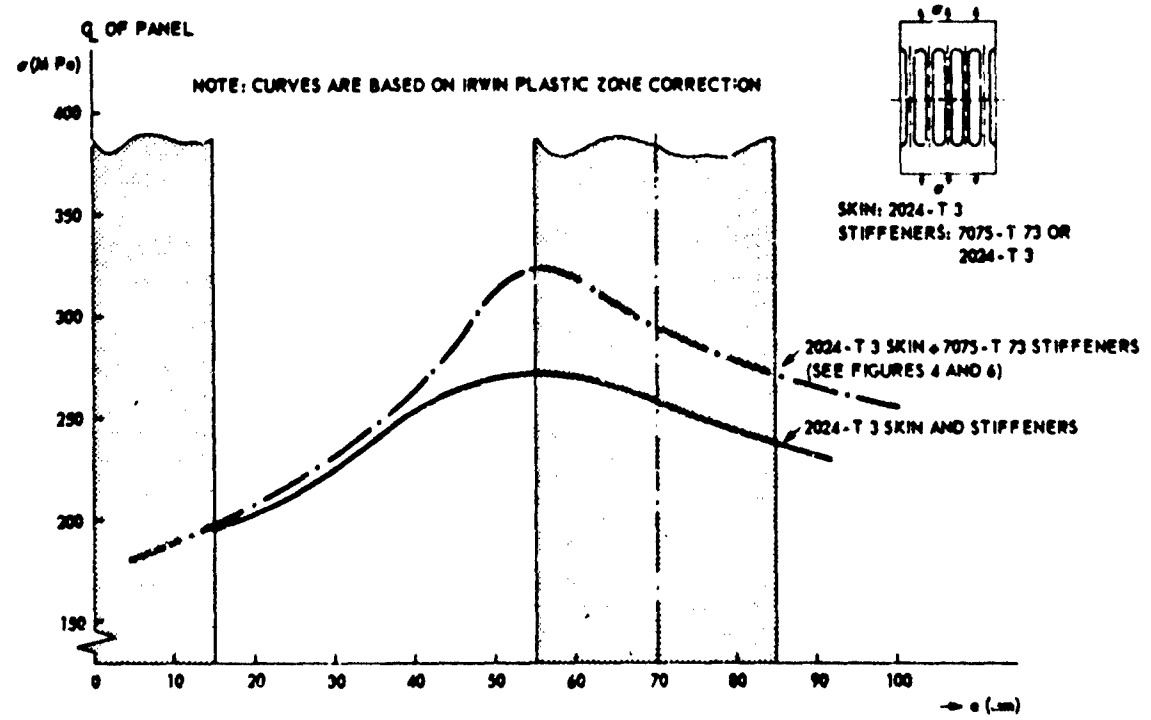

FIGURE 8 COMPARISON OF RESIDUAL STRENGTH OF PANELS WITH 2024-T 3 SKIN AND 2024-T 3 OR 7075-T73 STIFFENERS. CENTRAL STIFFENER IS BROKEN

EXAMPLE PROBLEM 3.3.3.7

RESIDUAL STRENGTH OF RIVETED PANELS WITH 7075-T6 OR 2024 SKINS AND 7075-T6 STIFFENERS

H. Vlieger

National Aerospace Laboratory NLR
Anthony Fokkerweg 2, 1059 CM Amsterdam
The Netherlands

1. STATEMENT OF THE PROBLEM

Residual strength calculations were carried out for centre-cracked panels with 2024-T3 or 7075-T6 skins of 2 mm thickness and provided with Z-stiffeners of 7075-T6. The stiffeners were riveted to the skin. More details about the structural configuration are given in Figure 1.
The panels contained skin cracks extending across the panel central stiffener. The cracks were symmetrical with regard to the stiffener rivet line and passed through rivet holes.
The residual strength calculations are compared with test data published earlier [1] .

2. METHOD OF ANALYSIS

The analysis applied is based on the stress intensity factor approach. The principles of this method as applied to stiffened panels are discussed in detail in sections 3.3.1.1 (b),(c) and (d) of this chapter. The panels with a 2024-T3 skin require a special treatment. This point is discussed comprehensively in section 2 of example problem 3.3.3.6.
The analysis requires the residual strength properties (σ_c versus a_c) of the unstiffened skin materials (2024-T3 and 7075-T6). These data can be found in Figure 7 of this chapter for a panel width of 300 mm. The 2024-T3 residual strength data are on the net section yield line (σ_{yield} = 357 MPa), while the 7075-T6 data are on a K_c = 67 MPa $\sqrt{m}$ curve.
To allow an elastic analysis for the 2024-T3 material (see section 3.3.1.1(d) of this chapter), a relation between σ_c and a_{eff} (= a_c + r_p, where r_p is a plastic zone correction) was determined using the Irwin and Dugdale plastic zone corrections. From these relationships values of K and r_p were determined. The results are presented in Table 1. The required K = const. curves in a stress versus crack length plot were found by using the analytical computer programme ARREST [2] , which enables the computation of the sheet-stiffener interaction coefficients C and L as functions of stress and crack length for panels with riveted stiffeners, taking into account the yielding of rivets and stiffeners. From the stress intensity correction factors, C, curves of K = const. in a stress versus crack length plot were determined. A set of these curves is plotted in Figure 2. Using these curves together with the K and r_p values presented in Table 1, the stiffened-sheet curves of the 2024-T3 skin can be found (see section 2.2 of example problem 3.3.3.6). These curves are plotted in Figures 2 and 3 of the present example (labelled ⓐ and ⓑ).
The stiffened-sheet curve of 7075-T6 can be found directly because for this material K is not a function of crack length (at least not for a certain range of crack lengths, see section 3.3.1.1(a) of this chapter). The stiffened-sheet curve of 7075-T6, i.e. K = 67 MPa $\sqrt{m}$ (= K_c of unstiffened 7075-T6 material), is plotted in Figure 4.
From the load concentration factors, L, the stiffener failure curves were determined assuming that failure occurs when the maximum stiffener strain attains the failure strain of the stiffener material. The stiffener failure curves of the 7075-T6 stiffeners are also plotted in Figures 3 and 4.
The calculations showed that for stress-crack length combinations corresponding with the region under the stiffener failure curves none of the rivets reached the maximum allowable rivet load. This means that with respect to residual strength prediction the possibility of rivet failure can be ruled out for these configurations.

3. TEST-ANALYSIS CORRELATION

The residual strengths for the panels with 2024-T3 and 7075-T6 skin are given in Figures 3 and 4 respectively. Also given in these figures are residual strength test data for panels of the same configuration [1] . For those panels that showed unstable crack growth followed by crack arrest the crack-tips were arrested in rivet holes of the adjacent stiffeners. With increasing external load the crack tips remained in the rivet holes until final panel failure. For this reason a vertical line has been drawn at a half crack length equal to the stiffener pitch plus half the rivet diameter. The intersection of this vertical line with the central stiffener failure curve (point B in Figures 3 and 4) was taken as the predicted panel failure stress. In other words, it was assumed that the arrested crack tips would remain in the rivet holes until failure of the central stiffener led to total panel failure. Without this assumption any point on the vertical line between A and B (see Figures 3 and 4) could have been taken as the panel failure stress, because (1) crack re-initiation from the rivet holes would immediately lead to panel failure (see shape of stiffened-sheet curve for crack lengths larger than s + $\frac{1}{2}$ d) and (2) a criterion for crack re-initiation after crack arrest is not available. The assumption that the panels were stiffener-critical is justified by the fact that all panels that showed crack arrest failed at approximately the same stress level, irrespective of the choice of skin material.
Comparing the analytical results with the test data, it can be concluded that the failure stresses were predicted within 5 % accuracy for both panel configurations. Because the investigated panel configurations appeared to be stiffener-critical, this result does not give an estimate of the accuracy of the predicted stiffened-sheet curves. However, considering the stresses and crack lengths at which unstable crack growth occurred (see Figures 3 and 4) it can be concluded that the observed instability points are all fairly close to the calculated curves.

4. CONCLUSIONS

(1) The residual strength of panels with a 7075-T6 or 2024-T3 skin and provided with riveted stiffeners can be predicted with sufficient accuracy using the stress intensity factor approach (see section 3.3.1.1 of this chapter).

(ii) The stress levels at which unstable crack growth in 7075-T6 and 2024-T3 skins occurs are predicted fairly well with the same approach.

5. REFERENCES

1. Vlieger, H., "Residual strength data of riveted panels with different stiffener configurations", NLR report TR 76033 U (1976).
2. Vlieger, H., Sanderse, A., "User's Manual of ARREST, a computer routine for prediction of residual strength of cracked stiffened panels", NLR report TR 75129 U (1975). Issue 2 of this report is being prepared.

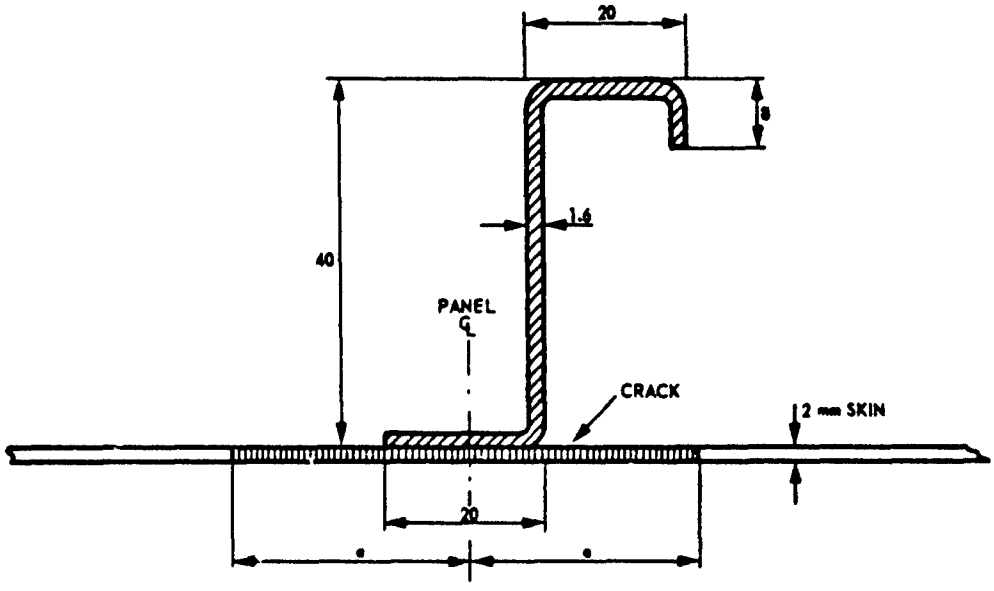

SKIN MATERIAL: 2024-T 3 OR 7075-T 6 (SEE FIGURE 7 OF THIS CHAPTER FOR RESIDUAL STRENGTH PROPERTIES)
STIFFENER MATERIAL: 7075-T 6 (σ_{yield} = 465 M Pa, σ_{ult} = 535 M Pa)
STIFFENER SPACING: 60 mm
RIVETS: d = 4.8 mm, PROTRUDING HEAD
RIVETS SPACING: 20 mm
PANEL WIDTH: 300 mm

FIGURE 1 STIFFENED PANEL CONFIGURATION. DIMENSIONS IN mm

	Irwin plastic zone correction				Dugdale plastic zone correction			
a_{eff} (mm)	σ_c (MPa)	$K=\sigma_c\sqrt{\pi a_{eff}}\cdot\sqrt{\sec\frac{\pi a_{eff}}{W}}$ (MPa $\sqrt{m}$)	$r_p=\frac{1}{2\pi}\left(\frac{K}{\sigma_{yield}}\right)^2$ (mm)	$a_c=a_{eff}+r_p$ (mm)	σ_c (MPa)	$K=\sigma_c\sqrt{\pi a_{eff}}\cdot\sqrt{\sec\frac{\pi a_{eff}}{W}}$ (MPa $\sqrt{m}$)	$r_p=\frac{\pi}{16}\left(\frac{K}{\sigma_{yield}}\right)^2$ (mm)	$a_c=a_{eff}+r_p$ (mm)
30	315	99	12.27	17.73	323	102	15.87	14.13
45	289	115	16.54	28.46	302	120	22.28	22.72
57.5	267	125	19.50	38.00	285	133	27.42	30.08
62.4	258	128	20.51	41.89	279	139	29.59	32.81
67.5	248	131	21.41	46.09	272	144	31.77	35.72
70	243	132	21.81	48.19	269	146	32.85	37.15
85	212	138	23.80	61.20	248	162	40.19	44.81

NOTE: σ_{yield} = 357 MPa, W = 300 mm

TABLE 1 CALCULATED VALUES OF K AND r_p FOR 2024-T 3 SKIN MATERIAL FOR TWO PLASTIC ZONE CORRECTIONS

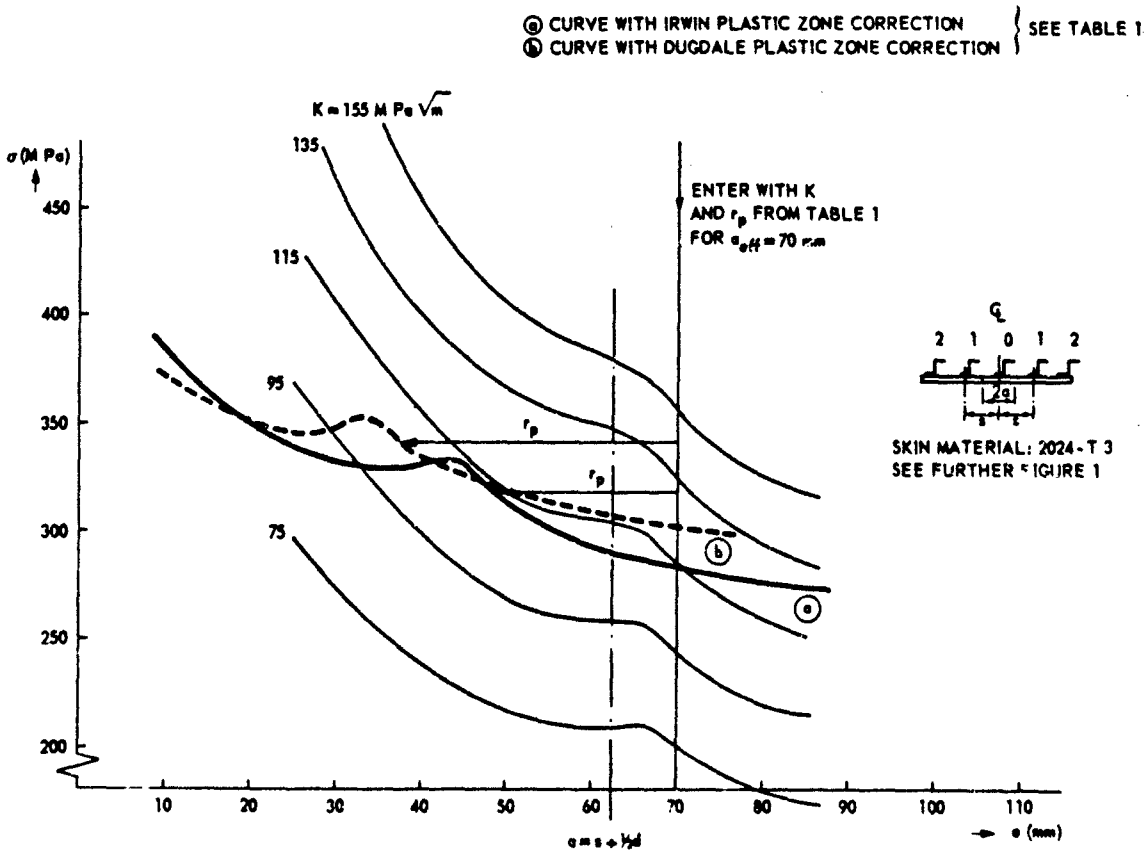

FIGURE 2 CALCULATION OF STIFFENED-SHEET CURVES (CURVES a AND b) FROM UNSTIFFENED PANEL DATA (SEE TABLE 1)

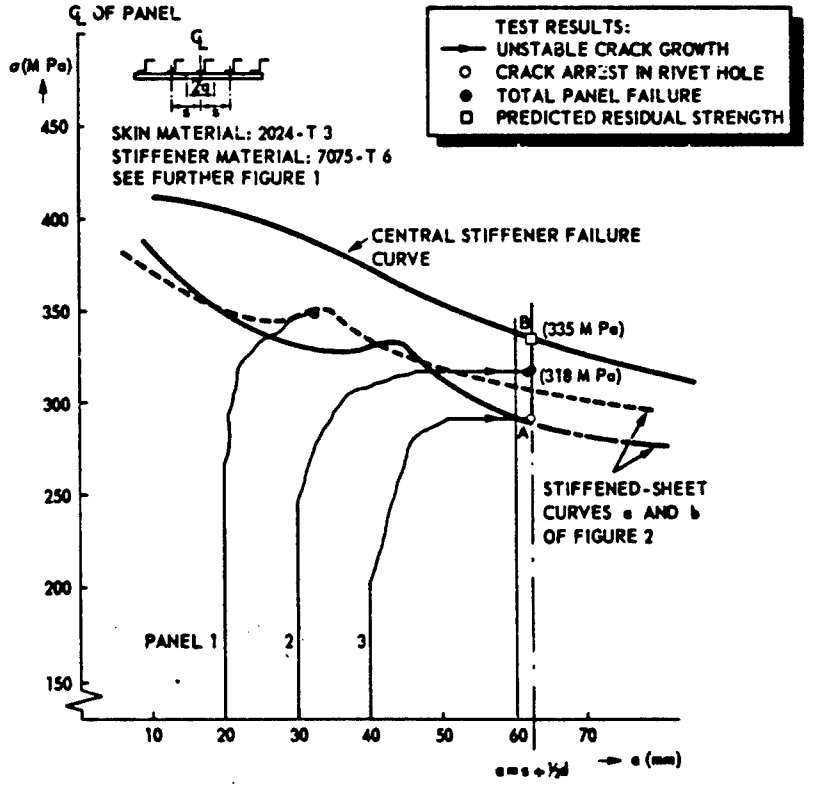

FIGURE 3 RESIDUAL STRENGTH DIAGRAM OF PANELS WITH 2024-T 3 SKIN AND 7075-T 6 STIFFENERS

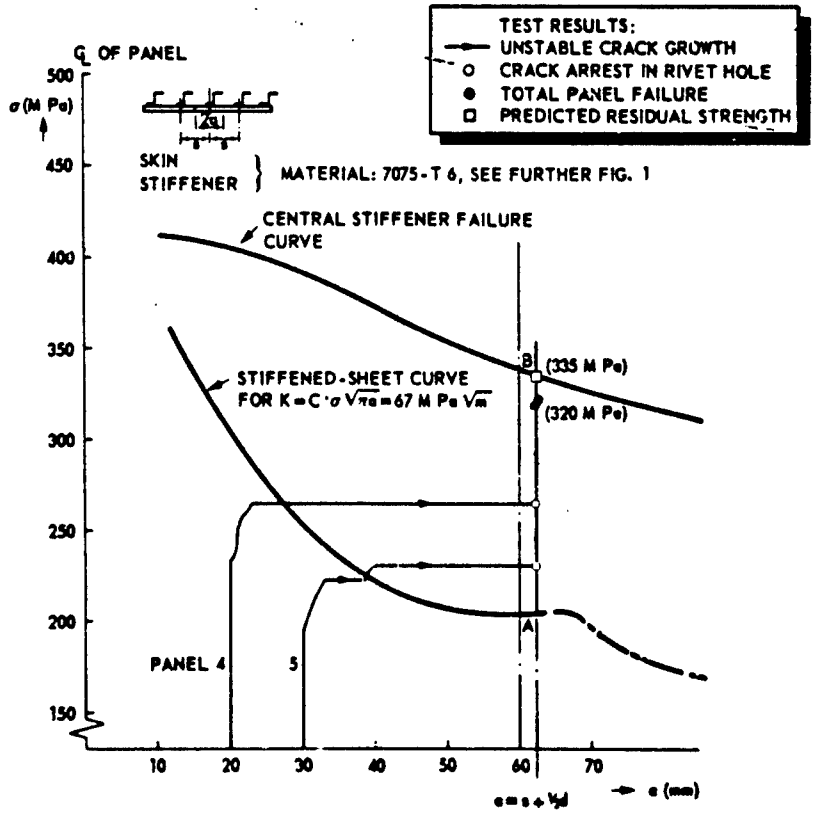

FIGURE 4 RESIDUAL STRENGTH DIAGRAM OF PANELS WITH 7075-T 6 SKIN AND STIFFENERS

3.4 FATIGUE CRACK PROPAGATION (D. BROEK)

3.4.1 Fatigue crack propagation in built-up skin-stringer structures

3.4.1.1 Introduction

As in the case of all structures and components, the damage tolerance analysis of skin-stringer combinations consists of three parts, viz. (1) the stress-intensity analysis, (2) the residual strength analysis, and (3) the crack-growth analysis. The unique residual strength characteristics of skin-stringer combinations are the justification for devoting an entire chapter of this handbook to this type of structure. By the same token, the larger part of Chapter 3 is devoted to the analysis of these unique residual strength properties and to the derivation of the stress intensity. Fatigue-crack growth behaviour of skin-stringer combinations lacks this uniqueness and can be dealt with in relatively short space. Some of the difficulties encountered in crack-growth analysis of built-up structures are associated with the presence of holes. These difficulties are reviewed in the chapter on fastened joints (Chapter 4); they will not be discussed here.
After determination of the stress intensity as a function of crack size, fatigue-crack-growth analysis is performed by a numerical integration of da/dN-ΔK data. The problems germane to this integration, such as retardation, integration routines, data variability, and crack-tip similitude requirements, will not be discussed here, because they are not different to crack-growth analysis of any other type of structure. Remaining problems are generally associated with damage development assumption. These will be the subject of this section.

3.4.1.2 The crack propagation curve

In previous sections, it was shown that the stress intensity is strongly affected by nearby broken or intact stringers. Clearly, this will be reflected in the crack-propagation curve as is illustrated in Figure 16. Complete arrest of a fatigue crack at a stringer should not be anticipated. A fast running crack can be arrested there if the stress intensity drops below the critical value. This is a go-no-go situation, which does not exist in fatigue. If the crack approaches an intact stringer, the stress intensity decreases which merely results in a deceleration of fatigue-crack growth (Figure 16b). Of course, this will automatically follow from the crack-growth integration and it presents no particular difficulty.
Naturally, in the case of decreasing stress intensity some retardation may occur. The decrease in stress intensity is slow, however, and retardation will likely be negligible. Moreover, if a retardation model is used during integration any retardation resulting from the stress intensity decrease will be automatically accounted for.
In the case of a broken stringer, the stress intensity will be increased and a higher crack-growth rate will result (Figure 16c).
It was shown in the foregoing sections that a proper residual strength analysis requires that fastener plasticity and stringer plasticity have to be accounted for in the calculation of the stress intensity. Usually, fatigue-crack propagation will take place at stresses substantially below the residual strength level. Consequently, these plasticity effects play only a minor role and the stress intensity for the crack-growth analysis can be determined from simple elastic K-analysis. One complication arises here. During some of the higher fatigue loads in the spectrum some plasticity may occur in the high load-transfer fasteners. This means that load transfer during subsequent cycling may be shifted somewhat to more remote fasteners, which may increase the stress-intensity factor. Hence, the stress-intensity factor becomes history dependent. Since it is not known in advance when these higher loads occur in actual service, it is difficult to account for this effect. The consequence is that crack-growth predictions that ignore this effect will tend to be unconservative.
When a crack reaches a stringer, it may run into a fastener hole. In the chapter on joints, it is shown that cracks running into holes in general do not show a longer crack growth life, because the reinitiation period is offset by increased growth rates when the crack approaches the hole and by the increased damage size due to the hole. Experimental data supporting this are provided in Reference [174] and an example is shown in Figure 17. Therefore, it seems prudent not to count on any beneficial effects. In this respect, the USAF airplane damage tolerance requirements of MIL-A-83444 can be considered realistic in that they assume continuing damage at the other side of the hole.

3.4.1.3 Damage development assumptions

The most obvious, and also most dangerous damage assumption is that of continuous crack growth in the skin. It is very likely that an undetected service crack will show discontinuous growth at some point close to the minimum in the skin-crack propagation curve. This is illustrated in Figure 18. Although the residual strength of the stiffened skin is generally as high as limit load, unstable crack growth can occur at much lower loads. When the crack remains undetected until a size at which the minimum in the skin crack propagation curve is reached, unstable crack growth can occur at loads encountered quite often during normal operation. Of course, arrest will occur (A to B in upper half of Figure 18), but at the expense of a much shorter crack growth life.
It cannot be anticipated whether instabilities will occur; or what the magnitude of these instabilities would be (C-D would be more serious, but less likely because of the higher required load, than A-B). Obviously, dangerously unconservative crack growth lives are obtained if continuous crack growth is assumed. Note that the absence of instabilities in a full-scale flight-by-flight test is no guarantee that they will not occur in service, since they depend upon the load history and upon whether high loads occur at smaller or larger damage sizes.
More complex damage development assumptions may be necessary at a crack initiating at a stringer. No general rules can be given here, but the problem may be illustrated by a particular example shown in Figure 19. The problem is one of cracking of a frame, frame tie clip, crack arrester strip, and skin. The cracking sequence is not known in advance, nor is it known what the initiation times in the other components will be, once the first component cracks. Therefore, it seems prudent to conduct the analysis with assumed initial damage in the uncracked components. Formally, it would then be possible to calculate how stress-intensity factors vary in the relevant components and to assess the development of the damage.
Obviously, any assumption on damage development in a complex case as in Figure 19 is arbitrary. It might be necessary to analyze which assumptions would lead to the shortest crack-growth life. Since this would

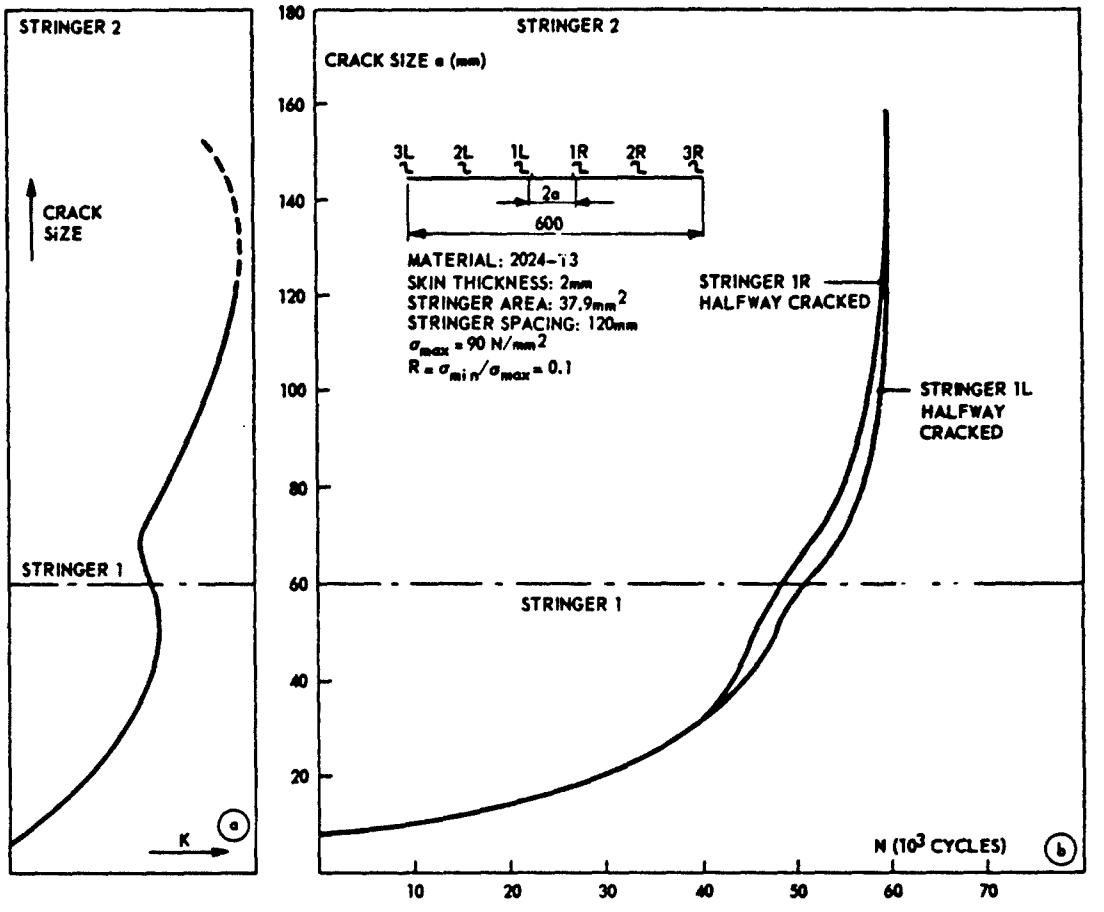

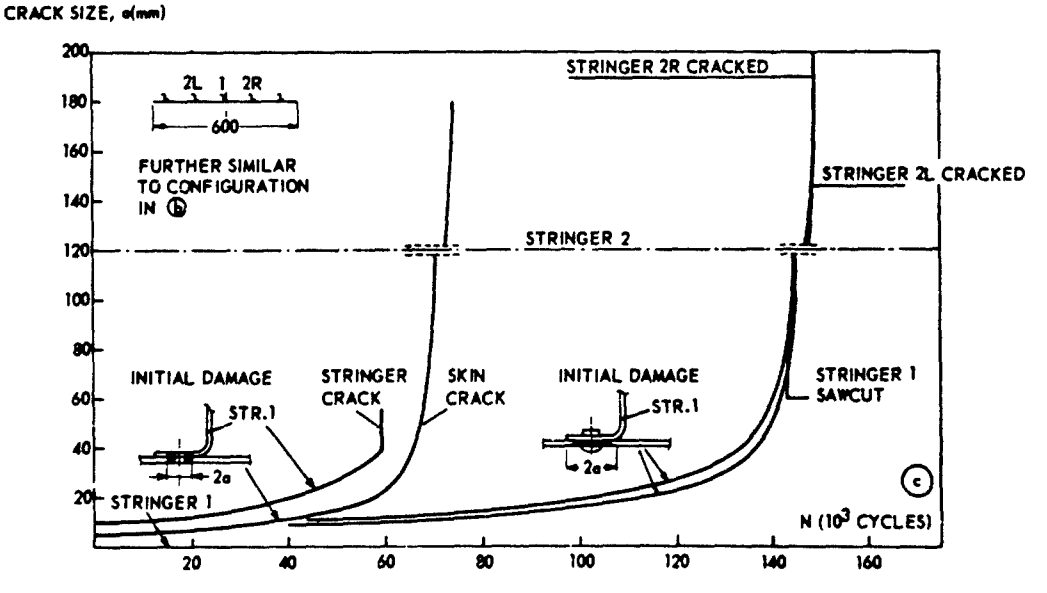

FIGURE 16 CRACK GROWTH IN STIFFENED PANELS (a) STRESS INTENSITY (SCHEMATIC); (b) CRACK BETWEEN STRINGER; (c) CRACK ACROSS STRINGER. (TEST DATA FROM REFERENCE [74])

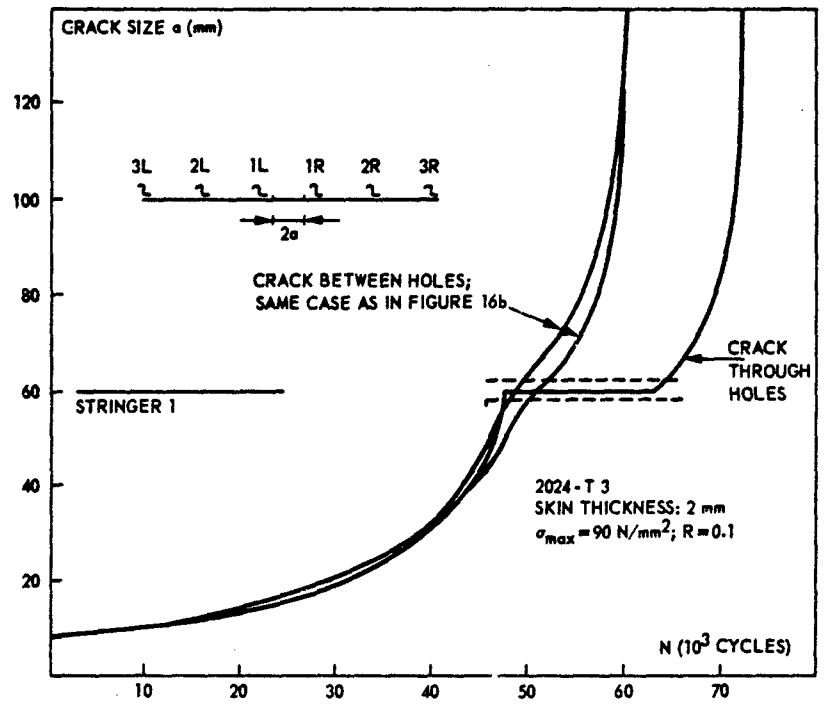

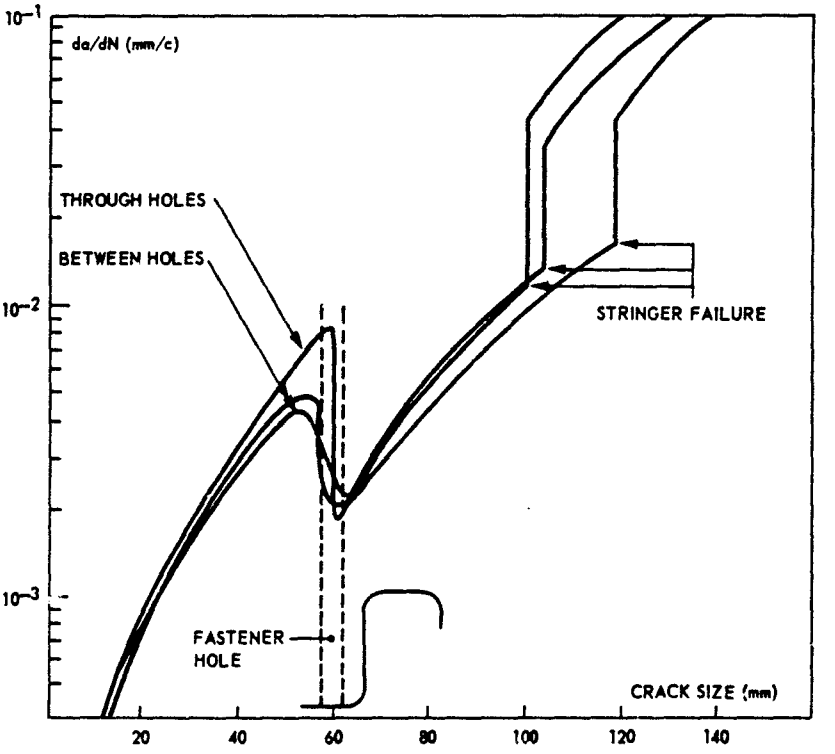

FIGURE 17 CRACK GROWTH THROUGH AND BETWEEN RIVET HOLES – (a) CRACK-GROWTH CURVES; (b) CRACK-GROWTH RATES. (DATA FROM REFERENCE [174])

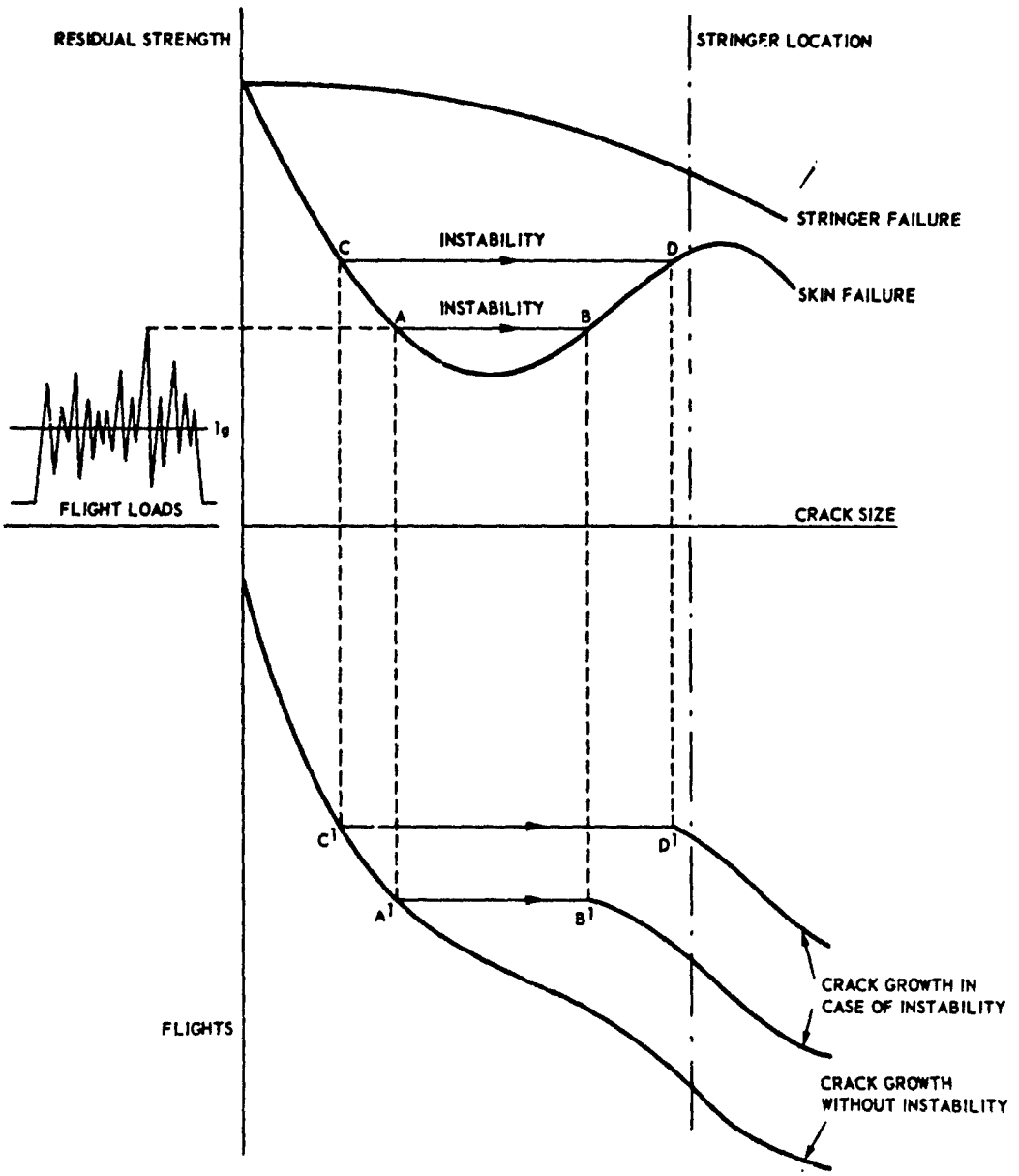

FIGURE 18 EFFECT OF INSTABILITY ON CRACK-GROWTH LIFE

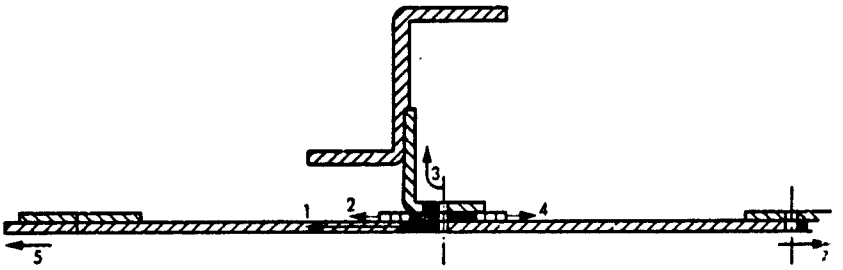

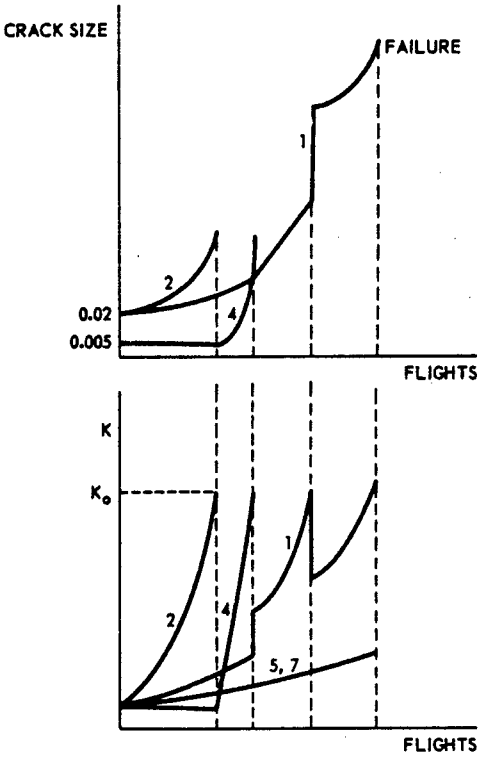

FIGURE 19 EXAMPLE OF DAMAGE DEVELOPMENT ASSUMPTIONS

be a monumental task, it is more practical to rely on damage development observed in the full scale or component tests and on engineering judgement.
An attempt has been made to illustrate the complexity of crack-growth analysis in skin-stringer combinations. The conclusion that can be drawn from these examples is that unconservative predictions are likely when too simple assumptions are made. Some interesting results of tests with different damage development are given in Reference [182] .

3.4.1.4 Integral Panels

Crack growth in integrally stiffened panels is somewhat easier to deal with. Also in this case, damage development assumptions are the major problem. A crack in the skin is usually assumed to be semi-circular, as a matter of convenience. Clearly, elliptical cracks with high aspect ratio would exhibit considerably faster growth.
The main damage development problem is encountered when considering cracks at the fasteners of the longitudinal splices between planks. This problem, however, is no different from that encountered in built-up structures. No general rules can be given and the analysis has to be based on natural damage development observed in tests and upon sound engineering judgement.

3.4.2 Application of fracture mechanics principles to real structures

(a) Information available from literature (see section 3.5)

In the literature a large number of examples can be found which illustrate the application of fracture mechanics principles to crack propagation predictions for real structures. These applications either deal with actual designs or are more general in nature. Applications to case studies are also available.
Without intending to give the impression of completeness, a list of relevant references is given here:

(a.1) Applications to actual designs or projects

Anderson, Chu, Malluck	[172]
Anon.	[174-176]
Barrois	[164]
Casalegno	[170]
Conley, Sayer	[169]
Crichlow, Wells	[119]
Ekvall, Brussat, Liu, Creager	[145]
Gökgöl	[171]
Heath, Nicholls, Kirkby	[147]
Hedrick, Wehle, Bell	[161]
Impellizzeri	[160]
Kaplan, Reiman	[167]
Lalli, Sergio	[158]
Lehmann	[162]
McHenry, Hensley	[163]
Murnane, Stronge, Davenport	[166]
Nelson, Melcon, Simons	[159]
Sanga	[144]
Stone, Swift	[68]
Swift	[39,65,67]
Thrali	[156]
Troughton, McStay	[157]
Toor	[85]
Various authors	[168]
Wood	[165]

(a.2) General studies

Anderson, Chu, McGee	[178]
Cartwright, Dowrick	[41]
Heller, Liu, Swift	[177]
Hunt, Denke, Eide	[150]
Poe	[46]
Salvetti et al.	[32-38]
Schwarmann	[82,83]
Schwarmann, Bauer	[154,179]
Smith, Porter, Engstrom	[153]
Sorensen	[148]
Ratwani	[61,62]
Vlieger	[75,77,79]
Wang	[152]

(a.3) Case studies and textbooks

Rich, Cartwright (Editors)	[155]
Broek	[1]
Rolfe, Barsom	[181]
Wilhem	[180]

(b) Practical examples

A number of investigators closely concerned with the application of fracture mechanics to actual designs were found willing to write up results of some of their recent crack propagation computations as examples in this handbook. These examples are presented in this section. They were left as much as possible in their original but edited form, to give full credit to the contributors. The way of presentation, the contents and the conclusions are the responsibility of the contributors. Each example is followed by some concise editorial comments.
It has to be noted that the examples must be considered as self-contained texts, i.e. they have their own numbering system of figures and references.

EXAMPLE PROBLEM 3.4.2.1

STIFFENED WING PANEL AT SPAR-PANEL JOINT

L. Casalegno
Aeritalia, Turin
Italy
(Literal)

1. STATEMENT OF THE PROBLEM

The wing panel considered (Figure 1) has integral stiffeners and is fastened to the U-shaped spar with Hi- loks. The material of both the panel and the spar is 2024-T351. Two quarter-circular corner flaws in a hole are considered, with an initial length of 2.5 mm.

2. STRESS INTENSITY

The stress intensity was derived on the basis of the solution by Poe [1] for a cracked sheet with riveted stringers. However, some important differences have to be taken into account, namely:

- The spar is riveted, the stringers are integral
- The stiffening ratio is different for the stringers to panel and for the spar to panel details
- The crack is not a central crack but tends to become an edge crack
- The crack starts as a corner crack, not a through crack.

In this particular example, however, it is found that the tip of the critical crack c_c is still close to the spar, so that the integral stringers play no role. Also, it is believed that considering the crack as a central crack in an infinite plate does not introduce a significant error. The spar area contributing to the stiffening was assumed to be the U-leg plus half the web area; the resulting stiffening ratio is $\mu = 0.33$. For this stiffening ratio Poe [1] gives the stress intensity as a function of the a/b (ratio between crack size and stringer spacing), and with p/b as a parameter (p/b is the ratio between rivet spacing and stringer spacing). The curve with $p/b = 1/6$ describes the reduction of the stress intensity factor due to the spar presence, relative to an unstiffened panel. It was assumed that a corner crack is equivalent to a through-crack by dividing its length by $\sqrt{2}$ (see [2]), i.e.

$$(a_{Th.c})_{eq.} = \frac{a_{c.c}}{\sqrt{2}}$$

In the range from $a_{c.c} = 2.5$ to 7 mm (the through the thickness range of the corner crack, see Fig.1), this results in $(\frac{c}{b})_{eq.} = 0.025$ to 0.048 (see Fig.1) and the spar effect is on the average a 3 percent reduction in K [1], which was conservatively ignored. The propagation of the corner crack to a through-the-thickness crack can then be studied as a corner crack in a hole in an unstiffened plate, using for example the Liu solution [2]. To study the propagation from 7 mm, the curve with $p/b = 1/6$ was approximated by steps with constant values of $\frac{K}{\sigma\sqrt{\pi a}}$ in $\frac{a}{b}$ intervals; these values were input to a crack propagation computer program for centre cracks in unstiffened plates with the same correction factors, i.e. $K = \alpha\,\sigma\sqrt{\pi a}$.

3. RESULTS

A critical crack length of $(2c_c)_{panel} > 140$ mm and a life greater than 450 blocks (Figure 2) was found for a panel stress $\sigma = 187$ Nmm^{-2} and $K_c = 2400$ Nmm$^{-1.5}$. However, the overload in the spar and in the fasteners due to the crack are also to be considered. The spar will fail when the stress reaches $\sigma_u = 398$ Nmm^2, (the material strength), so the maximum overload it can take is $L = 398/187 = 2.13$.
From Poe [1]: $(\frac{c}{b})_c = .68$, i.e. $c_c = .68 \times 140 = 95$ mm, and $(2c_c)_{stiff.} = 190$ mm. The criterion for the stiffener failure could be the yield strength instead of the tensile strength, because, for instance, of possible aerodynamic consequences of appreciable deformations. In this case, $L = \frac{290}{187} = 1.55$ and $(2c_c)_{stiff.} = 95$ mm.
The fastener's ($\phi = 5.0$ mm Hi-loks) strength is $P = 12800$ N, or, in terms of panel load, $\frac{P}{(bt)\sigma} = \frac{12800}{700 \times 187} = 0.10$. Assuming that this load has to be carried entirely by the rivet closest to the crack, this corresponds to $(\frac{c}{b})_c = 0.17$ [1], i.e. $(2c_c)_{fast.} = 47.6$ mm.
So the fasteners are the weakest item in the design. The critical crack length is then $2c_c = 47.6$ mm and the life (unretarded) to failure from an initial flaw of 2.5 mm is 350 blocks.

4. REFERENCES

1. Poe, C.C., "Stress intensity factor for a cracked sheet with riveted and uniformly spaced stringers", NASA TR R-358, May 1971.

2. Liu, A.F., "Stress intensity factor for a corner flaw", Engng. fract.mech., Vol.4 (1972), pp 175-179.

5. COMMENTARY

Practically everything discussed in Section 3.4.1 (Fatigue crack propagation in built-up skin-stringer structures) of this chapter can be considered as commentary on this example.

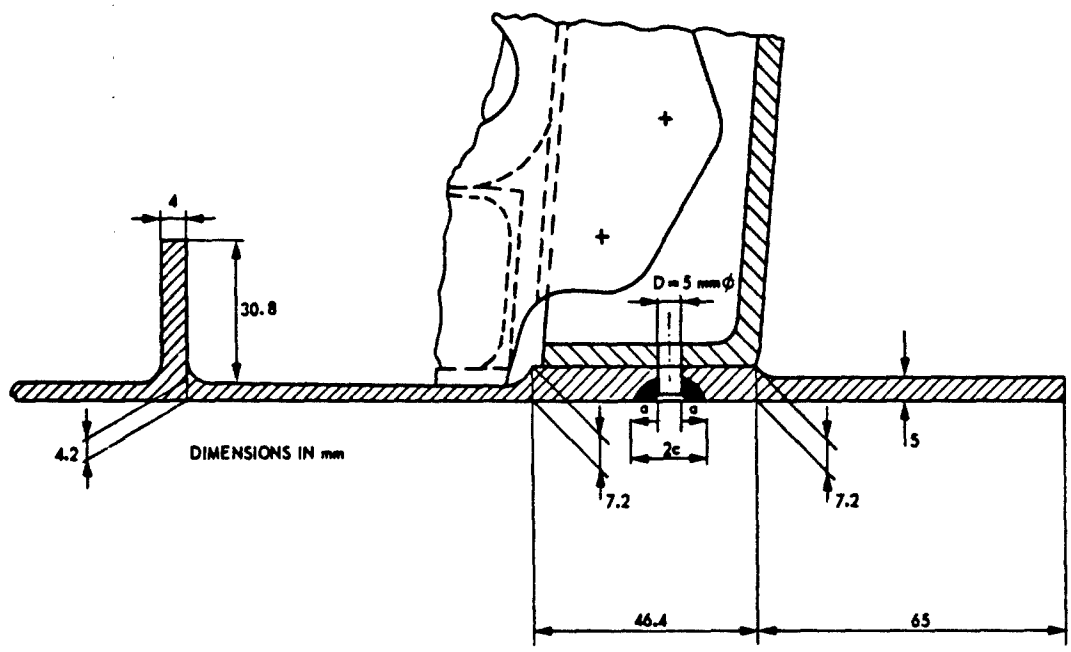

FIGURE 1 WING PANEL TO SPAR JOINT

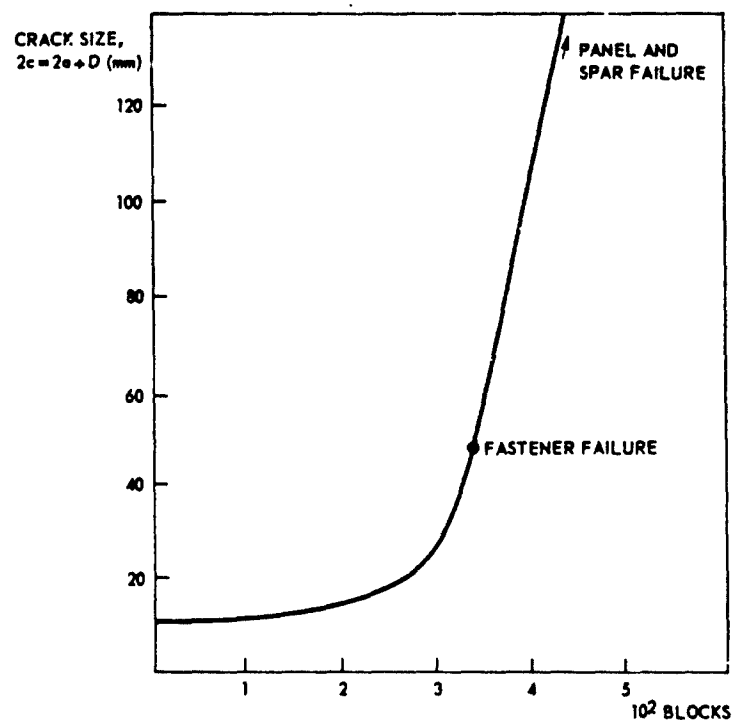

FIGURE 2 CRACK PROPAGATION IN PANEL AT A PANEL STRESS, $\sigma = 187$ MPa

EXAMPLE PROBLEM 3.4.2.2

CRACK PROPAGATION AND DECELERATION IN STIFFENED PANELS

J.N. Thomas
S.N.I. Aérospatiale
Toulouse
France
(Literal)

1. STATEMENT OF THE PROBLEM

The problem of crack propagation arises in the choice of design concepts of aircraft structures. It is a fundamental problem for stiffened panels, where it directly affects inspection frequencies and the means of crack detection used.
A comparative study has been made to measure the influence of integral or separate stiffeners and the contribution of fail-safe strips or reinforcements. The calculations were made using the finite-element method. Special crack tip elements directly provided the stress intensity factor. The crack propagation curve was calculated using the Forman equation associated with a Wheeler retardation model. The same constants were used in the Forman equation for all the comparative calculations, although in reality the thick plate (integral panel) and thin plate (separate stiffener panel) had slightly different propagation properties.
The panel material was AU2GN-T6 with a thickness of 2.2 mm in the pockets. The structure studied was a panel stiffened with nine stiffeners at a pitch of 133 mm (see Figure 1). In all cases the centre stiffener was assumed cracked, and the crack propagated on both sides of this stiffener.
The stiffener configurations studied are shown in Figure 2. In the case of separate stringers, the attachment can be considered to be either infinitely rigid or of finite stiffness to account for the fasteners. These two alternatives were both considered. In the case of rigid attachment, a point in the stiffener was rigidly coupled to a point in the skin in the finite element model. In the case of a flexible coupling, the two corresponding points were coupled by two sets of hinged bars, one set in the longitudinal, the other in the transverse direction.

2. RESULTS OF COMPUTATIONS

The results are shown in the following figures:

Figure 3 – Comparison of propagation for separate stringers if the crack propagates between, or through infinitely rigid attachments (arrest by the hole is not taken into account).

Figure 4 – Comparison of propagation for separate stiffeners if the crack propagates through either elastic or infinitely rigid attachments (arrest by the hole is not taken into account).

Figure 5 – Comparative study of an integrally stiffened panel under the same load spectrum.

A study was made of the effect of the introduction of titanium or AU4G1 fail-safe strips in the center of the pockets of the integral panels, in order to slow down crack propagation. These strips were 4.5 mm thick and 36 mm wide. The strips were connected to the sheet by means of adhesive bonding. The results obtained are shown in Figures 6 and 7.
In the case of heavily loaded areas, or for repair schemes, one could envisage the addition of reinforcing plates under which the crack would pass. Two types of reinforcements were considered, viz., a very thick local plate (to act as a crack stopper) or a thinner but larger plate (to slow down the crack propagation). In both cases, the reinforcement was riveted to the skin. This calculation exercise was made with:

- A 5.0 mm thick crack stopper fitted in the vicinity of the second stiffener (the centre stiffener was already cut).
- A 3.2 mm thick plate, joining five stiffeners (with the centre stiffener cut) to slow down the crack growth.

The various results are shown in Figures 8 and 9.

3. COMPARISON OF CALCULATIONS WITH TEST RESULTS

A comparison of calculations and test results was carried out for a 1.6 mm thick integrally machined panel. The geometric characteristics of the panel are shown in Figure 10. The panel was subjected to three different load spectra. The results of the comparisons are shown in Figure 11.

4. CONCLUSION

In general the integral stiffener is more effective in slowing down the crack than the separate stringer. For heavily loaded areas, the crack propagation can be limited by fail-safe strips or reinforcing plates. The results are very beneficial, but these schemes are impractical as they are heavy and costly.

5. COMMENTARY

This is an excellent example of the use of damage tolerance analysis to assess design alternatives. Unfortunately, many examples deal with the problem of inspection and operational safety. For such applications damage tolerance analysis is often discredited for its inaccuracy (since there is no other way to get the desired answers, the objections are somewhat naive). However, the greatest strength of damage tolerance analysis is not in such applications, but in trade-off studies during design as in the present example. Analytical trade-off studies for optimum damage tolerance are much more economical than component tests. With regard to skin-stringer combinations, the analytical tools developed by Vlieger and Swift provide an expeditious means for such trade-off studies.

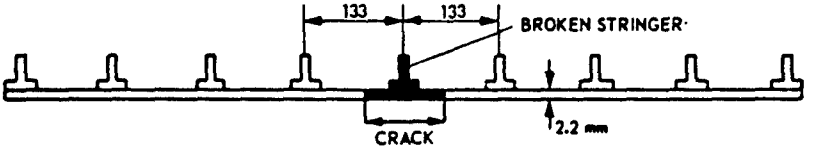

FIGURE 1 PANEL CONFIGURATION

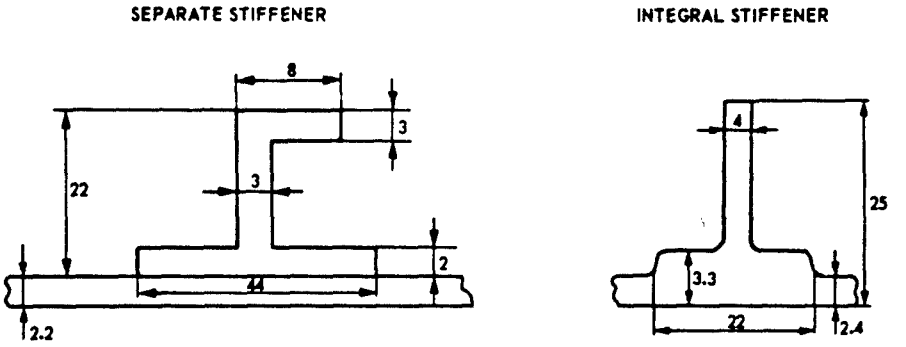

FIGURE 2 STIFFENER CONFIGURATION (DIMENSIONS IN mm)

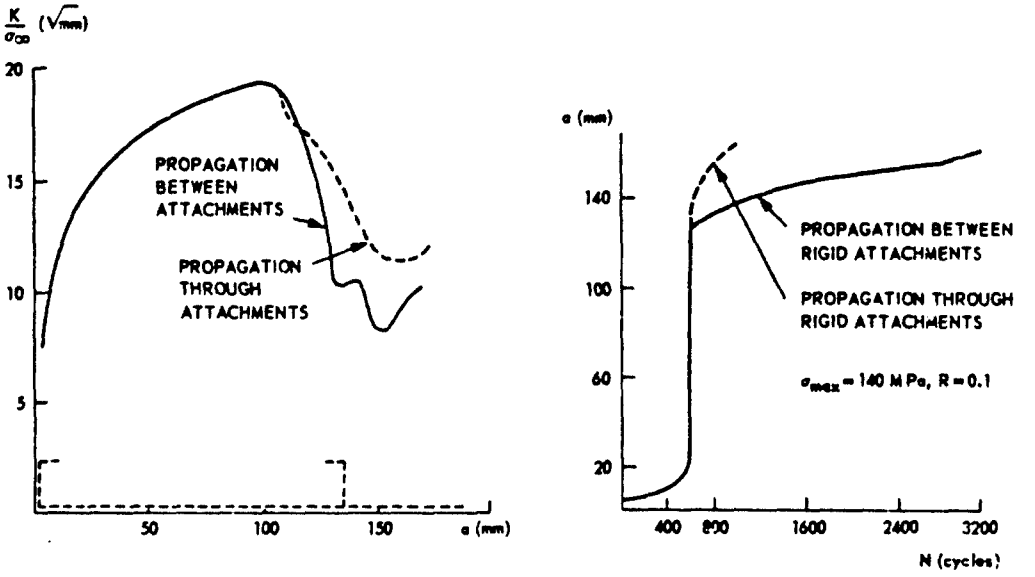

FIGURE 3 DIFFERENCE BETWEEN CRACK GROWTH THROUGH AND BETWEEN ATTACHMENTS FOR PANEL WITH SEPARATE STIFFENERS. LEFT STRESS INTENSITY, RIGHT CRACK GROWTH.

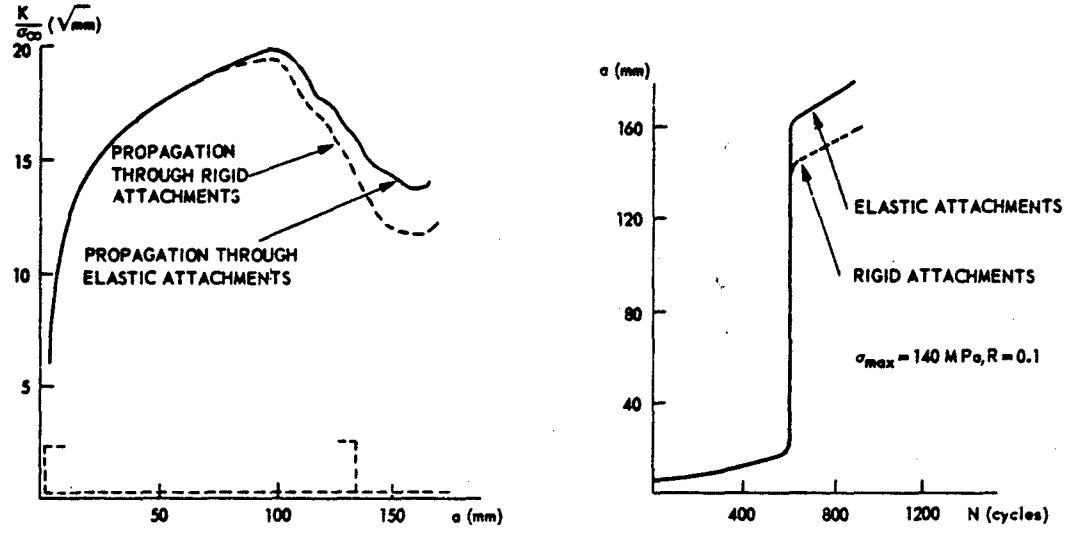

FIGURE 4 EFFECT OF ATTACHMENT STIFFNESS FOR PANEL WITH SEPARATE STIFFENERS
LEFT STRESS INTENSITY, RIGHT CRACK GROWTH

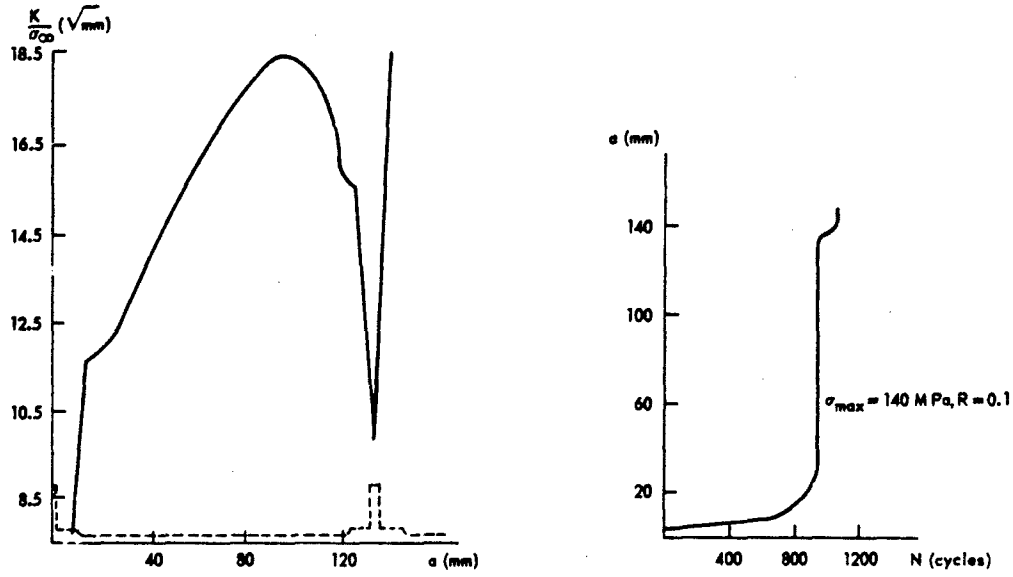

FIGURE 5 PANEL WITH INTEGRAL STIFFENERS. LEFT STRESS INTENSITY, RIGHT CRACK GROWTH.

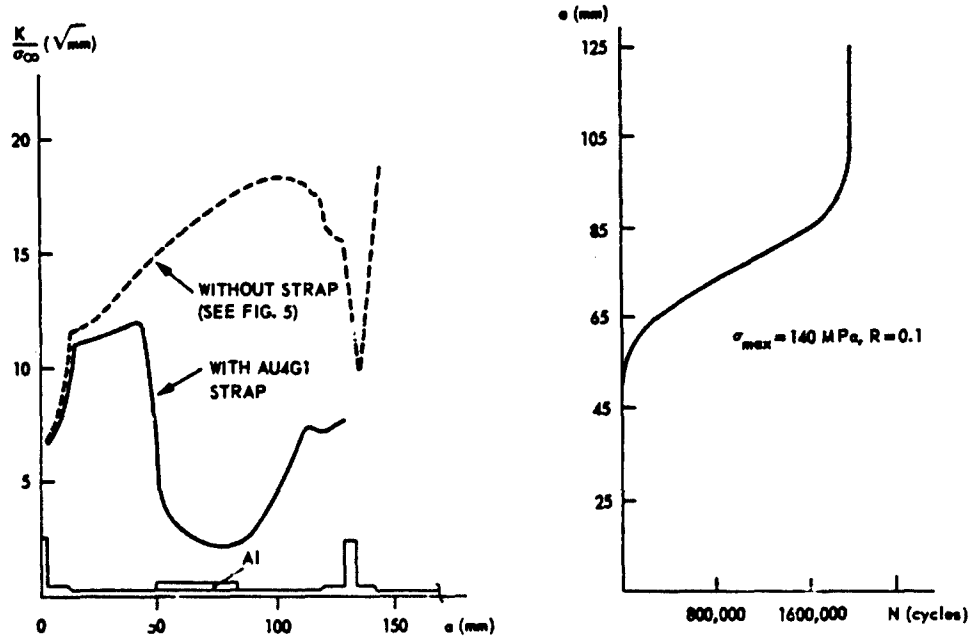

FIGURE 6 EFFECT OF ALUMINIUM CRACK STOPPER STRAP. LEFT STRESS INTENSITY, RIGHT CRACK GROWTH

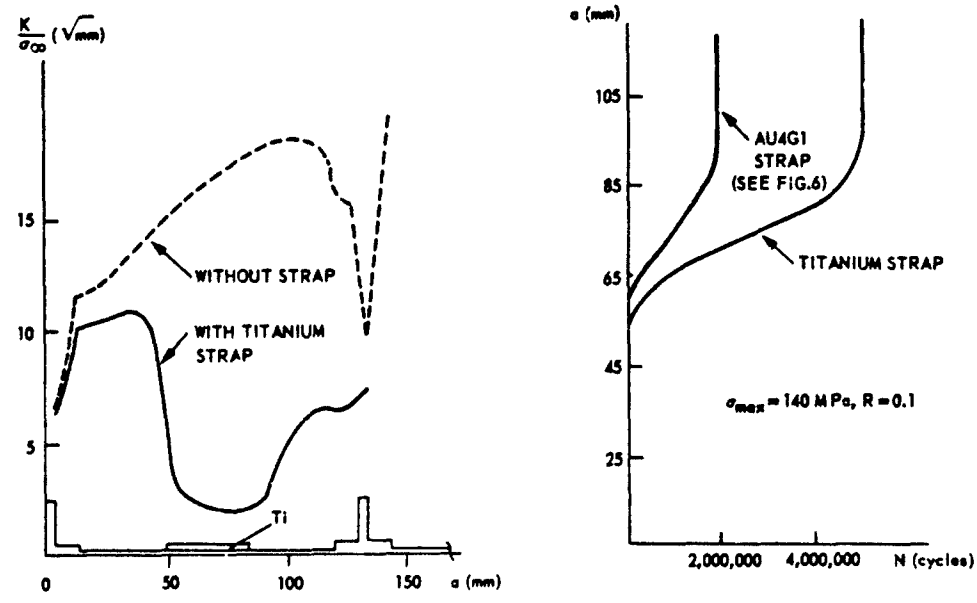

FIGURE 7 EFFECT OF TITANIUM CRACK STOPPER STRAP. LEFT STRESS INTENSITY, RIGHT CRACK GROWTH

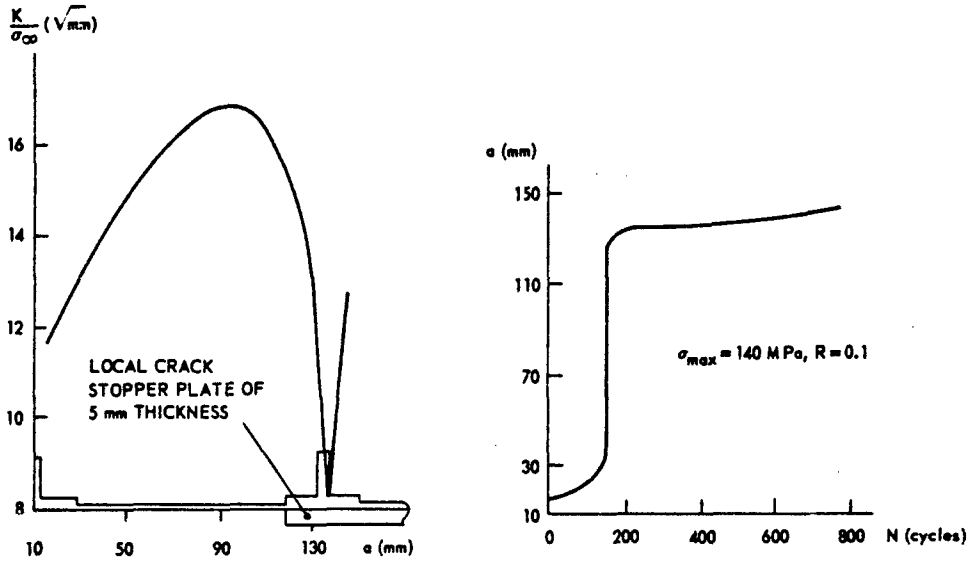

FIGURE 8 INTEGRALLY STIFFENED PANEL WITH CRACK STOPPER PLATE. LEFT STRESS INTENSITY, RIGHT CRACK GROWTH

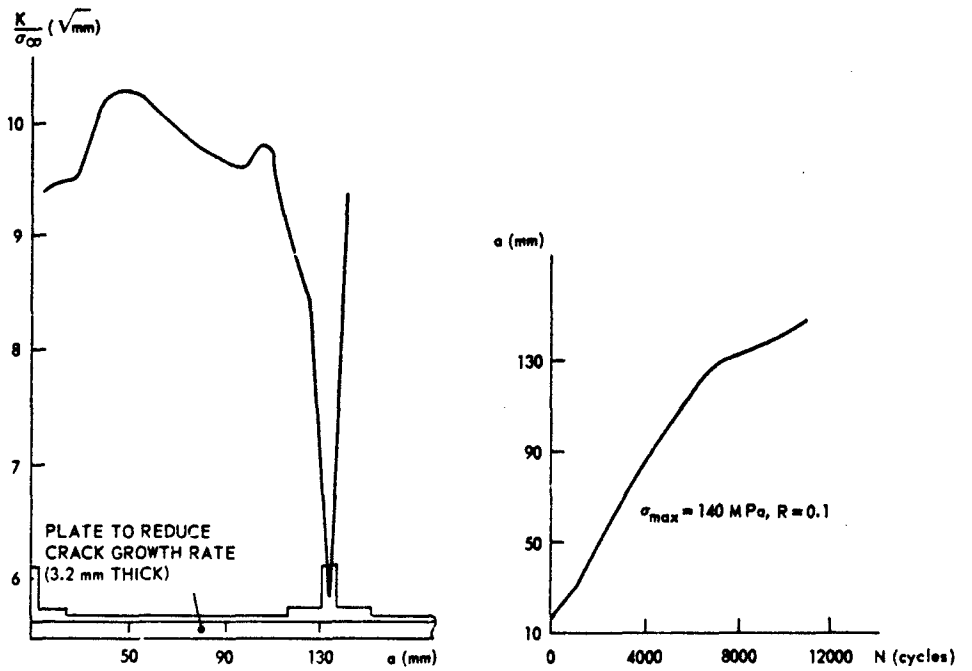

FIGURE 9 INTEGRALLY STIFFENED PANEL WITH CRACK RETARDATION PLATE. LEFT STRESS INTENSITY, RIGHT CRACK GROWTH

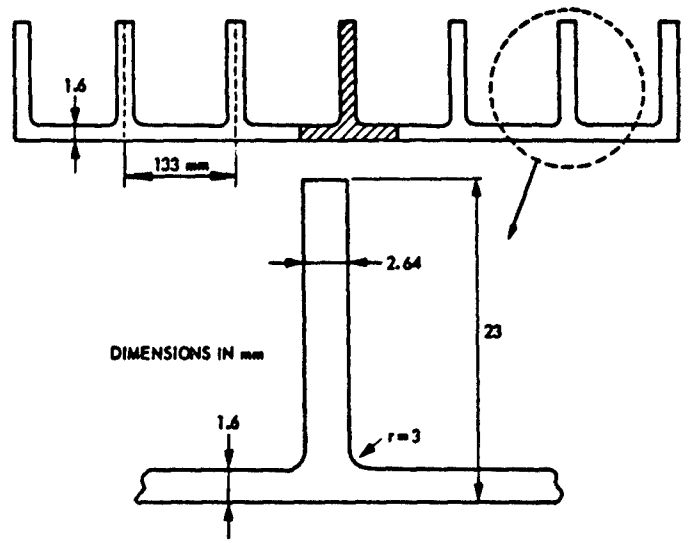

FIGURE 10 PANEL CONFIGURATION USED FOR INVESTIGATION OF CALCULATION-TEST CORRELATION

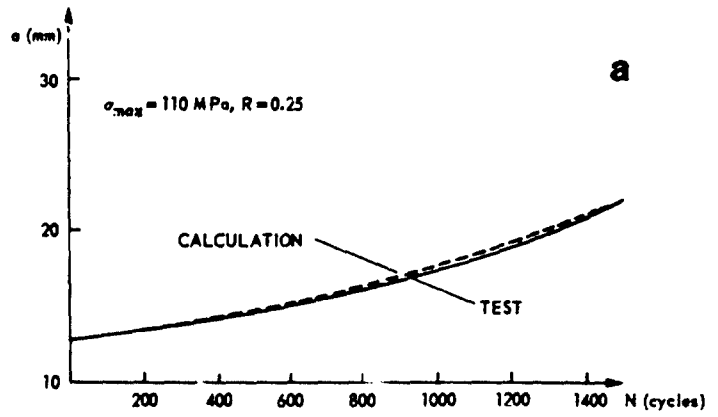

FIGURE 11 COMPARISON OF CALCULATIONS WITH TEST RESULTS FOR PANEL CONFIGURATION SHOWN IN FIGURE 10
(CONTINUED NEXT PAGE)

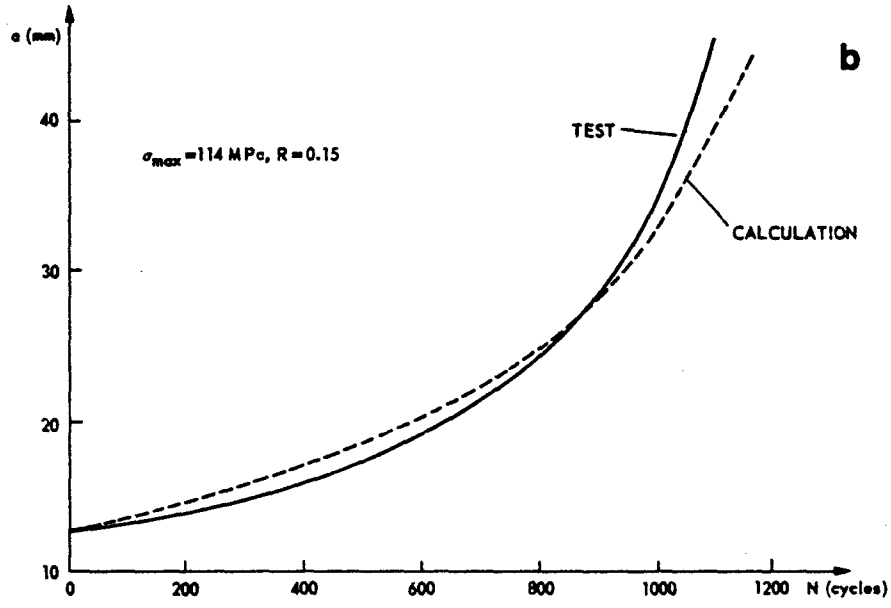

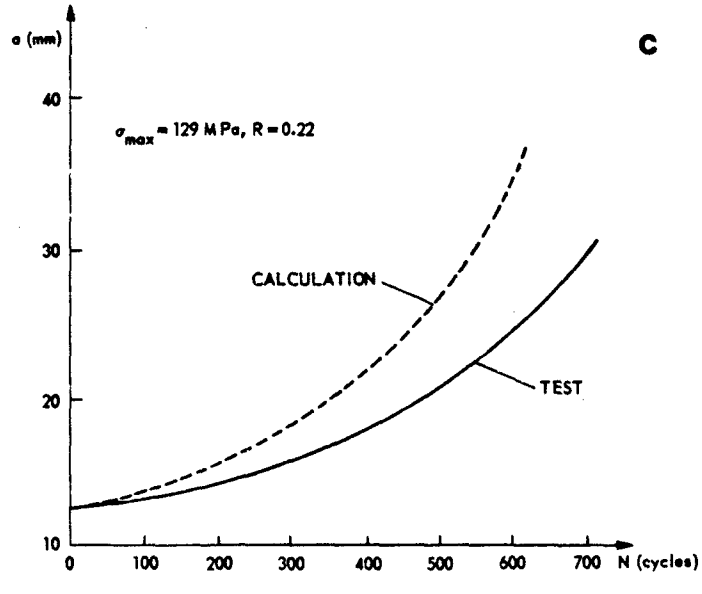

FIGURE 11 (CONCLUDED)

EXAMPLE PROBLEM 3.4.2.3

CRACK PROPAGATION IN WING STRINGER-SKIN PANEL

M. Bradley
British Aerospace
Manchester Division
U.K.
(Literal)

1. STATEMENT OF THE PROBLEM

The results of crack propagation tests on stringer-skin panels [1] were compared with theoretical predictions made for the same configuration. The panels represented the lower wing surface of a medium transport aircraft in the region of the engine ribs, details of which are shown in Figure 1. The crack sizes investigated were within the range 0.5 to 8.0 inches. The loading was of constant amplitude with a mean stress of 8800 psi and an alternating stress of $\pm$ 4000 psi. The skin material was L72 (2014-T3); the stringer material was L65 (2014-T6).

2. ANALYSIS

The stress-intensity solution employed was that by Poe [2] for a stiffener-skin combination with all stiffeners intact. The solution is based on an elastic analysis which does not account for stiffener attachment flexibility and stiffener offset. The solution assumes a crack in an infinite sheet with an array of equally spaced identical stiffeners. The crack is positioned symmetrically either at midbay or across a stiffener. In addition, a correction was included, item 1.1.1 of Reference[3], to allow for the panel's finite size, since the solution is for an infinite panel. To utilize the Poe solution, the structure was idealized as follows.
For the predictions relating to tip A, the solution for a crack originating at a stiffener was utilized (Figure 2).

$$K = \sigma \sqrt{\pi a} \left(K/K_{o\ \text{stringer}}\right)\left(K/K_{o\ FW}\right)$$

where σ = gross stress, $K/K_{o\ \text{stringer}}$ is a function of a_e/b and p/b and $K/K_{o\ FW}$ is the finite width correction.
For the predictions relating to tip B, the solution for a crack originating at midbay was utilized (Figure 3).

$$K = \sigma \sqrt{\pi a} \left(K/K_{o\ \text{midbay}}\right)\left(K/K_{o\ FW}\right)$$

where $K/K_{o\ \text{midbay}}$ is a function of a_e/b and p/b.
The baseline propagation data used were obtained from Reference[4]. Basically, the predictive calculations consisted of determining the stress intensity at the tip under consideration from the approach outlined above and then obtaining the corresponding propagation rate from the baseline data. Plots of da/dN as a function of crack size were made for both the predicted and test data.

3. RESULTS

Comparison of the test results with the predictions show that on average the latter are low by a factor of 3. The results are shown in Figure 4 and 5, where a factor of 3 is applied to the prediction. The discrepancy can be attributed to either scatter between the test panel material and material used for the generation of baseline data, or to the solution not adequately modelling the configuration, or a combination of both. Failure to cater for stiffener attachment flexibility and stiffener offset in the solution, both lead to underestimations of the stress intensity [5] , which in turn would yield the low predictions of propagation rates. The rate data used were based on the mean of the data, thus this also could contribute to the error. The predicted curves are drawn for clarity with a factor of 3. It can be seen that with the exception of the final portion of the curves, the correlation between the two is quite reasonable. The divergence over the final portion is probably due to errors arising from the difficulty in determining rates from the curves of cycles against crack size, at the end of the test.
A program was written for integration of the rate data. For reasons of expediency both crack tips were assumed to grow as the one under the most severe conditions. Crack propagation curves so obtained are shown in Figures 6 and 7. A conservative result would be ensured if an additional factor is taken to cover scatter.
Note - the divergence between predicted and experimental curves beyond N = 10,000 cycles is believed to be due to unequal growth at the two crack tips.

4. APPLICATION

The method was applied to the engine rib area of a full-scale fatigue test specimen of an aircraft at stringer 7. The structure is shown diagrammatically in Figure 8. The 0.144 inch reinforcement is an extension of a larger plate around an inspection hole between the engine ribs. The loading was as shown in Figure 9. The stresses were obtained from strain gauge measurements. The flight loading was idealized to one cycle A-B-A at R = 0 and 19.5 cycles B-C-B at R = 0.44.
The crack was assumed to grow from the nearest rivet hole to the large hole to stringer 7, and then from the other side of the hole to stringer 8. Reasonably accurate test data were available for a large part of the second stage of crack growth. This second stage was analysed in two parts (see Figures 8 and 10):
(i) From rivet hole to stringer 8.
Up to stringer 8, when the crack is inside the reinforcement, the stress level was reduced by the ratio of the cross sectional areas without and with reinforcement.

The parameters influencing the Poe factors were also calculated using a skin thickness equal to the skin and reinforcement. The crack length used in calculating the factor, which was for a broken stringer case, was a_e.
In place of the edge correction, a correction for a crack approaching a sudden change in section was applied using 2.1.4 of Reference[3]. The effect of the large hole was taken into account by using the well-known Bowie factor which expresses (K/K_o) as a function of a/D. The factor used was that for a hole with a crack at each side. The overall expression was therefore:

$$K = F_{Poe} \cdot F_{change\ of\ section} \cdot F_{Bowie} \cdot \sigma \sqrt{\pi a}$$

The major error in this idealization is the assumption of equal cracks at each side of the large hole. In this case, however, the crack does not become large compared with the diameter of the hole and the error is not great. As the error is always pessimistic the method should serve for design purposes in all cases.

(ii) From stringer 8 outwards.
The method was basically the same as above with the exceptions that the stress and Poe parameters were calculated for the basic structure (no reinforcement) and no edge factor was needed. When the crack passed through rivet holes, it was assumed that a .05 inch crack already existed on the other side of the hole (.05 inch had been found by experience to be large enough to cover MIL - SPEC requirements in all cases).

5. RESULTS

The graph shown in Figure 11 shows the comparison between theoretical prediction and test results for the starboard wing at the inboard and outboard engine ribs. It can be seen that there is a reasonable correlation in both cases when the beneficial effects of rivets have been removed. It is important that these effects are ignored as their presence cannot be guaranteed.

6. CONCLUSION

Compared with methods now beginning to become available in the form of sophisticated computer programs a method based on the Poe curves, which assumes elastic structures and rigid stringer corrections, seems relatively crude. It can be seen from this example, however, that provided a factor can be derived from a panel of similar structure and material, a reasonable prediction may be made even when the details of the structure and the loadings are changed to quite a large degree.
The possible beneficial effects of the rivets are also illustrated. It is unfortunate that they cannot be relied on.

7. REFERENCES

1. Internal British Aerospace Manchester report.
2. Poe, C.C., "Stress Intensity Factors for a Cracked Sheet with Riveted and Uniformly Spaced Stringers" NASA TR 358, 1971.
3. Rooke, D.R. and Cartwright, D.J., "Compendium of Stress Intensity Factors", HMSO, London (1976).
4. ESDU, Fatigue, Vol.4, Figure 2.
5. Swift, T., "Effects of Fastener Flexibility and Stiffener Geometry on the Stress Intensity in Stiffened Cracked Sheet", Delft Conference Paper, June 1974.

8. COMMENTARY

As mentioned in the example, more sophisticated computer programs than the Poe analysis are presently available. Closed form solution programs (Vlieger and Swift) are fast and cheap to run and eliminate the need for finite-element analysis.
The example is a good illustration of the calibration of the analysis of a complex structure by means of test data for a simpler configuration. The waviness of the calculated crack-growth curves is puzzling.

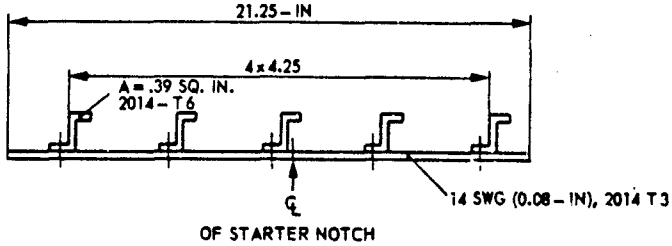

FIGURE 1 PANEL DIMENSIONS. RIVET PITCH = 1.0 inch. PANEL LENGTH = 48 inches

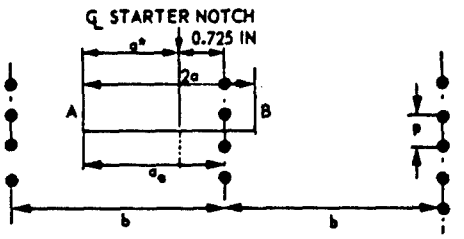

FIGURE 2 CRACK DIMENSIONS FOR CALCULATIONS RELATING TO CRACK TIP A

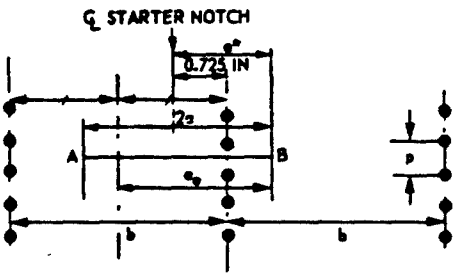

FIGURE 3 DITTO FOR CRACK TIP B

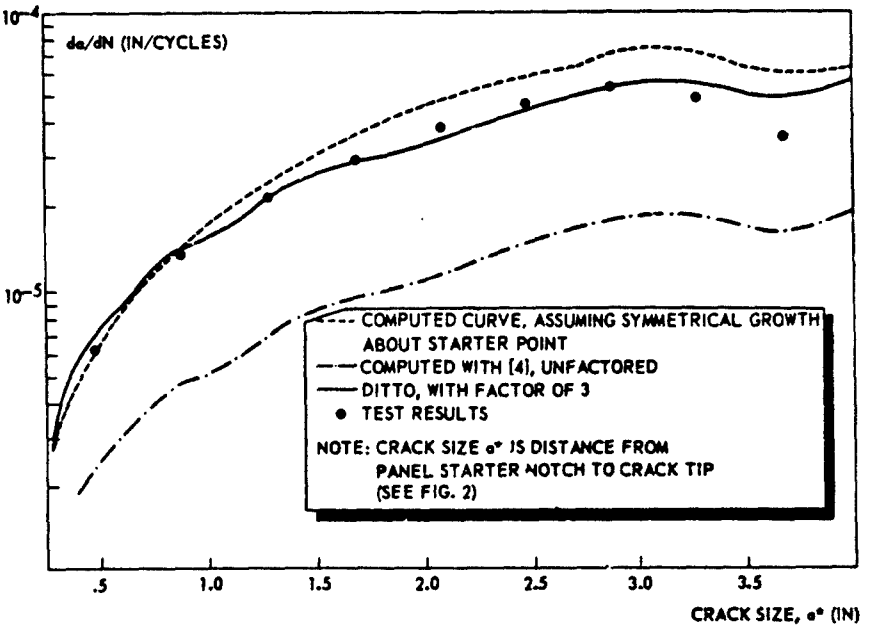

FIGURE 4 COMPARISON OF COMPUTATIONAL AND TEST RESULTS FOR AFT CRACK TIP

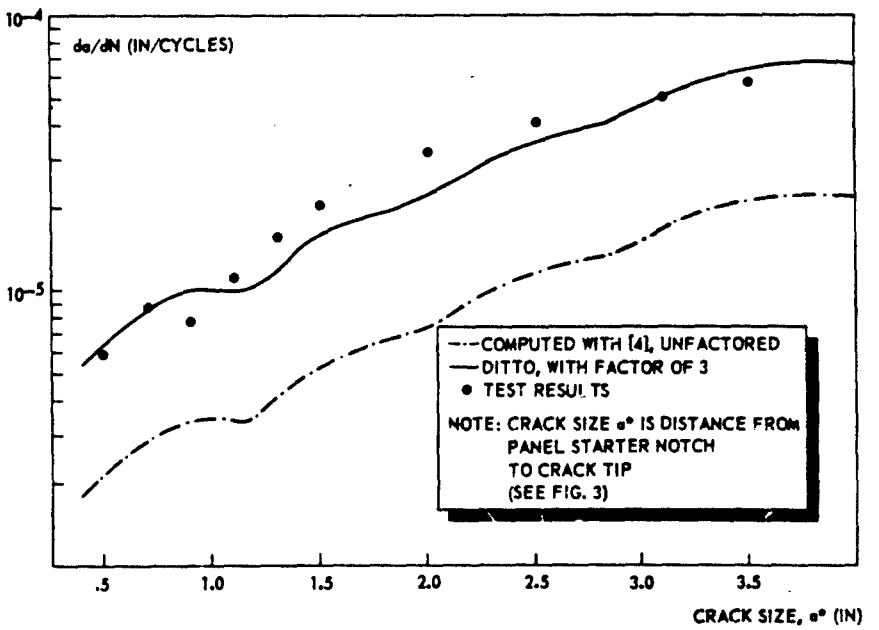

FIGURE 5 COMPARISON OF COMPUTATIONAL AND TEST RESULTS FOR FORWARD CRACK TIP

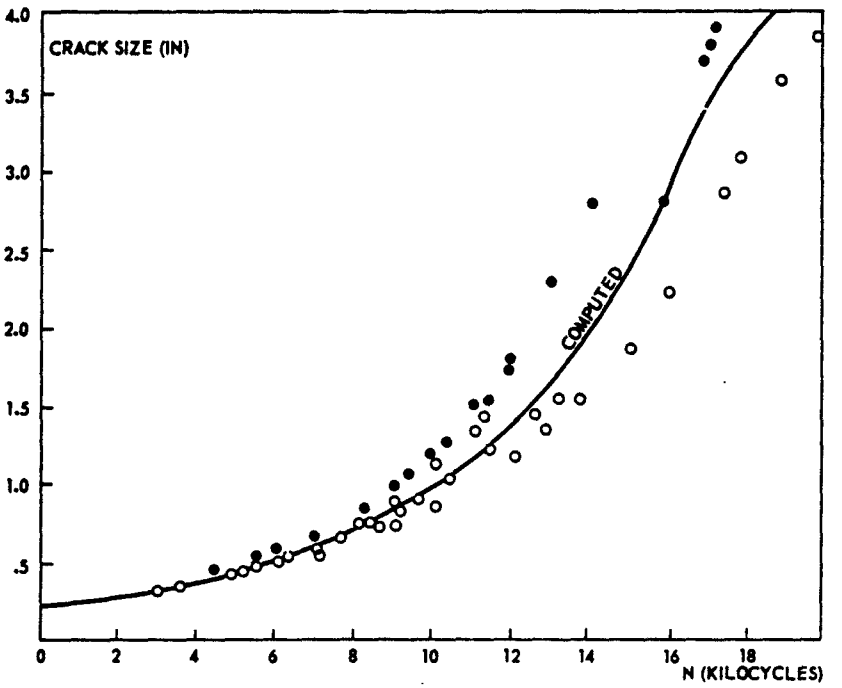

FIGURE 6 CRACK GROWTH CURVE (GROWING AFT; CRITICAL) COMPARISON BETWEEN COMPUTATION AND TEST

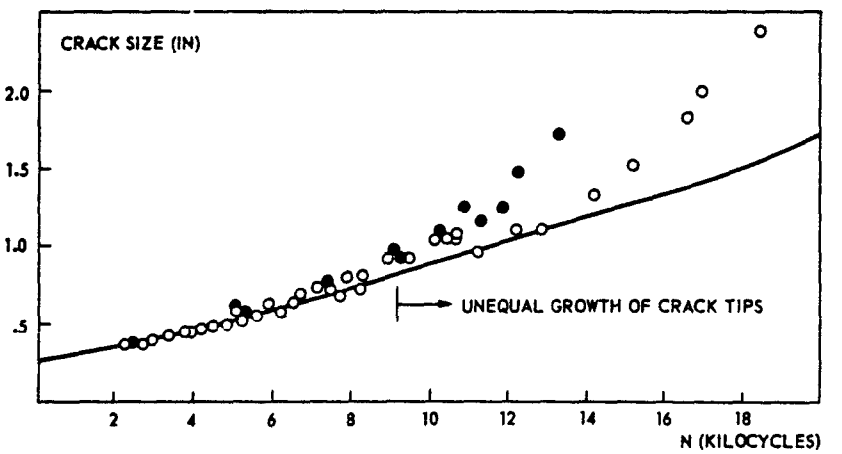

FIGURE 7 CRACK GROWTH CURVE (GROWING FORWARD; NONCRITICAL)

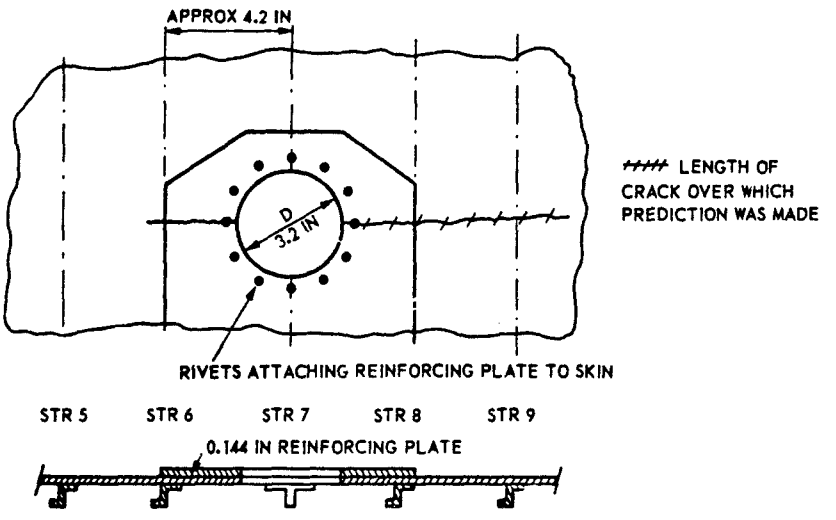

FIGURE 8 DIAGRAM OF STRINGER 7 STRUCTURE

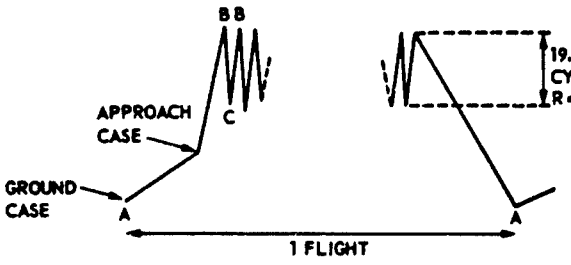

FIGURE 9 FLIGHT LOADING

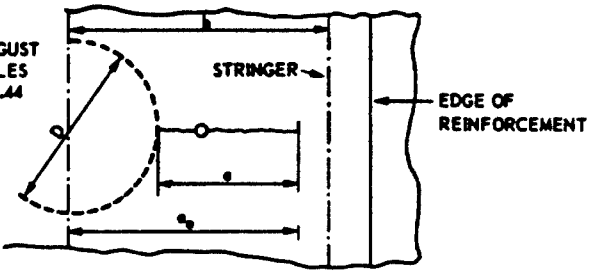

FIGURE 10 CRACK AND REINFORCEMENT (SEE ALSO FIG. 8)

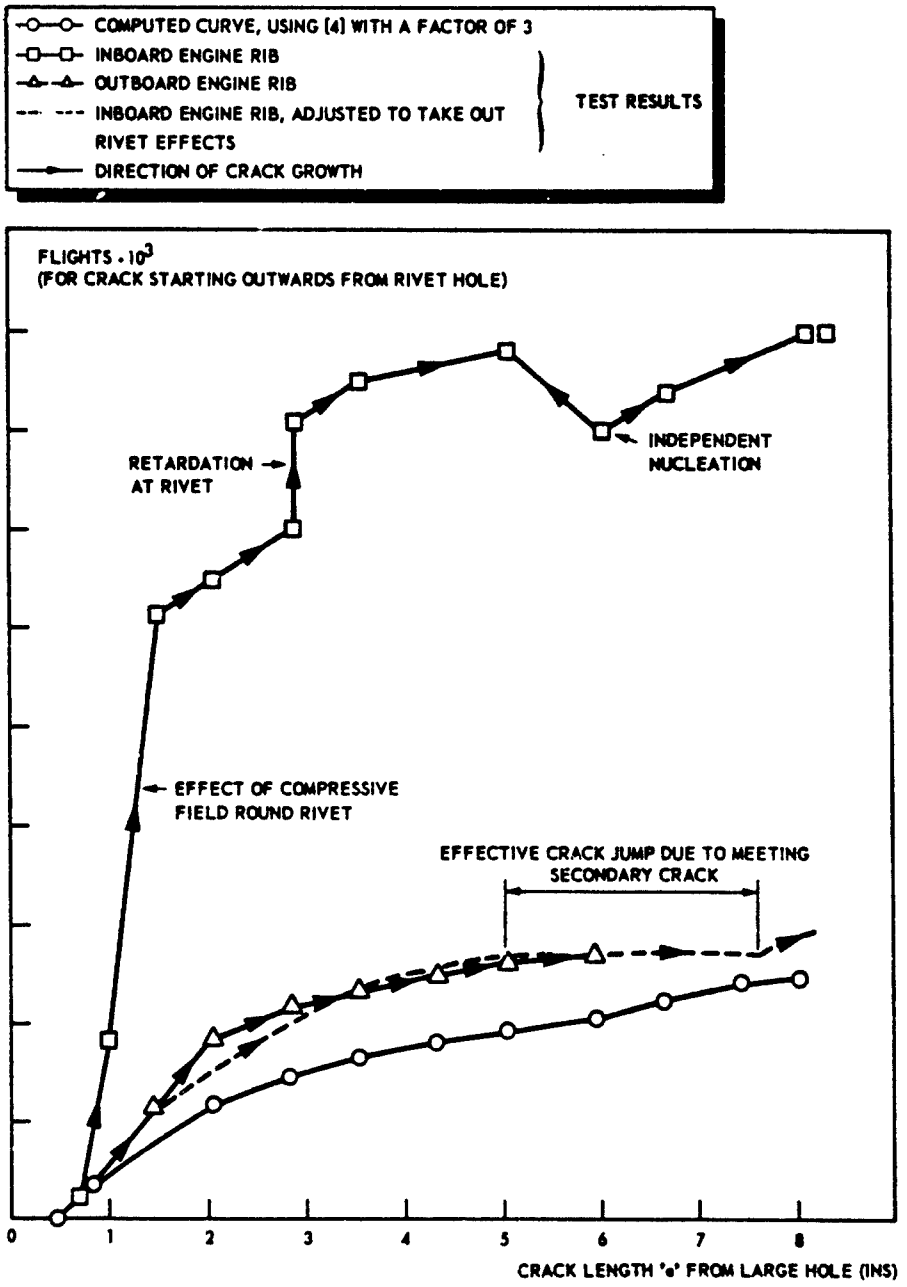

FIGURE 11 COMPARISON BETWEEN CALCULATED RESULTS AND RESULTS OF FULL-SCALE FATIGUE TEST SPECIMEN. CRACK GROWING FORWARD FROM STRINGER 7 (SEE FIG.8)

EXAMPLE PROBLEM 3.4.2.4

ENGINE PYLON OF MEDIUM TRANSPORT

D. Grange
British Aerospace
Manchester Division
U.K.
(Literal)

1. STATEMENT OF THE PROBLEM

The structure is shown in Figure 1. The structure is basically a box section of fabricated skin and stiffener configuration. Crack growth and residual strength predictions were required.

2. ANALYSIS

The structure was modelled as a stringer-skin panel using the Poe [1] closed form solution for a panel of infinite width with an array of equally spaced equal stiffeners. Although there was a physical break in the skin at the corners of the box section, it was considered reasonable to assume an infinite size since continuity was maintained with the adjoining side panels by the corner angles. Since the solution does not permit stiffeners of differing section, the panel was considered to have the light gauge stiffeners of the side under consideration. This is a conservative assumption.
The damage configuration considered was a crack growing equally about a stiffener. The Poe solution for this case is given as a function of p/b, μ, and a/b, where p = stiffener attachment pitch (i.e., bonded) b = stiffener pitch (= 5.7 inches), and μ is the stiffening ratio (0.32). The value of p/b was taken as 1/12 (bonded stiffener). A p/b of zero would be appropriate but the minimum value of p/b for which data were available was 1/12.
The propagation predictions were based upon a loading spectrum which covered both flight and ground loads. Preliminary calculations showed the flight loadings contribution to be insignificant, thus only the taxi spectrum and a ground-to-air cycle were considered. The spectrum was divided up into increments, for each of which the average value of stress range, $\Delta\sigma$, was obtained, together with the respective stress ratio, R, and the number of occurrences, n. The procedure adopted to evaluate the propagation of the crack under the spectrum loading is outlined diagramatically in Figure 2. An example of the calculation for one increment of crack growth is given in Table 1. A plot of crack length against flights is given in Figure 3. It has to be noted that no allowance was made for crack retardation.

3. RESULTS

The residual strength requirement was 2/3 of the design ultimate loading. The stress distribution across the section varies, thus to be conservative the peak value was taken, giving the residual stress level as σ = 21.920 lb/in^2 thus at a = 5 inches one finds $K = (K/K_o)_{POE} \cdot \sigma\sqrt{\pi a}$ = 0.654 x 21.920x 3.97 = = 56900 lb/in^2 $\sqrt{in}$. On the basis of handbook values of K_c [2] it was considered that at this level of stress intensity the crack would be stable. The crack growth curve is shown in Figure 3.

4. REFERENCES

1 Poe, C.C., "Stress intensity factors for a cracked sheet with riveted and uniformally spaced stringers"
NASA TR 358, 1971.

2 Anon.,"Damage Tolerant Design Handbook – A compilation of fracture and crack-growth data for high-strength alloys."
MCIC HB-01, Part 1, 1972.

3 Anon.,"Fatigue crack propagation in thin sheet aluminium alloy"
ESDU Vol.4, Sheet 73021, Fig.1

5. COMMENTARY

This example is a good illustration of the idealization of a complex structure to a much simpler configuration for which, on the basis of existing solutions for the stress intensity, a residual strength and crack propagation analysis can readily be carried out. Both the modelling of the structure and the analysis applied were kept simple, ensuring the achievement of a conservative result.

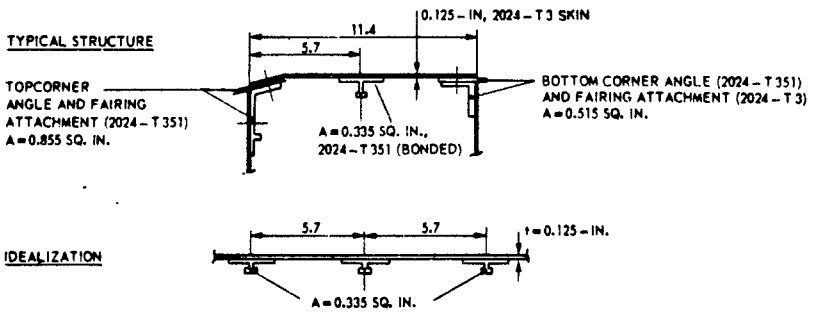

FIGURE 1 STRUCTURE AND IDEALIZATION

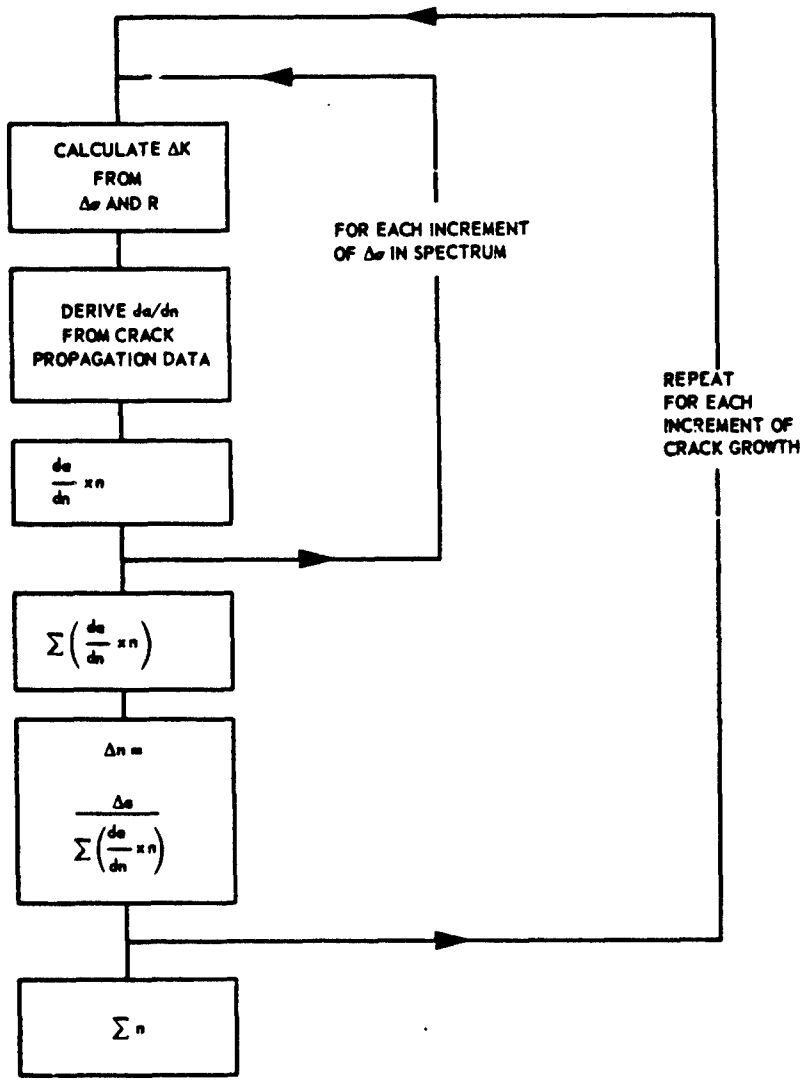

FIGURE 2 PROCEDURE ADOPTED TO EVALUATE CRACK GROWTH

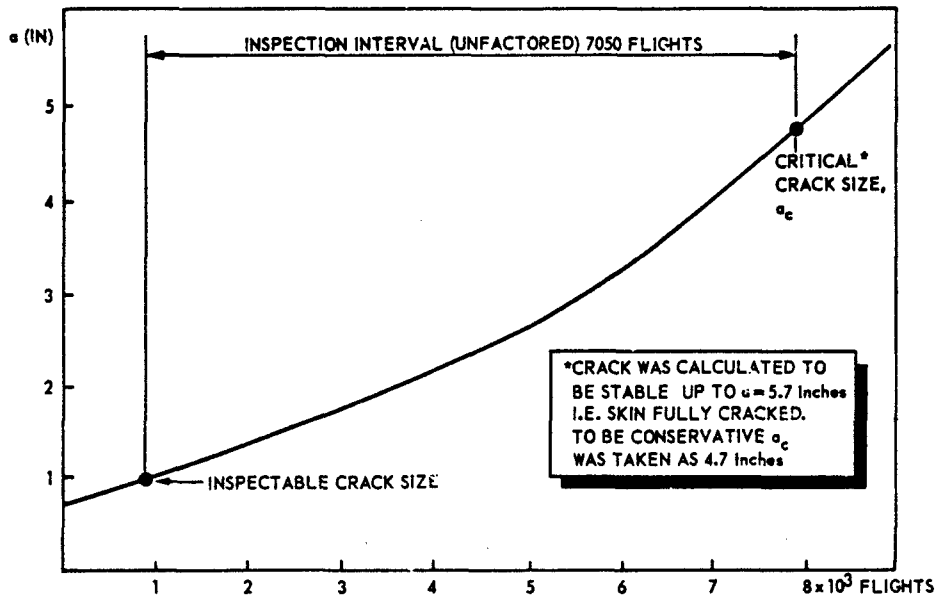

FIGURE 3 CRACK PROPAGATION CURVE

			a=.75 inch to 1.25 inch i.e. a_{MEAN}=1.0 inch		
Stress range, $\Delta\sigma$ (lb/in^2)	Stress ratio, R	Occurrences per flight, n	$\left(\frac{K}{K_o}\right)_{POE}$ $\Delta K = \Delta\sigma . \sqrt{\pi a}$ (lb/in^2 $\sqrt{in}$) Ref.[1]	da/dn inch per cycle Ref.[3]	da/dn inch per flight
5250	.237	.004	6704	$3.4x10^{-6}$	$1.3x10^{-8}$
4750	.284	.0189	6066	$1.8x10^{-6}$	$3.4x10^{-8}$
4250	.334	.137	5427	$1.7x10^{-6}$	$2.33x10^{-7}$
3750	.388	1.5	4789	$1.4x10^{-6}$	$2.1x10^{-6}$
3250	.447	9.3	4150	$1.3x10^{-6}$	$1.21x10^{-5}$
2750	.512	42.06	3512	$1.1x10^{-6}$	$4.63x10^{-5}$
2250	.582	101.9	2873	$0.9x10^{-6}$	$9.17x10^{-5}$
1750	.659	87.1	2235	$1.0x10^{-6}$	$8.17x10^{-5}$
1250	.744	46.0	1596	$0.9x10^{-6}$	$4.14x10^{-5}$
750	.838	53.6	958		
250	.943	107.3	319		
6150	0	1	7860		$1.3x10^{-6}$

$\sum = 28.3x10^{-5}$,
or $\Delta n = 1767$ flights
(for $\Delta a = 0.5$ inch)

TABLE 1 EXAMPLE OF CALCULATION PROCEDURE

EXAMPLE PROBLEM 3.4.2.5

DAMAGE TOLERANCE OF A PRESSURE BULKHEAD

D. Grange

British Aerospace
Manchester Division
U.K.

1. STATEMENT OF THE PROBLEM

The calculations in this example formed part of the preliminary analysis of the pressure cabin rear bulkhead of a light civil transport. The bulkhead is of spherical form having a radius of 90 in. Its construction is built up skin and stiffeners consisting of riveted top hat sections radially and bonded straps circumferentially (see Figure 1). The skin and stiffener material is L72 (equivalent to 2014-T3). Initially the skin thickness was 20 swg (.036 inch). On the basis of crack propagation calculations the skin thickness was changed to 18 swg (.048 inch).

2. DAMAGE SIZE, LOADING AND INSPECTION REQUIREMENTS

The initial damage considered is a circumferential crack of 2a = 4 inches, originating at a failed radial stiffener (see Figure 1). The maximum crack length considered is 2a = 14 inches. Up to this length comparison with an R-curve [4] shows the condition to be stable, but above this length negligible additional life will result. The foregoing implies that the inspection interval will correspond with crack growth from 2a = 4 inches to 14 inches.
The only loading on the bulkhead is that of pressure. This is made up of two components, internal cabin pressurization and external suction. For the fatigue calculations, loading applicable to normal operations is required, i.e. a maximum cabin operating pressure of 6.5 psi and an external suction under normal conditions of 1.25 psi. This results in a combined differential pressure of 7.75 psi. One pressurization per flight was assumed.
For the residual strength calculation, the following loading is applicable with a factor of 1.33, viz. a cabin relief valve pressure of 7.0 psi and an external suction due to air brake deployment of 2.0 psi. This yields a combined differential pressure of 12.0 psi. Owing to the spherical curvature the differential pressure will create hoop stresses of equal value in both the radial and circumferential directions. The hoop stress will be equal to

$$\sigma_{hoop} = \frac{\Delta p . R_C}{2t}$$

where Δp is differential pressure, R_C is bulkhead radius (= 90 inches) and t is skin thickness (= 0.036 inches). With the respective differential pressures it follows that

$$\sigma_{hoop,fatigue} = 9690 \text{ psi}$$

and

$$\sigma_{hoop,residual\ strength} = 15000 \text{ psi}$$

The annual inspection will be based on a utilization of 3670 flights per year and a scatter factor on propagation of 3.0, resulting in a factored value of 11010 flights per year.

3. STRESS INTENSITY SOLUTION

The solution used is that of Poe [1] for a built-up skin stiffener construction having a skin crack originating at a failed stiffener location. The solution is a function of stiffener pitch (or bay width), cross sectional area, attachment pitch and skin thickness, but does not cater for the flexibility of the stiffener attachment. In fact Poe provides stress intensity values for a certain crack size as a function of the attachment pitch to bay width ratio (p/b) and the stiffening parameter μ. The latter parameter is defined as the ratio of stringer stiffness to total stiffness per stiffener bay.
The bay width was taken here as 27 in. This represents the mean value of the outer bay. It was considered unreasonable to take the maximum width, since considerable restraint can be expected from the edge member. Using this bay width value, it follows for the bulkhead dimensions shown in Figure 1 (the attachment pitch is equal to 1.0 in.) that

$$\mu = \frac{A_{st}}{A_{st}+bt} = 0.199$$

and

$$p/b = 1/27$$

In the analysis the curve p/b = 1/12 is used since this is the minimum p/b-curve provided by Poe.
Since the pressure loading on the skin will cause a bulging effect on the crack, the correction as described by Kuhn is applied [2] . The bulging correction factor as given by Kuhn reads $(1+k\frac{a}{R})$, where a is semi-crack length, R is radius and k is a constant (= 5.0). (Kuhn uses the total crack length in his correction factor (see [2]), instead of the semi-crack length as applied here, editor). However, the presence of a stiffener was observed by Swift to reduce the bulging to unity [3] . Thus the distribution derived from this expression, is assumed to be fully effective at mid-bay, reducing to unity at the stiffener. For this particular configuration, where the stiffener is failed, the bay width will be considered effectively doubled. With these assumptions it follows for the stress intensity factor in the curved panel

$$K_{CURVED} = 1+\left(\frac{b-a}{b}\right)\frac{k.a}{R} \quad K_{FLAT}$$

It has to be noted finally that in calculating the value of K in the bi-axial stress field existing in a spherical bulkhead, it was assumed that the stresses parallel to the crack do not influence K.

4. RESULTS

The computation of the stress intensity factor, K, as a function of crack size and of the number of flights, N, it takes to grow the crack from 2a = 4 inches to 14 inches are carried out in Table 1 for a skin thickness of 0.036 inch. The computed values are plotted in Figures 2 and 3. The R-curves of [5] appear not to be tangential to the K-curve plotted in Figure 2 over the crack size region considered. Thus the residual strength properties are adequate. However, as can be seen from Figure 3, the crack propagation life from a = 2 inches to 7 inches provided an inadequate inspection interval (viz., 325 flights instead of the required 11010 flights). Therefore the same computations as presented in Table 1 were repeated but now for a skin thickness of 0.048 inch. These calculations are not given in this example, but the computed data are plotted in Figures 2 and 3. The 0.048 inch thickness yielded a life of 12800 flights (see Figure 2), i.e. an inspection interval of 1.16 years, which was considered adequate.

5. REFERENCES

1. Poe, C.C., "Stress Intensity Factor for a Cracked Sheet with Riveted and Uniformly Spaced Stringers" NASA TR R-358.

2. Kuhn, P., "Notch Effects on Fatigue and Static Strength", published in Current Aeronautical Fatigue Problems by Pergamon Press (1965).

3. Swift, T., "Application of Fracture Mechanics to the Design of Damage Tolerant Stiffened Aircraft Structures" Douglas Aircraft Paper 5981.

4. Bradshaw, F.J., Wheeler, C., "Crack Resistance of Some Aluminium Alloys and the Prediction of Thin Section Failure", RAE TR 73191, Fig.13.

5. Anon., "Fatigue Crack Propagation in Thin Sheet Aluminium Alloy" ESDU Vol.4, Sheet 73021, Fig.2.

6. COMMENTARY

An aircraft pressure cabin bulkhead, built up of skin and stiffeners, is a type of design that is pre-eminently suited to fracture mechanics analysis, because its loading is well-defined and simple, viz., one cycle per flight and of a constant amplitude. The present example clearly demonstrates both the benefit and necessity of carrying out a fracture mechanics analysis on such a type of structure already in the design stage. From the analysis it turned out that by applying a 30 % thicker skin in the design the crack propagation life associated with the defined crack size range increased by a factor of 40 (viz., from 325 flights to approximately 13,000 flights). This enormous increase in crack propagation life is due to the sensitivity of da/dn to ΔK variations (da/dn is a power function of ΔK). This implies that in general the reliability of a predicted life will strongly depend on the accuracy with which the stress intensity is determined. With a view to this it has to be remarked that the calculation of K as a function of crack size, as applied in the present example, is on the one hand unconservative (the Poe solution does not account for attachment flexibility) and on the other hand conservative (the p/b = 1/12 curve was used, while the actual p/b is equal to 1/27). Which of both effects (i.e. fastener flexibility and attachment spacing) prevails in the present design cannot be determined without carrying out a more refined analysis.

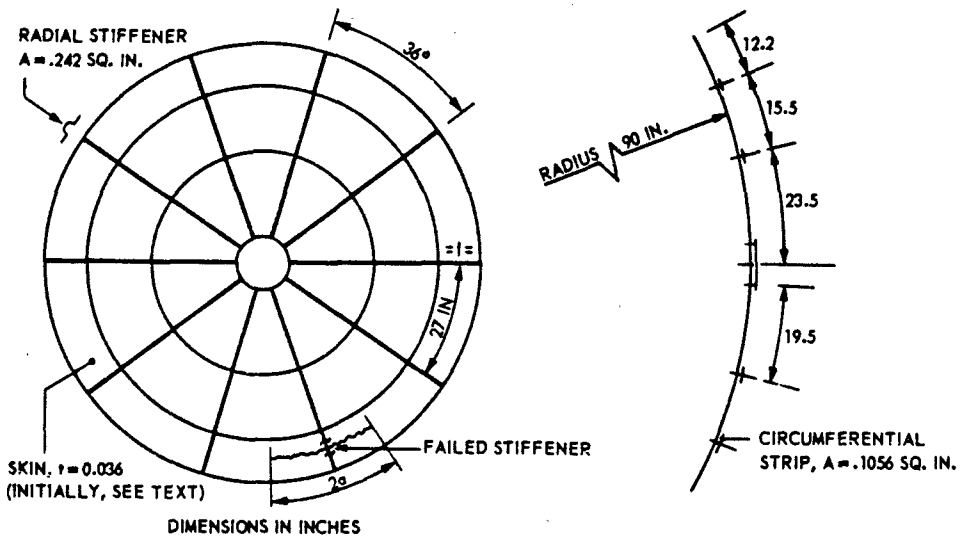

FIGURE 1 CONSTRUCTION DETAILS OF PRESSURE CABIN REAR BULKHEAD.
MATERIAL OF SKIN AND STIFFENERS: L 72 (2014 – T 3)

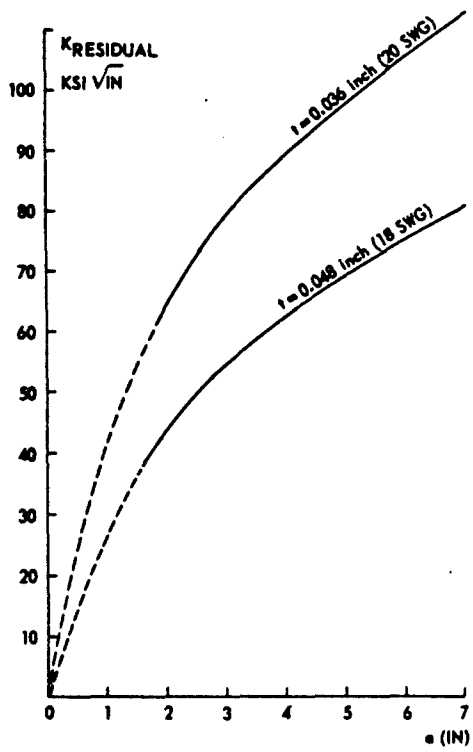

FIGURE 2 PLOT OF COMPUTED RESIDUAL STRENGTH DATA (SEE TABLE 1)

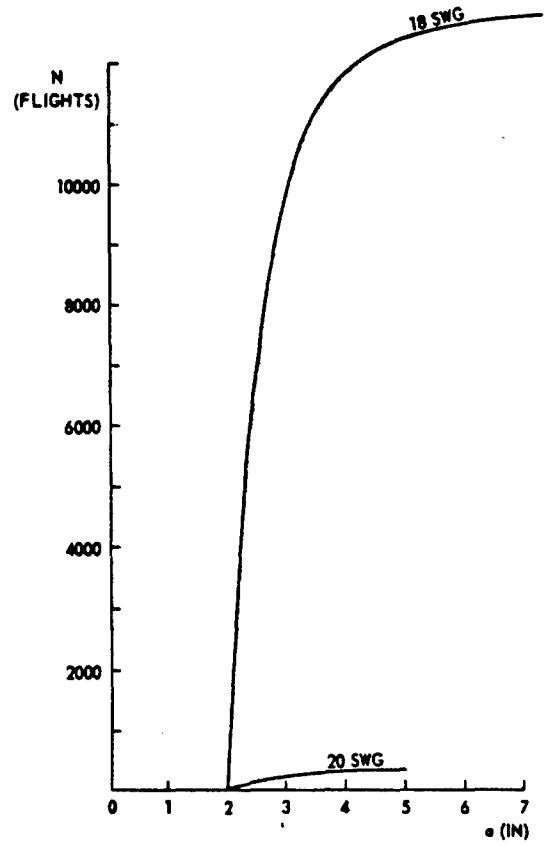

FIGURE 3 PLOT OF COMPUTED CRACK PROPAGATION DATA (SEE TABLE 1)

a (inch)	a_{AV} (inch)	$\frac{K_{curved}}{\sigma\sqrt{\pi a}} = 1+(\frac{b-a}{a})\frac{ka}{R}$	$\left(\frac{K}{\sigma\sqrt{\pi a}}\right)_{POE}$ Ref.[1]	$K_{RESID.} = K_{curved} \cdot K_{POE}$ (psi $\sqrt{in}$)	ΔK (fatigue) (psi $\sqrt{in.}$)	da/dN, R=0 (inch/cycle) Ref.[5]	dN da=.5 (Flights)	N (Flights)
2.0								0
	2.25	1.115	1.55	68,920	44,520	.0027	185	
2.5								185
	2.75	1.137	1.53	76,440	49,380	.0070	71	
3.0								256
	3.25	1.159	1.49	82,490	53,290	.0150	33	
3.5								289
	3.75	1.179	1.44	87,410	56,470	.0270	19	
4.0								308
	4.25	1.199	1.40	92,010	59,440	.0480	11	
4.5								319
	4.75	1.218	1.36	95,980	62,000	.080	6	
5.0								325
	5.25	1.239	1.32	99,300	64,150			
5.5								
	5.75	1.251	1.30	103,670	66,970			
6.0								
	6.25	1.267	1.28	107,800	69,640			
6.5								
	6.75	1.281	1.26	111,490	72,020			
7.0								

TABLE 1 COMPUTATION OF K_{RESID} AND ΔK FOR A THICKNESS OF 0.036 INCH

EXAMPLE PROBLEM 3.4.2.6

CRACK PROPAGATION ANALYSIS OF FLAT STIFFENED PANELS

L. Schwarmann

Vereinigte Flugtechnische Werke-Fokker GmbH
Bremen, Germany
(Literal)

1. STATEMENT OF THE PROBLEM

Crack propagation results obtained from constant amplitude tests on panels with riveted stiffeners are compared with corresponding analytical results. The influence of the stiffeners on the stress intensity factor has been calculated by using a semi-closed form solution. The crack propagation rates have been calculated by using the Forman equation. The constants in this equation were derived from test results of an unstiffened centre-cracked panel.

2. TESTING DETAILS

Details of the tested panel configurations are shown in Figure 1 and Table 1. Gross-sectional areas A of stiffeners were varied in order to obtain different values of the stiffening ratio, μ, which is defined as the ratio of stiffener cross section to total cross section per stiffener bay. The panels were subjected to constant amplitude loading with σ_{max} = 90 MPa (R=0.1). The frequency was 4.2 Hz, and testing was done in a laboratory environment. All cracks (total length 2a) were cut in the sheet under the panel central stiffener. Tests and calculations started at an initial crack length of 2 a_i = 24 mm. After applying cyclic loads the cracks were measured visually as a function of the applied load cycles N. The results of these measurements were the a = f (N) curves. Two different conditions of the central stiffener were considered, viz., intact and totally broken.

3. ANALYSIS METHOD

3.1 Crack propagation law

The crack length "a" as a function of the applied load cycles N was calculated using the following equation

$$a = a_i + \int_{a_i}^{a} \frac{da}{dN} \qquad (1)$$

The required analytical procedure was incorporated in a VFW-Fokker in-house computer programme [1]. For the determination of crack propagation rates, da/dN, the so-called Forman equation [2] was used, which is defined by

$$\frac{da}{dN} = \frac{C_F(\Delta K)^{n_F}}{(1-R)K_{C_F}-\Delta K} \qquad (2)$$

In equation (2) the symbols C_F , n_F , K_{C_F} are the so-called Forman constants, which were derived by the following:
from the measured "a" versus N curve of the unstiffened panel (panel 1A in Table 1, width = 440 mm) the crack propagation rate $(\frac{da}{dN} \approx \frac{\Delta a}{\Delta N})$ and the range of the stress intensity factor

$$\Delta K = (\sigma_{max} - \sigma_{min}) \sqrt{\pi a} \sqrt{\sec \pi \frac{a}{W}} \qquad (3)$$

were calculated. The crack propagation test was completed at a crack length of 2a = 286 mm and the panel had been loaded to failure. The maximum load for this case was F_{max} = 94333 N. From these data the Forman constant

$$K_{C_F} = \frac{94333}{2.440} \sqrt{\pi . 143 . \sec \pi \frac{143}{440}} = 3143 \ \text{Nmm}^{-1.5}$$

was derived. On log-log paper the values

$$\frac{da}{dN} \left((1-R)K_{C_F} - \Delta K\right) \quad \text{versus} \quad \Delta K$$

obtained from test results were plotted, see Fig.2. These data were approximated by a straight line, which can be described by the two other Forman constants n_F, C_F (see Fig.2). The accuracy of the Forman equation for the unstiffened panel was cross-checked. For results see Fig.3.

3.2 Stiffener influence

For the stiffened panels the influence of the stiffeners on the stress intensity factor and its range has to be taken into account

$$Y = \frac{\Delta K_{stiffened}}{\Delta K_{unstiffened}} \qquad (4)$$

The correction factor Y contains the influence of the intact or broken central stiffener on the stress intensity factor. In order to obtain these correction factors a special computer programme has been

developed [3] , in which the fundamental works by Poe [4] and Swift [5] have been incorporated. The computed correction factors for the stiffened panels are shown in Fig.4. The calculation of the crack propagation for the stiffened panels has been carried out by using the correction factors from Fig.4 and applying equations (1)-(4).

4. TEST-ANALYSIS CORRELATION

Comparing the experimental results [6] with the corresponding analytical results (see Figure 5), one observes that crack arrest, which occurs when the crack reaches a rivet hole, cannot be predicted by the analysis. However, for all stiffened panels a good correlation between test and calculated crack life results has been obtained.

5. CONCLUSIONS

The crack propagation behaviour, due to constant amplitude loading, can be predicted satisfactorily, provided that proper Forman constants (material behaviour) and a correction factor on ΔK for the presence of the stiffeners (specific for the structure) are available.

6. REFERENCES

1. Schwarmann, L. et. al, "DAMTOL - A computerprogram for damage tolerance analysis" VFW-Fokker, not published.

2. Forman, R.G., et. al, "Numerical analysis of crack propagation in cyclic loaded structures" Trans. ASME, Journal of Basic Engin., 1967, pp. 459-464.

3. Handbuch Struktur Berechnung, Band 2, Struktur Blatt 63611, "The influence of stiffeners on crack propagation and residual strength" IASB, Munich, 1975.

4. Poe, C.C., "Stress intensity factor for a cracked sheet with riveted and uniformly spaced stringers" NASA TR R-358, 1971.

5. Swift, T., "The effect of fastener flexibility and stiffener geometry on the stress intensity in stiffened cracked sheet". Douglas Paper 6211, Delft, 1974.

6. VFW-Fokker GmbH, "Crack propagation in aircraft structures" ZTL 2.20, Ministry of Defence, 1974-1975.

7. COMMENTARY

The present example shows that the crack propagation life of center-cracked panels with riveted stiffeners is to be predicted satisfactorily when the crack growth to the next stiffener is considered. Generally, the calculated results are then conservative. When the crack tips reach the rivet rows of the adjacent stiffeners, the crack path has two alternatives, viz., through or between rivet holes. In the former case the crack tips will be arrested in the rivet holes for a certain number of cycles, until a new crack initiates from the hole. The present analysis does not account for this possible crack arrest. However, because in the actual structure crack arrest in rivet holes is not guaranteed (see for example results of panels 11.3 and 12.3 in Figure 5), it is not allowable to account for this possible delay when predicting the crack propagation life of riveted structures for crack lengths extending beyond the next stiffeners. By ignoring this delay, in the present example in almost all cases a conservative estimate of the total crack propagation life (until fracture instability) was obtained.

PANEL	STIFFENER PROFILE	CROSS SECTION A_s (mm^2)	STIFFENING RATIO μ	CENTRAL STIFFENER
1A	-	-	-	-
5.2	Z 25 x 15 x 0.8	43.9	0.268	INTACT
5.3	Z 25 x 15 x 0.8	43.9	0.268	BROKEN
7.2	Z 30 x 20 x 1.5	101.0	0.457	INTACT
7.3	Z 30 x 20 x 1.5	101.0	0.457	BROKEN
11.2	Z 50 x 25 x 2.0	190.1	0.613	INTACT
11.3	Z 50 x 25 x 2.0	190.1	0.613	BROKEN
12.2	FLAT 25 x 4.0	100.6	0.456	INTACT
12.3	FLAT 25 x 4.0	100.6	0.456	BROKEN

TABLE 1 PANEL CONFIGURATIONS INVESTIGATED

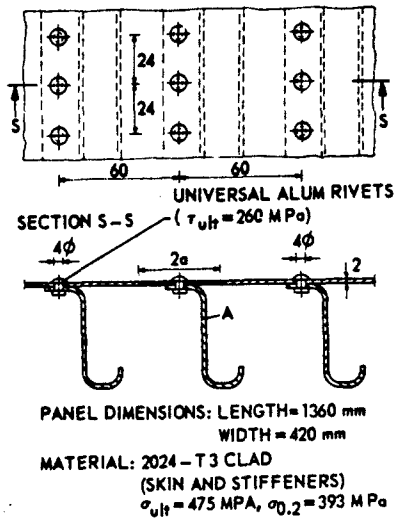

FIGURE 1 STIFFENED PANEL DIMENSIONS (mm) AND PROPERTIES

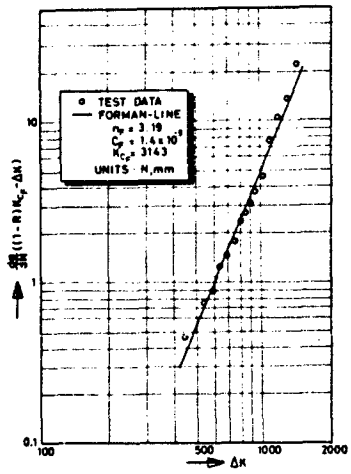

FIGURE 2 FORMAN DIAGRAM UNSTIFFENED PANEL 1A

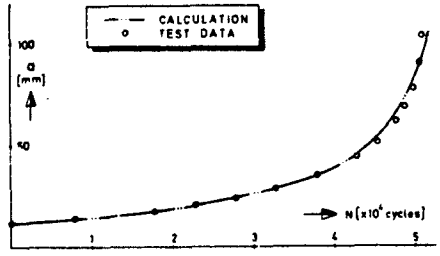

FIGURE 3 CRACK PROPAGATION CURVE UNSTIFFENED PANEL 1A

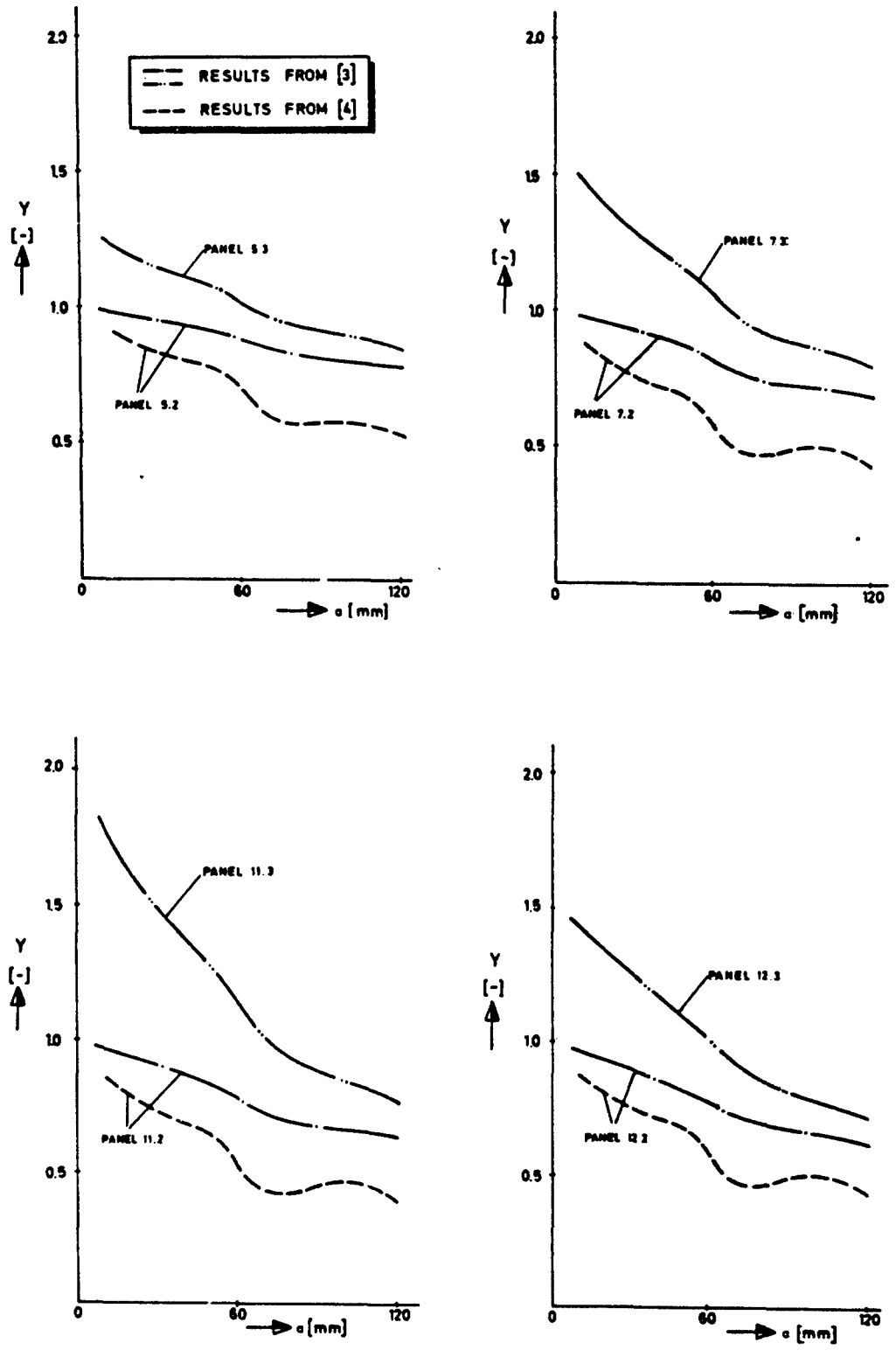

FIGURE 4 CORRECTION FACTOR Y. COMPARISON OF RESULTS FROM [3] AND [4].

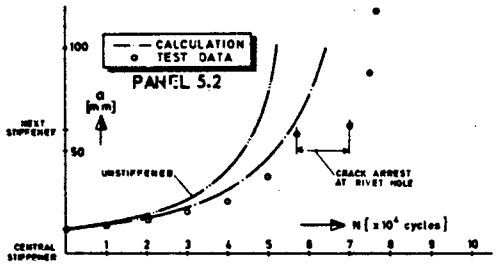

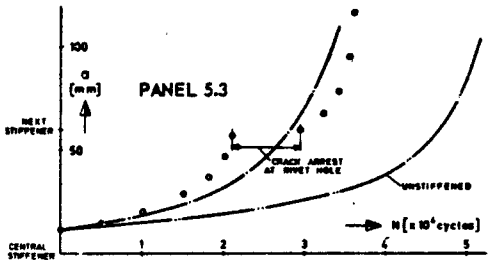

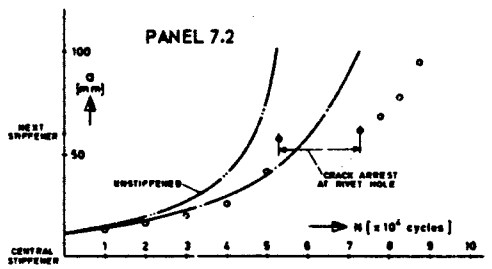

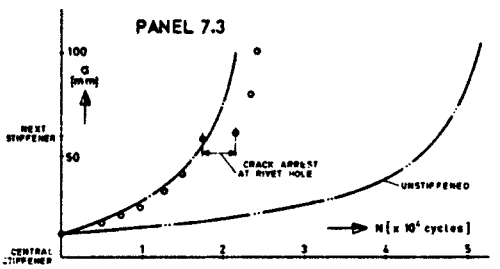

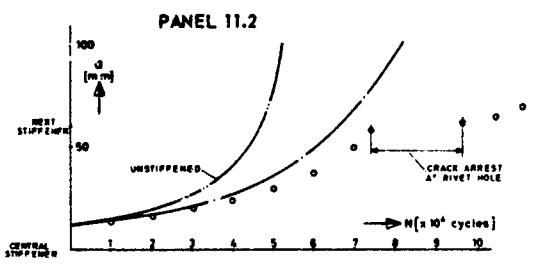

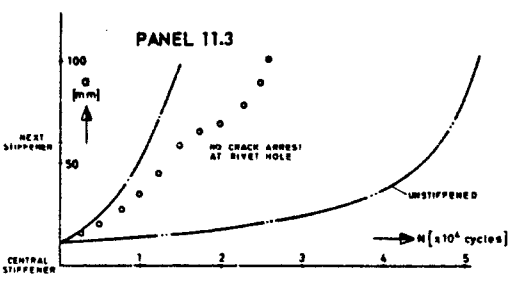

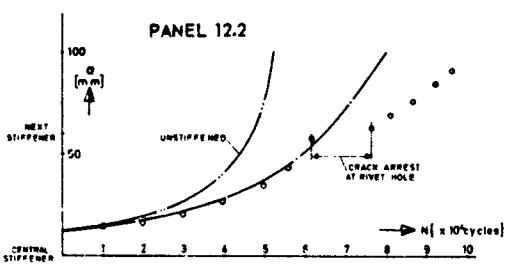

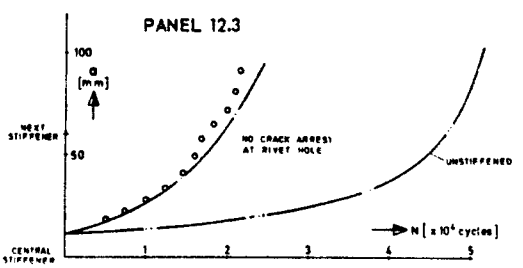

FIGURE 5 COMPARISON OF CALCULATED CRACK PROPAGATION CURVE WITH TEST DATA (SEE ALSO TABLE 1)

EXAMPLE PROBLEM 3.4.2.7

CRACK PROPAGATION ANALYSIS OF PRESSURIZED FUSELAGE STRUCTURE

L. Schwarmann
Vereinigte Flugtechnische Werke-Fokker GmbH
Bremen, Germany
(Literal)

1. STATEMENT OF THE PROBLEM

Crack propagation test results of a pressurized fuselage structure, in which different artificial cracks had been made, were compared with corresponding analytical results. The crack propagation rates have been calculated by using the so-called Forman diagram, which has been derived from test results of a flat, centre-cracked panel.

2. DESCRIPTION OF STRUCTURE AND TESTING DETAILS

The fuselage structure consists of a curved sheet (radius of curvature = 1435 mm, sheet thickness = = 0.8 mm) with riveted frames and bonded stringers, see Fig.1. The fuselage structure was manufactured from 2024-T3 clad material. Three different crack configurations have been considered (see Figure 1), viz.,

(i) Crack A (the crack is located in the sheet between two intact frames)
(ii) Crack B (the crack is located in the sheet below a frame. The strip and part of the clip have been cut).
(iii) Crack C (the crack is located in the sheet below a stringer).

The fuselage structure was loaded by constant amplitude internal pressure of $\Delta P = 470$ mbar under laboratory conditions.
All cracks have been made in the shell in the longitudinal direction. Tests and calculations start at total initial crack lengths of $2a_i = 50$ mm. The cracks were measured visually after applying internal pressure.

3. ANALYSIS METHOD

3.1 Crack propagation behaviour

The crack length 'a' as a function of the applied load cycles N was calculated by the following equation [1]

$$a = a_i + \int_{a_i}^{a} \frac{da}{dN} \tag{1}$$

The material behaviour, as far as crack propagation was concerned, was measured from constant amplitude tests of flat panels, the results of which are shown in Fig.2. The crack propagation rates for the fuselage structure can be found from Fig.2, provided that the range of stress intensity factor

$$\Delta K = \Delta P \sqrt{\pi a} \cdot Y_V \cdot Y_C \tag{2}$$

for the fuselage structure is known.

3.2 Correction factors

The correction factors in equation (2) have been determined as follows:

- Influence of frames → Y_V

  This correction factor has been calculated by using an existing computer programme [2], which has been developed based on the investigations of Poe [3] and Swift [4]. The results of the calculations are given in Fig.3.

- Influence of curvature → Y_C

  The influence of curvature and internal pressure has been taken into account by applying the following equation [5]:

$$Y_C = \frac{R_C}{t} \sqrt{1+1.61 \frac{a^2}{R_C^2} 50 \tanh \frac{R_C}{50\, t}} \tag{3}$$

  where R_C is radius of curvature and t is shell thickness.

4. TEST-ANALYSIS CORRELATION

From the comparisons of measured [6] and calculated crack propagation behaviour, see Fig.4-6, the following statements can be made:

- Crack A (see Figure 4)

  The analytical and test results conform with each other extremely well.

- Cracks B, C (see Figures 5 and 6)

  The analysis yields conservative crack propagation results as compared with test results. Taking into account possible scatter of material behaviour, as far as crack propagation is concerned, one can conclude that the recommended

analytical procedure enables the stress engineer to predict crack propagation rates of fuselage structure loaded by constant amplitude internal pressure.

5. REFERENCES

1. Schwarmann, L., et.al., "DAMTOL - A computerprogram for damage tolerance analysis" VFW-Fokker, not published.

2. Handbuch Struktur Berechnung, Band 2, Struktur Blatt 63611, "The influence of stiffeners on crack propagation and residual strength" IASB, Munich, 1975.

3. Poe, C.C., "Stress intensity factor for a cracked sheet with riveted and uniformly spaced stringers" NASA TR R-538, 1971.

4. Swift, T., "The effect of fastener flexibility and stiffener geometry on the stress intensity in stiffened cracked sheet" Douglas paper 6211, Delft, 1974.

5. Hahn, G.T., et.al., "Criteria for crack extension in cylindrical pressure vessels" Int. Journal of Fracture Mechanics, Vol.5, 1969, pp. 187-210.

6. VFW-Fokker GmbH report, "Evaluation of stress intensity factor of cracked fuselage structures" ZTL 2.01/5, Ministry of Defence, 1973.

6. COMMENTARY

This example demonstrates that the growth of longitudinal cracks in a pressurized fuselage structure (spacing of riveted frames is approximately 500 mm) can be predicted in a conservative (and not too conservative) way by applying fracture mechanics principles. The cracks in this example appear to become unstable at a total length of approximately 140 mm, so that possible arrest of the stably growing crack at the next frames (see the previous example) plays no part.
The crack propagation rates in the stiffened curved structure have been determined using the ΔK-da/dn relation of an unstiffened panel and correcting the stress intensity for the influences of frames and curvature. The correction due to the presence of the frames has been calculated by means of a computer programme especially developed for that purpose earlier [2] . This procedure is preferable to determining the effect of the stiffeners on the stress intensity using curves published in the literature, because these curves generally do not completely apply to the problem to be solved. Further, the effects of, for example, eccentricity, attachment flexibility, yielding of stiffeners and/or attachments are usually not accounted for in available stress intensity curves.

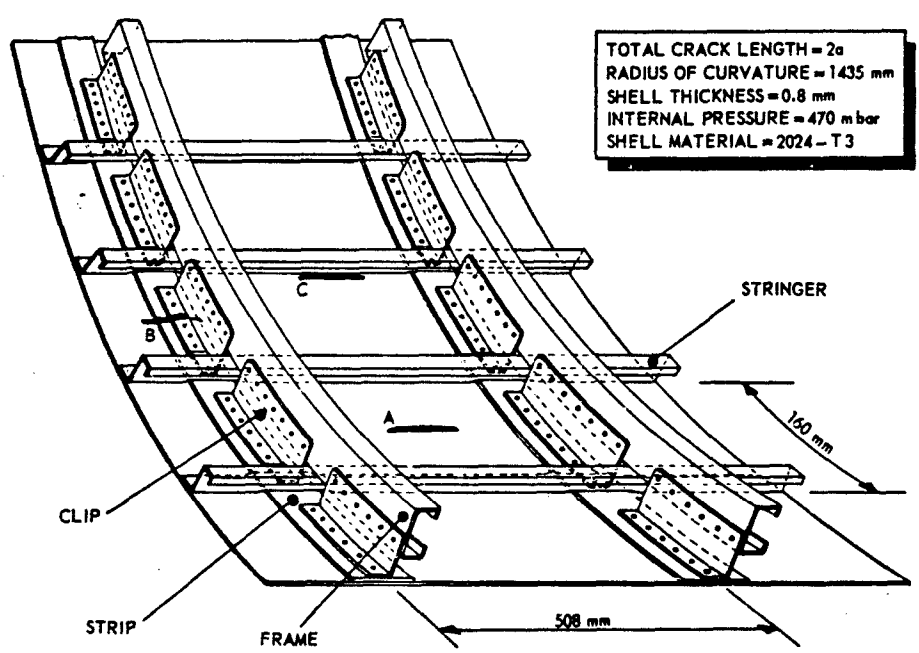

FIGURE 1 FUSELAGE STRUCTURE. CRACK CONFIGURATIONS

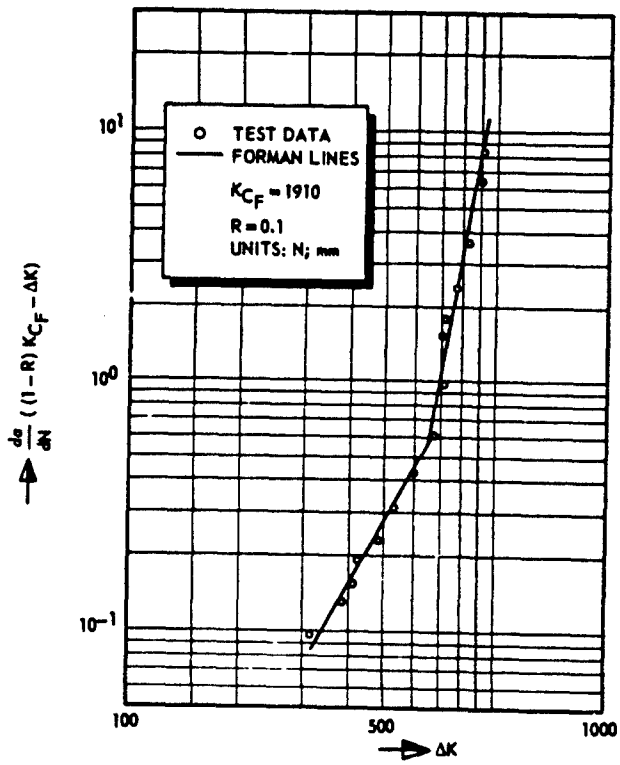

FIGURE 2 FORMAN DIAGRAM

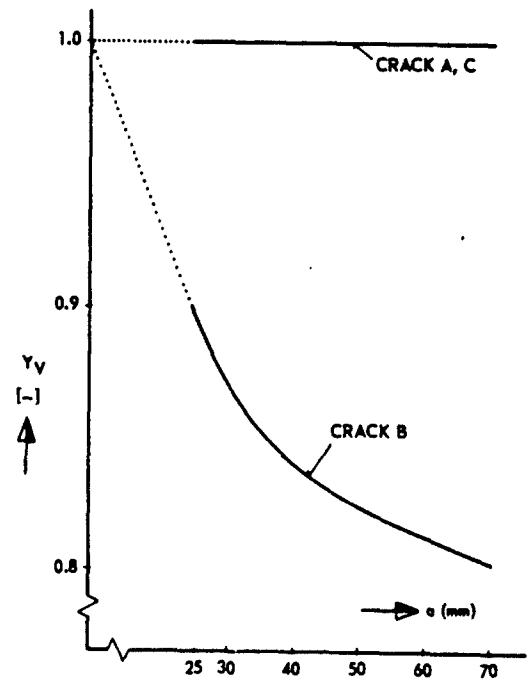

FIGURE 3 CORRECTION FACTOR DUE TO THE PRESENCE OF FRAMES

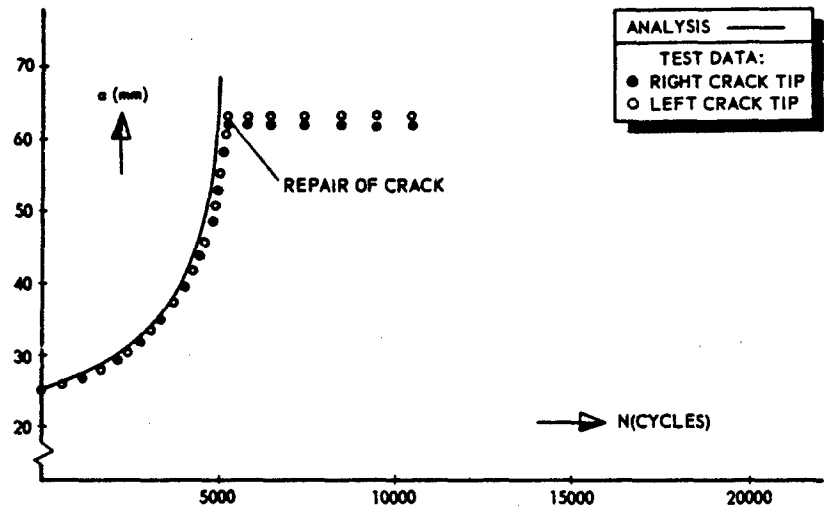

FIGURE 4 CRACK PROPAGATION BEHAVIOUR. CRACK A

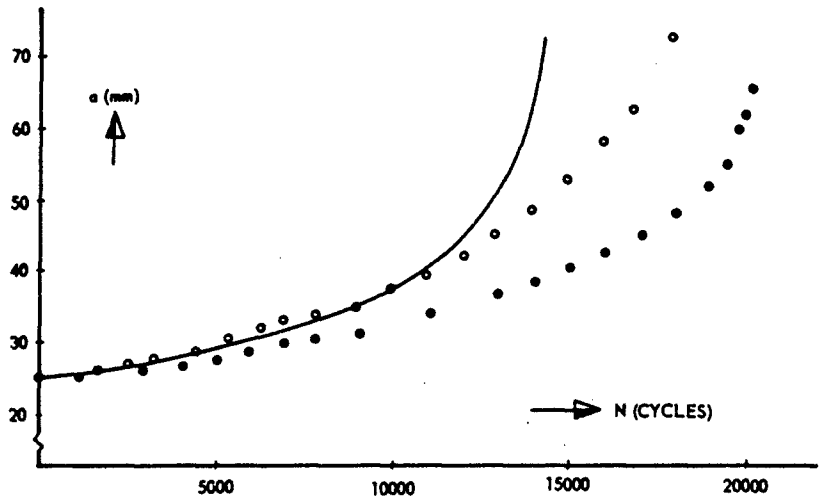

FIGURE 5 CRACK PROPAGATION BEHAVIOUR. CRACK B

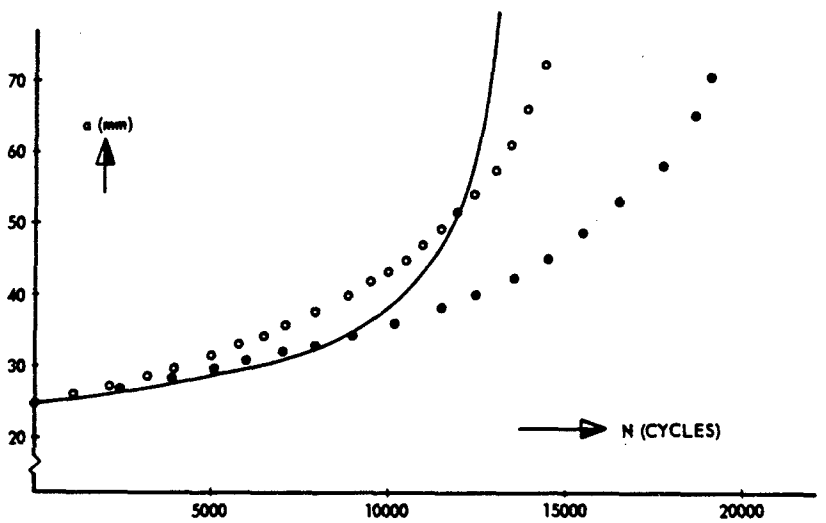

FIGURE 6 CRACK PROPAGATION BEHAVIOUR. CRACK C

EXAMPLE PROBLEM 3.4.2.8

FATIGUE CRACK PROPAGATION IN STRUCTURES WITH RIVETED STIFFENERS

A. Salvetti

Institute of Aeronautics
University of Pisa
Italy
(Literal)

FOREWORD

Although this note, strictly speaking, does not represent an example of application of fracture mechanics in design, it has still been included as a contribution to this handbook because it deals with the significant problem of the effects of fastener connection flexibility on the stress intensity factor (Editor).

1. INTRODUCTION

Recent developments in military specifications concerning safety with the introduction of "damage tolerant" structures as well as the contractual requirement on the use of sophisticated crack control techniques in spacecraft design have spurred research into cracked structure behaviour by favouring its growth out of the already large field of commercial aviation. Within that field of research the problem of fatigue crack propagation in stiffened structures is of particular importance because of its role in the structural design of air- and spacecraft. A correct solution of the problem is quite difficult even with constant amplitude loading because of the uncertainty connected with evaluation of the stress intensity factor.
In fact the value of the stress intensity factor relative to a given crack length depends mainly on the value of the mutual forces between stiffeners and skin and therefore it is possible to evaluate K correctly only when those forces can be determined with reasonable accuracy. This accurate theoretical determination is not easy because of the difficulty of representing the behaviour of the joining elements properly. In the case of a riveted joint, the rivet is considered as rigid element so there can be no relative displacement between the center of the holes in the skin and in the stiffener; this assumption allows a rather easy determination of mutual forces and then of K [1,2] .
Comparison with experimental data [3] has shown that the assumed pattern may be too unconservative for skin cracks (while being the opposite for stiffener cracks) since it gives too large rivet forces. In order to assume a better model the rivet was considered as an elastic element which allows some relative displacement between the centers of the holes; the value of rivet flexibility was also estimated by generalizing experimental results relative to riveted joints[4,5] and then fitting the experimental formulae into numerical models developed to evaluate K. The results which were obtained in such a way were not checked with the measured values of rivet forces for cracked stiffened structures. Therefore the proposed formulae do not seem to offer the same reliability in the different structural situations found in design practice.
This conclusion also stems from the intrinsic difficulty of formulating a reliable scheme of stiffener skin joint behaviour. Actually the mechanism of the so-called rivet flexibility, which depends upon the deformation of both rivet and hole is not fully understood. The global deformation (which also depends upon rivet type and setting) has different characteristics depending on whether it works in the elastic domain or shows local plastic regions around rivet holes due to the contact of the rivet on the hole edge. In the latter case characteristics are hard to determine. Friction forces which arise from skin stiffener contact because of rivet pressure further increase the difficulty of the problem.
In such a situation it is obvious that developing reasonably reliable methods for the prediction of crack growth rate in stiffened structures by theoretical evaluation of K requires research into the behaviour of those structures based on a set of experimental data covering the different structural situations of technical interest. On that ground, the Institute of Aeronautics, University of Pisa, as part of a wider research on the fatigue behaviour of cracked stiffened structures, has taken up the problem of defining the influence of structural configuration (stiffener geometrical shape, rivet type, crack starting point) upon crack growth. With this aim many fatigue crack propagation tests have been completed on stiffened panels of different configuration, and results have been processed using theoretical formulations of the K factor based on increasingly sophisticated models (rigid rivet, flexible rivet, taking friction into account). Through this work it has been possible to reach a classification of the behaviour of stiffened panel configurations explaining, at least qualitatively, the role played by the joint in the crack growth.

2. RESEARCH AIMS AND METHODOLOGY

The need to evaluate da/dn in stiffened structures with the same accuracy as in plates requires a knowledge based on experimental data of the mechanism through which the load is transferred from plate to stiffener (Fig.1,2). This knowledge can be gained essentially in two ways: a direct one based on measuring the forces which are exchanged between the two elements of the stiffened structure; an indirect one based on comparing results of crack propagation tests in stiffened structures and flat specimens and using for the stiffened structure a value of K given by increasingly sophisticated models of the riveted joint.
The first way is very accurate since it allows an evaluation of each rivet contribution to a K factor and also shows the distribution of mutual forces between rivets and the magnitude of the friction forces. However, it requires a large experimental effort in order to acquire all the meaningful data even for a single stiffened panel. Considering also the influence of random variables on the problem, it follows that a rigorous use of the direct way would cause a large waste of time and money.
The second method, which is based upon the relationship

$$\frac{da}{dn} = F(\Delta K, R) \qquad (1)$$

can only give global information showing the kind and the magnitude of the error affecting K [9] ;

however, it has the advantage of requiring reduced test time and costs if an efficient technique for testing and data evaluation has been previously developed. Therefore this method offers the possibility of gaining with reasonable experimental effort sufficiently wide information on the influence of different parameters concerning the geometrical shape and the type of joint.
At present both those methods are being developed at the Institute of Aeronautics, University of Pisa, as part of a wider research concerning the fatigue behaviour of cracked stiffened structures.
The first method, based on strain gauge measuring [7] has been used with some panel configurations with the multiple aim of setting up the method, getting an early picture of the force scattering among similar rivets relative to a given panel shape and comparing the force variation induced by crack growth with the different theoretical forecasts. The results of that early investigation, given in [7] , showed the variation in behaviour of the joint depending upon stiffener and rivet shape and emphasized the importance of the random effects induced by rivet setting.
From that point on the second method, which is employable on a wide range of structural configurations and required reasonable technical times, has been used to probe further into the problem. The first method may be used again for refinements and quantitative evaluations found at a later stage of the research.
In particular the research has followed both a theoretical and an experimental direction which interact and complete each other in reaching the desired aim. First of all, a modular numerical program has been prepared in order to process rationally and immediately the results of crack propagation tests on stiffened panels under constant amplitude loads. The first module of the program gives K as function of semi-crack length "a" for a given panel on the basis of increasingly sophisticated models: rigid joint, flexible joint, joint with friction. The flexible joint was modelled using the results of a stress and strain elastic analysis of the rivet hole contour taking simplifying assumptions like "hole wall free to warp and loaded with a given force distribution" [10] . The hole edge deformation given by this approach is much larger than that of the rivet, which is assumed to behave like a short beam, and may be considered as the only cause of joint flexibility. This approach, even though it is based on very strong simplifying assumptions, may give an acceptable size order of flexibility value and then of K. This analysis is meaningful since it gives a rational starting point for analysing experimental data on crack propagation towards more accurate formulation of the flexibility problem based on empirical corrections suggested by comparing the variation of da/dn as function of ΔK given by equation (1) with the one found using experimental values of da/dn and computed values of ΔK.
The evaluation of the friction effect on transferring forces from skin to stiffener is done at a preliminary stage, by replacing the continuous distribution of forces on the contact area by concentrated forces acting on chosen points and imposing strain consistency at those points as long as friction forces are less than dislocation limit values, while imposing constant friction forces beyond the dislocation limit condition. Evaluating the limit condition also depends upon the friction coefficient and the normal pressure between contact surfaces. In the absence of better experimental knowledge, K is calculated as a function of that pressure. About the meaning of those evaluations obviously the same considerations as in the case of the flexibility program hold.
The second module, using experimental a-n data, computes da/dn and, using the data from the first module, computes log da/dn = F (ΔK). With that processing technique and using the experimental results explained in the next section, curves da/dn = F (ΔK) were obtained for plain sheets (in this case they are supposed to give the correct trend of F) as well as for stiffened panels using in the latter case three different approaches in order to obtain K. By comparing the two kinds of data, those referring to plain sheets and those relative to stiffened panels with the rigid joint approach, the correction which must be given to K in order to regularize F for the stiffened panel can be evaluated. Afterwards that correction is interpreted in terms of flexibility and friction effects. Results which can be obtained by this methodology are discussed later.

3. EXPERIMENTAL PROGRAMME

The experimental side of the research consisted of a set of crack propagation tests on panels with and without stiffeners under an axial constant amplitude pulsating load. Tests are aimed at obtaining the propagation curve a = f (n), that gives for each crack length the number of load cycles which is necessary to produce it.
The specimens used for testing were panels of different geometry, with and without stiffeners, made of 2024-T3 and 7075-T6 alloys. They can be subdivided according to their geometrical shape into (see Table 1):
- stiffened panels with [-shaped stiffeners
- stiffened panels with strip stiffeners on one side
- stiffened panels with strip stiffeners on both sides
- unstiffened panels.

The joint between skin and stiffeners was made by hand clinched rivets. It was also necessary to differentiate joint geometry since both universal-head and countersunk-head rivets were used.
In each panel a crack is started by a notch artificially made with a thin small saw normal to the direction of the applied load. In the stiffened panels the crack was introduced between two joint rivets starting from the junction line (see Table 1).
Table 1 gives the panel configurations investigated with the main dimensions. Full details of test results can be found in [11] . All the panels were tested at the fatigue laboratory of the Institute of Aeronautics, University of Pisa following procedures given in [6] . All the results were processed according to the method described before [11] and they are summarized in the next section.

4. ANALYSIS OF FATIGUE TEST PROCESSING RESULTS

The results of the comparison of 52 da/dn-K curves, 42 of which are relevant to the stiffened panels (see [11]), are given in this section.
The analysis was divided into consecutive stages. At a first stage all the curves da/dn-K relevant to stiffened panels, with the assumption of rigid riveted joint, were divided into groups according to panel material and were compared with average curves (obtained as "Best-Fit" of da/dn-K data) of plates of the same material. Such a comparison (summarized in Fig.3) was used for an early check on the applicability of equation (1) to stiffened panels with the assumption of a rigid joint for evaluating K. The situation appears to be extremely scattered as can be seen on comparing the typical scatter band, showing confidence levels of 95 % and 99 % reached by a statistical analysis of sheet data made with the linear regression

technique [5] , and the scatter band for stiffened panels given by simply enclosing all the data between two lines parallel to the plate average curve (it was neither easy nor reasonable at that comparison stage to process statistically da/dn-K data relative to stiffened panels). The scatter band of stiffened panels is approximately in the ratio of 5/2 to the scatter band of sheet and is not symmetric as to plate average line. All that shows the presence of systematic errors (obviously due to the inadequacy of the rigid joint model) which can bring errors of different importance, depending upon panel geometry and rivet type, into K computation. In order to explain better this kind of systematic influence, a comparative analysis was taken of the K-da/dn curves, still assuming a rigid joint at the processing stage. It followed from the analysis that the curves, while looking scattered in a random way, actually behave systematically according with rivet type, stiffener shape and global joint geometry (stiffener plus rivet). Stiffened panel curves representing each single situation were compared in order to show up any peculiar characteristics of da/dn-K curves which could indicate qualitatively the kind of error affecting K and therefore could suggest which correction should be given to that quantity.

A first remark concerns the possible shape that F can have for stiffened panels as compared to unstiffened sheets. In the latter case (Fig.4a) both da/dn and K are increasing functions of "a" so that on a da/dn-K curve each point represents a definite value of the crack length. For stiffened panels (Fig.4b) both da/dn and K show subsequent maxima and minima due to stiffeners, so that the same point of the da/dn versus K curve may correspond to more than one value of crack length. With those conditions many anomalies of the curve da/dn-K are possible, due both to schematic errors in the numerical method for K (Fig.4b) and to small errors in evaluating da/dn due to data processing (Fig.4c).

In all those cases the da/dn-K curve is no longer unique (against the basic assumption of an unequivocal relation between da/dn and K) and it takes the shape 4b II, when underestimating K, or the shape 4b III when overestimating it. If there are small errors in the computation of da/dn, curves show the typical loops of Fig.4c. In general both causes may be present and consequently trends are possible which differ a little from the basic two given in Fig.4.

That being stated, the analysis based on the use of the factor K for a rigid joint showed the following effects:

a) Effects of rivet type and material

Fig.5 shows da/dn-K curves for two sets of stiffened panels which have the same geometrical shape but one having universal-head rivets and the other countersunk-head rivets. It is clear from the comparison that curves for countersunk-head rivets are shifted towards lower values of K under the same value of da/dn; that means that the theoretical solution is more deficient for countersunk-head rivets than for universal-head rivets. In other words, because of joint flexibility the stiffeners are less loaded than in the case of a rigid joint; therefore the actual stress intensity factors are larger than the one given by theoretical analysis. That "flexibility" effect is even more emphasized in the countersunk-head rivet joint. That effect appears to be affected by the material choice, as shown in Fig.6.

b) Stiffener geometry effect

The comparison of curves relating to panels which differ only in stiffener shape, having either a single strip stiffener or one with double strips, shows that the single strip panel behaves in a more flexible way (see Figure 7).

Panels with [-shaped stiffeners also behave in the same way as the single strip panels if K is evaluated taking into account stiffener flexural deformations due to eccentricity of the rivet force line of action. That effect can be computed closely through an "area reduction" to obtain "equivalent" strip stiffeners which should have the same deformations in the region where loads are transmitted as for actual stiffeners under the same load condition [6] .

c) Stiffener-rivet geometry effect

The comparison of results given up to this point and processed under a rigid joint assumption shows a different behaviour for the sheet average curve when the stiffener-rivet system is changed.

That situation is summarized in Fig.8, which shows the scatter bands containing results belonging to each geometry. In more detail it can be noted that double strip joints are the most rigid. Single strips and shaped stiffener joints with universal-head rivets are next, while single strip joints with countersunk-head rivets have high flexibility. Also it can be seen from Fig.8 that a double strip joint is more efficient in stress intensity factor reduction than it could be expected from the rigid joint assumption which was used to calculate K. That efficiency increase is most probably due to two concomitant causes. First, joint geometry, by giving considerably uniform contact pressure along the rivet hole axis, minimizes the deformation of the hole surrounding region for a given rivet force and shifts the beginning of transition to plasticity towards higher values of rivet forces; both those effects make the joint less flexible.

Second, friction forces of substantial importance are present due to the extent of contact surfaces which help rivets in conveying the load from cracked sheet to stiffener.

Obviously those two factors (i.e. flexibility and friction) have opposite effects on stiffener efficiency and consequently on K value. Results in Fig.8 show that friction has a prevailing effect since all the scatter band is on the left of the sheet average line. On the contrary the flexibility effect prevails in all the other rivet-stiffener configurations and that happens because of the lesser contact surface which lowers, under the same friction force, the friction force maximum and because of probable strong variability of contact pressure on hole walls in the axial direction of rivets which is inclined to increase hole deformation where pressure is higher, and to anticipate transition to plasticity under the same rivet force as in the symmetric case.

Concluding this discussion it can be noted that the analysis based on rigid joint assumption, even though it does not allow an accurate evaluation of K and therefore of da/dn, is an efficient tool to show and to classify the different anomalies which characterize the phenomenon. On the ground of those conclusions it was decided to undertake a new data evaluation organized in the following way:

K was evaluated

- for single strip and shaped stiffener panels with universal- and countersunk-head rivets accounting for flexibility, but not for friction,
- for double strip panels accounting for friction, but not for flexibility.

The results of that new evaluation are given in Fig.9 and 10. The left side of Fig.9 shows the typical change of curves da/dn-K when taking flexibility into account. The flexible joint curve shows substantial

improvements both qualitatively and quantitatively so that sheet propagation data (average curve) can be transferred to the stiffened panel with K values so calculated without introducing notable errors. That is further corroborated by data given in the two other diagrams of Fig.9 where the two scatter bands which are the envelope of all the da/dn-K curves worked out with the two assumptions of rigid and flexible joint, are compared. The flexible joint scatter band is very small and of the same magnitude as that of the unstiffened sheet; however, it is not perfectly symmetric about the sheet average line, and that agrees with the fact that the theoretical analysis of flexibility at present does not make any distinction between universal- and countersunk-head rivets. On the contrary they have different flexibility as shown by the experimental results. Fig.10 deals with double strip panels and compares the results of the analysis of rigid joint assumption with and without friction forces; in this case substantial improvements both in curve shape and in scatter band are apparent.
The two last figures are very heartening since they show the possibility of reaching substantial improvements in technique for fatigue crack growth forecasting in aircraft stiffened structures. Obviously those results must be regarded as preliminary and K computation techniques here illustrated cannot be used yet for engineering design.
It is, however, necessary to acquire further experimental data using mainly the first of the two methods described in section 3 in order to reach a better understanding of friction mechanism and behaviour differences among joint types in terms of flexibility. It seems to be reasonable that a numerical model could be developed which would take into account friction and flexibility with technically acceptable approximation so that the substantial improvements in forecasting already given by the present method can be valid in any situation even for geometries which differ substantially from those examined in the present research.

5. CONCLUDING REMARKS

Fatigue crack propagation in stiffened structures is a very important problem at the present stage of aerospace technique development. It is therefore of great importance to have accurate methods in order to evaluate crack growth time in keeping with modern design techniques.
Through a theoretical and experimental research, carried out at the Institute of Aeronautics, University of Pisa, it has been possible to give some contributions to the solution of the said problem.
On the theoretical side, numerical models for evaluating the stress intensity factor have been improved by introducing both joint flexibility and friction forces relative to sheet-stiffener contact.
On the experimental side, many crack propagation tests on stiffened panels of different geometry and rivet type have been carried out.
The analysis of experimental results in terms of da/dn-K curves, where K was evaluated according to joint type, has allowed a first evaluation of stiffener geometry and rivet type effects (Fig.4-7) and has shown the limits of the numerical method for K evaluation based on rigid joint assumption.
The foregoing analysis, based on K values calculated assuming both joint flexibility and friction forces, has explained the very important role those two phenomena can play in forecasting techniques for fatigue crack growth.

6. REFERENCES

1. Poe, C.C. Jr., The Effect of Riveted and Uniformly Spaced Stringers on the Stress Intensity Factor of a Cracked Sheet. M.S. Thesis, Virginia Polytechnic Institute, 1969.
2. Lazzarino, L. and Salvetti, A., A Theoretical and Experimental Research on the Fatigue Behaviour of Reinforced Sheets Performed at the Institute of Aeronautics, University of Pisa. The Seventh Congress of the International Council of the Aeronautical Sciences, Rome 1970, ICAS Paper 70-35.
3. Salvetti, A., On the behaviour of Cracked Riveted Stiffened Panels Undergoing Constant Amplitude Fatigue Loading. Proceedings of the fifth International Conference on Experimental Stress Analysis, Paper 21, CISM Udine, 1974.
4. Swift, T., Application of Fracture Mechanics in the Development of the DC-10 Fuselage. In AGARDograph no.176, 1974.
5. Cavallini, G., Lazzeri, L., Determinazione sperimentale delle leggi semiempiriche della velocità di propagazione di difetti passanti. Ricerca sulla Meccanica della Frattura in strutture spaziali pressurizzate e soggette a fatica acustica, R-25, III Rapporto Quadrimestrale, Giugno 1977.
6. Salvetti, A., Frediani, A., Grassi, E., Theoretical and Experimental Research on the Fatigue Behaviour of Cracked Stiffened Panels. Final Technical Report - February 1973. European Research Office, United States Army, London W. 1 England. Contract DAJA 37-72-C-1783.
7. Salvetti, A., Frediani, A., Grassi, E., Theoretical and Experimental Research of the Fatigue Crack Propagation in Stiffened Panels. An Evaluation of the Paris Theory. Final Technical Report, September 1974 European Research Office, United States Army, London W. 1 England, Contract Number DAJA 37-73-C-2821.
8. Salvetti, A., Del Puglia, A., Fatigue Crack Propagation in Stiffened Panels. The Eighth Congress of the International Council of the Aeronautical Sciences, Amsterdam 1972. ICAF Paper nr.72-40.
9. Salvetti, A., Fatigue Behaviour of Cracked Stiffened Panels. AGARD Structures and Materials Panel. Specialists Meeting on Fracture Mechanics Design Methodologies, London, Sept. 1976.
10. Arrighi , L., Linzi, P., Ricerca teorico-sperimentale sul comportamento delle giunzioni rivettate in strutture tolleranti il danneggiamento. Tesi di laurea - Istituto di Aeronautica dell'Università di Pisa, A.A. 1976-77.
11. Anon., Raccolta dei risultati delle prove di propagazione di fessure CSF, CFP, ALP. Documenti Istituto di Aeronautica dell'Università di Pisa, 1977.

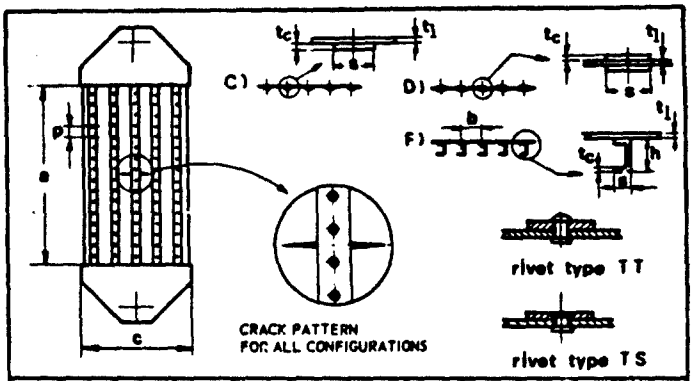

type	a mm.	c mm.	b mm.	p mm.	s mm	h mm.	t_1 mm	t_c mm	α_{c_s}	NUMBER OF PANELS 2024-T3	7075-T6
C_1	500	300	60	30	18.5	–	1.27	0 8	0.225	2	1
C_2	"	"	"	"	21.4	–	"	1.6	0.45	11	12
D_1	"	"	"	"	21.4	–	"	0.8	0.45	2	1
D_2	"	"	"	"	21.4	–	"	1.27	0.50	0	1
D_4	"	"	"	"	18.5	–	"	1.6	0.90	2	2
F_2	583	350	70	25	1.6	3 2	1.6	1.6	0.30	4	0
F_1	583	350	70	25	1.6	3 2	1.27	1.27	0.30	0	1

*$\alpha_c = \frac{A_{st}}{bt}$, WHERE A_{st} = STIFFENER CROSS-SECTIONAL AREA

TABLE 1 FATIGUE TEST PANEL GEOMETRY

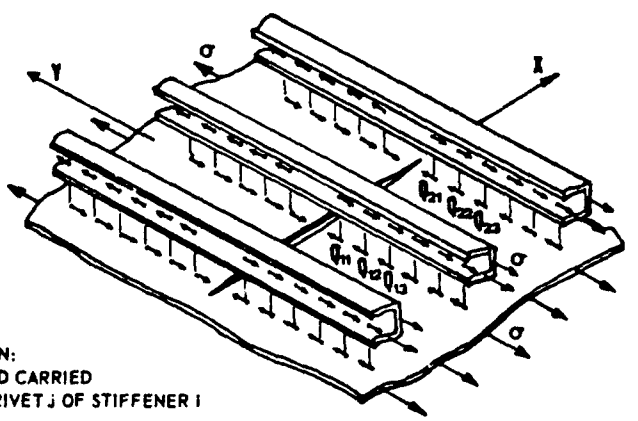

NOTATION:
Qij = LOAD CARRIED
BY RIVET j OF STIFFENER i

FIGURE 1 STIFFENED PANEL AS REDUNDANT SYSTEM

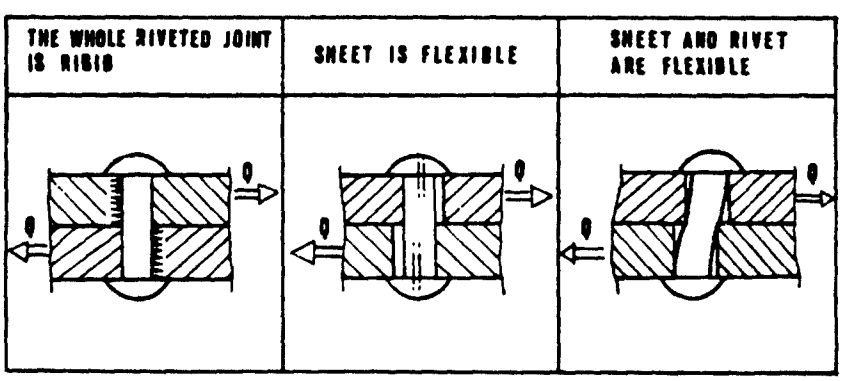

FIGURE 2 RIVETED JOINT WHEN LOADED

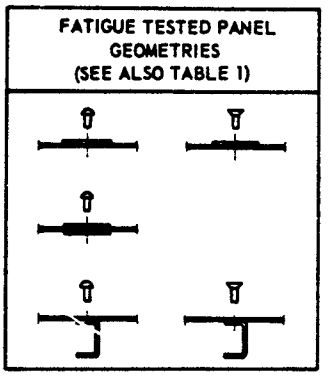

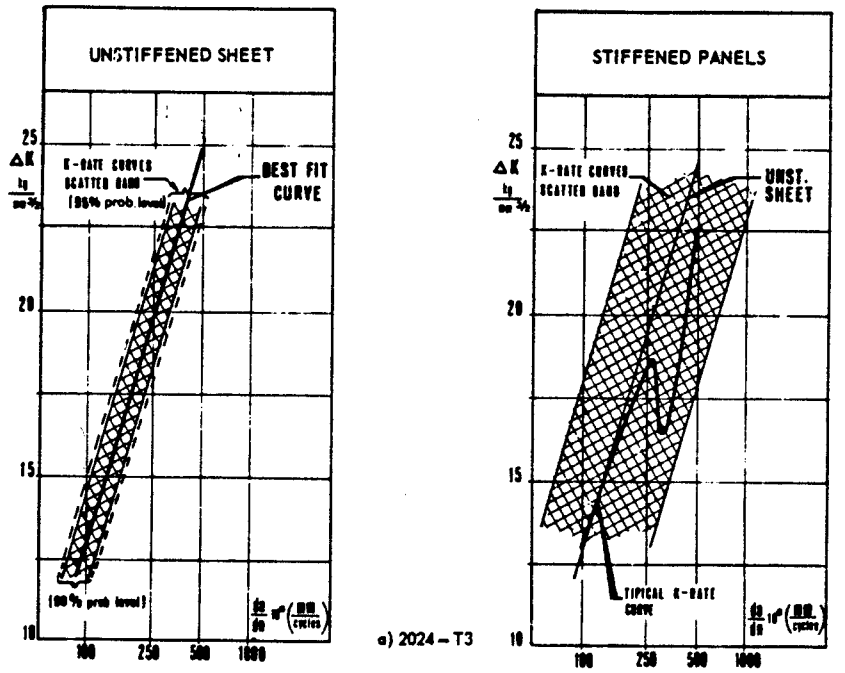

a) 2024 – T3

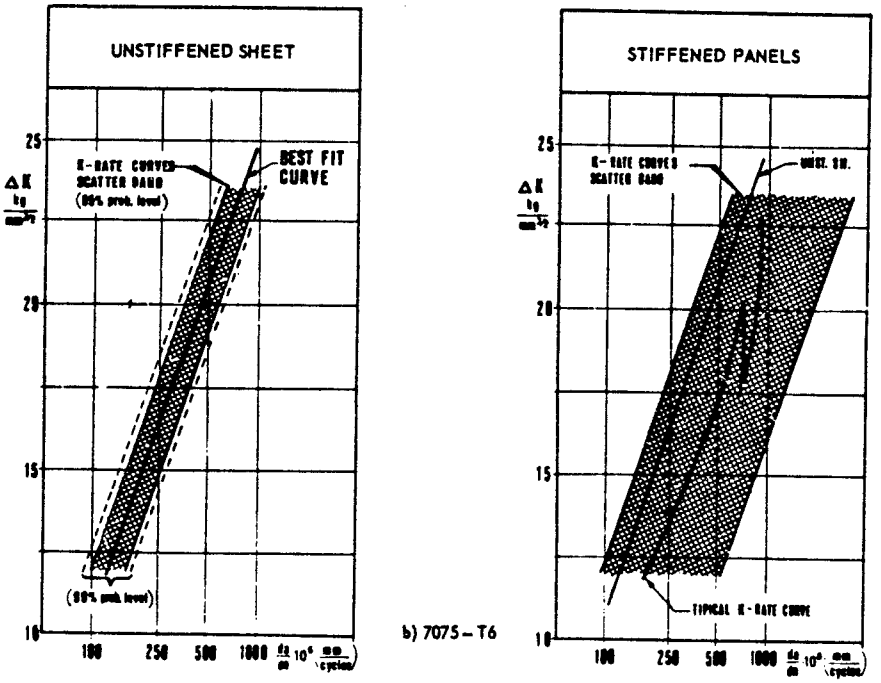

b) 7075 – T6

FIGURE 3 K – RATE CURVES SCATTER BAND

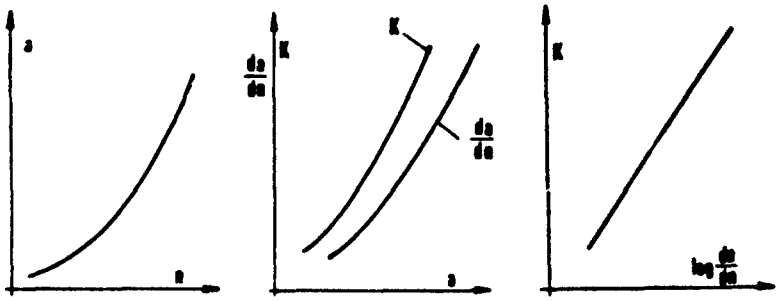

FIGURE 4a K – RATE CURVE OF UNSTIFFENED SHEET

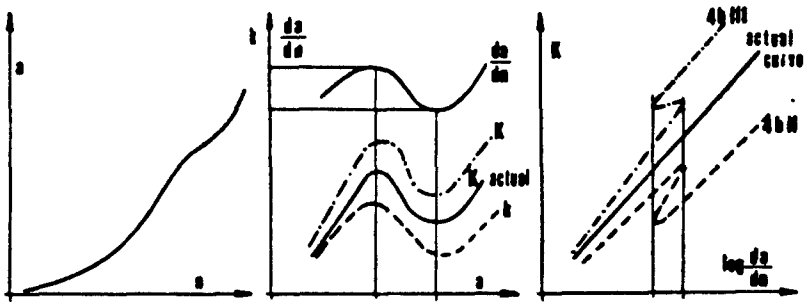

FIGURE 4b K EVALUATION AND K-RATE CURVE (Z-LIKE CURVE) OF STIFFENED PANELS

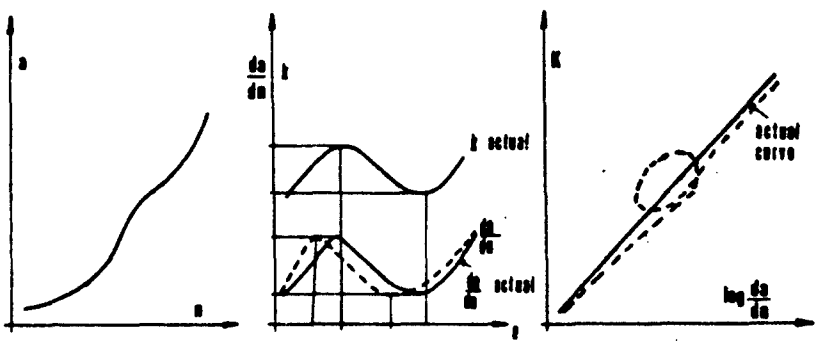

FIGURE 4c $\frac{da}{dn}$ EVALUATION AND K-RATE CURVE (LOOP-LIKE CURVE) OF STIFFENED PANELS

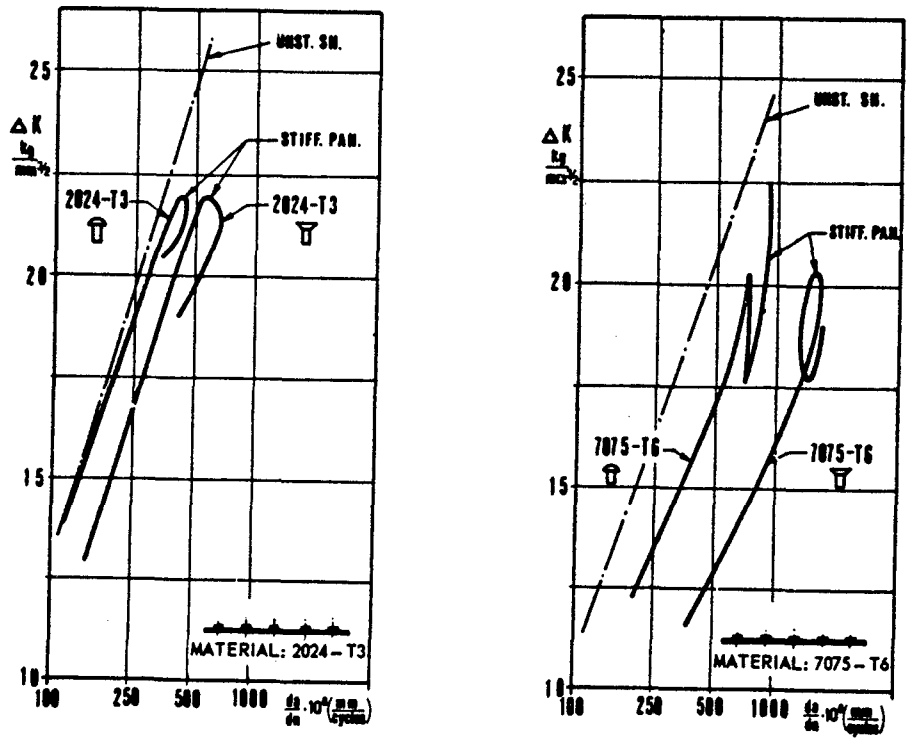

FIGURE 5 RIVET TYPE EFFECT

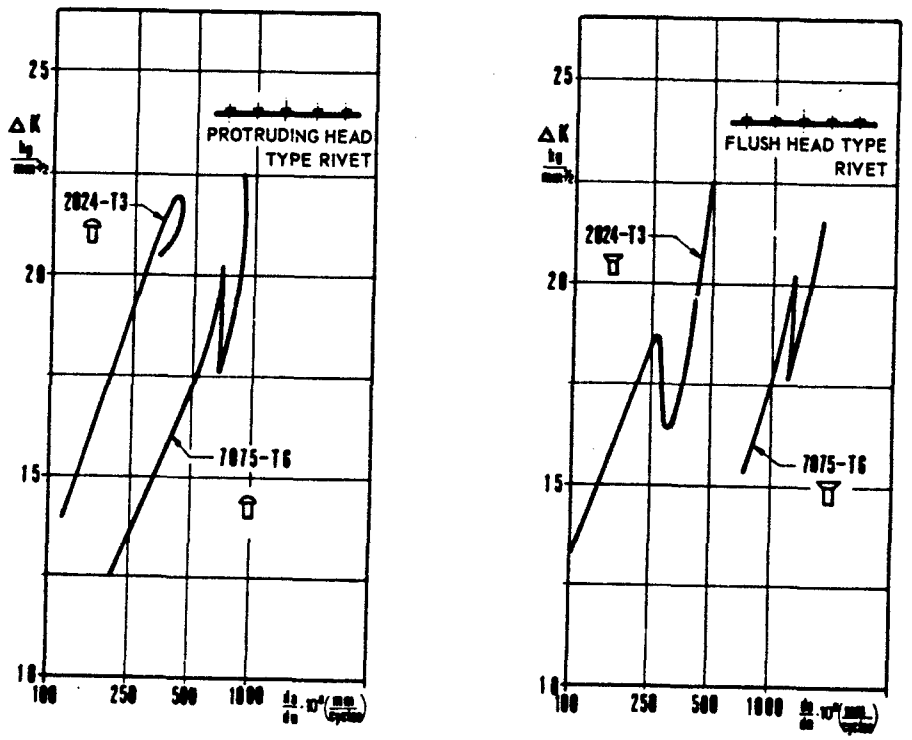

FIGURE 6 MATERIAL EFFECT

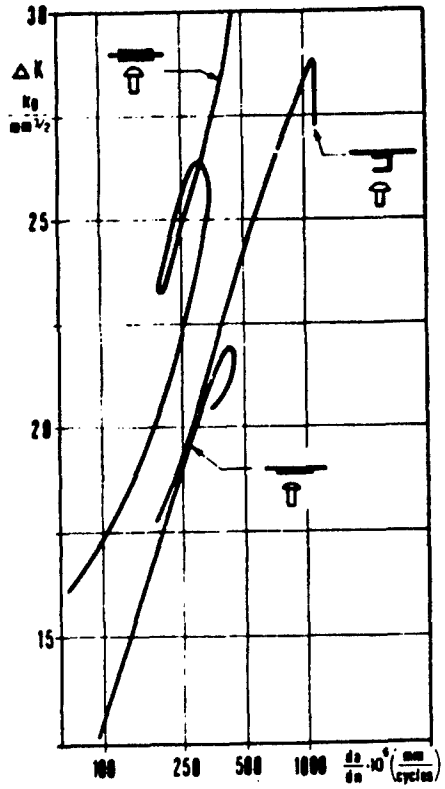

FIGURE 7 STRINGER GEOMETRY EFFECT (MATERIAL 2024 – T3)

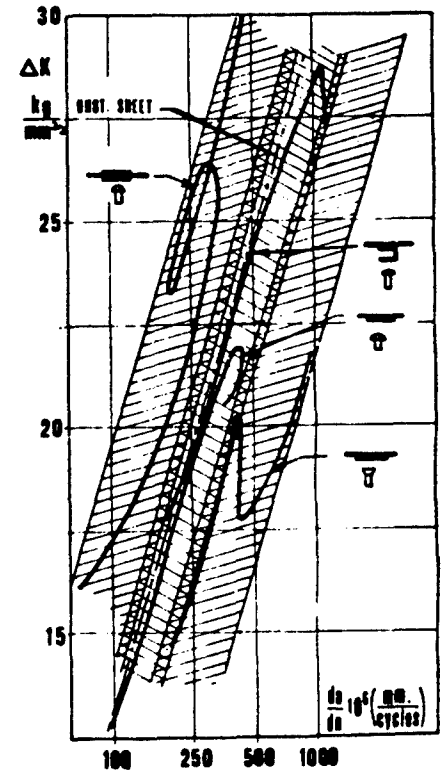

FIGURE 8 RIVETED JOINT GEOMETRY EFFECT (MATERIAL 2024 – T3)

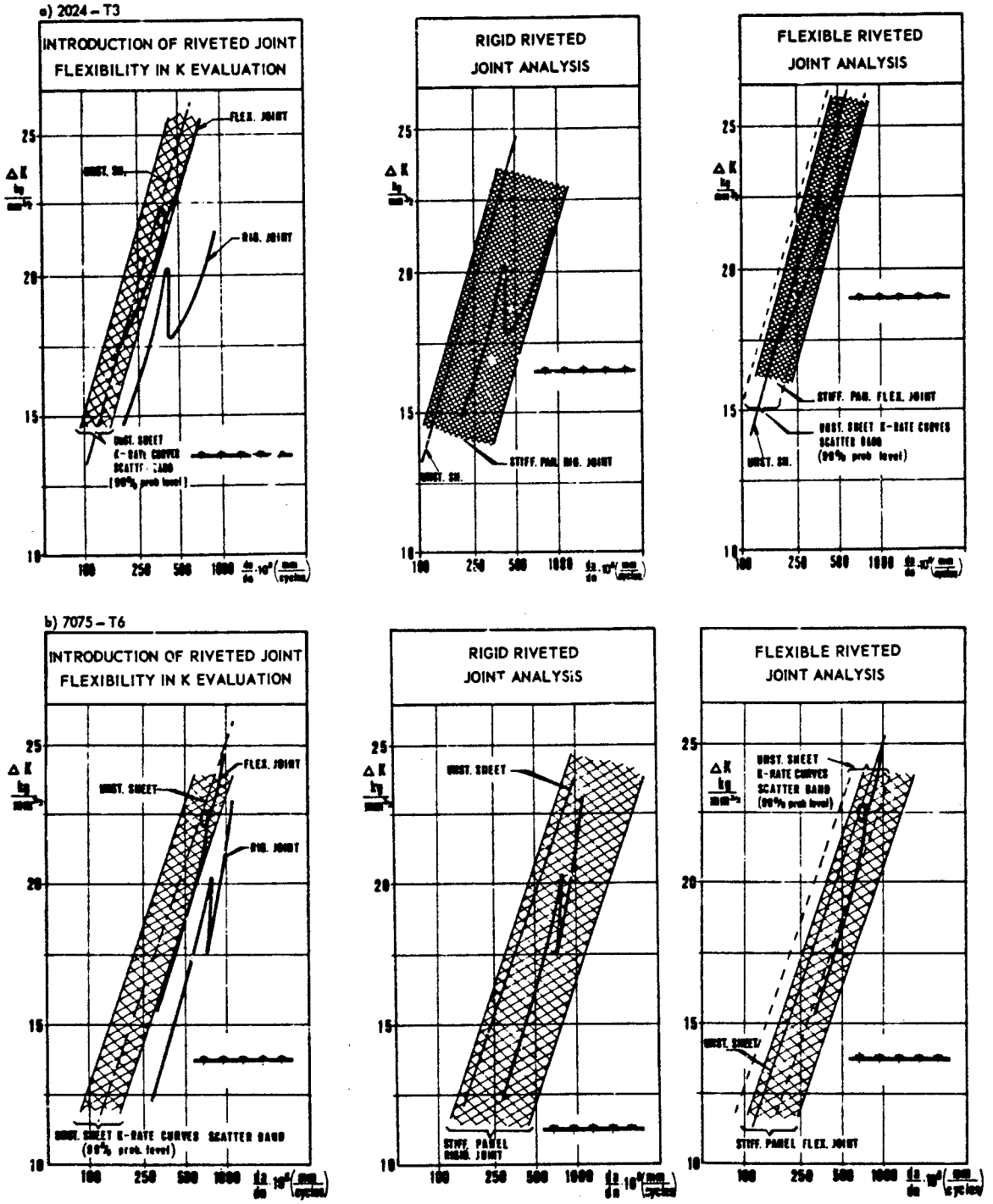

FIGURE 9 K – RATE CURVES SCATTER BANDS

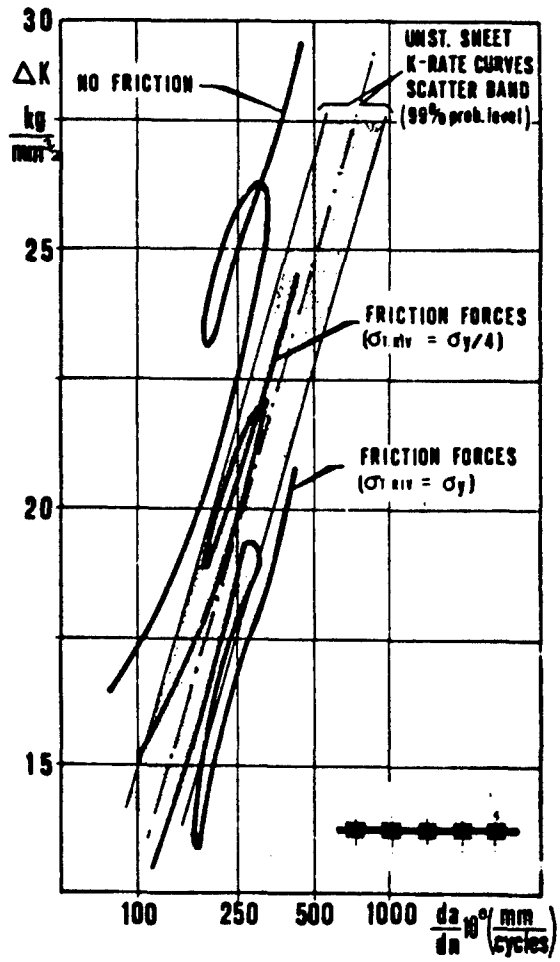

FIGURE 10 INTRODUCTION OF FRICTION FORCES IN K EVALUATION

3.5 REFERENCES

1. Broek, D., "Elementary engineering fracture mechanics", Noordhoff International Publishing, The Netherlands (1974).
2. Knott, J.F., "Fundamentals of fracture mechanics", Butterworths, London (1973).
3. Various authors, "Journal of strain analysis", Vol.10 (1975), pp 193-265.
4. Romualdi, J.P., Frasier, J.T., Irwin, G.R., "Crack-extension-force near a riveted stiffener", Naval Research Lab. Memo, Report no.4956 (1957).
5. Westergaard, H.M., "Bearing pressures and cracks", J.Appl.Mech., Vol.61 (1939), pp A49-A53.
6. Romualdi, J.P., Sanders, P.H., "Fracture arrest by riveted stiffeners", Proc.4th Midwestern Conf. on Solid Mechanics, University of Texas, Austin (1959), pp 74-90.
7. Romualdi, J.P., "Fracture arrest design considerations", Proc. of Crack Propagation Symposium, Cranfield (1961).
8. Romualdi, J.P., Sanders, P.H., "Dynamic considerations in fracture arrest by riveted stiffeners", Proc. 5th Midwestern Conf. on Solid Mechanics (1961).
9. Sanders, J.L.Jr., "Effect of a stringer on the stress concentration due to a crack in a thin sheet", NASA TR R-13 (1959).
10. Greif, R., Sanders, J.L.Jr., "The effect of a stringer on the stress in a cracked sheet", J.Appl.Mech., Vol.32 (1965), pp 59-66.
    Also: ONR Technical Report no.17, Harvard University (1964).
11. Bloom, J.M., Sanders, J.L.Jr., "The effect of a riveted stringer on the stress in a cracked sheet", J.Appl.Mech., Vol.33 (1966), pp 561-570.
    Also: ONR Technical Report no.20, Harvard University (1964).
12. Mushkelishvili, N.I., "Some basic problems of the mathematical theory of elasticity", McGrawhill Book Company, Inc., New York, N.Y. (1956).
13. Vlieger, H., Broek, D., "Residual strength of cracked stiffened panels", NLR Report S.653 (1967).
14. Isida, M., Itagaki, Y., "Stress concentration at the tip of a central transverse crack in a stiffened plate subjected to tension", Proc. 4th US Nat.Congr.Appl.Mech. (1962), pp 955-969.
15. Isida, M., Itagaki, Y., Iida, S., "On the crack tip stress intensity factor for the tension of a centrally cracked strip with reinforced edges", Dep.of Mech., Lehigh University, Bethlehem, Pa. (1965).
16. Isida, M., "The effect of a stringer on the stress intensity factors for the tension of a cracked wide plate", Dep. of Mech., Lehigh University, Bethlehem, Pa. (1965).
17. Isida, M., "On the determination of stress intensity factors for some common structural problems", Eng.Fract.Mech., Vol.2 (1970), pp 61-79.
18. Isida, M., "Analysis of stress intensity factors for the tension of a centrally cracked strip with stiffened edges", Eng. Fract. Mech., Vol.5 (1973), pp 647-665.
19. Isida, M., "Method of Laurent series expansion for internal crack problems", Mechanics of Fracture, Vol.1, Chapter 2 - Methods of analysis and solutions of crack problems (Ed. G.C. Sih), Noordhoff International Publishing, The Netherlands (1973).
20. Poe, C.C.,Jr., "The effect of riveted and uniformly spaced stringers on the stress intensity factor of a cracked sheet", Paper presented to Air Force Conference on Fatigue and Fracture of Aircraft Structures and Materials, Miami Beach, Florida (1969). AFFDL-TR-70-144 (1970), pp 611-634.
21. Poe, C.C.Jr., "Stress intensity factor for a cracked sheet with riveted and uniformly spaced stringers", NASA TR R-358 (1971).
22. Poe, C.C.Jr., "The effect of broken stringers on the stress intensity factor for a uniformly stiffened sheet containing a crack", Paper presented at the 10th Anniversary Meeting of the Society of Engineering Science, Raleigh, North Carolina (1973). NASA TM X-71947 (1973).
23. Rooke, D.P., Cartwright, D.J., "Compendium of stress intensity factors", Her Majesty's Stationary Office, London (1976).
24. Sih, G.C., "Handbook of stress intensity factors for researchers and engineers", Institute of Fracture and Solid Mechanics, Lehigh University, Bethlehem, Pa. (1973).
25. Tada, H., Paris, P., Irwin, G., "The stress analysis of cracks handbook", Del Research Corporation, Hellertown, Pa. (1973).
26. Cartwright, D.J., Rooke, D.P., "Methods of determining stress intensity factors", RAE Technical Report 73031 (1973).
27. Cartwright, D.J., Rooke, D.P., "Approximate stress intensity factors compounded from known solutions", Eng. Fract.Mech., Vol.6 (1974), pp 563-571.
28. Rooke, D.P., Cartwright, D.J., "A method of compounding stress intensity factors for complex configurations", RAE Technical Report 75063 (1975).
29. Rooke, D.P., Cartwright, D.J., Davis, E., "Stress intensity factors for cracks in stiffened sheets", RAE Technical Report 75072 (1975).
30. Rooke, D.P., Cartwright, D.J., "The compounding method applied to cracks in stiffened sheets", Eng. Fract. Mech., Vol.8 (1976), pp 567-573.
31. Rooke, D.P., Cartwright, D.J., "Stress intensity factors for collinear cracks in a stiffened sheet", Int. J. Fract., Vol.14 (1978), pp R 237 - R 240.
32. Lazzarino, L., Salvetti, A., "A theoretical and experimental research on the fatigue behaviour of reinforced sheets", Paper presented to 7th ICAS Congres, Rome, Italy, (1970), paper no.70-35.

33. Salvetti, A., Del Puglia, A., "Fatigue crack propagation in stiffened panels", Paper presented to 8th ICAS Congress, Amsterdam, The Netherlands (1972), paper no.72-40.

34. Salvetti, A., Frediani, A., Grassi, E., "Theoretical and experimental research on the fatigue behaviour of cracked stiffened panels", European Research Office Report, Contract no.DAJA 37-72-C-1783 (1973), London W.1, England. ICAF Doc.891.

35. Salvetti, A., Frediani, A., "Theoretical and experimental research on the fatigue crack propagation in stiffened panels - An evaluation of the Paris theory", European Research Office Report, Contract no.DAJA 37-73-C-2881 (1974), London W.1, England, ICAF Doc.892.

36. Salvetti, A., Frediani, A., Grassi, E., "Fatigue behaviour of stringers in stiffened panels", European Research Office Report, Contract no.DA-ERO-124-74-G0042 (1976), London W.1, England. ICAF Doc.893.

37. Salvetti, A., "On the behaviour of cracked riveted stiffened panels undergoing constant amplitude fatigue loading", Proc. 5th Int. Conf. Exp. Stress Analysis, paper 21, CISM Udine (1974).

38. Salvetti, A., "Fatigue behaviour of cracked stiffened panels", Agard Structures and Materials Panel, specialists meeting on Fracture Mechanics Design Methodology, London (1976), pp 7.1-7.22.

39. Swift, T., "The application of fracture mechanics in the development of the DC-10 fuselage", in Fracture Mechanics of Aircraft Structures AGARDograph 176 (1974), pp 227-287.

40. Swift, T., "The effects of fastener flexibility and stiffener geometry on the stress intensity in stiffened cracked sheet", in Prospects of Fracture Mechanics, Ed. by G.C. Sih, H.C. van Elst and D. Broek, Noordhoff International Publishing, The Netherlands (1974), pp 419-436.
Also: Douglas paper 6211.

41. Cartwright, D.J., Dowrick, G., "Effects of attachment deflection on fatigue crack growth rate in a stiffened sheet", in Fracture Mechanics in Engineering Practice, Proc. Annual Conference, Sheffield, England (1976). Published by Applied Science Publisher Ltd., London (1977), pp 361-372.

42. Ratwani, M.M., Wilhem, D.P., "Development and evaluation of methods of plane stress fracture analysis - A technique for predicting residual strength of structure", AFFDL-TR-73-42, Part II, Vol.I (1975).

43. Ratwani, M.M., Wilhem, D.P., "Development and evaluation of methods of plane stress fracture analysis - Application of the residual strength prediction technique to complex aircraft structures", AFFDL-TR-73-42, part III (1975).

44. Ratwani, M.M., Wilhem, D.P., "Factors affecting residual strength prediction of a cracked aircraft structure", J. Aircraft, Vol.16 (1979), pp 209-214.

45. Wang Ke-Jen, Cartwright, D.J., "A crack near doubly riveted stiffeners", Proc. 4th Int. Conf. on Fracture (ICF4), Waterloo, Canada, Vol.3 (1977), pp 647-656.

46. Poe, C.C.Jr., "Fatigue crack propagation in stiffened panels", ASTM STP 486 (1970), pp 79-97.

47. Kanazawa, T., Machida, S., Ohyagi, M., "Some basic considerations on crack arresters - Part V ", J.Soc.Naval Arch. Japan, Vol.122 (1967), pp 200-214.
Also: RAE Library Translation, No.1648 (1972).

48. Miller, M., Cartwright, D.J., "Stress intensity factors for a crack in two intersecting uniformly stressed sheets", Int. J. Engng. Sci., Vol.12 (1974), pp 353-359.

49. Cartwright, D.J., Miller, M., "Stress intensity factors for a crack in a sheet with a partially debonded stiffener", Int. J. Fracture, Vol.11 (1975), pp 925-932.

50. Arin, K., "A plate with a crack, stiffened by a partially debonded stringer", Eng. Fract. Mech., Vol.6 (1974), pp 133-140.

51. Arin, K., "A note on the effect of lateral bending stiffness of stringers attached to a plate with a crack", Eng.Fract.Mech., Vol.7 (1975), pp 173-179.

52. Arin, K., "A cracked sheet stiffened by several partially debonded intact or broken stringers", NASA CR-144952 (1975).
Also: a condensed version in the Proc.13th Ann.Meet.Soc.Engng. Sci.Inc., NASA CP 2001 (1976).

53. Arin, K., "Several intact or broken stringers attached to an orthotropic sheet with a crack", Eng.Fract.Mech., Vol.11 (1979), pp 1-8.

54. Hart Smith, L.J., "Adhesive bond stresses and strains at discontinuities and cracks in bonded structures", Transactions of the ASME, Journal of Engineering Materials and Technology, Vol.100 (1978), pp 16-24.

55. Wilhem, D.P., Fitzgerald, J.H., "Fracture resistance and material property characterization", Part II, Vol.II, AFFDL-TR-73-42 (1974).

56. Cartwright, D.J., Rich, T.P., "Plastic strip yielding for a crack in a stiffened sheet", Proceedings on the First Int. Conf. on Numerical Methods in Fracture Mechanics", (Ed. by A.R. Luxmore and D.R.J. Owen), Swansea (1978), pp 550-568.

57. Dugdale, D.S. "Yielding of steel sheets containing slits", J.Mech.Phys.Solids, Vol.8 (1960), pp 100-108.

58. Erdogan, F., Arin, K., "A sandwich plate with a part through and a debonding crack", Eng.Fract.Mech., Vol.4 (1972), pp 449-458.

59. Keer, L.M., Lin, C.T., Mura, T., "Fracture analysis of adhesively bonded sheets", J. Applied Mech., Vol.98 (1976), pp 652-656.

60. Anderson, J.M., Hsu, T.M., McGee, W.M., "Characterization of crack growth in bonded structures", Proc.Annual Meeting of Soc.of Engng.Science, University of Texas, Austin (1975), pp 1283-1292.

61. Ratwani, M.M., "Characterization of fatigue crack growth in bonded structures - Crack growth prediction in bonded structures", AFFDL-TR-77-31, Vol.I (1977).

62. Ratwani, M.M., "Characteristics of fatigue crack growth in bonded structures - Analysis of cracked bonded structures", AFFDL-TR-77-31, Vol.II (1977).

63. Ratwani, M.M., "A parametric study of fatigue crack growth behaviour in adhesively bonded metallic structures", J.Eng.Mat. and Techn., Vol.100 (1978), pp 46-51.

64. Ratwani, M.M., "Analysis of cracked, adhesively bonded structures", Proc.AIAA/ASME 19th Structures, Structural Dynamics and Materials Conference, Bethesda, Md.,(1978), pp 155-163.

65. Swift, T., Wang, D.Y., "Damage tolerant design - Analysis methods and test verification of fuselage structure", paper presented to Air Force Conference on Fatigue and Fracture of Aircraft Structures and Materials, Miami, Florida (1969), AFFDL-TR-70-144 (1970), pp 653-683.
Also: Douglas paper 5684.

66. Swift, T., "Development of the fail-safe design features of the DC-10", paper presented to ASTM symposium on Damage Tolerance in Aluminium Aircraft Structures, Toronto, Canada , (1970).
ASTM STP 486, pp 164-214.

67. Swift, T., "The application of fracture mechanics to the design of damage-tolerant stiffened aircraft structure", paper presented to American Society for Metals 1972 Westec Conf., Los Angeles, California (1972). Also: Douglas paper 5981.

68. Stone, M., Swift, T., "Structural integrity through damage-tolerance design practices", 15th Meeting International Committee on Aeronautical Fatigue, Darmstadt, Germany (1977).
Also: Douglas paper 6608.

69. Swift, T., "Fracture analysis of adhesively bonded panels", ASME paper no.77-WA/MAT. Published in Journal of Engineering Materials and Technology, Vol.100 (1978), pp 10-15.

70. Swift, T., "Damage tolerance analysis of redundant structures", paper presented to Fracture Mechanics Design Methodology, AGARD-NATO Lecture Series, Delft, Netherlands; Munich, Germany; Lisbon, Portugal (1978).

71. Swift, T., "Design of redundant structures", paper presented to Fracture Mechanics Design Methodology, AGARD-NATO Lecture Series, Delft, The Netherlands; Munich, Germany; Lisbon, Portugal (1978).

72. Vlieger, H., "Residual strength of cracked stiffened panels", NLR Report TR 71004 U (1971).

73. Vlieger, H., "The residual strength characteristics of stiffened panels containing fatigue cracks", paper presented at the Symposium on Fracture and Fatigue, George Washington University, Washington (1972). Published in Eng. Fract. Mech., Vol.5 (1973), pp 447-477.

74. Vlieger, H., Broek, D., "Residual strength of built-up sheet structures", in Fracture Mechanics of Aircraft Structures, AGARDograph no.176 (1974), pp 195-225.

75. Vlieger, H., "Fail-safe characteristics of built-up sheet structures", paper presented to 9th ICAS congres, Haifa, Israel (1974), ICAS paper no.74-08.

76. Vlieger, H., Sanderse, A., "User's manual of ARREST, a computer routine for prediction of residual strength of cracked stiffened panels", NLR Report TR 75129 U (1975).

77. Vlieger, H., "Application of fracture mechanics in designing built-up sheet structures", Agard Structures and Materials Panel, specialists meeting on Fracture Mechanics Design Methodology, London, England (1976), Agard Conf. Proc. no.221, pp 5.1-5.18.

78. Vlieger, H., "Prediction of fail-safe strength of realistic stiffened skin aircraft structures", Proc.4th International Conference on Fracture (ICF4), Waterloo, Canada, Vol.3 (1977), pp 699-704.

79. Vlieger, H., "Residual strength and crack propagation properties of panels with bonded stiffeners", NLR report to be published shortly.

80. Lehrke, H.P., Huth, H., "Rechenprogramm zur Ermittlung der Beanspruchungsgrössen von versteiften, rissbehafteten Blechfeldern unter Zugbelastung, LBF-Bericht, to be published (autumn, 1975, according to [81]).

81. Huth, H., Gerharz, J.J., Schütz, D., "Ueber den Einfluss von Versteifungen auf den Rissfortschnitt", LBF-Bericht Nr.FB-122 (1975).

82. Schwarmann, L., "Spannungsintensitätsfaktoren von ebenen, versteiften Blechstrukturen", VFW-Fokker, GK-Untersuchung Bruchmechanik (1974).

83. Schwarmann, L., "Bruchmechanische Kennwerte von ebenen, versteiften Blechstrukturen mit Zentralriss", VFW-Fokker, GK-Untersuchung Bruchmechanik (1976).

84. Broek, D., "The residual strength of cracked sheet and structures", NLR report M.2135 (1964).

85. Toor, P.M., "A review of some damage tolerance design approaches for aircraft structures", Eng.Fract.Mech., Vol.5 (1973), pp 837-880.

86. Feddersen, C.C., "Evaluation and prediction of the residual strength of center cracked tension panels", ASTM STP 486 (1971), pp 50-78.

87. Anon., "Damage Tolerant Design Handbook", A compilation of fracture and crack growth data for high-strength alloys, part 1, MCIC-HB-01 (1972).

88. Broek, D., Vlieger, H., "The thickness effect in plane stress fracture toughness", NLR report TR 74032 (1974).

89. 't Hart, W.G.J., Nederveen, A., Stoffels, E., Tromp, P.J., "Fracture toughness and fatigue properties of the new aluminium alloy 7475-T76", NLR report TR 75168 (1975).

90. 't Hart, W.G.J., "Residual strength of the aluminium alloy 7475-T76 at low temperatures", NLR report TR 76103 (1976).

91. 't Hart, W.G.J., "Supplementary residual strength investigation of the aluminium alloy 7475-T76", NLR report TR 77007 (1977).

92. Broek, D., "Residual strength and fatigue crack growth in two aluminium alloy sheets at temperatures down to -75°C", NLR report TR 72096 (1972).

93. McClintock, F.A., Irwin, G.R., "Plasticity aspects in fracture mechanics", ASTM STP 381 (1965), pp 84-113.

94. Krafft, J.M., Sullivan, A.M., Boyle, R.W., "Effect of dimensions on fast fracture instability of notched sheets", Proc. Crack Propagation Symposium , Cranfield, Vol.I (1961), pp 8-28.

95. Broek, D., Vlieger, H., "The thickness effect in plane stress fracture toughness", NLR report TR 74032 U (1973).

96. Heyer, R.H., McCabe, D.E., "Plane-stress fracture toughness testing using a crack-line loaded specimen", Eng.Fract.Mech., Vol.4 (1972), pp 393-412.

97. Heyer, R.H., McCabe, D.E., "Crack growth resistance in plane-stress fracture testing", Eng.Fract. Mech., Vol.4 (1972), pp 413-430.

98. Various authors, "Fracture toughness evaluation by R-curve methods", ASTM STP 527 (1973).

99. Bradshaw, F.J., Lacey, D., Wheeler, C., "The effect of section thickness on the crack resistance of aluminium alloy L93, with measurements of plastic strain", RAE Technical Report 72039 (1972).

100. Bradshaw, F.J., Wheeler, C., "The crack resistance of some aluminium alloys and the prediction of thin section failure", RAE Technical Report 73191 (1973).

101. Wheeler, C., Wood, R.A., Bradshaw, F.J., "Some crack resistance curves of sheet compact tension specimens of aluminium alloys 7475-T761, 2024-T3 and 2024-T81", RAE Technical Report 74086 (1974).

102. Anon., "Tentative recommended practice for R-curve determination", E561-76T, ASTM Annual Book of Standards, Part 10 (1976), pp 539-557.

103. Irwin, G.R., Kies, J.A., "Critical energy rate analysis of fracture strength", Welding Journal Research Suppl., Vol.19 (1954), pp 193-198.

104. McCabe, D.E., "Determination of R-curves for structural materials using nonlinear mechanics methods", Flaw growth and fracture, ASTM STP 631, (1977), pp 245-266.

105. McCabe, D.E., Landes, J.D., "Elastic-plastic R-curves", J.Engng Mat. and Techn., Vol.100 (1978), pp 258-265.

106. Creager, M., Liu, A.F., "The effect of reinforcements on the slow stable tear and catastrophic failure of thin metal sheet", paper presented to AIAA 9th Aerospace Sciences Meeting, New York (1971), AIAA Paper 71-113.

107. Rice, J.R., "A path independent integral and the approximate analysis of strain concentration by notches and cracks", J.Appl.Mech., (1968), pp 379-386.

108. Verette, R.M., Wilhem, D.P., "Development and evaluation of methods of plane stress fracture analysis, review and evaluation of structural residual strength prediction techniques", AFFDL-TR-73-42 (1973).

109. Wilhem, D.P., "An improved technique for residual strength prediction - A modified crack growth resistance approach", Proc.Intern.Conf. on Prospects of Fracture Mechanics, Delft University of Technology, The Netherlands, G.C. Sih, H.C. van Elst and D. Broek, editors (1974), pp 389-404.

110. Hayes, D.J., Williams, J.G., "A practical method for determining Dugdale model solutions for cracked bodies of arbitrary shapes", Inter.J.Fract.Mech., Vol.8 (1972), pp 239-256.

111. Rice, J.R., "Fracture - An advanced treatise", ed. H. Liebowitz, Academic Press, N.Y. (1968).

112. Wilhem, D.P., Ratwani, M.M., Zielsdorff, G.F., "A J-integral approach to crack resistance for aluminium, steel and titanium alloys", Journal of Engineering Materials and Technology, Vol.99 (1977), pp 97-104.

113. Ratwani, M.M., Wilhem, D.P., "Application of resistance curves to residual strength prediction", Journal of Engineering Materials and Technology, Vol.100 (1978), pp 138-143.

114. Wilhem, D.P., Ratwani, M.M., "Crack growth resistance at low stress intensities", Journal of Engineering Materals and Technology, Vol.100 (1978), pp 134-137.

115. Wilhem, D.P., Ratwani, M.M., "Application of the R-curve concept to fatigue crack growth", Journal of Engineering Materials and Technology, Vol.100 (1978), pp 416-420.

116. Peters, R.W., Kuhn, P., "Bursting strength of unstiffened pressure cylinders with slits", NACA TN 3993 (1957).

117. Kuhn, P., "Notch effects on fatigue and static strength", presented at the Symposium on Aeronautical Fatigue, Rome, Italy (1963), Published in Current Aeronautical Fatigue Problems, Ed. by J. Schijve, J.R. Heath-Smith, E.R. Welbourne, Pergamon Press (1965).

118. Anderson, R.B., Sullivan, T.L., "Fracture mechanics of through-cracked cylindrical pressure vessels", NACA TN D-3252 (1966).

119. Crichlow, W.J., Wells, R.H., "Crack propagation and residual static strength of fatigue cracked titanium and steel cylinders", ASTM STP 415 (1967), pp 25-70.

120. Duffy, A.R., et al., "Studies of hydrostatic test levels and defect behaviour", Symposium on pipeline research, American Gas Assoc., New York (1967).

121. Folias, E.S., "A finite line crack in a pressurized spherical shell", Int.J.Fract.Mech., Vol.1 (1965), pp 20-46.

122. Folias, E.S., "An axial crack in a pressurized cylindrical shell", Int.J.Fract.Mech., Vol.1 (1965), pp 104-113.

123. Folias, E.S., "A circumferential crack in a pressurized cylindrical shell", Int.J.Fract.Mech., Vol.3 (1967), pp 1-11.

124. Copley, L.G., Sanders, J.L.Jr., "A longitudinal crack in a cylindrical shell under internal pressure", Int.J.Fract.Mech., Vol.5 (1969), pp 117-131.

125. Duncan, M.E., Sanders, J.L.Jr., "The effect of a circumferential stiffener on the stress in a pressurized cylindrical shell with a longitudinal crack", Int.J.Fract.Mech., Vol.5 (1969), pp 133-155.

126. Folias, E.S., "On the effect of initial curvature on cracked flat sheets", Int.J.Fract.Mech., Vol.5 (1969), pp 327-346.

127. Hahn, G.T., Sarrate, M., Rosenfield, A.R., "Criteria for crack extension in cylindrical pressure vessels", Int.J.Fract.Mech., Vol.5 (1969), pp 187-210.

128. Folias, E.S., "On the prediction of catastrophic failures in pressure vessels", Proc.Intern.Conf. on Prospects of Fracture Mechanics, Delft University of Technology, The Netherlands, G.C. Sih, H.C. van Elst and D. Broek, editors (1974), pp 405-418.

129. Lemaitre, J., Turbat, A., Loubet, R., "Fracture mechanics analysis of pressurized cracked shallow shells", Eng.Fract.Mech., Vol.9 (1977), pp 443-460.

130. Joshi, S.R., Schewchuk, J., "Fatigue crack propagation in biaxial-stress field", Exp.Mech., Vol.10 (1970), pp 529-533.

131. Wilson, I.H., White, D.J., "Cruciform specimens for biaxial fatigue tests: an investigation using finite element analysis and photo-elastic coating techniques", J.Strain Anal., Vol.6 (1971), pp 27-37.

132. Kibler, J.J., Roberts, R., "The effect of biaxial stress on fatigue and fracture", J.Engineering for Industry, Vol.70 (1970), pp 727-734.

133. Adams, N.J., "Some comments on the effect of biaxial stress on fatigue crack growth and fracture", Eng.Fract.Mech., Vol.3 (1973), pp 983-991.

134. Ogura, Keiji, Ohji Kiyolsugu, Okhubo Yoshiji, "Fracture crack growth under biaxial loading", Int.J. Fract.,Vol.10 (1974), pp 609-610.

135. Miller, K.J., Kfouri, A.P., "An elastic-plastic finite element analysis of crack tip fields under biaxial loading conditions", Int.J.Fract., Vol.10 (1974), pp 393-403.

136. Hilton, P.D., "Plastic intensity factors for cracked plates subjected to biaxial loading", Int.J. Fract., Vol.9 (1973), pp 149-156.

137. Smith, S.H., "Analysis of energy quantities for fracture under biaxial stresses", Proc.Int.Conf. on Prospects of Fracture Mech., Delft University of Technology, The Netherlands, (Ed. G.C. Sih, H.C. van Elst and D. Broek), (1974), pp 367-388.

138. Shah, R.C., "Stress intensity factors for through and part-through cracks originating at fastener holes", presented at the 8th Nat.Symp. on Fract.Mech., Brown University, Providence, R.I. (1974)

139. Erdogan, F., Kibler, J.J., "Cylindrical and spherical shells with cracks", Int.J.Fract.Mech., Vol.5 (1969), pp 229-237.

140. Beck, E.J., "Fatigue flaw growth behaviour in stiffened and unstiffened panels loaded in biaxial tension", NASA CR-128904 (1973).

141. Ratwani, M.M., Wilhem, D.P., "Influence of biaxial loading on analysis of cracked stiffened panels", Eng.Fract.Mech., Vol.11 (1979), pp 585-593.

142. Liu, A.F., Ekvall, J.C., "Material toughness and residual strength of damage tolerant aircraft structures", ASTM STP 486 (1971), pp 98-121.

143. Ekvall, J.C., Brussat, T.R., Liu, A.F., Creager, M., "Engineering criteria and analysis methodology for appraisal of potential fracture resistant primary aircraft structure", AFFDL-TR-72-80 (1972).

144. Sanga, R.V., "The 747 fail-safe structural verification program", paper presented to 7th ICAF symposium, London, England (1973).

145. Ekvall, J.C., Brussat, T.R., Liu, A.F., Creager, M., "Preliminary design of aircraft structures to meet structural integrity requirements", AIAA/ASME/SAE 14th structures, structural dynamics and materials conference, Williamsburg, Va. (1973), AIAA paper no.73-374.
Also: J.Aircraft, Vol.11 (1974), pp 136-143.

146. Nanduri, V.G., Radzins, K., "The crack containment capability of stiffened bonded panels", Canadian Aeronautics and Space J., Vol.21 (1975), pp 388-400.

147. Heath, W.G., Nicholls, L.F., Kirkby, W.T., "Practical applications of fracture mechanics techniques to aircraft structural problems", Agard Structures and Materials Panel, specialists meeting on Fracture Mechanics Design Methodology, London, England (1976), Agard Conf.Proc.no.222, pp 1.1-1.22.

148. Sorensen, A., "Some design considerations for tear-resistant airplane structures", paper presented at the IAS 24th Annual meeting, New York (1956), preprint no.618.

149. Crichlow, W.J., "The ultimate strength of damaged structure - Analysis methods with correlating data", ICAF-AGARD symposium, Amsterdam, The Netherlands (1959).

150. Hunt, R.T., Denke, P.H., Eide, G.R., "Crack propagation and residual static strength of stiffened and unstiffened sheet", paper presented at the Joint AGARD/ICAF Meeting, Rome, Italy (1963).

151. Eide, G.R., "Fail-safe design of stiffened panels", Douglas report no.LB-32056 (1964).

152. Wang, D.Y., "An investigation on fatigue crack propagation and failsafe design of stiffened large aluminum alloy panels with various crack stoppers", Proc.10th ASME/AIAA structures", structural dynamics and materials conf., New Orleans, La., (1969).

153. Smith, S.H., Porter, T.R., Engstrom, W.L., "Fatigue crack-propagation behaviour and residual strength of bonded strap reinforced, lamellated and sandwich panels", Proceedings of the Air Force Conf. on Fatigue and Fracture of Aircraft Structures and Materials, Miami Beach (1969). AFFDL-TR-70-144, pp 611-634.

154. Schwarmann, L., Bauer, J., "Ermittlung von bruchmechanischen Kennwerten ebener, versteifter Schalen, mit Hilfe der Finite-Element Methode", Vortrag IKOSS-Finite Element Kongress, Baden-Baden (1977).

155. Various authors, "Case studies in fracture mechanics", Ed. by T.P. Rich and D.J. Cartwright, Army materials and mechanics research center, Watertown, Massachusetts (1977).

156. Thrall, E.W.Jr., "Failures in adhesively bonded structures", Agard Lecture series no.102: Bonded Joints and Preparation for Bonding, presented Oslo, Norway; the Hague, the Netherlands (1979).

157. Troughton, A.J., McStay, J., "Theory and practice in fail-safe wing design", in Current Aeronautical Fatigue Problems, pp 429-462, Schijve, Heath-Smith, Welbourne, Eds., Pergamon Press (1965).

158. Lalli, D., Sergio, G., "Design and certification for executive type aircraft", paper presented to 5th ICAF Symposium, Melbourne, Australia (1967).

159. Nelson, L.W., Melcon, M.A., Simons, H., "The Lockheed L-1011 Tristar fatigue and fail-safe development program", paper presented to the 7th ICAF Symposium, London, England (1973).

160. Impellizzeri, L.F., "Structural fatigue analysis and testing for fighter aircraft", paper presented to Agard Specialists Meeting on "Design against Fatigue", the Hague, the Netherlands (1973).

161. Hedrick, I.G., Wehle, L.B., Bell, P.D., "Fatigue and fracture considerations for tactical aircraft", paper presented to Agard Specialists Meeting on "Design against Fatigue", the Hague, the Netherlands (1973).

162. Lehmann, H., "Use of the fracture mechanics in the design of the European Airbus A300B", paper presented to 39th Meeting of the AGARD Structures and Materials Panel, Munich (1974).

163. McHenry, H.I., Hensley, E.K., "Evaluation of damage tolerance in aircraft structures", AIAA/ASME/SAE 15th Structures, Structural Dynamics and Materials Conference, Las Vegas, Nevada (1974), AIAA Paper no.74-347.

164. Barrois, W., "Practical use of the "equivalent" measured stress intensity factor to control fatigue crack propagation rates in aircraft full-scale fatigue tests - First assessment of the method in testing of a pressurized aircraft fuselage", paper presented to the 39th AGARD Structures and Materials panel, Munich (1974), Published in Eng.Fract.Mech., Vol.7 (1975), pp 673-688.

165. Wood, H.A., "Application of fracture mechanics to aircraft structural safety", Eng.Fract.Mech., Vol.7 (1975), pp 557-564.

166. Murnane, S.R., Stronge, T.D., Davenport, O.B., "Northrop/United States air force durability and damage-tolerance assessment of the F-5E/F aircraft", Agard Structures and Materials panel, specialists meeting on Fracture Mechanics Design Methodology, London, England (1976), Agard Conf.Proc.no.221, pp 4.1-4.33.

167. Kaplan, M.P., Reiman, J.A., "Use of fracture mechanics in estimating structural life and inspection intervals", J.Aircraft, Vol.13 (1976), pp 99-103.

168. Various authors, "Rissfortschritts- und ergänzende Betriebsfestigkeitsversuche an der dynamischen Bruchzelle der Transall C160", Aerospatiale/VFW-Fokker/MBB-UH Report (1977).

169. Conley, F.M., Sayer, R.B., "Correlation of predicted and actual crack growth in a transport wing", AIAA/ASME 18th Structures, Structural Dynamics and Materials Conf., San Diego, Calif. (1977), AIAA Paper no.77-381.

170. Casalegno, L., "Project and experimental fatigue test of the wing of a modern combat aircraft", paper presented to AIFA Meeting on Fatigue in Aerospace Structures, Turin, Italy (1978).

171. Gökgöl, A., "Crack free and cracked life of the pressurized cabin of the A300B - Calculation, tests and design measurements to improve damage tolerance", paper presented to 11th ICAS Congress, Lisbon, Portugal (1978).

172. Anderson, J.M., Chu, C.S., Malluck, J.F., "A fail-safe analysis of a spanwise wing-panel splice", AIAA/ASME 19th Structures, Structural Dynamics and Materials Conf., Bethesda, Md. (1978), AIAA paper no.78-487.

173. Anon., "Experimentell-theoretische Bestimmung der Spannungsintensitätsfaktoren von rissbehafteten Rumpfbauteilen unterschiedlicher Bauweisen", VFW-Fokker Report 2.01/5, Part 2, Progress Report (1973).

174. Anon., "Rissfortschritt in Kampfflugzeugbauteilen unter betriebsähnlichen Bedingungen", VFW-Fokker Report 2.20/1, Part 1, Progress Report (1974).

175. Anon., "Rissfortschritt in Kampfflugzeugbauteilen unter betriebsähnlichen Bedingungen", VFW-Fokker Report 2.20/2, Part 1, Progress Report (1975).

176. Anon., "Rissfortschritt in Kampfflugzeugbauteilen unter betriebsähnlichen Bedingungen", VFW-Fokker Report 2.20/3, Part 1, Progress Report (1976).

177. Heller, R.A., Liu, C.T., Swift, G.W., "Fatigue damage analysis and life prediction of a composite laminate", AIAA/ASME/SAE 16th Structures, Structural Dynamics and Materials Conf., Denver, Colorado (1975), AIAA paper no.75-768.

178. Anderson, J.M., Chu, C.S., McGee, W.M., "Growth characteristics of a fatigue crack approaching and growing beneath an adhesively bonded doubler", Journal of Engineering Materials and Technology, Vol.100 (1978), pp 52-56.

179. Schwarmann, L., Bauer, J., "Ueber die Anwendung der finite-element Methode in der Bruchmechanik", Vortrag der 10. Jahrestagung der Deutschen Gesellschaft für Luft- und Raumfahrt, Berlin (1977), DGLR Vortrags Nr.77-055.

180. Wilhem, D.P., "Fracture mechanics guidelines for aircraft structural applications", AFFDL-TR-69-111 (1970)

181. Rolfe, S.T., Barsom, J.M., "Fracture and fatigue control in structures - Applications of fracture-mechanics", Prentice-Hall, Englewood Cliffs, New Jersey (1977).

182. Pettit, D.E., et al., "Flaw growth in complex structure", AFFDL-TR-77-79 (1977).

4. FASTENED JOINTS

DAVID BROEK
Battelle's Columbus Laboratories
505 King Avenue
Columbus, Ohio 43201

SYMBOLS 4-2

4.1 INTRODUCTION. 4-3

4.2 STATE OF THE ART OF STRESS-INTENSITY ANALYSIS 4-3

4.2.1 Through Cracks at Holes Under Remote Loading 4-3
4.2.2 Part-Through Cracks at Holes 4-5
4.2.3 Holes With Fasteners 4-9
4.2.4 Joints 4-11

4.3 DAMAGE TOLERANCE ANALYSIS 4-11

4.3.1 Scope 4-11
4.3.2 Residual Strength. 4-11
4.3.3 Propagation of Cracks at Holes 4-13
4.3.4 Crack Growth in Fastened Joints. 4-15

4.4 EXAMPLES. 4-18

4.4.1 Introduction 4-18

4.5 REFERENCES. 4-18

4.6 EXAMPLE PROBLEMS. 4-20

4.6.1 Crack Propagation in Lugs on Aft Flap Links. 4-20
(M. Bradley)

4.6.2 Corner Defects at Holes of Wing Spar Booms 4-24
(D. Grange and M. Bradley)

4.6.3 Residual Strength Predictions for Corner Defects
at Holes in Spar Booms (D. Grange). 4-26

4.6.4 Damage Tolerance Estimated for a Landing Gear Component. 4-28
(D. Grange)

4.6.5 Crack Growth and Fracture of a Loaded Hole in Aircraft
Boom End (M. Bradley). 4-35

4.6.6 Titanium Alloy Wing Lug
(L. Casalegno) 4-42

4.6.7 Flight-by-Flight Crack Propagation Investigation
on MRCA Tornado Components (W. Geier and K. O. Sippel) 4-44

4.6.8 Aircraft Horizontal Stabilizer Lug 4-49
(S. H. Smith, T. P. Forte, H. J. Malik, N. D. Ghadiali)

4.6.9 Damage Tolerance Analysis of an Aircraft Structural. . . 4-52
(S. H. Smith, F. A. Simonen)

Symbols

a	crack size; depth of corner crack or surface flaw
a_a, a_{eff}	effective crack depth
b	edge distances (example problems only)
B	thickness
c	surface length of corner crack or surface flaw
c_a, c_{eff}	effective crack length c
C, C_1, C_2, C_3	constants
d	hole diameter (example problems only)
D	hole diameter
F	function
K	stress intensity
K_c, K_{Ic}	fracture toughness
ΔK	stress intensity range
$M_f M_k$	stress intensity magnification factors (example problems)
n	exponent in rate equation
N	cycle number
p	crack depth (example problems)
p_{eff}	effective p (example problems)
P	load
q	crack length (example problems)
q_{eff}	effective q (example problems)
Q	flaw shape parameter
R	stress ratio of cyclic loading
t	thickness (example problems)
W	width
$\alpha, \alpha_b, \alpha_f$	stress intensity magnification factors
β	stress intensity geometry factor
Φ	elliptical integral
θ	angle
λ	stress intensity correction factor (example problems)
σ	stress
σ_R	residual strength
σ_{ult}	ultimate tensile strength
$\Delta\sigma$	stress range

4. FASTENED JOINTS

David Broek
Battelle's Columbus Laboratories
505 King Avenue
Columbus, Ohio 43201

4.1 INTRODUCTION

Holes in lugs and joints are common locations for crack initiation. Holes are a source of stress concentration which in many joints is enhanced by load transfer through the pin or fastener. Thus, it is not surprising that a review of aircraft structural failures[1] revealed that about 30 percent of the crack origins were bolt or rivet holes. As a consequence, holes in joints are the subject of a considerable part of aircraft damage tolerance analyses, and therefore a substantial number of examples of application of fracture mechanics to joints and lugs was anticipated. Nevertheless, the number of examples was low. On the other hand, if many examples would be available, it could be concluded that analysis of joints was common practice, such that a handbook of this nature would be superfluous. Thus, the scarcity of examples may be considered a justification for a handbook that presents such examples, although at the same time it prohibits the possible publication.

The present chapter deals first in general terms with the stress-intensity analysis of joints. Any damage tolerance analysis at present is based on the stress intensity. Hence, the problem of determining stress-intensity factors is of paramount importance. Since the subject of stress-intensity analysis is dealt with extensively in other chapters of this handbook, only a brief discussion will be presented here to highlight some of the specific complications arising in the case of joints in general, and cracks at holes in particular.

Thereafter follows a discussion of damage-tolerance analysis of fastened joints. Here again, many of the problems are generic to damage-tolerance analysis. Therefore only those problems will be reviewed that are particular to joints. The discussion will only be brief, partly because no satisfactory solutions exist to many of the problems associated with cracks at holes in joints.

The second part of this chapter consists of the examples made available by various sources. These examples are presented as much as possible in their original form in order to give full credit to the contributors. Each example is concluded with some critical comments.

4.2 STATE OF THE ART OF STRESS-INTENSITY ANALYSIS

4.2.1 Through Cracks at Holes Under Remote Loading

Every damage-tolerance analysis starts out with the determination of the applicable stress-intensity solution. Since fastened joints all contain holes, the stress-intensity solution for a crack emanating from a hole is of great interest.

On the basis of the work by Bowie[2], the stress-intensity factor for a through crack at a hole in an infinite plate (Figure 1) is given by

$$K = \sigma \sqrt{\pi a}\, f_B\left(\frac{a}{D}\right) \tag{1}$$

where a is the size of the crack as measured from the edge of the hole, and D is the hole diameter. The function f_B (a/D) can be given in tabular or graphical form as f_{B1} for a single crack and f_{B2} for the symmetric case with two cracks. Grandt[3] has recently developed a least square fit to f_B of the form

$$f_B\ (a/D) = \frac{C_2}{C_2 + a/D} + C_3 \tag{2}$$

where C_1, C_2, and C_3 have values as given in Figure 1.

If the crack is not too small with respect to the hole size, the hole may be considered part of the crack. The total defect size is then given by the physical crack length plus the hole diameter (Figure 1). The stress intensity is simply

$$K = \sigma \sqrt{\pi a_{eff}} \quad . \tag{3}$$

By developing Equation (3) as

$$K = \sigma \sqrt{\pi a_{eff}} = \sigma \sqrt{\pi a}\sqrt{\frac{D}{2a} + \frac{1}{2}} = \sigma \sqrt{\pi a}\, f_{E1(a/D)} \tag{4}$$

for the asymmetric case, and

$$K = \sigma \sqrt{\pi a_{eff}} = \sigma \sqrt{\pi a}\sqrt{\frac{D}{2a} + 1} = \sigma \sqrt{\pi a}\, f_{E2}(a/D) \tag{5}$$

for the symmetric case, it follows that f_{B1} and f_{B2} in Equation (1) are replaced by f_{E1} and f_{E2}. A comparison of these functions is made in Figure 2. It appears that the differences between the exact functions and the engineering functions are small, if a/D >0.1. In view of the accuracy of fracture-mechanics analysis and the scatter in raw data, the simple Equation (3) can be used in many applications.[4,5,6]

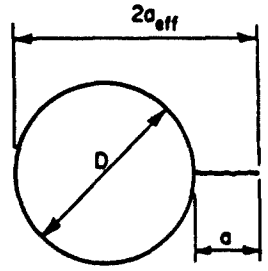

a. Asymmetric case (single crack)

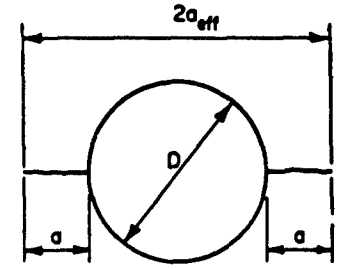

b. Symmetric case (two cracks)

$$f_B\left(\frac{a}{D}\right) = \frac{C_1}{C_2 + a/D} + C_3$$

	f_{B1} Asymmetric	f_{B2} Symmetric
C_1	0.4367	0.3433
C_2	0.1623	0.1386
C_3	0.6762	0.9439

c. Least square fit to f_B

FIGURE 1. THROUGH CRACKS EMANATING FROM A HOLE AND THE BOWIE FUNCTION

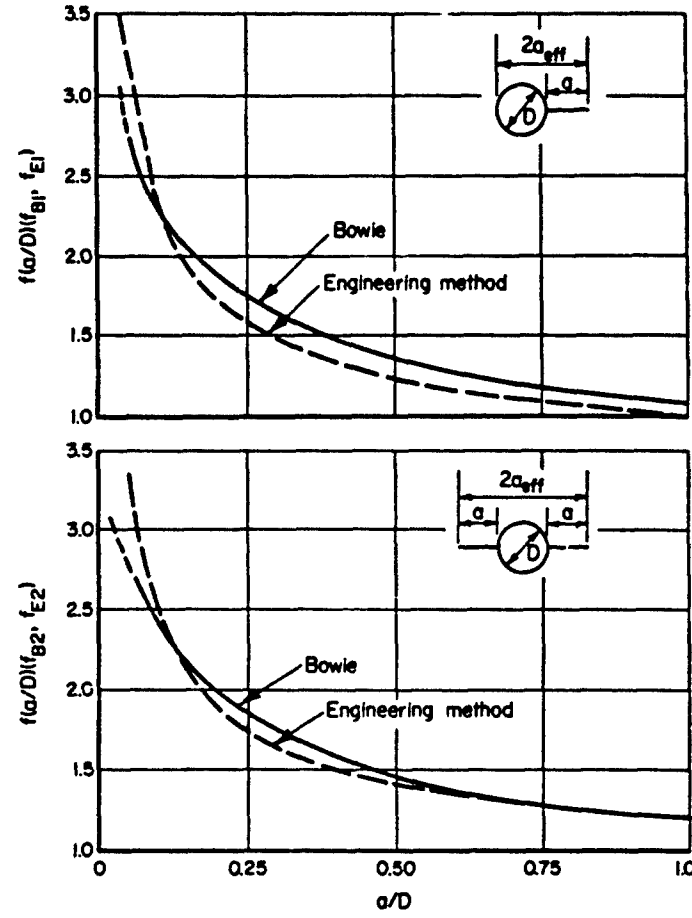

FIGURE 2. BOWIE'S ANALYSIS AS COMPARED TO ENGINEERING METHOD

For the practical case of finite panels, the Isida (and Feddersen) width correction can be applied to Equations (1) and (3) as was shown by the finite-element calculations by Owen and Griffiths[7]. Results for a finite-size strip were obtained also by Cartwright and Ratcliffe[8], who conducted compliance measurements.

A few attempts were made[3,8,9] to analyze the case of a loaded hole. A simple approximate analysis[9] based on the superposition principle is presented in Figure 3. According to the figure, the stress-intensity factor for a loaded hole is given by

$$K_A = \frac{K_B + K_D}{2} \quad . \tag{6}$$

The Bowie solution of Equation (1) can be taken for K_B. The expression for K_D is well known to be $K_D = P/\sqrt{\pi a}$, if the hole is considered part of the crack. A standard finite size correction can be applied.

Figure 4 allows a comparison of Equation (6) with the results of the compliance measurements made by Cartwright and Ratcliffe[8]. The stress intensity first rises sharply and then decreases, since the second term in Equation (7) is a decreasing function of a_{eff}. This is in agreement with the results of the compliance measurements. It is also confirmed by the analysis of Grandt[3]. If the cracks grow longer, K increases again as a result of the finite size correction.

Pin loading creates minor shear stresses along the crack line. Consequently, there will be combined K_I and a K_{II} loading modes. The compliance measurements can only determine G and cannot uncouple K_I and K_{II}. But as pointed out by Cartwright and Ratcliffe, the error in equating $K_I = \sqrt{EG}$ is less than 1 percent. Grandt[3] accounted for this by taking the crack perpendicular to the maximum principal stress. The crack is then at an angle of 81 degrees (instead of 90 degrees) to the loading axis.

4.2.2 Part-Through Cracks at Holes

A corner crack at a hole is an important case in the fracture safety control of structures. A "rigorous" solution for flawed holes requires a complicated three-dimensional finite element analysis. However, stress-intensity estimates have been reported(10,11) employing elliptical crack solutions and correction factors to account for the hole. For some configurations, stress-intensity factors were determined experimentally(12,13). A number of these solutions are described in subsequent paragraphs.

An approximate solution acceptable for rough calculations uses the standard elliptical flaw solution and applies the Bowie correction factor, as if it were a through crack,

$$K = \frac{\sigma}{\phi}\sqrt{\pi\frac{a^2}{c}}\, f_B\left(\frac{c}{D}\right) \quad , \tag{7}$$

where ϕ is the well-known elliptical integral applicable to elliptical cracks, c is along the surface, and f_B is the Bowie function given in Figure 2, but with the abscissa given as c/D instead of a/D. The equation is limited to cases where a/B <0.5, B being the thickness, unless a back-free surface correction would be applied.

Hall and Finger[10] derived an empirical expression on the basis of failing stresses of specimens with flawed holes, assuming the specimens failed when K reached the standard K_{Ic}. They arrived at

$$K = 0.87\,\sigma\sqrt{\pi c_e}\, f_B\left(\frac{c_e}{D}\right) \quad . \tag{8}$$

In this equation, c_e represents an effective crack size, which has to be found from empirical curves. It incorporates the influence of both flaw shape and back-free surface, but it is limited to a/c <1. The Bowie function, f_B, is also based on the effective crack size, c_e.

Liu[11] considered a quarter-circular flaw, such that the flaw shape parameter ϕ equals $\pi/2$. He arbitrarily based the Bowie function on an effective crack, $a_e = 1/2\ a\sqrt{2}$. His equation then is

$$K = \alpha_b\alpha_f\frac{\sigma}{\phi}\sqrt{\pi a}\, f_B\left(\frac{a_e}{D}\right) \quad . \tag{9}$$

A corner flaw has two free surfaces, which can be accounted for by a free surface correction of 1.26. Since the edge crack surface correction is already included in the Bowie function, Liu took the free surface correction $\alpha_f = 1.26/1.12 = 1.12$. Taking the back-free surface correction, α_b, equal to unity and noting that $\phi = \pi/2$, the final equation is

$$K = \frac{2.24\sigma}{\pi}\sqrt{\pi a}\, f_B\left(\frac{a_e}{D}\right), \quad \text{with} \quad a_e = \frac{1}{2}\sqrt{2}\, a \quad . \tag{10}$$

Hall and Engstrom[14] presented an analysis method for dual elliptical cracks emanating from holes. They used the solution for a pressurized elliptical crack with a pressure distribution in the form of a polynomial. They fitted the polynomial roughly to the stress distribution around an uncracked hole in a plate under tension. Then they solved the problem of an elliptical crack (without a hole) with the calculated pressure distribution. The result is (see Figure 5 for notations),

$$K = \frac{\sigma}{\phi}\sqrt{\pi a}\left[\cos^2\beta + \frac{a^2}{c^2}\sin^2\beta\right]^{1/4} F\left(\frac{c}{D}, \beta\right) \quad . \tag{11}$$

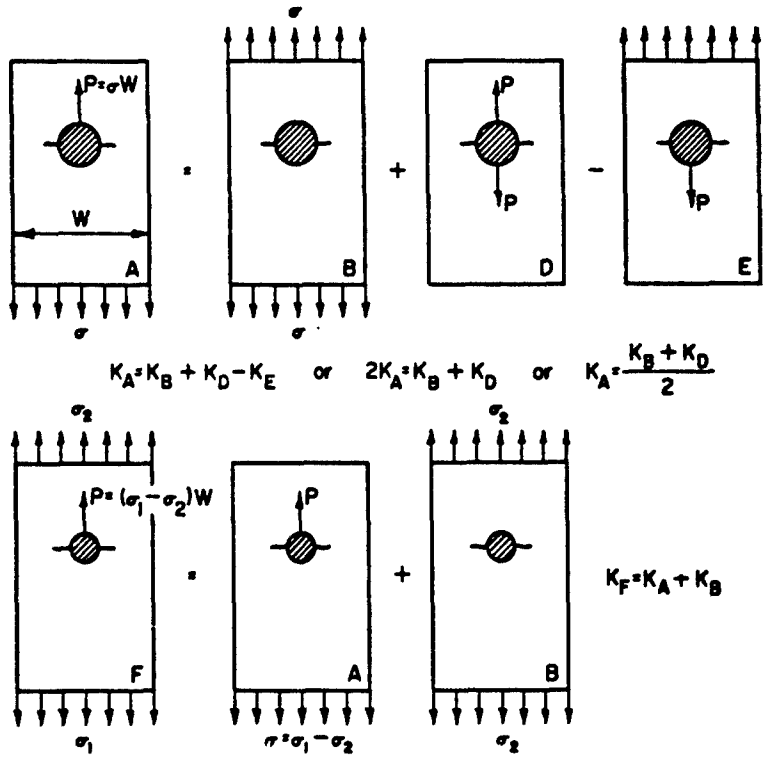

FIGURE 3. STRESS INTENSITY FOR PIN-LOADED HOLE FROM SUPERPOSITION

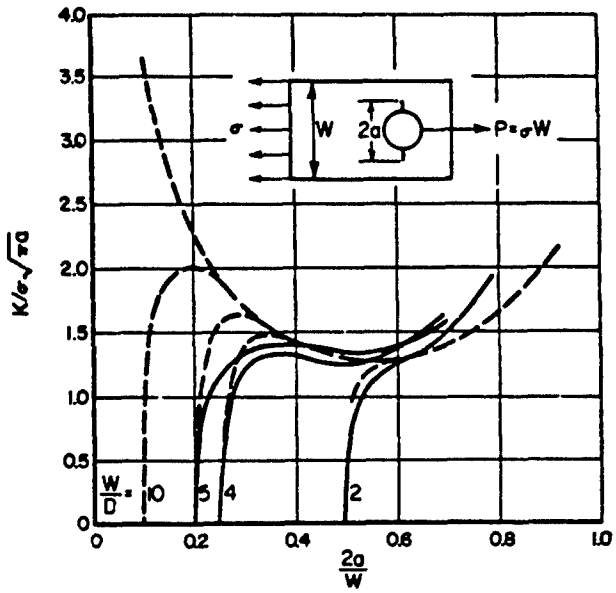

FIGURE 4. STRESS-INTENSITY FACTOR FOR PIN-LOADED HOLE ACCORDING TO COMPLIANCE MEASUREMENTS (REFERENCE 8) (SOLID LINES) AND ACCORDING TO SUPERPOSITION (DASHED LINES)

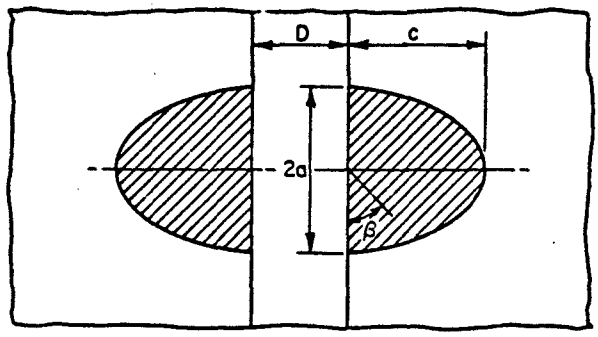

FIGURE 5. PROBLEM SOLVED BY HALL AND ENGSTROM

$$K=\frac{\sigma}{\phi}\sqrt{\pi a}\left[\cos^2\beta+\frac{a^2}{c^2}\sin^2\beta\right]^{1/4}F\left(\frac{c}{D},\beta\right) \qquad a>c$$

$$K=\frac{\sigma}{\phi}\sqrt{\pi a}\left[\sin^2\beta+\frac{c^2}{a^2}\cos^2\beta\right]^{1/4}F\left(\frac{c}{D},\beta\right) \qquad a<c$$

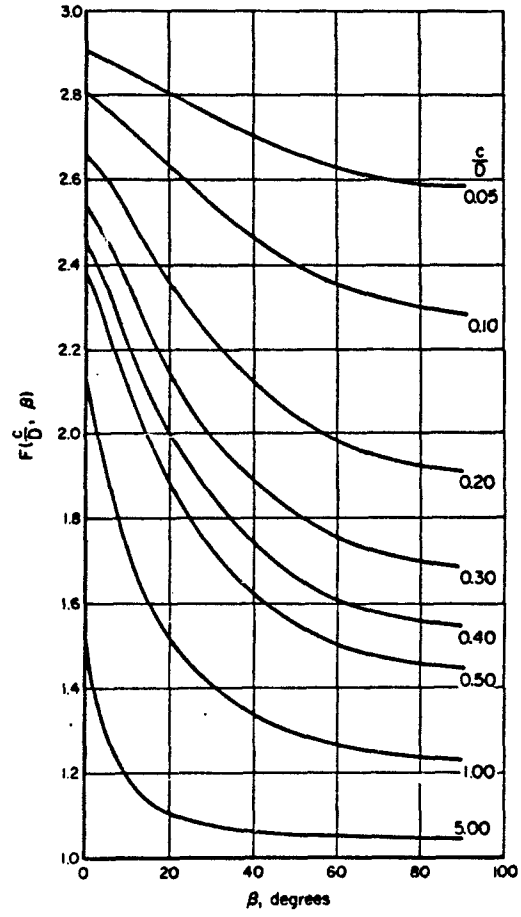

FIGURE 6. EFFECT OF HOLE ON STRESS INTENSITY ACCORDING TO HALL AND ENGSTROM

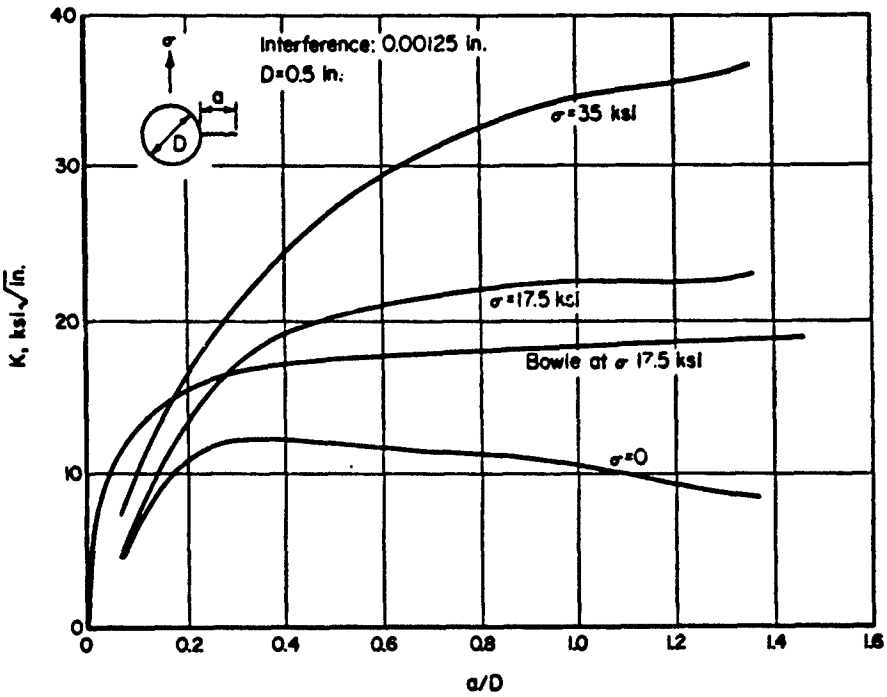

FIGURE 7. STRESS INTENSITY FOR THROUGH CRACKS AT HOLE WITH INTERFERENCE FIT FASTENER (REFERENCE 3)

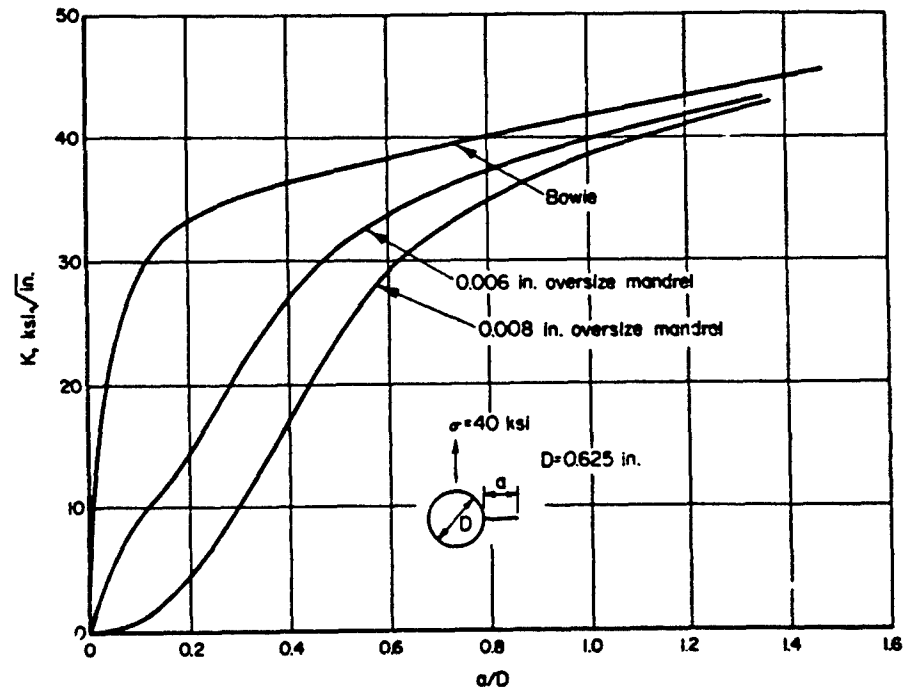

FIGURE 8. STRESS INTENSITY FOR THROUGH CRACKS AT COLD WORKED HOLES

The function F(c/D,β) is given in graphical form in Figure 6. It is also slightly dependent on a/c, but the variations are within 6 or 7 percent as compared with the case of a/c = 0.6 for which Figure 6 holds.

Hall and Engstrom checked their procedure by applying it to a through crack and found it applicable. They also showed that the case of an elliptical crack reduces to the Bowie solution for a/c approaching infinity. The stress-intensity factor is then $K = \sigma\sqrt{\pi c}\, F(c/D,90°)$, implying that values of F(c/D,90°) in Figure 6 should be equal to the Bowie function f_B. This is indeed the case.

The solution of Equation (11) was made suitable for corner cracks by applying free-surface correction factors and an extra correction factor for the case of a single corner crack. The results for a single corner crack is

$$K = \alpha_f \alpha_b \frac{\sigma}{\phi} \sqrt{\pi a} \left[\cos^2 \beta + \frac{a^2}{c^2} \sin^2 \beta\right]^{1/4} F\left(\frac{c}{D}, \beta\right) \sqrt{\frac{D+\pi ac/4B}{D+2\pi ac/4B}} \quad . \tag{12}$$

Some of the above work provides engineering solutions for the stress intensity of corner cracks and elliptical cracks of arbitrary shape. Such solutions are essential for damage tolerance analysis, since the crack changes shape during propagation as discussed in a later section. The problem of a corner crack of arbitrary shape was treated by means of three-dimensional finite-element analyses by Raju and Newman[15]. Stress-intensity factors were derived for a range of values of the relevant parameters; crack depth to thickness ratio ranged from 0.2 to 0.8, crack depth to length ratio ranged from 0.2 to 2, but the hole radius to plate thickness ratio was kept constant at 0.5. Raju and Newman have presented their results in graphical form.

Fujimoto also presented a solution for corner cracks and elliptical cracks of arbitrary shape at the edge of a hole. Fujimoto idealized the cracked plate by a number of slices each containing a through-the-thickness crack of different length. Springs between the slices were used to represent shear coupling. The solution was presented in terms of closed form polynomial expressions which contain the relevant ratios of crack depth to thickness, crack size to hole radius, etc. Fujimoto also provided extensive tables with coefficients for these polynomials for different kinds of cracks, such as corner flaws at unloaded and loaded holes, and embedded cracks at unloaded and loaded holes.

4.2.3 Holes With Fasteners

When considering a crack emanating from a fastener hole, the influence of the fastener has to be taken into account. If the fastener is a loose fit in an otherwise untreated hole, and when there is no load transfer, it is likely to have little effect on the behavior of a crack emanating from the hole. In general, however, the fastener has a tight (interference) fit. In many cases it does transfer some load. Moreover, the holes are often cold worked to improve fatigue resistance. All these things have an effect on cracking behavior, since they induce a redistribution of local stresses to the effect that the stress intensity is different from that at a cracked open hole.

Application of fracture mechanics principles to cracks at filled fastener holes requires knowledge of the effect of interference, cold work, and load transfer on the stress-intensity factor. Grandt[3] calculated stress-intensity factors for cold worked and interference fit holes by solving the problem of a cracked hole with an internal pressure distribution equal to the hoop stress surrounding an uncracked fastener hole.

Figures 7 and 8 show the observed trends. Since the shape of the curves depends upon the applied stress, the calculation has to be repeated for different stresses. Consequently, the results cannot be presented nondimensionally. The results in Figure 7 may be slightly misleading, because the hoop stress will be partly released when the bolt gets more clearance as the crack grows (decreasing stiffness). This effect was not accounted for in Grandt's solution.

It appears from Figures 7 and 8 that both an interference fit and cold work significantly affect the stress intensity. Mandrelizing is more effective, since it gives a larger reduction of the stress intensity over a wider range of a/D values.

For large a/D the stress intensity of the interference fit becomes larger than that of an open hole (compare the Bowie solution and interference fit curves for σ = 17.5 ksi in Figure 7). As explained above, the difference may be smaller in reality as the interference decreases due to the lower stiffness resulting from the larger crack. Yet, this phenomenon is considered typical for an interference fit. It also constitutes the essential difference between an interference fit and a mandrelized hole, as discussed in the following paragraph.

During mandrelizing the rim of the hole is plastically expanded. After removal of the mandrel the surrounding elastic material is allowed to contract, and thus it exerts compressive stresses to the rim. The plastic expansion of the rim does occur upon installation of an interference fastener. But the fastener stays in place, and hence, no contraction of the surrounding elastic material occurs. As a matter of fact, there exist tensile stresses around the hole, instead of compressive stresses. This is confirmed by the positive stress intensity of significant magnitude that remains at σ = 0 (Figure 7).

Shah[16] derived an approximate elastic-plastic solution for the stress distribution at holes with interference fit fasteners and also developed stress-intensity factors for the case of a loaded plate with a through crack at a hole containing an interference fit fastener. His results show trends similar to those by Grandt[3]. Increasing interference gives lower values for the peak stress intensity (by interference alone); if the plate is loaded the stress intensity becomes virtually independent of the amount of interference if the crack size is larger than the hole diameter.

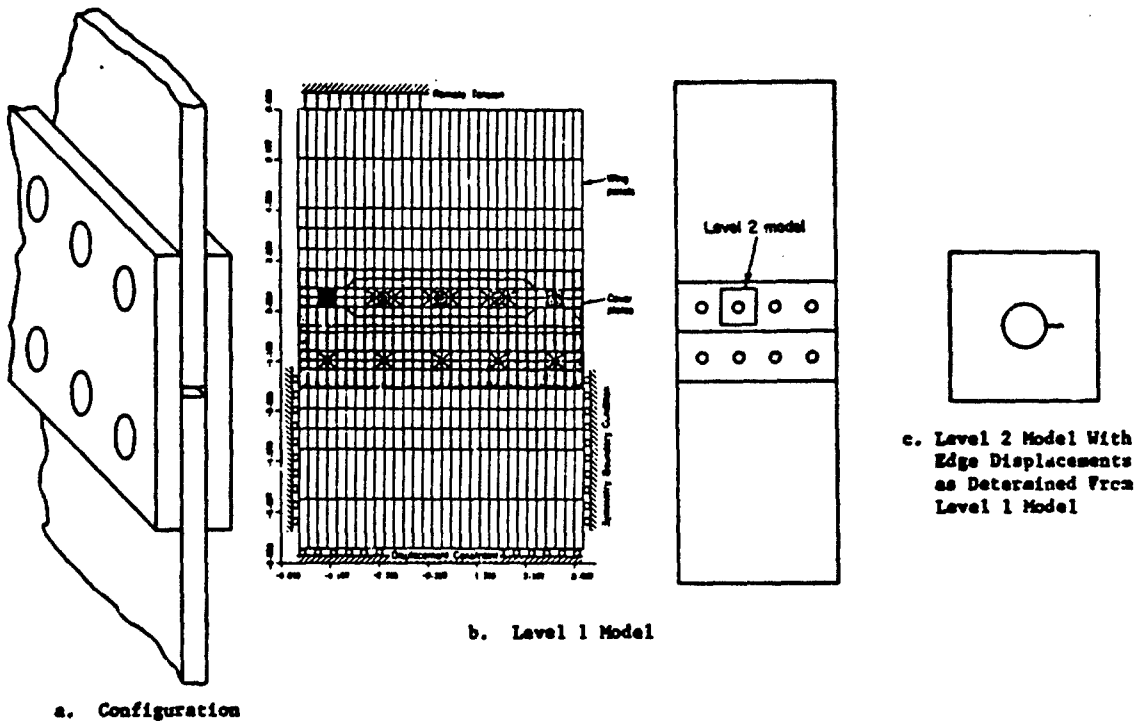

a. Configuration

b. Level 1 Model

c. Level 2 Model With Edge Displacements as Determined From Level 1 Model

FIGURE 9. SUBMODELING

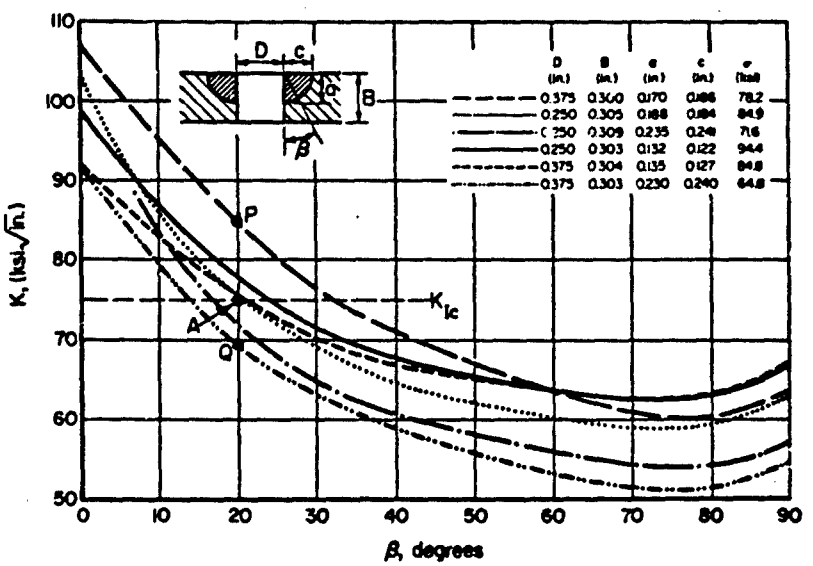

FIGURE 10. FRACTURE INDUCED BY SYMMETRIC CORNER CRACKS AT HOLES IN 4340 STEEL (REFERENCE 14)

4.2.4 Joints

In many cases joints transmit little or no load. That is, the joints between stringers and skin in a stiffened panel transmit moderate shear loads only. Somewhat higher shear loads are transmitted by e.g., a spanwise splice. However, due to the presence of a cracked hole, load will be transmitted from the cracked material into the underlying reinforcements. Usually, this will not affect the fastener in the cracked hole; the load transfer occurs through the adjacent fasteners, which may not carry any load in the absence of the crack. The result is twofold. In the first place, the cracked element experiences a lower stress, to the effect that growth rates are reduced. However, the load transfer through adjacent fasteners may induce other cracks. These cracks may occur in the same element, which leads to multiple parallel cracks. Also, they may occur in the underlying reinforcements. In case that load transfer occurs through the fastener in the cracked hole (lap joints, stringer run outs), the cracking tends to reduce the load transfer. This reduces the stresses at the cracked fastener at the expense of higher stresses at adjacent fasteners, which again may develop multiple cracks. A rigorous damage tolerance analysis might have to consider these possibilities.

An extreme case of load transfer to reinforcing elements occurs in stiffened panels if the cracks grow long. A skin crack across a stringer leads to extremely high growth rates in the stringer once it cracks. Cracks extending to the next stringer induce a high load transfer also, leading to low fatigue endurance of that stringer.

Many joints are designed for the specific purpose of load transfer, e.g., most pin-lug joints, chordwise splices, etc. Analysis of these joints requires the determination of the amount of load transfer through each of the fasteners. Lap joints and load bearing splices contain eccentricities. The bending stresses due to these eccentricities will have to be accounted for. Finally, a crack occurring at one of the holes in the joint will change the local stiffness and cause a redistribution of load transfer, which in turn will affect the stress intensity.

In most cases, a conventional stress analysis will be adequate to provide the necessary information for a damage tolerance assessment. The conventional stress analysis provides the stresses at the relevant fastener holes. One of the solutions discussed in the previous sections can then be used to determine the stress-intensity factor. In this manner, it can be established which joints have ample damage tolerance and which are marginal. The marginal joints could be redesigned; however, if the existing design is accepted a more elaborate analysis may be in place for these critical locations. A finite-element analysis would then be required.

In general, the finite-element analysis will be of the sub-model type. First, a relatively large, but coarse model is made of all elements of the joint and the surrounding structure. No cracks are assumed yet. Subsequently, a finer sub-model is analyzed that contains only the structural elements in the critical area. The boundary conditions for this sub-model are obtained from the large model. A crack is assumed at the critical location in the most critical structural element. However, an extremely fine mesh around the crack is not yet necessary, since this first sub-model is used only to determine the effect of the crack on load transfer. Finally, another sub-model is made of only the critical structural element at the critical location. Again, the boundary conditions follow from the previous model. A refined mesh at the crack tip is made for an adequate calculation of the stress-intensity factor.

Alternatively, instead of the last sub-model, one of the solutions discussed in the previous sections can be used to determine the stress-intensity factor, since the last sub-model has reduced the complex joint to the basic case of a crack emanating from a hole in a plate.

The procedure of sub-modeling is illustrated in Figure 9. The technique is discussed also in one of the example problems later in this chapter.

4.3 DAMAGE TOLERANCE ANALYSIS

4.3.1 Scope

In principle, the actual damage-tolerance analysis of a joint is no different than for any other structural detail. A crack-growth calculation and a residual-strength calculation are required. In this respect, similar difficulties are encountered as in any damage-tolerance calculation. These are associated with the stress spectrum, stress history, crack-growth-integration technique, retardation modeling, etc. Although these problems may be of more significance than any other of the problems encountered in the analysis of joints, they are not specific for joints. They are adequately treated elsewhere[9,18] and they are beyond the scope of this chapter.

A number of problems specific for the damage-tolerance analysis of joints will be discussed in the following subsections. The details of how to perform crack growth and residual-strength analysis will be assumed well-known.

4.3.2 Residual Strength

In the case of through cracks, particularly when plane stress prevails, the critical crack size is usually on the order of the hole diameter or larger. Then the simple engineering solution for the stress intensity that considers the hole part of the crack, is adequate for residual-strength analysis. The accuracy is much better than the scatter in material behavior, so that more refined analysis is not necessary. This was demonstrated by experimental data on large panels with through cracks at holes.[5,6]

In the case of corner cracks and embedded cracks in plane strain, the effect of the hole and the crack shape has to be accounted for. Solutions for K were discussed in the previous section. In all cases, the stress intensity varies along the crack front. It is usually assumed that fracture occurs when the maximum stress intensity (anywhere along the periphery of the crack) is equal to the fracture toughness.

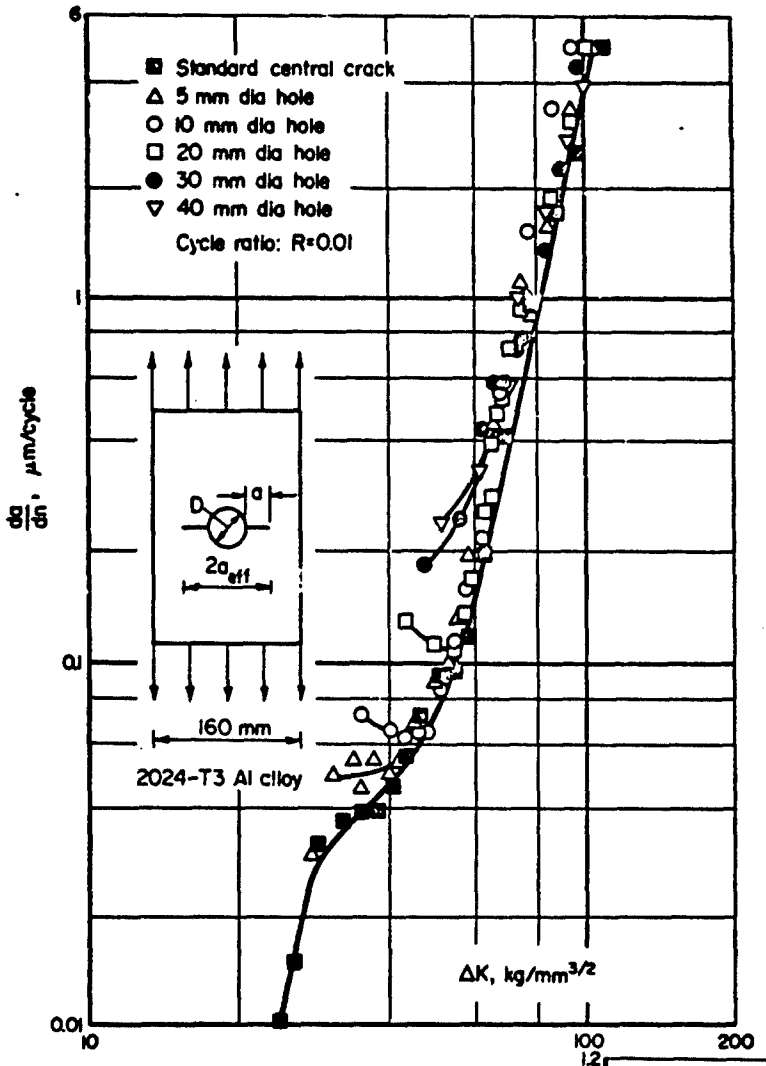

FIGURE 11. CRACK-GROWTH RATES FOR THROUGH CRACKS AT HOLE (REFERENCE 4)

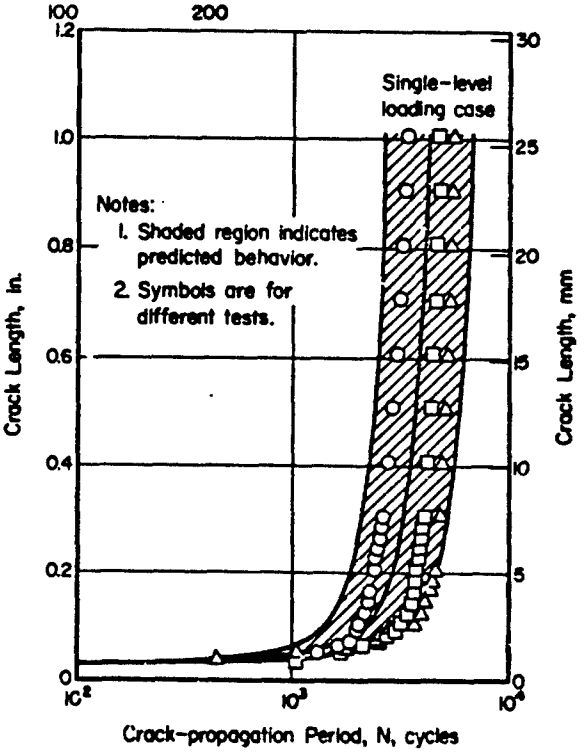

FIGURE 12. COMPARISON OF PREDICTED AND EXPERIMENTAL CRACK GROWTH (REFERENCE 20)

Despite the technical importance of the problem, a large scale experimental study to check the usefulness of the stress-intensity solutions to predict the residual strength, has never been performed. Several investigations were conducted in which limited ranges of the relevant parameters were considered. Almost all analysis methods gave good results when applied to such limited sets of data. However, the differences among the various solutions are large enough[9,18] to state that most of them must have limited applicability. To some extent this may be caused by the assumption that the highest stress intensity is a measure for the residual strength.

In this respect, the solution by Hall and Engstrom[14] is interesting, because it provides the variation of the stress intensity along the crack front. Some fracture test data provided by Hall and Engstrom are reproduced in Figure 10. The figure shows the calculated variation of K along the crack front at the onset of fracture for this flaw shape. If the analysis is assumed correct, it follows from Figure 10 that fracture occurred when the material at $\beta \approx 20°$ was subjected to a K equal to K_{Ic}.

Now the difficulty involved in the method becomes apparent. In order to be able to predict the residual strength of a given configuration, one has to know which K to use. If one chose to assume that K at $\beta = 20°$ is the significant quantity, failure would be predicted at point A for the given K_{Ic}. Actual test data vary between P and Q. If any other crack configuration were to be analyzed by the same method, the significant value of β for that particular case would have to be known. It is obvious from Figure 10 that a different choice of β would affect the outcome of the prediction. Not only the stress-intensity factor varies along the crack front, also the fracture toughness may be different in different directions. Materials with greater anisotropy than 4340 steel may exhibit another critical β, if K_{Ic} in the direction of that β is significantly lower than in other directions. In order to make the method useful for engineering applications, test programs are required to establish the fracture condition in terms of the angle, β. The tests would have to cover different configurations, and do so for a wide range of the geometrical parameters B, D, a, and c. Of course, any other analysis procedure would be faced with the same problem. The approaches discussed in the previous sections either assumed $\beta = 0$ or 90° to be critical, or they empirically established an effective crack size which implicitly accounts for the correct β.

The data in Figure 10 can be analyzed easily by considering the hole as part of the crack. The defect then would be a surface flaw of approximately semielliptical shape, with major axis $2\bar{c} = 2c + D$ and minor axis $\bar{a} \approx a$. The flaw shape parameter, ϕ, is to be based on $\bar{a}/2\bar{c}$. Since these are shallow flaws, the backfree surface correction is fairly large and cannot be neglected. Applying this correction, assuming $\sigma/\sigma_{ys} \approx 0.5$ for the determination of the flaw shape parameter, and taking $K_{Ic} = 75$ ksi$\sqrt{\text{in.}}$, the fracture stresses, σ, of the specimens in Figure 10 are predicted as 82, 94, 79, 114, 100, and 68 ksi. The actual fracture stresses are listed in the same order in Figure 10. The estimates are unconservative by only 6 to 12 percent. Thus, this simple procedure may be suitable for a quick appraisal of the order of magnitude of the failure stress.

The lesson to be learned from this discussion is that the problem of calculating the residual strength of a joint is not solved by having a solution for the stress-intensity factor. Indeed, it is doubtful whether a rough approximate solution for the stress-intensity factor is worse than a rigorous solution obtained from expensive finite-element analyses. Therefore, such rigorous solutions need to be generated for the most critical cases only. However, regardless of the sophistication of the K-solution, one still is left with the assumption that the maximum K will dictate fracture. Since this will generally be a conservative assumption, it is the one adopted in virtually all residual-strength analyses.

4.3.3 Propagation of Cracks at Holes

Fatigue through cracks emanating from holes were studied by Rau and Burck[9]. They used specimens of Udimet 700, containing small holes. In their analysis, they used the Bowie solution with an appropriate width correction.

Due to the smallness of the holes, the crack size is soon on the order of the hole diameter. Hence, the effect of the hole can only be found at low ΔK values. In this region the data were close to the reference curve, indicating that the Bowie analysis worked well.

Test data[4] for 2024-T3 aluminum sheet show[4,6,9] that crack growth from holes is very similar to the growth of a central crack, the differences being of the order of magnitude of the usual scatter in crack growth. This means that the hole can well be considered part of the crack if the amount of crack extension covered is on the order of one or a few times the hole diameter, depending upon the hole size.

Some da/dN data of the specimens are given in Figure 11, based on the Bowie analysis. According to Figure 11, the cracks emanating from holes grow slightly faster initially than normal central cracks at the same ΔK. This may be due to the fact that crack closure is less effective due to the presence of the hole.

Since a relatively large part of the crack-growth life is spent while the crack is still small compared to the hole, predictive calculations often should make use of the Bowie solution. By the same token, if much of the life is spent while the cracks are small, the accuracy of the solution is of great impact for the accuracy of the prediction. However, as shown above, discrepancies may not so much be a result of inaccurate stress intensities as well as of the lack of similitude. Small cracks at holes have a different history than the cracks used for derivation of the baseline da/dN data. As a result, conditions of equal K are associated with different plastic histories, closure, and residual stress. Thus some differences in growth rates should be expected. However, in general, damage-tolerance analysis assumes that equal K is enough guarantee for similitude, so that baseline data are applicable to all cases. Although this is a general problem in crack-growth analysis, it is more pronounced in the case of cracks at holes. Nevertheless, the prediction of crack growth can be reasonably accurate as shown by Crews and White[20]. Their predicted crack-growth curves (based on Bowie and on center crack basic data) are compared with actual test results in Figure 12.

With respect to corner cracks and elliptical cracks at holes, the accuracy is more difficult to assess. Fatigue-crack propagation of elliptical flaws is a problem for which a generally accepted analysis method is

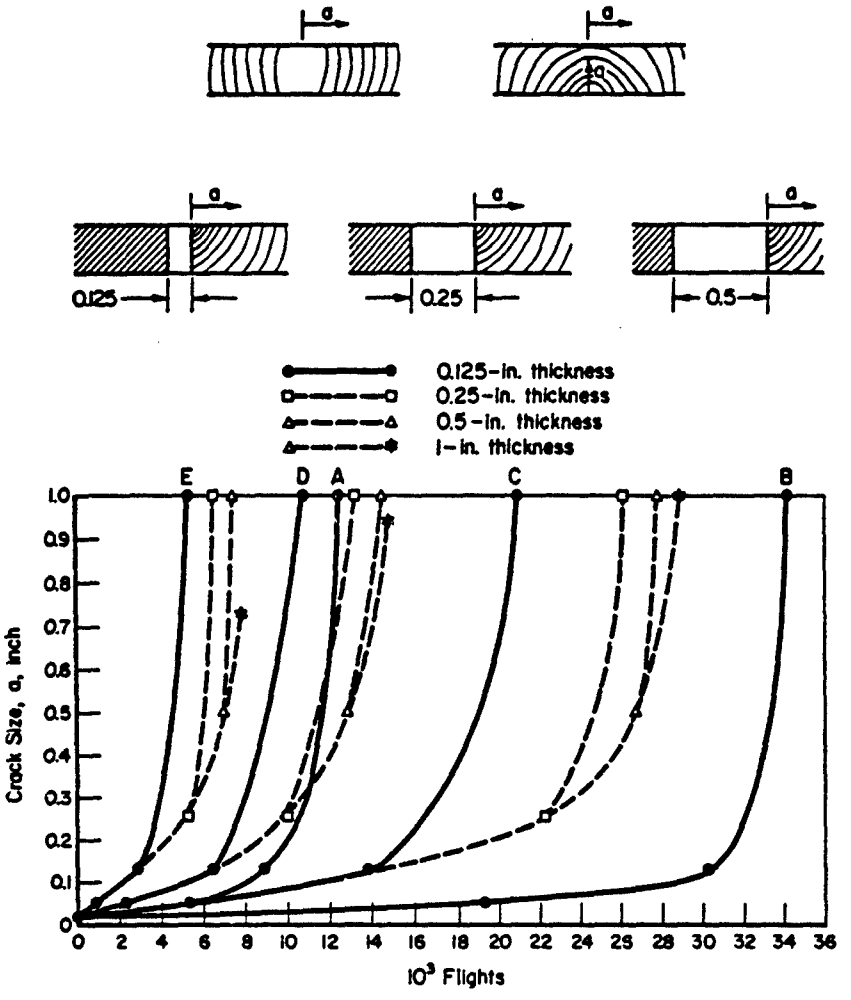

FIGURE 13. DIFFERENT FLAW SIZE ASSUMPTIONS

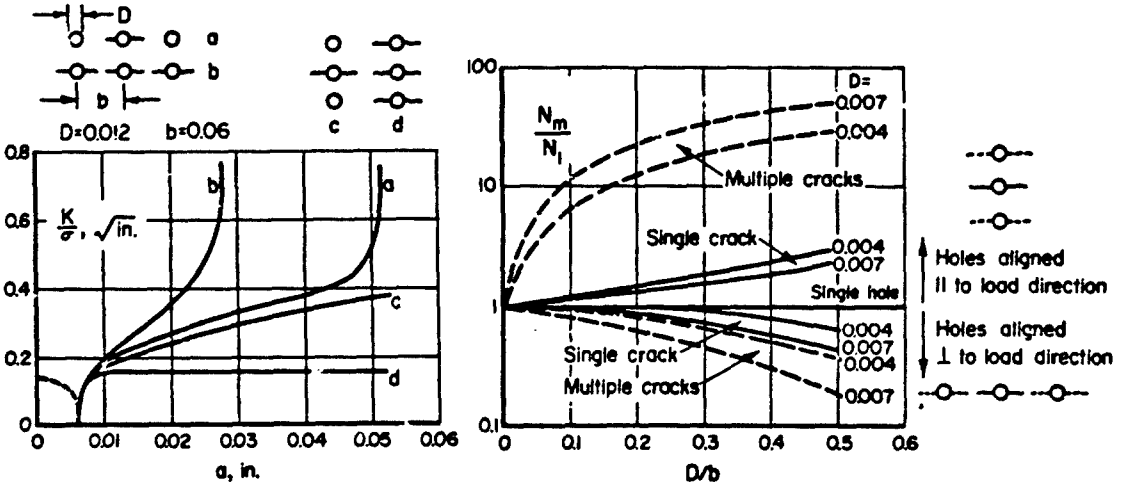

a. Stress-Intensity Factor as a Function of Crack Size b. Crack Propagation Life for Multiple Holes, N_m, Related to Life for Single Hole, N_1

FIGURE 14. EFFECT OF MULTIPLE HOLES AND MULTIPLE CRACKS (REFERENCE 24)

not yet available. The complication of the presence of a hole seems only minor. More than in the case of fracture, the variation of K along the crack front is of concern for fatigue-crack propagation.

A semielliptical surface flaw has its highest stress intensity at the end of the minor axis, the stress intensity at the surface being lower by a factor $\sqrt{a/c}$. Assuming that fatigue-crack growth in all directions is governed by the same relation between da/dN and ΔK, the crack will grow faster inward than along the surface, thus increasing its ratio a/c. When $a \gtrsim c$, the stress intensity is essentially constant along the crack front. Consequently da/dN will be the same at any crack tip element and the crack remains semicircular.

This tendency of cracks to become semicircular was observed by Mukherjee and Burns[21] in plexiglas sheet, a material not showing directional effects. Irrespective of the initial c/a ratio, the cracks changed shape until $c/a \gtrsim 0.96$. Similar results were obtained by Corn[22] for an aluminum alloy, two steels and two titanium alloys. Marked deviations from this behavior occurred in the case of bending, when the crack depth approached midthickness. Deviations may also occur when the crack-growth properties in the thickness direction differ from those in width direction. Finally, there is an increasing effect of the back-free surface when the crack moves further inward, resulting in an extra variation of K along the crack front.

If standard fracture mechanics approaches apply to surface flaws, there is a basis to assume that they apply to elliptical flaws at holes as well. Due to the larger variation of K along the crack front (Figure 10), the change of shape must be expected to be more pronounced than in the case of surface flaws. Therefore it is unlikely that crack growth can be reliably predicted if a flaw of constant shape is assumed. It is probably even insufficient to consider both the growth of c and a; one or two intermediate positions may be required.

Once the scene is set for a reliable prediction of crack growth, there remains one technical problem. This concerns the assumption of initial flaw shapes. Depending upon the assumed damage, machining practice, fastener type, etc., an endless variation of initial flaw shapes can occur. For a surface flaw, the crack-propagation life until critical size is reached, depends more on flaw shape than upon initial flaw size and fracture toughness[23]. The same holds for flaws at holes.

It might be argued that the flaw shape giving the shortest life should be prescribed. Most likely this would call for too frequent inspections or for inefficient weight penalties. As in all damage tolerance requirements, a certain risk of premature failure will have to be accepted. Therefore, the most likely initial flaw shapes may have to be disregarded. Establishment of a prescription for one or more initial flaw shapes would require an analysis of many configurations along the lines discussed above.

At this point it should be emphasized that the selection of a conservative but arbitrary size and shape of initial flaw, may not produce the same degree of conservatism in all cases. This is clearly demonstrated in Figure 13 which shows crack-growth curves for flight-by-flight loading for five different crack geometries. The cracks start at an assumed initial crack size of 0.02 inch.

Consider first Case E. If for reasons of conservatism the initial crack was assumed to be 0.05 inch, the crack-growth life would be approximately 16,000 flights. Crack growth from 0.02 to failure covers roughly twice as many flights. Thus the assumption of the larger initial crack buys a factor of 2 in conservatism.

In Case B, however, the life of an 0.02 crack is approximately 6,000 flights, and the life of an 0.05 crack is 5,000 flights. Thus, the assumption of the larger initial crack buys only a factor of 1.2 in conservatism. The difference is due to the fact that the stress-intensity factor for a small crack at the edge of a hole increases very rapidly with crack size (much more so than for the elliptical crack).

The conclusion to be derived from Figure 13 is that assumptions that provide conservative predictions in some cases, may provide only marginally conservative predictions in other cases. Generally, this can easily be foreseen (as in the example of Figure 13). Therefore each case should be considered by its own merits. Attempts to cover all crack problems with general assumptions can lead to dangerous optimism.

4.3.4 Crack Growth in Fastened Joints

Some special problems occur in the analysis of crack growth in fastened joints. These are

- Residual stresses due to interference fit fasteners and mandrelizing (hole expansion)
- Crack growth through rows of holes in multiply fastened joints
- Multiple cracks and merging of cracks in rows of holes
- Fretting.

The question may be raised whether it is practical to deal with these detailed problems. At present, it may be premature in view of the following reasons:

(a) The analysis of a cracked hole is still not satisfactory.

(b) The scatter in raw data makes predictions inaccurate anyway.

(c) There is still no reliable methodology to account for load interaction and retardation.

(d) There are additional unknowns in the load history, temperature history, and the effect of environment.

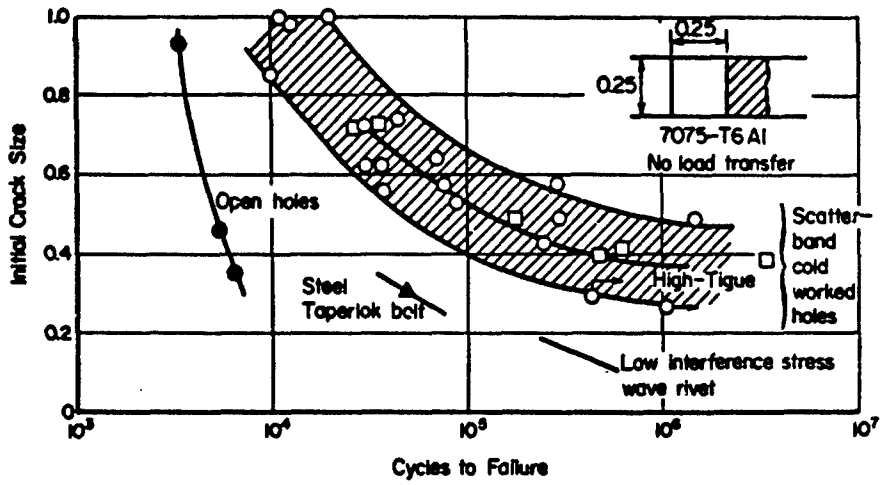

FIGURE 15. EFFECT OF FASTENERS AND COLD WORK ON CRACK GROWTH FROM HOLES (REFERENCE 25); σ_{max} = 30 KSI, R = 0.5

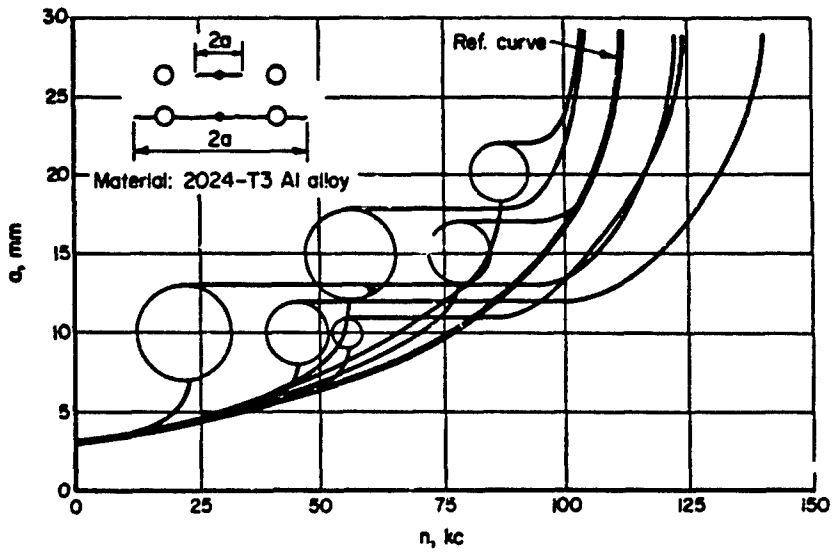

FIGURE 16. FATIGUE CRACKS GROWING INTO HOLES (REFENCE 26)

Therefore, a general analysis of the listed problems may suffice. It would provide an appreciation of the relative significance of each of them. Then they could be dealt with in an approximate way, without the necessity of costly detailed analysis of each particular structural geometry.

The case of multiple cracks at holes was analyzed by Burck and Rau[24]. They determined stress-intensity factors for single and multiple cracks at linear arrays of holes, either perpendicular or parallel to the load path. The result is shown in Figure 14(a). Multiple colinear cracks soon attain a high stress intensity. The single crack in this configuration would only reach a high K when approaching the neighboring hole (see also the section on arrest capabilities of holes). If multiple cracks are aligned in the loading direction, there is an important shadow effect giving a significant reduction of K.

On the basis of Figure 14(a), Burck and Rau predicted crack-growth lives for wrought Udimet 700. Their results are given in Figure 14(b). Due to the presence of multiple holes, the lifetime of single cracks appears to be influenced by a factor of 0.5 - 3 as compared with a single crack at a single hole. Multiple cracks show an even larger difference in growth lives. The case of multiple cracks in an array parallel to the load axis is unstable. If one of the cracks becomes longer than the others, its K increases, while K of the other cracks decreases. The effect is larger for longer cracks, so that the array is likely to promote one crack to grow to failure. For colinear cracks, the K for all cracks increases if any one crack becomes larger.

Some data[25] regarding the effect of fasteners are presented in Figure 15. They show the large beneficial effect of interference and cold working. In the case of load transfer, the crack-propagation rates were significantly higher[25]. Large interference leads to slower growth rates. Equal amounts of growth of a corner crack at an unloaded taperlok bolt in 2219-T851 aluminum took 29, 21, and 12 kilocycles at interferences of 0.0060, 0.0038, and 0.0024, respectively[14]. In the case of the open hole, the same crack growth occurred in only 6 kilocycles.

These data indicate some trends, but they cannot be generalized. Other stress levels, other fastener systems, and load transfer may change these results considerably. So many parameters are involved that systematic test data are hard to find, if at all available. Investigations to the effect of fasteners all tend to include too many of these parameters, to an extent that even elaborate test programs often fail to give generalizable results. Another shortcoming of the tests is inherent in the production of specimens. In order to obtain the required starter crack, the specimens are precracked before the interference fit fastener is installed or before the hole is cold worked. Both procedures are liable to build additional residual stresses into the crack tip area. A different stress system would exist at the crack tip if it had grown after fastener installation or hole expansion. Conceivably, also, crack-growth behavior would be different.

Fastener holes usually occur in rows. A crack initiated at one of them may interact with other holes in the crack path. If a fatigue crack runs into a hole, it may be arrested there for a considerable time. Therefore, holes are often considered as useful crack stoppers. Unfortunately, it turns out that this is seldom true.

Isida[30] has determined stress-intensity factors for cracks approaching holes. If the crack tip is in the vicinity of the hole, the stress intensity tends to infinity. This can be observed also in Figure 14(a). Consequently, the fatigue crack must run into the hole at an extremely fast rate. If the crack reaches the hole, the defect size is suddenly increased by the hole diameter. When the crack reinitiates at the other side, there is a much larger crack with an inherently higher growth rate. These two effects appear to offset the gain in life from the dormant period necessary for reinitiation.

This is confirmed by the test data[26] shown in Figure 16. Irrespective of the size and spacing of the holes, the crack-propagation curve is practically identical to the reference curve, the differences being on the order of the normal scatter. Crack-growth rates as a function of ΔK (on the basis of Isida's solution) satisfy the reference curve[26]. Hence, the case can be treated with normal fracture mechanics procedures (that do not include the dormant period). In the USAF damage tolerance requirements[27], the dormant period is completely neglected. The requirements assume the existence of an 0.005 inch crack at the other side of the hole when a crack runs into a hole.

Probably, the beneficial effect of the hole is much larger in the case of mandrelized holes. Crack growth into the hole is not likely to be affected much by the expansion, but the residual compressive stresses will certainly lengthen the reinitiation period. There are no test data available to prove this point. It is confirmed indirectly by tests on expanded stopholes[28].

Arrest of fatigue cracks can be attained in three different ways:

(a) Reduction of stress concentration.

(b) Introduction of residual compressive stresses.

(c) Reduction of stress-intensity factor.

Reduction of the stress concentration occurs when the crack runs into a hole. As shown previously, this may not be beneficial unless there are also residual stresses as a result of mandrelizing. Reduction of the stress-intensity factor occurs when the crack approaches a reinforcement element (e.g., a stringer). The result is that the crack-growth rates are drastically reduced, although a total arrest may not occur. Since stringers are usually attached to the skin by means of fasteners; total arrest can occur if the crack runs into a fastener hole.

The capability of holes to arrest post-instability crack growth is a matter of great interest. The problem is a complicated one because it has to be treated on the basis of dynamic stress intensity and

elastic energy release rates, while there may also be a contribution of kinetic energy. A qualitative analysis of dynamic crack arrest can be made in principle[19], and this could be extended to give a qualitative formulation of the effect of holes. From an investigation by Kobayashi, et al[29,30], it can be concluded that the arrest power of small holes is probably poor. Therefore, the arrest capability of holes in general is probably not of great technical importance.

A particular case of arrest at holes occurs in stiffened panels, where the arrest may be essential to the fail-safe strength. This subject is dealt with in the chapters on stiffened structures.

4.4 EXAMPLES

4.4.1 Introduction

The number of examples received was small. Also, there was no uniformity in their presentation, nor in the amount of detail provided. Therefore, it was virtually impossible to cast all examples in a similar format. Instead, it was decided to present the brief examples in their original but edited form, without attempts to arrive at some uniformity. Examples for which more details were provided were abbreviated to provide an abstract that still retains the essential features of the analysis. It is emphasized that the way of presentation, the contents and conclusions are the responsibility of the contributors. No changes were made other than for the sake of legibility. At the end of each example, a brief comment is provided by the editor.

4.5 REFERENCES

1. Gran, R. J., Orario, F. D., Paris, P. C., Irwin, G. R., and Hertzberg, R. W., "Investigation and Analysis Development of Early Life Aircraft Structural Failures", AFFDL-TR-70-149 (1971).

2. Bowie, O. L., "Analysis of an Infinite Plate Containing Radial Cracks Originating at the Boundary of an Internal Circular Hole", J. Math. and Phys., 35, 1 (1956), pp 60-71.

3. Grandt, A. F., Jr., "A General Stress Intensity Factor Solution for Through-Cracked Fastener Holes", Submitted for publication in Int. J. of Fracture.

4. Broek, D., "The Propagation of Fatigue Cracks Emanating From Holes", Nat. Aerospace Lab., Amsterdam, Report TR 72134 (1972).

5. Broek, D., and Vlieger, H., "Cracks Emanating From Holes in Plane Stress", Int. J. Fract. Mech. 8 (1972), pp 353-356.

6. Broek, D., "Fail Safe Design Procedures", Fracture Mechanics of Aircraft Structures, Chapter V, Liebowitz, editor, AGARDograph No. 176 (1974).

7. Owen, D.R.J., and Griffiths, J. R., "Stress Intensity Factors for Cracks in a Plate Containing a Hole and in a Spinning Disc, Int. J. of Fracture, 9 (1973), pp 471-476.

8. Cartwright, D. J., and Ratcliffe, G. A., "Strain Energy Release Rate for Radial Cracks Emanating From a Pin Loaded Hole", Int. J. of Fracture Mech., 8 (1972), pp 175-181.

9. Broek, D., Elementary Engineering Fracture Mechanics, Noordhoff (1974).

10. Hall, L. R., and Finger, R. W., "Fracture and Fatigue Growth of Partially Embedded Flaws", Air Force Conference on Fatigue and Fracture, AFFDL-TR-70-144 (1970), pp 235-262.

11. Liu, A. F., "Stress Intensity Factor for a Corner Flaw", Eng. Fracture Mech. 4 (1972), pp 175-179.

12. Grandt, A. F., Jr., and Hinnerichs, T. D., "Stress Intensity Factor Measurements for Flawed Fastener Holes", U. S. Army Symposium on Solid Mech., 1974.

13. McGowan, J. J., and Smith, C. W., "Stress Intensity Factors for Deep Cracks Emanating From the Corner Formed by a Hole Intersecting a Plate Surface", Virginia Polytechnic Institute, Report VPI-E-74-1 (1974).

14. Hall, L. R., and Engstrom, W. L., "Fracture and Fatigue-Crack-Growth Behavior of Surface Flaws and Flaws Originating at Fastener Holes", Boeing (1973). To be issued as AFFDL technical report.

15. Raju, I. S., and Newman, J. C., "Stress Intensity Factors for Corner Cracks at the Edge of a Hole", NASA Tech. Mem. 78728 (1978).

16. Fujimoto, W. T., "Determination of Crack Growth and Fracture Toughness Parameter for Surface Flaws Emanating From Fastener Holes", McDonnell Aircraft Company Report MCAIR 76-005 (1972).

17. Shah, R. C., "Through Cracks at Interference Fit Fasteners", ASME Paper No. 76 PVP-5 (1976).

18. Fracture Mechanics of Aircraft Structures, Liebowitz, editor, AGARDograph No. 176 (1974).

19. Rau, C. A., Jr., and Burck, L. H., "Fatigue of Ni-Base Superalloy Sheets Containing Various Diameter Small Holes", Eng. Fract. Mech., 2 (1971), pp 211-223.

20. Crews, J. H., and White, N. H., "Fatigue-Crack Growth from a Circular Hole With and Without High Prior Loading", NASA TN D-6849 (1972).

21. Mukherjee, B., and Burns, D. J., "Growth of Part-Through-Thickness Fatigue Cracks in Sheet PMMA", Eng. Fract. Mecn. 4 (1972), pp 675-685.

22. Corn, D. L., "A Study of Cracking Techniques for Obtaining Partial Thickness Cracks of Preselected Depths and Shapes", Eng. Fract. Mech. 3 (1971), pp 45-52.

23. Schra, L., et al, Private communication, Nat. Aerospace Inst., Amsterdam.

24. Burck, L. H., and Rau, C. A., "Fatigue-Crack Propagation From Small Holes in Linear Arrays", Int. J. Fract. 9 (1972), pp 43-51.

25. Tiffany, C. D., Stewart R. P., and Moore, T. K., "Fatigue and Stress-Corrosion Tests of Selected Fasteners/Holes Processes", ASD-TR-72-111 (1973).

26. Van Oosten Slingeland, G. L., and Broek, D., "Fatigue-Cracks Approaching Circular Holes" (in Dutch), Delft University (1973).

27. Wood, H. A., "The Use of Fracture Mechanics Principles in the Design and Analysis of Damage Tolerant Aircraft Structures", Fract. Mech. of Aircraft Structures, AGARDograph No. 176 (1974), pp 18-31.

28. DeRijk, P., and Otter, A.A.M., "Empirical Investigation on Some Methods for Stopping the Growth of Fatigue Cracks", Nat. Aerospace Inst., Amsterdam, Report TR 70021 (1970).

29. Kobayashi, A. S., Wade, B. G., and Maiden, D. E., "Photoelastic Investigation on the Crack-Arrest Capability of a Hole", Exp. Mech. (1972), pp 32-37.

30. Kobayashi, A. S., and Maiden, D. E., "Stress Intensity Factor for a Straight Crack Approaching a Circular Hole", Air Force Conference on Fatigue and Fracture", AFFDL-TR-70-144 (1970), pp 217-223.

4.6 EXAMPLE PROBLEMS

EXAMPLE PROBLEM 4.6.1

CRACK PROPAGATION IN LUGS ON AFT FLAP LINKS

M. Bradley, British Aerospace
(Literal)

1. STATEMENT OF THE PROBLEM

This calculation was undertaken in order to obtain an inspection crack size for lugs on the aft flap links of a medium transport aircraft. The Hall and Finger method of analysis for a crack at a hole was first compared with some data for shackles from another aircraft, but of the same material, and a factor deduced to give the correct K_{Ic} value at failure.

The aft flap link is shown in Figure 1. The load spectrum consisted of two cycles per flight, each ascending from zero to a certain maximum value.

2. INTERPRETATION OF SHACKLE DATA FROM A PREVIOUS AIRCRAFT

The shackle data were available only in terms of failure stress as a function of cracked area, as shown in Figure 2. Assuming the cracks were of elliptical shape, their area is $\pi pq/4$, and $q = 0.83\ p$. So p and q can be derived for any point on the curve.

K was calculated for 5 points on the curve without using an edge factor. The K_{Ic} value of the material was then divided by the calculated K to give the required edge factor value for each point. A curve was then plotted of edge factor against $(d+2q_{eff})/D$ as shown in Figure 3.

3. STRESS-INTENSITY FACTOR

The formula used for the stress-intensity factor was the one proposed by Hall and Finger:

$$K = .87\ \sigma\sqrt{\pi q_{eff}}\ F_B\ (q_{eff}/d)\ F_E\left(\frac{2q_{eff} + d}{D}\right)$$

(crack at both sides of hole) q_{eff} is the length of a through crack equivalent to the corner crack and is derived using a plot of q_{eff}/q against P/B for the required P/q ratio.

F_B is the Bowie Factor which caters for the effect on the hole on the crack.

F_E is an edge factor based on the diameter of the hole plus the two equivalent through crack lengths being equal to the length of a crack in a center cracked panel. This factor was derived empirically from the shackle data and then used for the flap lugs.

4. CALCULATION OF CRACK GROWTH AND CRITICAL CRACK SIZE

The required residual strength was equal to the cyclic stress.

Using the method derived above, the K values were calculated for the midpoints of successive .05-inch increments. The values of q_{eff} were also calculated for the edge points of the increment. It was found that the K_{Ic} value of the material was not reached at the outer edge of the lug. As the theory is not applicable after this point and the shape of the graph of K against q was very steep, it was decided to take the failure point as the edge of the lug.

The R value for the load cycle was zero and so the max K values calculated above were also the ΔK values for the propagation calculation. Crack-growth data for the S99 material were obtained from the National Physical Lab Report MG/EF/365/72. The data were represented by

$$da/dN = 1.6 \times 10^{-14}\ \Delta K^{1.9} \quad .$$

Since a refers to the length of a through crack, it follows that $a = q_{eff}$. From this dq/dN values were calculated at .05 in increments.

Hence for each segment:

$$\text{Cycles to grow through segment} = \frac{q_{eff}\ (\text{end}) - q_{eff}(\text{start})}{dq_{eff}/dN} \quad .$$

The cycles for each segment were added to the sum of the previous ones to give the number of cycles from zero to that length. A curve was then plotted through the points obtained by the method above. When a desired inspection period had been decided this was stepped back from the failure point and the corresponding crack length read off (Figure 4). This crack length then had to be of sufficient length to be detectable.

5. DISCUSSION

Unfortunately no test results are available for the flap links so that no comment can be made on the accuracy of this method. However, the example illustrates the general philosophy used: wherever possible

the given equations are modified using test data from components similar to the one to be analyzed. This approach has been used because experience has shown that no one method is capable of covering all cases adequately. The choice of the Hall and Finger method as a base for the calculation stems from the limited amount of data available. The method advocated by Broek, although theoretically superior requires several corrections of a complicated nature which would require large amounts of data to fully cover them and this amount of data is not generally available. A numerical example follows which will help clarify the foregoing outline.

6. NUMERICAL EXAMPLE

A. Shackle

D = 3.64; d = 1.328; B = 0.8. Ultimate design stress is 80 tons/in.^{2}. % stress is expressed as net stress; gross stress = net stress x (D - d)/D; q = 0.83 p.

For loss of area of 10%

$$\text{area lost per side} = \frac{0.1 \times (2.64-1.328) \times .8}{2} = .105$$

$$= \pi pq/4 = \pi \times .83\ p^2/4;\ p = 0.2835;\ q = 0.2353$$

% ultimate stress = 76.5.

Hence, gross stress = $76.5 \times 80 \times 2240 \times \frac{2.64 - 1.328}{2.64}$ = 68024 psi; p/q = 1.2048; p/B = 0.3544.

From Hall and Finger Curve; $q_{eff}/q = .66$

$$q_{eff} = .66 \times .2353 = .1538;\ \frac{q_{eff}}{d} = \frac{.1533}{1.328} = .1154.$$

From Bowie Curve for crack each side of hole: $F_B = 2.32$

$$.87\ \sigma\sqrt{\pi q_{eff}}\ F_B = .87 \times 68024 \times \sqrt{\pi \times .1533} \times 2.32 = 95{,}283\ \text{psi}\sqrt{\text{in.}}$$

For S99 $K_{Ic} = 80{,}000/\text{psi}\sqrt{\text{in.}}$; $F_E = 80{,}000/95{,}283 = 0.8396$

$$\frac{d + 2q_{eff}}{D} = \frac{1.328 \times 2 \times .1533}{2.64} = 0.6192.$$

Results for various values of $(d+2q_{eff})/D$ are plotted in Figure 3.

B. Aft Flap Link Top Lug

d = 1.125; D = 1.6; B = 0.5. Gross stress = 6693 psi. K was calculated using the same method as for the shackle but with the edge factor. Since the case considered now is a single crack at a hole, a different Bowie curve is used. Use of the derived edge factor is slightly pessimistic but acceptable for design purposes.

Summary of Results

q	q_{eff}	K
.025	.0043	2,215
.05	.016	
.075	.0311	5,793
.10	.051	
.125	.0744	9,078
.15	.0997	
.175	.1243	12,715
.20	.151	
.2188	.1718	19,104
.2375	.1193	

Propagation:

$$\frac{dq_{eff}}{dN}\ (\text{for } 0 - .05 \text{ inc.}) = 1.6 \times 10^{-14} \times 2215^{1.9} = 3.6335 \times 10^{-8}$$

$$\text{Cycles for increment} = \frac{.016 - 0}{3.6335 \times 10^{-8}} = 4.4035 \times 10^5.$$

Summary of Results (plotted in Figure 4)

Crack Inc	Cycles in Inc	Cumulative Cycles
0 - .05	4.4035×10^5	440,350
.05 - .10	1.5494×10^5	595,290
.10 - .15	9.1887×10^4	687,180
.15 - .20	5.1024×10^4	738,200
.20 - .2375	1.9917×10^4	758,120

Required inspection period was 1 year (=15,040 cycles with factor of 2). From Figure 4 it follows that the crack length which must be inspectable is 0.2068 in.

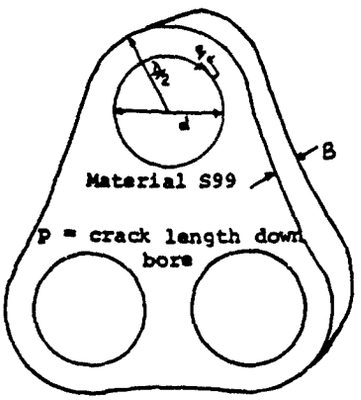

FIGURE 1. AFT FLAP LINK

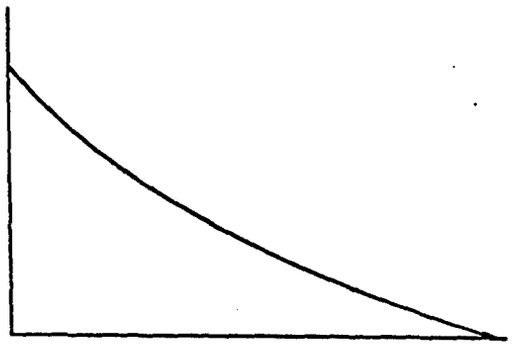

FIGURE 2. SHACKLE DATA

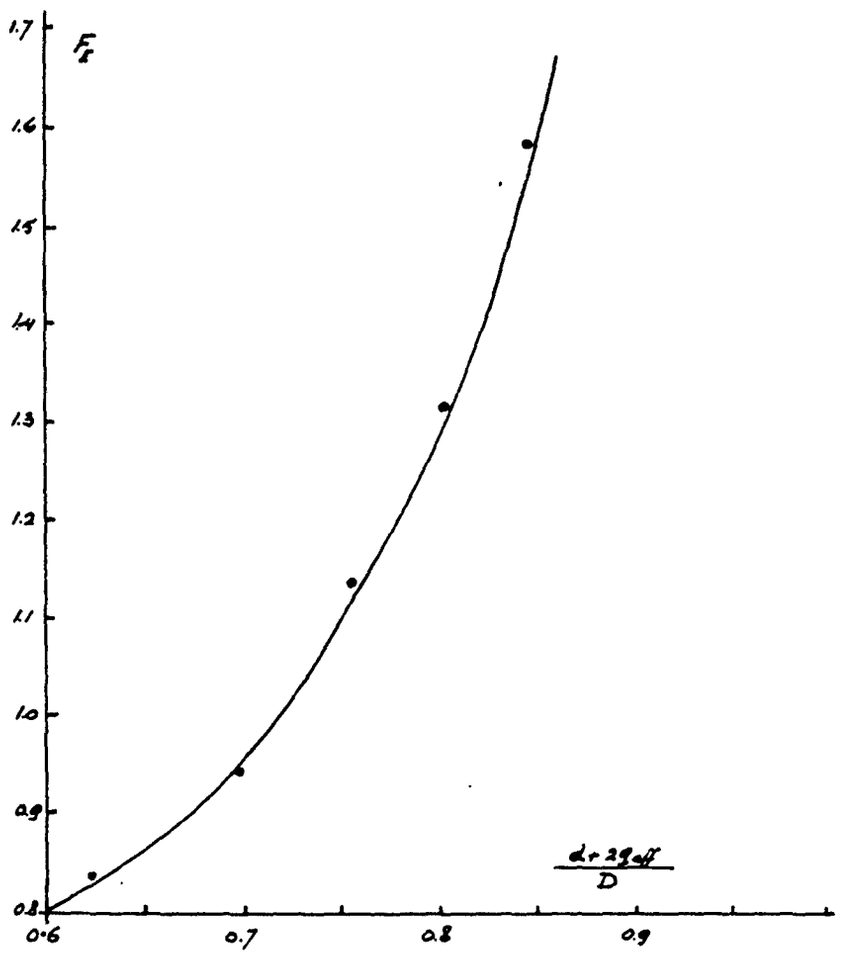

FIGURE 3. THE EDGE FACTOR

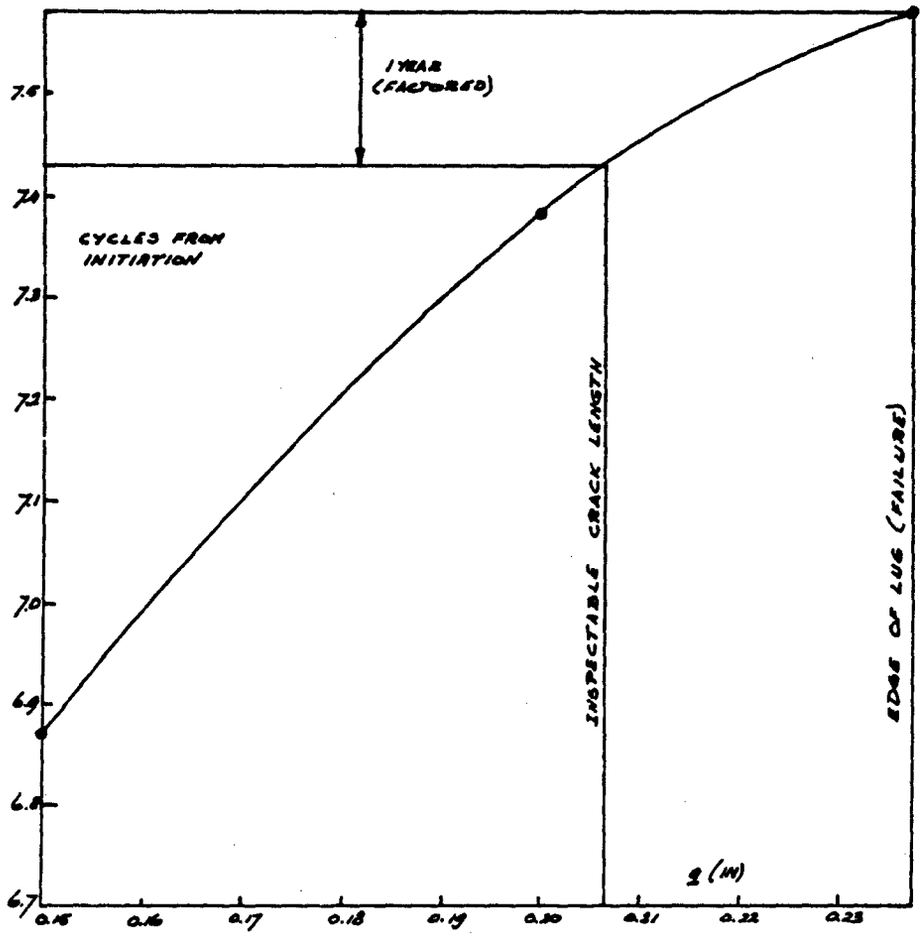

FIGURE 4. PROPAGATION CURVE FOR FLAP LINK LUG

7. COMMENTARY

Calibrating β in $K = \beta\sigma\sqrt{\pi a}$ by adjustment to test data is a cost-effective solution. The difficulty here is the (high) K_{Ic} of 80 ksi$\sqrt{\text{in}}$. If the yield strength of S - 99 is 70 ksi, the failures of the shackle occurred while the plastic zone (plane strain) was $(80/70)^2/6\pi = 0.07$ inch, which is 25 percent of the crack size in the numerical example. The failure stress calculated in the numerical example is 68 ksi, so that the entire net section was probably yielding. Thus, applying the calculated equivalent stress-intensity factors for fracture to fatigue-crack propagation (small plastic zone) is a violation of similitude requirements. The stress-intensity factors are probably too low. (In the case of net section yield fracture takes place at apparent stress-intensity factors well below those for elastic fracture.) Therefore the calculated crack growth should be considered with reservation. Nevertheless, if no better information is available, the method illustrated in the example can be very useful.

EXAMPLE PROBLEM 4.6.2

CORNER DEFECTS AT HOLES OF WING SPAR BOOMS

D. Grange and M. Bradley
British Aerospace
(Literal)

1. STATEMENT OF PROBLEM

Corner cracks occurred at holes in the wing spar booms (Figure 1) of a heavy military aircraft during its full scale fatigue test. As a result, estimates of the residual strength and permissible inspection periods were required. The residual strength estimates were based on the plane strain toughness for the material and the Hall and Finger stress-intensity solution for a corner defect at a hole. Inspection periods were based on propagation data deduced from the fractographic examination of the fatigue test specimen failure. The predictions assume the damage to be corner defects of quarter circular form at each side of the hole.

2. STRESS INTENSITY

The solution utilized was that by Hall and Finger for a corner defect at a hole, where the defect is idealized as an equivalent through the thickness crack. This solution caters for a finite condition with regard to thickness, but not with regard to width, thus a correction to cover the latter was included. Since no test evidence for defect sizes approximating those anticipated as being critical under the residual strength loading were available, an additional factor of 1.5 was included to cover possible scatter. This value was deduced from some previous work on these booms, where predictions made using the above solution were compared with plane strain toughness values, measured from the same material.

$$\text{i.e., } K = 0.87\,\sigma\sqrt{\pi q_{eq}} \cdot f(q_{eq}/D) \cdot f\left(\frac{R+q_{eq}}{w}\right) \cdot 1.5$$

where $f(q_{eq}/D)$ is the Bowie function to allow for the presence of the hole

and $f\left(\frac{R+q_{eq}}{w}\right)$ is a finite width correciton.

q_{eq} is obtained from empirically derived curves which are a function of P/B and q/P ref. AFFDL TR 70-144.

3. RESIDUAL STRENGTH

The residual strength requirement was 80% of the design ultimate, resulting in a stress of 26,160 psi. The plane strain material toughness for the boom material in the longitudinal direction is 27.0 ksi$\sqrt{\text{in}}$. The stress intensity as a function of crack size was determined for the above loading, and the crack size appropriate to the above toughness obtained. Critical crack size was 0.125 inch.

A typical evaluation of K follows. Considering q = 0.1 evaluate the size of the equivalent through crack from

$p/2 = 0.1/2.24 = 0.0446 \quad p/q = 1.0.$

The curves provide: $q_{eq}/q = 0.118$, so that $q_{eq} = 0.118 \times 0.1 = 0.0118$.

The Bowie function for $q_{eq}/D = \frac{0.0118}{0.625} = 0.0189$.

The finite width correction follows from $\frac{R + q_{eq}}{w} = \frac{0.3125 + 0.0118}{0.75} = 0.432$, giving $f\left(\frac{R+q_{eq}}{w}\right)$ 1.12.

Thus: $K = 0.87 \times 26{,}160 \sqrt{0.0118\pi} \times 3.08 \times 1.12 \times 1.5 = 22.67$ ksi$\sqrt{\text{in}}$.

A plot of K against a is given in Figure 2.

3.1. Permissible Inspection Period

This was based on the propagation data deduced from a fractographic examination of the fatigue failure. The results should be directly applicable since the loading was the actual service spectrum. The permissible inspection period is the period of growth from the crack reaching a size deemed as inspectable a_i to the size at which unstable growth would result under the residual load a_c. The size of crack deemed to be inspectable under this configuration was 0.05 inch, thus the permissible inspection period will be the time for the crack to grow from 0.05 inch to 0.125 inch.

From the fractographic examination, it was known that to grow from 0.05 inch to 0.10 inch requires 460 flights. It was necessary to estimate the additional time for growth from 0.10 inch to 0.125 inch. This is deduced by estimating the difference in average rate between the two growth periods.

Considering growth from 0.05 inch to 0.10 inch takes N = 460 flights, the average $da/dN = 0.05/460 = 1.087 \times 10^{-4}$ in./cycle.

Considering growth from 0.10 inch to 0.125 inch, the difference in average rate can be obtained from the difference in K for each of the mean crack sizes of the two growth periods: For 0.05 – 0.10 inch the average is 0.075 inch and for 0.10 – 0.125 inch the average is 0.1125 inch.

From Figure 2 it follows that the ratio of the K-values for these two crack sizes is 1.42. To obtain the difference in rate over the two periods, a $da/dN \sim \Delta K$ curve for the material was used. The average rate for the growth period covered by the test (0.05 inch to 0.10 inch) was 1.087×10^{-4} in./cycle. According to the rate data, these represented an effective ΔK of 21.0 ksi$\sqrt{in}$. However, for the growth period 0.10 inch to 0.125 inch the effective ΔK value would be expected to have been $21.0 \times 1.42 = 29.82$ ksi$\sqrt{in}$.

The $da/dN - \Delta K$ curve provides the rate applicable to this growth period.

$da/dN = 3.54 \times 10^{-4}$ in./cycle, or $N = \frac{0.025}{3.54 \times 10^{-4}} = 70.6$ flights, and $N_{tot} = 460 + 71 = 531$ flights.

To cover scatter in propagation, a factor of 3 is applied, making the inspection period 177 flights.

4. COMMENTARY

It is considered reasonable practice to take crack increments of 5 percent (sometimes 10 percent) of the current crack size. The increment taken in the example is 25 percent; however, the remaining life of 7 flights is so small that the rough approximation is well justified in this case.

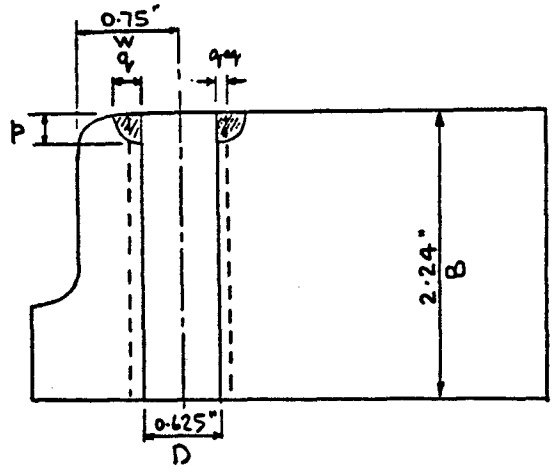

Material DTD 683

duplex precipitated to DTD 5104

FIGURE 1. CRACKS IN SPAR BOOM

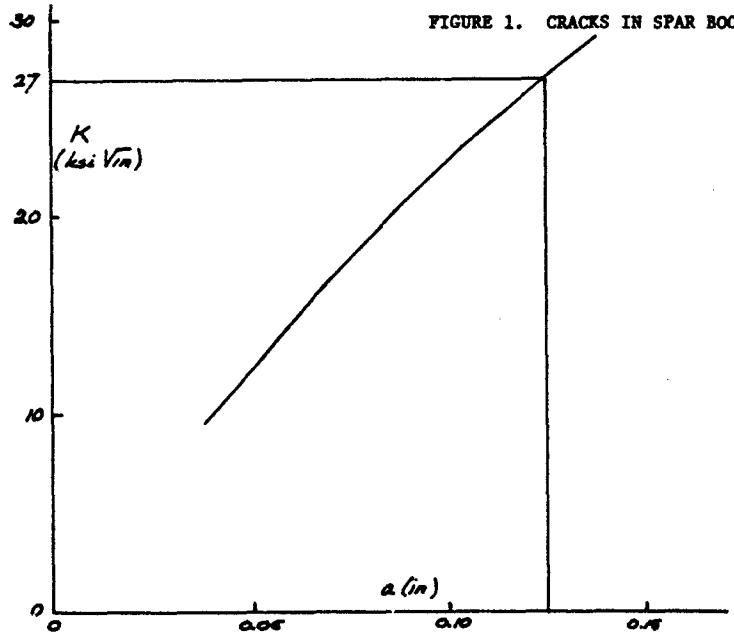

FIGURE 2. K VERSUS a FOR σ = 26.2 KSI

EXAMPLE PROBLEM 4.6.3

RESIDUAL STRENGTH PREDICTIONS FOR CORNER DEFECTS AT HOLES IN SPAR BOOMS

D. Grange, British Aerospace
(Literal)

1. STATEMENT OF THE PROBLEM

Residual strength predictions were made for test specimens having corner flaw type defects at holes. The predictions were based on conventional through-the-thickness crack-toughness data, obtained from specimens manufactured from the same material. Various stress-intensity solutions were considered, to see which was the more appropriate. The test results were previously published by Kirkby in Agardograph 176, Chapter VC.3 but in that instance predictions were only made for one particular solution.

2. TOUGHNESS

The specimens were manufactured from sections of wing spar booms, having material specifications DTD683 and DTD5074, respectively (Figure 1). The through-the-thickness toughness data for the type 1 Boom Material (DTD683) were quoted as K_{Ic} = 24.6 to 31.8 ksi$\sqrt{in}$. from results of 16 specimens cut from 2 residual strength specimens, and for the type 2 Boom Material (DTD5074) as K_{Ic} = 24.0 to 35.0 ksi$\sqrt{in}$. from results of 36 specimens from 9 booms.

The crack orientation for these specimens was not quoted but since crack orientation in the residual strength specimens was longitudinal, it should be concluded that they were likewise. Which of the two subdirections they represented (L-T or L-S) was not known. Possibly they were some of each. More recently, some additional toughness measurements have been made on the type 1 Boom Material, the results were

L-T K_{Ic} = 26.7 ksi$\sqrt{in}$. average of 4 specimens

L-S K_{Ic} = 29.0 ksi$\sqrt{in}$. average of 4 specimens

3. STRESS INTENSITY

Three different stress-intensity solutions were considered.

(a) The procedure discussed by Broek in NLR-TR71033U, where the defect and hole are idealized as a large surface flaw. K is calculated at the end of the major and minor axis (Figure 2(a)).

(b) The procedure discussed by Hall and Finger in AFFDL TR 70-144 where the defect is idealized as a through-the-thickness crack of equal severity (Figure 2(b)).

(c) The procedure discussed by Kirkby in Agardograph 176 where the defect is treated as a quarter circular corner crack, using the surface dimension as the radius (Figure 2(c)).

The failure stresses calculated by using the above stress-intensity solutions and the quoted K_{Ic}-values are plotted in Figure 3 versus the actual failure stress in the test. Of course, a 1-to-1 relation in this figure would be an exact prediction.

The solution that was finally applied to the type 1 booms was $K = 0.795\,\sigma\sqrt{\pi \cdot a}$, and the solution applied to the type 2 booms was $K = 0.795\,\sigma\sqrt{\pi \cdot a}/1.75$. The factor 1/1.75 was introduced to allow for the increase in restraint imposed on the crack due to the relatively smaller holes.

4. COMMENTARY

This example shows (Figure 3) how difficult it is to justify any stress-intensity solution for cracks at holes. To a large extent this is caused by the large scatter in residual strength usually observed in test specimens with corner cracks at holes. The results are compared on the basis of a fixed K_{Ic} value for the material. Thus a stress-intensity solution that appears to give a poor correlation for a particular test may not be at fault, but the particular test specimen may have exhibited an extremely low or high K_{Ic} as compared to the fixed K_{Ic} value taken for the evaluation. To some extent, justification is difficult, because of the problems discussed in association with Figure 10 in the main chapter.

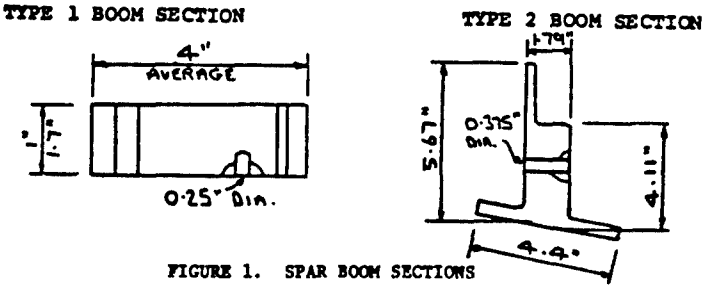

FIGURE 1. SPAR BOOM SECTIONS

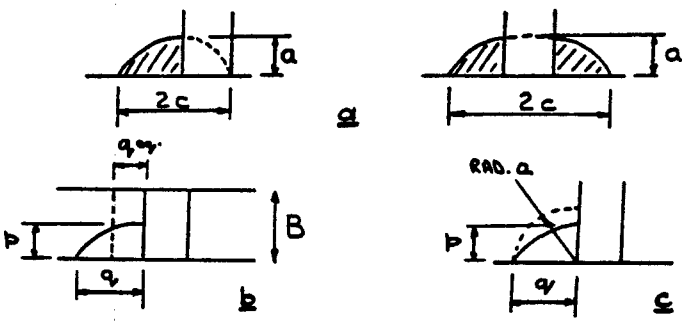

FIGURE 2. DEFECT IDEALIZATION

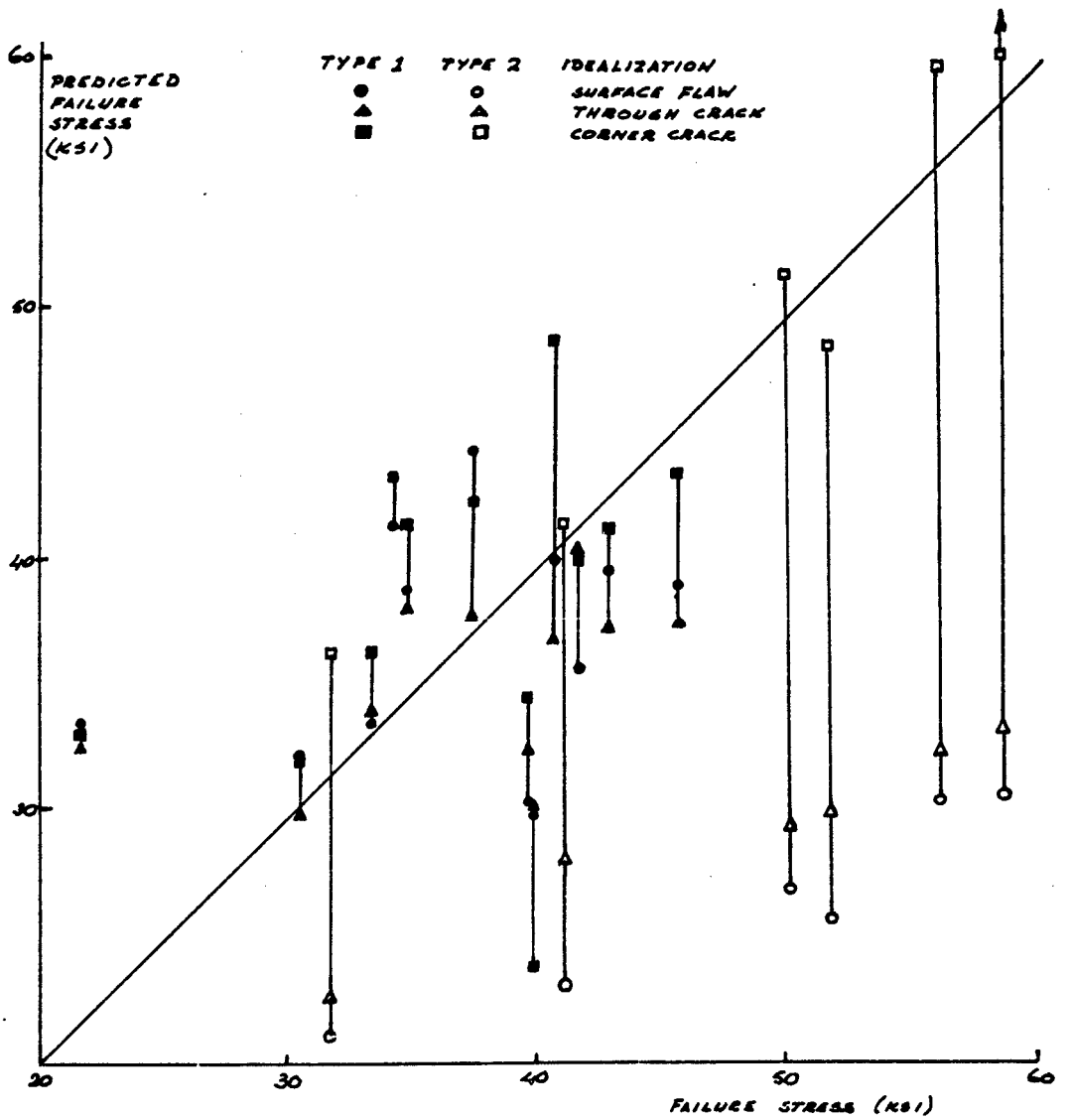

FIGURE 3. CALCULATED VERSUS ACTUAL FAILURE STRESS FOR THREE FLAW IDEALIZATIONS

EXAMPLE PROBLEM 4.6.4

DAMAGE TOLERANCE ESTIMATES FOR A LANDING GEAR COMPONENT

D. Grange, British Aerospace
(Literal)

1. STATEMENT OF PROBLEM

The analysis concerns a component of the main wheel landing gear of a medium transport aircraft, which during the testing of the fatigue test specimen, developed corner defects at a drain hole. Calculations were made for the basic design and also for a range of hole diameters, to cover the eventuality of the hole being increased in size to remove the crack. The damage assumed was a corner defect of quarter circular form, at both sides of the hole. The component is made of DTD5104 (U.S. equivalent approximately 7075-T7; duplex aged). A section through the component at the drain hole is shown in Figure 1.

2. DAMAGE-TOLERANCE PHILOSOPHY

Two philosophies are considered. A fail-safe approach based on growth from the inspectable size to the critical size, and a safe life approach, where the hole having been found clear, is increased in size by an amount equal to the inspectable size. The object of the latter is to remove any defect still existing of a size less than the inspectable size. Thus only defects of effectively zero size need then be considered and the safe-life approach is therefore based on the growth from a size just greater than zero to the critical size. This latter approach would be chosen in preference to the former, when the inspection interval would be prohibitively short.

If defects are found, the general procedure is to increase the size of the hole in increments, until a clear indication is achieved from the inspection technique. The appropriate philosophy is then chosen on the basis of the resulting hole size.

The detectable defect size was considered to be 0.10 inch. A scatter factor on life of 4.0 was assumed.

3. STRESS-INTENSITY SOLUTION

The solution chosen was the one by Hall and Finger, where the corner defect at a hole is idealized by an equivalent through-the-thickness crack at a hole. The equivalent crack is obtained from empirically derived curves which relate corner cracks to through cracks. This solution caters for a finite condition with regard to thickness, but not with regard to width, thus a correction to cover the latter was included (i.e., Item 1.1.5 of the Compendium of Stress Intensity Factors by Rooke and Cartwright HMSO 1976). The stress intensity is (see Figure 2 for notations):

$$K = 0.87\,\sigma\sqrt{\pi q_{eq}}\cdot f(q_{eq}/D)\cdot f(d/b,\ a/d)$$

where $f(q_{eq}/D)$ is the Bowie function which relates q_{eq} to the hole diameter D and $f(d/b, a/d)$ is a finite width correction.

4. FRACTURE TOUGHNESS

In an attempt to obtain a realistic estimate of the critical stress intensity value, relevant to the defect configuration, toughness tests were conducted on specimens with corner defects at holes of equal diameter as the drain hole (i.e., 3/16 inch). The specimens (Figure 3) were manufactured from material obtained from other identical components with the defect in the specimens arranged such that it had the same orientation as the defect in the fatigue test specimen.

The values of stress intensity at failure, were evaluated using the above solution. The results for 6 specimens showed a minimum K_{Ic} of 30.9 ksi$\sqrt{\text{in.}}$, an average value of 32.65 ksi$\sqrt{\text{in.}}$ and a standard deviation of 2.25 ksi$\sqrt{\text{in.}}$ The value used in the subsequent analysis was 30 ksi$\sqrt{\text{in.}}$

5. CRACK-PROPAGATION DATA

The data used were obtained from a fractographic examination of the fatigue failure. The specimen had been loaded randomly to the service spectrum, thus the data were in the form of crack size versus flights, as shown in Figure 4.

These data are applicable only to the hole diameter of the test component. To make it applicable to defects at other hole diameters a correction must be made. The correction takes the form of a factor on rate equal to the ratio of the stress intensity for a defect at a 3/16-inch hole, to the stress intensity for that defect at the hole diameter under consideration.

6. RESIDUAL STRENGTH

For each diameter of drain hole considered, the relationship between strength and crack size was established, using the solution previously detailed. However, for small crack sizes, errors can be expected, and a correction was applied as in the Feddersen approach (Figure 5), using:

$$\sigma \text{ limit} = \sigma \text{ ult} \times \frac{2b-D}{2b}$$

where σ limit is the gross stress to produce a net stress equal to σ ult, and σ ult is the material ultimate stress (69.44 ksi).

The correction takes the form of a tangent drawn from the curve based on K = 30 ksi$\sqrt{in}$. to $\sigma = \sigma$ limit at q = 0. The critical crack size was then obtained from the corrected plot of σ against 'a' at the residual strength level of σ_R = 44.59 ksi. A plot of critical crack size as a function of hole diameter is shown in Figure 6.

7. CRACK GROWTH

To obtain crack lives at hole diameters other than 3/16-inch, propagation data relevant to these diameters were required. They were obtained by the following procedure. Consider, e.g., a hole diameter of 0.25 inch and a starter size of 0.10 in for the fail-safe philosophy. From Figure 6 the critical crack size is obtained as q crit = 0.132 inch, which means that the total amount of fatigue crack growth is 0.032-inch. From the crack growth data for the 3/16-inch hole (Figure 4), it follows that growth from 0.1 — 0.18 inch takes 585 flights. Then the average rate of growth is da/dF = 0.08/585 = 1.37×10^{-4} inch/flight.

From ESDU Fatigue, Vol. 4, Item 75029, Figure 11, using the 7075-T7351 curve as a basis, the equivalent value of ΔK for that rate is found to be 18.2 ksi$\sqrt{in}$. An estimate is now made of what the value of ΔK would be, if the diameter was 0.25 inch (i.e., considering q = 0.125 inch).

$$\Delta K_{D = 0.25 \text{ inch}} = \frac{1.007 \times 2.08 \times 0.87\ \sigma\ \sqrt{\pi a}}{1.006 \times 1.89 \times 0.87\ \sigma\ \sqrt{\pi a}} \times 18.2 = 20.05 \text{ ksi}\sqrt{in}.$$

Referring back to the da/dN - ΔK curve, this is equivalent to a da/dN = 2.2×10^{-4} inch/flight. Therefore, the number of flights for the crack to grow from 0.10 inch to 0.132 inch at a 0.25-inch-diameter hole will be N = 0.032/0.0022 = 145 flights.

This procedure was repeated for various values of hole diameter, and a plot obtained of crack growth life from a detectable crack size of 0.10-in to failure against hole diameter (see Figure 7).

By repeating the above procedure, but with a starter length of effectively zero, the relationship between hole diameter and life was obtained for the safe-life philosophy. In Figure 7 this relationship is shown, but D is plotted as D - 0.20 inch. This was done to obtain the relationship in terms of the diameter of the hole found to be clear of defects.

8. SUMMARY

The damage tolerance philosophy regarding this component may be summarized as follows. The hole is inspected for defects, and with the technique employed, it is not expected that defects greater than 0.10 inch will be missed. If during inspection no indication of a defect is observed, then it is assumed that at that hole, at that point in time, there are no defects present greater than 0.10 inch. However, there could be defects present less than 0.10 inch. Reference is then made to Figure 7, from which is obtained the inspection interval and safe life for the two philosophies. A decision is then made as to which philosophy is the most practicable. If the safe life is chosen, then the hole must be opened up by 0.20 inch on diameter, to ensure the hole is then free of defects. If however, on inspection a defect is observed, then the hole in question is opened up in increments until found to be clear. Reference is then made to Figure 7 to determine what the subsequent inspection interval or safe life will be.

APPENDIX A. ADDITIONAL TOUGHNESS DATA

In addition to the toughness results described, data were obtained from two compact tension specimens with the objective to determine the difference in results if through-crack data were used as opposed to corner-crack data.

The specimens were manufactured from material obtained from identical components, with the same crack orientation as the other specimens. The toughness values measured were 25.46 ksi$\sqrt{in}$. and 23.57 ksi$\sqrt{in}$. (the latter could be considered valid as per the BS.5447:1977). The first value was suspect since cracking did not occur in the same plane over the full width of the crack front.

It is obvious that, with the solution used, an overconservative result would have been achieved with the compact tension data.

APPENDIX B. CRACK GROWTH UNDER RANDOM LOADING

If the loading spectrum is modified, then the propagation data, deduced from the fractographic examination of the fatigue test specimen failure, will not be relevant. Therefore, to cover this eventuality, a study was undertaken to assess what degree of accuracy could be achieved for predictions of crack growth under random loading.

The study utilized the results of propagation tests under random loading, which were conducted on the same specimens that subsequently yielded the residual strength results previously discussed. The calculations were based on the solution previously discussed, using baseline propagation data deduced from specimens tested under constant-amplitude loading. The applied loading was the same spectrum as applied to the specimens. The Willenborg retardation model was used to account for load interaction.

The specimens were as detailed in Figure 3. During the tests records were kept of cycles and crack growth along the surface. However, to evaluate propagation rates, an estimate of the growth down the bore was required. From the appearance of the fracture surface and the final crack front shape, it was decided that it would not be unreasonable to assume that the growth down the bore approximately equalled the growth along the surface.

The two cracks at opposite sides of the hole did not grow at the same rate. Therefore, since the solution only caters for an equal crack condition, a concession was required to evaluate values of ΔK. Values of ΔK were evaluated for each tip, based on the crack size for the tip being considered. Evaluating ΔK in this manner assumes that the other tip is of equal size. The rate for the tip being considered is plotted against this value of ΔK, the other tip is treated likewise.

A plot of dq_{eq}/dN against ΔK for constant amplitude is shown in Figure 8. This data is for R = 0. The data were extended over a wider range than that covered by the test results, by fitting each end of the curve to the equation.

$$dq_{eq}/dN = C \cdot \Delta K^{n} \quad .$$

In the prediction of the results of the spectrum tests allowance was made for load interaction by means the Willenborg retardation model, using:

$$K \text{ effective} = ZK_{n} - K_{max}$$

where K_n is the K level under consideration and K_{max} is the maximum K reached in the spectrum.

The modified spectrum was as follows:

Δσ	R	N
8,460	0	1
26,950	0	1
12,480	0	1
6,030	0	1
2,850	0	1
720	0	1
26,680	0	1
11,310	0	0.5
11,310	0	0.5

A computer program was used for the integration. The calculated results, i.e., q_{eq} against failure, are plotted together with the spectrum test results in Figure 9. The calculated values are, on average, a factor of 1.6 on life, lower calculated values were also obtained for the fatigue test specimen, the loading is 1.17 times greater than the latter. Comparison of the calculated with the fatigue test specimen values are shown in Figure 12; the difference is again of a similar order.

9. COMMENTARY

This is a good example of the technique sometimes referred to as stripping, by which non-inspectable cracks are removed by cutting away material. The example accounts for a detectable defect of 0.1 inch. This means that a defect of 0.1 inch can escape detection. Thus, a hole found clear at inspection still has to be oversized by 0.2 inch to eliminate defects that were missed.

In view of the inaccuracy of predictions for cracks at holes (see previous example) it would still be necessary to apply ample factors on calculated action intervals.

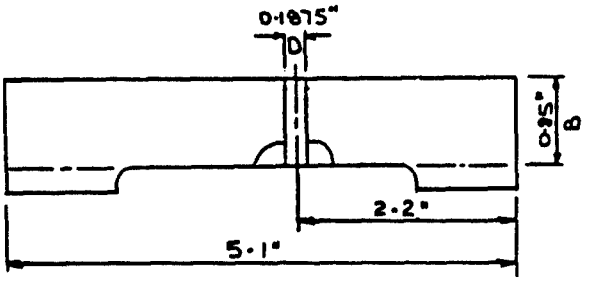

FIGURE 1. SECTION THROUGH COMPONENT AT DRAIN HOLE

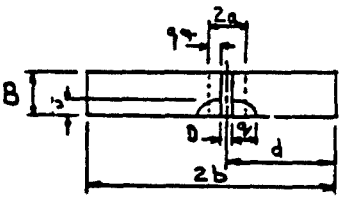

FIGURE 2. STRESS INTENSITY

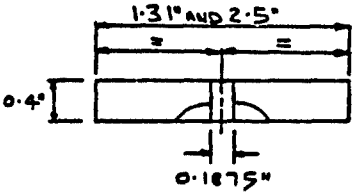

FIGURE 3. TOUGHNESS SPECIMEN

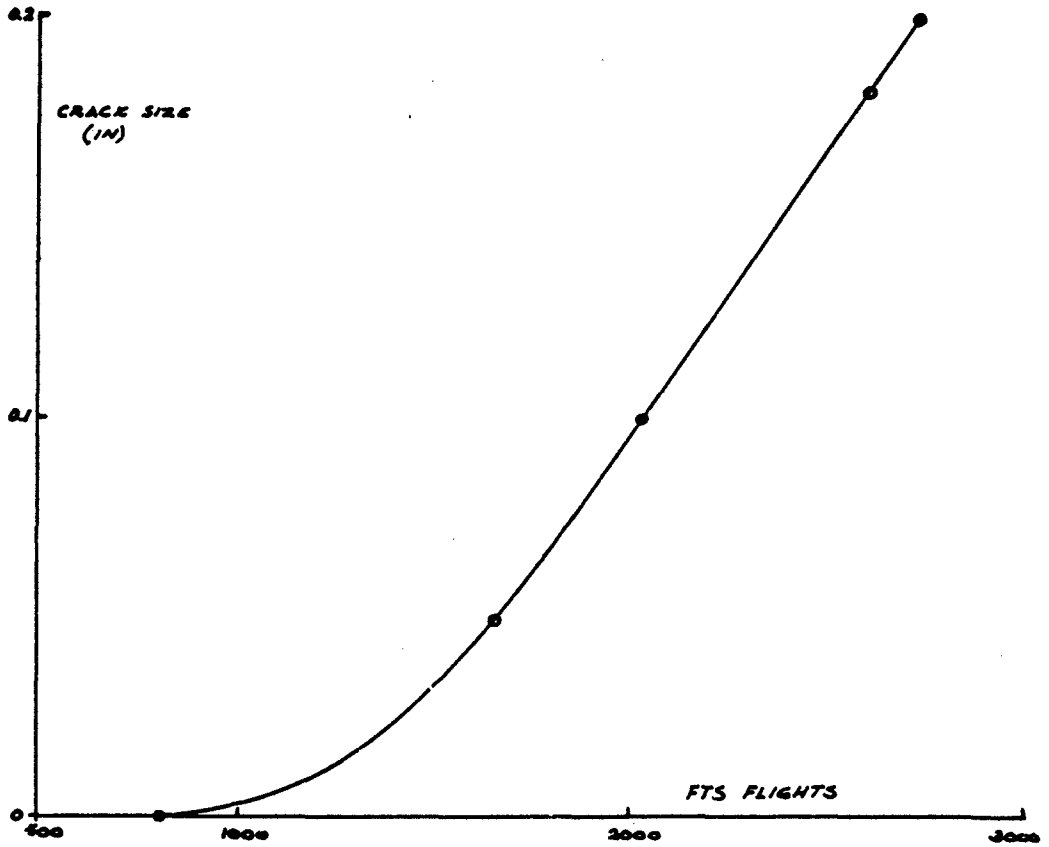

FIGURE 4. RESULTS OF FRACTOGRAPHY

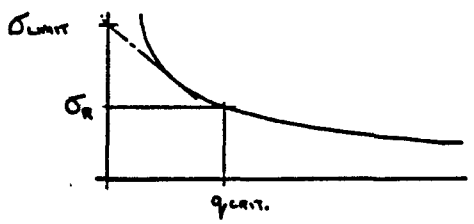

FIGURE 5. FEDDERSEN APPROACH

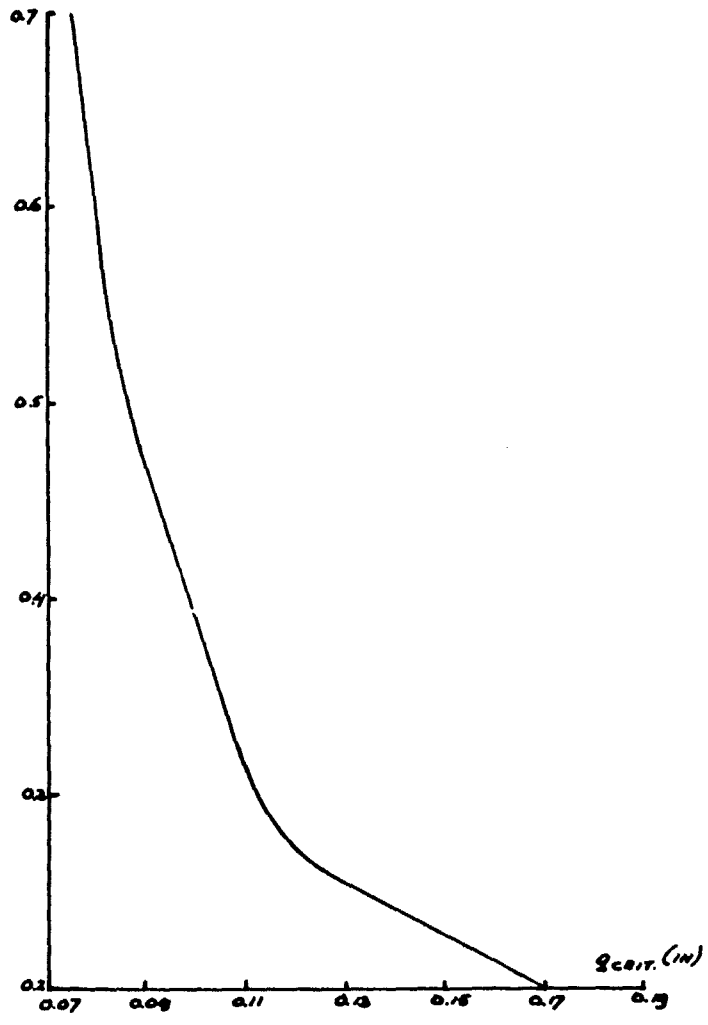

FIGURE 6. HOLE DIAMETER VERSUS CRITICAL CRACK SIZE

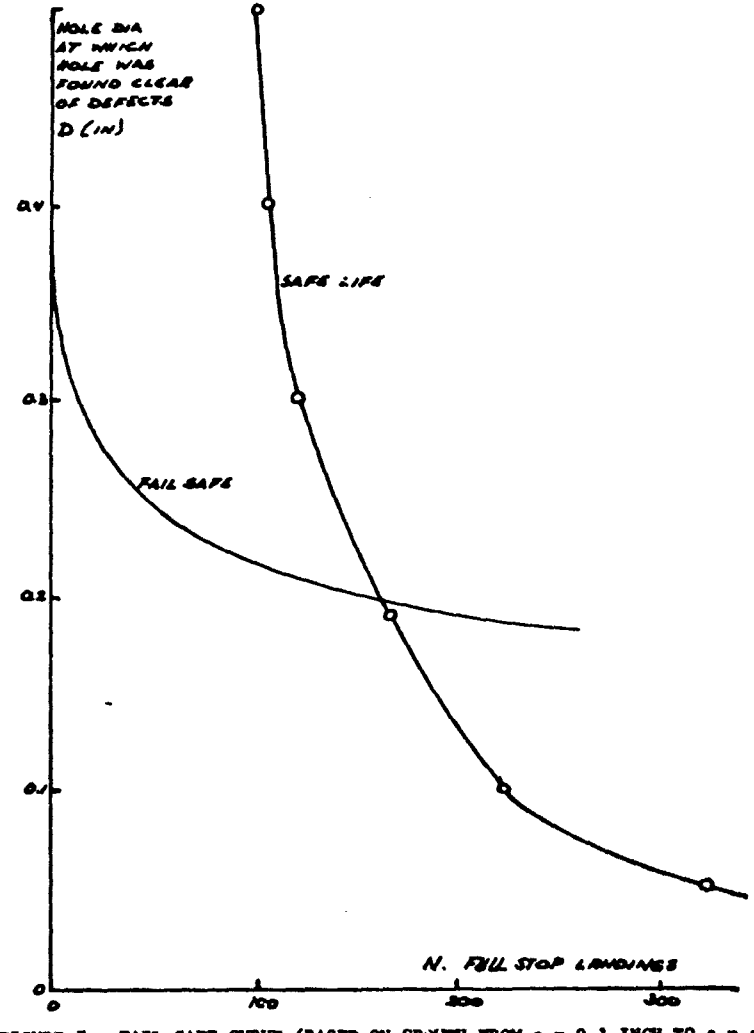

FIGURE 7. FAIL SAFE CURVE (BASED ON GROWTH FROM a = 0.1 INCH TO a = a_c) AND SAFE LIFE CURVE (BASED ON GROWTH FROM a = o TO a = a_c). NOTES: HOLES OPENED UP 0.2-INCH FROM THE SIZE FOUND TO BE CLEAR: INSPECTABLE DEFECT SIZE 0.1-INCH; SCATTER FACTOR 4

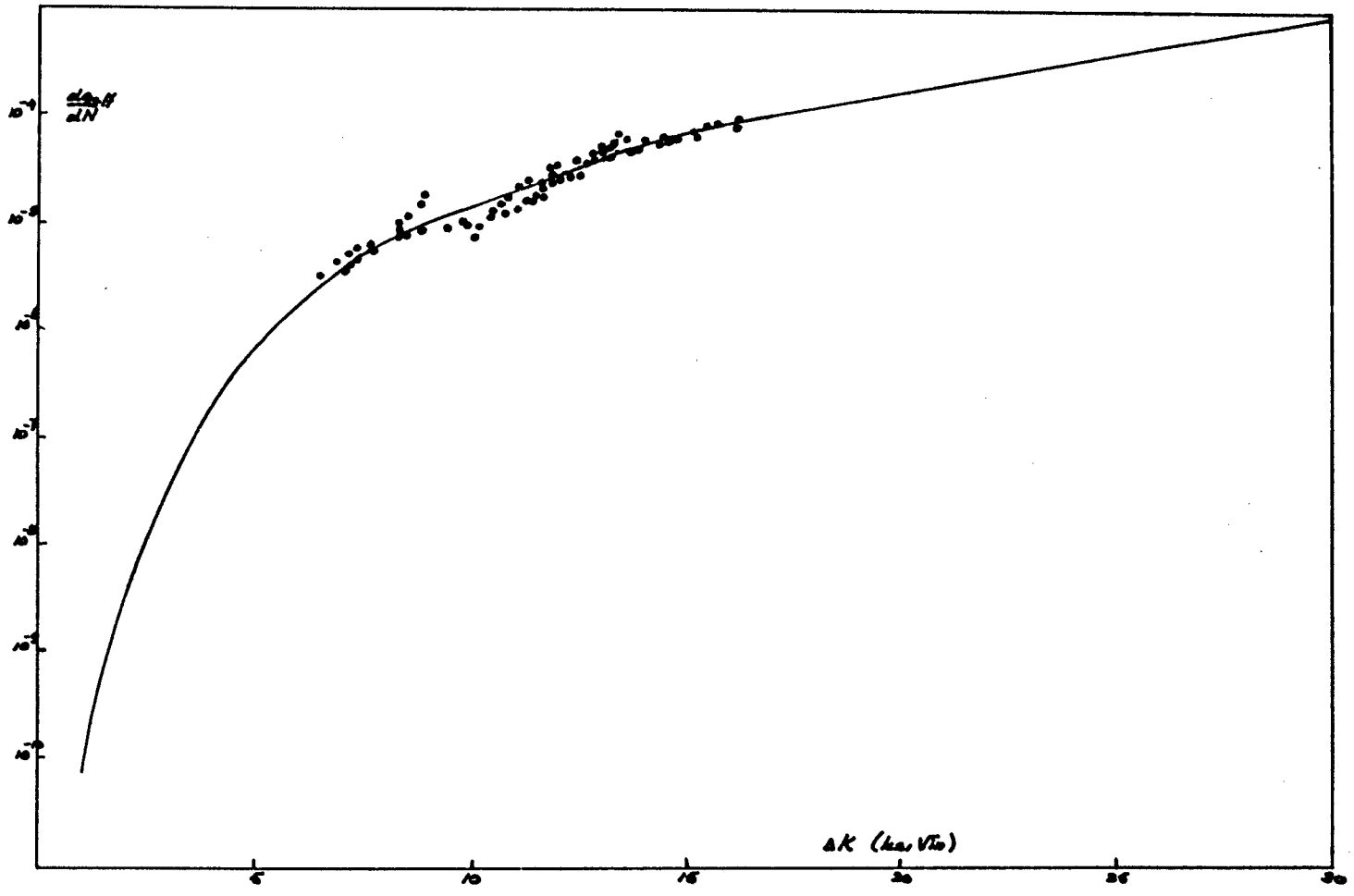

FIGURE 8. CRACK-GROWTH RATE. (CURVE WAS USED IN COMPUTER PROGRAM)

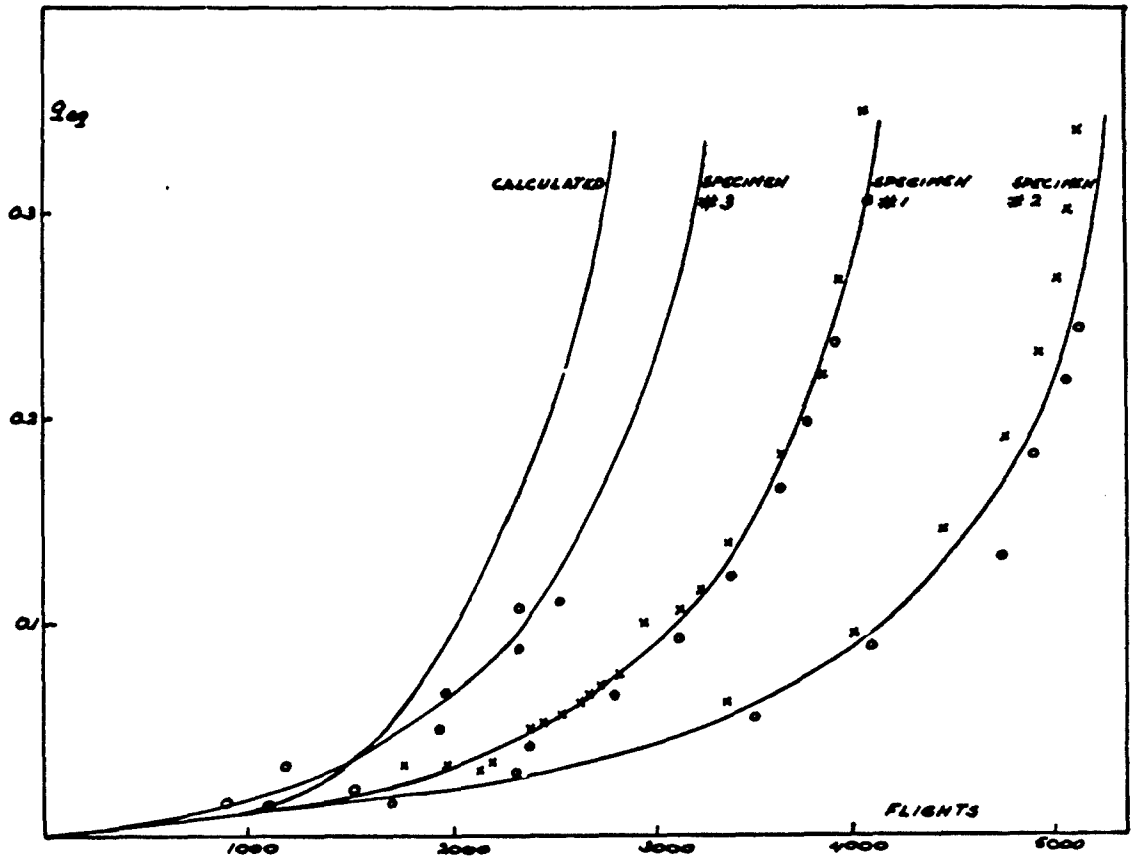

FIGURE 9. COMPARISON OF CALCULATIONS WITH TEST RESULTS

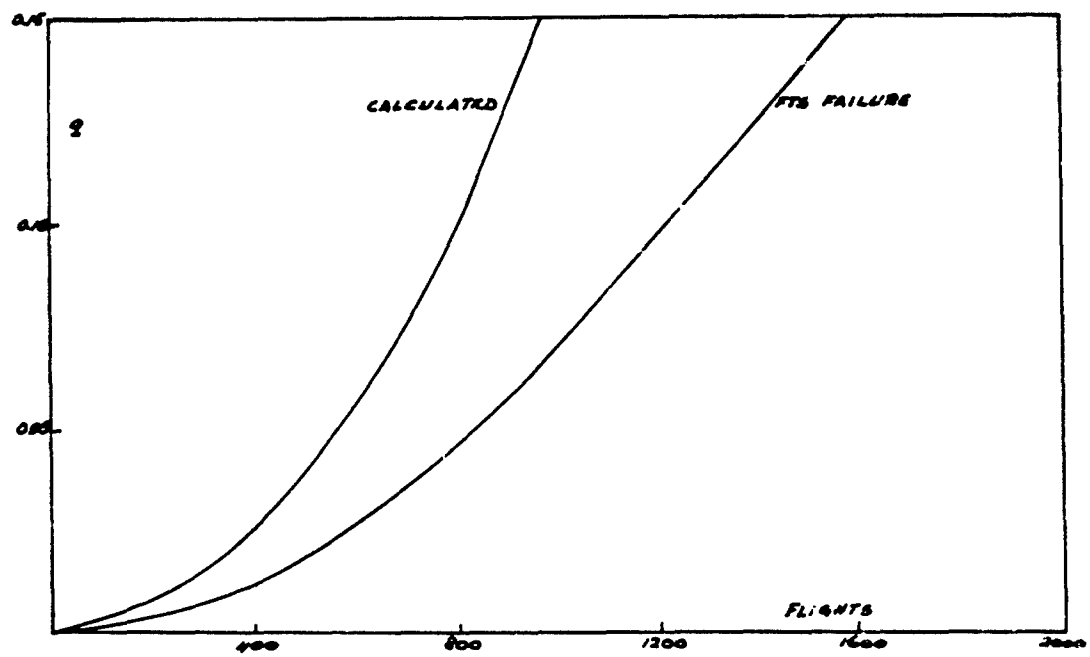

FIGURE 10. COMPARISON OF CALCULATED AND FTS FAILURE

EXAMPLE PROBLEM 4.6.5

CRACK GROWTH AND FRACTURE OF A LOADED HOLE IN AN AIRCRAFT BOOM END

M. Bradley, British Aerospace
(Literal)

1. STATEMENT OF THE PROBLEM

Calculations undertaken to find the inspection period for a hole at a boom end, loaded by a pin are described. The aircraft involved was a geriatric medium transport aircraft. The boom end is shown in Figure 1.

The problem was to derive an easy to use method of analyzing a corner crack in a hole containing a loaded pin. A solution along the lines of the Hall and Finger method for cracks at holes with a remote loading was sought.

2. STRESS-INTENSITY FACTOR

Using the idealization shown in Figure 2, the crack at the hole was idealized as a crack of length equal to the hole diameter plus crack length, i.e., $2a = D + q$. This crack was loaded with sinusoidally distributed forces along the length covered by the diameter of the hole.

From Sih and Liebowitz's analyses (1968) for a crack with a distributed load along its length, it follows that:

$$K_A = \frac{1}{\sqrt{\pi a}} \int_{-a}^{a} \sigma_x \left(\frac{a+x}{a-x}\right)^{1/2} dx$$

The bearing stress is given as:

$$\sigma_B = \frac{1}{D} \int_{-a}^{D-a} \sin \frac{\pi(x+a)}{D} = \frac{2}{\pi} \quad .$$

It was desired to derive a function λ

$$K_A = \lambda \times \sigma_B \times \sqrt{\pi q} \quad \text{or} \quad \lambda = K_A/\sigma_B \sqrt{\pi q} \quad \text{with } \lambda = f\left(\frac{q}{R}\right) \quad .$$

Using a numerical approximation to calculate K_A with a large number of increments, λ was derived as indicated above. A graph of λ against q/R appears in Figure 3.

The above analysis, of course, assumes an infinite sheet. To produce a correction to allow for a finite environment, some experimental results by Cartwright and Ratcliffe were utilized. They were in the form of an overall factor plotted against q/R for a specimen with a width to hole diameter ratio of 2. The overall factor was divided by λ at comparable positions of q/R and the result plotted against $2(R+q)/W$, where W = specimen width. A graph showing the factor appears in Figure 4.

As stated before, the above analysis is for a through crack. The problem that we must solve is for a corner crack at a hole. This was done by converting the corner crack to an equivalent through crack using the Hall and Finger curves. Hence, formula for K for a corner crack at a hole was taken as:

$$K = \lambda \times \sigma_B \times \sqrt{\pi q_{eff}} \times F_E$$

where q_{eff} = equivalent or effective crack length, F_E = edge factor from Figure 4, and λ is from Figure 3.

NOTE: After completion of this job, it has been realized that a better idealization would have been achieved if the sine distribution on one side of the crack had been replaced by a constant distribution of $2D/W$ over the length of the crack to cater for the remote loading on the other side of the hole. However, as the D/W ratio for Cartwright and Ratcliffe's specimens, our specimens, and the actual components are all substantially the same the final results should not be affected.

3. EXPERIMENTAL VERIFICATION

In order to check the theory derived above, some tests were performed on scaled down versions of the boom ends. The test pieces consisted of a tie with a loaded hole at each end with a corner crack at each hole. An alternating load at $R = 0.5$ was applied and the growth of the crack, both down the hole and along the surface was monitored. Also several compact tension specimens for the same material were tested and propagation curves derived to obtain $da/dN - \Delta K$ data.

Using the Hall and Finger curves, with the values of p and q for the test pieces, values of q_{eff} can be derived from

$$q_{eff} = fn\ (P/B \cdot P/q) \times q$$

where P = crack length down hole, q = crack length along surface, and B = specimen thickness.

For the test pieces a graph of q_{eff} against endurance, N (cycles), was drawn and dq_{eff}/dN evaluated at each data point. The value of dq_{eff}/dN could then be read across to the propagation curves from the compact tension specimens to give a value of ΔK for each data point in the growth of the corner cracks.

K for the corner cracks was also calculated by the expression

$$\Delta K = \lambda \times \Delta\sigma_B \times \sqrt{\pi q_{eff}} \ .$$

which is the expression derived above without the edge factor. The ΔK derived from the compact tension specimens was divided by the ΔK calculated from the expression above to give a value of F_g for each data point. F_g was then plotted against $2(q_{eff}+R)/W$.

The graph obtained appears in Figure 5. It will be noticed that all the points follow the slope of the Cartwright and Ratcliffe line fairly well but a constant factor seems to be required for the line to go through the mean of the points. A factor of 0.87 was selected as this also appears in the Hall and Finger expression. This fits fairly well.

This method, when used to calculate the propagation and failure of the crack in the component being investigated cannot handle a variable p/q and so a value of p/q for the calculation must be selected. The graph in Figure 6 shows the results for several runs using different crack ratios and constants on some of the specimens. It can be seen that a combination of p/q = 1.5 and a constant of .87 gives a very good correlation between the computer results and the test pieces. The results for two specimens with a higher loading are shown on Figure 7. Again, the correlation is quite reasonable.

Figures 8 and 9 show the propagation result from the same program. These are not quite as good, mainly because the variance in p/q ratios in the specimens (1.2 to 2) has a greater effect on propagation than K value. They do show, however, that the method gives mostly "safe" answers.

On the basis of these results, it was decided that a factor of 2 on life would be sufficient to use with this method.

The final formula was taken as:

$$\Delta K = .87\ \Delta\sigma_B\ \lambda\ F_g\ \sqrt{\pi q_{eff}} \text{ with } p/q = 1.5 \ .$$

The propagation curves used were developed from the compact tension specimen results. As they were only for R = 0.5, the relationship

$$\frac{da}{dN} = C \left(\frac{\Delta K}{1 - R}\right)^m \Delta K^n$$

was used to generate curves for other values of R. From a review of available aluminum data m was deduced to be 2.

In order to get a reasonable correlation between the formula and the compact tension specimens data, the curve was split into two parts, each part with a different n-value.

4. PROPAGATION AND FAILURE PREDICTIONS

The calculation for the component followed almost exactly the same method as the check calculations on the test specimens. The major difference was that a complicated load spectrum was applied, representing the service loading of the component. The load spectrum was derived from both gust loading and ground loading during taxi. It is of a random nature between takeoff and landing and during the taxi.

Crack growth was numerically integrated. The dq_{eff}/dN values were simply summed to give the total dq_{eff}/dN for each crack increment. This is not strictly correct as there will be some retardation effect owing to small loads being preceded by large ones. Owing to the random nature of the loading, however, it is not possible to make an assessment of the retardation. It was therefore decided to ignore it, which at least gives a safe answer.

The results of the calculations for the component appear in Figures 10 and 11. No comment can be made on the accuracy except that an inspection period of 12 flights was adopted and this proved to be satisfactory.

5. DISCUSSION

One major source of error in these calculations is that the propagation data was extrapolated from a curve for a single R-value. The formula used is one of many propagation equations, none of which is really reliable.

Unless reliable propagation data are available from another source, it is suggested that at least two propagation curves should be produced from compact tension specimens, one at a high R-value and one at R = 0. Then at least the boundary values of any selected propagation equation can be properly evaluated.

6. COMMENTARY

The example would have been more valuable if the proposed stress-intensity solution for a lug with a through crack would have been compared with other solutions (see main chapter).

The short crack propagation period and short inspection interval (12 flights) are reason to believe that the crucial point in this analysis is the flight load history. When crack growth covers thousands of flights, the flight load statistics are rather dependable. However, one series of 12 flights can be largely different from the next series of 12 flights, so that the calculated growth curve will be an average of a very broad band of actual service behavior. Rather than taking an arbitrary factor on life, in a case like this it seems almost imperative that a parametric analysis is made, by repeating the calculation for different types of flights (weather). This would at least give a feel for the variability in service behavior to be anticipated, and it would give a more rational bases for establishing an inspection interval. (Since the inaccuracies of the method would equally apply to all parametric results, the relative life under various weather and loading conditions would still provide useful information on variability.)

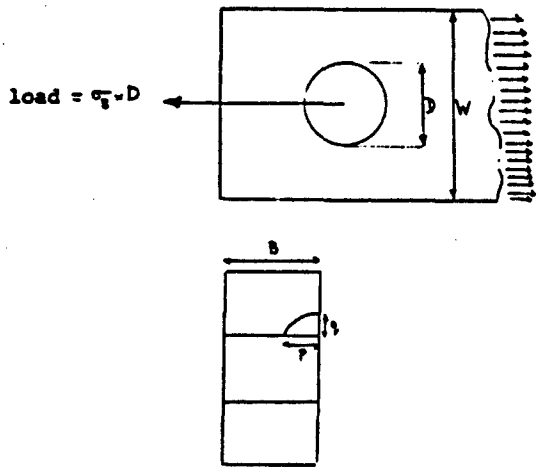

FIGURE 1. DIAGRAM OF BOOM END

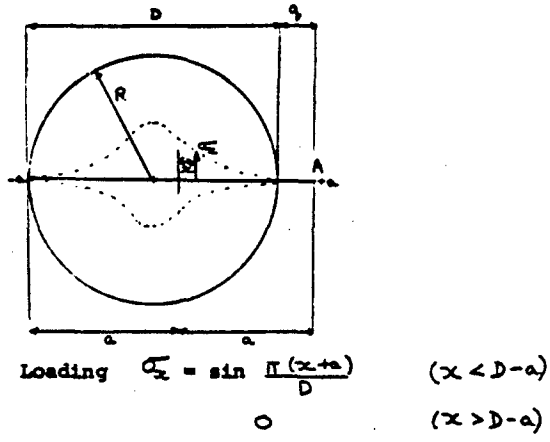

FIGURE 2. IDEALIZATION OF CRACK AT LOADED HOLE

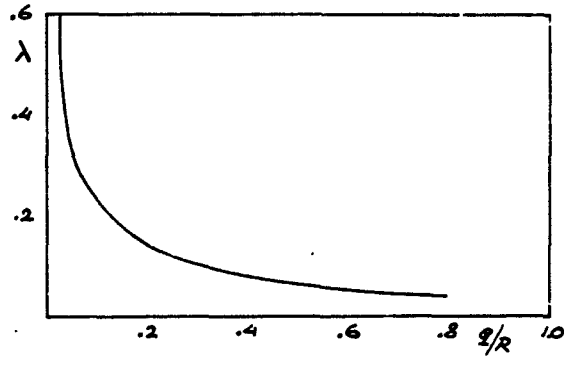

FIGURE 3. GRAPH OF λ VERSUS q/R

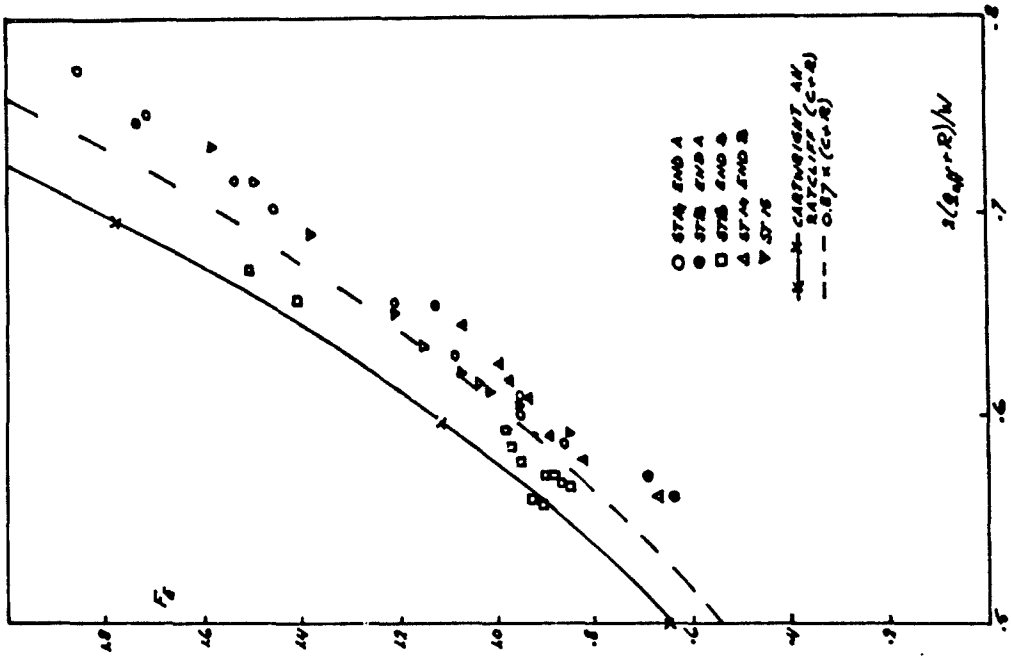

FIGURE 5. CALCULATED EDGE FACTOR AND EXPERIMENTAL DATA

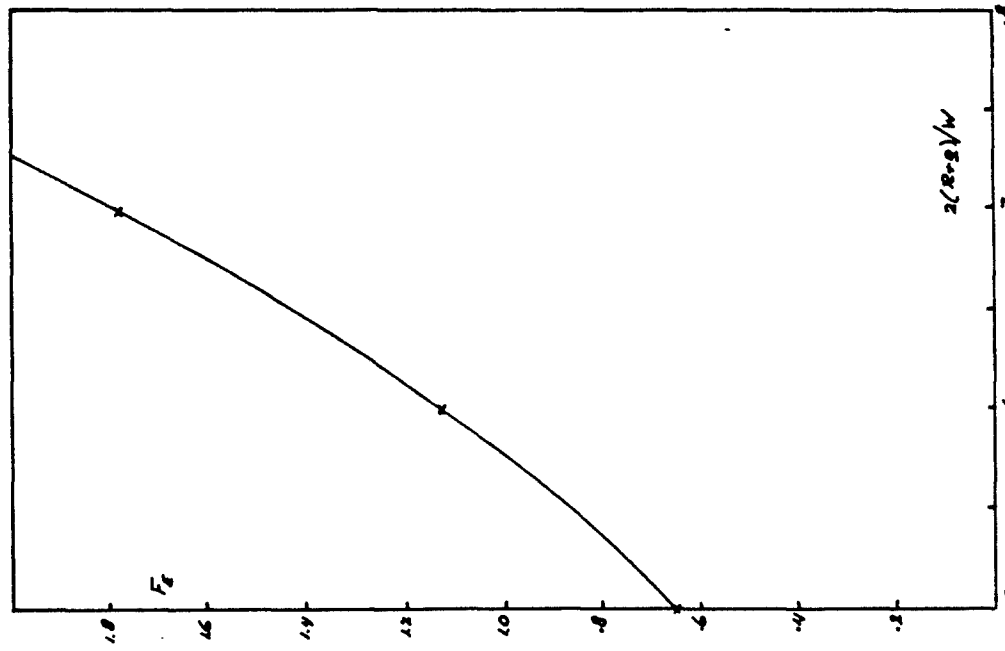

FIGURE 4. EDGE FACTOR AS A FUNCTION OF (R+q)/W

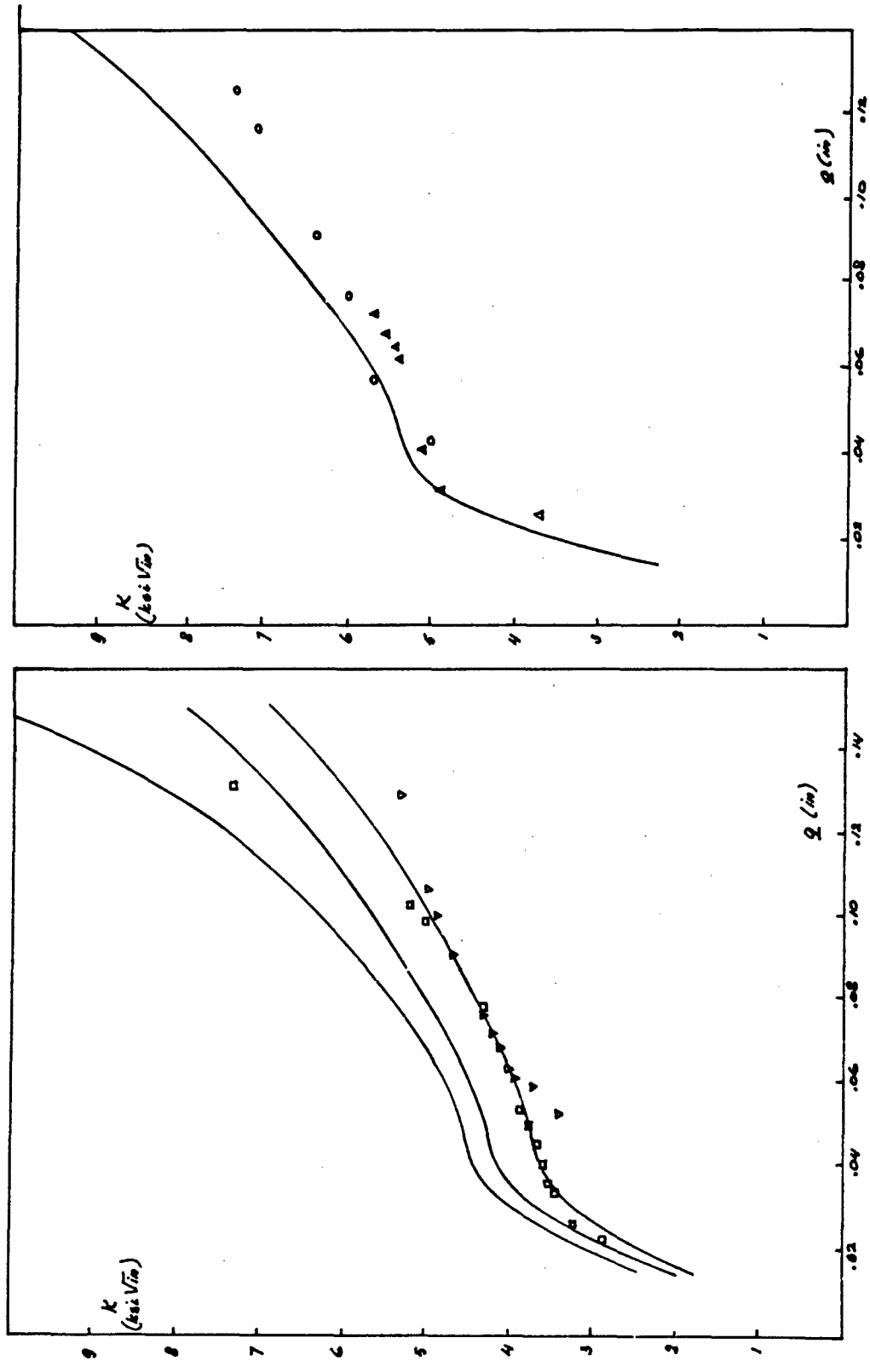

FIGURE 6. K AS A FUNCTION OF q. COMPARISON OF COMPUTED RESULTS AND TEST DATA

FIGURE 7. COMPARISON OF COMPUTER AND TEST RESULTS

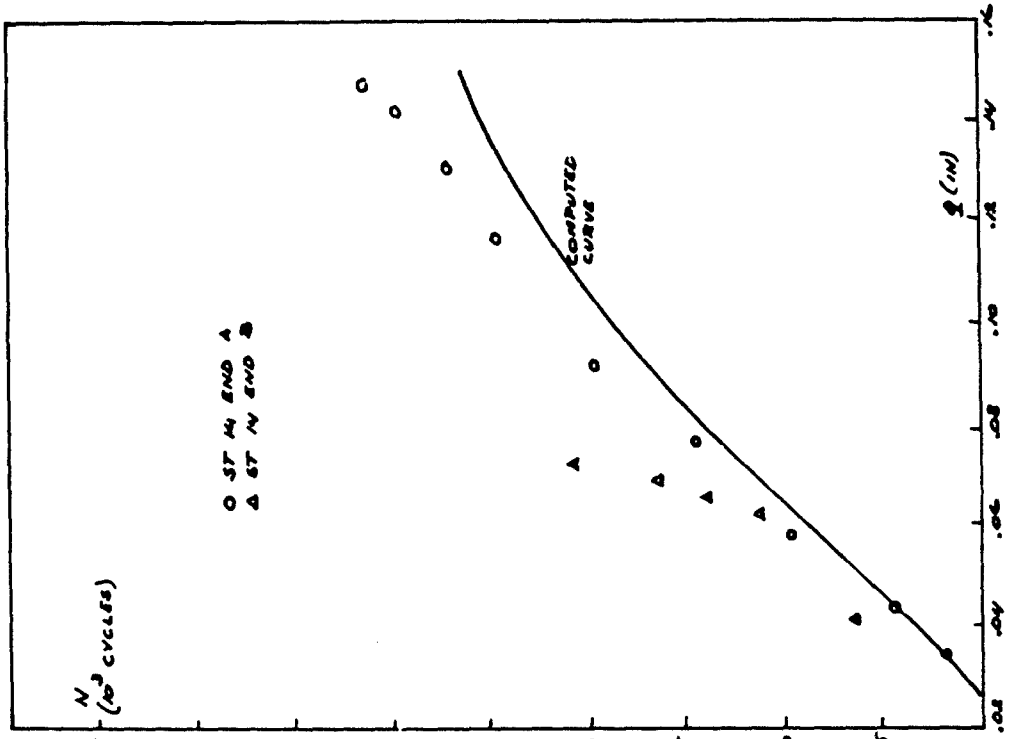

FIGURE 9. COMPARISON OF COMPUTED RESULTS AND TEST DATA N VERSUS q

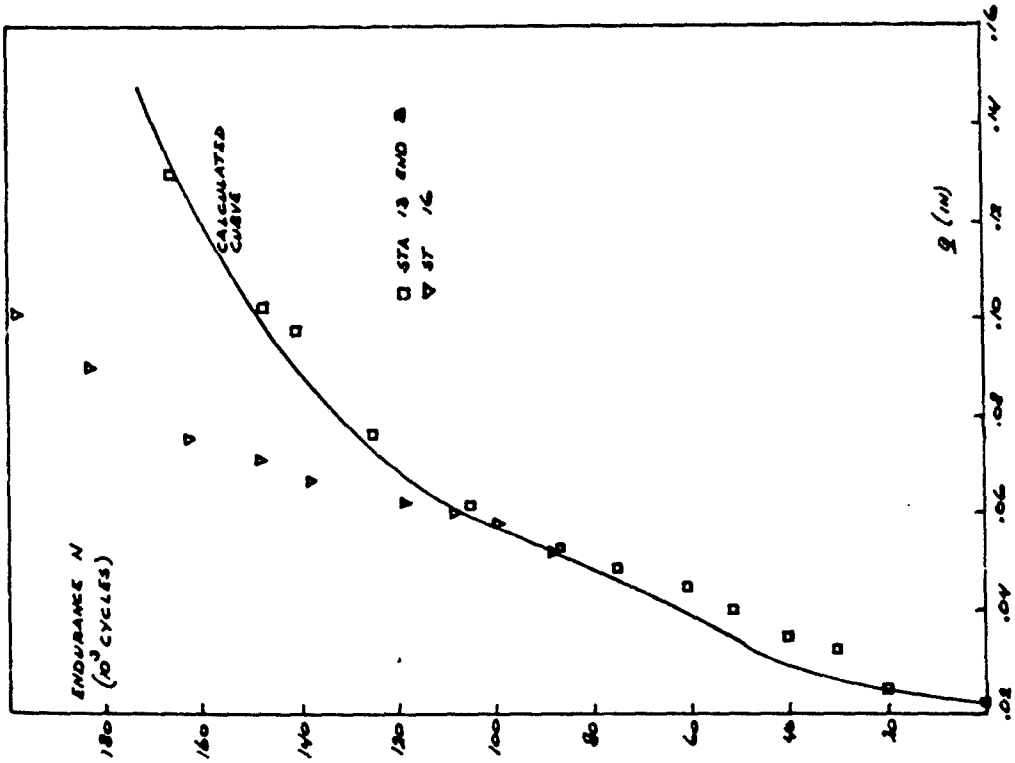

FIGURE 8. ENDURANCE AS A FUNCTION OF q

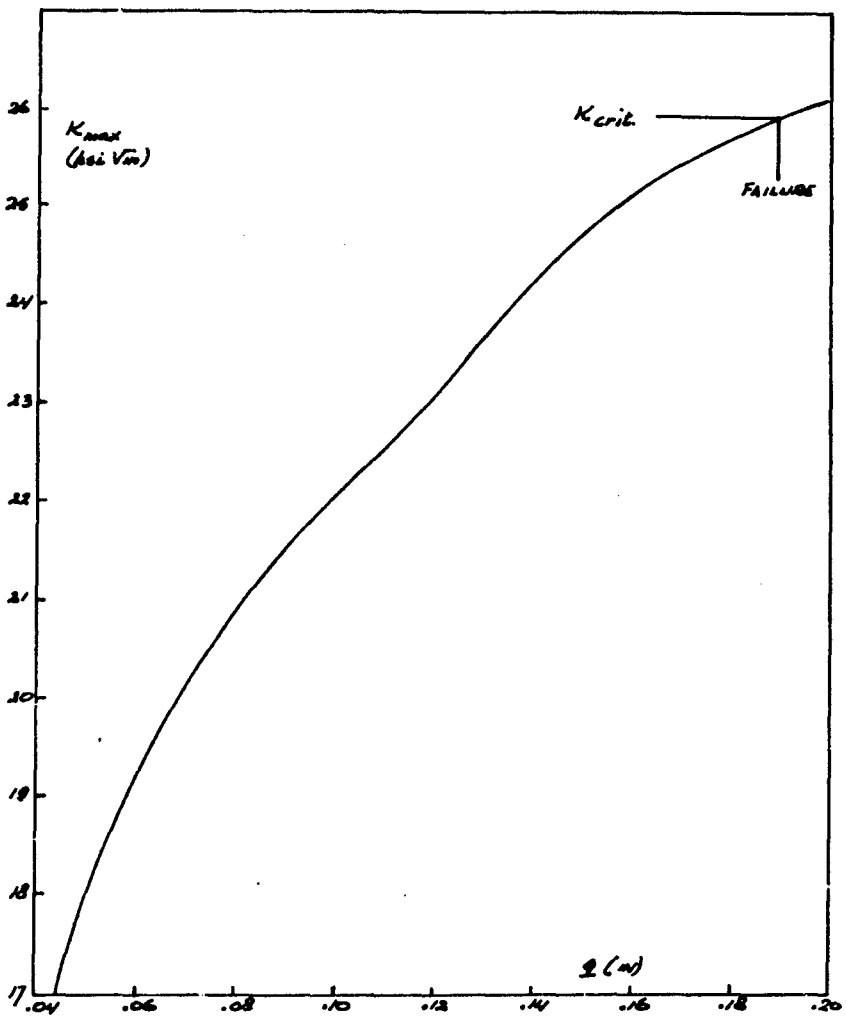

FIGURE 10. K_{max} VERSUS q

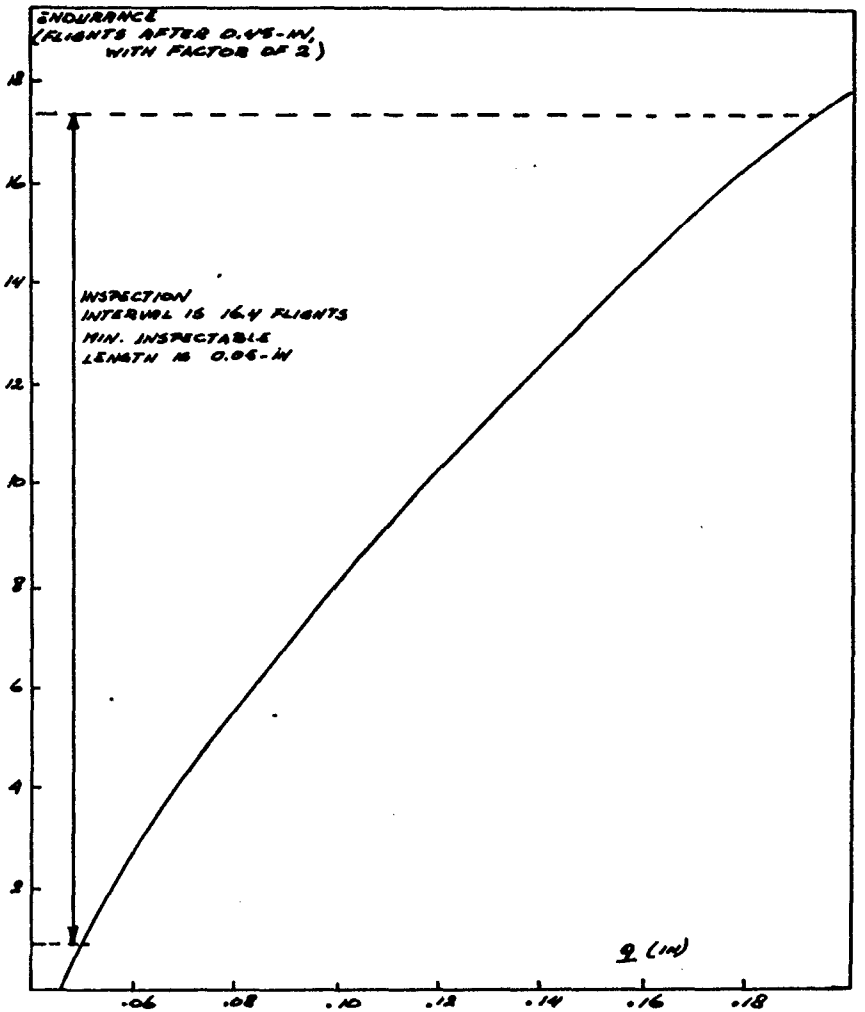

FIGURE 11. ENDURANCE FROM 0.045-INCH AS A FUNCTION OF q FOR COMPONENT

EXAMPLE PROBLEM 4.6.6

TITANIUM ALLOY WING LUG

L. Casalegno, Aeritalia
(Literal)

1. STATEMENT OF THE PROBLEM

The wing lug considered (Figure 1) is in titanium 6Al-4V and is loaded by a steel pin. The quarter-circular corner flaw has been positioned on the lower edge of the lug bore, where the stress is about 10 percent higher than the average net section stress due to in-plane bending caused by the eccentric pin loading. This bending stress (σ = 330 N/mm^2) has been taken as the section stress, because of the small depth of the critical crack size resulting from the calculations.

2. STRESS-INTENSITY FACTOR

Four solutions for the stress-intensity factor of a corner flaw in a lug have been considered from the literature:

(a) Liu's solution (Reference 1) for a hole in an infinite plate in tension, corrected for finite width

$$K_I = 0.713\ \sigma_G\sqrt{\pi a}\cdot F\left(\frac{L}{R}\right)F\left(\frac{a}{t}\right)\sqrt{\sec\frac{\pi D}{2W}} \quad .$$

where $F\left(\frac{L}{R}\right)$ is the Bowie function with $L = a/\sqrt{2}$ and $F\left(\frac{a}{t}\right)$ is the back face correction factor, which Kobayashi and Moss (Reference 2) have approximated by the polynomial $F\left(\frac{a}{t}\right) = 1 + 0.05021\left(\frac{a}{t}\right) - 0.5604\left(\frac{a}{t}\right)^2 + 2.201\left(\frac{a}{t}\right)^3 - 3.3879 \times \left(\frac{a}{t}\right)^4 + 1.9472\left(\frac{a}{t}\right)^5$.

(b) MBB interim solution (Reference 3) for a lug

$$K_I = 0.7\ \sigma_N\sqrt{\pi a}\cdot k_T\cdot\left(\frac{g}{g+a}\sqrt{\frac{b}{b-a}}\right) .$$

where σ_N is the net stress, k_T the geometric stress concentration factor and the quantity in parenthesis is the finite width correction, with g being a function of k_T and b the lug arm.

(c) Newman's solution (Reference 4) for a pin loaded hole

$$K_I = \sigma_G\sqrt{\frac{\pi a}{Q}}\cdot M_e\cdot f_b\sqrt{\sec\frac{\pi D}{2W}}\times\left[0.5 + \frac{W}{\pi(D+a)}\sqrt{\frac{D}{D+2a}}\right]$$

where Q is the shape parameter, f_b is the Bowie function and M_e is a front and back-face correction factor.

(d) Wanhill and Lof's solution (Reference 5), from a Lockheed formula

$$K_I = 1.12\ \sigma_G\sqrt{\frac{\pi a}{Q}}\left[1 + \frac{1}{2}\left\{\frac{D}{D+a}\right\}^2 + \frac{3}{2}\left\{\frac{D}{D+a}\right\}^3\right]\times\left(1.26 + 2.65\cdot\frac{a^2\pi}{2(W-D)t}\right) \quad .$$

3. CRITICAL CRACK SIZE

For the particular design and material (K_c = 2200 Nmm$^{-1.5}$) and a stress σ = 330 N/mm^2, the four solutions give the following critical crack lengths:

Solution (a) — a_c = 8.5 mm; Solution (b) = 6.0 mm; Solution (c) = 8.2 mm; and Solution (d) = 7.3 mm.

4. CRACK-PROPAGATION CURVE

The crack propagation curves, calculated for the anticipated service spectrum with the Forman's equation $da/dN = c\Delta K^n/\{(1 - R)K_c - \Delta K\}$ are shown in Figure 2. Three of the four solutions gives comparable results, while the fourth gives only half the life of the others. An average life of 25 blocks can be assumed. The effect of load interaction (retardation) can be estimated from tests performed at MBB on a different component, but with similar material and spectrum, to be a three to five times increase in life. Nondestructive inspection specialists are to assess inspection techniques for this component, and the minimum crack size detectable with adequate confidence. Inspection intervals will be prescribed based on half the calculated life or on test results (when available) and the nondestructive inspection method applicable.

5. REFERENCES

1. Lin, A. F., Engineering Fracture Mechanics, Vol. 4, (175), 1972.

2. Kobayashi and Moss, "International Conference on Fracture", Brighton, 1969.

3. Geier, W., MBB/UFE FE 217/5/75.

4. Newman, J. C., NASA TN D-8244, June, 1976.

5. Wanhill, R.J.H., and Lof, C. J., AGRAD CP-221.

6. COMMENTARY

The comments to Example 3 apply here as well. In addition, the analysis is limited to quarter-circular flaws. There is no guarantee that actual flaws in service will not be elliptical, which would result in rather drastic changes in crack-growth behavior. It would be worthwhile to assess the magnitude of such changes in a parametric analysis. Obviously, this applies to all analyses of surface flaws and corner cracks. Apart from the flaw size, the flaw shape is of great influence on anticipated life (see main chapter). An arbitrary shape may be useful for comparative (design) studies, but may be unconservative as a basis for decisions regarding operational safety.

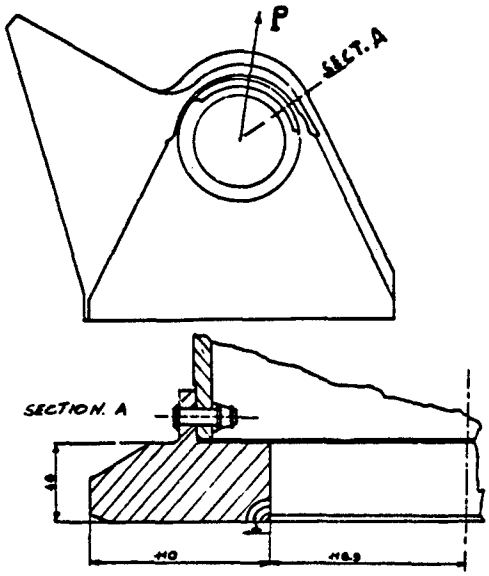

FIGURE 1. LOWER WING LUG

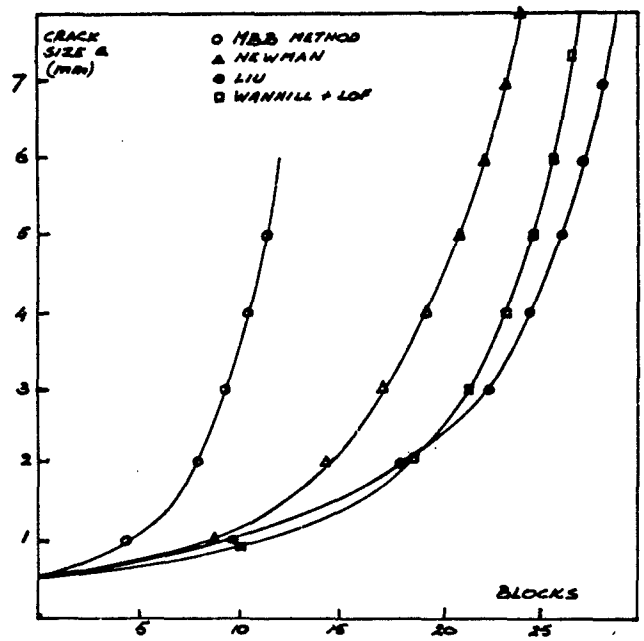

FIGURE 2. CRACK PROPAGATION CURVES

EXAMPLE PROBLEM 4.6.7

FLIGHT-BY-FLIGHT CRACK PROPAGATION INVESTIGATION ON MRCA TORNADO COMPONENTS

W. Geier and K. O. Sippel
Messerschmitt-Bolkow-Blohm GMBH
Military Aircraft Division
Department of Material and Fatigue
(Literal)

1. STATEMENT OF THE PROBLEM

Inspection intervals for the MRCA Tornado have, inter alia, been established on the basis of crack propagation calculations. A comparison between calculations and tests carried out on the structure will be made to check if the results obtained from calculations are reliable. The results thus obtained may help to make better assumptions for similar crack propagation calculations. This applies in particular to the transfer of simple known stress-intensity solutions to components of a complex structure. Calculations of the crack propagation in various components have revealed that the known stress-intensity solutions can in many cases only be applied by considerably simplifying the structural components.

Various effects on the crack propagation such as those caused by the rigid structure in the vicinity of the crack or by the type of load introduction, i.e., the stress distribution can in most cases not be taken into account in the stress-intensity solutions known in the literature.

Within the scope of the production investment phase various components were subjected to flight-by-flight crack propagation tests. The test results were compared with crack propagation calculations carried out after Forman.

Although calculations made after flight-by-flight crack propagation tests on center crack specimens were very much on the safe side (factor ~ 4.5) this cannot be taken as a general rule for components. In the case of crack propagation calculations carried out on components, simplifying assumptions must be made frequently. In the case of flight-by-flight crack propagation calculations carried out after Forman, the results may be on the unsafe side even if the retardation effect has not been taken into account.

2. CRACK-PROPAGATION TESTS

Following the life endurance tests on various components and assemblies, crack starter notches were made with a saw at critical points, e.g., at points having a high nominal stress level or a high stress concentration.

The crack propagation under flight-by-flight loading was observed by means of crack wire gauges. The test results are shown in Figures 1, 2, and 3. In this case, the components investigated were the lower load plate of the wing carry-through box, the outboard aft post of the wing carry-through box, and the pertaining link. In the case of the lower load plate, the crack starter notch was made on the integral reinforcement inside the wing box. During the life endurance test on the outboard aft post, a fatigue crack appeared. It was an edge crack at the critical lug diameter. In the link an edge crack was made with a saw.

3. CALCULATION OF THE CRACK PROPAGATION AND THE CRITICAL LENGTH

3.1. Procedure

For the following examples the crack propagation was calculated using the Forman equation:

$$da/dN = \frac{C\,\Delta K^n}{(1-R)K_c - \Delta K} \quad .$$

For various reasons which will be dealt with later, the crack propagation retardation caused by the flight-by-flight load sequence was not taken into account.

The load spectra needed for the calculation (Figures 4 and 5) were determined for each component. Each load spectrum consisted of three sub-spectra which corresponded to the respective wing sweep positions. For the calculation of the crack propagation, only fatigue loadings were used whereas the calculation of the critical crack length was based on the maximum loading.

The crack propagation values C, n, and K_c to be used in the Forman equation were determined using center cracked specimens. Normally, the thickness of the specimen is not the same as that of the component to be calculated.

3.2. Lower Load Plate of Wing Carry-Through Box

The part is shown in Figure 6. It was made of Ti-6Al-4V, annealed. The constants in the Forman equation were

$C = 2.27\ E\text{-}10$; $n = 3.35$; and $K_c = 3688\ N/mm^{3/2}$.

The Forman values were determined from 120 mm wide, 400 mm long center cracked specimens of 8 mm thickness, tested at $\sigma_m = 176\ N/mm^2$, $\sigma_a = 147.5\ N/mm^2$.

The crack model assumed was a semielliptical surface crack with transition to center crack[1,2]. The maximum fatigue stress was $\bar{\sigma}_o$ = 452 N/mm^2 and the maximum static load was σ_{max} = 452 N/mm^2, both gross area stresses.

3.3. Link — Outboard Aft

The part is shown in Figure 7. It was made of HP 9-4-30. Constants for the Forman equation were:

C = 5.19 E-5; n = 1.48; and K_c = 6775 N/mm$^{3/2}$. The Forman values were determined from center cracked specimen, 400 mm inch length; 100 mm inch width; and 5 mm inch thickness, tested at σ_m = 176.5 N/mm^2 and σ_a = 147.5 N/mm^2.

The critical crack length was calculated from K_{Ic} = 3600 N/mm$^{3/2}$. The crack model assumed was an edge crack in a lug[3]. The maximum fatigue stress was $\bar{\sigma}$ = 443.5 N/mm^2 and the maximum static stress: σ_{max} = 478 N/mm^2, both are nominal net stresses given by $^{o}\sigma_N$ = P/(W-D)t.

3.4. Post Outboard Aft

The part is shown in Figure 8. Forman values and crack model were as in Section 3.3. The maximum fatigue stress was $\bar{\sigma}_o$ = 443.5 N/mm^2, and the maximum static stress: σ_{max} = 478 N/mm^2, both are nominal net stresses from σ_N = P/(W-D)t

4. DISCUSSION

Crack growth in a given load cycle will be retarded when the load cycle was preceded by a higher load level. Since in flight-by-flight crack-propagation tests a multistep variable amplitude load sequence is applied where high loads are frequently followed by small ones, considerable crack propagation retardation is encountered. Retardation is dependent mainly on the type of material and load spectrum.

If the flight-by-flight crack propagation is calculated using a procedure that does not take the retardation effects into account, the life obtained will always be on the safe side. However, an important prerequisites are that (1) the damage calculation is carried out using the overall g-spectrum and (2) the constants used in the Forman equation are determined in crack-propagation tests with constant load amplitude where R is greater than 0.

Flight-by-flight crack-propagation tests using a typical combat aircraft n_z-spectrum and center cracked specimens revealed that the life endurance calculated without retardation is on the safe side by the factor of 4.9 and 4.5 in the case of Ti-6Al-4V and high-strength steel, respectively, when compared with the results obtained from tests.

The fact that the difference between the crack propagation lives obtained from tests and calculations is considerably less for the components investigated here (lower load plate: 1.63, post: 1.06, and link: 2.3) may be due to the following reasons:

(a) Using the same n_z-spectrum, the form of the stress spectrum may be different for various components. Thus the spectrum used for the test specimen need not be identical with that used for the component. As has been mentioned above the crack propagation retardation effect is dependent on the form of the spectrum.

(b) A different stress-intensity distribution in the test specimen and the component may also lead to different crack propagation retardations.

(c) The selection of the Forman constant has a considerably greater influence on the crack-propagation life. Various investigations have revealed that in the case of plane stress the crack-propagation life decreases with increasing material thickness[5,6,7].

The lack of crack-propagation data often necessitates the use of Forman constants from thin specimens for thick-walled components and vice-versa as in Section 3. The resulting inaccuracies may be of the order of 1.5 and more.

(d) The decisive factor for the quality of the crack-propagation calculation, however, is that the stress intensity in the crack model used for the calculation and the actual stress intensity in the component are of the same magnitude.

There are a great number of stress-intensity solutions in the literature; however, there are only a few cases that take the structure used in aircraft into account. The inaccuracies existing in those cases can be compensated for only by the most conservative assumptions.

5. CONCLUSION

As has been shown in the comparison between the test results and the respective calculations as well as in the discussion, the accuracy of crack-propagation calculations of an aircraft structure depends on a number of factors that cannot be quantified. These inaccuracies could be greatly compensated for — at least in the case of the three components in quesion — by applying a rather conservative crack propagation calculation procedure, i.e., conservative at least when comparing the results obtained from flight-by-flight crack-propagation tests and calculations on center cracked specimens. If the retardation effect obtained for center cracked specimens was to be taken into account in the component calculations — be it in the form of a retardation factor, be it by using a crack propagation retardation model — the result might be considerably optimistic.

In principle, the same result was obtained by Stephens when investigating crack propagation retardation[8]. During the 9th ICAF Meeting in Darmstadt in May, 1977, he made the following appropriate statement:

> "The desirable effect of fatigue-crack-growth retardation has become most impressive to the aeronautical industry. Inclusion of the fatigue-crack-growth retardation models into aircraft life prediction is a very fashionable concept today. This inclusion can be quite irresponsible, however, depending upon the actual service spectrum, environment, thickness, and crack geometry relative to conditions under which the retardation data were originally obtained."

This is why the crack propagation retardation effect under flight-by-flight loadings should only be taken into account when the most important factors have been obtained in the form of proper quantities.

6. REFERENCES

1. Newman, J. C., "Predicted Failure of Specimens With Either Surface Cracks or Corner Cracks at Holes", NASA TN D 8244.

2. Tada, H., "The Stress Analysis of Cracks Handbook", Del Research Corporation, Hellertown, Pennsylvania.

3. Geier, W., "Stress Intensity Solution for Lugs", MBB TN FE 217/5/75 (not published).

4. Sippel, K. O., and Weisgerber, D., "Crack Propagation in Flight-by-Flight Tests on Different Materials", ICAF Lausanne, June 5, 1975.

5. Weisgerber, D., and Keerl, P., "Beurteilung und Bewertung der bekanntesten Rißfortschrittsberechnungsmodelle anhand von experimentell ermittelten Rißfortschrittskurven an verschiedenen Werkstoffen und Kollektivformen", ZTL 1875 MBB UFE 1236.

6. Feddersen, C. E., and Hyler, W. S., "Fracture and Fatigue-Crack Propagation Characteristics of 7075-T7351 Aluminum Alloy Sheet and Plate".

7. Schijve, J., Jacobs, F. A., and Tromp, P. J., "Environmental Effects on Crack Growth in Flight-Simulation Tests on 2024-T3 and 7075-T6 Material", NLR TR 76104 U.

8. Stephens, R. J., "Fatigue Crack Growth Retardation: Fact and Fiction", presented at the 9th ICAF, Darmstadt, 1977.

7. COMMENTARY

It is "bon ton" to discredit crack-growth calculations that account for retardation. No engineer seriously involved in the problem will deny the limitations of such analysis. However, discrediting them without making the comparison for the case under consideration, is subjective. A statement that retardation was conservatively ignored, would have sufficed. As pointed out correctly, the da/dN data were not applicable to the case under consideration. This, and the limited accuracy of the stress-intensity solutions and scatter could cause the small discrepancy between linear integration and test data. (This comes out clearly in Figure 1, where the different shapes of calculated and test curves indicate that the stress intensity used in the calculation was quite different from the one in the tests.) Thus, it was prevalent to ignore retardation (although retardation did occur in the tests and the test data were used to determine inspection intervals). When using crack growth analysis in matters concerning safety, it is good to ignore retardation. However, most damage tolerance analyses are performed in the design stage to arrive at the best design option. In those cases, retardation has to be accounted for, since linear analysis might show the worst design to be the best option.

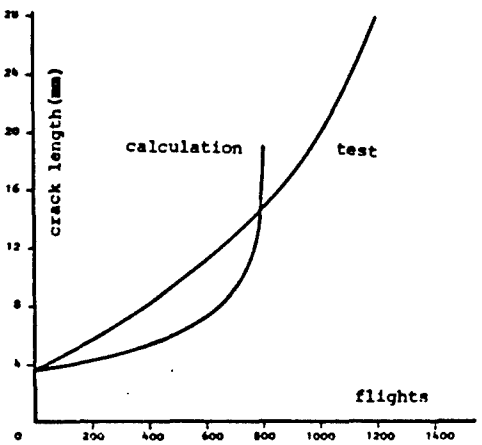

FIGURE 1. CRACK PROPAGATION IN THE LOWER LOAD PLATE

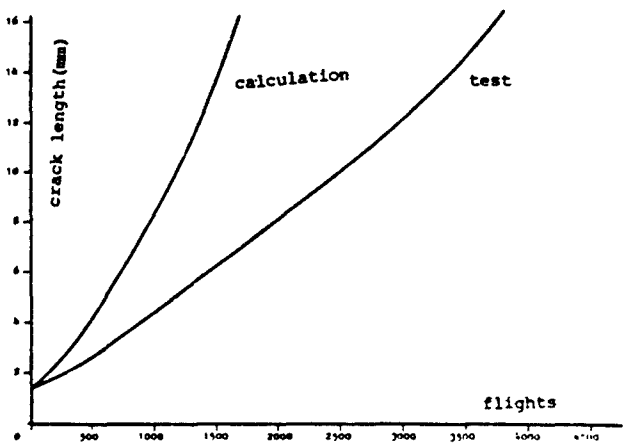

FIGURE 2. CRACK PROPAGATION IN OUTBOARD AFT LINK

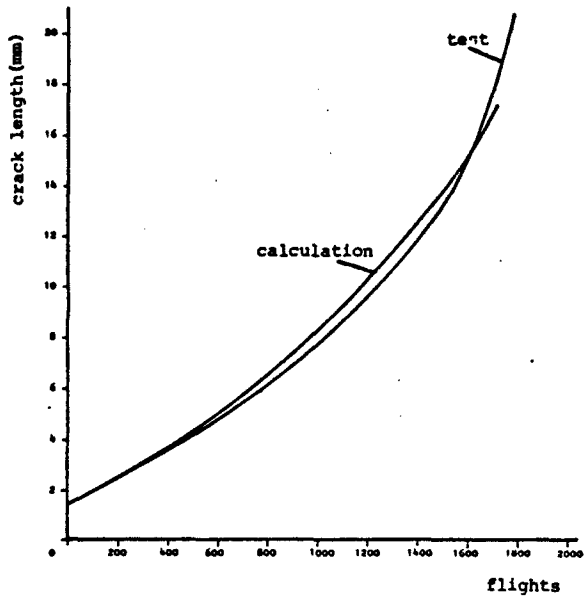

FIGURE 3. CRACK PROPAGATION IN OUTBOARD AFT LINK

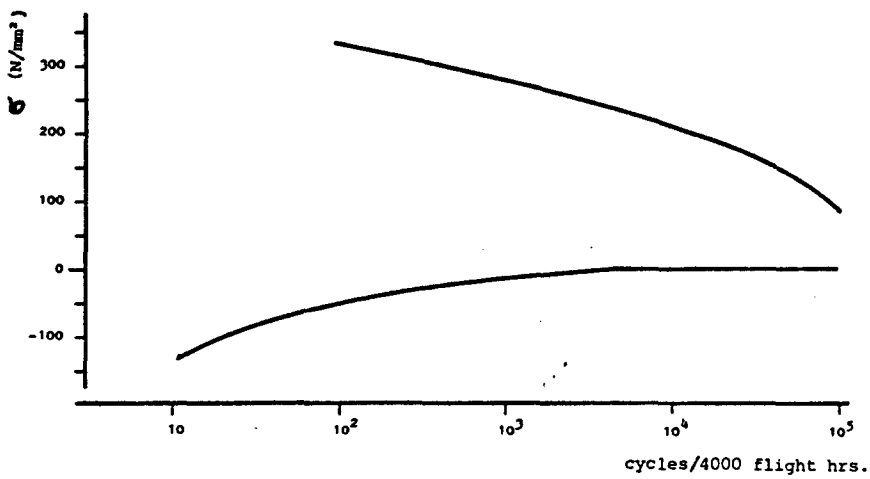

FIGURE 4. LOWER LOAD PLATE STRESS SPECTRUM

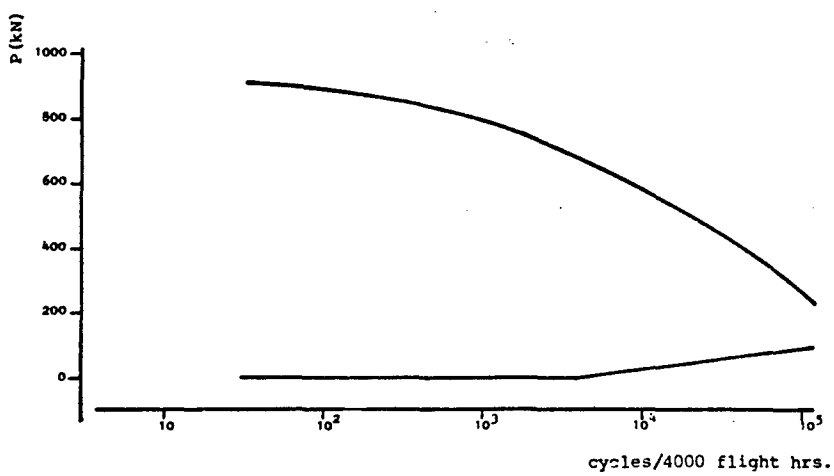

FIGURE 5. LOAD SPECTRUM FOR POST AND LINK

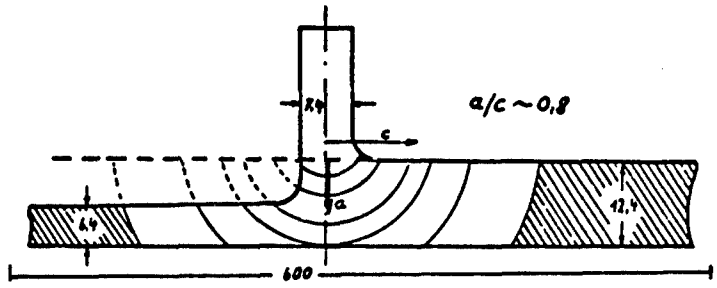

FIGURE 6. LOWER LOAD PLATE OF WING CARRY-THROUGH BOX

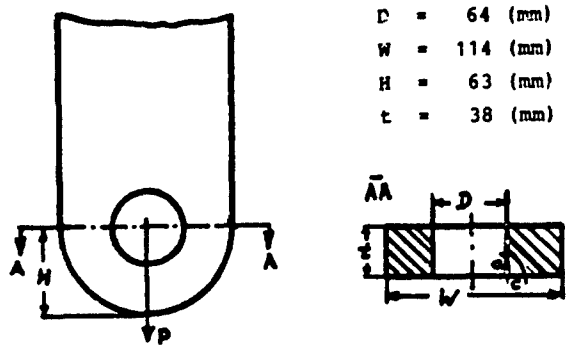

D = 64 (mm)
W = 114 (mm)
H = 63 (mm)
t = 38 (mm)

FIGURE 7. OUTBOARD AFT LINK

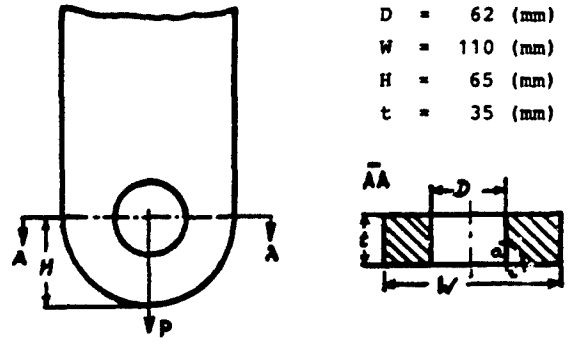

D = 62 (mm)
W = 110 (mm)
H = 65 (mm)
t = 35 (mm)

FIGURE 8. OUTBOARD AFT POST

EXAMPLE PROBLEM 4.6.8

AIRCRAFT HORIZONTAL STABILIZER LUG

S. H. Smith, T. P. Forte, H. J. Malik, and N. D. Ghadiali
Battelle's Columbus Laboratories

The following is a brief exerpt of a paper
presented at the 1978 SESA Spring Meeting

1. STATEMENT OF THE PROBLEM

A fatigue-crack growth and residual-strength analysis was made of horizontal stabilizer lugs (Figure 1) of high time aircraft. Finite-element-stress analysis was performed to determine stress-intensity factors.

2. STRESS-INTENSITY FACTOR

The stress-intensity factor was obtained from finite element submodeling using the NASTRAN code. The full structural model consisted of 481 nodes and 677 elements (Figure 2). A submodel was used for the general area around the lugs (Figure 3). Finally, the detailed model of Figure 4 was used to derive stress-intensity factors for cracks at the lug holes. Through cracks were assumed and K was calculated from crack opening displacement as well as from crack closure energy. The results were obtained in the form of $\beta = K_I/\sigma\sqrt{\pi a}$. In order to arrive at the stress intensity for a corner crack the calculated values for the through crack were modified by taking

$$K_I = \beta\sigma M_f \sqrt{\pi a} \quad \text{with} \quad M_f = \frac{1.12\, M_k}{[Q]^{1/2}}$$

where M_k is the back surface correction and Q is the flaw shape parameter.

3. FATIGUE-CRACK-GROWTH ANALYSIS

The stress spectrum consisted of a flight-by-flight history representing a random mix of seven basic missions used in monitoring the aircraft's service experience. Crack-growth analysis was performed using the CRACKS III integration program with the Willenborg retardation model. Retardation within each flight was taken into account but was not carried over to subsequent flight. Crack-growth baseline data were taken for 7075-T651 forging tested in humid air. The highest rates of the scatter band were used and represented by the Forman equation. Examples of calculated growth curves for different mission mixes is shown in Figure 5.

4. COMMENTARY

This example illustrates the method of submodeling discussed in the main chapter. (See the comments to Example 9 with regard to detailed modeling.)

The example (Figure 5) also provides a good illustration of parametric analysis as mentioned in the comments to Examples 5 and 6.

Finally, it provides an alternative to a normal crack-growth analysis with retardation. Rather than ignoring retardation completely, it is accounted for within a flight, but not carried over to the next flight. This is based on the argument that possible compressive stress hold-periods during ground time could wipe out retardation due to previous overloads. In addition, the baseline crack-growth data used are the upper boundary of the scatterband. Both of these precautions are in fact as arbitrary as ignoring retardation, but it would be interesting to perform a combined analytical and experimental study to investigate whether this would consistently lead to more realistic predictions.

In Figure 4, the crack at hole 1 will never be subjected to compressive stresses, since a negative V_1 will be supported by the left edge of the hole. However, the same negative V_1 will cause compressive stresses over the crack at hole 2. Thus, the argument concerning carry-over of retardation does not equally apply to both holes of the lug. This shows how every conservative assumption is not equally conservative in all cases (see also the discussion with regard to Figure 10 in the main paper). Thus, in following the present example, each case should be considered by its own merits and the fact remains that engineering judgment is more important than fracture mechanics formalities.

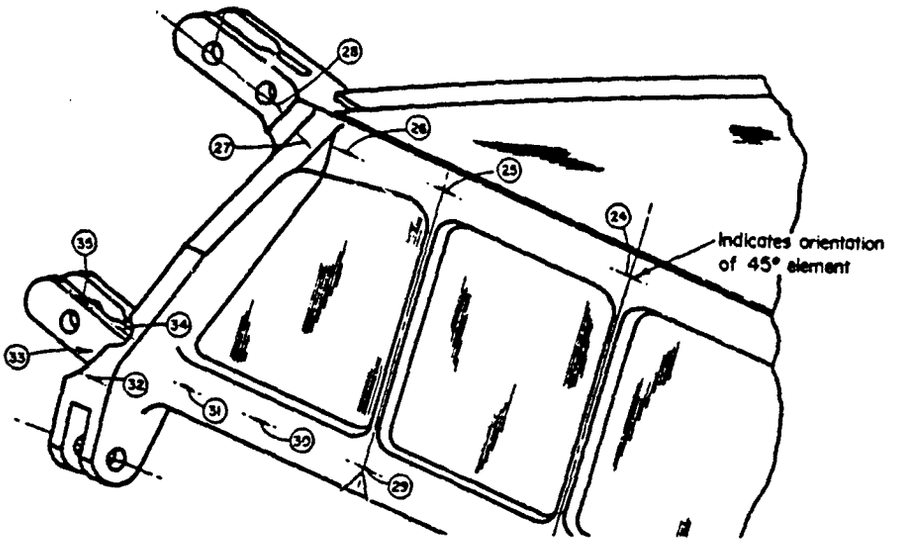

FIGURE 1. HORIZONTAL STABILIZER WITH ATTACHMENT LUGS (NUMBERS INDICATE STRAIN GAGE LOCATION)

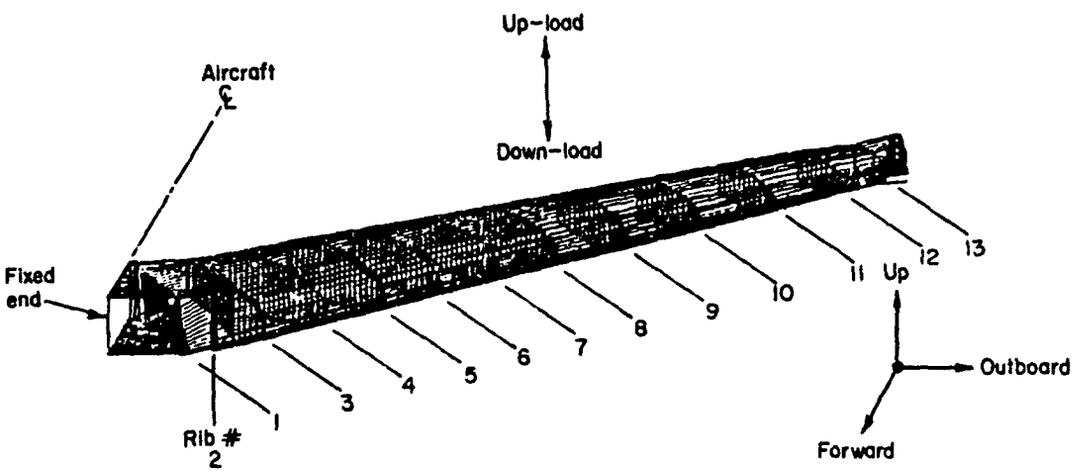

FIGURE 2. FINITE-ELEMENT MODEL OF FULL STRUCTURE

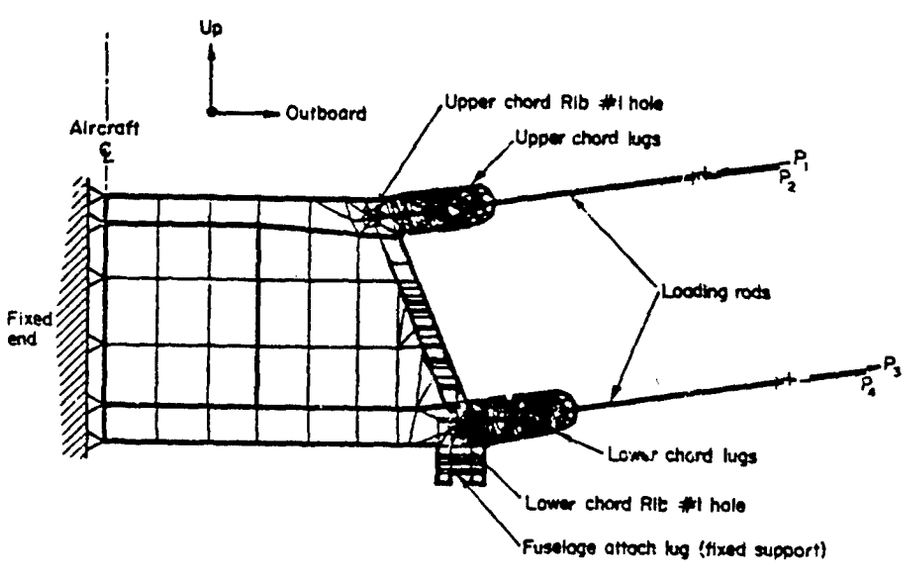

FIGURE 3. SUBMODEL, 933 NODES, 647 ELEMENTS (NASTRAN)

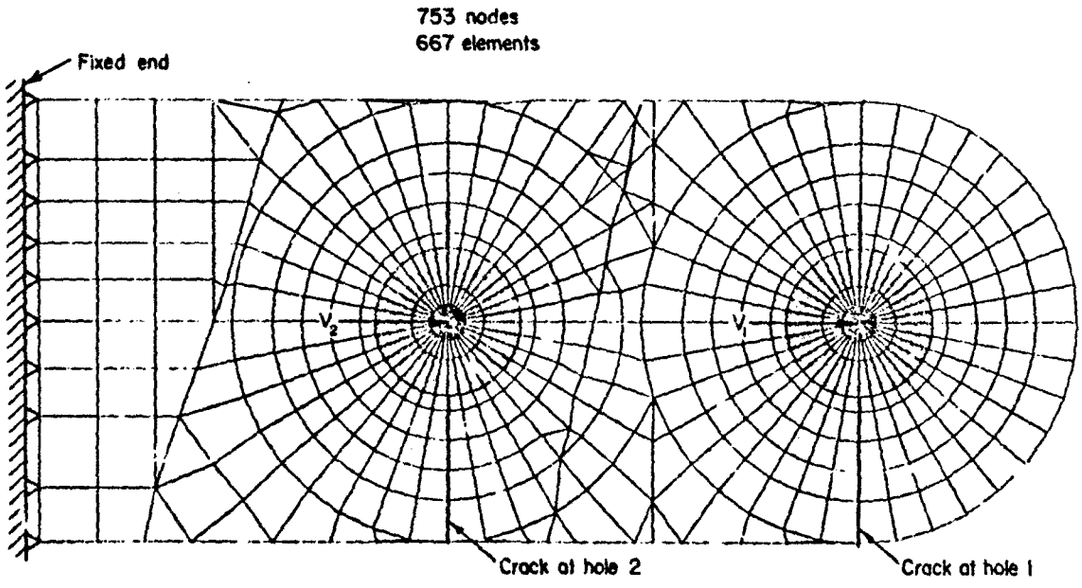

FIGURE 4. DETAILED MODEL

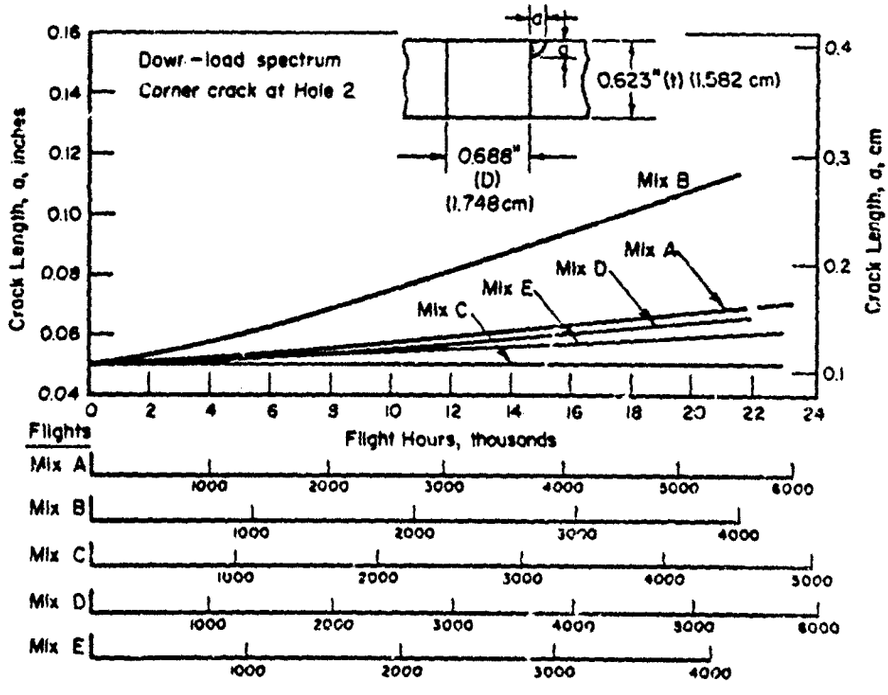

FIGURE 5. FLIGHT-BY-FLIGHT FATIGUE-CRACK GROWTH FOR DIFFERENT USAGE (PREL ITED)

EXAMPLE PROBLEM 4.6.9

DAMAGE TOLERANCE ANALYSIS OF AN AIRCRAFT STRUCTURAL JOINT

S. H. Smith and F. A. Simonen
Battelle's Columbus Laboratories

The following is an excerpt from a paper presented at the
4th Army Materials Technology Conference

1. STATEMENT OF THE PROBLEM

Crack growth and residual strength were calculated for a chordwise splice joint (Figure 1).

2. STRESS-INTENSITY FACTOR

Finite-element analysis and submodeling were used to determine load transfer through the bolts and the stress in the vicinity of the fastener holes (Figure 2). A final detailed finite-element model of the area around the hole was subjected to the boundary conditions obtained from the larger scale models. Stress-intensity factors were calculated from crack opening displacement and crack closure energy. Results are shown in Figure 3. K for corner cracks was obtained as in the previous example.

3. CRACK GROWTH

Crack growth was calculated using upper-bound baseline data represented by the Forman equation. Linear integration was performed as well as retarded integration using the Willenborg model. Some results are shown in Figure 4.

4. COMMENTARY

This is another good example of submodeling. Before following this and the previous example, it should be decided whether or not such a detailed analysis is justifiable from an economical point of view. Generally speaking, it is advisable to perform a simple hand analysis first to determine the criticality. If it turns out that crack-growth life is ample in the presence of cracks of inspectable size, the hand analysis (with an appropriate factor) is perfectly acceptable. Only if the case was marginal an elaborate analysis should be contemplated. However, even then, it would be sensible to assess how much could be gained in accuracy from the elaborate analysis. If in the end approximate stress-intensity solutions have to be used, the detailed analysis would only be necessary, if there were serious doubts about the stress obtained from simpler analysis.

The example shows an interesting case of multiple cracks. Note that the stress intensity of a given crack depends upon the length of other cracks. Thus crack-growth analysis for a given crack cannot be performed independently. If two cracks grow simultaneously, the growth of one is affected by the growth of the other. This means that one has to know the growth of the other crack during a certain crack increment, before one can calculate the growth of the first crack during the next increment.

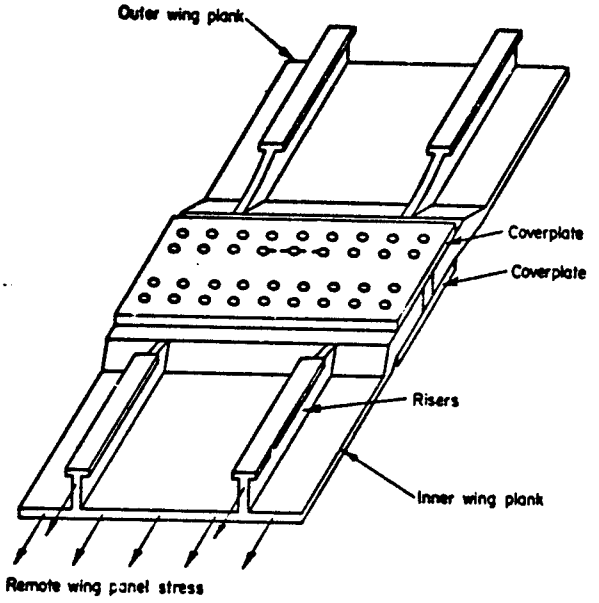

FIGURE 1. STRUCTURE OF JOINT

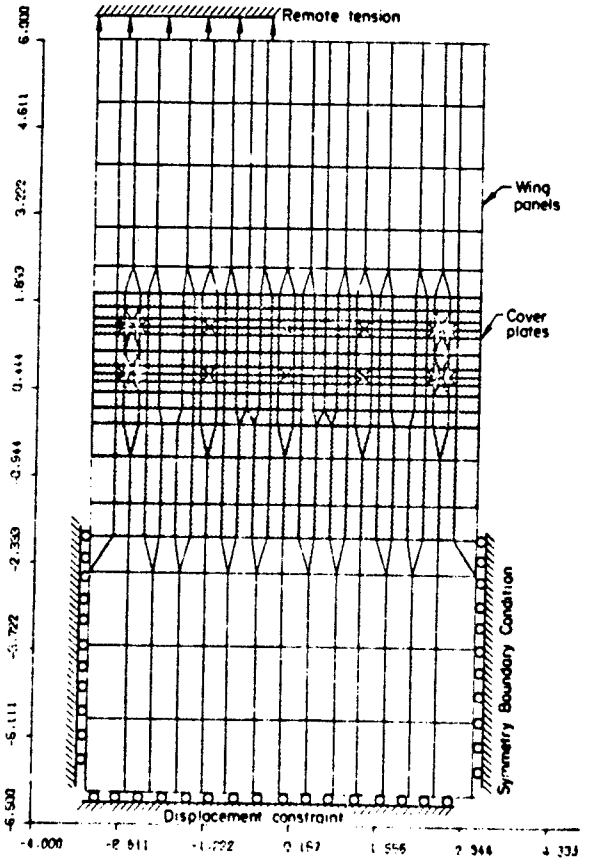

FIGURE 2. FINITE-ELEMENT MODEL

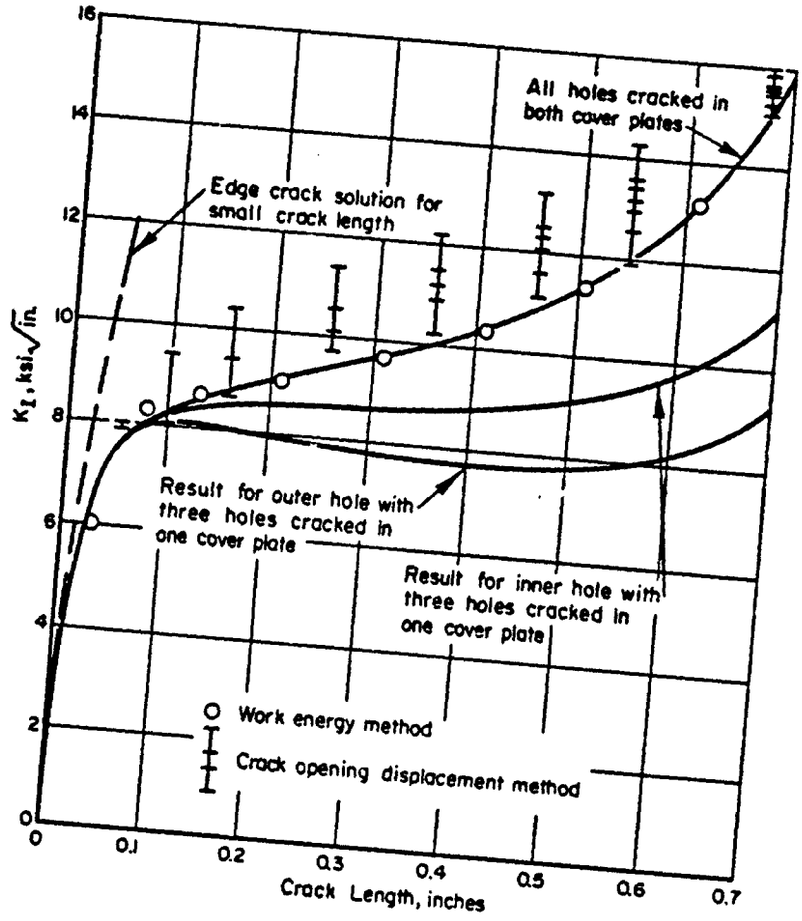

FIGURE 3. STRESS-INTENSITY FACTORS

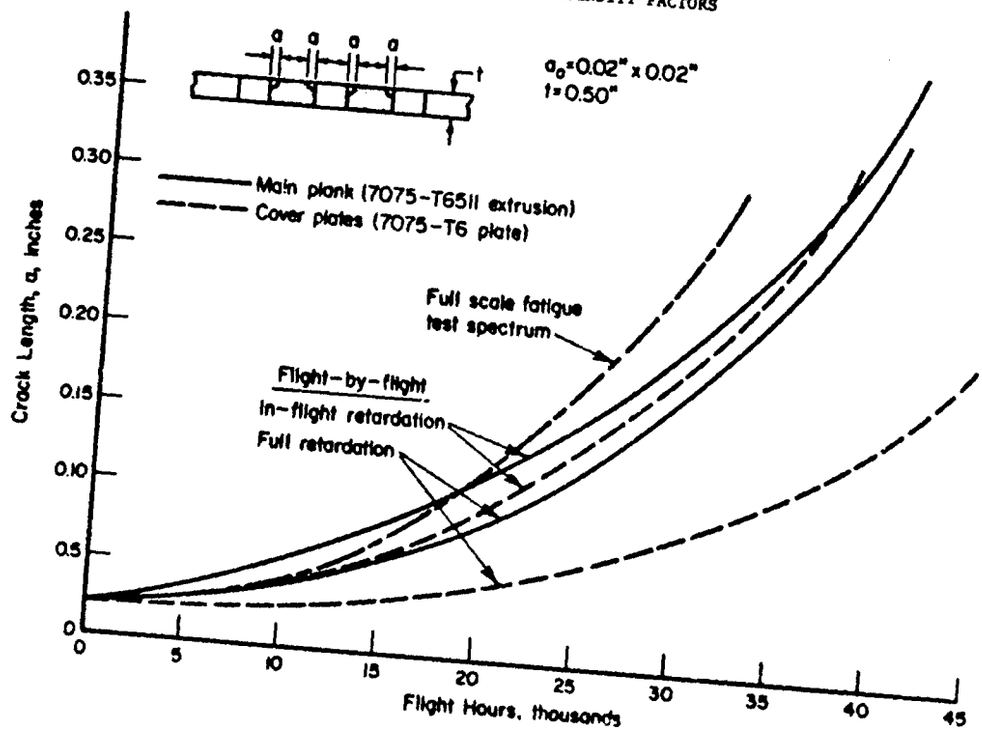

FIGURE 4. CRACK-GROWTH CURVES

5 INTEGRAL STRUCTURES

L.F. NICHOLLS, British Aerospace, Bristol, U.K.

A. JEFFERSON, University of Southampton, U.K.

C.I.P. MARTIN, British Aerospace, Bristol, U.K.

CONTENTS

SUMMARY

5.1 Introduction 5-3

5.2 Fracture Mechanics in the Design of Integral Stiffened Structures 5-3

5.2.1 A Review of the Influence of Stiffeners on S.I.F. 5-3
5.2.2 Comparison with Flat Panel Test Data 5-5
5.2.3 Summary 5-5

5.3 Application of Fracture Mechanics in the Fail-Safe Design of Integrally Stiffened Structures 5-6

5.3.1 Review of Further Factors Influencing Fail-Safe Design 5-6
5.3.2 Comparison with Component Tests 5-6

5.4 Discussion and Conclusions 5-7

SUMMARY

In this chapter the basic formulae for the determination of stress intensity factors,appropriate to integral structures on the basis of the Linear Elastic Fracture Mechanics (L.E.F.M.) approach,are outlined. The effectiveness of the fracture mechanics approach is demonstrated by comparison with results from crack propagation and residual strength tests.

Particular difficulties associated with integrally stiffened structures in relation to accurate stress intensity factor determination and the more general problems of curvature, loading history and bi-axial stressing are discussed and areas of further investigation suggested.

SYMBOLS USED

a, a'	Half crack length
A_s	Cross sectional area of stringer
b	Half stiffener pitch
C	Constant in crack growth equation
C^*	K_I/K_o For crack symmetrical about a failed stiffener
C_p	Retardation Parameter
C_{poe}	K_I/K_o For mid-bay crack between stringers
e	Distance of crack tip from adjacent stringer
E	Young's modulus for plate
E_s	Young's modulus for separate stiffener
K	Stress intensity factor
K_I	" " " opening mode
K_o	" " " in the absence of boundaries
K_c	Critical stress intensity factor
ΔK	Range of stress intensity factor
n	Constant in crack growth equation
N	Number of cycles of applied stress
p	Rivet pitch
R	Stress ratio $\sigma_{MIN}/\sigma_{MAX}$
t	Plate thickness
w	Half plate width
x	Co-ordinate from centre line of panel
α	Bending stiffness of stiffener
β	Ratio $e/(2a+e)$
λ	Stiffness parameter
μ	Stiffener parameter
σ, σ_o	Applied stress
σ_y	Yield stress
σ_{MIN}	Minimum stress in stress cycle
σ_{MAX}	Maximum stress in stress cycle

5.1 INTRODUCTION

Integrally stiffened structures have been extensively employed in the construction of present day civil and military aircraft. Whilst integral construction will, in general, give an increase in overall fatigue life due to the reduction in the number and degree of stress concentration introduced into the structure, a conflict arises between the increase in 'safe-life' and the requirement for a damage tolerant structure. Designers have long been aware of the fact that the most effective way of slowing the rate of propagation of a crack in a plate is to introduce a surface boundary. In this way crack growth is delayed until a new fatigue crack is initiated. In a similar way the use of separate crack stopper straps to meet damage tolerance requirements has been increasingly employed, the delay in crack growth being effective until the fatigue life of the strap has been exhausted. For integrally stiffened structures there are few surface boundaries at which cracks can be arrested and delayed until further fatigue crack initiation has taken place. However, integral stiffeners do have the effect of reducing the rate of crack propagation of an approaching crack by reducing the stress intensity factor (S.I.F.). The retardation in crack growth depends upon the size and spacing of the stiffeners, amongst other things, and a degree of optimisation is therefore necessary in the design of such panels to meet damage tolerance requirements.

In the following sections of this chapter the basic fracture mechanics formulae employed and developed for the analysis of crack propagation and residual strength of stiffened structures are presented. The extension of these formulae to the design of integral structures is then shown by reference to a few practical examples. Finally problems, perhaps not exclusive to integral structures, have been addressed in the hope of eliciting further consideration on these subjects and stimulating interest in those areas in which further research is necessary.

5.2 FRACTURE MECHANICS IN THE DESIGN OF INTEGRAL STRUCTURE

Integrally stiffened structures contain various geometrical features of interest, apart from the raised stiffener, such as holes and stringer run-outs; attention will however be focused on the influence a continuous integral stiffener has on the S.I.F. for a crack located in an integrally stiffened plate. The practical application of the solution to this problem is in the damage tolerant design of wing structure and pressure cabins, where machined skin panels, having multiple stiffeners, are employed.

5.2.1 A Review of the Influence of Stiffeners on S.I.F.

In the literature equal attention has been given by researchers to consideration of a flat sheet having either continuously attached or discretely attached (i.e. riveted) stiffeners. Romualdi[1] et al (1957) considered the influence of a riveted stiffener, making a number of simplifying assumptions which limited the extent of its applicability, however it was the first of such papers and served to indicate the way in which a solution might be found to the S.I.F. for a cracked panel having an intact stiffener.

Sanders[2] (1959) considered the problem of a continuously attached stiffener to an infinite sheet subjected to uniaxial tensile stress, the crack being normal to and located symmetrically about the stiffener. The two possible conditions of either a broken or unbroken stiffener were investigated. The case of the broken stiffener is essential to the consideration of integrally stiffened panels and this work by Sanders is, therefore, directly relevant to this problem. The S.I.F. solution K_I, given as a ratio of K_o the S.I.F. for the crack in the absence of the stiffener, is commonly referred to as C*. Table 1 gives C* as a function of the stiffener parameter

$$\text{where } \lambda = \frac{2atE}{A_s E_s}$$

which for integral panels reduces to

$$\lambda = \frac{2at}{A_s} = \frac{\text{cracked area of plate}}{\text{area of stiffener}}$$

In the analysis the stiffener was taken to be a single line stiffener of cross-sectional area A_s lying in the plane of the plate with zero in-plane bending stiffness. In practice the stiffener will have thickness, bending stiffness and will be offset from the plane of the plate.

The early work by Sanders was extended later by Grief and Sanders[3] to consider an asymmetric crack with respect to the stiffener. This has application where one end of the crack is approaching an integral stiffener. The results of K_I/K_o for this case are shown in Figure 1. However, the same limitation with regard to zero thickness stiffeners etc., implies that the solutions have to be considered somewhat approximate in practice, particularly in the case of a crack tip very close to the stiffener.

Isida[4] has considered the case of a cracked plate in tension with edges reinforced by stiffeners and also of a cracked plate stiffened by a single stiffener. In both cases the in-plane bending stiffness of the stiffener was taken into account (see Figure 2).

In an analysis of a sheet stiffened by a number of equally spaced parallel stiffeners, Poe[5] derived S.I.F's for two symmetrical cases of crack location involving riveted stiffeners - the case of a crack extending equally on both sides of a stiffener and the case of a crack located mid-bay i.e. between two stiffeners. The information was presented in the form of design graphs and covered the variables of rivet pitch, stiffener spacing and stiffness and crack length. The basis of the analysis was that of force and displacement matching at the rivets. The in-plane bending stiffness of the stiffener was taken to be zero and all forces were taken as acting in the plane of the plate. Relative displacement between the rivet and the sheet (i.e. rivet flexibility)was not considered. Although the theory could not be applied directly to the problem of zero length rivet pitch, comparison with results from tests on integrally stiffened panels has shown good correlation with prediction based on the low rivet pitch given by P/2b = 1/12. Figure 3 shows the S.I.F. for a crack extending equally between two stiffeners, according to Poe, for a rivet pitch to stiffener pitch ratio of 1/12 over a range of stiffener stiffness, given by

$$\mu = \frac{A_s E_s}{A_s E_s + 2\ btE}$$

The close agreement between the design curves of Poe for rivet to stiffener pitch ratio of 1/12 and that for a crack approaching an integral stiffener given by Grief and Sanders is also indicated on Figure 3 using the results of Figure 1 and the Compounding Technique of Rooke and Cartwright [6] (See also Chapter 10). The relationship between S.I.F. and crack length when the crack extends beyond the adjacent stiffener, given by Poe,[7] is shown in Figure 4. The crack growth rate is assumed to be equal in the plate and stiffener so that the stiffener is not severed completely until the crack in the plate has advanced an additional distance equal to the height of the stiffener. Poe found that this assumption caused only slight disagreement between measured and predicted crack growth rate on integrally stiffened test panels. For the analysis and design of integrally stiffened panels according to damage tolerance requirements these two S.I.F. solutions, one for the failed stiffener from Table 1 and the analysis of Poe given in Figure 3,were the ones most generally employed by the authors. They may be combined, using the compounding technique, for the analysis of a panel having mutiple stiffeners. It will be observed, by reference to Table 1 and Figure 3, that the influence of a failed or intact stiffener on the S.I.F. is of a localised nature, becoming significant only when the crack tip and stiffener are in close proximity. An approximate solution for a crack centred on a failed stiffener may be obtained by combining factors such that:

$$\frac{K_1}{K_o} = C^*.\ C_{Poe}$$

However, as discussed by Rooke et al in Chapter 10 this simplification is not directly applicable if the crack crosses one of the boundaries. In this case the crack, plus the boundary which it crosses, must be replaced by an equivalent crack of a size a' which will give an equal S.I.F. in the absence of other boundaries. This equivalent crack then interacts with the remaining boundaries.

From the foregoing basic S.I.F. solutions a fracture mechanics analysis of residual strength and crack growth rate can be performed for integrally stiffened panels given the appropriate fracture and crack growth properties of the basic material. This type of analysis can be used to demonstrate conformance with damage tolerance requirements, for the determination of inspection intervals and for setting the standard for maximum permissible defect sizes.

5.2.2 Comparison with Flat Panel Test Data

A number of tests have been conducted on flat machined fuselage-type panels by BAe as part of the Concorde development test programme. The test panels were of three types and details of their cross sections are given in figure 5. The panels were of a seven stiffener design and tests with symmetrical cracks were conducted on a central stiffener. The tests in general consisted of a period of fatigue crack growth at typical fatigue stress levels followed by a residual strength test. Tensile and fracture properties of the material BACM76, (RR58 plate) indicated that plastic zone sizes for this material under fatigue and residual strength loading would be small and hence L.E.F.M. would be applicable. The stress distribution across the centre section of the test panel was determined from strain gauges and is shown in Figure 6. The distribution may be represented by an equation of the form

$$\sigma\left(\frac{x}{w}\right) = \sigma_o\left[\, 0.0317\left(\frac{x}{w}\right)^4 - 0.1657\left(\frac{x}{w}\right)^2 + 1.05 \,\right]$$

When calculating the S.I.F. resulting from such a stress distribution a factor was applied which took the same form as the stress distribution. This is equivalent to assuming a uniform stress across the panel of magnitude $\sigma(a/w)$ equal to that which would exist at the crack tip location in the absence of the crack. This approximation had been found to give satisfactory agreement with test results. However, S.I.F. solutions are now available for centre and edge cracks with arbitrary loading[8], which if applied to the above distribution differ by less than 3% from the above approximation.

The results of the residual strength tests on the stiffened panels are shown on Figure 7 for the cases in which the cracks were grown out to the adjacent stiffeners. For comparison a calculated residual strength is also plotted using the method explained in para 5.2.1 , together with the stress distribution outlined above, and a K_c value derived from coupon testing. Figure 8 shows the variation in residual strength across a stiffener bay, for three values of stiffener parameter, as a function of crack length. It will be observed from this figure that for a material with a given fracture toughness (K_c) there is a crack size shorter than the bay width which is critical at a lower stress. However the propagating crack is arrested as it extends towards the stiffener into a region of reducing S.I.F.

Figures 9 (a) and 9(b) compare measured and calculated crack growth rates in flat panels. The calculated crack propagation rates are based on a crack growth equation of the form proposed by Forman, Kearney and Engle: [9]

$$\frac{da}{dN} = \frac{C\,\Delta K^n}{(1-R)K_c - \Delta K}$$

The equation was derived from crack propagation tests on flat coupon specimens. Favourable agreement is shown between test and calculation.

5.2.3 Summary

The development tests showed the suitability of the L.E.F.M. approach for this material under uniaxial loading in the damage tolerance design of the Concorde pressure cabin and other primary structure. However when related to actual components further consideration must be given to the possible influences which bi-axial loading, pressure, curvature and the fatigue spectrum may have on the crack growth rate and residual strength.

In the following section consideration is given to the application of fracture mechanics in the fail-safe design of more typical integral stiffened aircraft structures.

5.3 APPLICATION OF FRACTURE MECHANICS IN FAIL-SAFE DESIGN OF INTEGRAL STRUCTURES

The application of the methods developed for flat panels in section 5.2 to cover more typical aircraft structures will now be discussed. These structures could differ from the flat panels, on which good correlation between test and theory was achieved, by perhaps having significant curvature, being subject to spectrum loading and having the possibility of cracks in a bi-axial stress field. What follows is a review of some of the possible solutions for dealing with these differences and the effect these solutions may have on the prediction of crack propagation and residual strength.

5.3.1 Review of Further Factors Influencing Fail-Safe Design

A parameter which should be taken into consideration is that of curvature and its possible influence on residual strength and crack propagation. Folias[10], Duncan and Sanders[11] and Adams[12] obtained correction factors for the case of circumferential cracks in unstiffened cylinders. It will be observed that there is a large variation in the curvature correction factors between the various researchers.

The effect of spectrum loading on crack propagation must also be considered because a fatigue load preceded by a load of higher magnitude produces less crack propagation than it would in the absence of such a load. This retardation effect is mainly attributed to a combination of residual deformation and stress around the crack tip and the effect on crack closure due to the plastic deformation left in the wake of the crack front.

There are several models treating retardation in a quantitative way, most are semi-empirical, the two best known are due to Wheeler[13] and Willenborg et al[14].

Using the Wheeler model, the retarded crack growth can be determined from the relationship,

$$\frac{da}{dN} = C_p f(\Delta K)$$

where $f(\Delta K)$ is the usual crack growth function and Cp is a retardation parameter based on experimental data.

Another factor to be considered when carrying out crack propagation tests on a component, such as a fuselage which includes internal pressure, is the resulting bi-axial stress field. Anstee and Morrow[15] have reported on the effects of bi-axial loading and have concluded that bi-axial tension stresses reduce the crack growth rate. They used panels made from the same material and of almost identical configuration to those discussed in this report. Their results indicate a reduction in crack growth rate of 55% when the stress parallel to the crack is equal to the longitudinal stress and some 33% reduction when the parallel stress is half the longitudinal. However, these findings call into question the use of ΔK (calculated as a function of applied stress normal to the crack) as the parameter for correlating with crack growth rate. If bi-axial effects, displacements and strain energy related quantities are to be adequately represented then, as discussed by Eftis et al[16], an additional non-singular constant term should appear in the local stress components parallel to the crack.

5.3.2 Comparison with Component Tests

Crack propagation and residual strength tests on curved integrally stiffened panels, with circumferential cracks, see fig.10, have been conducted on a representative fuselage component specimen. Two residual strength tests were taken to failure, both were carried out without pressure but the bending moment applied to the specimen was such that the total tension stress, including that due to pressure, was developed at the top centre line. The tests were done with the crack centred on a failed stiffener and extending to adjacent stiffeners. The results are shown on Figure 11. Also plotted is a line of constant stress intensity for the curved panels which has been calculated using the compounding technique, taking into account the failed stiffener, the influence of the intact stiffeners adjacent to the crack tips and a value of K_c derived from coupon tests. The results from fig.7, for the flat panels are also plotted for comparison. Bearing in mind that there was no pressure applied on the fuselage tests, i.e. the stresses being predominantly uniaxial, it was assumed that any variation between the flat panel on the fuselage results would be due to curvature. As the results

showed little variation a curvature correction factor of 1.0 was applied in all subsequent analyses.

All crack propagation tests on circumferential cracks in curved panels were carried out under a cycle of loads representing a complete spectrum of on-ground and in-flight stresses. A typical spectrum representing a single flight cycle is shown on Figure 12. The results of two such crack propagation tests are shown on figs.13 (a) and 13 (b) together with the results of calculations using the methods for flat panels derived in section 5.2, taking a linear accumulation of crack growth under each individual load in the spectrum.

Although this analysis does not give correlation with the test results it can be further improved by the consideration of retardation effects. The method used was that due to Wheeler(13) and the results of such an analysis are also shown on figs.13 (a) and 13 (b).

The crack propagation tests on curved panels also included at the appropriate times the effect of internal pressure and its resulting bi-axial stress field. As the hoop stress in these tests was circa 8600 lb/in^2 it can be seen from the spectrum of normal stress that during the time that pressure was applied (see fig.12) the stresses parallel to the crack are generally about the same as the peak stresses normal to the crack. The work of Anstee and Morrow (14) indicates that this degree of bi-axiality would give a factor on life of around 1.5 and a further improvement in correlation between prediction and test would be obtained by the application of a factor of this magnitude to the crack propagation life during the time pressure was applied.

Obviously a more rigorous approach to the effect of a fatigue spectrum of bi-axial stresses on crack propagation needs to be developed. In the meantime the best course is to perform tests in the most representative manner if accurate results are required.

5.4 DISCUSSION AND CONCLUSIONS

Despite the simplifications inherent in the two-dimensional analysis for the determination of S.I.F.s and the idealisation of the structure which is necessary good agreement between test results and calculation can be shown for flat panels under uniaxial loading. Improvements are clearly required in the determination of the S.I.F. for an integrally stiffened panel for the case where the crack tip is adjacent to an intact stiffener and beginning to propagate into it. Poe (7) gives a linear approximation to the S.I.F. for cracks growing through integral stiffeners.

The influence of curvature on the effective S.I.F. requires further investigation. Residual strength tests on curved panels under essentially uniaxial loading have given results comparable to those obtained on flat panels, also tested under uniaxial loading, indicating the effect of curvature to be small for the type of structure tested.

Crack growth in curved panels under a spectrum of biaxial stresses differs significantly from that which would be predicted using a simple linear damage approach. Further investigation is required into the effect of biaxial stresses, in particular the influence on crack growth of the resulting variation in magnitude and direction of principal stress which occurs during a spectrum of fatigue loading.

REFERENCES

1. J.P. ROMUALDI, J.F. FRASIER, G.R. IRWIN "Crack-extension Force Near a Riveted Stiffener" NRL Report 4956, October 1957.

2. J.L. SANDERS "Effect of a Stringer on the Stress Concentration due to a Crack in a Thin Sheet" NASA Technical Report R-13, Langley Research Centre, 1959.

3. R. GRIEF, J.L. SANDERS "Effect of a Stringer on the Stress in a Cracked Sheet" ONR Technical Report No.17, June, 1963; J.App.Mech. Vol.32 (1965) p.59.

4. M. ISIDA "Analysis of Stress Intensity Factors for the Tension of Centrally Cracked Strip with Stiffened Edges" Journal of Engineering Fracture Mechanics, Vol.5, No.3.

5. C.C.POE "Stress Intensity Factor for a Cracked Sheet with Riveted and Uniformly Spaced Stringers" NASA Technical Report R-358, Langley Research Centre, May,1971.

6. D.P. ROOKE & D.J. CARTWRIGHT "A Method of Compounding Stress Intensity Factors for Complex Configurations" RAE Technical Report TR75063, June, 1975.

7. C.C.POE "Fatigue Crack Propagation in Stiffened Panels" ASTM S.T.P.486, 1971 p.79.

8. G.G. CHELL "Stress Intensity Factors for Centre and Edge Cracks with Arbitrary Edge Loading Applied Distant from the Crack" International Journal of Fracture Mechanics 12 (1976) p.33-46.

9. R.G. FORMAN, V.E. KEARNEY, R.M. ENGLE, "Numerical Analysis of Crack Propagation in Cyclic Loaded Structures", Trans. ASME, J. Basic Engineering, Vol.89, p.459 (1962).

10. E.S. FOLIAS "A Circumferential Crack in a Pressurized Cylindrical Shell" International Journal of Fracture Mechanics, Volume 3, March 1967, p.1-12.

11. M.E. DUNCAN & J.L. SANDERS "A Circumferential Crack in a Cylindrical Shell under Tension" International Journal of Fracture Mechanics, Vol.8 March 1972, p.15.

12. N.J.I.ADAMS "The Influence of Curvature on Stress Intensity at the Tip of a Circumferential Crack in a Cylindrical Shell" presented at the 1970 Annual Meeting of the Am.Soc. Testing and Materials, Toronto, June 1970.

13. O.E.WHEELER "Spectrum Loading and Crack Growth" Trans. ASME, Journal of Basic Engineering, Vol.94 (1972) pp.181-186.

14. J.D. WILLENBORG, R.M. ENGLE & H.A. WOOD "A Crack Growth Retardation Model Using an Effective Stress Concept" Air Force Flight Dynamic Laboratory, Rep. No. TM FBR-71-1, 1971.

15. R.F.W. ANSTEE & SARAH M. MORROW "The Effects of Biaxial Loading on the Propagation of Cracks in Integrally Stiffened Panels" Presented at the 10th Symposium of the ICAF, Brussels, May, 1979.

16. J. EFTIS, N. SUBRAMON, A.N. & H. LIEBOWITZ, Engng. Fracture Mechanics, Vol.9 (1977) p.189-210.

TABLE 1

VARIATION OF S.I.F. WITH STIFFNESS PARAMETER λ

FOR A CRACK IN A PLATE SYMMETRICAL ABOUT A

FAILED STIFFENER, (REF. 2)

λ	C*	λ	C*	λ	C*
0.1	4.06	1.5	1.297	15	1.033
0.2	2.73	2.0	1.228	20	1.025
0.3	2.23	3.0	1.15?	30	1.017
0.4	1.960	4.0	1.119	50	1.010
0.5	1.791	5.0	1.096	100	1.005
0.6	1.676	6.0	1.080		
0.7	1.590	7.0	1.069		
0.8	1.524	8.0	1.061		
0.9	1.472	9.0	1.054		
1.0	1.430	10.0	1.049		

FIGURE 1 - INFLUENCE OF A STIFFENER ON THE S.I.F. AT AN APPROACHING CRACK TIP (REF. 3.)

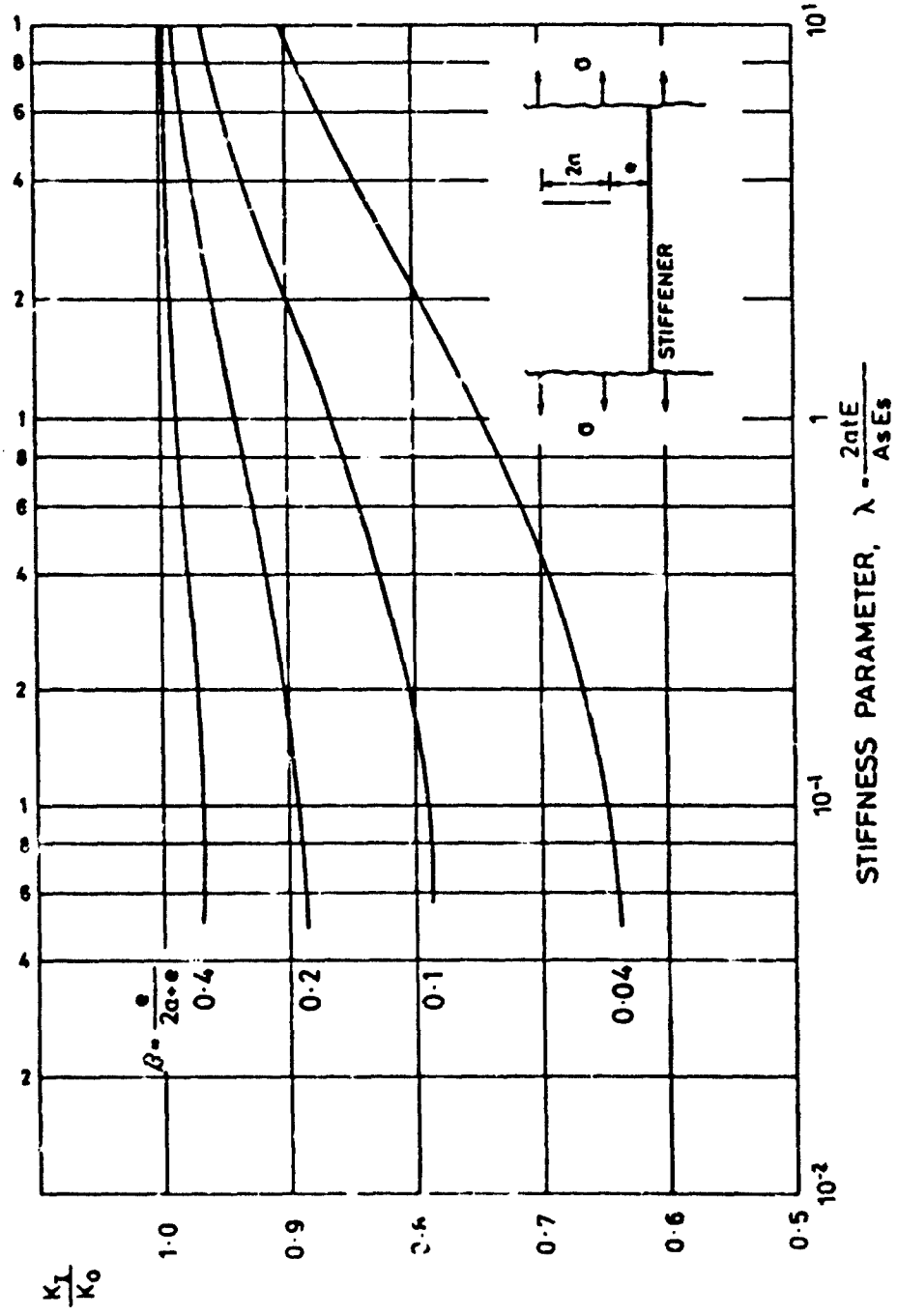

FIGURE 2 - INFLUENCE OF A STIFFENER ON THE S.I.F. AT AN APPROACHING CRACK TIP (REF:4)

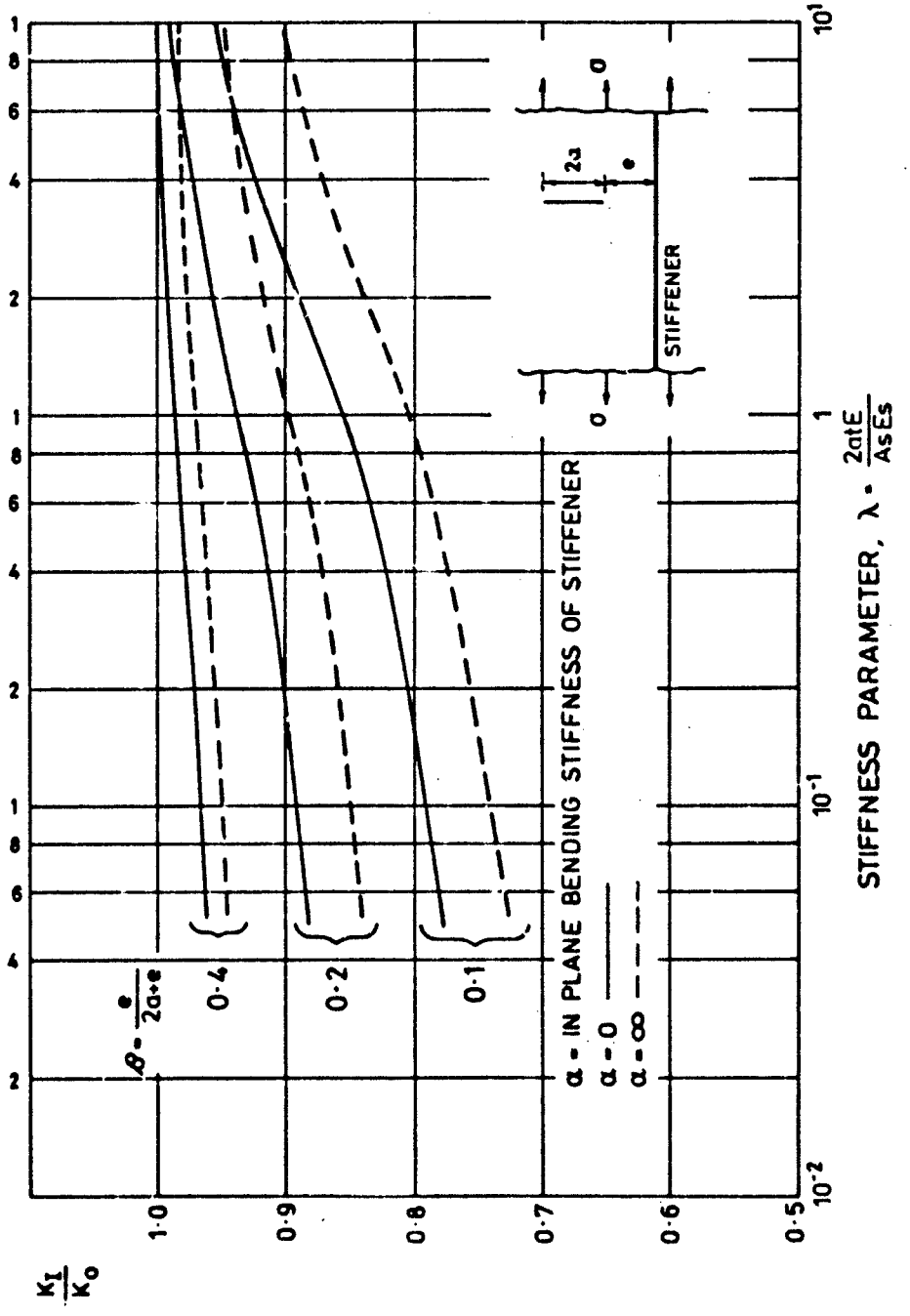

FIGURE 3 -S.I.F. FOR A CRACK EXTENDING EQUALLY BETWEEN TWO STRINGERS (REF. 5)

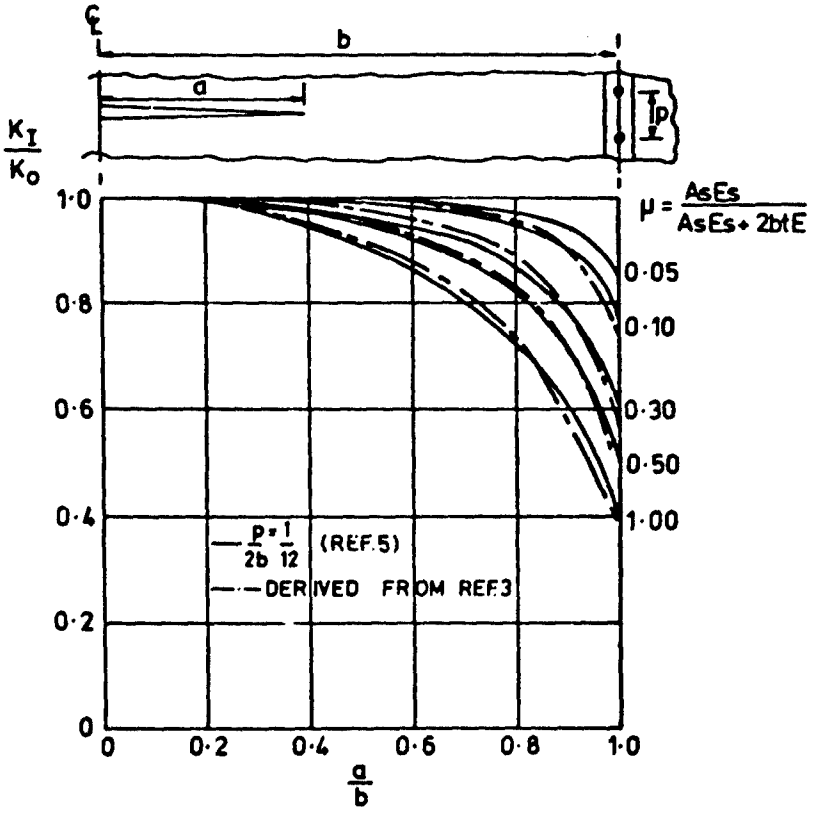

FIGURE 4 S.I.F. FOR A CRACK EXTENDING BEYOND THE ADJACENT STRINGER

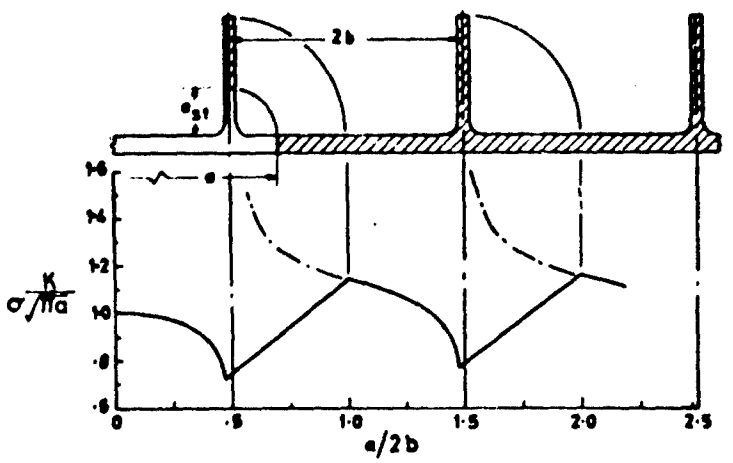

FIGURE 5 -FLAT PLATE TEST PANELS

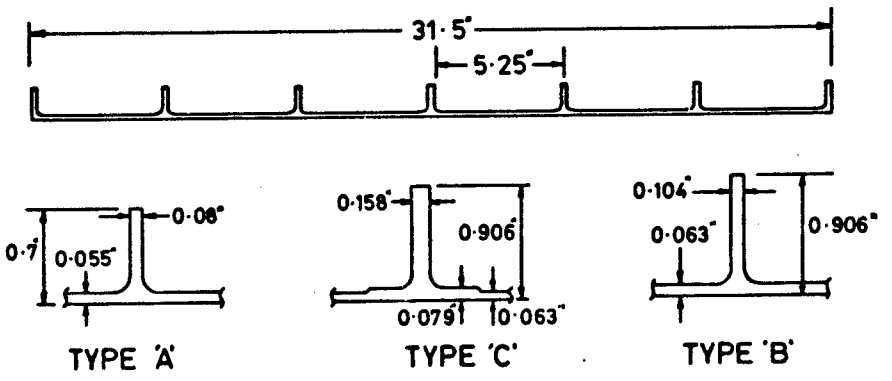

FIGURE 6 -MEASURED STRESS DISTRIBUTION ACROSS PANELS

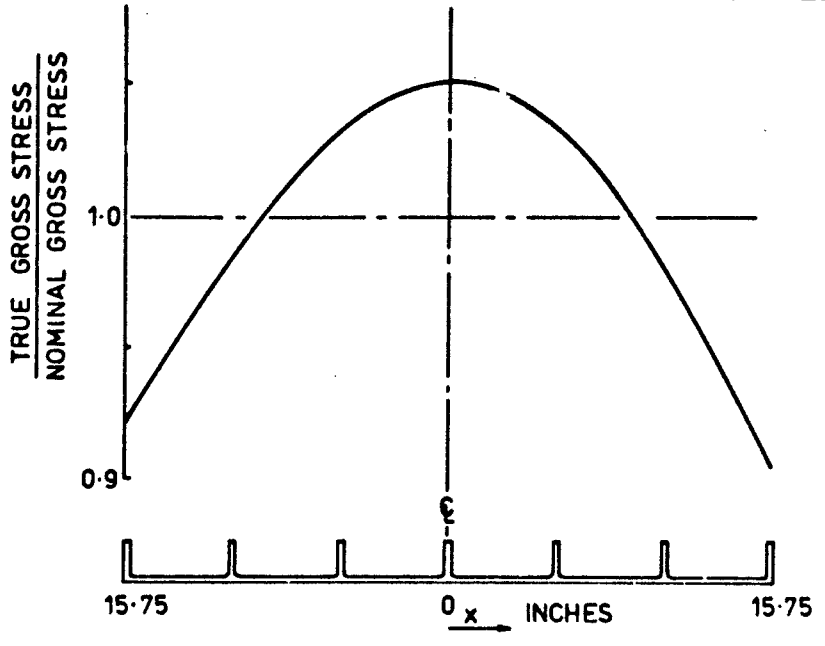

FIGURE 7 RESIDUAL STRENGTH OF FLAT STIFFENED PANELS FOR A SYMMETRICAL CRACK CENTRED ON A FAILED STIFFENER AND EXTENDING TO ADJACENT STIFFENERS

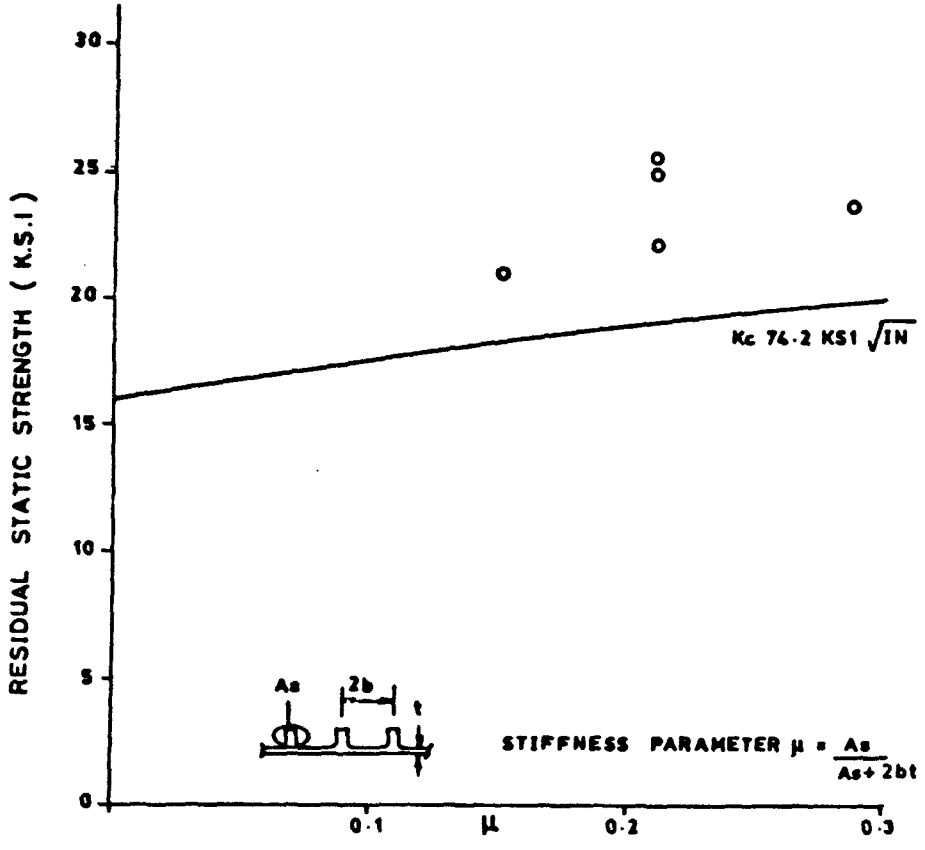

FIGURE 8 - RESIDUAL STRENGTH OF INTEGRALLY STIFFENED PANEL AS A FUNCTION OF K_c AND μ FOR A CRACK SYMMETRICAL ABOUT A FAILED STIFFENER

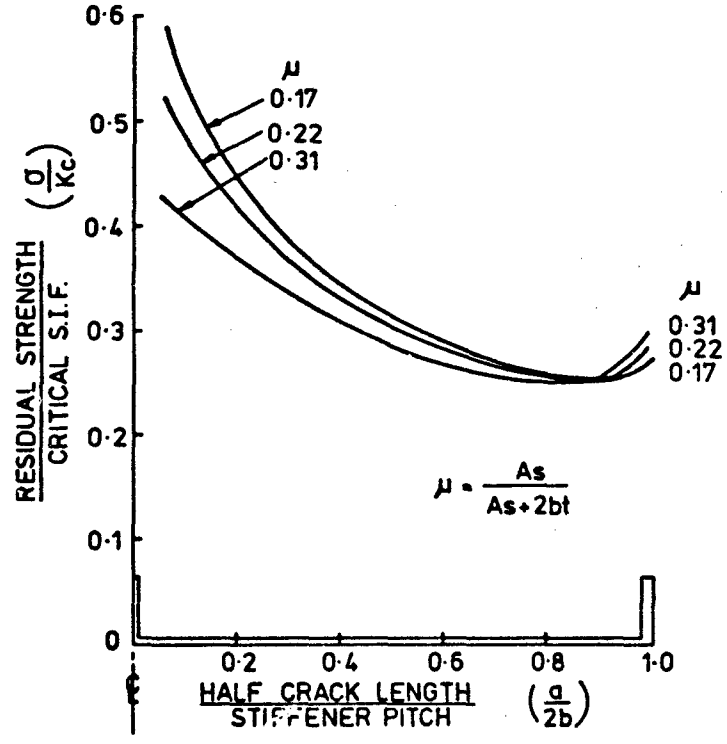

FIGURE 9(a)- MEASURED AND CALCULATED CRACK GROWTH FOR INTEGRALLY STIFFENED PANEL WITH CRACK SYMMETRICAL ABOUT A FAILED STIFFENER

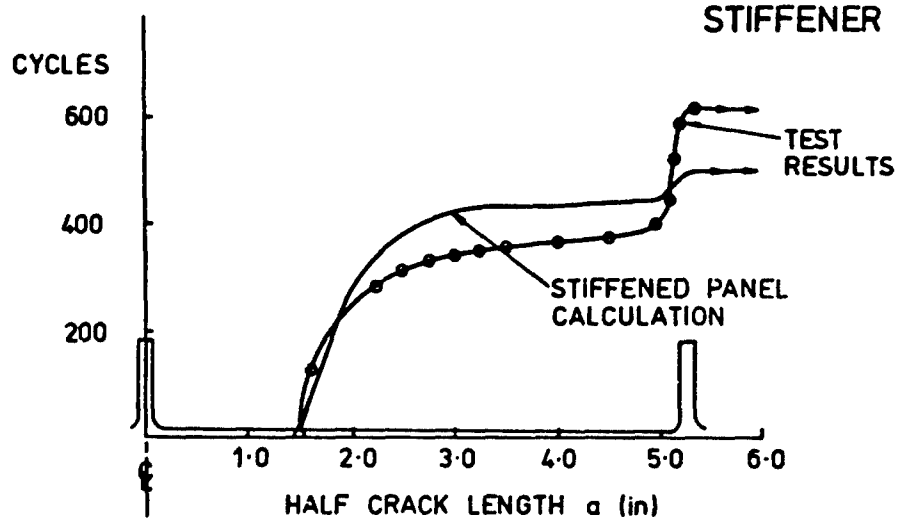

FIGURE 9(b)- MEASURED AND CALCULATED CRACK GROWTH

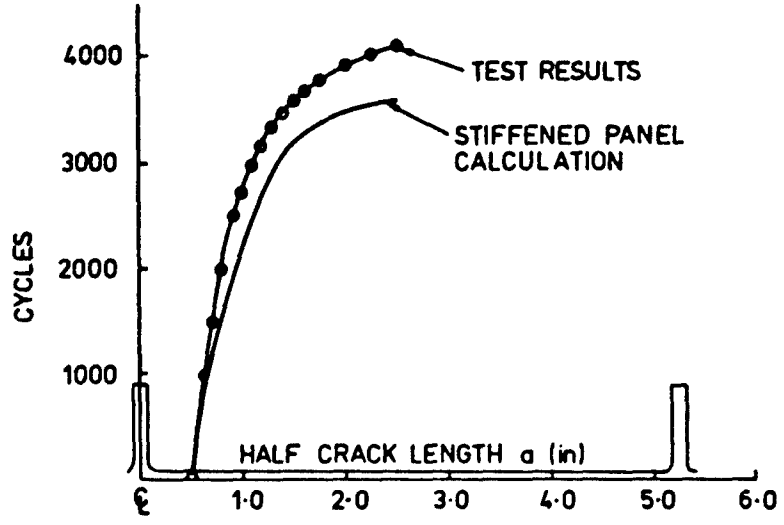

FIGURE 10 - CURVED FUSELAGE TEST PANELS

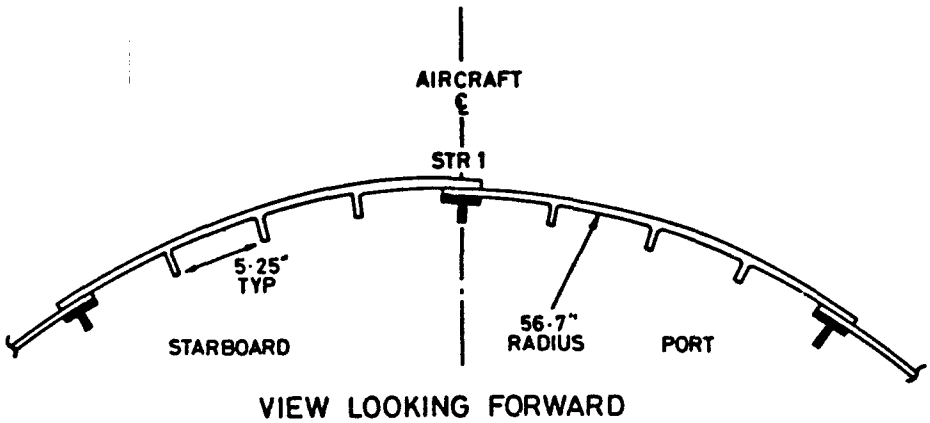

VIEW LOOKING FORWARD

TYPE A

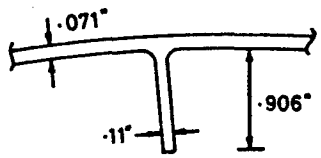

TYPE B

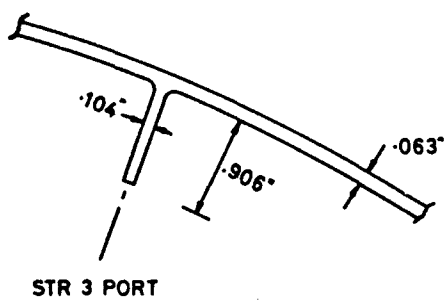

FIGURE 11 RESIDUAL STRENGTH OF FLAT AND CURVED STIFFENED PANELS FOR A SYMMETRICAL CRACK CENTRED ON A FAILED STIFFENER AND EXTENDING TO ADJACENT STIFFENERS.

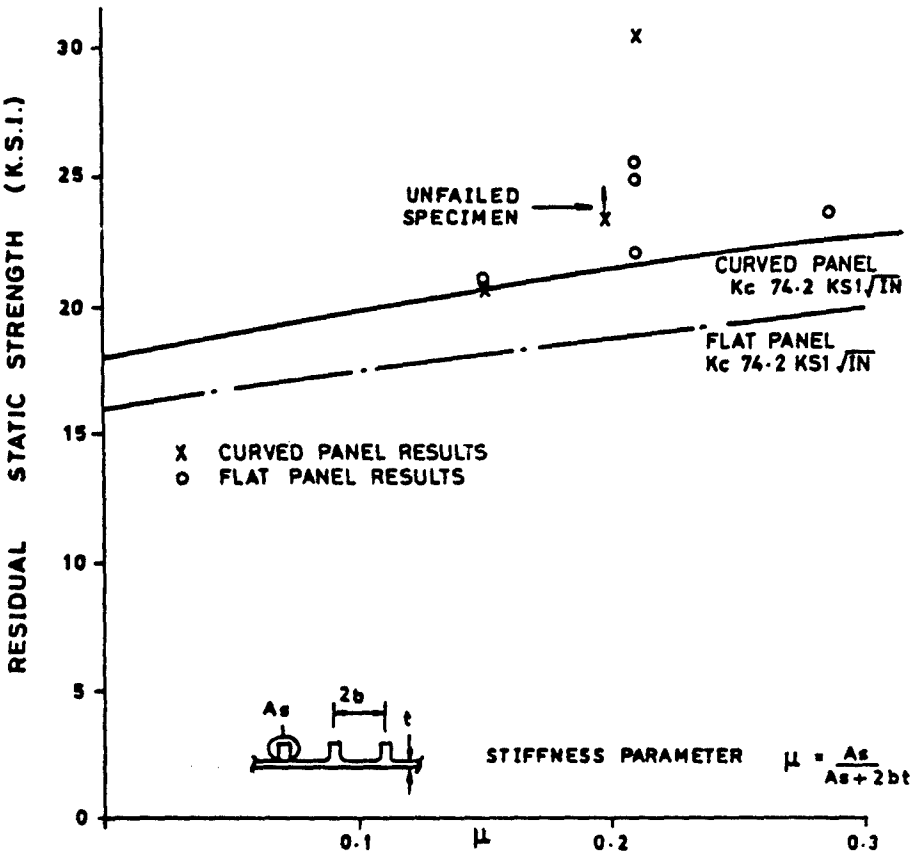

FIGURE 12 - TYPICAL FATIGUE SPECTRUM FOR A SINGLE FLIGHT REPRESENTED AS A SERIES OF PEAKS AND TROUGHS

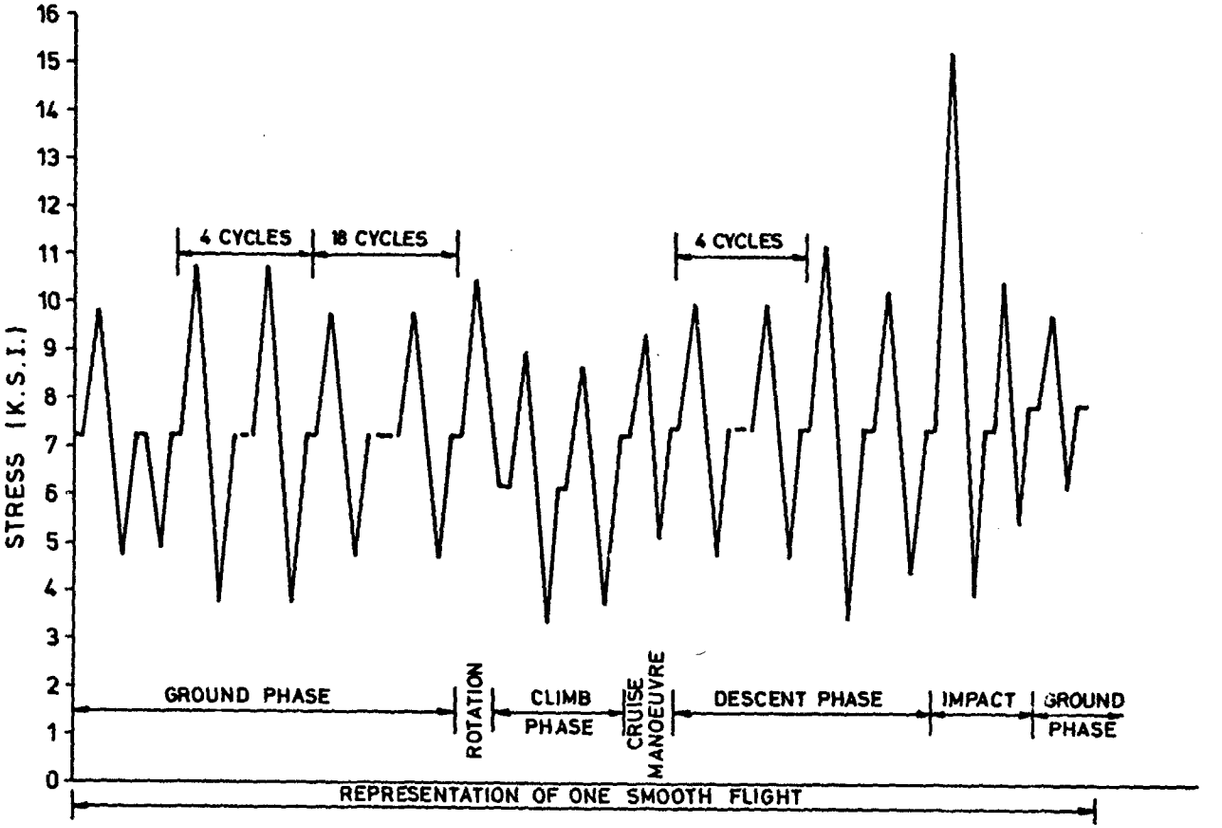

FIGURE 13(a)- CRACK PROPAGATION IN CURVED FUSELAGE PANEL UNDER BLOCK SPECTRUM LOADING

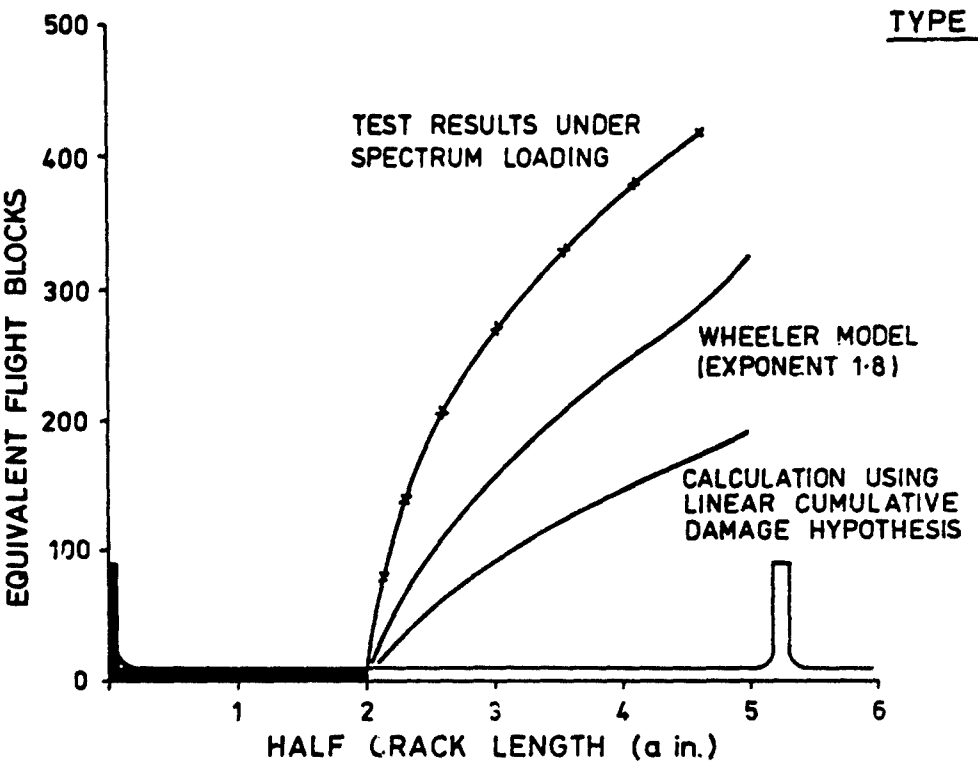

FIGURE 13(b)- CRACK PROPAGATION IN CURVED FUSELAGE PANEL UNDER BLOCK SPECTRUM LOADING

TYPE 'B'

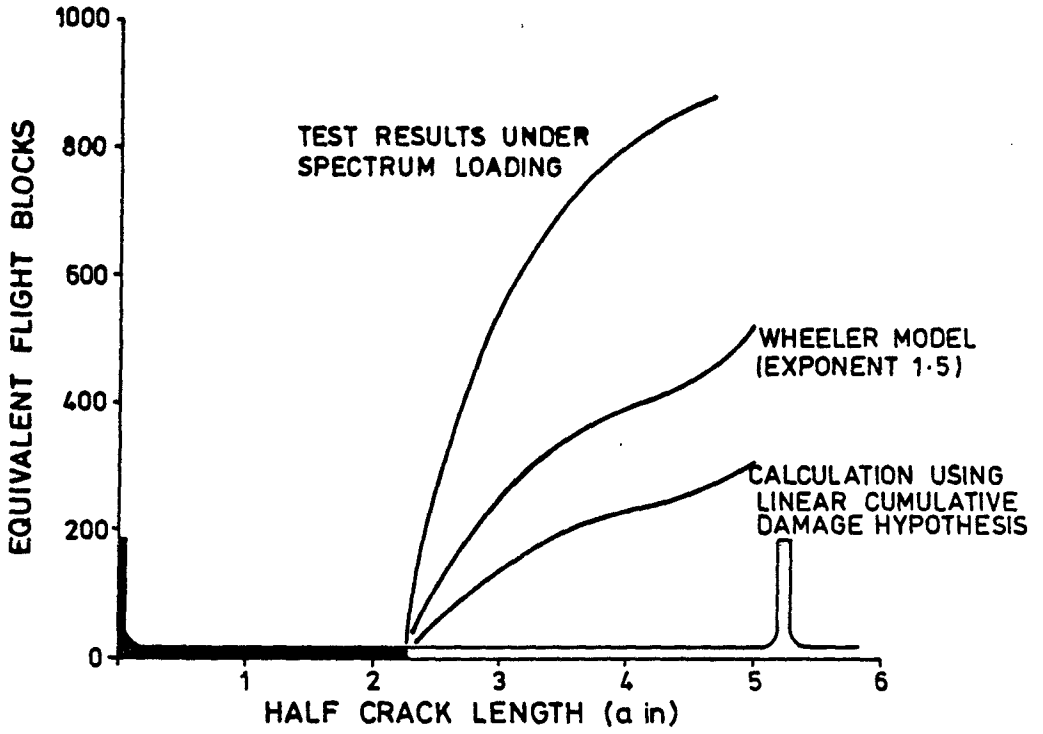

6. FORGINGS, INCLUDING LANDING GEARS

by

Dr.-Ing WALTER SCHÜTZ
Industrieanlagen-Betriebsgesellschaft mbH
Einsteinstraße 20, 8012 Ottobrunn, Germany

6.1 INTRODUCTION 6-3

6.2 STATE OF THE ART OF UTILIZING FRACTURE MECHANICS FOR THE DESIGN OF FORGINGS 6-3

6.2.1 Special Considerations. 6-3

6.2.2 Basic Formulae to be Applied. 6-4

6.2.3 Laboratory Tests and Specimens Utilized 6-5

6.3 EXAMPLES OF APPLICATION OF FRACTURE MECHANICS TO FORGINGS. 6-6

6.3.1 Forgings Designed According to Fracture Mechanics Principles. 6-6

6.3.2 Forgings from Aircraft in Service or Under Development 6-6

6.3.3 Tests on Forged Components to Determine their Fracture Properties and Comparison with Specimen Data 6-8

6.3.3.1 General Remarks. 6-8

6.3.3.2 Nose Landing Gear Strut. 6-8

6.3.3.3 Forged Wing Attachment Fitting 6-11

6.3.3.4 Hinge Rib Forging. 6-12

6.3.3.5 Full Scale Fatigue Test on a Main Landing Gear 6-13

6.3.4 Fracture Mechanics Tests on Standard Specimens cut from Forged Components. 6-13

6.4 CONCLUSIONS. 6-15

6.5 REFERENCE. 6-17

6. FORGINGS, INCLUDING LANDING GEARS

by

Dr.-Ing. Walter Schütz

Industrieanlagen-Betriebsgesellschaft mbH
Einsteinstraße 20, 8012 Ottobrunn, Germany

6.1 Introduction

Forgings are employed at many different locations in an aircraft structure. Some examples which come to mind are wing spars, root ribs, bulkheads, frames, wing or empennage attachment fittings etc. It is typical for these components to be fully machined, the weight of the finished part sometimes being only a few percent of that of the original forging. This machining will disrupt the grain flow, which may have been highly irregular to start with, see Fig. 1.

Compressor or turbine disks, as well as gun barrels or helicopter rotor heads are examples of fully machined forgings from other fields.

Other forged components such as undercarriage legs are not machined over most of their surfaces. However, they may still have an irregular grain flow within the forgings and much more so between individual forgings of identical shape.

The large amount of machining on most aircraft structural forgings can be reduced by so-called "precision" forgings. The aim is to reduce costs by forging the net shape, requiring no machining except for drilling attachment holes etc. Precision forgings are said to offer additional benefits such as better mechanical properties and fatigue characteristics due to the higher degree of work during forging, better grain orientation and other metallurgical advantages retained when the as-forged surfaces are not removed.

Forged components are monolithic, they usually have a single load path and their failure may result in a catastrophic accident. This obviously has been recognised in the relevant MIL-Standard 1587 of the USAF [37], because all surfaces of structural forgings used in fatigue critical applications must be completely shotpeened or placed into compression by other suitable means after final machining and heat treatment. Furthermore, all forgings made of steel with 1400 N/mm² ultimate tensile strength and above must be shotpeened. The objective apparently is to avoid cracks altogether.

Forgings were formerly designed to the "safe life" philosophy; nowadays they have to meet the "slow crack growth" requirements, at least if the USAF damage tolerance requirements [1, 37] are applicable. Therefore the residual static strength and the crack propagation properties of forgings are important to the designer, the airworthiness authorities and the operator of the aircraft.

6.2 State of the Art of Utilizing Fracture Mechanics for the Design of Forgings

6.2.1 Special Considerations

When utilizing fracture mechanics for the design of new or the damage tolerance assessment of in-service components, the following procedure is usually followed:

1. Establish the fracture toughness K_{Ic} of the material (if thickness is sufficient for plane strain conditions) by standard ASTM tests on specimens machined out of the component. For simplicity's sake or if the component is not yet available, "typical" K_{Ic}-values are often taken from the literature [3, 17].

2. Calculate the residual static strength of the component in the cracked condition assuming
   - a "typical" crack shape expected in service
   - a crack size which is certain to be detected with the NDI method employed
   - the critical section and its maximum nominal stress at, say, limit load and, last but not least
   - that the fracture toughness K_{Ic} as per 1. is valid for the component.

   If the residual static strength is too low, the procedure is repeated, using for example a higher K_{Ic}-value or a smaller crack length, meaning that a higher-toughness material or better NDI methods must be employed.

This is the procedure for designing new components, neglecting for the moment the much more difficult problem of crack propagation under service loads. For the damage tolerance assessment of components which have cracked in service at least the critical section and the crack shape are known. Also the specimen can be taken out of the component near this location. The result of the computation is thus more reliable.

However, the crack may turn out to be of a complex shape, for which no "textbook" solutions are available. In that case a finite element solution may be called for.

PRECEDING PAGE BLANK-NOT FILMED

Even then, it should be realized that in the procedures described above one basic assumption is still employed, which is the mainstay of fracture mechanics, so to speak: "The fracture toughness of a small standard specimen is a quantitative measure of the residual static strength (in the cracked condition) of the component from which the specimen was taken". If one goes a step further, even the scatter of the fracture toughness of the specimens would have to be equal to (or larger than) the scatter of the residual static strength of the component.

For calculating the crack propagation, da/dN vs. Δ K-curves are produced, again utilizing specimens. Here the basic assumption is: The range of stress intensity Δ K at a certain stress ratio R determines the crack propagation rate", that is, at equal Δ K and R the crack propagation rate in a specimen and in the corresponding component are equal.

In the author's opinion, it has not been shown conclusively that the above basic assumptions are correct in a l l cases. In the case of f o r g i n g s , one might intuitively expect some special problems due to the following reasons:

- The heavy sections of forgings cannot be worked as uniformly or as thoroughly as, for example, sheet or plate.
- Particulars of the forging procedure, for example if only a finishing die is used, may heavily influence the residual static strength of a forging resulting in extreme differences in critical crack sizes.
- The grain flow will be disrupted by machining; furthermore it may be irregular within the forging. This might lead to different fracture toughnesses and to peculiar crack shapes. Two nominally identical forgings, having been forged by the same company in the same die, may have widely different grain flow patterns and fracture surfaces, see Figures 2 to 5. Thus the requirement in the applicable MIL-Standard [5] "the first production forging shall be sectioned and etched to show the grain flow pattern .." may not be meaningful.
- Many forged components are large and contain widely different section thicknesses. It will therefore be difficult if not impossible to attain similar fracture toughness properties all over the forging.

The above problems are valid even for only one forging; they may be more marked for a large number of only nominally identical forgings.

On the other hand it should be easy to use fracture mechanics procedures on forgings because the sections are usually thick enough for plane strain conditions to apply, avoiding the difficulties associated with plane stress conditions such as gross plastic yielding and/or inexact solutions for the applicable stress intensity factor K. In this respect the solution should be simple, because the forging is, so to speak, in one piece and the problems with, for example, stress intensity factors for sheet with riveted-on stiffeners do not exist.

So it would appear that most of the problems of using fracture mechanics for the design and damage tolerance assessment of typical forged components do not come from the fracture mechanics side and therefore cannot be solved by improvements in fracture mechanics theory, better formulae for K etc. Rather they come from the production procedures and materials properties side.

In other words, the difficulties lie not so much in the calculation procedures, but in the input data - as in many other engineering problems - and there might be large differences in fracture toughness behaviour between specimens and complete components. In any case a larger than normal variability of fracture toughness has to be expected. Only comparative fracture toughness tests with specimens and complete forged components can answer these questions. Because of the enormous costs of such programs little data on the fracture toughness and crack propagation properties of complete forged components are available [6 to 16], which are described in section 6.3. In contrast, a very large number of standard ASTM tests with specimens machined from forgings can be found in the literature [17 to 33].

For the rest of this chapter, an attempt will be made to condense what <u>is</u> available from IABG and other sources, in order to present some quantitative data and to summarize in a qualitative way what the designer of forged components should know and be aware of with regard to their fracture toughness properties.

6.2.2 Basic Formulae to be Applied

The "typical" crack in a forging is of the quarter- or half-elliptical shape, the K-solutions of which can be found in any of the well known handbooks [34 to 36]. In real life forgings, the actual crack shape may deviate more or less from these ideal shapes; however, this will be known only if service cracks are known or at least if laboratory tests with realistic load sequences have been carried out. In the example of Figure 6 a sufficiently exact solution can most probably be found using the procedures described in chapter 10 of this handbook.

In an extreme case, such as shown in Figure 7 it will indeed be difficult to calculate anything! The only consolation is that this forging had a far longer crack propagation life and a far larger critical crack length than three other nominally identical forgings, which showed "normal" crack shapes.

A method for determining a K-solution for a case which is not to be found in any handbook will be described shortly: If a stepped shaft with a shoulder fillet is loaded by a realistic torsional load sequence, a large number of small 45 degree-cracks will initiate in the fillets. At first these are independent of each other; see Figure 8. When the test is continued, they will eventually join up and form the continous jagged outline shown in Figure 9. For several reasons it is very difficult to formulate a stress intens ity factor solution for this case. For examole, when applying torsion in one direction the 45-degree surfaces of these multiple cracks will come into contact and friction will occur. What is more, when reverse torsion is applied, the cracks are opened.

The problem was solved [37] in the following way:
The compliance of the shaft will increase as the cracks grow. Therefore at different crack lengths the compliance was determined by measuring the decay of the torsional eigen-frequency of the cracked shaft, exciting it by a large massloaded lever. This method was chosen in preference tc the usual deflection measurement, because the latter proved to be not sensitive enough. Care had to be taken to excite only the cracked section of the shaft.

The energy necessary to produce new crack surfaces can be expressed on one hand by the change of the spring energy dE_F divided by the incremental growth of cracked area dA.

$$\frac{dE_F}{d_A} = 1/2 \cdot T^2 \frac{dC_p}{d_A} \qquad (1)$$

where C_p compliance
T torsional moment
$E_F = \frac{1}{2 C_p} \cdot T^2$ spring energy.

Another energy equation can also be deduced (according to Irwin) from the stress intensity K_I for plane strain conditions:

$$\frac{dE_p}{d_A} = \frac{K_I^2}{E} (1 - \nu^2) \qquad (2)$$

By equating (1) and (2)

$$K_I = T \sqrt{\frac{dC_p}{d_A}} \cdot \sqrt{\frac{E}{2 (1 - \nu^2)}}$$

After some further transformations:

$$K_I = \sqrt{\pi \frac{dC_p}{d_A}} \frac{D_o^3}{16} \sqrt{\frac{\pi G}{1 - \nu}}$$

where D_o shaft diameter
A crack area
G shear modulus
ν Poisson's ratio

6.2.3 Laboratory Tests and Specimens Utilized

Normally the standard ASTM specimen according to ASTM E-399 [38] is used to determine the fracture toughness K_{Ic} of forgings and in many cases also their crack propagation properties expressed as da/dN vs. ΔK. No more need be said about this well known specimen except that besides the "normal" ratio of thickness to width D/W = 0,5 other ratios are also allowed in the standard, namely B/W from 0,25 to 1,0.

This will allow us to take larger standard specimens out of some forgings. It should be a prerequisite to machine as large a specimen as possible out of the section in question. Some of the difficulties mentioned before with regard to the use of specimen data for components will then be minimized.

For testing the fracture toughness of thickwalled cylinders, for example forged gun barrels or high-pressure vessels, a C-shaped specimen has been standardized in the latest edition of the ASTM fracture toughness standard [38]. It is shown in Figure 10 and has been successfully used in a number of investigations [26, 28, 39 to 41]. One important advantage is that this specimen can simply be cut from the existing cylinder with no additional machining of inside and outside diameters.

6.3 Examples of Application of Fracture Mechanics to Forgings

6.3.1 Forgings Designed According to Fracture Mechanics Principles

No example of this type was found in the literature or furnished by the AGARD nations.

6.3.2 Forgings from Aircraft in Service or under Development

Here a number of examples is available:
First, for a modern tactical aircraft which was originally designed to the "safe-life" philosophy, a damage tolerance assessment was carried out by the manufacturers during the development phase. To this end, a number of critical components were selected throughout the structure, some of them being forgings. For an especially critical aluminum forging no less than five possible critical sections were analysed, four of them for two or more different flaw types (i. e. corner flaw and through crack). The materials data - K_{Ic} or K_c, as the case was, as well as da/dN vs. ΔK - were determined with specimens.
Some numerical examples: For 2014-T6 forgings, the fracture toughness was determined as $K_{Ic} = 778$ N/mm$^{3/2}$ in the T-L direction and as 683 N/mm$^{3/2}$ in the S-T direction. For Ti6Al4V forgings in the annealed condition, the corresponding values were:

$K_{Ic} = 1890$ N/mm$^{3/2}$ (S-T)
$= 1783$ N/mm$^{3/2}$ (L-T)
$= 1708$ N/mm$^{3/2}$ (T-L)

Besides ASTM standard specimens, for crack propagation tests rectangular specimens with a central crack were manufactured from sheet, plate, or forgings in the appropriate thickness.

These tests established the materials "constants" necessary for the subsequent damage tolerance assessments, namely K_{Ic} or K_c for critical crack length a_c and C and n in the Forman equation [42]

$$\frac{da}{dN} = \frac{C \cdot \Delta K^n}{(1 - R)\, K_c - \Delta K}$$

where a crack length
N number of cycles
C constant
n constant
R stress ration $= \frac{\sigma_{min}}{\sigma_{max}}$

which was used for calculating crack propagation under service loads, neglecting the retardation effect of the high loads in the spectrum. Next the stress intensity factor formulae for the various typical crack shapes expected in the different critical components were agreed upon between the firms building the aircraft, for example

"corner crack"
"elliptical internal flaw"
"through crack at a hole"
"through-crack at a pin loaded hole", etc.

The appropriate formulae for K were mostly taken from the literature [4 to 16]; some of them were derived or existing ones improved or adapted by the firms themselves.

The crack propagation life starting from an assumed initial crack length a_o was then calculated under the stress spectrum applicable to the component. The assumed initial crack lengths varied from 0,25 to 10 mm, in most of the bases being 2,5 mm.

The procedure was the same in principle for all components from thin sheet to heavy-section forgings. No special measures were employed to take into account, for example, the potentially higher scatter of K_{Ic}- or da/dN-values of forgings or other heavy-section components.

A second example is the application of fracture mechanics to the damage tolerance assessment of an older tactical aircraft [42] which has been in service for more than 15 years. A number of critical locations and the associated crack shapes are therefore known; compared to the first example this damage tolerance assessment thus had the benefit of hindsight in these two important aspects. Among the 39 critical locations selected, five were in forgings.

It is not intended to cover these damage tolerance assessment procedures in any detail; they have been well documented [42, 43] and are in principle similar to those in the example described before. Again specimen tests were used to establish the constants necessary for the subsequent crack propagation and critical crack length calculations for components, forgings being dealt with in the same way as sheet, extrusions or plate.

The third example concerns a lug from the Heavy Lift Helicoper (HLH) [47] rotor hub, which was manufactured from an alpha-beta 6Al-4V titanium forging in the solution treated and aged (STOA) condition. During fatigue tests of three rotor hub and crossbeam assemblies premature fatigue cracks occurred in the rotor hub lower lugs, cross beam bosses and bushings. The failure of the rotor lug was thought to be attributable to one of the following three possibilities:

- low fracture toughness K_C
- rapid fatigue crack propagation at all stress level of the spectrum applied
- fretting as crack initiator.

A fracture mechanics assessment was carried out showing that the fracture toughness met specifications and that indeed all the stresses in the spectrum led to crack propagation.

Again specimen data were used for arriving at both answers. The fracture toughness of the lugs at failure in the fatigue test was calculated, assuming a uniaxial stress existed normal to the fracture surface. Depending on which stress was assumed to be decisive, that at the chamber of the lug or the average gross stress, a K_C of 4.850 $N/mm^{3/2}$ or 3.020 $N/mm^{3/2}$ was calculated. These two values were then averaged to give a K_C of 3.920 $N/mm^{3/2}$. By comparison with specimen data determined in the HLH Titanium Materials Evaluation Program it was found that even on the basis of the lower above mentioned fracture toughness the material met specifications.

The da/dN vs. Δ K data were established in the same evaluation program with specimens taken from the center of the forging and tested at the stress ratio R = 0 .43, encountered at the lug during fatigue testing. Using these data, the crack propagation in the lug was calculated employing two different models, labelled "conservative" and "unconservative". The former accounted for the stress concentration magnification effect of the lug geometry, while the latter did not and "was the most optimistic representation of the crack which could possibly be made" [47]. Calculating back from the known conditions at failure, the crack growth rates associated with each stress level of the applied spectrum were determined.

Several more examples were furnished by working group members from other countries: The first concerns a forged main undercarriage leg of a military aircraft, which had developed cracks in service. Its residual static strength was calculated employing fracture mechanics. Two non-standard specimens were machined from the arms of the forging and a semielliptical surface notch was milled into the surface. The fracture toughness K_{Ic} of the material was established with these specimens, applying the well known ASTM thickness and crack depth criteria. One of the specimens gave a valid K_{Ic}-value, which was then used to calculate the residual static strengths at several locations where service cracks had shown up. In addition the crack growth rate applicable for the material was taken from the literature and the crack propagation per landing impact was computed. The result was not checked by a residual static strength test of the landing gear.

In another example [45] the failure cause and the reclamation possibilities of stress corrosion cracked vertical stabilizer beam forgings was analysed using fracture mechanics. Standard ASTM specimens were taken from the forgings. The direction of crack propagation in the specimens were selected on the basis of a microscopic examination of the grain flow in the outer surfaces of the forging near to the service crack region in order to use relevant fracture toughness data. Valid K_{Ic}-data of 630 - 650 $N/mm^{3/2}$ were developed from these specimen data. Using a somewhat conservative number of 600 $N/mm^{3/2}$ the critical stress at failure for corner cracks, through cracks and surface flaws was calculated depending on crack length. Again no check of this calculation was possible since no residual static strength tests on the complete forging were performed.

Another case [11, 12] concerns the residual static strength of a forged horizontal stabilizer rear attachment fitting, see Figure 11, which had failed in flight, resulting in a fatal accident. Here a slightly different procedure was followed: Five cracked and two uncracked fittings were statically loaded to failure in a test rig. All the cracked fittings failed through the fatigue cracks present.

However, the fracture toughness values for the material in question, 7075-T6, were taken from the literature to be 607 $N/mm^{3/2}$ and 1.101 $N/mm^{3/2}$ in the T-L and L-T direction respectively. Three slightly different formulae for the stress intensity factor K of the crack shape prevalent in the failed fittings were also taken from the literature to be

$$K = 0{,}799\,\sigma\cdot\sqrt{\pi a}$$

$$K = 0{,}705\,\sigma\cdot\sqrt{\pi a}$$

$$K = 0{,}815\,\sigma\cdot\sqrt{\pi a}$$

Thus the failure of the leg according to fracture mechanics could be assumed to be bounded by the conditions

$$1010 = 0{,}705\,\sigma\cdot\sqrt{\pi a} \quad \text{and} \quad 607 = 0{,}815\,\sigma\cdot\sqrt{\pi a}$$

These predictions are based on the assumption of a uniform stress on the surface, a condition not valid in the test. The problem of deciding which dimension should be used to represent the crack length was solved by selecting the value which gave the least scatter in the predicted failing load vs. the actual failing load. Thus the prediction in a way was fitted to the test results.

6.3.3 Tests on Forged Components to Determine their Fracture Properties and Comparison with Specimen Data

6.3.3.1 General Remarks

As mentioned before, one basic assumption has been used in all the above cases: Fracture toughness properties of components, such as crack propagation or critical crack lengths were calculated using materials constants derived from specimen tests. Test programs to verify this assumption can therefore be very useful. The author has carried out two such programs on aluminum forgings [9, 10, 13] (a third one on a titanium forging being underway). These will therefore covered in detail.

6.3.3.2 Nose Landing Gear Strut

By chance, some years ago the nose landing gear strut of a certain tactical aircraft type was replaced throughout the fleet because of suspected stress corrosion cracks; a large number of (originally) expensive forgings thus became available at no cost for test purposes.

The material was 7075-T6, which is no longer used in modern aircraft due to its well known disadvantages. However it was (and still is) felt by the author that the results of fatigue and fracture test would still be generally representative of typical aluminum aircraft forgings: The nose landing gear strut would nowadays probably be manufactured of 7075-T73; it is not at all likely that this small change in heat treatment would fundamentally alter the behaviour of the forgings in question in the cracked condition under static or repeated loading, especially the associated scatter. Another objection was the fact that the various nose landing gear struts had been in service for different, but unknown numbers of flying hours. However, during flying service different sections were highly stressed than in the tests carried out in the laboratory. The third, most serious, objection was that the forgings were manufactured about 20 years ago and the forging procedures thus did not represent modern tandards.

One purpose of this test program was to provide reliable data on the behaviour of typical aluminum forgings in the cracked condition under static and repeated loading. A second purpose was the use of fracture mechanics to predict this behaviour; in other words: Is fracture mechanics able to predict the residual static strength of and the fatigue crack propagation in these aluminum forgings?

To this end, a large number of nose landing gear struts was obatined, enabling us to determine the scatter of residual static strength. The forgings (see Figure 12) had been manufactured to identical drawings by four different forges in three different countries. Thus, we were also able to determine the influence of manufacturing on the above properties. The forgings were first notched by sawcuts in three locations, see Figure 13. Fatigue cracks were then grown in locations 1, 2 and 3 by applying constant load amplitudes at the points shown in Figure 13 until a predetermined crack length was reached. The nose landing gear strut was then broken by increasing the load until failure occurred, the COD being registered. Finally the fracture toughness of the forging was computed, using the formula of Irwin [46] which is based on [47]. The limited width of the component was accounted for according to [48], bending according to [49]. It was then determined if the thus calculated value K_Q could be considered a valid K_{Ic} using the following criteria:

- $K_{fmax} \leq 0{,}6\ K_Q$ [38]
- $\frac{K_{max}}{F_Q} \leq 1{,}1$ (5-per cent secant) [38] and
- $\frac{\text{crack depth}}{\text{component width}} \leq 0{,}5$

Near locations 1 and 2, CT-specimens according to ASTM-E 399 [38] were then cut from the forgings (see Figure 11) and the fracture toughness determined. Near location 2 C-shaped specimens (see Figure 14) were machined from the forging. This specimen type was originally developed by the Watervliet Arsenal of the US Army [40, 41]. For the dimensions shown in Figure 14 the calibration formulae given in [41] were not applicable; therefore the compliance of the specimen was measured and the formula for K calculated by fitting a 3rd degree polynominal. The applicable conditions of ASTM-E 399 [38] were observed with regard to crack front straightness, length of crack, generation of the fatigue crack, 5-per cent secant method etc.

Crack propagation tests were carried out for location 3 only; again the crack starter notch was machined; two different realistic load sequences were used:

- a flight by flight sequence simulating the stresses of the lower wing surface in the wing root area of a tactical aircraft, called "TCTP spectrum" [50]. The sequence has pronounced ground to air cycles; a sample is shown in the upper half of Figure 15. One repeat period consists of 803 flights with an average of 100 cycles per flight.

- a landing gear sequence, simulating the loads acting in the X-direction, such as spin-up and spring-back on landing, taxying, braking, engine run up etc. This was called "landing gear spectrum"; a sample is shown in the lower half of Figure 15. One repeat period consists of 200 flights with an average of 300 cycles per flight

The stresses were selected such that 1.000 to 4.000 flights to complete failure of the nose landing gear strut were obtained. Crack growth was observed visually on the surface only.

Using the USAF retardation model of Willenborg et al [51] crack propagation under the landing gear spectrum was then calculated. The constants necessary for this calculation (C and n in the Forman equation [42]) were determined by three constant amplitude crack propagation tests on CT-specimens. Three of them were machined from the edge of forgings failed in the crack propagation tests; three further CT-specimens were taken from the center, in both cases near the fatigue crack. The constants C and n were different for both locations, probably because of the different grain structure. The calculation according to the Willenborg model was carried out with the average $\bar{C}$- and $\bar{n}$-values of the CT-specimens taken from the center. The K_{Ic}-values required in the Forman equation were obtained from CT-specimens cut from the forging near the crack location.

The results are shown in detail in Tables 1 to 6; some are also given in Figures 16 to 21:
The mean fracture toughness of CT-specimens was $\bar{K}_{Ic} = 1020$ N/mm$^{-3/2}$ for the LT-direction, see Table 5, which agreed closely with literature data on this material [3, 15]. The scatter of K_{Ic}, see Figure 16, was about identical to that for CT-specimen taken from aluminum plate [24, 52].

The C-shaped specimens, see Table 6, again agreed quite well with literature data on a similar type of specimen taken from a forging [15]; scatter was rather high. As there was no measurable difference in fracture toughness between the two fatigue crack locations (in the flash line and beside the flash line, see Figures 22 and 23), all valid C-shaped specimens were statistically evaluated together in Figure 16.

The fracture toughness of the complete f o r g i n g s for location 1, using only the valid tests as described above, gave a higher mean value (1375 as compared to 1020 N/mm$^{-3/2}$) and a m u c h l a r g e r coefficient of variation ($v = 0{,}21$ compared to $v = 0{,}04$) than the CT-specimens, see Figure 17. This means that the mean ($P_s = 50$ per cent) residual static strength of the component would have been predicted conservatively using the fracture toughness of CT-specimens taken from the forging itself. However, this conservatism is only true for probabilities of survival $P_s \leq 90$ per cent, see Figure 16. At the much higher P_s values necessary for safe life parts the prediction would have been highly unconservative.

For location 2 no valid fracture toughness K_{Ic} was obtainable with the forgings, see Table 2.

Four valid tests were possible at location 3, see Table 3. Again the mean fracture toughness was higher ($\bar{K}_{Ic} = 1130$ vs. 717 N/mm$^{-3/2}$) and the scatter was also higher ($v = 0{,}16$ vs. $v = 0{,}10$) Figure 17); the estimate of the residual static strength of the forging would have been conservative up to $P_s \leq 99{,}95$ per cent.

All the data discussed in the preceding paragraphs are summarized in Figure 17.

The residual static strength on net area σ_{NR} of some of the forgings (including those which had not given valid K_{Ic}-values) were extremely high, see Tables 1 to 3, surpassing the tensile ultimate of about $F_{tu} = 550$ N/mm^2 in some cases, even for quite large cracks. No explanation can be given at the moment for these results. They were not due to gross plastic yielding, as proved by COD-measurements on all forgings tested in this way. +)

Anyway, the load at failure was very much different for similar sizes and shapes of the crack, see e.g. Table 2: Forgings 3R2-1 and 3R3-3 had very nearly the same size and shape of crack, yet their failing load was 23.000 N and 15.700 N respectively. Again in Table 1 forgings 1R2-19 and 1R7-38 had failing loads of about 28.000 and 18.000 N. This result obviously cannot be explained by any calculation method. Also any possible errors in the formulae for K used cannot account for these results.

There was no discernible difference between the residual static strength of forgings of manufacturers A, B and C. Manufacturer D (3 forgings only) lay on the lower limit of the scatter band, see Table 2.

The results of the crack propagation tests are summarized in Table 4 and Figures 18 and 19: It can be seen that the scatter again was extremely large. This is true for the number of flights to failure (crack initiation plus crack propagation period) as well as the crack initiation or the crack propagation period alone, see Figure 18.

+) For the calculation of the residual static strength at location 1 the formula for a curved beam in pure bending in [53] was used. The stress calculated in this way was then used for the determination of the residual static strength and of K_Q in Table 1. The gross stresses at location 1 and 3 were measured with strain gages and found to agree quite well with the calculated stresses.

A scatter $\overline{T} = N_{90}/N_{10}$ of 1 : 5,2 (landing gear spectrum) or 1 : 7,7 (TCTP-spectrum) for the crack propagation period is most unusual. The IABG has carried out many tests with similar or identical load sequences on axially loaded sheet and plate specimens of aluminum-, titanium- and steel alloys. In every case the scatter was much smaller than T = 1 :2,0.

As for the scatter of fatigue life, a similar comparison is possible: the forgings gave $\overline{T}$ = 1 : 6,0 for the TCTP-spectrum. Applying the identical sequence to an axially loaded bolted joint of aluminum alloy AZ 74 resulted in $\overline{T}$ = 1 : 3,5, while two types of notched specimens of 7075-T6 gave a still smaller scatter [50].

Moreover, there is no discernible correlation between the number of flights to failure and the crack initiation or crack propagation period. In other words, a forging having a long fatigue life to failure did not necessarily have a long crack propagation period and vice versa. For example, see Table 4, forging 1Ri2-54 had a fatigue life of 7.604 flights under the TCTP-spectrum while the crack propagation period was only 620 flights; on the other hand forging 1Ri3-49 had a fatigue life of 3.620 flights and the crack propagation period was nearly the same at 640 flights; finally forging 1Ri4-12 had a very similar fatigue life at 3.843 flights, but its crack propagation period was much longer at 2.940 flights.

For the landing gear spectrum only two tests were carried out with identical maximum loads (30 000 N), see Table 4: the other two forgings were tested with higher and lower maximum loads respectively. Assuming a slope of 1 : 6,0 of the σ-N-curve the life of these other two forgings under a maximum load of 28 000 N can be calculated (figures in parentheses in Table 4).

The corresponding crack propagation curves are shown in Figures 20 and 21. The upper end of these curves indicates failure of the forging. Figure 20 also contains the calculated crack propagation according to the Willenborg model [51], which was highly conservative in this case: it predicts a crack propagation life from a 1,5 mm crack to failure of 170 flights. The actual mean life of two forgings, however, was about 750 flights.

The IABG has also used the Willenborg model in another test program [54] on axially loaded sheet specimens. Under the identical load sequence it was almost exactly right for maraging steel and conservative by a factor of 1,5 for 2024-T3.

However, in several other load sequences the Willenborg model generally gave quite unconservative results. For a tactical aircraft lower wing surface load sequence it predicted, for example, a four times longer life than actually occurred in the test (material 7075-T7351) [54]. Similar findings were reported by Weissgerber et al in [55] and the author [51]. So the above results should not be generalized.

No influence of the manufacturer on crack propagation behaviour could be found. The three extreme examples discussed above (1Ri2-54, 1Ri3-49 and 1Ri4-42) all came from the same forge.

The fracture surface of some of the forgings looked quite usual, see Figure 7. This forging had a fatigue life of 4.400 flights, a crack propagation life of 3.510 flights and a crack initiation life of 890 flights under a maximum load in the spectrum of 28 000 N. The forging shown in Figure 24 (2Ri2-34) under a maximum load of 30 000 N gave 2.045, 860 and 1.185 flights respectively, see Table 4. That is, the percentages of the life spent for crack initiation and for crack propagation were grossly different, the forging shown in Figure 7 having a short crack initiation and a long crack propagation life. These two forgings came from manufacturers A and B. The other forgings also could be identified as to their origin by viewing their fracture surfaces: Manufacturer A's forgings always had shear type failures like 2Ri1-9, Figure 7, while B's forgings had the usual brittle failure like 2Ri-2-34, Figure 24. However, a shear type fracture surface was not a definite sign of a long crack propagation period as B's forgings gave the longest as well as the shortest of such periods, see Table 4, TCTP-spectrum.

The conclusions from this test program were as follows:

- The fracture toughness of complete forgings was higher in all three locations than that of specimens taken out of the forgings at these locations.
- The scatter of fracture toughness was much larger for the forgings than for the specimens. This scatter of the forgings could not be explained by the usual metallographic procedures.
- Nominally identical forgings with cracks of very similar dimensions can have grossly different ultimate failing loads. This cannot be explained by <u>any</u> calculation method.
- Crack propagation was considerably slower under a landing gear spectrum than predicted by the Willenborg retardation model. This may be due to the load sequence employed; for other sequences the Willenborg model gave unconservative results in some other test programs.
- The scatter of
  - fatigue life to failure as well as
  - the crack initiation and
  - the crack propagation period

  was extremely large for the forgings under two different but realistic load sequences.

- Forgings with a long fatigue life can have very short crack propagation periods and vice versa.

- The fracture surface and crack shapes in forgings may be highly irregular.

- The important forging properties determined in this test program - residual static strength, fatigue life and crack propagation life - may be subject to an extremely large scatter, much larger than for sheet or plate components. In order to attain equal probabilities of survival, larger safety coefficients would therefore have to be observed for forgings than for sheet or plate components. For a fatigue test on a structure consisting of forgings and of sheet and plate components, there obviously exists a dilemma: If the test is stopped at some multiple (say 4) of the required lifetime, the probability of survival is higher for the sheet and plate components than for the forgings.

- A long fatigue life of a forged component on test is no guarantee for a long crack propagation period. This again has obvious implications for the full scale fatigue test.

- Forgings are often used in internal structure and are therefore difficult to inspect. Every effort should be made to improve NDI techniques for such applications.

6.3.3.3 Forged Wing Attachment Fitting

After the somewhat disturbing results of the test program on forgings described in section 6.3.3.2 the author advocated the continuation of this work. In 1978 a large number of forged wing attachment fittings became available as scrap due to an error in the machining operations. The material was AZ74, a silver bearing alloy of the AlZnMgCuAg-type developed in Germany. Thus, all the objections voiced against the program described in section 6.3.3.2 were not valid here: The material was a modern high-strength aluminum alloy, the forgings were new and the forging procedure certainly was modern, the forgings having been produced after 1970. The seven fittings used for this program came from two different heats of material with different yield strength, viz. 456 against 512 N/mm^2.

After some further machining a shallow semielliptical flaw was introduced into the tension flange by electrical discharge machining, see Figure 25. The fitting was attached via the four fuselage frame attach bolts to the IABG strongback and loaded in bending as shown in Figure 25. Three forgings were loaded by the wellknown "Falstaff" load sequence /56/ and the crack propagation was monitored visually. In two additional forgings, also loaded by the Falstaff sequence the crack started at an erroneously machined notch of a much lower stress concentration factor. The crack propagation in these two forgings was not monitored. All five forgings were run to complete failure, the failing load being determined.

Then standard CT-specimens were cut from the broken forgings at different locations in the tension and compression flange and at different angles to the grain orientation. An example is shown in Figure 26. Further CT-specimens were machined from two additional forgings.

Six CT-specimens were used for crack propagation tests to determine the materials constants which would be required for a subsequent calculation of crack propagation in the forgings themselves under the Falstaff load sequence. In other words, the materials constants which would typically have been utilized for assessing the damage tolerance of the wing attach fitting - namely K_{Ic} and da/dN vs. ΔK - were determined.

The statistical evaluation of the fracture toughness of CT-specimens from two forgings is shown in Figure 27. The scatter (coefficient of variation) of K_{Ic} is on the high side for aluminum (see Chapter 9), though not unduly so; however, the extremely large difference between the fracture toughness with the crack parallel to the grain flow and that with the crack at right angles to the grain flow is notable. Besides, a large percentage of the CT-specimens did not give strictly valid K_{Ic}-values, mostly because of the direction which the crack took; some very peculiar ones occurred, see for example Figure 28.

The crack propagation under constant amplitude loading in CT-specimens is plotted in Figure 29, starting from a notch plus crack length of 8 mm. The specimen numbering system is as follows: The first digit designates the number of the forging; the letter o means "taken from the tension flange", u means "from the compression flange" and the last digit is the consecutive number.

Overall, the scatter of the crack propagation properties is large, even for the moment neglecting specimen 7o8 What is more, there is no discernible correlation between the position of the specimen in the fitting, or the direction of the crack and the crack propagation properties. The two specimens from forging 6 had a similar and quite fast, crack growth, although one came from the tension and the other from the compression flange. Even more disturbing is the fact that 7o7 and 7u9 are very similar, although one was cut from the flange and the other from the web at a different crack orientation, compare Figures 30 and 31; 7o8, which should be identical with 7o7 because both are situated symmetrical to the parting plane of the forging, see Figure 30, showed a completely different behaviour. If the damage tolerance of the forging to a transverse crack in the region of 7o7 and 7o8 were assessed using by chance the curve of specimen 7o8 a completely different answer would obviously result than if the curve of 7o7 had been employed.

The crack propagation curves of the complete fittings 4, 5 and 6 under the Falstaff load sequence are shown in Figure 32, including the fracture surfaces: Scatter again is large; with sheet and plate under the identical load sequence three tests usually fall within a narrow scatter band bounded by about 1 : 1,5. Also fitting 6 at first was very similar to 4 and 5, but at about 1.000 flights the crack rate suddenly accelerated.

The failure load of fittings 4, 5 and 6 was then calculated using the mean fracture toughness K_{Ic} = 1330 N/mm$^{3/2}$ shown in Figure 27. Fittings 4 and 5 had failed in test at the same load step of Falstaff, namely at 80 000 N, fitting 6 at 74 000 N. However, fitting 4 had a crack length of 53 mm, fitting 5 of only 32 mm, fitting 6 of 50 mm. Assuming a half elliptical crack no width correction factor and no rear wall correction factor

$$K = \sigma \sqrt{\frac{\pi \cdot 1}{Q}}$$

with Q = 2,35 for a/21 = 0,4 and σ/σ_y = 0,47

a failing load of 82 000 N was calculated - almost exactly right - for fitting 4; for fitting 5 the calculated load was 96 000 N, about 20 % more than actual; for fitting 6 77 500 N was calculated, slightly more than actual. In fitting 1 a crack originated beside the EDM flaw, the failing load being 80 000 N, however, the calculated failing load was no less than 114 000 N, almost 50 % higher.

The fracture surfaces and corresponding grain flow patterns for fittings 5 and 6 are compared in Figures 2 to 5.

The results of the crack propagation tests are shown in Table 7. Except for the large scatter already mentioned, no peculiarities occurred. Fitting 5 was best in life to failure as well as in crack initiation and crack propagation. Its critical scatter was especially large in the crack initiation period.

These fittings were also found to be critical in the course of the full scale fatigue test of the tactical aircraft in question [16]. They were therefore replaced by redesigned ones made of AZ74 with thicker sections. These were the fittings tested in the program described above; the critical location was a bolt hole. The crack propagation from this hole was monitored in 3 fittings of 7079-T6 and 4 fittings of AZ 74 by removing the bolt at frequent intervals and inspecting the hole by eddy-current. The results are shown in Figure 33. The load sequence applied was a complex flight-by-flight test. The large scatter in crack propagation found when testing the fittings alone as described above (and with an EDM notch, not a bolt-filled hole) was not quite so large in the full scale fatigue test. Even so, it was quite irregular and it would be interesting to calculate it on the basis of the materials data developed in the above program.

6.3.3.4 Hinge Rib Forging

The primary objective of the program [6] from which this example is taken was to establish the mechanical properties and economic advantages of precision forging. Only that part of the program which is relevant to fracture toughness of forgings will be mentioned here.

The hinge rib forging shown in Figure 34 is made from 7075-T7352; it was selected as a typical forged component. As a conventional die forging it is fully machined; it is located at the wing leading edge of the Boeing 747, supporting the variable-camber for flap. Two hand forgings, twelve conventional forgings and eleven precision forgings were made.

Of these eight conventional and seven precision forgings, as well as one hand forging, were fatigue tested to failure under a two step load program with marker loads interspersed. Crack length versus cycles curves were regenerated from the marker load locations by fractographic analysis near the crack origin where striations could be resolved. As the current MIL-A-83444 specifies a 1,27 mm deep semicircular surface flaw in the primary failure region of a fail-safe structure, the crack propagation life to failure from such a crack length was determined and found to be in all cases less than 21 % of the life from the start of the fatigue test to failure. For one forging this percentage was only about 8 %. The percentage of life from a 0,64 mm deep crack to failure was less than 30 per cent in all eight forgings, in two cases it was only about 15 per cent, see Table 8, which contains most of the data, brought together in a similar way as in Table 4 and 7. Again it is seen that good crack propagation properties do not necessarily coincide with a long fatigue life, see for example forging AC 15: It is best in both crack propagation periods (from 0,67 mm and from 1,27 mm to failure), but it is the third of four in fatigue life.

Furthermore forging AP 04 had the shortest critical crack length, but was best (of four) in crack propagation and in fatigue life; and forging AP 05 had the longest critical crack length (of thirteen) and the best crack propagation but the shortest fatigue life (of three). Both the shortest and the longest critical length occurred in precision forgings !

Additionally a 0,64 mm deep semicircular crack was electrically discharge machined into one precision and one conventional forging at the location where the cracks were thought to have started in the unflawed forgings. Under the identical load sequences as described above the flaw was grown to a crack length of 1,27 mm and then to failure. The two forgings with the EDM flaw, however, did not fail at 15 to 30 per cent of the life of the unflawed forgings, as was to be expected. Instead they failed at 50 to 73 per cent. This was due to a crack growth rate lower than in the other forgings with the natural cracks. Apparently the EDM flaws had been placed in a lower stress region than the fatigue crack origins of the other forgings, i.e. the natural cracks occurred about 10 mm away. This illustrates the importance of correct preflaw location.

Although the fracture toughness K_{Ic} of the forging material was determined by a sufficient number of ASTM standard tests, no attempt was made in this program to correlate these results with the residual static strength of the complete forgings.

6.3.3.5 Full Scale Fatigue Test on a Main Landing Gear

The F-104 G main landing gear was tested at the IABG /87 by a complex flight-by-flight load sequence. It originally was made of 7079-T6 and consisted of a largely unmachined forging; because of stress corrosion cracks the material was later changed to AZ74, the alloy mentioned in section 6.3.3.3 In all, three forged main gear legs of each alloy were tested. All of them failed between about 5.200 and 8.000 landings. Superficially this means low scatter. However, the landing gears failed at three completely different sections; one additional main gear leg of 7079-T6 failed at a fortuitous forging flaw at the king pin' support. This was repaired and the test continued to 12.000 landings without failure or cracking of the leg. Thus the actual result of three tests was that one had endured 12.000 landings without failure or cracking at any of the critical locations, while another had failed at only 5.200 landings, with crack having started at less than 4.000 landings.

This example again demonstrates that large scatter of the fatigue life to failure, the crack initiation and the crack propagation period may be an inherent characteristic of forgings.

6.3.4 Fracture Mechanics Tests on Standard Specimens cut from Forged Components

As mentioned in section 6.3.2 it is current practice in damage tolerance assessments of aircraft to determine the required materials constants by specimen tests. Indeed this is the only way possible because otherwise complete components would have to be tested at enormous costs and the whole idea of fracture mechanics would be jeopardized. However, the scatter to be expected in these materials constants should be taken into account; in the opinion of the author perhaps more so than has been done up to the present. It was therefore thought worthwhile to devote one section of this chapter to fracture tests on specimens with due regard to the associated scatter. The reader is also referred to Chapter 8 of this book for a general discussion on how to treat scatter and for some more examples.

The literature abounds with data on fracture toughness of standard specimens machined from forgings, only a few which are mentioned in the references /3, 4, 15, 17, 18, 20 to 37/.

Recently a cooperative fracture toughness program on C-shaped specimens /28/ took place with 8 laboratories participating. All 48 specimens were machined from one cylindrical forging; the results are statistically evaluated in Figure 35: The scatter of the K_{Ic}-values is remarkably low, especially when considering that 8 different laboratories carried out the tests.

The IABG conducted such a program on a similar steel (of a slightly lower yield strength) several years ago /26/ also utilizing C-shaped specimens; however, they were machined from 5 cylindrical forgings with slightly different heat treatments; the results are shown in Figure 36. Again the scatter is quite low. However, the slight variations in heat treatment (mainly the temperating temperature was varied between 520° and 565° C) resulted in quite large differences in fracture toughness, although the yield strengths differed only between 1210 and 1280 N/mm^2.

The forgings for these two programs were very simple, probably resulting in a well defined uniform grain flow pattern, symmetrical all around the circumference of the cylinders. Also, the fact that

- they were gun barrel forgings which for obvious reasons are worked very thoroughly during manufacture and
- the steels were vacuum degassed

may have helped in obtaining the low scatter and for their yield strength the quite high fracture toughness.

A typical aircraft steel forging of complex shape was tested in Australia /30/. It is a component in the F-111 structure and consists of D 6ac steel which is known for its high variability of fracture toughness. Together with the inherent variability of the fracture toughness of forgings, this gave the result shown in Figure 38: Within one

forging the fracture toughness varied almost by a factor of two! Taking only specimens in one direction does not decrease this variability. Rather it is seen that there is a distinct grouping of fracture toughness, the thick-section lug area having a low fracture toughness, the thin-section web and speed brake area a high fracture toughness. If such a component were designed according to fracture mechanics criteria, two entirely different K_{Ic}-values would have to be used, a low one for the thick sections, a high one for the thin sections. Compared to these large differences in fracture toughness, the orientation of the specimens notch did not have any measurable influence on fracture toughness.

In Figure 38 five more of these forgings were evaluated, all specimens being machined from the thin section web and speed brake areas: The scatter of fracture toughness within any individual forging was very low; however, the mean fracture toughness of the thin-section areas, also taking the forging shown in Figure 37 into account, varied between about 2100 $N/mm^{3/2}$ and about 2800 $N/mm^{3/2}$.

For titanium forgings, a large body of fracture toughness data is available from Alcoa [29, 23] containing no less than 1229 valid ASTM specimen results from so-called lot prolongation tests of three different Ti6Al4V forgings of similar size and complexity. As shown in Figure 39, which was taken over from [32], the mean fracture toughness and the associated coefficient of variation varied widely, depending on intentional processing variables. Scatter is again quite high, even if it is considered that the tests cover a large number of lots with probably only one or two K_{Ic}-tests per lot. Even so, according to curve 1 five per cent of 561 tests had a fracture toughness below about 1500 $N/mm^{3/2}$, while the mean was $K_{Ic} \approx 2050$ $N/mm^{3/2}$.

References [29] und [32] contain a good deal more data on the fracture toughness of large structural forgings of Ti6Al4V and Ti6Al6V 2Sn and the effect of processing / composition options. Figure 40, taken directly from [29], is a summary of this work, illustrating that low oxygen content (0,13 % max.) and a recrystallisation annealing is beneficial primarily at low yield strengths, compared to standard oxygen content (0,20 % max.) and mill annealing; it is also beneficial in reducing the scatter of fracture toughness, as was to be seen in Figure 39. A more detailed explanation of the effect of these composition / forging process / heat treatment "options" on fracture toughness is given in Table 9 [32], showing that a wide range of typical guaranteed minimum properties including fracture toughness is available in Titanium forgings, even some with the derivable combination of high static properties and high fracture toughness, albeit at a cost premium.

The IABG has recently carried out some fracture toughness tests on six C-T-specimens machined from a large Titanium hand forging, a section through which is shown in Figure 1. The preliminary results are evaluated in Figure 41, scatter is quite low. Another Titanium forging investigated at the IABG was the compressor disc shown in Figure 42; the associated statistical evaluation of the C-R specimens is given in Figure 43. It is seen that

- on the average fracture toughness is higher in the hub area than in the rim area and
- there is no discernible difference between R-C and C-R orientation of the specimens.

Scatter again is quite low, even if all the C-R-specimens (from the hub and the rim area) are evaluated together as in Figure 43. By the way the manufacturer of the jet engine in question requires a minimum fracture toughness for this compressor disc of 1650 $N/mm^{3/2}$ in the C-R orientation, the control specimen being taken from the rim area. One specimen did not meet this requirement, see Figure 42.

The crack propagation properties of the discwere also determined utilising three discs, they were practically identical with those of a large Ti6Al4V-plate, see Figure 44, both curves being the mean of several tests. The scatter obtained from six specimens machined from three discs is shown in Figure 45; it is quite low, all specimens falling in a scatter band of less than 1 : 2.

As for aluminum forgings, another large test program is available from Alcoa [20], a comparison between the modern forging alloys 7175, 7050 and 7049. Many different structural die forgings were produced from these alloys. They were mainly of two types, heavy section landing gear type forgings and web-flange type forgings, having highly directional grain flow. In addition several different hand forgings were produced. The results of this investigation are summarized in Figure 46, taken directly from [20]. However, this presents too simplistic a picture: On closer inspection of the results several peculiarities become apparent. For example, a 75 mm hand forging has the highest fracture toughness in the LT-direction of fourteen forgings of 7050, namely 1562 $N/mm^{3/2}$. In the SL-direction it is, however tenth at 736 $N/mm^{3/2}$. This large difference is apparently <u>not</u> typical for handforgings, because two other 75 mm handforgings of the same material the same shape and the same heat treatment were ninth and tenth in the LT-direction at 1093 $N/mm^{3/2}$ and 1041 $N/mm^{3/2}$ as well as ninth and eleventh in the SL-direction at 760 and 729 $N/mm^{3/2}$. The heavy section 7050 forgings also tended to have relatively high fracture toughness in the SL-direction while in the LT-direction the web-flange type forgings were generally superior. In 7049, two web-flange forgings of a certain shape gave both the highest and the lowest fracture toughness in the LT-direction of twenty forgings produced in eight different dies. The best and worst forging had very similar yield strengths. In the SL-direction the rating was practically identical; however, the yield strengths of the best and worst forgings were grossly different!

In 7175 the rating was very similar in both specimen orientations. However, while in the SL-direction the forging with the highest K_{Ic} had the lowest yield strength and vice versa in the LT-direction, the picture is not so clear: The forging with highest fracture toughness had the second highest yield strength.

A general conclusion whether a web-flange type forging or a thick-section type forging resulted in higher fracture toughness was not possible from this program.

In Figures 47 and 48 the fracture toughnesses of all forgings of one material in this investigation /20/ are evaluated statistically. The extremely large coefficients of variation are remarkable. Except for 7050, they are not reduced when only die forgings are included and hand forgings are left out. This goes for both specimen orientations. All this goes to show that it may be quite misleading to speak of "the fracture toughness of 7XXX forgings"; rather the fracture toughness of any individual forging may depend much more on as yet unknown variables than on the forging type, the material and the heat treatment. In addition, the problems of the applicability of specimen data to complete forgings, as discussed in section 6.3.3, arise.

A large amount of additional specimen data on the fracture toughness of aluminum, titanium and steel forgings can be found in /3/. As no further details about the forgings are given from which the specimens were machined, these data must be considered with caution, in view of the above reservations.

The MIL-Handbook 5 c /4/ contains a table of "typical" fracture toughness data for Aluminum alloys, showing minimum, average and maximum K_{Ic}-values for two to five forging lots per material. The variability of the forgings fracture toughness, that is the quotient maximum/minimum fracture toughness, is on the average larger than that of plate or extrusions.

6.4 Conclusions

The following conclusions are based on the test programs described in section 6.3.3. and 6.3.4

- The application of fracture mechanics to structural forgings of Aluminum, Titanium and steel alloys is difficult - to put it mildly. This does not reflect so much on fracture mechanics theory - and therefore cannot be improved by better theory - but results from the peculiar characteristics of forgings.
- The one outstanding feature of the fracture behaviour is the large variability of the relevant properties - fracture toughness and crack propagation - in specimen tests or (much more so) in tests on complete typical structural forgings. Even if normal scatter is obtained in specimen tests, the complete forged component may show very large variability.
- Only if the shape of the forging is simple with a well defined symmetrical grain flow pattern - as in gun barrel or in compressor disc forgings - a normal variability of fracture toughness is obtainable.
- If the forging procedure results in thorough working of the material and if the forging process controls are extensive - as in gun barrels and especially in compressor and turbine discs - in addition very high fracture toughness for the respective yield strength are obtainable.
- The difference in fracture toughness (within one forging) between different actual or nominal crack orientations can be large.
- There may also be large difference in fracture toughness within one forging between thin and thick sections.
- Nominally identical forgings can have a very similar fracture toughness in one crack orientation and a very dissimilar one in another crack orientation.
- Nominally identical forgings with cracks of very similar dimensions can have grossly different failing loads.
- A long fatigue life in a test on a complete forged component does not necessarily mean a long crack propagation period. Thus a crack may initiate very late in the life and then propagate very quickly.
- Forgings with short critical crack lengths can have favourable crack propagation properties as well as long crack initiation periods.
- The fracture toughness of complete forgings can be higher or lower than the fracture toughness of specimens machined from the forgings at the failure location. Thus, the calculation of the residual static strength or the crack propagation properties of a complete forging based on specimen tests may be far on the conservative or on the unconservative side.

In view of the above conclusions, it is not recommended to depend on specimen data only if critical forgings are designed according to fracture mechanics criteria. Rather, full scale tests with such forgings are advocated and, in addition, a comparison between their results and fracture mechanics calculations based on tests with

- specimens machined from the forging as well as
- "typical" K_{Ic}- and da/dN-values taken from the literature.

If full scale tests are not possible and the dimension of the forgings must be based on specimen tests only, at least the larger variability of the fracture properties of forgings must be accounted for in the calcualtions.

Acknowledgements:

The author is grateful to the members of the working group, especially Messrs Dunsby and de Jonge, for supplying useful examples.

6.5 References

[1] N.N.: Military Specification: Airplane Damage Tolerance Requirements. MIL-A-83444 (USAF) 2 July 1974, USAF

[2] N.N.: Military Standard: Aircraft Structural Integrity Program - Airplane Requirements. MIL-STD-1530 A, 11 December 1975, USAF

[3] N.N.: Damage Tolerant Design Handbook, Parts 1 and 2, MCIC-HB-01, September 1973

[4] N.N.: Military Standardization Handbook. Metallic Materials and Elements for Aerospace Vehicle in Structures. MIL-HDBK 5 C, 15 September 1976

[5] N.N.: Materials and Processes Requirements for Air Force Systems. MIL-STD 1587 (USAF), July 1976

[6] Hyatt, M.V., H.D. Pasley, I. Goodlet and C.P. Yohn: High Integrity Forgings of Aluminum and Titanium Alloys. AFML-TR-77-81, 1977

[7] Larsson, S.E.: Fatigue Experience from Tests Carried out with Forged Beam and Frame Structures in the Development of the Saab Aircraft Viggen, in Advanced Approaches to Fatigue Evaluation, NASA SP 309, 1971

[8] Gierke, H., R. Schütz and K. Ahrensdorf: Hauptfahrwerksermüdungsversuch F 104 G. IABG-Report B-TF-418/2, 7 October 1975

[9] Schütz, W.: Crack Propagation and Residual Static Strength of Typical Aircraft Forgings, in: Fracture Mechanics Design Methodology. AGARD-CP-221, 1977

[10] Heidenreich, R. and W. Schütz: Restfestigkeits- und Rißfortschrittsversuche an Schmiedeteilen aus 7075-T6. IABG-Report TF-437, 1974

[11] Wiebe, W. and R.V. Dainty: Fractographic Analysis of Tutor Horizontal Stabilizer Attachment Fittings. National Aeronautical Establishment LTR-Report-ST-1023, Ottawa, August 1978

[12] de Waal, J.F., J.A. Dunsby, B. Shaver and A.C. Walker: Static Strength of the Horizontal Stabilizer Rear Attach Fitting of the Tutor Aircraft with and without Fatigue Cracks. NAE LTR-ST-1005, Ottawa, July 1978

[13] Oberparleiter, W. and W. Schütz: Bauteilspezifische Werkstoffuntersuchungen. Untersuchungen an Gesenkschmiedestücken der silberhaltigen Aluminiumlegierung 3.4354.7 (Fuchs AZ74.61). IABG-Report B-TF-861, 1979

[14] Woithe, K., R. Schütz and K. Ahrensdorf: Gesamtzellen-Ermüdungsversuch F-104 G. Schaden an den Flügel-Rumpf-Anschlußfittingen. IABG-Report TFS 81/21.8, 1 July 1972

[15] Moore, R.L., G.E. Nordmark and J.G. Kaufmann: Fatigue and Fracture Characteristics of Aluminum Alloy Cylinders under Internal Pressure. April 1, 1970, Alcoa Research Laboratories, New Kensington, Pennsylvania

[16] Gierke, H., R. Schütz and K. Ahrensdorf: Gesamtzellen-Ermüdungsversuch F-104 G. Fitting-Schäden am Retrofit-Flügel. IABG-Report TFS 81/21.9, January 1974

[17] Zenner, H. and W. Schütz: Bauteilspezifische Werkstoffuntersuchungen. Untersuchungen an Triebwerksscheiben aus Ti6Al4V. IABG-Report TF-676.3, 1977

[18] Schimmelbusch, H.W.: Metallurgical Evaluation of 7175-T736 and 7175-T66 Die Forgings. The Boeing Company, Report D6-24480

[19] Wanhill, R.J.H., J. Schijve, F.A. Jacobs and L. Schra: Environmental Fatigue under Gust Spectrum Loading for Sheet and Forging Aircraft Materials. NLR MP 75037 U, October 1975

[20] Staley, J.T.: Comparison of Aluminum Alloy 7075, 7049, MA52 and 7175-T736 Die Forgings. Technical Report AFML-TR-73-34, May 1973

[21] Wagner, W.: Werkstoffuntersuchungen an verschiedenen Ti- und Al-Legierungen. MBB-Bericht UFE-710-71

[22] Oberparleiter, W. and W. Schütz: Rißfortschrittsverhalten von 7075-T7351, MP 9-4-30, 300 M und Ti6Al4V unter Einzelflug- und Einstufenbelastung. IABG-Report TF-549, 1975

[23] N.N.: Statistische Auswertung der 1975 und 1976 an ungeknickten Trägerplatten ermittelten Bruchzähigkeitswerte. Krupp Metall- und Schmiedewerke, Essen, 1977

[24] Oberparleiter, W., H. Kratzer and W. Schütz: Zusammenstellung bruchmechanischer Kennwerte. IABG-Report TF-645, 1977

[25] Oberparleiter, W. and W. Schütz: Rißfortschritts- und Restfestigkeitsversuche an 6 mm dicken Titanplatten. IABG-Report TF-360, 1973

[26] Oberparleiter, W. and W. Schütz: Bruchzähigkeits- und Rißfortschrittsverhalten des Geschützrohrstahles 35 NiCrMoV 14 6. IABG-Report TF-436, 1974

[27] N.N.: Technical Information 7175-T736 and 7175-T66 Premium Strength Forgings. Aluminum Company of America, February 1970

[28] Underwood, J.H. and D.P. Kendall: Cooperative Plane Strain Fracture Toughness Tests with C-shaped Specimens. Journal of Testing and Evaluation, September 1978, pp. 296 - 300

[29] Kuhlmann, G.W. and F.R. Billmann: Processing Options for High Fracture Toughness Airframe Forgings. Society of Manufacturing Engineers SME Paper MR 77-250, 1977

[30] Ellis, R. and B.E. Anderson: The Fracture Toughness of Large Structural Fatigue Specimens of D6Ac Steel. Aeronautical Research Laboratories ARL, Structures and Materials Note 410, August 1974

[31] Zenner, H. and W. Schütz: Bauteilspezifische Werkstoffuntersuchungen. Untersuchungen an Triebwerksschreiben aus Inconel 718, IABG-Report TF 766.3, 1977

[32] Kuhlmann, G.W. and F. Billmann: Selecting Processing Options for High-Fracture Toughness Titanium Airframe Forgings. Metal Progress, March 1977, pp. 39 - 49

[33] Oberparleiter, W., W. Scharfenberger and W. Schütz: Bauteilspezifische Werkstoffuntersuchungen. Untersuchungen an TiAl6V4 Freiformschmiedestücken. IABG-Report B-TF-862, 1978

[34] Rooke, D.P. and D.J. Cartwright: Compendium of Stress Intensity Factors. Her Majesty's Stationery Office, 1976

[35] Tada, H., P. Paris and G. R. Irwin: The Stress Analysis of Cracks Handbook. DEL Research Corporation, 1973

[36] Sih,G.C.: Handbook of Stress Intensity Factors. Lehigh University 1973

[37] Griese, F.W., G. Schöne, W. Schütz und M. Hück: Rißfortschritt torsionsbeanspruchter Walzwerkswellen bei Betriebsbeanspruchungen. IABG-Report TF-727, IPH-Bericht 87/78, February 1978

[38] N.N.: Standard Test Method for Plane Strain Fracture Toughness of Metallic Materials. ASTM-399-78 Annual Book of ASTM Standards, Part 10, 1978

[39] Underwood, J.H. and D.P. Kendall: Fracture Toughness Testing Using the C-shaped Specimens, in: ASTM STP 632, 1977

[40] Underwood, J.H., R.D. Scanlon and D.P. Kendall: K Calibration for "C" Shaped Fracture Toughness Specimens of Various Geometries. Watervliet Arsenal, N.Y. 12189, Technical Report, April 1973

[41] Kendall, D.P., J.H. Underwood and D.C. Winters: Fracture Toughness and Crack Growth Measurements with "C" Shaped Specimens", Watervliet, FY 72, 1973

[42] Mc Carthy, J.F., C.F. Tiffany and O. Orringer: The Application of Fracture Mechanics to Decisions on Structural Modifications of Existing Aircraft Fleets, in: Case Studies in Fracture Mechanics, AMMRC MS 77-5, June 1977

[43] Tiffany, C.F.: Durability and Damage Tolerance Assessments of United States Air Force Aircraft in: Fatigue Life of Structures under Operational Loads, Proceedings of the 9th ICAF Symposium, Darmstadt 1977, LBF-Report TR-136

[44] Zola, J.C.: Analysis of Heavy Lift Helicopter Rotor Hub Lower Lug, in: Case Studies in Fracture Mechanics, AMMRC MS 77-5, 1977

[45] Vlieger, H. and E.A.B. de Graaf: Analysis of the Failure Cause and the Reclamation Possibilities of Cracked Starfighter Vertical Stabiliser Beams. NLR-M 72-89, Dec. 1972

[46] Irwin, G.R.: Crack Extension Force for a Part-Through Crack in a Plate. Journal of Applied Mechanics, Vol. 84 E, No. 4, Dec. 1972

[47] Green, A. and J.N. Sneddon: The Distribution of Stress in the Neighbourhood of a Flat Elliptical Crack in an Elastic Solid, Proc. Cambridge Phil. Soc. 46 (1950), pp. 159 - 164

[48] Grandt, A.F. jr. and G.M. Sinclair: Stress Intensity Factors for Surface Cracks in Bending. ASTM STP 513, American Society for Testing and Materials, 1971, pp. 37 - 57

[49] Brown, W.F. jr. and J.E. Srawley: Plane Strain Crack Toughness Testing of High Strength Metallic Materials. ASTM STP 410, 1976

[50] Schütz, W.: The Fatigue Life under Three Different Load Spectra - Tests and Calculations, in: Symposium on Random Load Fatigue, AGARD-CP-118, 1972

[31] Willenborg, J., R.M. Engle and H.A. Wood: A Crack Growth Retardation Model Using an Effective Stress Concept. AF Flight Dynamics Laboratory, TM-71-1-Fbr., 1971

[32] Schütz, W.: Versuchsmethoden der Bruchmechanik. Der Maschinenschaden, Heft 5, 1975

[33] Luftfahrttechnisches Handbuch Strucktur Berechnung. Blatt 31330, Ausgabe B, 1974

[34] Schütz, W. and W. Oberparleiter: Berechnung des Rißfortschrittes an Bauteilen bei veränderlichen Spannungsamplituden. IABG-Report B-TF-508, August 1976

[35] Weissgerber, D., P. Keerl and K. Sippel: Theoretische und experimentelle Rißfortschrittsuntersuchungen für Metallstrukturen; Rißfortschritt in Kampfflugzeugbauteilen unter betrieblichen Bedingungen. MBB-Bericht UFE 1236, 1975

[36] Aicher, W., J. Branger, G.M. van Dijk, J. Ertelt, M. Hück, J.B. de Jonge, H. Lowack, H. Rhomberg, D. Schütz and W. Schütz: Description of a Fighter Aircraft Loading Standard for Fatigue Evaluation "Falstaff". (Common Report of F+W Emmen, LBF, NLR, IABG, March 1976).

[37] Schütz, W.: Calculation Methods for Fatigue Life and Crack Propagation, in AGARD-AG 231, 1978

Table 1: Fracture Toughness and Residual Static Strenght of Forgings - Location 1

Forging No	Manu-facturer	Crack Area A_A [mm²]	Failing Load F_{max} [N]	F_Q [N]	Residual Static Strenght on gross area σ_{BR} [N/mm²]	net σ_{NR} [N/mm²]	Stress Intensity K_Q [N/mm^-3/2]	Fracture Toughness K_{Ic} [N/mm^-3/2]
1 R 1-21	A	76	70 600	70 600	697	765	2 995	-
1 R 2-19	B	1 034	28 350	24 250	240	642	2 430	-
1 R 3-25	B	310	25 000	25 000	247	343	1 130	1 130
1 R 4-29	B	208	65 700	53 700	531	667	2 420	-
1 R 5-30	B	200	69 150	56 900	562	696	2 480	-
1 R 6-31	C	497	29 300	28 700	283	463	1 380	1 380
1 R 7-38	A	1 184	18 400	17 750	176	679	2 545	-
1 R 8-41	B	310	34 800	34 800	343	488	1 620	1 620
1 R 9-43	B	410	-	-	-	-	-	-
1 R 10-46	B	830	38 150	33 850	334	578	2 500	-

- in the last column means that a valid fracture toughness K_{Ic} could not be obtained

Table 2: Fracture Toughness and Residual Static Strength of Forgings - Location 2

Forging No	Manu-facturer	Crack Area A_A [mm²]	Failing Load F_{max} [N]	F_Q [N]	Residual Static Strenght on gross area σ_{BR} [N/mm²]	net σ_{NR} [N/mm²]	Stress Intensity K_Q [N/mm^-3/2]	Fracture Toughness K_{Ic} [N/mm^-3/2]
3 R 1-26	A	341	51 975	48 540	387	669	1 750	-
3 R 2- 1	A	943	23 045	23 045	186	569	1 670	-
3 R 3- 3	D	964	15 690	15 300	117	389	1 055	-
3 R 4- 5	A	787	25 010	24 520	192	535	1 480	-
3 R 5-33	B	404	39 960	38 100	302	488	1 515	-
3 R 6-40	D	206	37 510	37 510	289	353	995	-
3 R 7-36	D	398	10 590	10 000	76	422	1 085	-

Table 3: Fracture Toughness and Residual Static Strenght of Forgings - Location 3

Forging No	Manu-facturer	Crack Area A_A [mm^2]	Failing Load F_{max} [N]	F_Q [N]	Residual Static Strenght on gross area σ_{BR} [N/mm^2]	net σ_{NR} [N/mm^2]	Stress Intensity K_Q [Nmm$^{-3/2}$]	Fracture Toughness K_{Ic} [Nmm$^{-3/2}$]
4 R 1-25	B	195	3 450	3 450	277	368	1 060	1 060
4 R 2-19	B	216	4 750	4 750	380	504	1 455	-
4 R 3-21	A	168	5 950	5 950	476	603	1 890	-
4 R 4-43	B	346	3 500	3 250	259	452	1 325	1 325
4 R 5-29	B	299	3 900	3 900	312	494	1 475	-
4 R 6-31	C	510	2 050	2 050	164	368	995	995
4 R 7-41	B	452	2 500	2 500	197	412	1 165	1 165
4 R 8-39	C	15	4 850	4 850	388	373	625	-
4 R 9-46	B	665	2 450	2 350	196	574	1 465	-

Table 4: Results of Crack Propagation Tests on Nose Landing Gear Strut

Forging No	Manu-fact.	Max. Load of the Spectrum [N]	Max. Stress in the Spectrum [N/mm²]	Number of Flights to Failure	Number of Flights from a Crack Length of 1,5 mm to Failure	Number of Flights to a Crack Length of 1,5 mm
TCTP - Spectrum						
1 Ri 1-22	A	22 000	211	3 137	1 980	1 157
(calculated)		(24 000)	(234)	(1 800)	(1 130)	(670)
1 Ri 2-54	B	24 000	234	7 604	620	6 984
1 Ri 3-49	B	24 000	234	3 620	640	2 980
1 Ri 4-42	B	24 000	234	3 843	2 940	903
Scatter $\bar{T} = \frac{N_{90}}{N_{10}}$				1: 6,0	1: 7,7	1: 22,0
Landing Gear Spectrum						
2 Ri 1- 9	A	28 000	274	4 400	3 510	890
(calculated)		(30 000)	(293)	(2 950)	(2 330)	(620)
2 Ri 2-34	B	30 000	293	2 045	860	1 185
2 Ri 4-10	A	30 000	293	1 063	620	443
2 Ri 5-28	B	33 000	322	1 910	870	1 040
(calculated)		(30 000)	(293)	(3 400)	(1 850)	(1 550)
Scatter $\bar{T} = \frac{N_{90}}{N_{10}}$				1: 3,5	1: 5,2	1: 6,2

Table 5: Fracture Toughness Determined with CT-Specimens

Specimen No	Direction	Stress Intensity K_Q and Fracture Toughness K_{Ic} [Nmm$^{-3/2}$]	Manufacturer
1 B 1-38	L - T	992 K_{Ic}	A
1 B 2-38	L - T	1 059 K_{Ic}	A
1 B 3-19	L - T	1 284	B
1 B 4-29	L - T	1 360	B
1 B 5-25	L - T	1 002 K_{Ic}	B
1 B 6-30	L - T	1 315	B
1 B 7-41	L - T	1 023 K_{Ic}	B
K_{Ic} - arithmetic mean value	L - T	1 020 K_{Ic}	
1 B 8-35	T - L	773	B
1 B 9-21	T - L	1 013 K_{Ic}	A
1 B 10-46	T - L	836	B

A K_{Ic} in the third column means that a valid K_{Ic}-value according to [38] was obtained.

Table 6: Fracture Toughness, Determined with C-shaped Specimens

Specimen No	Stress Intensity K_Q and Fracture Toughness K_{Ic} [Nmm$^{-3/2}$]	Manufacturer
4 B 1-44 S	632 K_{Ic}	C
4 B 3-35 S	693 K_{Ic}	B
4 B 5- 7 S	804 K_{Ic}	A
4 B 7-47 S	657	C
4 B 9-48 S	930	B
4 B 2-44 N	635	C
4 B 4-35 N	745 K_{Ic}	B
4 B 6- 7 N	710 K_{Ic}	A
4 B 8-47 N	403	C
4 B 10-48 N	880	B
K_{Ic} - arithmetic mean value	717	

S = Fatigue crack in the flash line
N = Fatigue crack beside the flash line

A K_{Ic} in the second column means that a valid K_{Ic}-value according to [38] was obtained.

Table 7: Results of Crack Propagation Tests on Wing Attachment Fittings

Forging No	Max. Load of the Spectrum [N]	Critical Crack Length $2\,l_{cr}$ [mm]	Number of Flights to Failure	Number of Flights from a Crack Length of 13 mm to Failure	Number of Flights to a Crack Length of 13 mm
	- Spectrum -				
4	80 955	53.0 (1)	5 170 (2)	2 670 (2)	2 500 (2)
5	80 995	37.0 (3)	6 450 (1)	2 950 (1)	3 500 (1)
6	80 995	50.0 (2)	2 495 (3)	1 595 (3)	900 (3)
	Scatter $\bar{T} = \frac{N_{90}}{N_{10}}$		1: 3.6	1: 2.4	1: 6.1

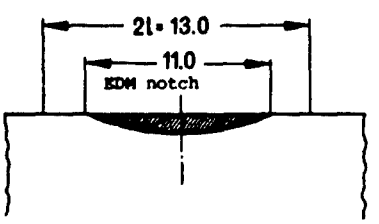

Table 8: Results of Fatigue Tests on Hinge Rib Forging [6]

Forging No	Peak Stress in Spectrum N/mm^2	Number of Cycles to Failure	Number of Cycles to 0,64 mm Crack	Number of Cycles to 1,27 mm Crack	Number of Cycles from 0,64 mm to Failure	Number of Cycles from 1,27 mm to Failure	Critical Crack Length (mm)
AC 14	280	81 000 (2)	68 000 (2)	75 000 (2)	13 000 (3)	6 000 (3)	6,2 (3)
AC 15	280	52 000 (3)	38 000 (3)	41 000 (3)	14 000 (1)	11 000 (1)	10,1 (1)
AC 16	280	90 000 (1)	76 000 (1)	81 000 (1)	14 000 (1)	9 000 (2)	7,5 (2)
AC 17	280	48 000 (4)	35 000 (4)	39 000 (4)	13 000 (2)	9 000 (2)	6,2 (3)
AC 18	238	85 000 (1)	61 000 (1)	69 000 (1)	24 000 (1)	16 000 (1)	6,3 (2)
AC 19	238	71 000 (2)	52 000 (2)	60 000 (2)	19 000 (2)	11 000 (2)	10,0 (1)
AP 01	280	65 000 (3)	51 000 (3)	56 000 (3)	14 000 (1)	9 000 (3)	15,9 (1)
AP 02	280	55 000 (4)	40 000 (4)	46 000 (4)	9 000 (3)	9 000 (3)	12,5 (2)
AP 04	280	76 000 (1)	55 000 (2)	62 000 (1)	14 000 (1)	14 000 (1)	3,8 (4)
AP 09	280	71 000 (2)	57 000 (1)	61 000 (2)	10 000 (2)	10 000 (2)	8,2 (3)
AP 05	238	99 000 (3)	70 000 (3)	84 000 (3)	29 000 (1)	18 000 (1)	15,0 (1)
AP 08	238	115 000 (1)	93 000 (1)	101 000 (1)	22 000 (2)	14 000 (2)	14,2 (2)
AP 10	238	101 000 (2)	83 000 (2)	90 000 (2)	18 000 (3)	11 000 (3)	11,2 (3)

AC = Die Forgings

AP = Precision Forgings,

Numbers in Paretheses Designate the Rating

Table 9: Typical Guaranteed Minimum Properties for Composition/Processing Options in Titanium Structural Forgings [32]

Alloy	Option	Room Temperature Tensile Properties				Fracture Toughness
		0,2 % Y.S. N/mm^2	U.T.S. N/mm^2	EL (4D) %	RA %	$N/mm^{3/2}$
Ti-64	Conv.	830 - 860	900 - 930	10	20 - 25	1290 - 1740
	1 a	790 - 830	860 - 900	10	20 - 25	1910 - 2260
	1 b	760 - 790	830 - 860	10	20 - 25	2430 - 2780
	2 a	790 - 860	930 - 1000	6 - 8	10 - 15	260 - 2950
	2 b	760 - 830	830 - 860	6 - 8	10 - 15	2780 - 3120
	3 a	810 - 850	900 - 930	10	20 - 25	2080 - 2430
	3 b	810 - 850	860 - 900	8 - 10	15 - 20	2260 - 2780
	4	760 - 790	830 - 860	6 - 8	10 - 15	2600 - 2950
Ti-662	Conv.	930 - 970	1000 - 1030	8 - 10	20 - 25	1040 - 1390
	1 a	900 - 970	970 - 1030	8 - 10	20 - 25	1390 - 1740
	1 b	-	-	-	-	-
	2 a	860 - 910	970 - 1030	6 - 8	10 - 20	1740 - 2080
	2 b	-	-	-	-	-
	3 a	900 - 930	1000 - 1030	8 - 10	15 - 20	1390 - 1740
	3 b	900 - 930	970 - 1030	6 - 8	12 - 20	1740 - 2080
	4	-	-	-	-	-

Option	Chemical Composition	Forging Process	Heat Treatment
Conventional	Standard	$\alpha + \beta$	Mill Anneal (MA)
1a	Standard	$\alpha + \beta$	Recrystallization Anneal (RA)
1b	Special	$\alpha + \beta$	Recrystallization Anneal (RA)
2a	Standard	$\alpha + \beta$	β Solution Treatment + Anneal (β A)
2b	Special	$\alpha + \beta$	β Solution Treatment + Anneal (β A)
3a	Standard	β Preform, $\alpha + \beta$ Block & Finish	Mill Anneal (MA)
3b	Standard	β Preform, β Block, $\alpha + \beta$ Finish	Mill Anneal (MA)
4	Special	β Preform, β Block, $\alpha + \beta$ Finish	Duplex Solution Treatment + Anneal (Duplex STAN)

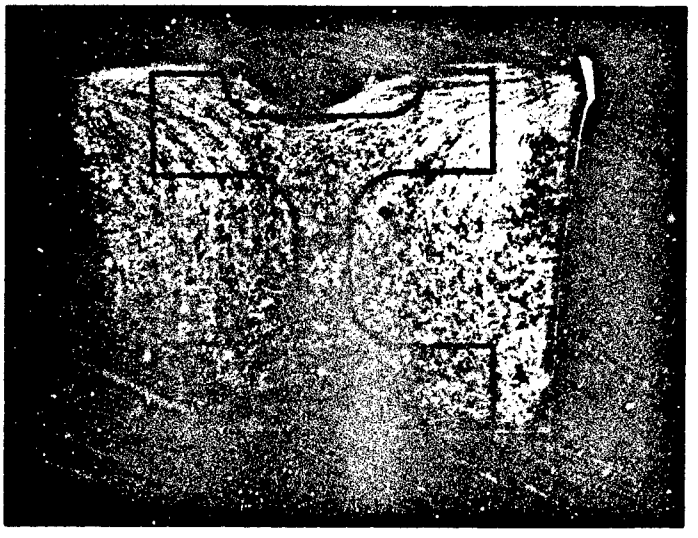

Fig.1 Titanium forging

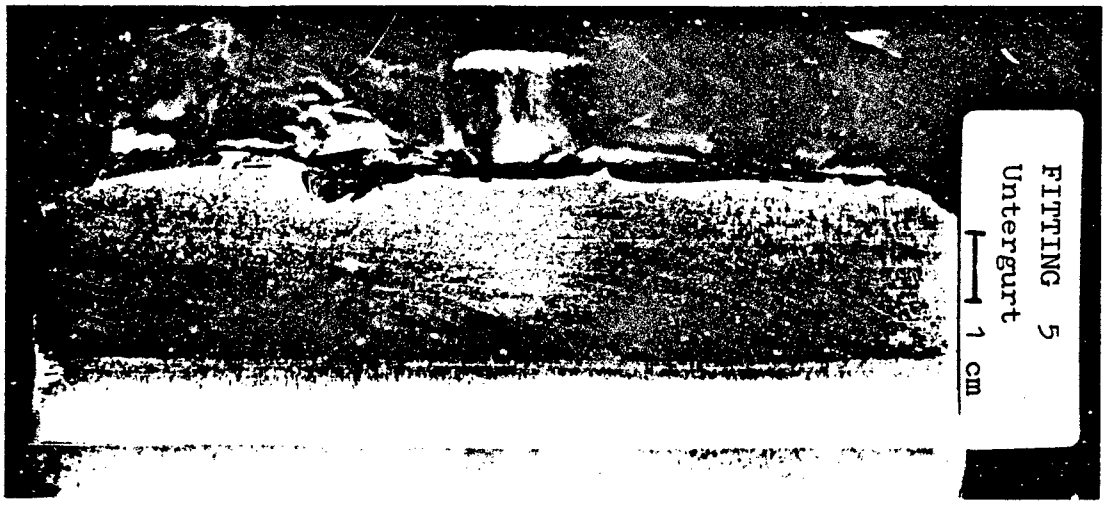

Fig.2 Grain flow pattern on the surface of a forged wing attachment fitting

Fig.3 Fracture surface of the wing fitting shown in Figure 2. Note the almost complete absence of shear lips

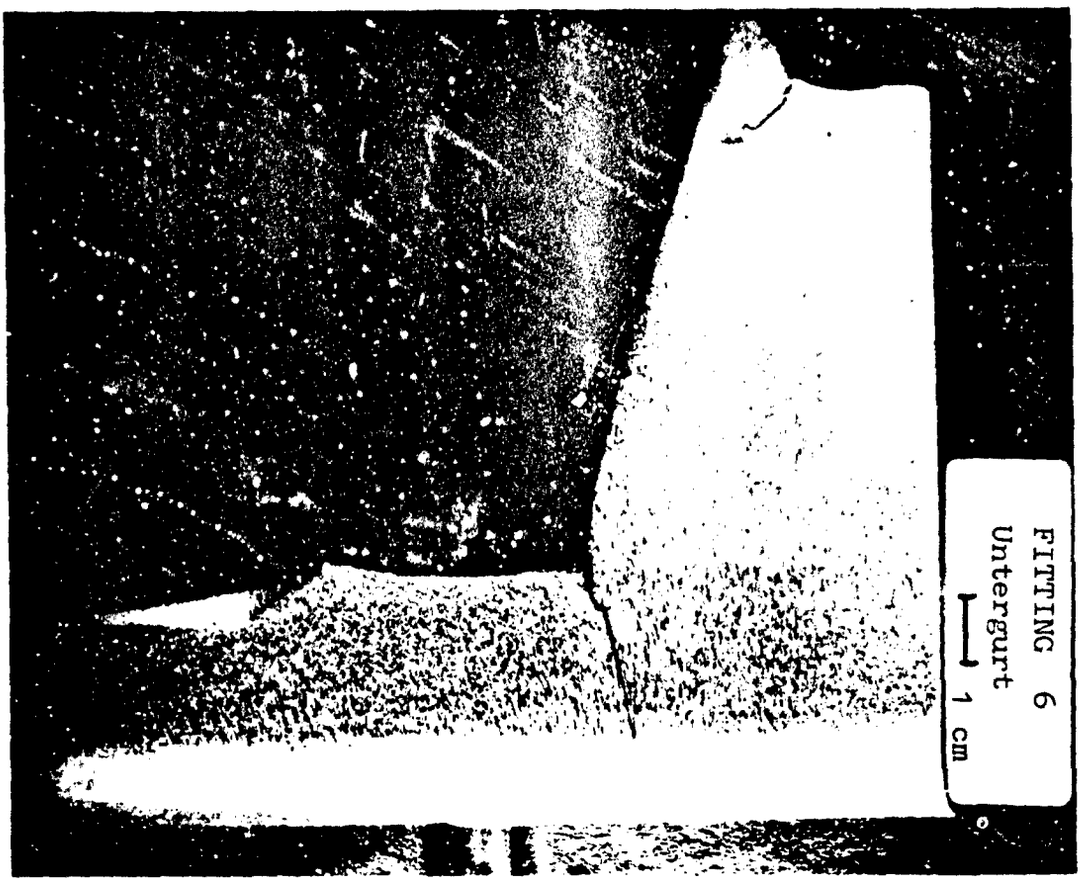

Fig.4 Grain flow pattern on the surface of a wing attachment fitting. Note grain flow and course of the failure are dissimilar to Figure 2, although forging is nominally identical to that of Figure 2

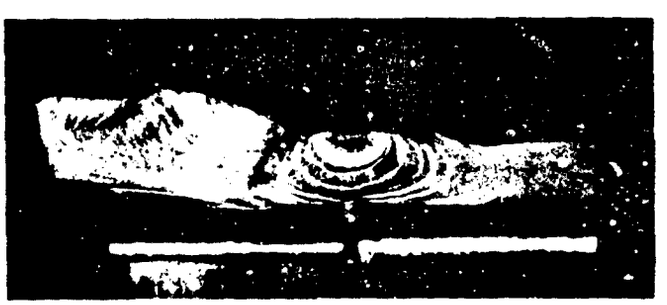

Fig.5 Fracture surface of the wing fitting shown in Figure 4. Note the complete shear failure of the left half of the section

Fig.6 Irregular crack shape in an aluminum forging

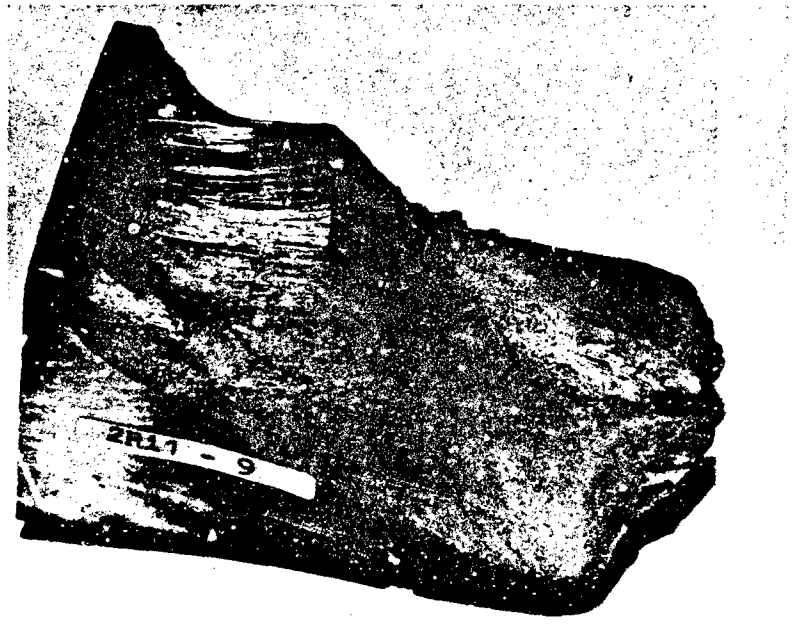

Fig.7 Crack propagation along the grain flow in an aluminum forging

Fig.8 Small 45-degree cracks in a fillet due to torsional loading

Fig.9 Appearance of the torsionally loaded shaft of Figure 8 after fracture

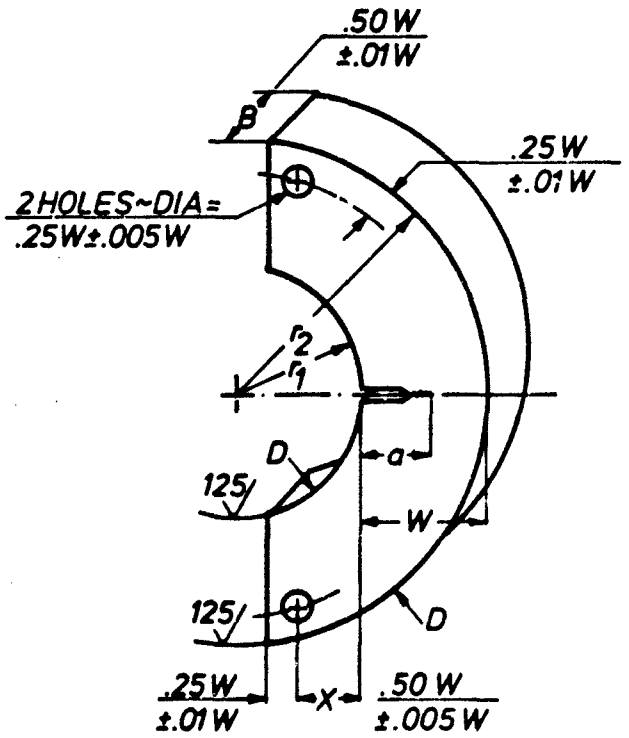

Fig.10 Standardized C-shaped specimen [38]

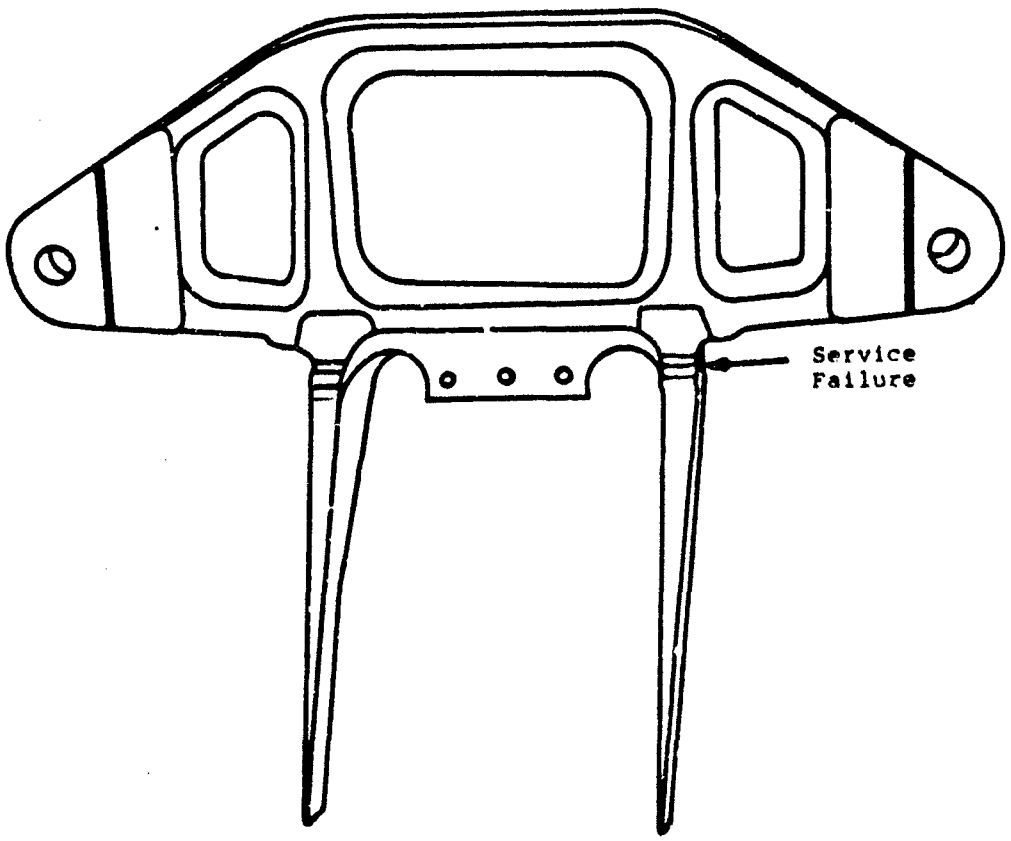

Fig.11 Horizontal stabiliser rear attachment fitting [12]

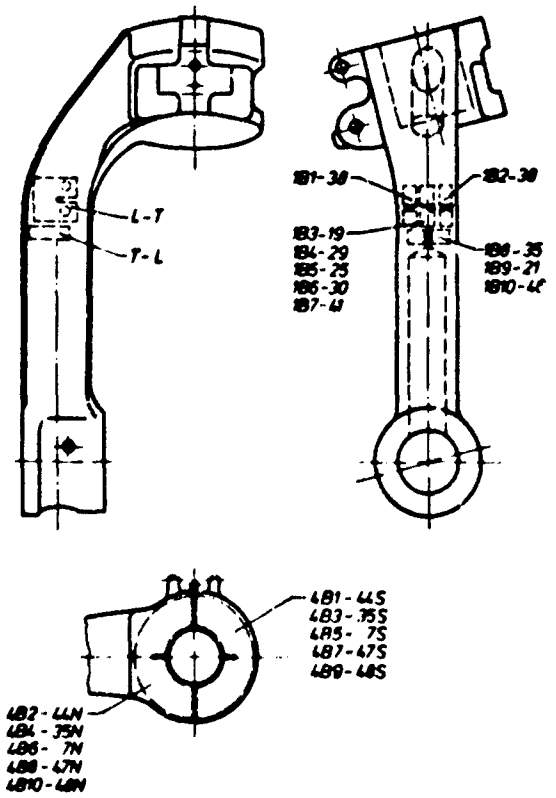

Fig.12 Nose landing gear strut and location of fracture toughness specimens

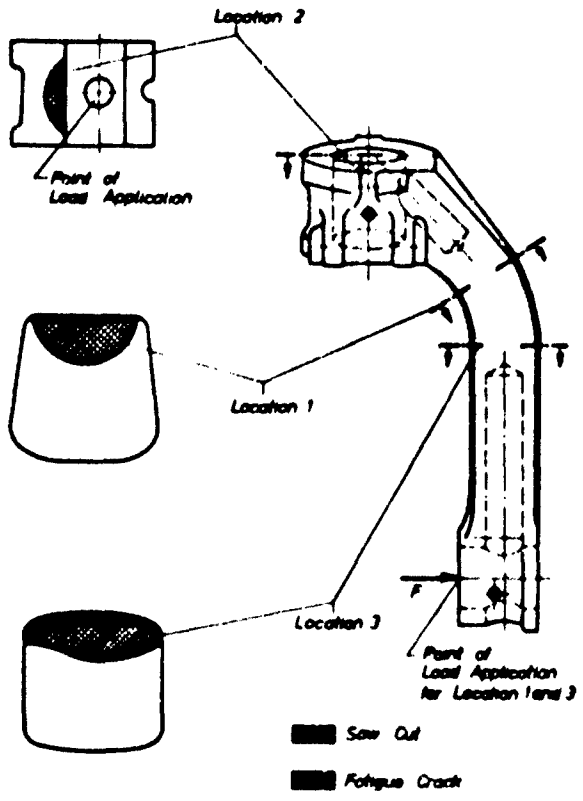

Fig.13 Artificially induced cracks in the component

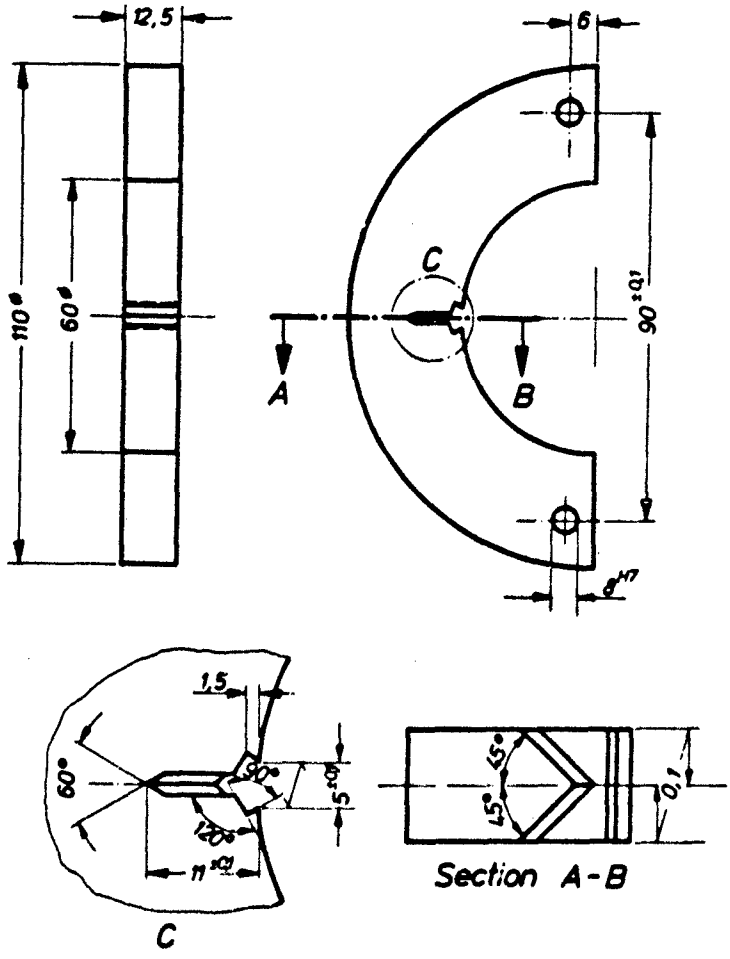

Fig.14 C-shaped fracture toughness specimen

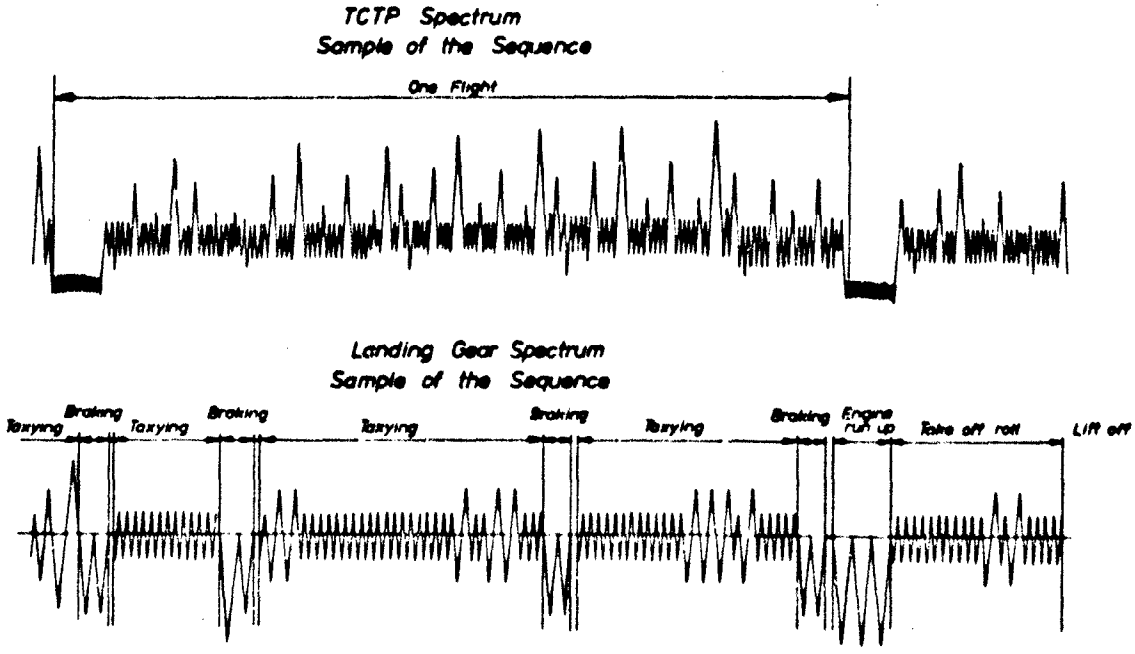

Fig.15 Samples of the two realistic load sequences used

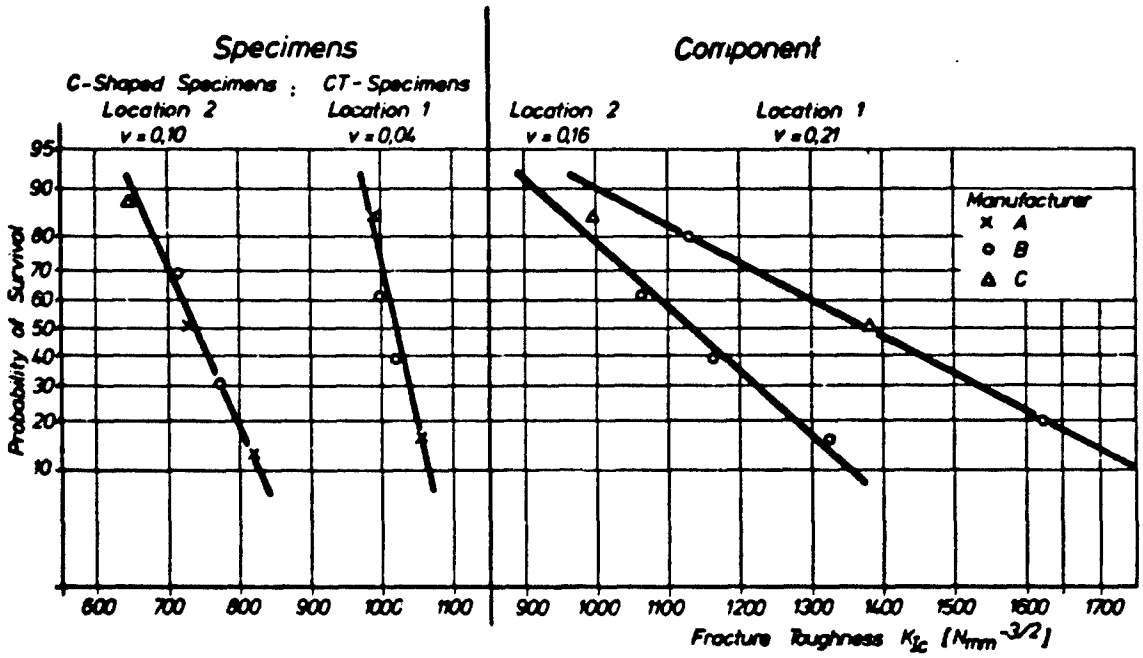

Fig.16 Statistical evaluation of fracture toughness K_{IC}

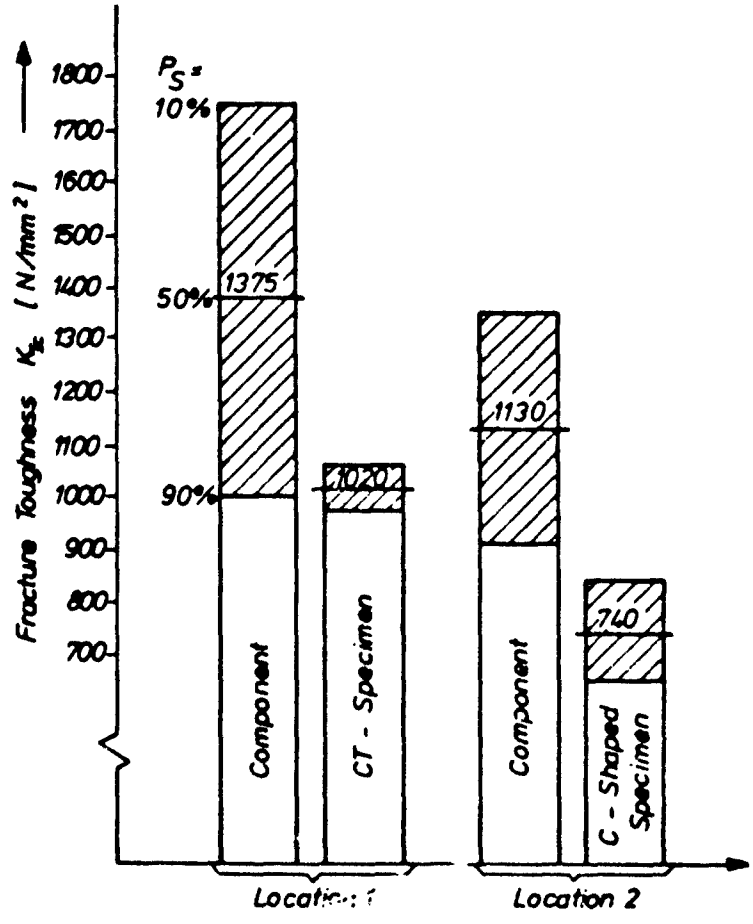

Fig.17 Fracture toughness of specimens and of components

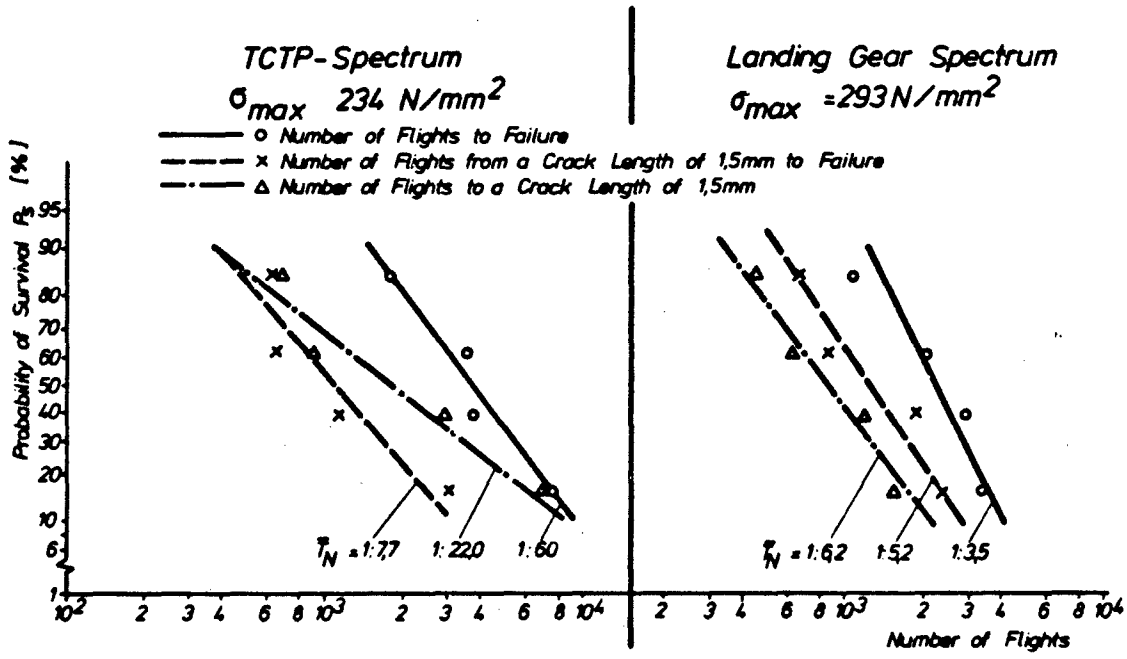

Fig.18 Statistical evaluation of crack propagation tests

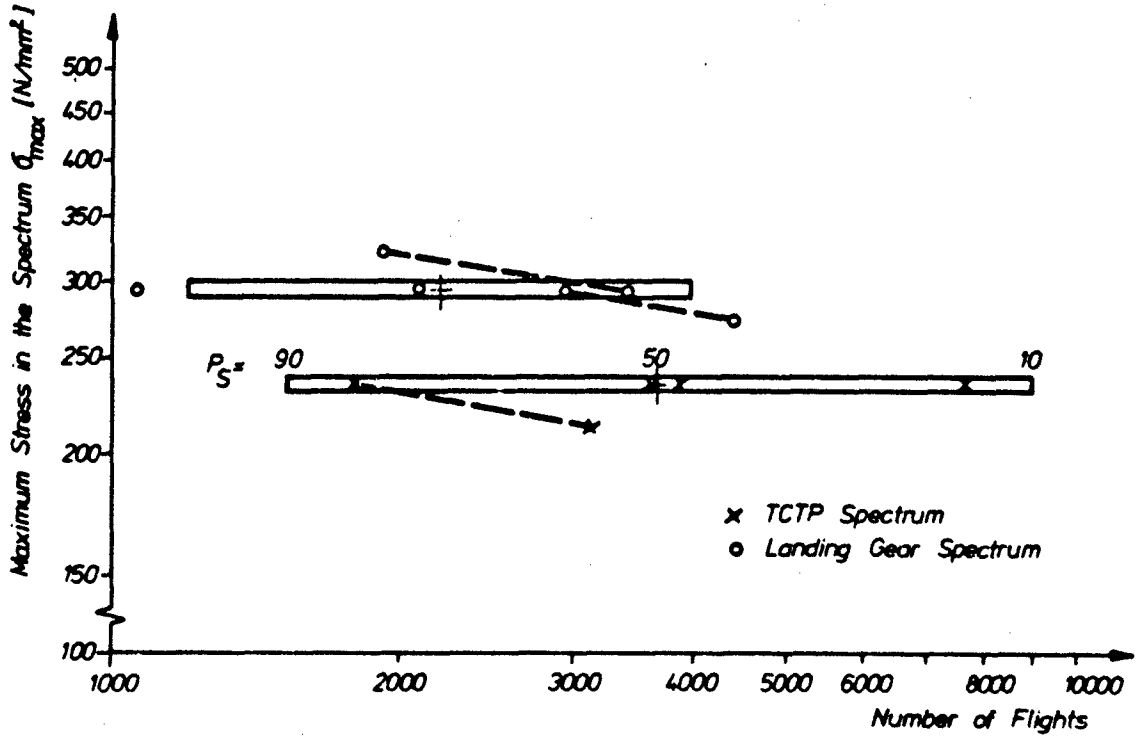

Fig.19 Fatigue life to complete failure
(crack initiation plus crack propagation period)

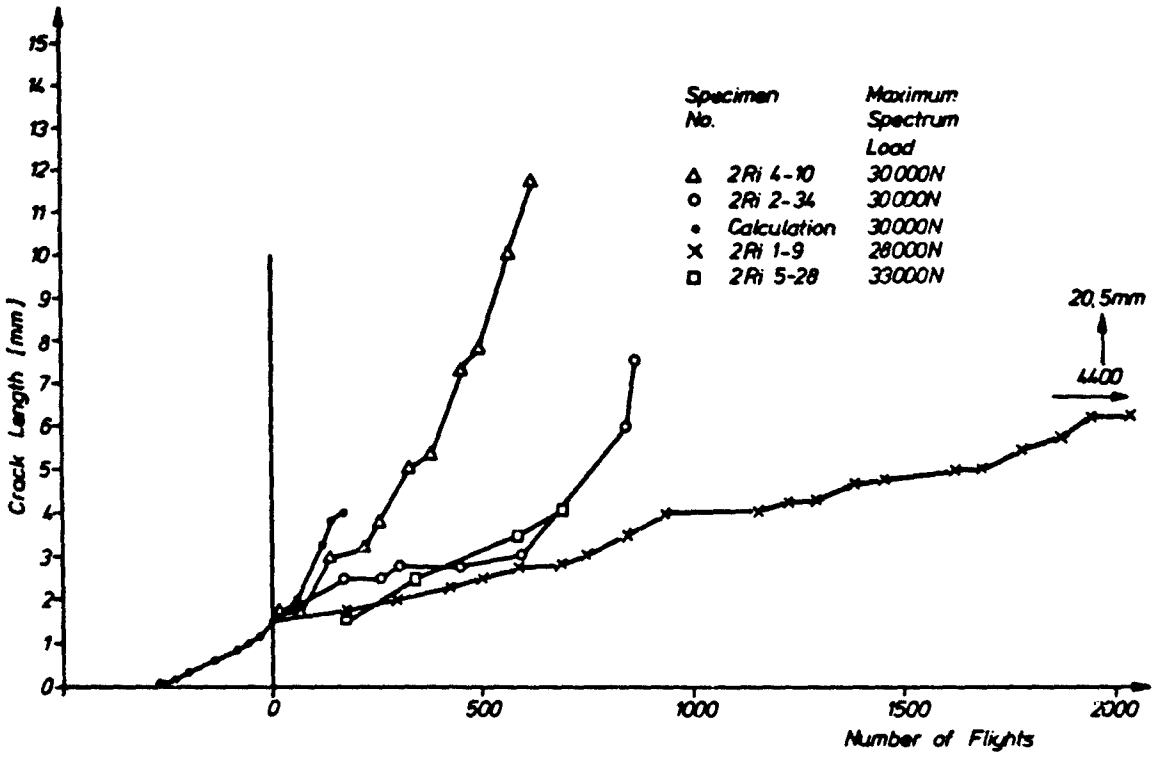

Fig.20 Crack propagation under the landing gear spectrum

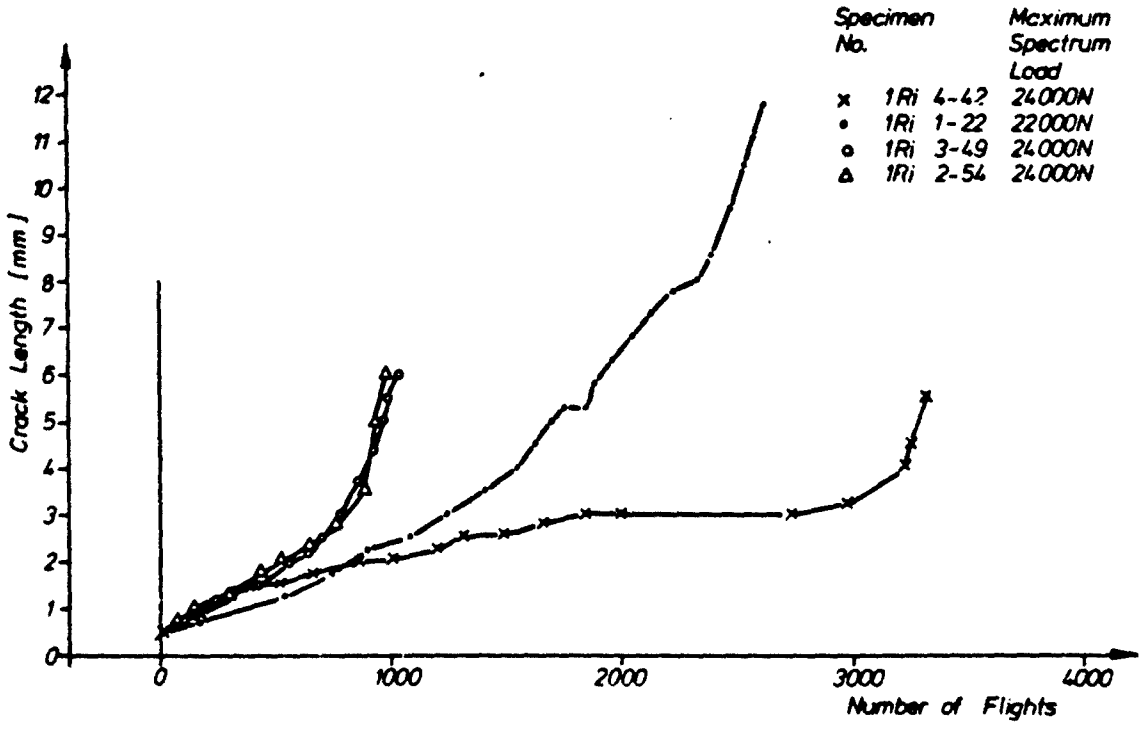

Fig.21 Crack propagation under the TCTP-spectrum

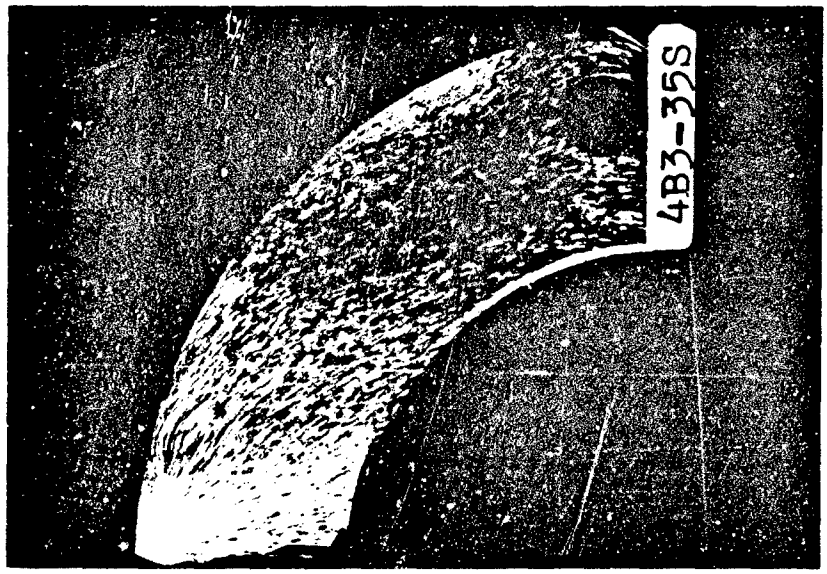

Fig.22 Location of the fatigue crack in the forging seam

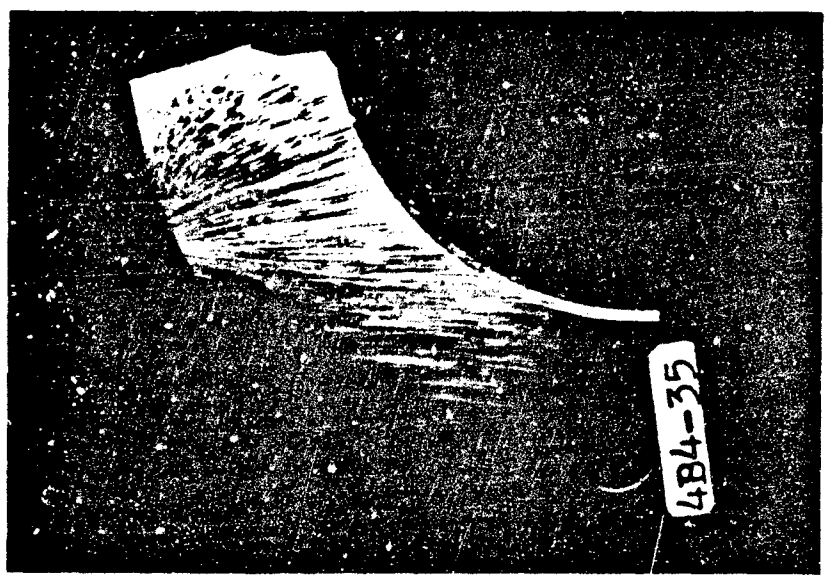

Fig.23 Location of the forging seam away from the fatigue crack

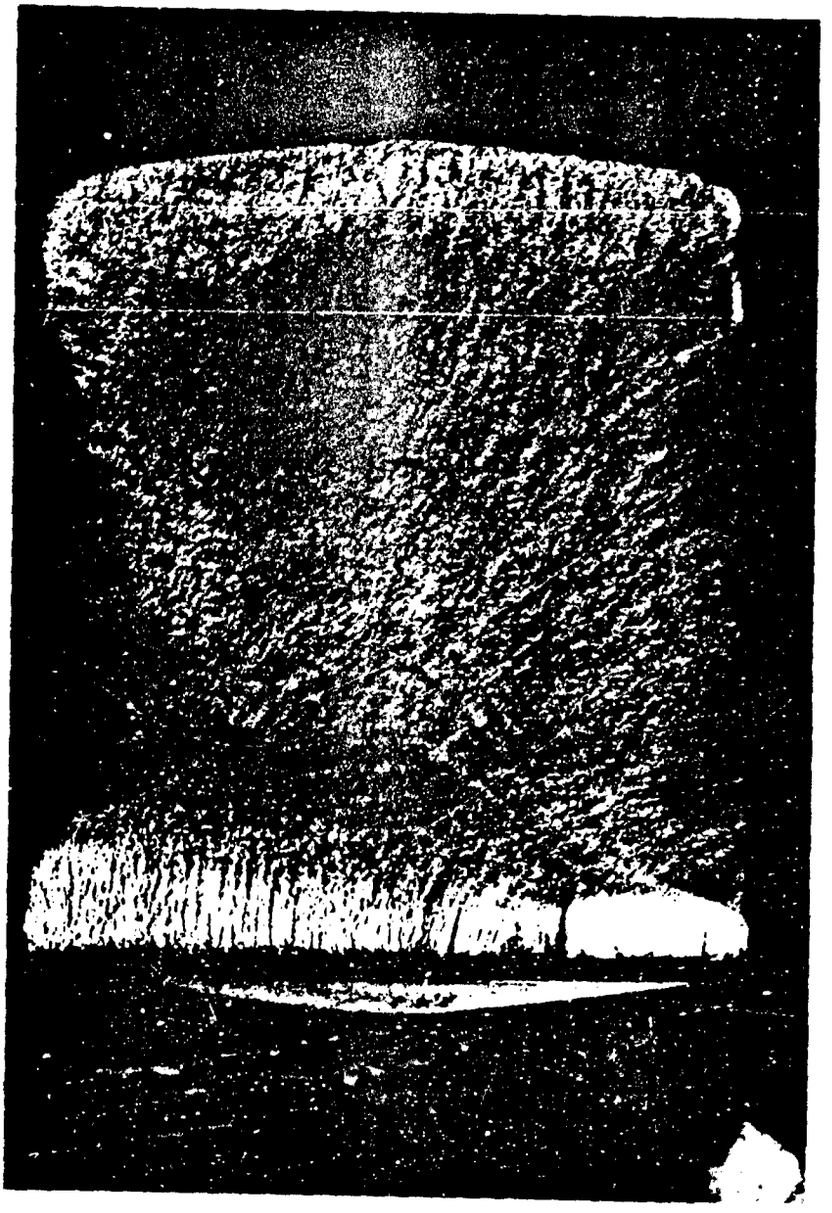

Fig.24 Forging 2 R: 2–34 fracture surface

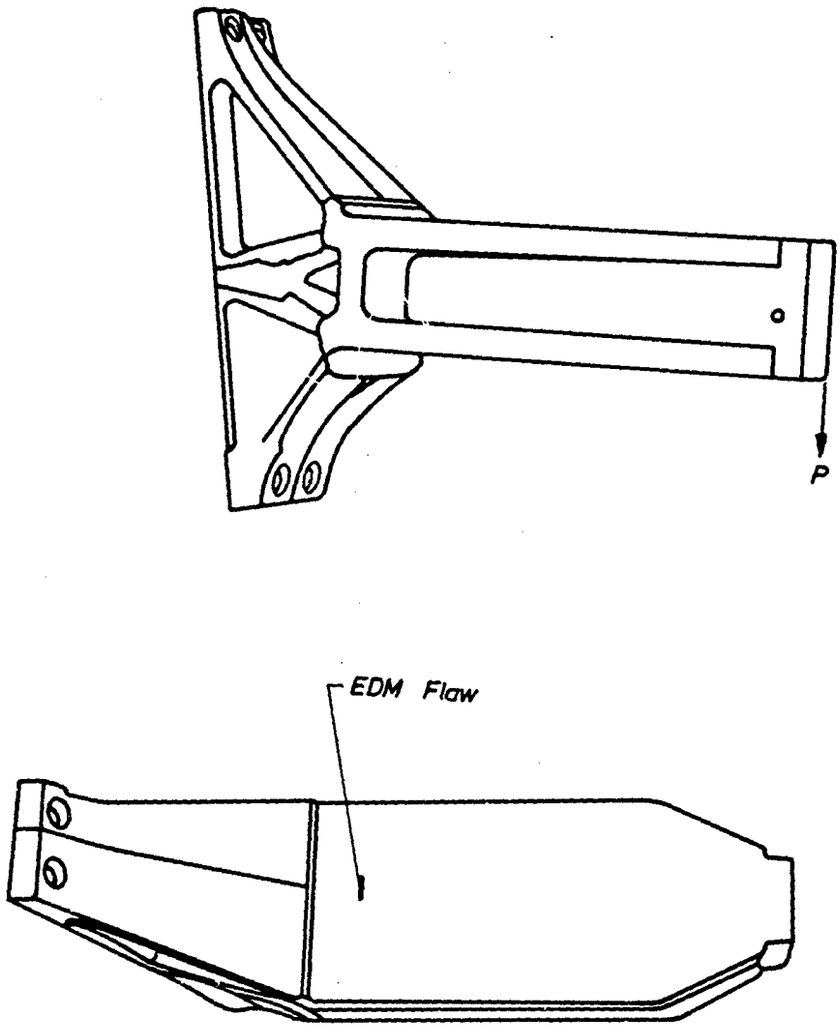

Fig.25 Wing attachment fitting

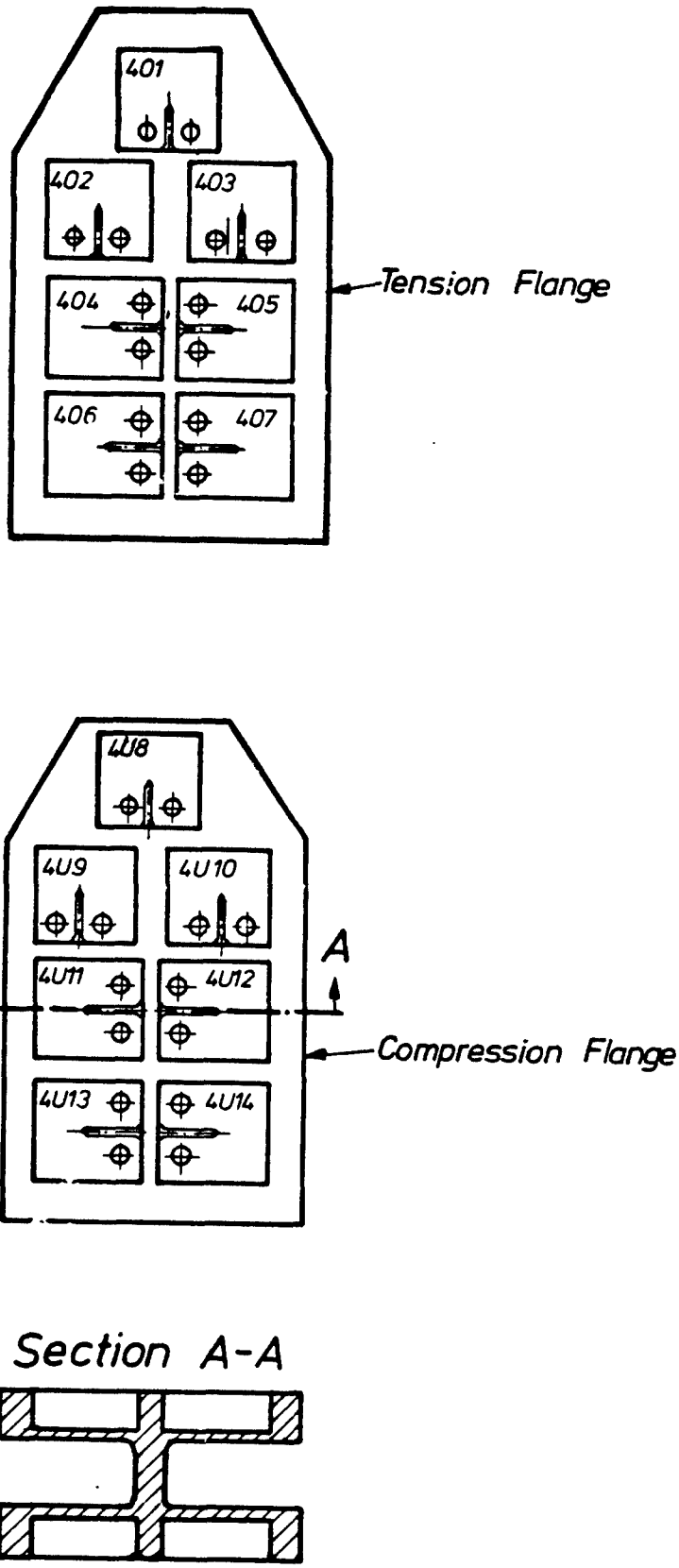

Fig.26 Specimen orientation in fitting 4

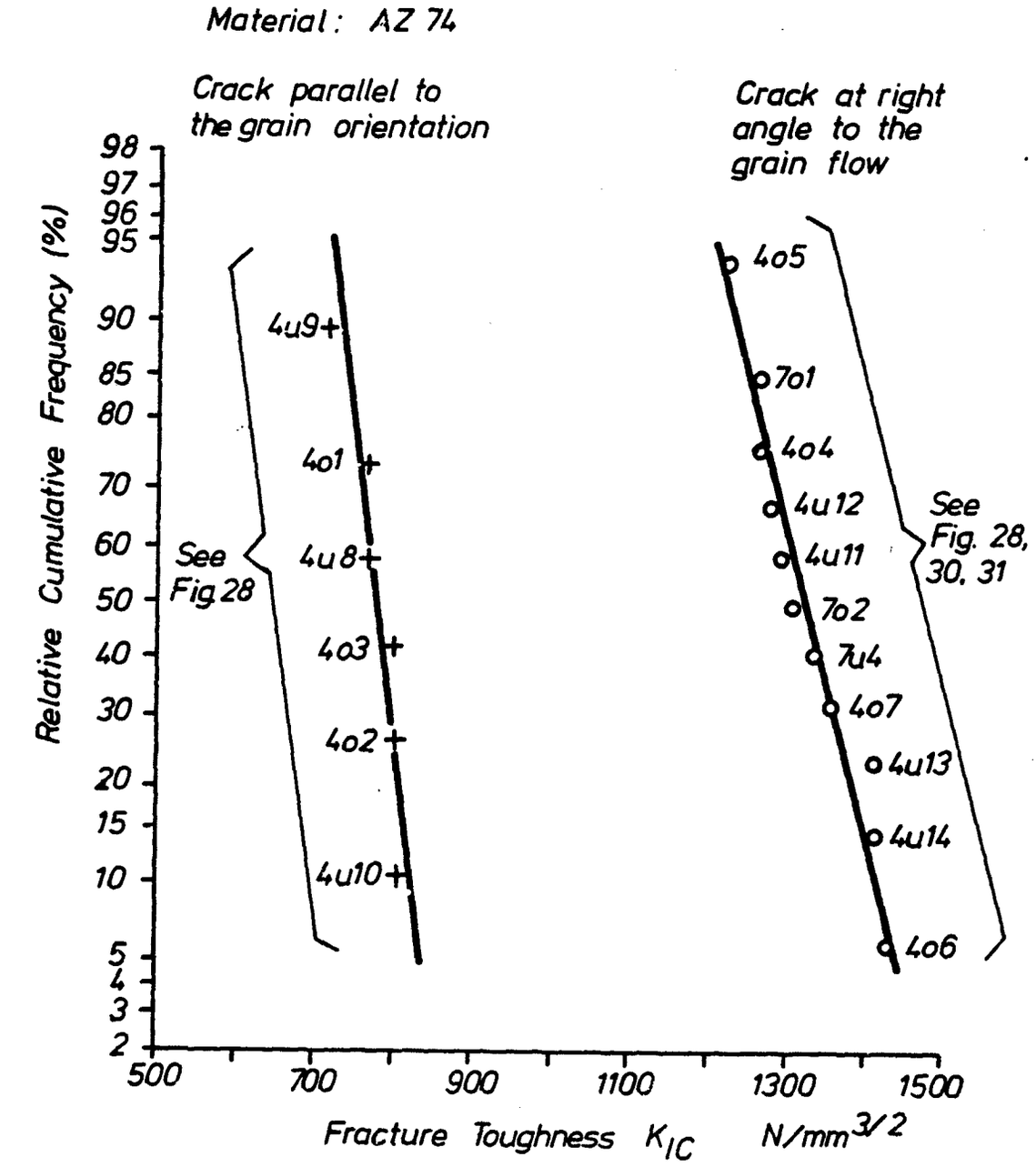

o P_S 50 % = 1330 N/mm$^{3/2}$ v = 0.054

+ P_S 50 % = 780 N/mm$^{3/2}$ v = 0.045

Fig.27 Statistical evaluation of fracture toughness

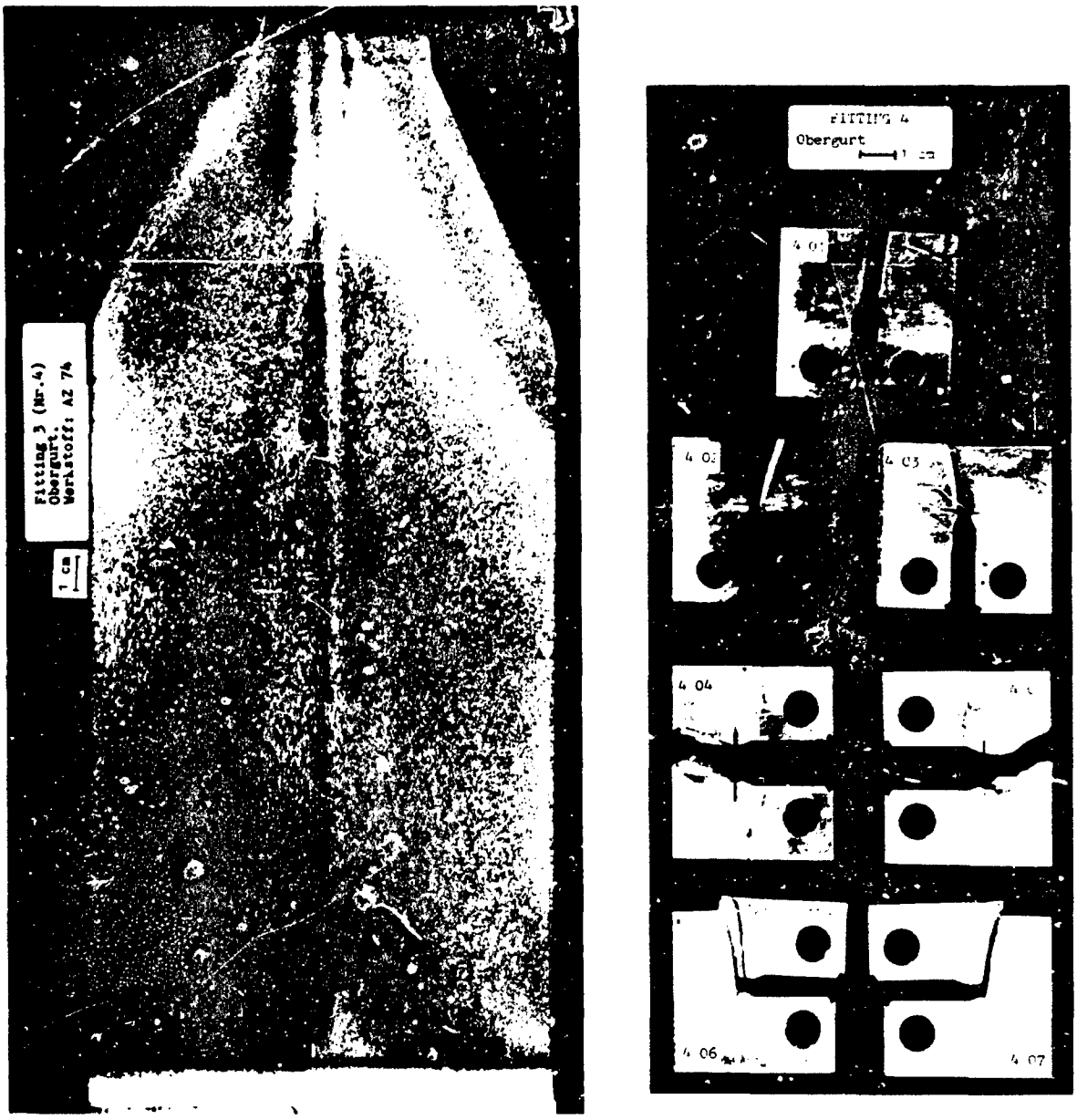

Fig.28 Grain flow pattern in the compression flange of fitting 4 (left side) compared to the crack direction in CT-specimens machined from fitting 4. Note: 402 and 403; 406 and 407

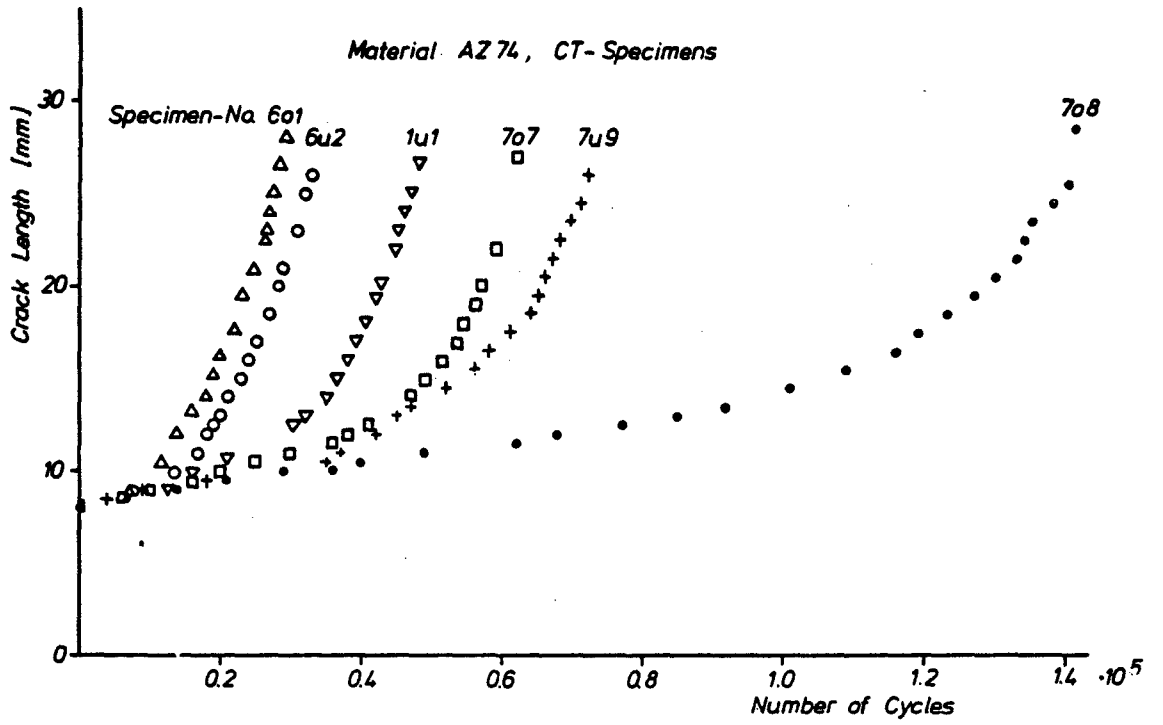

Fig.29 Crack propagation under constant amplitude loading, CT-specimens

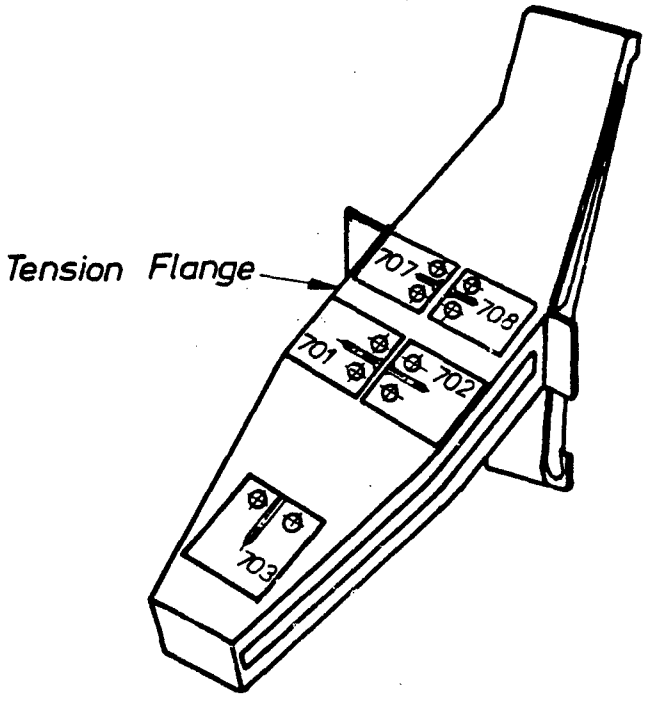

Fig.30 Specimen orientation in the forging tension flange

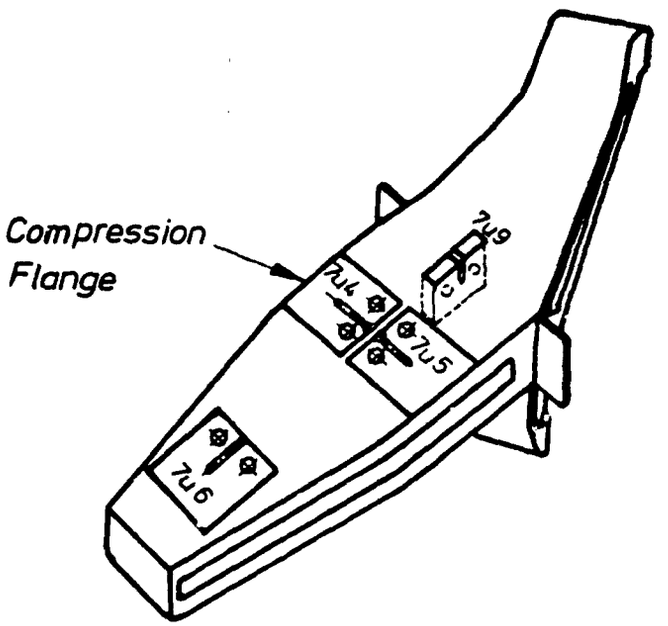

Fig.31 Specimen orientation in the forging compression flange

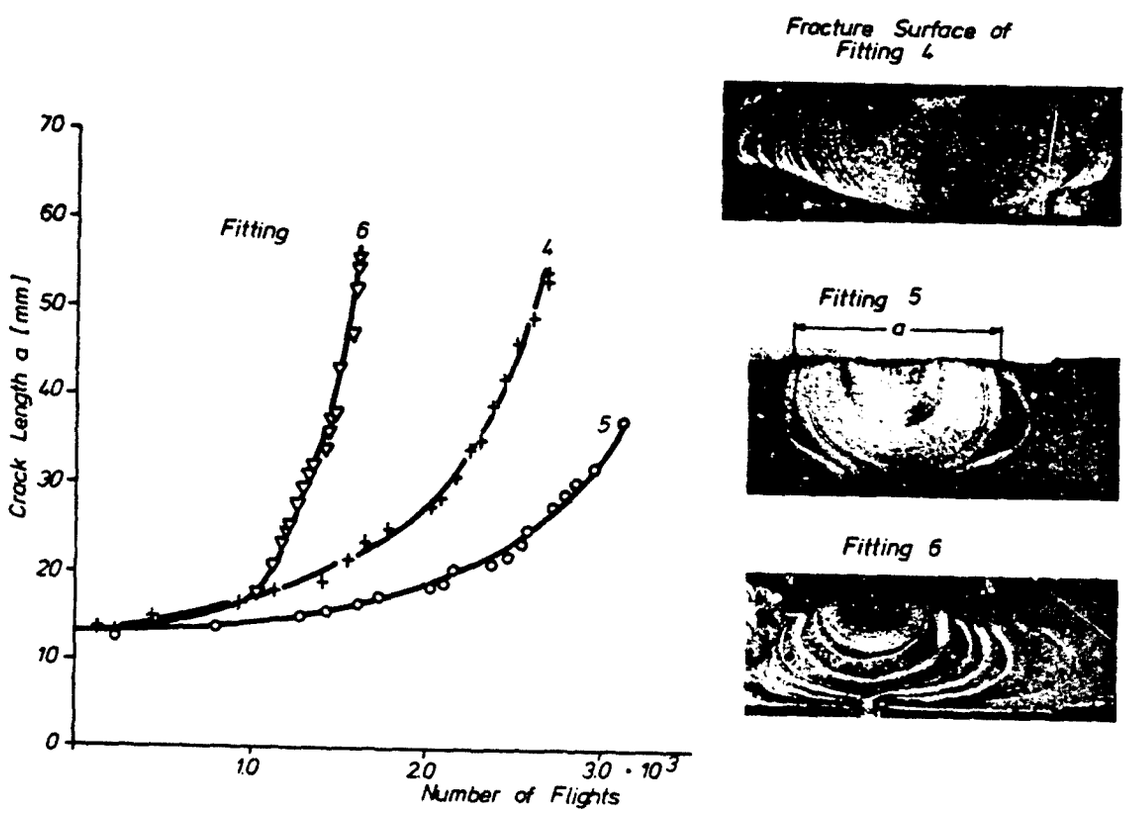

Fig.32 Crack propagation in fittings 4, 5 and 6 under the FALSTAFF load sequence

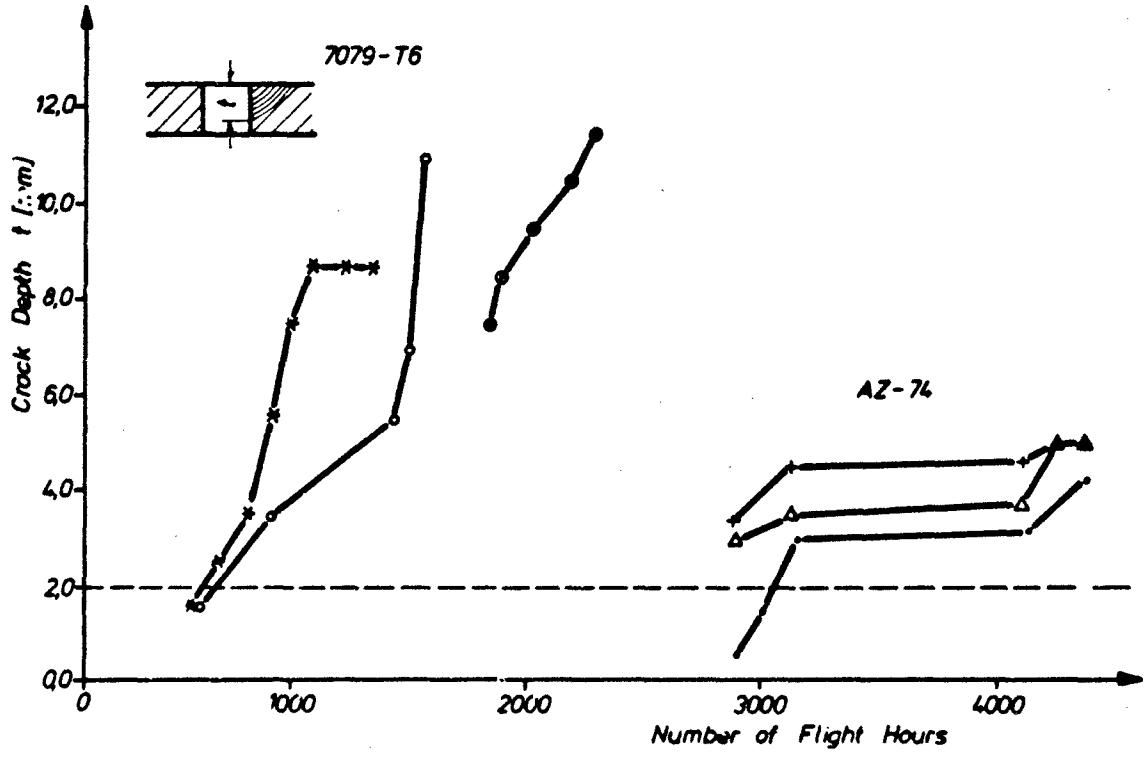

Fig.33 Crack propagation in wing attachment fittings in a full scale test

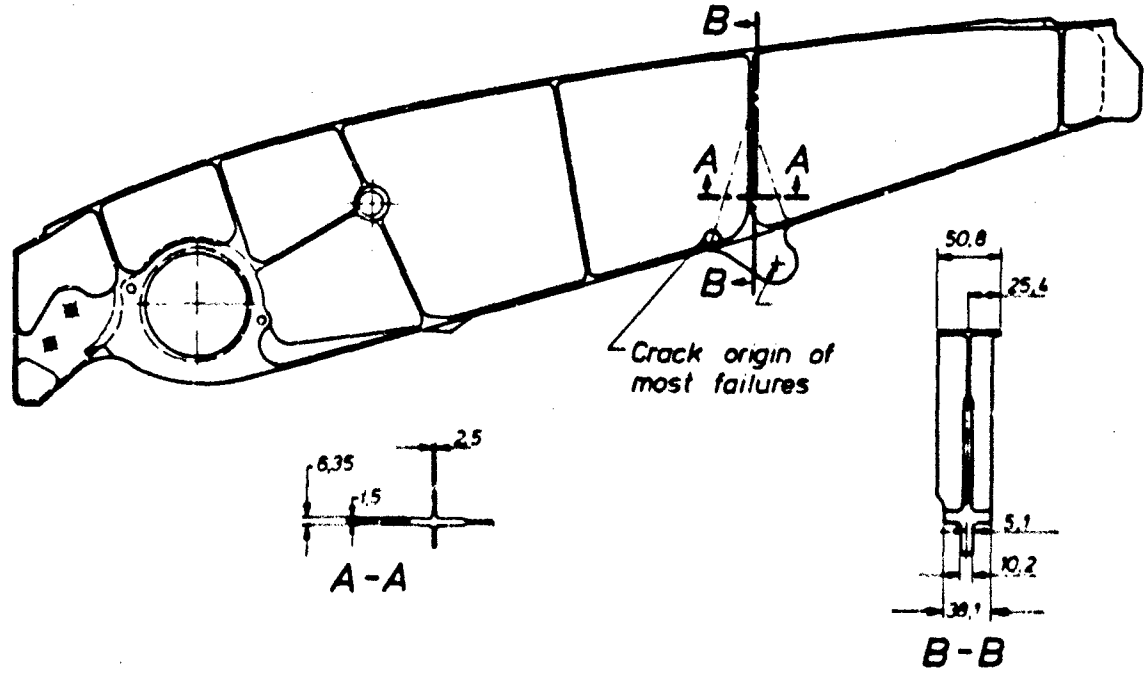

Fig.34 Hinge rib forging [6]

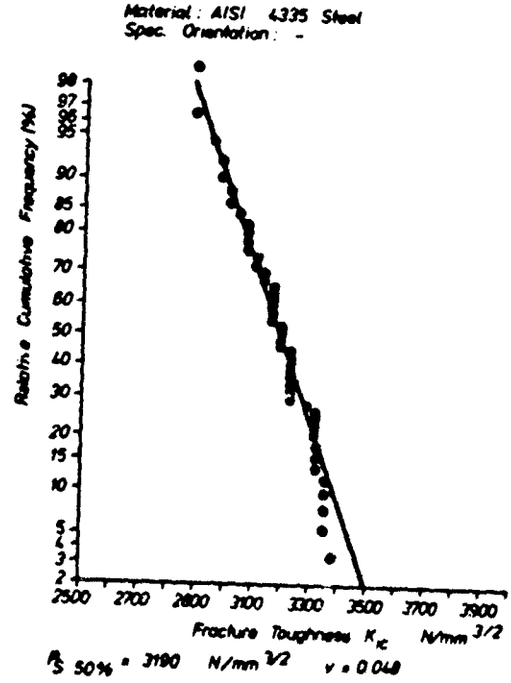

Fig.35 Fracture toughness of C-shaped specimens cut from one forging [28]

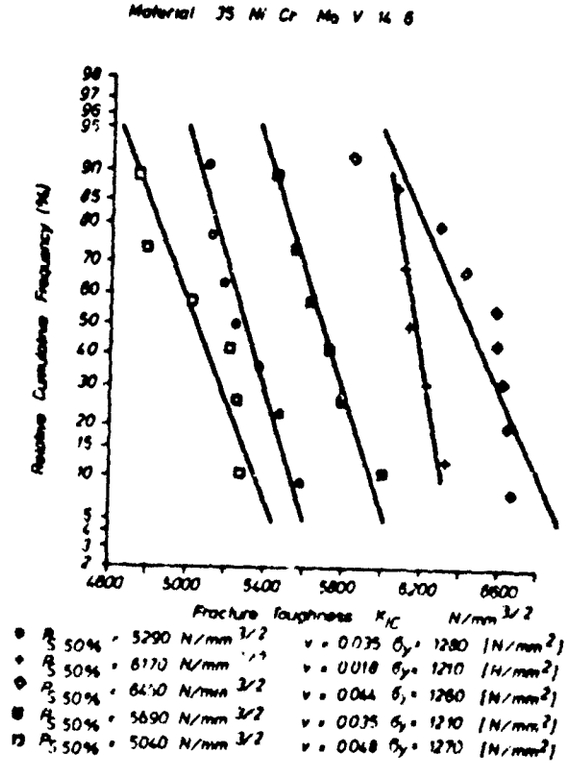

Fig.36 Fracture toughness of five forgings of different heat treatments, C-shaped specimens

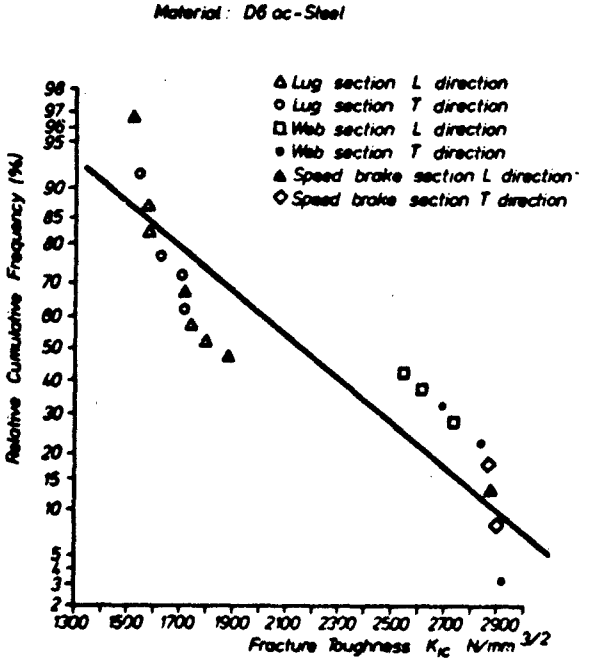

Fig.37 Fracture toughness of specimens taken from one large forging DCac [30]

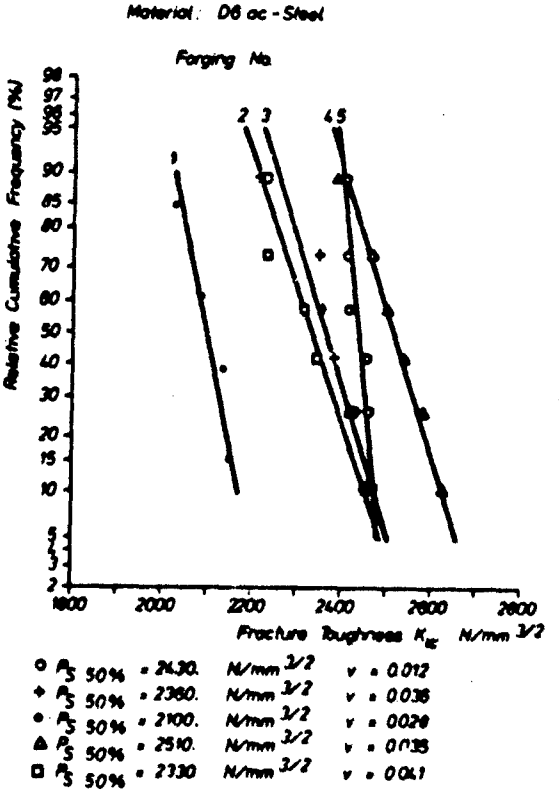

Fig.38 Fracture toughness of specimens taken from several large D6ac-forgings. Specimens taken from the web and speed brake sections [30]

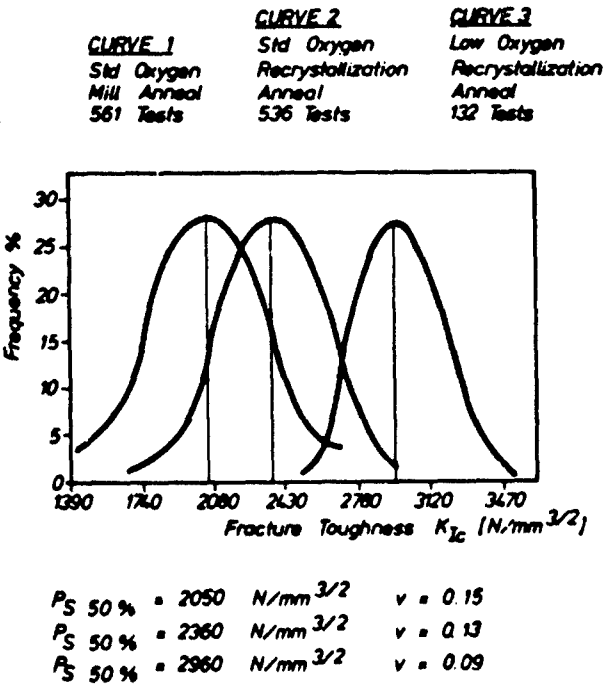

Fig.39 Frequency distribution of the fracture toughness of three Ti 6Al 4V-forgings from lot prolongation tests [29] Effect of processing variables

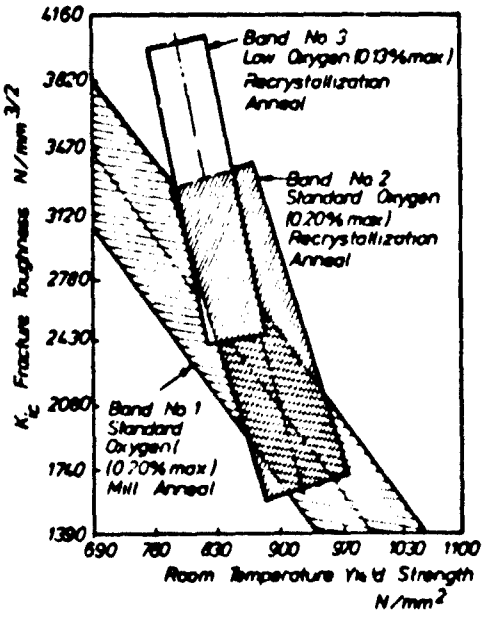

Fig.40 95% confidence bands and least squares Lines for Ti 6 Al 4V structural forgings [29]

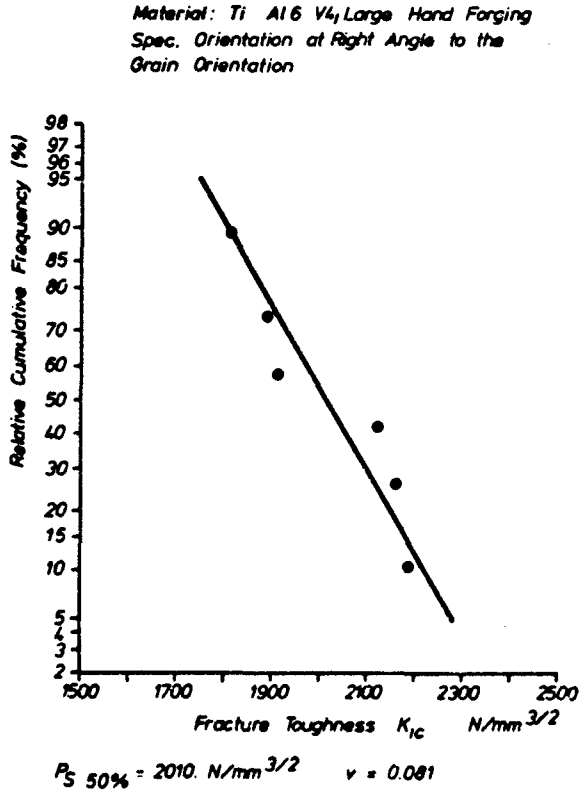

Fig.41 Statistical evaluation of fracture toughness

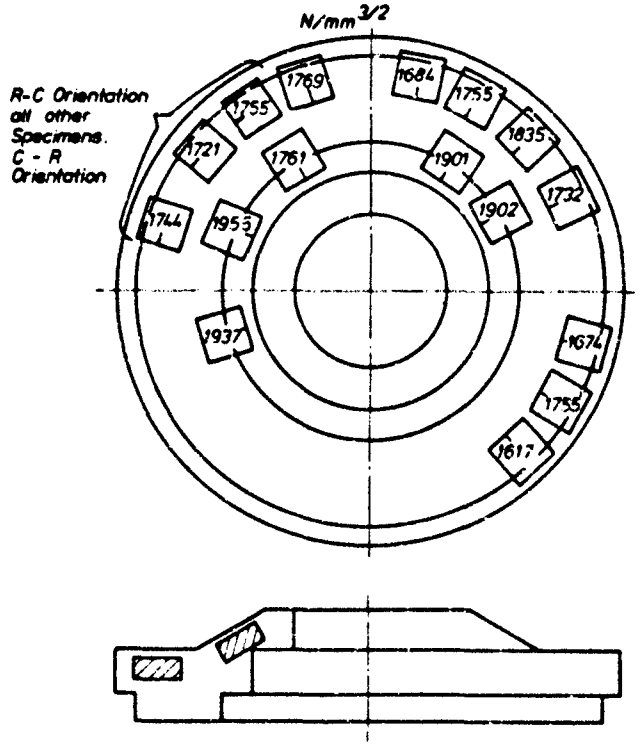

Fig.42 Fracture toughness within one compressor disc forging. Influence of location and crack orientation

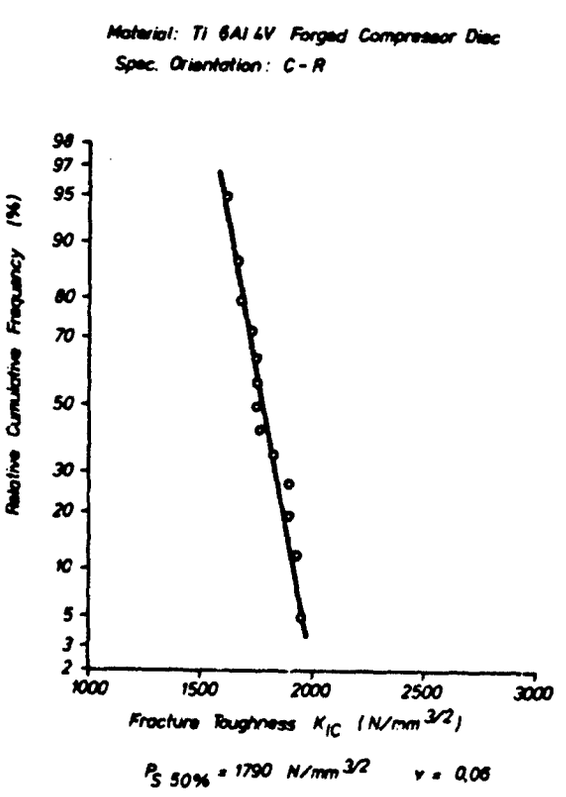

Fig.43 Statistical evaluation of fracture toughness

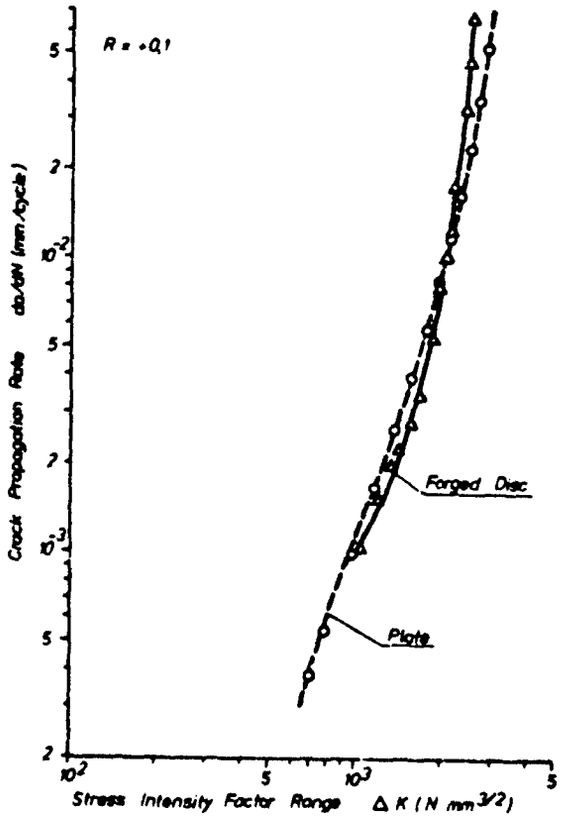

Fig.44 Comparisen of crack propagation rate of Ti 6Al 4V plate and forged disc

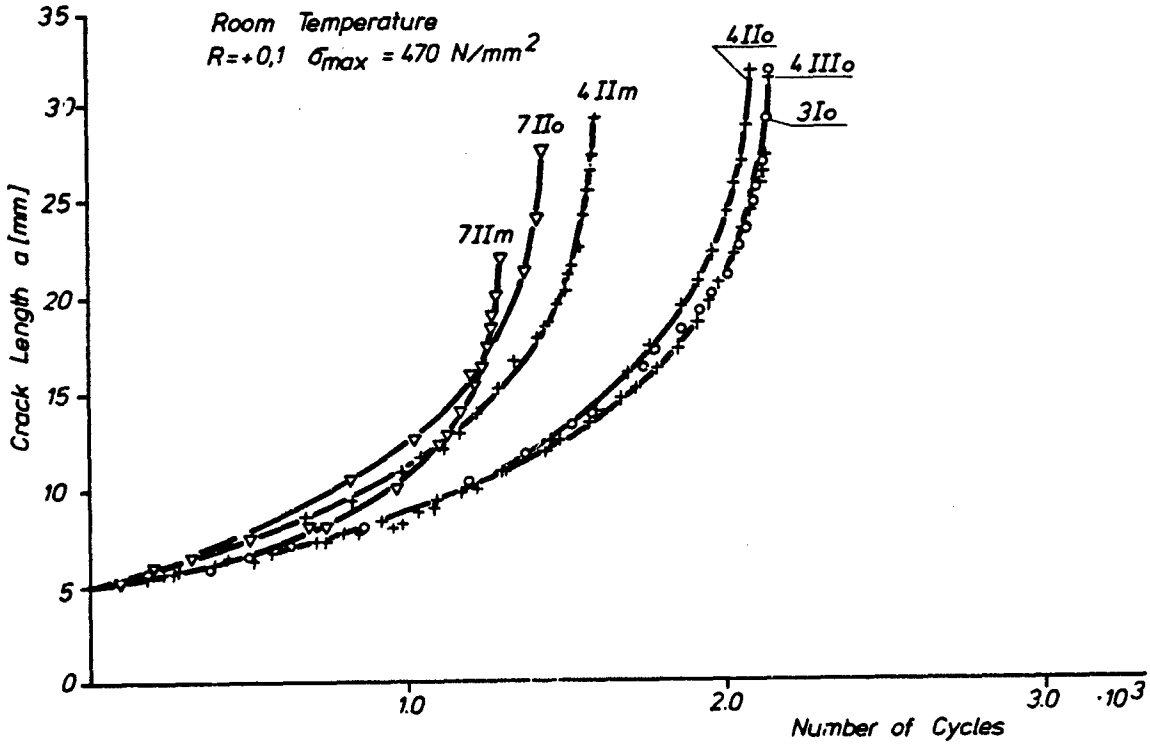

Fig.45 Crack propagation of specimens machined from three Ti 6Al 4V compressor discs

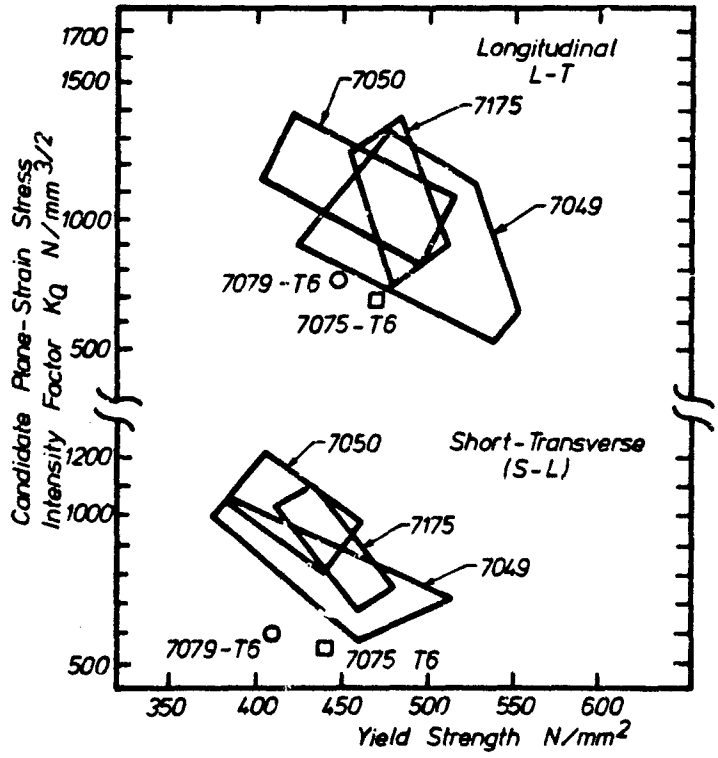

Fig.46 Fracture toughness of die forgings of three different materials [20]

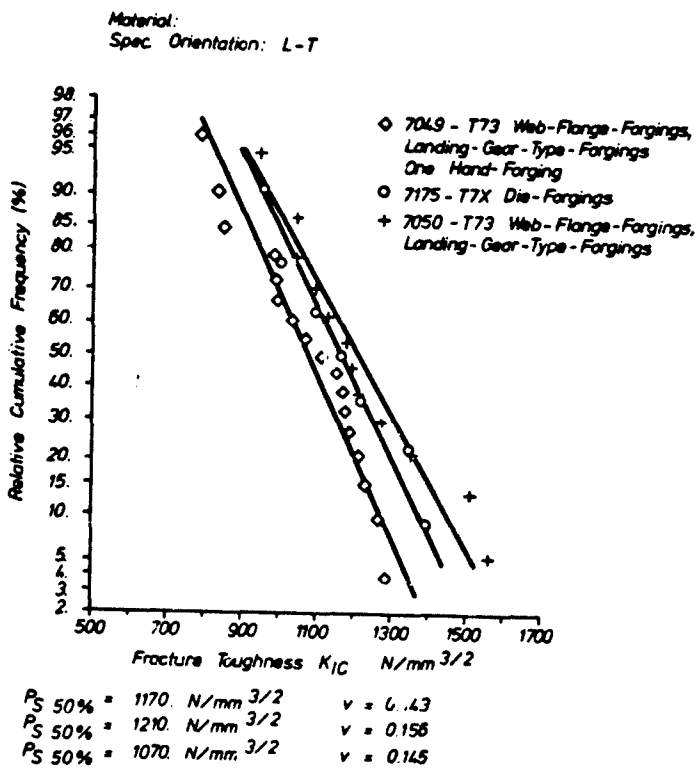

Fig.47 Statistical evaluation of fracture toughness of several forgings in three materials [20]

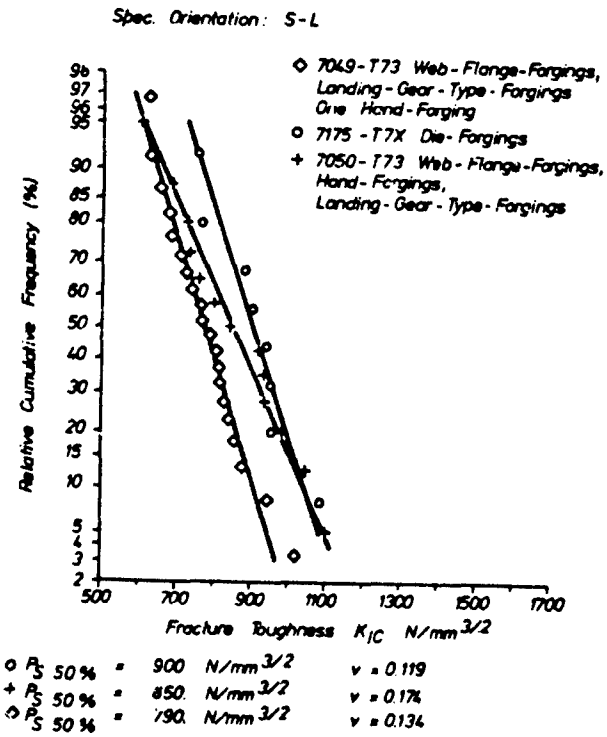

Fig.48 Statistical evaluation of fracture toughness of several forgings in three materials [20]

7. FATIGUE CRACK PROPAGATION UNDER VARIABLE LOADS

W. GEIER
Materials and Fatigue Department

K. H. SIPPEL
Head-Materials and Fatigue Department

Messerschmitt-Bolkow-Blohm GmbH
Unternehmensbereich Flugzeuge
Postfach 80 11 60, 8000 Munchen 80

SUMMARY

7.1 INTRODUCTION. 7-3

7.2 PROBLEMS ENCOUNTERED IN CALCULATING THE CRACK PROPAGATION 7-4

7.2.1 Basic Considerations 7-4

7.2.2 Difficulties in Predicting the Crack Propagation Under Variable Loads 7-11

7.3 METHODS OF CALCULATION THE CRACK PROPAGATION UNDER VARIABLE LOAD SEQUENCE. 7-15

7.3.1 Description of Current Models. 7-15

7.3.2 Future Approaches. 7-19

7.4 ASSESSMENT OF CURRENTLY USED CALCULATION PROCEDURES . 7-22

7.4.1 Comparison Between Test and Calculation. . . 7-22

7.4.2 Suggestions for Practical Application. . . . 7-30

7.5 CONCLUSION. 7-31

7.6 REFERENCES. 7-32

FATIGUE CRACK PROPAGATION UNDER VARIABLE LOADS

by

W. Geier
Materials and Fatigue Department

K. O. Sippel
Head-Materials and Fatigue Department

Messerschmitt-Bölkow-Blohm GmbH
Unternehmensbereich Flugzeuge
Postfach 80 11 60, 8000 München 80

SUMMARY

It is the purpose of this treatise to draw attention to some of the problems involved in calculating crack propagation under constant and multi-step amplitude load sequences and point the way to the solution.

By considering a number of factors influencing the crack propagation behaviour, it is shown that the selection of a suitable calculation formula is only one of several possible ways of improving the prediction of crack propagation.

For this reason a first estimation of the crack propagation life may be made with the aid of a simple calculation procedure such as the Forman equation, which in general yields conservative results. The Wheeler model which requires a considerably higher expenditure of computing time and cost compared with the Forman equation is recommended if more accuracy is required. Finally, calculation models based on the crack closure concept are also considered.

7.1 INTRODUCTION

It has been shown, on the one hand by improved NDI methods applied in the course of production and during inspections of the aircraft, and on the other hand by damage arising during operation, that cracks in aircraft components cannot be discounted even before the aircraft goes into service. When a component is checked for cracks it is usually only possible to detect cracks above a certain size, and even then only with a certain degree of probability. In order to guarantee the safe operation of an aircraft even when non-detectable cracks are present, every effort is made to forecast the propagation of cracks up to the failure of the component.

These efforts have already become established as damage tolerance requirements in MIL 83444 of the USAF.

The use of fracture mechanics in aircraft construction, be it to fulfil damage tolerance requirements, as already mentioned, or to determine inspection intervals, must at present still be regarded as a relatively new field of engineering in which there are a number of gaps yet to be closed.

A consequence of this is that forecasts of crack propagation life may involve various problems which at present can often only be overcome by fairly conservative estimates.

It is therefore the aim of this paper to make the engineer aware of various problems and as far as possible to point the way to suitable solutions.

Nomenclature

a_o	=	initial crack length
a	=	crack length
da/dN	=	crack propagation rate
C_p	=	retardation factor for the Wheeler calculation method
C, n	=	crack propagation parameters
c_1, c_2	=	crack propagation parameters for the crack propagation calculation method of Collipriest
F	=	correcting function for the stress intensity
K	=	stress intensity
ΔK	=	range of stress intensity factor
K_{min}	=	maximum stress intensity } for one load cycle
K_{max}	=	minimum stress intensity } for one load cycle
K_o, K_{th}	=	threshold value
K_c	=	fracture toughness under plane stress conditions
K_{IC}	=	fracture toughness under plane strain conditions
K_{eff}	=	effective stress intensity
m	=	retardation exponent for the Wheeler method

PRECEDING PAGE BLANK-NOT FILMED

m_w = crack propagation parameter for the Walker calculation procedure
n_z = multiple of gravitational acceleration
N = number of load cycles
N_c = number of load cycles until fracture
N_F = number of flights until fracture
R = stress ratio
R_y = radius of the plastic zone
R_{eff} = effective stress ratio
U = non-dimensional effective stress intensity
V = retardation factor
W = width of specimen
ζ = retardation function for the calculation method of Habibie
Λ = control function for the retardation according to Habibie
σ_B = ultimate strength of material
σ_y = yield strength of material
σ = gross stress
σ_{max} = maximum stress
σ_{min} = minimum stress
} of one load cycle
σ_a = amplitude stress
$\Delta\sigma$ = $2\,\sigma_a$
σ_o = maximum spectrum stress
σ_{op} = crack opening stress according to Elber
σ_m = mean stress

7.2 PROBLEMS ENCOUNTERED IN CALCULATING THE CRACK PROPAGATION

7.2.1 Basic considerations

In the mechanics of linear elastic fracture, the stress field around the crack tip can be described in terms of the stress intensity K [1].

$$K = \sigma\sqrt{\pi a}\,F \tag{2.1}$$

σ represents the gross stress, a the crack length and F a correcting function dependent on the geometry of the crack and the component and on the type of load introduction. In the literature there already exist stress intensity solutions, or correcting functions [2;3] for a number of different types of crack.

The stress intensity is used in the known procedures as a basis for calculating the crack propagation and the critical crack length.

Crack propagation tests under constant amplitude load have shown that, at the same stress intensity, cracks of differing geometry display the same rates of crack propagation. For this purpose it is assumed that for a certain material the stress ratio and the environmental conditions remain unchanged.

$$\frac{da}{dN} = f\,(\Delta K) \tag{2.2}$$

$$\Delta K = K_{max} - K_{min} \tag{2.3}$$

The experimentally determined crack propagation rate da/dN, as a function of the stress intensity factor range ΔK, produces approximately, on double-log arithmic paper, an S-shaped curve.

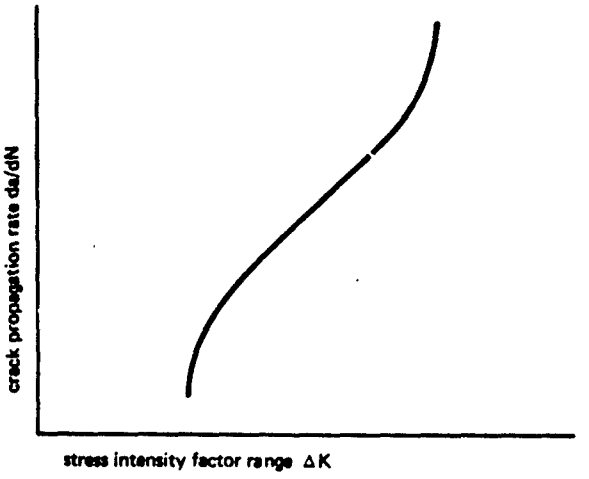

sketch: a typical curve of da/dN vs. ΔK

Where the rate of crack propagation is very small, ΔK approaches the threshold value K_{th}, below which no further crack propagation occurs [4].

Within the medium range, the relation between da/dN and ΔK can be extensively expressed by an exponential equation. An accelerated increase in the rate of crack propagation can be noted shortly before the critical crack length is reached.

7.2.1.1 Expressing the connection between da/dN and ΔK with the aid of various crack propagation calculation formulae

– Paris' calculation formula

Paris [5] was one of the first to state this connection by a simple exponential function

$$\frac{da}{dN} = C\,\Delta K^n \qquad (2.3)$$

C and n are parameters which primarily depend on the material and are determined by crack propagation tests under constant amplitude load.
The Paris equation only takes into account the central, i.e. linear area (see fig. 2.1). On the other hand, the marginal areas and the influence of the stress ratio R are not considered.

– Walker's calculation formula

Walker was among those who, to take proper account of the stress ratio R, proposed the following equation

$$\frac{da}{dN} = C\,K_{max}^{m_W} \cdot \Delta K^n \qquad (2.4)$$

– Forman's calculation formula

The accelerated increase in the crack propagation rate close to the critical crack length was first taken into account in the Forman equation [7].

$$\frac{da}{dN} = \frac{C\,\Delta K^n}{(1-R)\,K_c - \Delta K} \qquad (2.5)$$

– Richards and Lindley's calculation formula

The formula of R & L also includes the threshold value [8].

$$\frac{da}{dN} = E\left[\frac{\Delta K - \Delta K_{th}}{\sigma_B^2\,(K_c^2 - K_{max}^2)}\right]^m \qquad (2.6)$$

E and m are crack propagation parameters to be determined in crack propagation tests under constant amplitude load. σ_B indicates the ultimate strength and K_{th} the threshold value. K_{th} is available for a number of materials in reference [4].

– Collipriest's calculation formula

Instead of the much-used exponential formula to express crack propagation under constant amplitude load sequence, Collipriest uses a hyperbolic tangential function [9].

$$\log \frac{da}{dN} = C_1 + C_2 \tan h^{-1} [\phi (Keff)] \tag{2.7}$$

The material parameters C_1 and C_2 are likewise to be determined in crack propagation tests under constant amplitude load. For the independent variable K_{eff}, Collipriest uses the stress intensity factor range ΔK.

$$\phi (K_{eff}) = \phi (\Delta K) \tag{2.8}$$

– Davies and Feddersen's calculation formula

Davies and Feddersen [10] extend Collipriest's formula by

$$\varphi (K_{eff}) = \frac{\log (K_c \cdot K_o / K_{eff}^2)}{\log (K_o / K_c)} \tag{2.9}$$

For K_{eff}, Walker's formula is used.

$$K_{eff} = (1 - R)^{m_w} K_{max} \tag{2.10}$$

The methods just cited only represent a small section of the numerous methods known from the literature. It is intended, through this systematic selection from the best-known calculation methods, to illustrate the individual stages of development. The aim of all the formulae, beginning with the Paris formula, is to express the correlation between the crack propagation rate and the stress intensity as precisely as possible.

To achieve this the stress ratio R, the fracture toughness K_c and finally the threshold value K_{th} were included in the calculation formulae.

7.2.1.2 Valuation of the Forman equation with the aid of crack propagation tests under constant amplitude load

Present-day practice often uses the Forman equation to show the correlation between da/dN and ΔK.
The Forman equation has yielded fairly good results, at least in the range $R > 0$, for the aluminium, titanium and steel alloys commonly used in aircraft construction [12].

Fig. 2.1 shows a comparison between test results and the calculation after Forman. For the calculation, average Forman parameters were determined from the test results, and then the individual crack propagation test were calculated with these average C, n values. The test values were from [13].

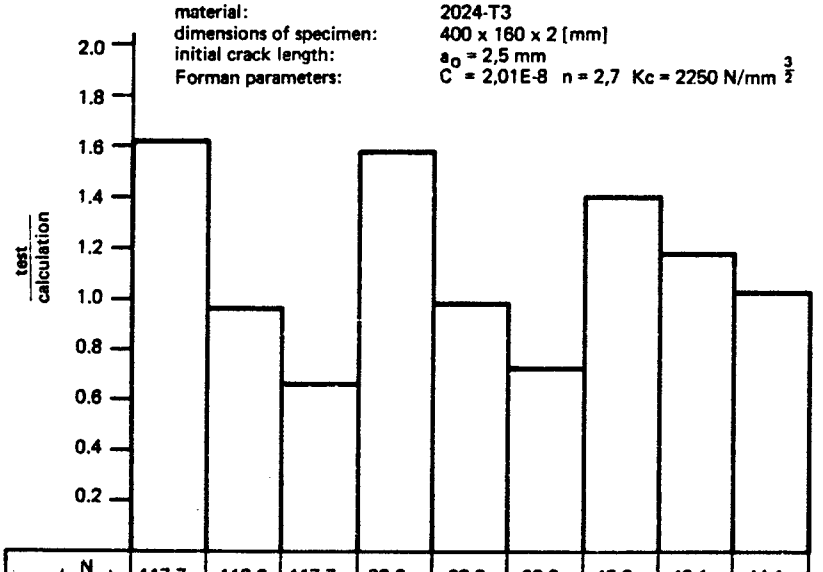

σ_m ($\frac{N}{mm^2}$)	117.7	118.2	117.7	88.3	88.2	88.2	45.2	46.1	44.1
R	0.65	0.5	0.29	0.56	0.38	0.16	0.29	0.19	0.05

Fig. 2.1 Calculation of crack propagation tests under constant amplitude load after Forman, using average C, n values

However, when comparing crack propagation tests under constant amplitude load in the range $R < 0$ with the calculation of crack propagation after Forman, major divergences may occur [12] if the calculation is made with those Forman parameters which were determined for $R > 0$.

The magnitude of the divergence between the test and the calculation in the $R < 0$ range depends not only on the stress ratio but also on the range of stress $\Delta\sigma$, i.e. the crack propagation life decreases from $R = 0$ to $R = -1$ in proportion to the increase of $\Delta\sigma$.

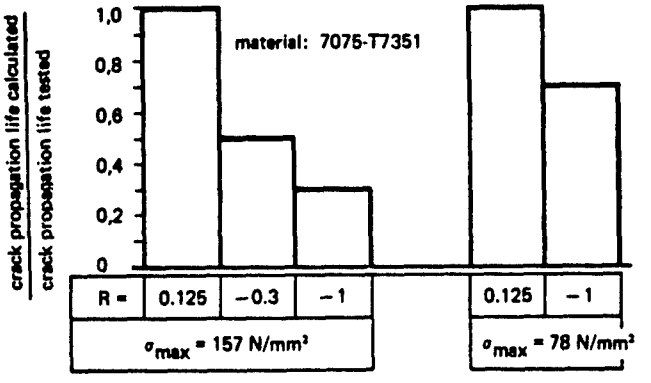

Fig. 2.2 Decrease of crack propagation life from $R = 0.125$ to $R < 0$ at various stresses σ_{max}/12/

As a general rule, though, it may be said that the Forman calculation always yields conservative results in the $R < 0$ range. Appropriate Forman parameters determined at $R < 0$ may yield a more reliable statement.

7.2.1.3 Influence of additional factors on the prediction of crack propagation life

The accuracy of the crack propagation calculation does not only depend on the method of calculation but also on the necessary input data such as material characteristics and stress intensity, not to mention the environmental conditions. This applies in particular to the calculation of components. It is well-known that the crack propagation behaviour of any given material depends not only on ΔK and R but also on the thickness of the specimen or component.

- Material thickness

  Particularly when calculating crack propagation for structural components it is found again and again that the appropriate crack propagation parameters are not available for every thickness of component material. The usual resort is to take the crack propagation parameters of specimens which are thicker than the component to be calculated. In the reverse case, the comoutation may be as much as factor 2 on the unsafe side.

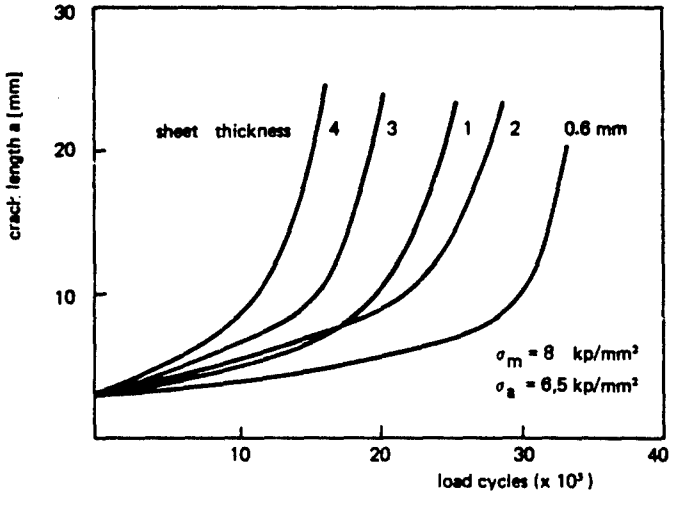

Fig. 2.3 Influence of specimen thickness on crack propagation in 2024-T3 /1/

– Fracture toughness dependent on the component

In addition to the crack propagation parameters, various calculation procedures use the fracture toughness Kc or K_{1c}. However, as tests have shown [14 , 15], the fracture toughness Kc depends not only on the thickness of the material but also on the width of the specimen and the length of the crack if elasto-plastic material behaviour is present (see fig. 2.4).

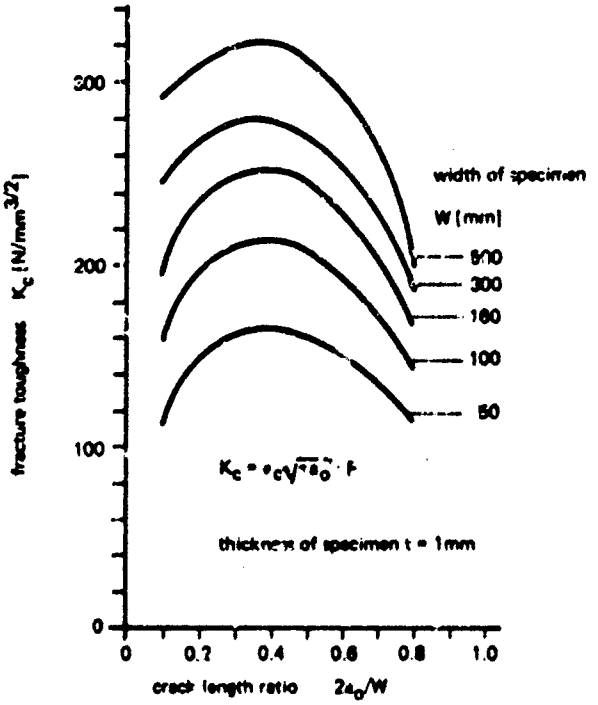

Fig. 2.4 Influence of crack length and specimen width on the fracture toughness Kc of Al 7475-T761 /14/

This may cause difficulties in calculating the crack propagation after Forman, since the parameters C and n always hold good in conjunction with the Kc value derived from the residual strength of the test specimen.

If C and n, which were determined from a crack propagation test under a constant amplitude load with a particular test specimen were to be used in calculating the crack propagation in components of a different size, it would falsify the calculation if the C and n values were used in connection with the Kc value for that particular case.

It would be possible to avoid this problem by calculating the crack propagation and the critical crack length independently of each other i.e. the critical crack length would first be found, then the crack propagation up to this critical length would be worked out. The crack propagation might for instance be determined after Walker or Forman, in the latter case using C, n values which have already been determined in connection with a Kc value which was as high as possible (large test specimen).

It can be seen from fig. 2.5 that the crack propagation rate is merely a function of the stress intensity. Not until it reaches the range of the critical crack length does the crack propagation rate in smaller specimens increase more rapidly. This range is virtually insignificant as regards crack propagation life.

– Environmental conditions

Crack propagation can be considerably influenced by environmental conditions such as temperature, humidity, corrosive agents and load frequency. Temperature increases can accelerate crack propagation, whilst lower temperatures appear to improve the crack propagation behaviour [17].

The following diagram, fig. 2.6, shows the influence of temperature on the crack propagation in 2024 T3 as a function of the load frequency.

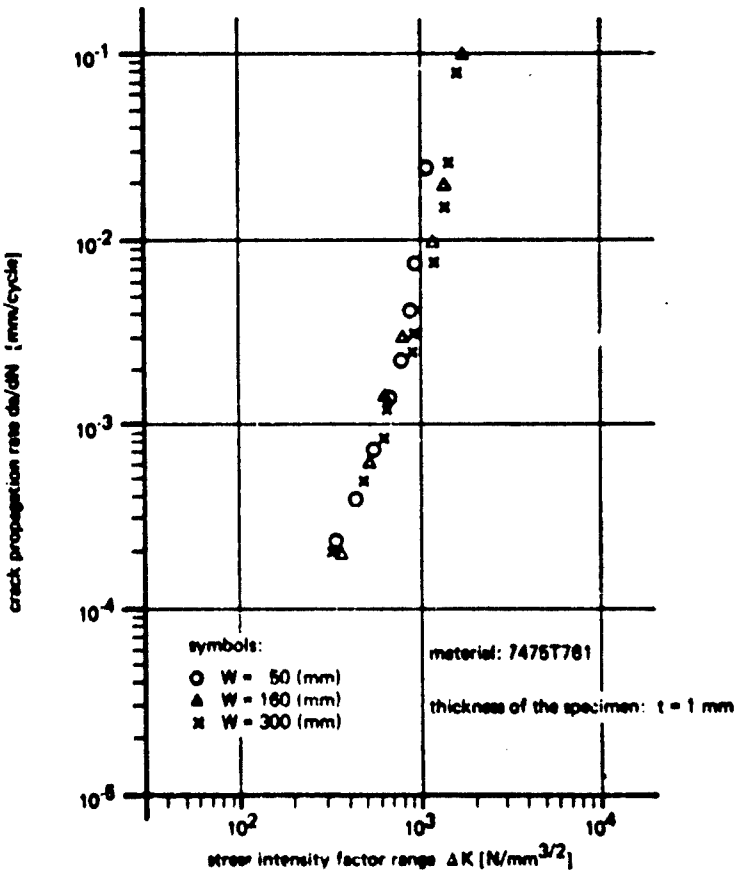

Fig. 2.5 Influence of the specimen width on the crack propagation behaviour in a 1.0 mm thick centre crack specimen

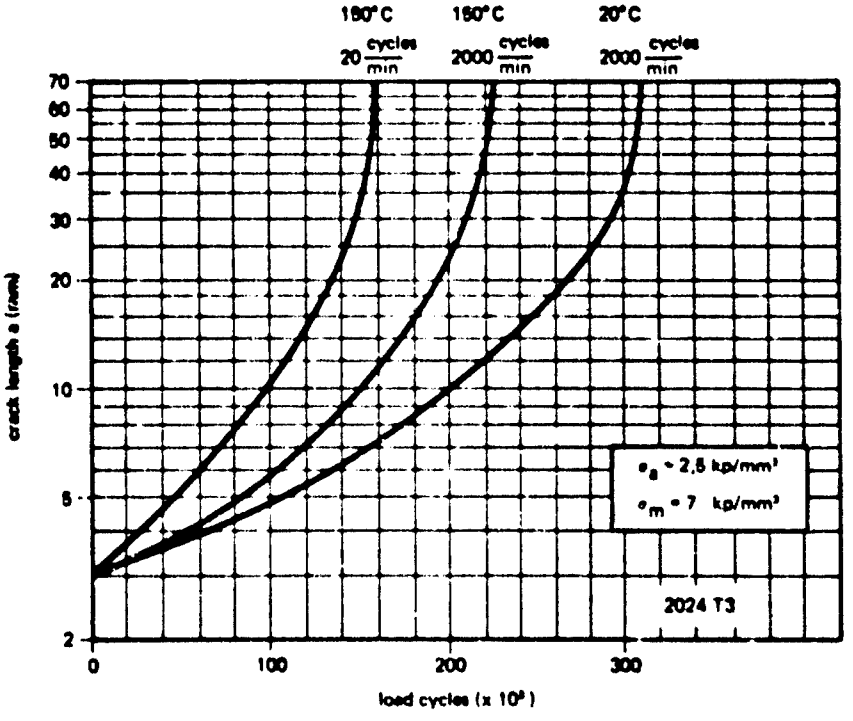

Fig. 2.6 Influence of temperature and frequency on the crack propagation in 2024-T3

Further investigations show that the influence of environmental factors such as temperature, humidity and corrosive agents on the propagation of cracks depends to a considerable extent on the load frequency. It can be generally noted that as load frequency increases, crack propagation becomes less dependent on environmental conditions [18].

Fig. 2.7 shows the influence of various environmental conditions on the crack propagation at various load frequencies.

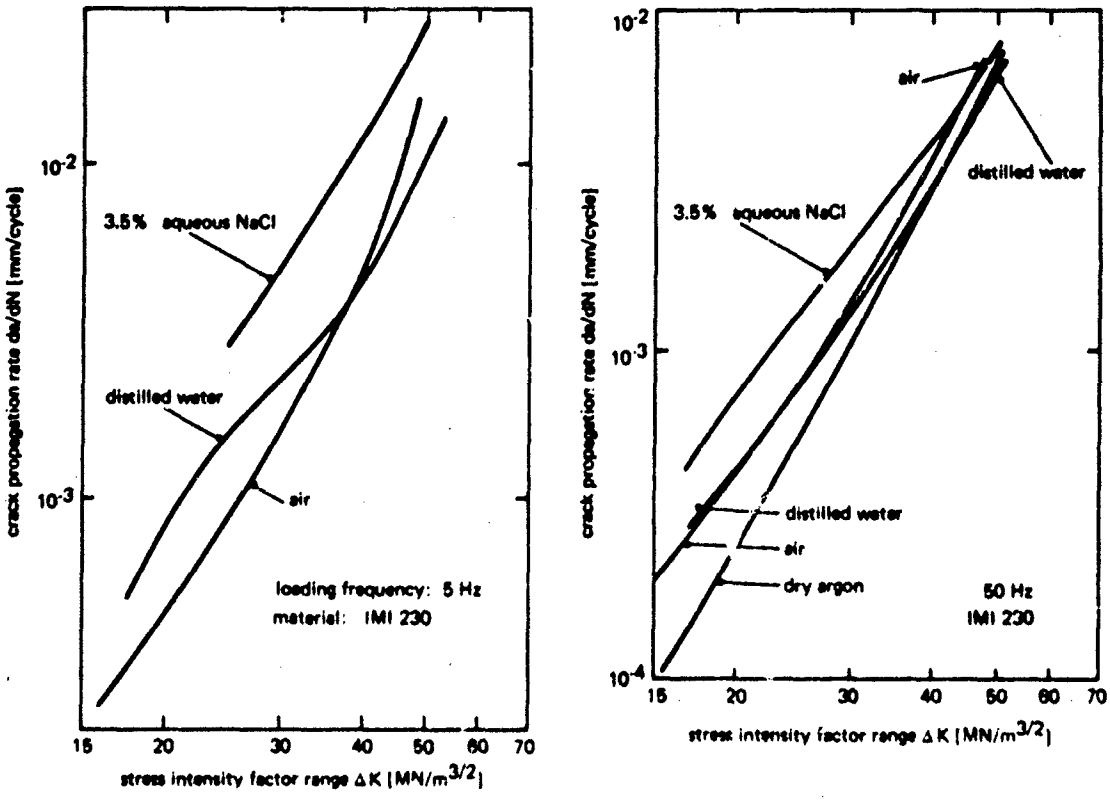

Fig. 2.7 Crack propagation behaviour under differing environmental conditions at various load frequencies /18/

Influences of this kind can be covered either by determining the crack propagation parameters under the respective environmental conditions or by taking the influence of environmental conditions into account by means of an adequate safety factor.

- Production process

A further influence on crack propagation behaviour can stem from the stretching, drawing and bending of semi-finished products during the production process. The extent to which this causes an improvement or deterioration of crack propagation behaviour certainly depends on the material, its heat treatment and shaping conditions.

To give an example, the crack propagation behaviour of 2024 sheet metal is improved by 1 – 3% stretching [19]. Further stretching, however, may result in accelerated crack propagation [19]. MBB tests (unpublished) showed the same result. In this case, 3% and 6% stretching of 2024 T3 caused acceleration of the crack propagation. In sheets made of 7475 T 761 alloy, though the effect of 3% and 6% stretching was only very slight.

- Stress intensity or correcting function for components

One of the main factors in calculating the crack propagation and residual strength is the stress intensity. Those who analyse structural components are continually confronted with the problem of finding a suitable stress intensity solution for the geometry of the component. In general, already known stress intensity solutions are then used [2], [3]. Nevertheless, it will seldom be possible to find a solution which corresponds exactly to the conditions actually inherent in the component such as its geometry, rigidity and load transfer. The component almost always has to be idealised to a greater or lesser extent. If a suitable stress intensity solution for a given case is not available in the literature, it will have to be determined specially. There are a number of possible procedures for doing so, which have been enumerated in ref. [16] in connection with the lug problem and their applications discussed.

Basically there are analytical, numerical and experimental procedures available for determining the stress intensity. In practice, however the analytical procedures are unimportant, since the marginal conditions in structural components are far too complex. Analytical procedures can therefore only be used for cases such as a plate of infinite size with a centre crack or an infinite plate with a crack starting from a hole.

For more complex components, the stress intensity can be determined numerically, for instance by the finite element method, or experimentally by crack propagation or compliance measurements [16].

There is no single correct answer as to which of the various methods is best suited for determining the stress intensity. The selection of a suitable procedure is generally decided by two criteria, namely the type of component and the technical possibilities.

The preceding explanations have shown the various parameters such as

- material (heat-treatment, manufacturing process, component thickness and size)
- $\Delta\sigma$, R
- Kc, K_{th}
- K (geometry of component and crack, load introduction)
- environment (temperature, humidity, corrosive agents)

effect the propagation of cracks.

The calculation procedure used is thus only one of several factors which may effect the accuracy of a prediction as to crack propagation life.

The use of a more complex calculation equation, which usually requires additional tests, does not necessarily bring about a corresponding improvement in the forecast of crack propagation life. The important thing is to take account of all influencing factors equally.

7.2.2 Difficulties in predicting the crack propagation under variable loads

The prediction of crack propagation in real structures is often additionally complicated by the multistep amplitude load sequence. It has been shown in a series of tests [20 ; 21] that crack propagation following peak loads can be considerably retarded. There are two ways of defining the term "retardation".

Retardation relative to the crack propagation Δa:
A smaller load following a peak load causes less crack propagation than does a constant amplitude load sequence.

Retardation relative to the load cycle number.
After a peak load, considerably more load cycles are needed to reach a given crack length than under a constant amplitude load sequence.

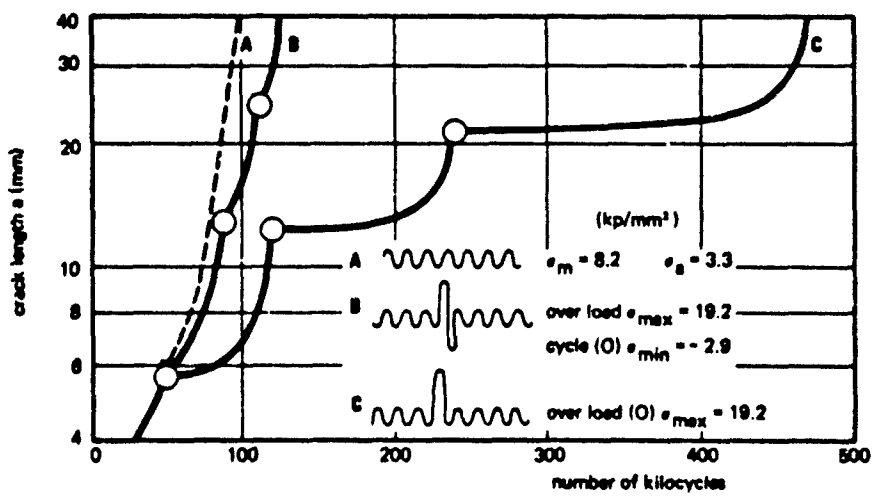

Fig. 2.8 Retardation through peak loads in 2024-T3 /1/

As can be seen from fig. 2.8, the retardation is considerably lessened by a compression load succeeding the peak load.

In the crack propagation calculation models which take account of retardation, such as the Wheeler and Willenborg models (see section 7.3.1), the retardation mechanism is only considered within the plastic zone situated in front of the crack tip. According to this procedure a large plastic zone is created by means of an overload. When the load is removed, a compressive stress is set up in the area of the plastic zone. This compressive stress is the main contributing factor in reducing the crack propagation under a smaller succeeding load cycle. Various tests, as for instance in ref. [22], have in fact shown that the retardation due to an overload may even be effective after the crack tip has already extended beyond the plastic zone created by the overload. Recent findings on this matter will be discussed at greater length in section 7.3.2.

Flight-by-flight crack propagation tests have shown that the retardation magnitude mainly depends on the following parameters [12]:

material
type of load spectrum
stress level
stress distribution

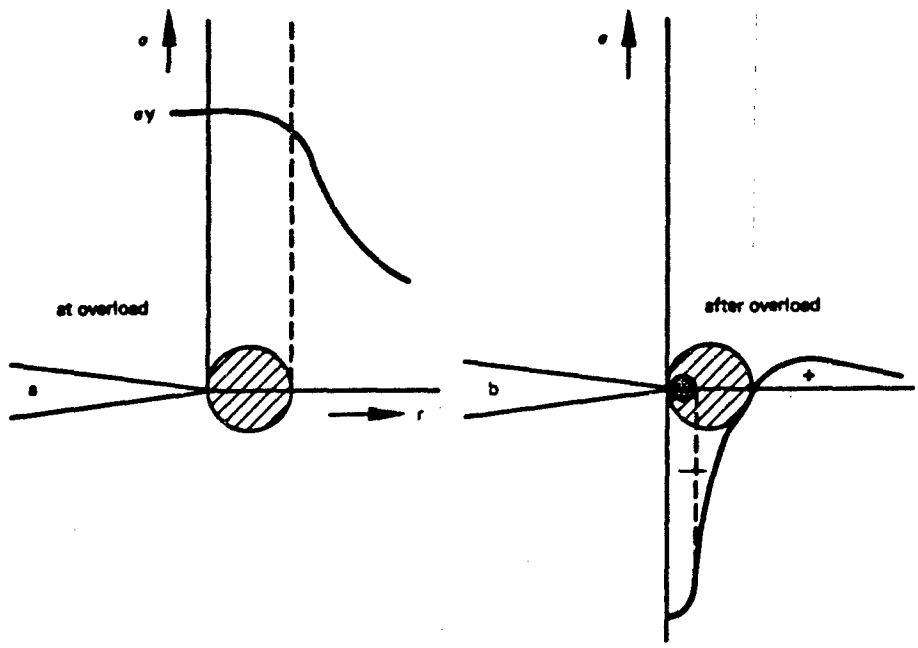

Fig. 2.9 Inherent stress at the crack tip following an overload

If the retardation is defined as

$$V = \frac{\text{crack propagation life found in test}}{\text{crack propagation life after Forman}}$$

the following retardation values for aeronautical materials are found, taking a typical fighter spectrum as a basis and a critical crack length of 2,5 mm.

material	$\bar{\sigma}_o$ (N/mm²)	σ_B (N/mm²)	$\bar{\sigma}_o/\sigma_B$	V	ref.
7075-T7351	136	463	0.42	3.4	/23/
300M	373	2102	0.18	4.16	/12/
HP 9-4-30	686	1579	0.43	4.68	/12/
Ti6Al4V	373	995	0.37	5.4	/23/
7075-T7351	273	463	0.59	1.9	/23/
Ti6Al4V	549	995	0.55	4.83	/23/

Table 2.1 Retardation effects of various materials

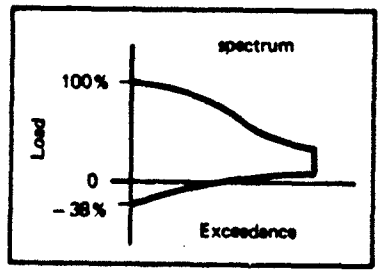

Fig. 2.10 Typical fighter spectrum

The values obtained for the aluminium and titanium alloys show that, at least for these two materials, the retardation decreases as the maximum spectrum load increases.

It can also be seen from the above table that the various materials display a different retardation rate at the same relative load δ_o / σ_B.

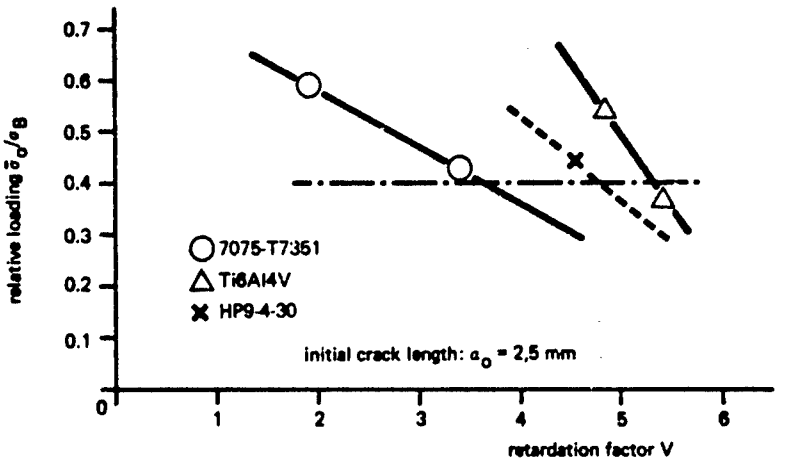

Fig. 2.11 Retardation effect of different materials as a function of the relative load

In fig. 2.11, the relative load σ_o / σ_B, which is roughly comparable for the materials 7075 T 7351, Ti 6Al4V and HP-9-4-30, is plotted vs. retardation V.

At a medium relative load of σ_o / σ_B = 0.4, the retardation in 7075 T 7351, HP-9-4-30 and Ti 6Al4V in that order, increases. Ti 6Al4V would then display a retardation 1.47 times as great as that of 7075 T 7351, which shows that the effect depends on the material.

The retardation V decreases in proportion not only to increases in maximum spectrum load but also to an increased initial crack length. This is illustrated in fig. 2.12 below.

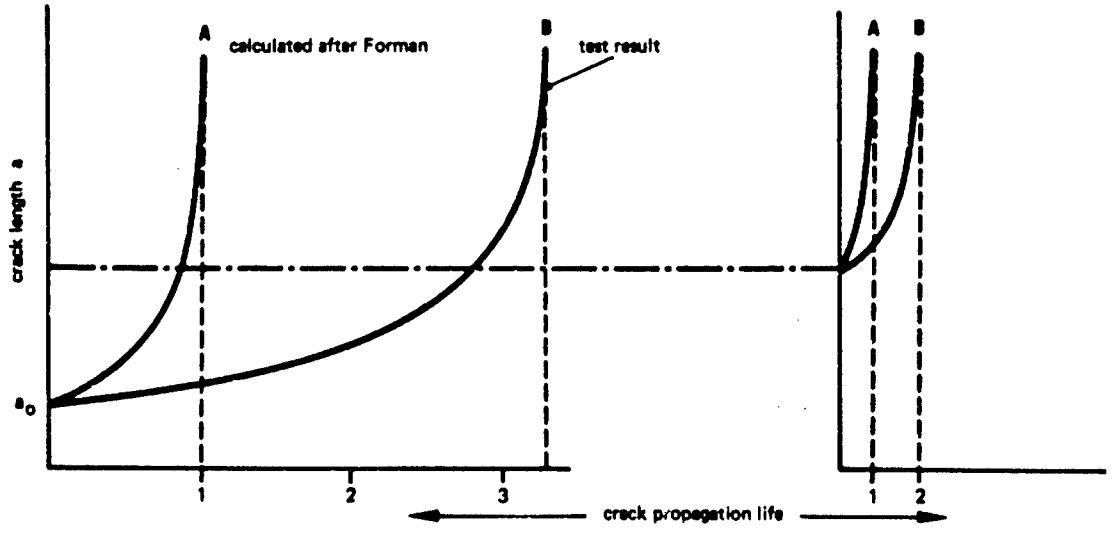

Fig. 2.12 Influence of initial crack length on retardation

Fig. 2.12 shows typical flight-by-flight crack propagation curves, first calculated after Forman and then determined experimentally.

From the shape of the two curves it can be concluded that most of the retardation occurs where the cracks are not very long. If, then, the retardation is dependent upon the load and the crack length in such a way that retardation is lessened as stress and crack length increase, it springs to mind that the retardation depends on the stress intensity. Retardation factors found in plates with a centre crack thus cannot unreservedly be taken to apply to components with a completely different stress intensity.

However, the retardation effect for any given material depends to a large extent on the type of load spectrum and also, to some extent, on the type of load sequence.

To find the influence of the load sequence, flight-by-flight crack propagation tests were carried out in [23] under various load sequences, using a typical combat aircraft spectrum.

spectrum	number of steps	flights and load cycles per period	number of different flights	load sequence
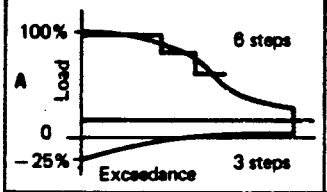	9	200 flights 14026 load cycle	15	defined flight by flight load sequence with gag (ground air ground) cycle (normal flight by flight program)
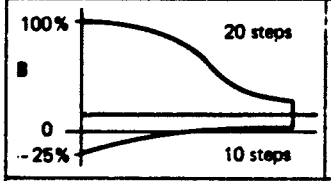	30	400 flights 28.052 load cycle	400	quasi randomisad (I) flight by flight load sequence with gag cycle
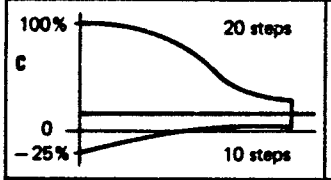	30	400 flights 28.032 load cycle	400	randomised (II) flight by flight load sequence with gag cycle
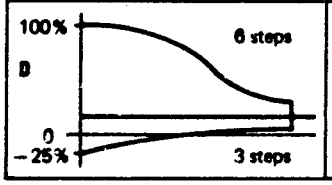	9	400 flights 28.052 load cycle	–	blocked program with gag cycle

Fig. 2.13 Various load sequences used in flight-by-flight crack propagation tests /23/

The next diagram, fig. 2.14, shows the average crack propagation curves for different load sequences. Basically, fig. 2.14 shows that, as far as crack propagation life is concerned, randomised load sequences may be twice as damaging as blocked load sequences as shown in fig. 2.13. This finding is particularly significant for the experimental damage tolerance qualification test.

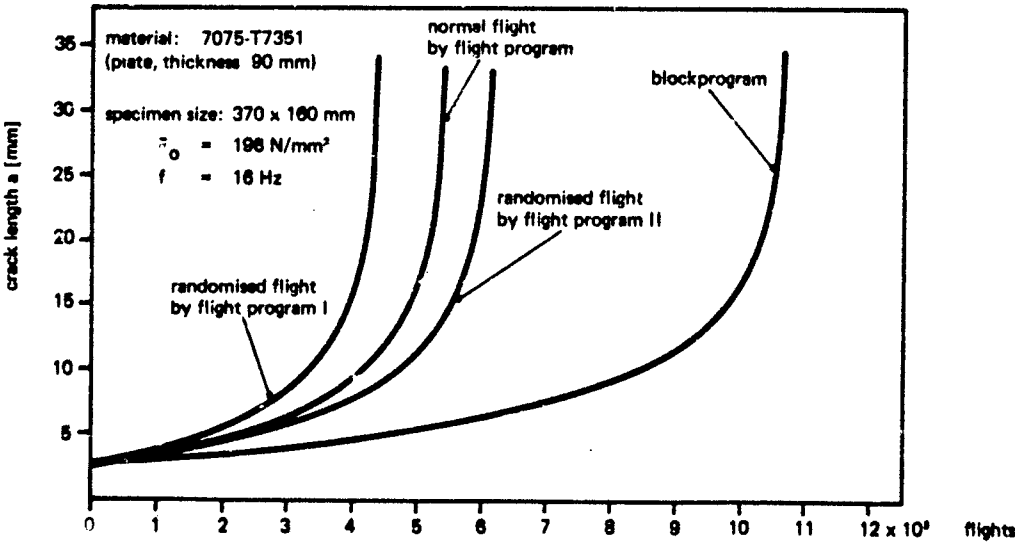

Fig. 2.14 Influence of load sequence on crack propagation /12/

The retardation effect, and with it the crack propagation life, can decrease considerably if the peak loads of a spectrum are truncated. Cutting the peak loads of a typical combat aircraft n_z spectrum down to about 57.5% of the load limit may lead in Ti 6Al4V to a decrease of crack propagation life, and thus of the retardation effect, by a factor of 2 [12].

The influence of truncation on the retardation effect depends of course on the type of load spectrum. Schijve [24], for instance, showed that in a gust spectrum, truncation of the peak loads by only 16% in 2024 and 7075 brings about a reduction of the retardation effect by approximately a factor of 2. Flight-by-flight crack propagation tests carried out on a particular spectrum chosen to meet certain requirements display a retardation effect which it may not be possible to achieve again during flight if for instance the originally-assumed high operating loads do not occur.

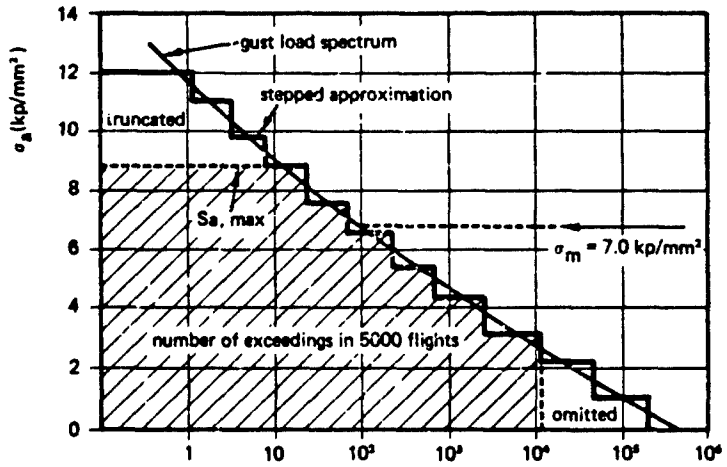

Fig. 2.15 Gust spectrum /24/

The retardation effect may also be considerably reduced due to compression loads. Using a typical taileron spectrum of a combat aircraft, it was possible to show that in 7075T7351 aluminium alloy, by dropping the compression loads, the crack propagation life was increased by a factor of 2.7 [12].

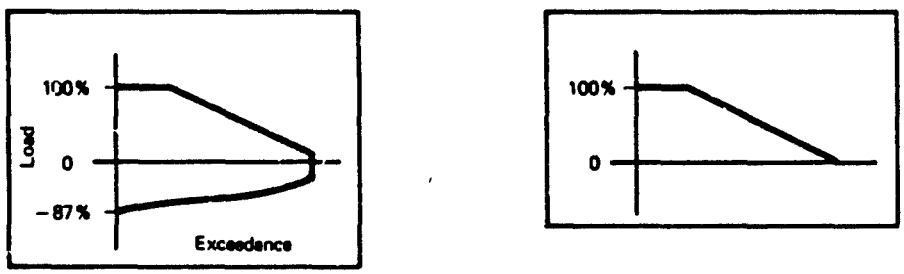

Fig. 2.16 Taileron spectrum with and without compression loads

7.3 METHODS OF CALCULATING THE CRACK PROPAGATION UNDER VARIABLE LOAD SEQUENCE

7.3.1 Description of current models

Although the Forman equation was only developed for calculating the crack propagation under constant amplitude load, it is nevertheless frequently used for working out the crack propagation under flight-by-flight load sequences. This means that retardation effects are not normally considered in flight-by-flight crack propagation.

$$da/dN = \frac{C\,\Delta K^n}{(1-R)\,Kc - \Delta K} \qquad (3.1)$$

As already mentioned under 2.1, the Forman characteristics C, n and Kc are determined from crack propagation tests under constant amplitude load in the R > 0 range. The correcting function F used in

$$\Delta K = \Delta\sigma \sqrt{\pi a} \cdot F \qquad (3.2)$$

is to be taken from solutions suitable for the component to be calculated and usually already existing in the literature.

The crack growth Δa per load cycle is usually calculated in steps corresponding to flight-by-flight conditions. The calculation can only be made with the aid of a computer.

Since the Forman equation does not consider retardation effects, the load sequence can be disregarded. It is thereby possible to combine the individual load levels to obtain a blocked spectrum (see fig. 3.1).

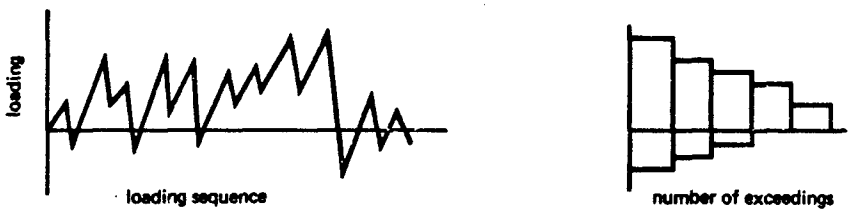

Fig. 3.1 Load sequence with blocked spectrum

For doing this, an approximation solution in the form of a numerical integration of the Forman equation was developed in [25]. This procedure is based on the following considerations.

By first considering the crack propagation under constant amplitude load, the number of load cycles between an initial crack length a_o and the critical crack length a_c can be found from the following integral.

$$N_c = \int_{N_o}^{N_c} dN = \int_{a_o}^{a_c} \frac{(1-R)\,Kc - \Delta K}{C\,\Delta K^n}\, d_a \qquad (3.3)$$

Due to the often complex correcting function F, which accounts for crack geometry, boundary effects and loading conditions, there is no analytical solution to the integral. However, instead of calculating the crack propagation for every load cycle, the function can be numerically integrated by an approximation procedure (Simpson's rule).

$$f(a) = \frac{(1-R)\,Kc - \Delta K}{C\,\Delta K^n}$$

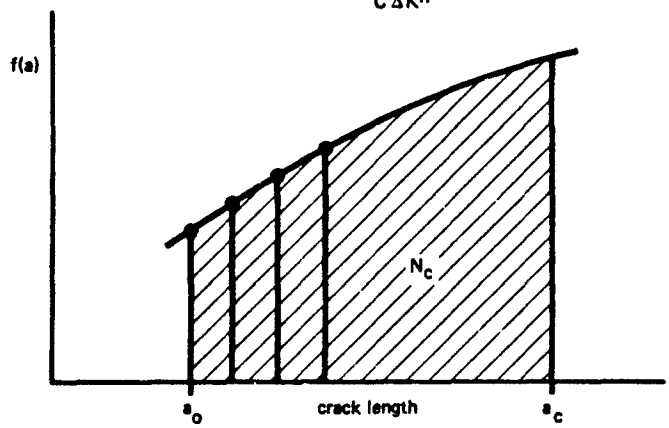

Fig. 3.2 Numerical integration of the Forman equation with the aid of the Simpson's rule (2nd-degree polynomial)

The area under the function f between a_o and a_c corresponds to the load cycle number until fracture. With about 20 integration steps, the deviation is usually approximately 1 – 2%.

If the computer time has hitherto been approximately proportional to the number N of load cycles, then – independently of N – only the computer time required to perform 20 integration steps is necessary.

Incidentally, it is noted that, using this method, crack propagation under constant amplitude load can be computed with a pocket calculator (e.g. HP67) with any correcting function. However, to deal with multi-step amplitude load sequences in the same way, a procedure was developed in [25] for determining a substitute load cycle instead of the blocked spectrum. With the aid of this substitute load cycle which causes the same extent of damage it is possible to treat the life calculation like that of the crack propagation under constant amplitude load. This can considerably reduce the cost of computation, particularly in working out the crack propagation in aircraft structures. The errors arising in this approximation are less than 5%.

Special calculation methods were developed for the multi-step load sequence to make provision for the crack propagation retardation. The methods which are best-known in the literature are those developed by Willenborg [26] and Wheeler [27].

The principle of these two procedures is described below.

The method developed by Willenborg could almost be termed a model, since no additional values of fracture mechanics are required in order to calculate the crack propagation with retardation. One of the known formulae

$$da/dN = f(\Delta K)$$

can be used as a basis for Willenborg's retardation model. In the following, the Willenborg model will be considered in conjunction with the Forman equation. If, using the Willenborg model, retardation occurs, then the stress intensity factor range ΔK and the stress ratio R are replaced in the Forman equation by what are known as effective values.

without retardation

$$da/dN = \frac{C\,\Delta K^n}{(1-R)\,Kc - \Delta K}$$

with retardation

$$da/dN = \frac{C\,\Delta K_{eff}^n}{(1-R_{eff})\,Kc - \Delta K_{eff}}$$

The effective values are determined by the following scheme. If, during a multi-step load sequence, a peak load causing σ_1 occurs, the already existing crack a_0 is extended to a_1. At the same time, in front of the crack tip of a_1, a plastic zone Ry of the size

$$Ry = a_{p1} - a_1 \tag{3.4}$$

is created.
The size of the plastic zone depends on the stress intensity K and the yield stress of the material.

The value obtained from [28] for the spectrum of plane stress is

$$Ry = \left(\frac{K}{\sigma_y}\right)^2 \cdot \frac{1}{2\pi} \tag{3.5}$$

and from [29] for the spectrum of plane strain is

$$Ry = \left(\frac{K}{\sigma_y}\right)^2 \cdot \frac{1}{4\sqrt{2\pi}} \tag{3.6}$$

For the subsequent load cycle causing σ_2, it should first be ascertained whether $\sigma_2 < \sigma_1$ is applicable. If not, the crack propagation is calculated without retardation after Forman

Otherwise (see fig. 3.3) the stress σ_{ap} necessary to obtain a plastic zone of the size $Ry = a_{p1} - a_1$ is calculated.

The stress σ_{ap} is determined with the aid of the equations 3.4 and 3.5.

$$\sigma_{ap} = \sigma_y \sqrt{\frac{2\,(a_p - a_1)}{a_1}} \tag{3.7}$$

The difference between σ_{ap} and σ_2 yields a stress σ_{red}, which is used to establish the effective values. No physical explanation for the derivation of σ_{red} is known.

$$\sigma_{red} = \sigma_{ap} - \sigma_2 \tag{3.8}$$

σ_{red} is made equivalent to zero, if $\sigma_2 > \sigma_{ap}$.

$$\left.\begin{aligned} \sigma_{o_2\,eff} &= \sigma_{o_2} - \sigma_{red} \\ \sigma_{u_2\,eff} &= \sigma_{u_2} - \sigma_{red} \end{aligned}\right\} \quad \sigma_{eff} > 0 \tag{3.9}$$

It follows that

$$\Delta K_{eff} = (\sigma_{o\,eff} - \sigma_{u\,eff})\sqrt{\pi a} \cdot F \tag{3.10}$$

$$R_{eff} = \sigma_{u\,eff} / \sigma_{o\,eff} \tag{3.11}$$

Complete crack stoppage is achieved when

$$\sigma_{o_2\,eff} = 0 \tag{3.12}$$

This is the case for

$$\sigma_{o_2} = \sigma_{red} \tag{3.13}$$

By inserting equation 3.13 in 3.8, the correlation between σ_{ap} and σ_2 is expressed as $\sigma_{ap}/2 = \sigma_2$. Since σ_{ap} is identical to σ_1, crack stoppage usually occurs when the stress following a peak load is only half as great.

If a further load causing σ_3 ensues, it is again checked whether the condition $\sigma_3 < \sigma_1$ is fulfilled. This presupposes. though, that retardation occurred in the case of σ_2.

If σ_2 was greater than σ_1, σ_2 replaces σ_1 as peak load for further crack propagation. We are assuming, however, that crack propagation was retarded in the case of σ_2. After load cycle σ_2, there is a crack length of a_2. Now the effective values are calculated once again with equations 3.4 – 3.11, crack length a_1 being replaced by a_2 and σ_2 by σ_3. This procedure will be terminated if the succeeding loads causing σ_i are less than σ_1, even where

$$a_{i-1} + Ry_i > a_p \tag{3.14}$$

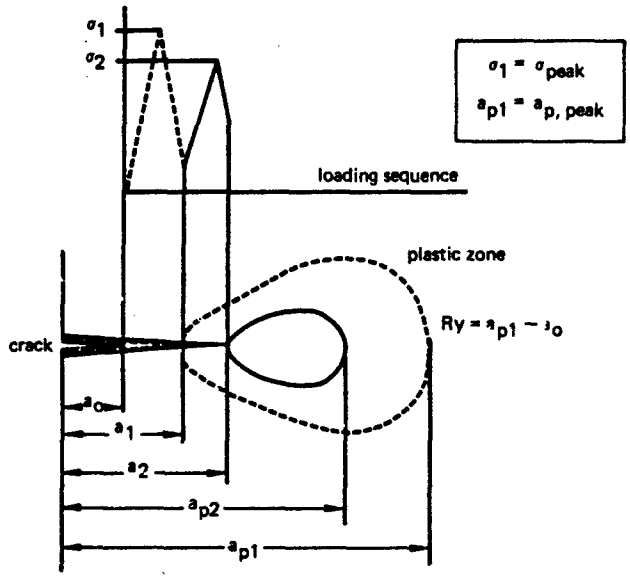

Fig. 3.3 Crack with plastic zone in multi-step amplitude load sequence

Wheeler and Willenborg used the same model to decide whether crack propagation will be retarded or not.

In this scheme, retardation takes place as long as the crack a with its accompanying plastic zone remains within the plastic zone created by the peak load (outer limit = ap).

The difference between the two procedures is that Willenborg takes account of the retardation effect by reducing the stress $\sigma \longrightarrow \sigma_{eff}$ whilst Wheeler takes account of the retardation effect by direct reduction of the crack propagation using a retardation function. Secondly, Wheeler requires an additional material value, which has to be determined through a multi-step test.

Like Willenborg, the Wheeler method is also based on a crack propagation law of the formula

$$da/dN = f(\Delta K).$$

Wheeler will be considered below in conjunction with the Forman equation.

$$da/dn = Cp \frac{C \Delta K^n}{(1 - R) Kc - \Delta K} \tag{3.15}$$

To determine the crack growth per load cycle, the factor Cp is inserted:

$$Cp = \left(\frac{Ry}{a_p - a}\right)^m \tag{3.16}$$

The crack growth is retarded if $Cp < 1$, i.e. $a + Ry < a_p$. However, as soon as $a + Ry > a_p$, then $Cp = 1$.

According to Wheeler, the exponent is to be a material constant determined in a multi-step experiment.

m is therefore fixed so that there is conformity between the crack propagation calculation after Wheeler and the crack propagation test under multi-step amplitude load sequence.

Less well-known in the literature is a retardation procedure proposed by Habibie [30], which is designed in particular to provide for truncation effects.

This method is likewise based on the Forman equation. The crack growth is reduced, as in the Wheeler method, by a retardation function which is determined by means of a multi-step crack propagation test.

$$da/dN = \varphi \frac{C \Delta K^n}{(1-R) Kc - \Delta K} \tag{3.17}$$

$$\varphi = a K^{-\gamma} \quad \varphi < 1 \tag{3.18}$$

a and γ are to be established experimentally.

An additional function Λ helps to determine from load cycle to load cycle whether retardation with φ will take place or not. This criterion corresponds to the plastic zone model used by Willenborg and Wheeler; thus, retardation takes place when $a + Ry < a_p$. In practice, however, the method developed by Habibie is of no great significance.

7.3.2 Future approaches

The above described methods of calculating the crack propagation under operating loads, which have been in practical use for many years, deal mainly with retardation effects which are caused by overloads and are confined to the region of the plastic zone in front of the crack tip.

On the other hand, crack propagation acceleration and the influence of compression loads have not been satisfactorily taken into account.

One promising way of correcting these inadequacies would be by considering the material behaviour, mainly in the wake of the moving crack.

A recognised precursor of this approach was Elber, with his crack closure concept. Elber [31] was one of the first to attempt to describe, with the aid of a physical model, the connection between load sequence, plastic deformation (by way of crack closure) and crack extension.

The experiments carried out by Elber on 2024T3 sheet metal have shown that crack closure still occurs under tensile stress.

Elber assumed that the closure of cracks under tensile stress could be attributed to the deformation of the crack plane remaining behind the crack tip, and that crack expansion cannot take place under cyclic loads until the crack is opened. In this case it is not the entire stress intensity area ΔK which affects crack propagation, as assumed in all the crack propagation calculation methods described hitherto, but a value ΔK_{eff} reduced by the crack opening tension or stress intensity

$$\Delta K_{eff} = (\sigma_{max} - \sigma_{op}) \sqrt{\pi a} \cdot F \tag{3.19}$$

Elber was able to show by experiment that the effective stress intensity, or the non-dimensional quantity U

$$U = \frac{\Delta K_{eff}}{\Delta K} \qquad \frac{\sigma_{max} - \sigma_{op}}{\sigma_{max} - \sigma_{min}} \tag{3.20}$$

in 2024T3 is mainly dependent on the stress ratio R.

The function $U = f(R)$ can be represented for 2024T3 by a linear equation

$$U = 0.5 + 0.4\,R \quad -0.1 < R < 0.7 \tag{3.21}$$

To calculate the crack propagation under constant amplitude loads, taking into account the crack closure concept, Elber proposes the following formula:

$$da/dN = C (U \Delta K)^n \tag{3.22}$$

C and n are material characteristics which can be determined by a crack propagation test under constant amplitude load for a given value U. The crack opening stress, or U as a function of R, is measured by Elber immediately behind the crack tip with the aid of a crack opening displacement gauge. Fig. 3.5 shows the positioning of the COD gauge and the relationship between applied stress and displacement.

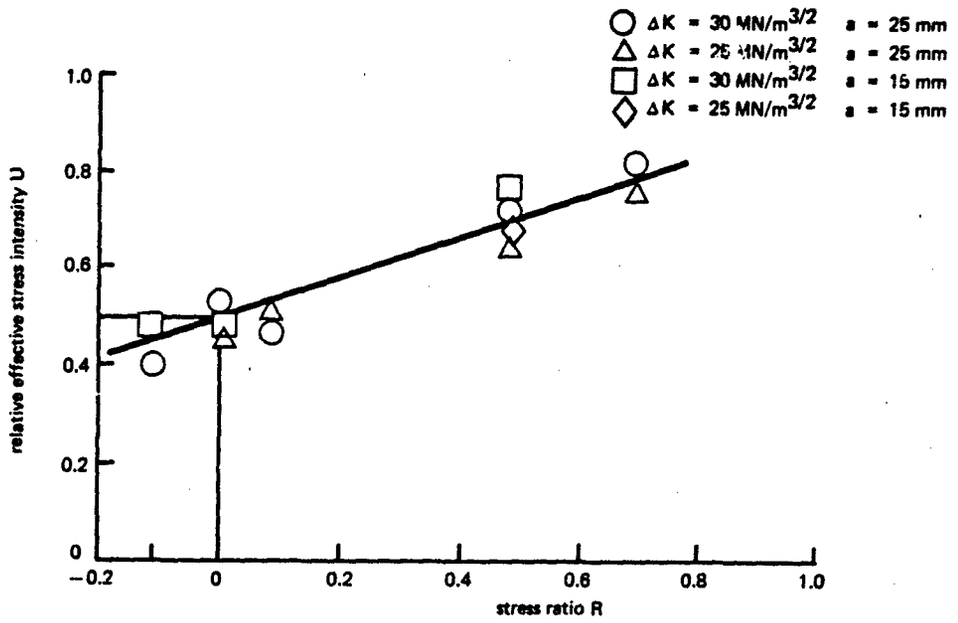

Fig. 3.4 Relationship between effective stress range ratio and stress ratio for 2024-T3 aluminium alloy

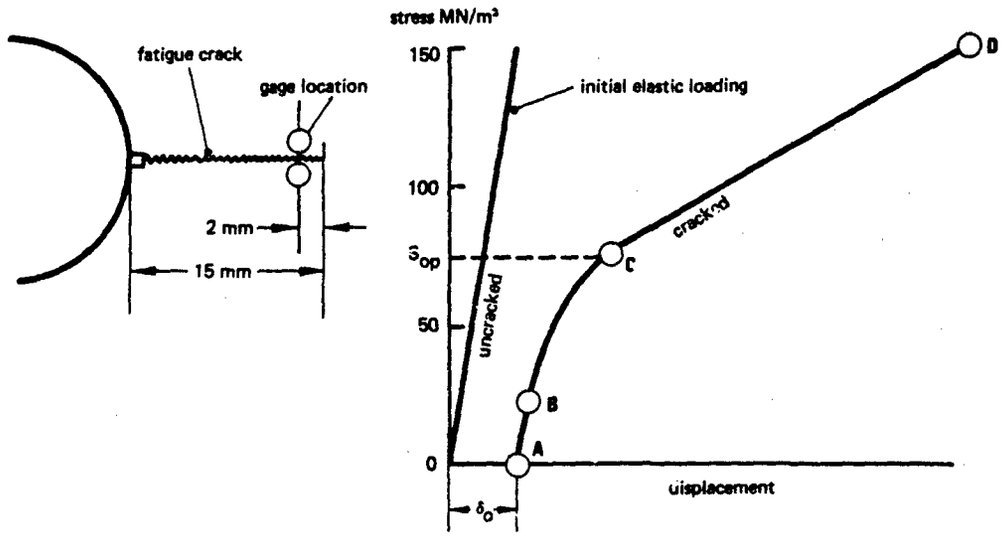

(a) crack configuration and gage location (b) applied stress – displacement relation

Fig. 3.5 Crack configuration and applied stress – displacement relationship

The stiffness of the linear range AB corresponds to that of the metal sheet which has no crack. The stiffness of the range CD is likewise linear and corresponds to that of a metal sheet with a saw-cut of the same length as the fatigue crack. In the intervening area BC, according to Elber, the crack is opened and closed. Führing [32] points out that the crack opening load normally will be underestimated following the Elber procedure.

In a comparison with the crack propagation calculation methods of Forman and Erdogan, Elber achieved a better conformity between test and calculation at various stress ratios using his crack closure concept. One of Elber's aims with the crack closure model was to provide a basic physical explanation for retardation and acceleration effects.

On the basis of Elber's crack closure concept Eidinoff and Bell [33], Führing and Seeger [34; 35], and Newman [36] all proposed methods for calculating the crack propagation under multi-step amplitude load sequence.

- Eidinoff and Bell method [33]

  The crack opening stress required for determining the effective stress intensity was established by Eidinoff and Bell not by direct measurements, like Elber, but indirectly by means of crack propagation tests under constant amplitude load and various R. According to ref. [33] the indirect determination of crack opening stress was preferred because, in the direct measurement, the scatter was too great. In applying the indirect measurement of crack opening stress, Eidinoff and Bell rely on Elber's results, according to which the crack opening stress σ_{oo} is only a function of the stress ratio R. It was further assumed in this method, for the sake of simplicity that crack opening stress and crack closure stress are identical. This calculation method also provides for two experimentally-determined functions which are intended to take into account the influence of several successive peak loads on the retardation effect on the one hand and the acceleration in transition from small to large loads on the other.

  By means of flight-by-flight crack propagation tests with typical combat aircraft spectra, Eidinoff and Bell were able to demonstrate a high degree of consistency between tests and calculation in aluminium and titanium alloys.
  Although the Eidinoff and Bell calculation procedure for multi-step amplitude load sequences, based on the crack closure concept, has come closer to practical application than any other, its general adoption would require further extensive investigations, i.e. comparison between tests and calculations. However, the expenditure involved in experimentally determining the retardation and acceleration functions has probably become, even today, a serious obstacle to the practical use of this method.

- Führing and Seeger method [34; 35]

  Whilst the previous method requires experimental determination of the crack opening stress, the Führing and Seeger method provides the possibility of calculating the crack opening stress analytically with the aid of an expanded Dugdale model [37].

  To simplify the procedure, the material behaviour is assumed to be elastic-perfectly-plastic. An important advantage of this calculation method as regards its future practical application is to be seen in that it is not necessary when considering crack propagation under multi-step amplitude load sequence to experimentally determine any additional crack propagation data. The essential input data for this calculation procedure are the da/dN curve, the yield stress and the modulus of elasticity. Here too, extensive investigations, i.e. comparisons between crack propagation tests under operating loads and calculations, must be made in order to discover how far this calculation method can be used for structural calculations. Investigations of this kind are being conducted. The corresponding computer program is based on simplified models of the crack closure concept and can describe both retardations and accelerations in crack propagation. As far as its practical application is concerned, the program being tested is considerably faster than the more accurate Dugdale method and can also be used more generally wherever random loads and various crack problems are involved.

- Newman method [36]

  In this method the crack closure and crack opening stresses are determined with the aid of a two-dimensional, non-linear calculation using the method of finite elements.

  Newman was able to achieve a high degree of consistency between numerically- and experimentally-determined crack closure behaviour in the constant and two-step amplitude block experiment.

  In the Newman calculation method, as in that of Führing and Seeger, the crack opening stress is used to determine the effective stress intensity in order to obtain a simple law of crack propagation. The Newman method also necessitates no further tests (such as those required by Eidinoff and Bell) in order to calculate the crack propagation under multi-step amplitude load sequence. As with Führing and Seeger, the material is assumed to have the elastic-perfectly-plastic behaviour. However, this method would appear unsuitable for future application because of the prohibitive computing costs involved in numerically determining the crack closure behaviour. For this method too, extensive comparisons between tests and calculations have yet to be made.

The extent to which any of the above-summarised calculation procedures will be adopted in future practice depends, in the last resort, on whether these calculation procedures offer any major advantages over traditional methods such as the Wheeler method. The decisive criteria are accuracy, computing costs and simplicity of use. As well as comprehensively examining the various calculation methods, however, it would also seem necessary to examine whether the basis they have in common, namely the crack closure concept, can be accepted as generally valid.

Although, for the purposes of developing the calculation methods, the validity of the crack closure concept was more or less taken for granted, a closer survey of the literature reveals a series of test results which, at least in part, show the crack closure concept in a more dubious light.

Shih and Wei [38], for instance, when examining Ti6Al4V by the electropotential method, discovered that crack closure does not only depend on R, as Elber found, but is also dependent on K_{max} which is in agreement with the theory [35]. In this examination, moreover, no crack closure was found for $R > 0.3$.

According to Shih and Wei, neither the influence of R on the crack propagation nor the retardation can be completely explained by crack closure.

As an example, retardation was observed even in cases where there was no crack closure. The difference between these and Elber's results lies mainly, according to Shih and Wei, in the fact that Elber did not carry out enough tests, and that those he did make were in the net section yielding range.

Bachman and Munz [39] likewise conducted crack closure measurements on samples of Ti6Al4V, using an extensometer. Unlike Shih and Wei, Bachmann and Munz were not able to discover any influence of K_{max} on crack closure behaviour, which in turn would seem to confirm Elber's results.

It was not only Bachmann and Munz, but also Schijve and Arkema [40], who showed that different environmental media may indeed have a considerable effect on the crack propagation behaviour, but not on the crack closure behaviour. Schijve and Arkema used the same measuring method as Bachmann and Munz, the tests being conducted on the 2024-T3 and 7075-T6 materials.

Irving, Robinson and Beevers [41], who conducted their examinations on α-titanium and EN24 steel using the electropotential method, observed crack closure only in vacuo but not in air. Irving et al. also assumed that crack closure is confined to low ΔK values.

Lindley and Richard [42] conducted crack closure measurements on various steels with the d.c. and a.c. resistance technique. They found that crack closure above K_{min} does not occur under plane strain, but only under plane stress conditions.

The test results of various authors cited in the foregoing display, at least superficially, a number of contradictions. It may be supposed that the contradictions stem in part from the different test methods and their accuracy of measurement.

It has evidently not yet been clearly established what influence the material, the stress condition and the surrounding medium have on crack closure.
The examinations mentioned also show that crack closure behaviour alone cannot completely explain the crack propagation in respect of mean stress retardation, acceleration and threshold.
It can be assumed, though, that crack closure is to be regarded as a significant factor in expressing these values.

7.4 ASSESSMENT OF CURRENTLY-USED CALCULATION PROCEDURES

It can be categorically stated that the calculation procedures used in practice are a long way from taking in the physical processes in the area of the crack tip. This is particularly true of inherent stresses after tensile or compressive load application and of strain hardening and softening processes within the plastic zone.
The assessment of the various calculation procedures therefore takes place mainly in the comparison between test and calculation.

7.4.1 Comparison between test and calculation

Most of the investigations known in the literature which involved a comparison between test and calculation were confined either to one material, one typical type of spectrum, or to a single crack propagation retardation procedure [26], [27], [30], [43], [44].

Ref. [23] is one of the few investigations where the crack propagation life was calculated after Forman, Willenborg, Habibie and Wheeler for different spectra and materials and was compared with flight-by-flight crack propagation tests.

The assessment of these calculation procedures therefore relies mainly on this investigation.

Fig. 4.1 shows the comparison between test and calculation using various procedures for 4 different types of spectrum in the 7075-T7351 aluminium alloy.

Spectra A to D occur as stress spectra in a combat aircraft in the following structural areas:

A: Wings and wing root area
B: Link and post of wing carry-through box in variable-sweep aircraft
C: Taileron
D: Taileron without compression loads

Fig. 4.1 shows that the life duration determined after Forman can lie on the safe side by as much as a factor of 4. Since the Forman equation does not take into account any retardation effects, the life duration calculated generally does lie on the safe side. If, however, wide fluctuations in the mean stress occur during one load sequence, the Forman calculation may also lie on the unsafe side, as is shown by the experiment with spectrum B.

It would be false to conclude that no retardation effect occurs in load sequences with a wide mean stress variation.

What should in fact be assumed is that the load sequence applied in the test is not taken into account in the same way as is the case with the crack propagation test.

For this reason the build-ups and drops of stress between marked mean stresses ought to be included as an additional load cycle in the Forman calculation.

As will be shown later, the Forman calculation is always on the safe side when the calculation is based on the overall g spectrum.

The calculation methods with retardation, such as those of Willenborg, Wheeler and Habibie may, according to the type of the spectrum, lie on the safe or the unsafe side. The Habibie retardation function and the Wheeler exponent were determined for spectrum A. When the tests were calculated with spectrum B it was shown that all retardation models were on the unsafe side, some quite considerably. This can probably be explained by the fact that the additional load cycles between the various mean stress levels were disregarded.

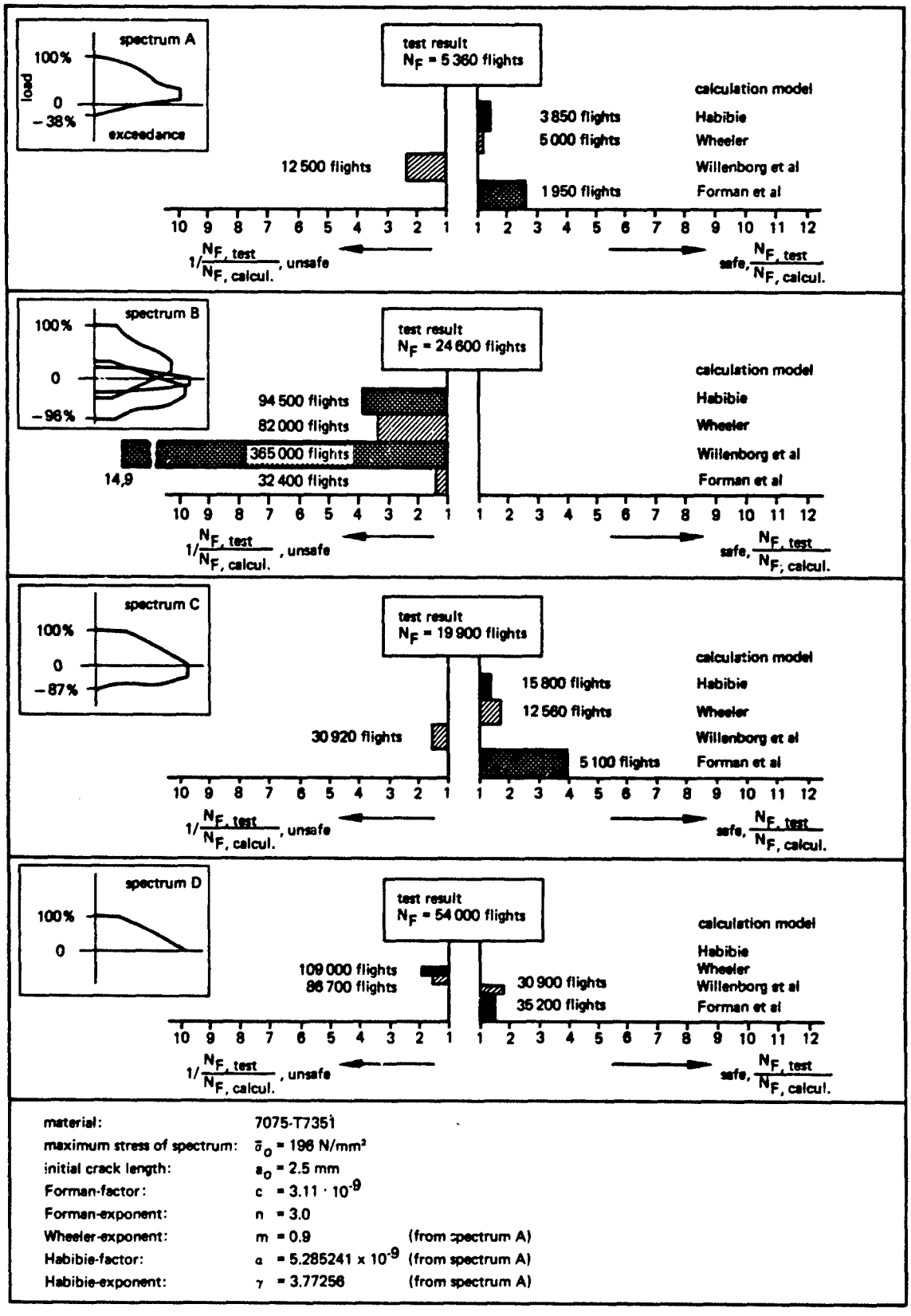

Fig. 4.1 Comparison between test and calculation for Al 7075-T7351 according to /12/

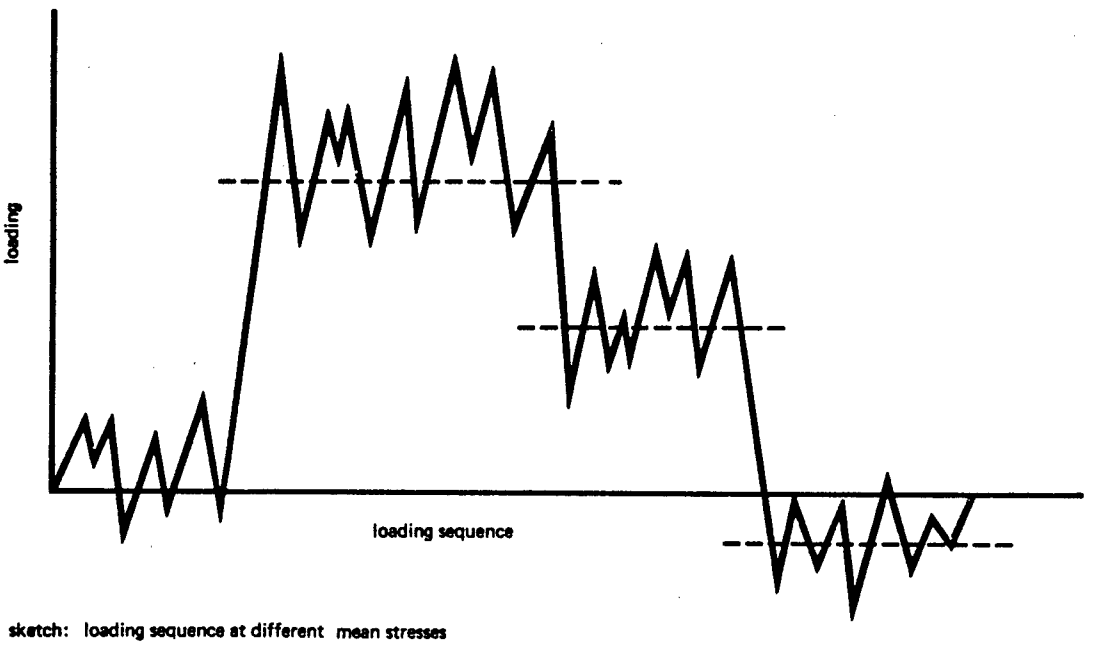

sketch: loading sequence at different mean stresses

From a study of the tests made on Ti6Al4V it will be found that the crack propagation retardation is about twice as great as in A17075T7351 (see fig. 4.2). This is shown by the fact that the Forman calculation is much more decidedly on the safe side. As a result, the life duration determined after Willenborg also tends more strongly towards the safe side.

If Willenborg still lays on the unsafe side by the factor 2.33 for the aluminium alloy in spectrum A, this value is reduced for titanium to about 1.66. For spectrum C, too, Willenborg is well on the safe side with titanium.

As for life prediction for Ti6Al4V after Wheeler, a marked displacement towards the safe side can be discerned here too. It is not possible, however, to take the greater retardation effect in Ti6Al4V as an overall explanation. It is likely that the compressive loads in spectrum C reduce the retardation in Ti6Al4V to a lesser extent than is the case in Al7075T7351.

It can be categorically stated that the life prediction, with or without retardation, tends more strongly to the safe side in Ti6Al4V than in Al7075T7351.

When considering the tests made on the 300 M high-tensile steel (see fig. 4.3), for spectra A und C, the retardation effect in this material appears to be slightly less than in Ti6Al4V. Incidentally, the measure of retardation can be seen not only from the comparison between the Forman calculation and the test result, but also from the Wheeler exponent. As may be gathered from figs. 4.1, 4.2 and 4.3, the Wheeler exponent takes the highest value as m = 1.95 in Ti6Al4V and the lowest value as m = 0.9 in Al7075-T7351. The 300 M high-tensile steel comes in between with m = 1.8.

The relatively great retardation effect in 300 M can in this case be attributed to the low stress level selected for the tests.

For spectrum A, the Willenborg life prediction is on the unsafe side, not only for aluminium and titanium but also for high-tensile steel.

In spectrum C, Willenborg is on the unsafe side only for steel and titanium, but not for aluminium.
This can presumably be explained by the lower retardation effect of the aluminium alloy on the one hand and by the greater reduction of retardation due to compressive loads on the other hand.

The life prediction after Wheeler is bound to conform to the test results for all materials in spectrum A, since the Wheeler exponent was established accordingly.

If, as in spectrum C, heavy compression loads occur, a comparatively conservative life estimate is to be expected whatever the material may be. This can chiefly be explained by the fact that both Wheeler and Forman make too much allowance for compressive loads.

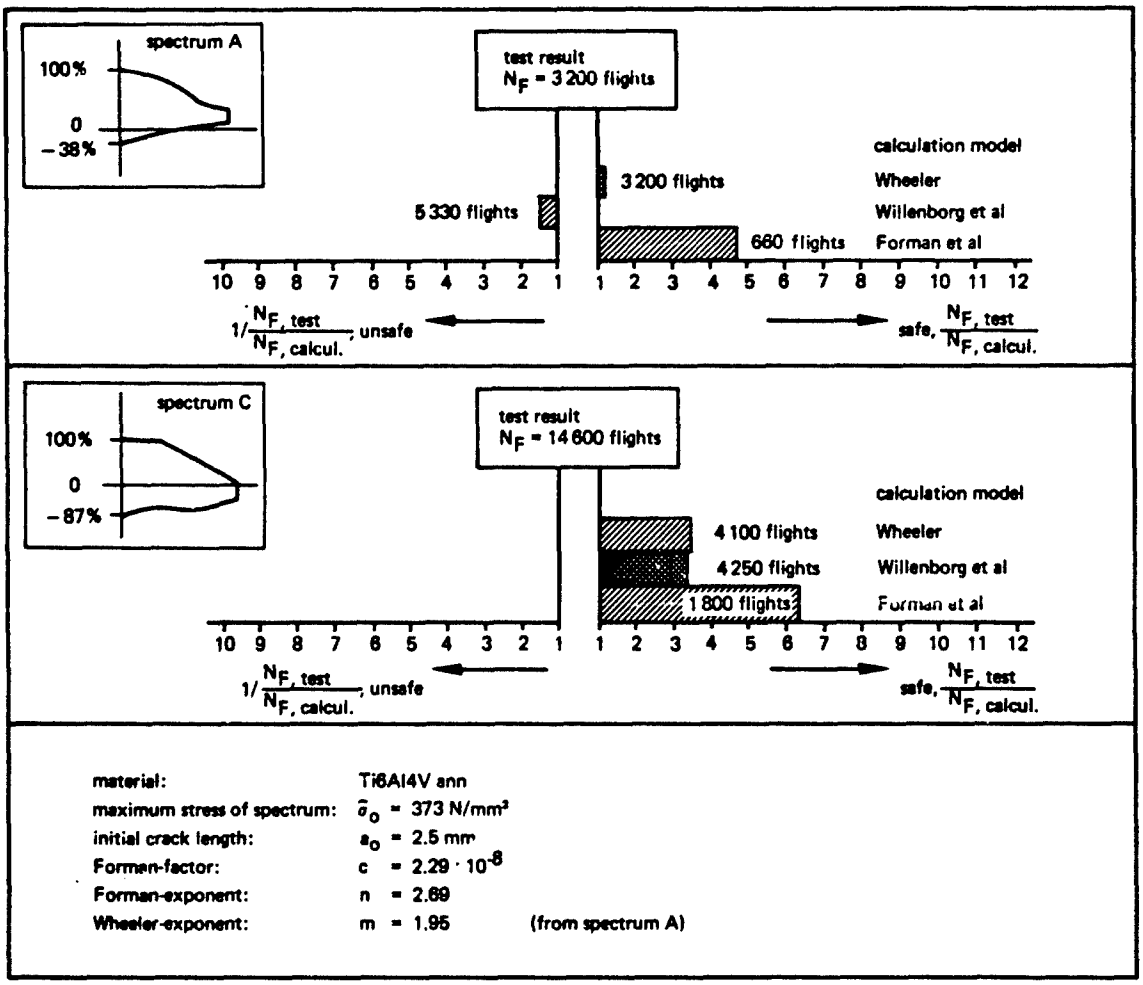

Fig. 4.2 Comparison between test and calculation for Ti6Al4V from /12/

If a final assessment of the various calculation procedures were to be made on the basis of this investigation alone, none of the procedures would display any significant advantage over the others.

Broadly speaking, if there is any major change in the spectrum it is uncertain whether the calculation will be on the safe or the unsafe side.

The Forman equation constitutes an exception. If, in a load sequence, account is taken of wide fluctuations in mean stress by introducing additional load cycles or by means of the overall g-spectrum, the life prediction after Forman will always be on the safe side.

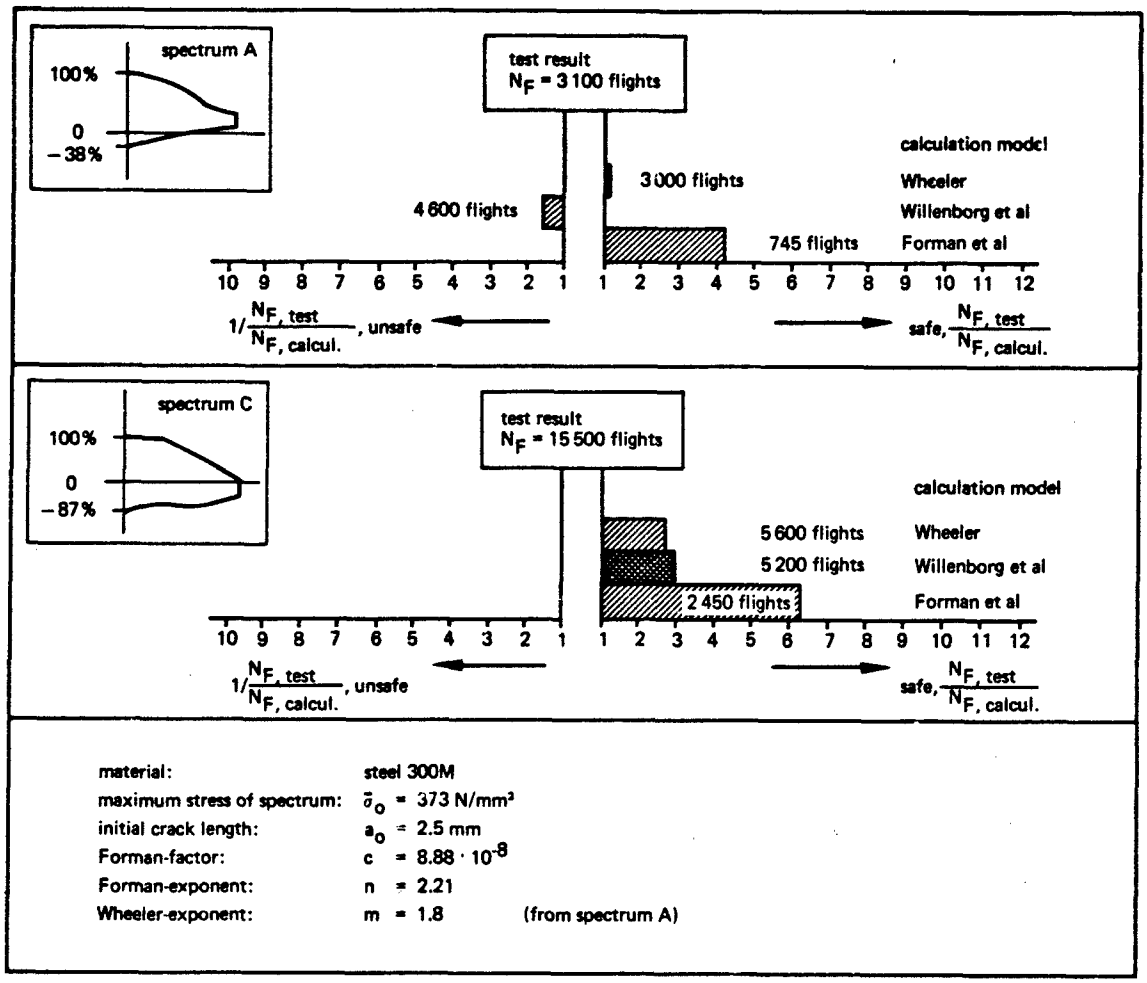

Fig. 4.3 Comparison between test and calculation for 300M steel, from /12/

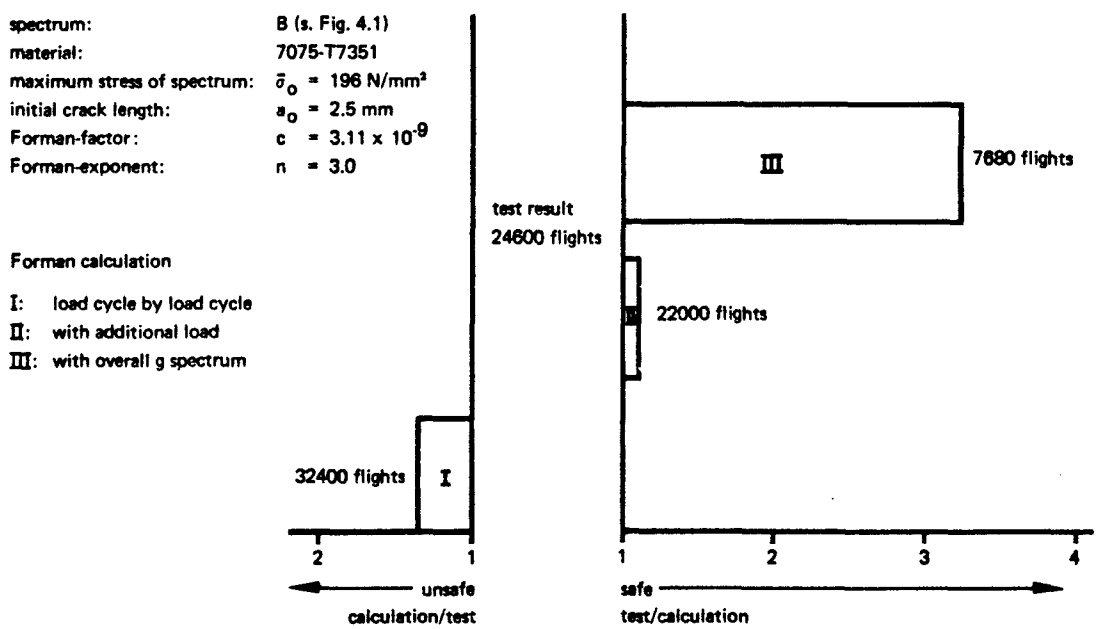

Fig. 4.4 Comparison between test and Forman calculation taking into account various load cycles, from /12/

key	variation
A	basic spectrum (σ_{max} = 106 ksi)
A1	low to high order
A2	high to low order
A3	truncated spectrum (σ_{max} = 100 ksi)
A4	truncated spectrum (σ_{max} = 91 ksi)
A5	basic spectrum (all stresses increased 10%)

Table 4.1 F-111 spectrum variations

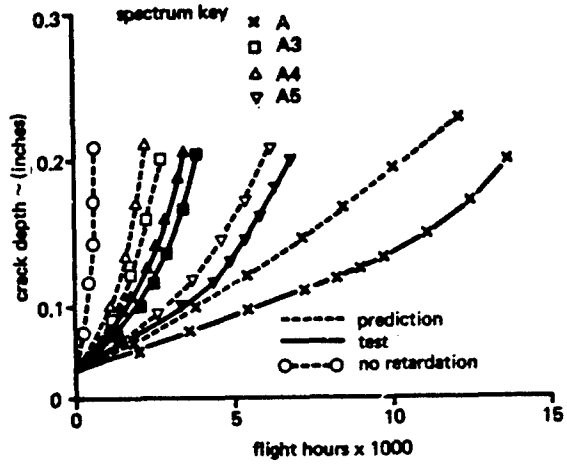

Fig. 4.5 F-111 spectrum, stress level variations

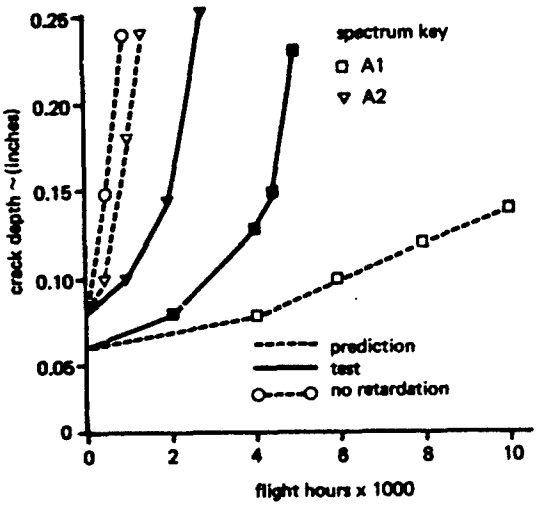

Fig. 4.6 F-111 spectrum, ordering variations

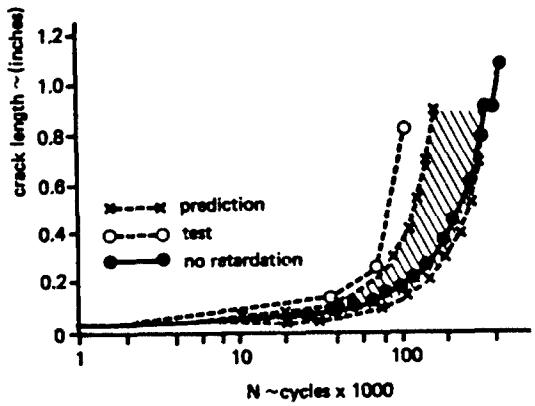

Fig. 4.7 C-5A flight-by-flight spectrum

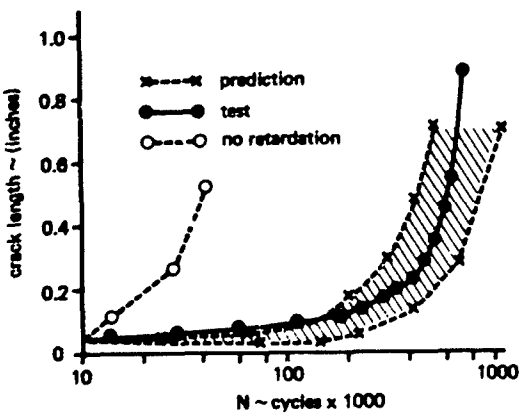

Fig. 4.8 C-5A blocked flight-by-flight spectrum

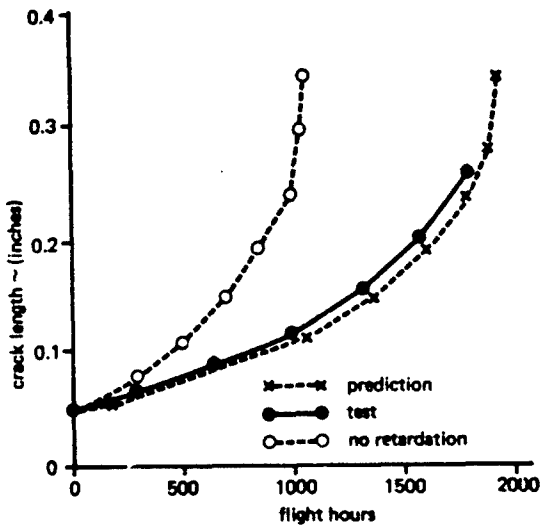

Fig. 4.9 F-4E flight-by-flight spectrum

Fig. 4.4 shows that the life calculated for spectrum B (see fig. 4.1) after Forman is on the safe side by a factor of about 3.2 when taking account of the overall g-spectrum and by a factor of 1.1 when taking account of additionally introduced load cycles.

Turning now to the life prediction according to Willenborg, we find that, in comparison with the test, the calculation is in most cases on the unsafe side in the investigation conducted in [12], the more so where the retardation effect of the material is less marked. This means that life duration determined after Willenborg displays a much stronger tendency to the unsafe side in Al7075-T7351 than in Ti6Al4V. It may be concluded that the yield stress σ_y included in the Willenborg model does not adequately represent the retardation behaviour specific to the material. In addition compressive loads cannot be taken into account.

As already demonstrated in the description of the Willenborg model, no crack propagation occurs when it is true that $\sigma_{i+1} = \sigma_{i/2}$. Investigations by Gallagher [45], on the other hand, have shown that in general it is not an overload by a factor of 2 which causes crack stoppage, but that a factor of 2.3 is applicable for aluminium and 2.8 for titanium. It follows that in titanium more load cycles would contribute to crack propagation than in aluminium. An investigation by Engle and Rudd [46] using the Willenborg model as modified by Gallagher resulted in a closer conformity to test results than in [12] (see fig. 4.5 to 4.9, table 4.1). This investigation [46] used the load sequences typical of F 111, C5A and F-4E, with the 7075-T6511 aluminium alloy as material.

Whether a similarly close conformity between the test and the modified Willenborg model can be excepted for other spectra and other materials cannot be predicted on the basis of this investigation.

A statistical evaluation of the deviation of crack propagation life predicted after Wheeler, Willenborg and Forman from actual test results yields a similar scatter for all three methods. The test results for the statistical evaluation were taken from [12]. As is evident from figs. 4.1 to 4.4, the investigation conducted in [12] used various materials, and spectra which in some cases differed quite substantially.

As shown in fig. 4.10, the crack propagation life determined after Forman is mainly on the safe side, that of Willenborg extensively on the unsafe side. Where the scatter behaviour is similar, though, the crack propagation life as determined after Wheeler may equally well be on the safe or the unsafe side.

A close conformity with the test result can only be excepted from the crack propagation life calculated after Wheeler if the spectrum on which the test was based, or one very similar, was used to determine the Wheeler exponent.

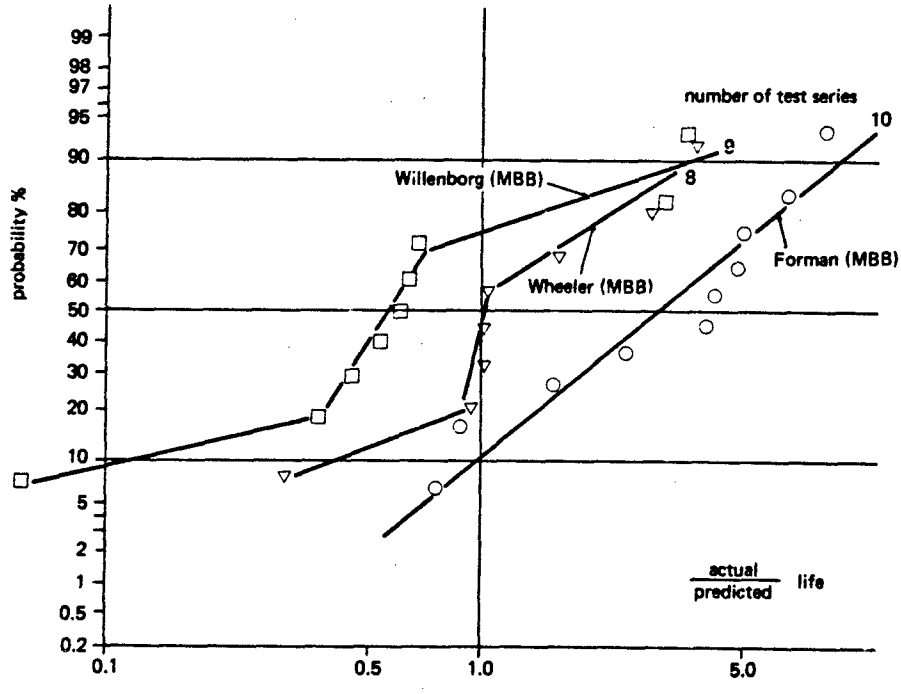

Fig. 4.10 Comparison of predicted and experimental crack growth for tactical aircraft. Fitted m.

Note: Extreme unconservative results were for tests with many compressive stresses, from /43/

Note: This type of comparative representation of different crack propagation calculation methods and their consistency with test results was first used by Schütz in [47].

Broek [43] conducted a calculation, using Wheeler, for a series of flight-by-flight crack propagation tests on 7075-T73 and Ti6Al4V with a typical combat aircraft spectrum.

Since the stress spectrum was only very slightly altered, as shown in fig. 4.11, the comparison between test and calculation yielded a high degree of consistency.

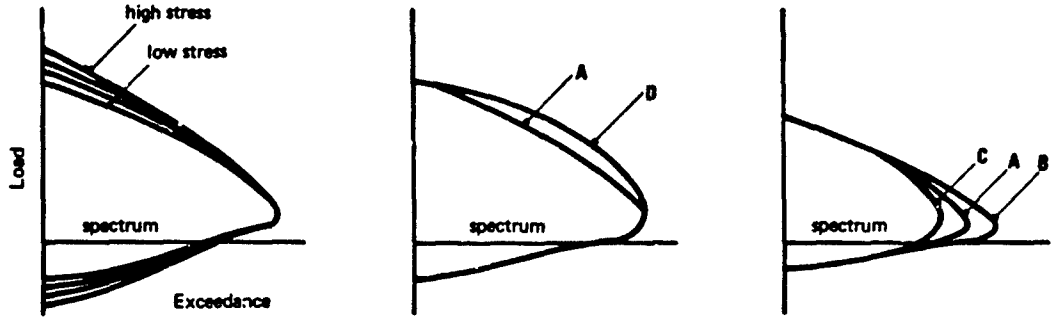

Fig. 4.11 Variation of the spectrum for investigations of crack propagation /43/

An investigation by Schütz [47] likewise made flight-by-flight crack propagation tests on aluminium, titanium and steel alloys with the Falstaff, Tornado and F 104 (wing and landing gear) spectra, comparing them with Forman, Wheeler and Willenborg.

A statistical representation of the deviation between test and calculation (see fig. 4.12) again shows results essentially comparable to those of the investigation conducted in [12].

Fig. 4.12 also contains the results of Broek's comparison between Wheeler and the tests.

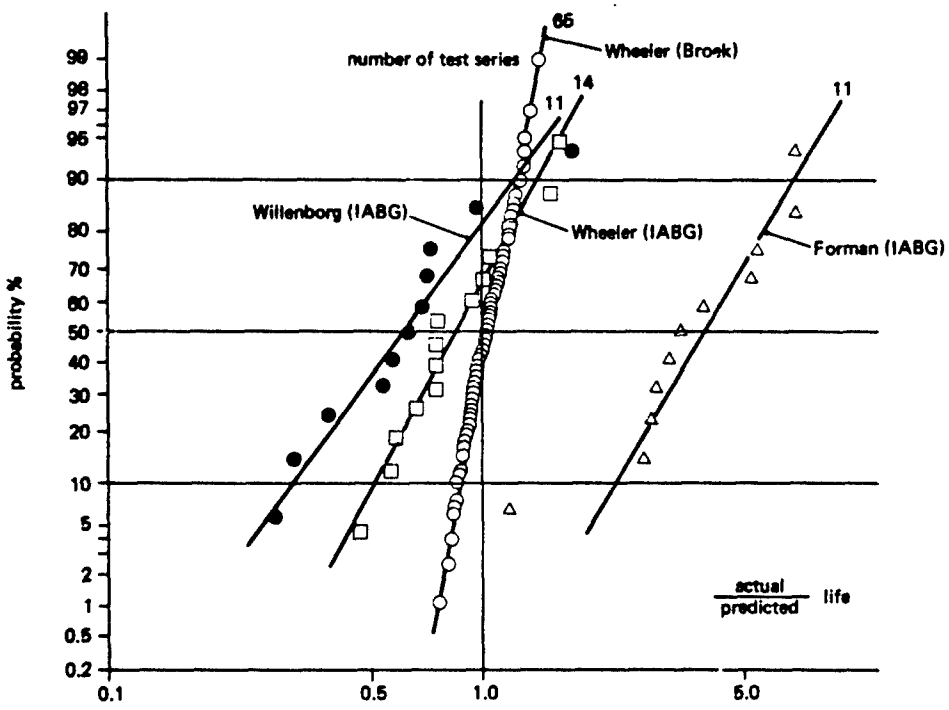

Fig. 4.12 Comparison of predicted and experimental crack growth.

Note: Wheeler m for IABG results was taken same as for Broek's results, from /43/

A comparison of fig. 4.10 and 4.12 reveals that in both investigations, Forman is on the safe side and Willenborg on the unsafe side.

It is also noticeable that the scatter of the results achieved with the respective calculation procedures is greater in fig. 4.10 than in fig. 4.12.
A considerable difference as regards scatter can be found between the Wheeler-MBB calculation results (see fig. 4.10) and the Wheeler-Broek calculation results (see fig. 4.12). The reason may be seen in the fact that Broek only very slightly varied the spectrum in his investigations (see fig. 4.11), whereas the investigation by Sippel and Weisgerber [12] used fundamentally different spectra for the comparison between test and calculation (see fig. 4.1).

The same may be said of the investigation conducted by Schütz (IABG) [47] (see fig. 4.12), in which the differences between the various spectra were by no means as great as in [12].

7.4.2 Suggestions for practical applications

When the various calculation procedures are compared in the light of a wide range of applications including different types of spectra and different materials, none of the methods considered offers any notable advantages as regards accuracy of prediciton, as has already been stated in section 7.4.1

The calculation only corresponds exactly to the test when it has been adapted to the test result by an additional empirical value such as the Wheeler exponent. This type of adaptation can on principle be undertaken in the Willenborg and Forman models as well. In the Willenborg model this is possible by virtue of the fact that crack stoppage does not come about at an overload of factor 2 but only, as Gallagher [45] has shown, at a greater load.

The crack propagation calculation after Forman could for instance be adapted to a flight-by-flight test result by a factor of

$$k = \frac{\text{test}}{\text{calculation}} \quad (= \text{relative Miner})$$

There would still be a high degree of consistency between the test and the calculation if either the maximum spectrum stress changed or if slight variations occurred in the type of spectrum. Spectrum changes of this kind can come about when for instance the requirements originally made on the aircraft are changed or the spectrum used in the design phase has to be corrected by later inflight measurements.

The improvement of calculations of crack propagation life in aircraft components is not, at present, merely a question of the calculation method in itself; it is also a question of cost. This is even more the case when the calculation method for life prediction is considered not in isolation but in the context of all the necessary calculation factors such as stress intensity, material characteristics, environmental influences, operating loads etc.

In view of the cost involved in calculating crack propagation, the Forman equation, in which the sequence of load cycles is only of secondary importance, affords a decisive advantage over the retardation models.

The computer cost of a retardation procedure, in which the crack growth must be ascertained load cycle by load cycle, is considerably higher than with the Forman equation.

It was also proved in section 7.4.1. that the crack propagation calculation after Forman is always on the safe side. This does presuppose, however, that wide mean stress fluctuations in the load sequence are taken into account either by additional load cycles or by the overall g-spectrum.

For the reasons stated, the Forman equation, which was originally developed to calculate crack propagation under constant amplitude load, can be used as a first approximation for predicting the crack propagation under flight-by-flight load sequences.

The application of this rather conservative calculation procedure at the same time covers a number of uncertain factors connected with the life prediction such as scatter of material and load, imprecise location of stress, stress intensity, environmental influences etc.

If it should prove, however, that the crack propagation life as determined after Forman is not long enough to establish an economic inspection interval, this would be the time to start improving the prediction of crack propagation.

There exist a number of suitable steps, such as exact determination of the stress acting on the component by strain gauge measurements, determining the stress intensity for the component with the aid of the finite elements method etc.

Improvement of the calculation procedure itself, for instance by expanding the Forman equation to include an experimentally determined retardation function (= Wheeler model) is only one of several possible measures.

If one is prepared to accept the cost of flight-by-flight crack propagation tests and long computation times, and if no substantial changes occur in the stress spectrum from one component to another, then, as Broek [43] showed, it is possible to achieve sufficient accuracy of life prediction using the Wheeler procedure.

As soon as greater divergences occur in the spectrum, however, Wheeler offers no particular adventage over Forman (see fig. 4.10) which might at least justify the greater expenditure involved in making the test and the calculation.

The investigations known in the literature usually only used typical aircraft spectra, usually center gravity spectra. On closer consideration of an aircraft structure, however, it will be seen that, depending on the overall concept of an aircraft (e. g. fixed wing or variable-sweep wing), the stress spectrum can change its form substantially not only from one assembly to another (e.g. wings, fuselage, taileron, landing gear) but also within one assembly.

An example of this are spectra A, B and C in fig. 4.1. These stress spectra all occur in a single aircraft. Whilst spectrum A is still identifiable as a typical combat aircraft spectrum, this is no longer the case with spectrum B. This example also shows that the Wheeler exponent determined for spectrum A is no longer of any use for spectrum B.

Based on the above considerations, the following procedure can be recommended to the engineer.

First of all, the crack propagation should be calculated without retardation using conservative hypotheses.

If the crack propagation life should prove to be too short for a reasonable inspection interval, it should be checked to what extent the comparatively conservative hypotheses used for the first calculation can be improved upon. The following possibilities are available:

- shorter initial crack length due to improved NDT methods
- improved stress analysis, possibly stress measurement on the component using strain gauges
- deriving local stress spectra
- development of a stress intensity solution for a specific component
- taking account of environmental conditions
- taking account of the retardation effect.

If the calculation is to be verified by making provision for the retardation effect, the Wheeler method can be recommended. It will have to be checked, however, to what extent the Wheeler exponent can be used for other stress spectra. Some initial indications will be found in the investigations from references [12], [23] and [43].

7.5 CONCLUSION

It is the purpose of this treatise to draw attention to some of the problems involved in calculating crack propagation under constant and multi-step amplitude load sequences and point the way to the solutions.

In particular, the relationship between da/dN and ΔK is demonstrated, appropriate calculation formulae such as those of Paris, Walker, Forman etc. being described.

It appears that none of the methods considered has any decisive advantage over the others. Even a negligible improvement in the expression of da/dN as a function of ΔK generally necessitates a much greater expenditure for the determination of additionally required material data.

By considering a number of factors such as material thickness, environmental conditions, temperature, correcting function for components, manufacturing process etc., which also influence the crack propagation behaviour, it is shown that the selection of a suitable calculation formula is only one of several possible ways of improving the prediction of crack propagation.

Crack propagation tests under multi-step amplitude load sequences are used as a basis to demonstrate that the retardation effect which appears depends essentially on the material, the type of spectrum, the stress level, the stress intensity and the load sequence. To calculate the crack propagation under multi-step amplitude load sequence various methods such as those of Willenborg, Wheeler etc. are described, and their principle explained; the method is then rated using a comparison between experimental and calculated values.

Here, too, it appears that none of the procedures investigated has any particular advantage over the others. For this reason a first estimation of the crack propagation life may be made with the aid of a simple calculation procedure such as the Forman equation, which in general yields conservative results.

One of the calculation methods which allows for the retardation effect is that of Wheeler. However, it is only possible to attain sufficient accuracy by this method if the type of spectrum for a particular material which is used to determine the Wheeler exponent is not substantially changed for the calculation of aircraft components. In comparison to the Forman equation, however, the use of the Wheeler method requires a considerably higher expenditure of computing time and experimenting costs, which are incurred by the determination of the Wheeler exponent for various materials and stress spectra.

Finally, calculation models based on the crack closure concept are also considered. The investigations studied here reveal that on the one hand some promising approaches have been made, such as that of Führing and Seeger, towards a better physical explanation of the retardation effect. On the other hand, though, there remain a number of questions concerning the crack closure concept which will have to be answered by extensive experiments before any of the procedures dealt with can be applied in future practice.

7.6 REFERENCES

[1] D. Broek; Elementary Engineering Fracture Mechanics, Nordhoff International Publishing

[2] D.P. Rooke, D.J. Cartwright; Compendium of Stress Intensity Factors, Printed in England for Her Majesty's Stationary Office by the Hillingdon Press, Uxbridge, Middx. Dd288672 K24 10/75.

[3] M. Tada, P. Paris, G. Irwin; The Stress Analysis of Cracks, Handbook, Del Research Corporation, Hellertown, Pennsylvania 1973

[4] Donahue, R.J., Clark, H.McJ., Atanmo, P., Kumble, R., and McEvily, A.J., "Crack Opening Displacement and the Rate of Fatigue-Crack Growth." International Journal of Fracture Mechanics, Vol. 8, June 1972, pp. 209-219.

[5] P.C. Paris; The Growth of Fatigue Cracks Due to Variations in Load, Ph. D. Thesis, Lehigh University (1962)

[6] Walker, K., The Effect of Stress Ratio During Crack Propagation and Fatigue, Spec. Tech. Publ. 462, 1970. ASTM, pp. 1-14.

[7] Forman, R.G. Kearney, V.E., Engle, R.M.; Numerical Analysis of Crack Propagation in Cyclic-Loaded Structures. Journal of Basic Engineering, Trans. AMSE, Series D, Vol. 89, 1976.

[8] Richards, C.E. und T.C. Lindley: The Influence of Stress Intensity and Microstructure on Fatigue Crack Propagation in Ferritic Materials. Engineering Fatigue Mechanics 4 (1972) S. 961.

[9] Collipriest, J.E., An Experimentalist's View of the Surface Flow Problem ASME, 1972, pp. 43 – 62.

[10] K.B. Davies, C.E. Feddersen, Inverse Hyperbolic Tangent Model of Fatigue-Crack Growth; Journal of Aircraft, Vol. 12, No. 12,December 1975

[11] W. Elber, The Significance of Fatigue Crack Closure; ASTM STP486

[12] K.O. Sippel, D. Weisgerber; Flight by Flight Crack Propagation Test Results with Several Load Spectra and Comparison with Calculation According to Different Models; ICAF Symposium, Darmstadt, 12. Mai 1977.

[13] NLR-TN M.2111

[14] W. Geier, Rißwachstum und Restfestigkeit, TZL 1976,MBB-UFE 1291.

[15] C.E. Feddersen, W.S. Hyler; Fracture and Fatigue Crack Propagation Characteristics of 7075T7351 Aluminium Alloy Sheet and Plate; Battelle Memorial Institute, Rep. No. G-8901, March 1970

[16] W. Geier,Spannungsintensitätslösung für den Augenstab, TN MBB UFE 214-4/79

[17] J. Schijve, P. De Rijk; The Effect of Temperature and Frequency on the fatigue crack propagation in 2024-T3 Alclad Sheet Material, NRL-TR M.2138

[18] R.J.H. Wanhill; Environment and Frequency Effects During Fatigue Crack Propagation in Ti-2.5 Cu (IMI230) Sheet at Room Temperature. Corrosion-Nace, Vol. 30, No. 1, January 1974

[19] Broek, D. and Bowles, C.Q.; The effect of precipitate size on crack propagation and fracture of an Al-Cu-Mg alloy; J. Inst. Metals, 99 (1971) pp. 255-257.

[20] Schijve, J. and Broek, D.; Crack-propagation-tests based on a gust spectrum with variable amplitude loading;Aircraft Engineering, 34 (1962) pp. 314-316.

[21] Hudson, C.M. and Hardrath, M.F.; Investigation of the effects of variable amplitude loadings on fatigue crack propagation pattern, NASA-TN-D-1803 (1963)

[22] W. Geier, Untersuchung des Proof-Loadverfahrens hinsichtlich seiner Anwendungsmöglichkeit im Flugzeugbau, ZTL-75 MBB-UFE 1216.

[23] K.O. Sippel, D. Weisgerber; Crack Propagation in Flight by Flight Tests on Different Materials; ICAF 1975 Lausanne.

[24] J. Schijve, F.A. Jacobs, P.J. Tromp; Crack-Propagation in Aluminium-Alloy Sheet Materials under Flight Simulation Loading, NRL-TR68117.

[25] W. Krimmel; Rißfortschritt verkürzt; MBB-UFE 214 (unveröffentlicht)

[26] J. Willenborg, R.M. Engle, H.A. Wood, Crack Growth Retardation Model, Using an Effective Stress Concept, Air Force Flight Dynamics Laboratory, Wreight Patterson Air Force Base Ohio. TM 71-1-FBR.

[27] O.E. Wheeler, Spectrum Loading and Crack Growth, Journal of Basic Engineering, March 1972/181

[28] Fracture Testing of High Strength Sheet Materials. First Report of Special ASTM Commitee, ASTM Bulletin, Jan. 1960.

[29] J.E. Srawley; Plastic Zone Near a Crack and Fracture Toughness. 7th Sagamore Ordunance Materials Research Conference, August 1960.

[30] Habibie, B.J.; Rißfreie und rißbehaftete Lebensdauer von modernen Leichtbauweisen, ZTL 74, MBB-UH 27-74.

[31] W. Elber; The Significance of Fatigue Crack Closure; Damage Tolerance in Aircraft Structures, ASTM STP 486, American Society for Testing and Materials, 1971, pp.230-242

[32] H. Führing; On the Determination of Crack Opening Loads, Int. J. Fracture 12, 1976, 917-920

[33] H.L. Eidlinoff, P.D. Bell; Application of the Crack Closure Concept to Aircraft, Fatigue Crack Propagation Analysis; Grumman Aerospace Corporation, Bethage, N.Y.11714, USA

[34] H. Führing, T. Seeger; Remarks on Load-Interaction Effects Based on Fatigue Fracture Mechanics Calculations, 9th ICAF Symposium on Aeronautical Fatigue, Darmstadt, 1977

[35] H. Führing, T. Seeger; Dugdale Crack Closure Analysis of Fatigue Cracks under Constant Amplitude Loading; Engineering Fracture Mechanics; Volume 11 Number 1 1979

[36] J.C. Newman; A Finite-Element Analysis of Fatigue Crack Closure, Mechanics of Crack Growth, ASTM STP 590, American Society for Testing and Materials. 1976, pp 281-301

[37] H. Führing; Berechnung von elastisch-plastischen Beanspruchungsabläufen in Dugdale-Rißscheiben mit Rißuferkontakt auf der Grundlage nichtlinearer Schwingbruchmechanik, Report Nr. 30 (1977), Technische Universität Darmstadt.

[38] T.T. Shih, R.P. Wei; A Study of Crack Closure in Fatigue, Engineering Fracture Mechanics, 1974, Vol. 6,pp. 19-32

[39] V. Bachmann, D.Munz; Crack Closure in Fatigue of a Titanium Alloy, Int. Journal of Fracture 11 (1975)

[40] J. Schijve, W.I. Arkema; Crack Closure and the Environmental Effect on Crack Growth, Delft University of Technology, Department of Aerospace Engineering, Report VTH-217

[41] P.E. Irving, J.L. Robinson, C.J. Beevers; A Study of the Effects of Mechanical and Environmental Variable on Fatigue Crack Closure, Engineering Fracture Mechanics, 1975, Vol. 7, pp. 619-630

[42] T.C. Lindley, C.E. Richards; The Relevance of Crack Closure to Fatigue Crack Propagation, Materials Science and Engineering, 14 (1974) 281-293

[43] D. Broek; Fatigue Crack Growth Analysis; Agard Lecture series No. 97, Fracture Mechanics Design Methodology.

[44] Effects of Fighter Attack Spectrum on Crack Growth; AFF DL-TR-76-112

[45] J.P. Gallagher; A. Generalized Development of Yield Zone Models; Air Force Flight Dynamics Laboratory, Wreight Patterson AFB, Ohio, AFFDL-TM-74-28-FBR, Jan. 1974

[46] R.M. Engle, J.L. Rudd; Spectrum Crack Growth Analysis Using the Willenborg Model; Journal of Aircraft, Vol. 13 No. 7

[47] W. Schütz; Calculation Methods for Fatigue Life and Crack Propagation; Chapter 4 Fatigue Design of Fighters, AGARD ograph No. 231

CHAPTER 8

ACCOUNTING FOR VARIABILITY IN MATERIALS PERFORMANCE

8A Treatment of Scatter of Fracture Toughness Data for Design Purpose 8-2

Dr-Ing Walter Schütz IABG.

8B Allowance for Variability in Crack Propagation Data. 8-14

R F W Anstee RAE

APPENDIX Statistical Methods 8-33

Engineering Science Data Unit Fatigue Sub-Series.

A. An Introduction to Statistical Terms and Methods Used in Analysing Data (Item 68013) 8-34

B. The Analysis of Normally Distributed Data (Item 68014) 8-41

C. The Analysis of Data Conforming to an Extreme Value Distribution (Item 68015). 8-52

Grateful acknowledgement is made to the Engineering Science Data Unit (ESDU) for permission to reproduce the basic data items on statistical methods as an Appendix to this Chapter.

8A. TREATMENT OF SCATTER OF FRACTURE TOUGHNESS DATA FOR DESIGN PURPOSES (Schütz)

1. INTRODUCTION 8-3

2. TREATMENT OF SCATTER IN FRACTURE MECHANICS CALCULATION .8-3

   2.1 General Remarks 8-3

   2.2 Necessary Input Data and Assumptions. 8-3

3. NUMERICAL DATA FOR THE COEFFICIENT OF VARIATION OF FRACTURE TOUGHNESS AND CRACK PROPAGATION 8-4

   3.1 Procedure and Data for K_{Ic}. 8-4

   3.2 Procedure and Data for K_c 8-5

4. RECOMMENDED VALUES OF FRACTURE TOUGHNESS PROPERTIES FOR DESIGN PURPOSES 8-6

   4.1 General Remarks 8-6

   4.2 Procedure and Numerical Data for K_{Ic}. 8-6

5. REFERENCES 8-6

CHAPTER 8A

TREATMENT OF SCATTER OF FRACTURE TOUGHNESS DATA FOR DESIGN PURPOSES

by

Dr.-Ing. Walter Schütz

Industrieanlagen-Betriebsgesellschaft mbH
EinsteinstraBe 20, 8012 Ottobrunn, Germany

1. INTRODUCTION

The numerical values used in fracture mechanics calculations (ie K_{Ic}, da/dN) depend on material properties. Therefore they have an inherent scatter - like all material data. For design purposes, this scatter must be accounted for either by "safety factors" or by suitable statistical procedures.

The mathematical procedures as such are relatively simple and well known; it is, however, a most difficult question which numerical values to use in such a calculation, for example for the coefficient of variation of fracture toughness K_{Ic}; this is so because such numerical values are still very scarce, as they are much more difficult and expensive to determine than, for example, F_{tu}-values.

Also, fracture toughness may be much more sensitive to slight variations in heat treatment than the normal mechanical properties; this may result in large differences of fracture toughness between different heats of a nominally identical material. This may be another reason why in most cases only "typical" values of K_{Ic} are given in handbooks (1).

2. TREATMENT OF SCATTER IN FRACTURE MECHANICS CALCULATION

2.1 General Remarks

Numerical values of mechanical properties determined by tests cannot be used directly for design purposes because that would imply a large percentage of failures. They have to be lowered, that is a certain "safe" distance has to be kept between the stress endured by the test specimen(s) and the stress allowable for design. Historically this "safe" distance was obtained by a consensus of the parties concerned and called a "safety factor". This factor was assumed to cover all eventualities so that practically no failure would occur. Two examples are the factor of 1.5 against ultimate strength for aircraft and of 1.5 against yield strength for ships. This factor usually has to be kept against the "book value" of the mechanical property concerned, which may be a minimum value, as in the Federal Republic of Germany's Aircraft Materials Handbook (2) or, as in the MIL-HDBK 5 (1), a statistical value assigned a certain probability with a certain confidence.

In recent years the probabilistic approach has gained acceptance which recognises that a certain probability of failure is inherent in any engineering structure and that by proper use of statistics this probability can be calculated - in contrast to the safety factor approach - and therefore kept at an acceptably low level.

However, it should be kept in mind that any statistical calculation requires as input numerical constants - for example the coefficient of variation of K_{Ic} - and therefore depends on the degree of accuracy of these input data and assumptions. In other words; the real difficulties lie not so much in the mathematics of the problem, but in using correct input data and in making the right assumptions - as in many other engineering problems. In the end, even when a high-grade statistical treatment is employed, engineering judgment will be decisive - as it was with the old "safety factor" approach. Therefore the advantage of using a probabilistic approach is smaller than one would at first think.

Nevertheless in this paper some numerical values to be used as input data for fracture toughness calculations will be suggested which in the author's opinion can be used for design purposes. They were collected from the literature and from IABG data.

Also some suggestions will be made as to other necessary assumptions, ie the required probabilities of survival, the kind of distribution to use, etc.

2.2 Necessary Input Data and Assumptions

Theoretically the mean, the scatter (standard deviation or coefficient of variation) and the distribution are necessary to be able to calculate the necessary factor by which the mean value must be reduced in order to arrive at the required probability of survival.

The Distribution

The determination of the distribution requires an extremely large number of tests, which will certainly not be available for fracture toughness data for a long time to come, if ever. Therefore, it is necessary to assume the distribution. Usually the Normal distribution is used for strength of materials, for example for the tensile strength or the fatigue strength*. For fatigue life on the other hand, the

---

* The well known staircase or up-and-down method assumes a Normal distribution for the fatigue strength.

log-normal distribution is often employed.

One disadvantage of the normal distribution is that for high probabilities of survival very low allowable stresses are calculated if the scatter is high. One example; the often-used "mean minus three sigma" value, corresponding to a probability of survival of about 99.8 per cent is half as high as the mean value for a coefficient of variation of .166. For still higher probabilities of survival and coefficients of variation the allowable stress would become zero or even negative.

Therefore many statisticians have developed distributions which give a lower limit at which the probability of survival reaches 100 per cent, for example the Weibull distribution, the arc sin $\sqrt{P}$ distribution developed by Rossow and co-workers[3] or a distribution developed by the IABG[4].

However, in the region between 50 and 95 per cent probability of survival there is no practical difference between any of the above distributions and for simplicity's sake the Normal distribution is therefore suggested as good enough for fracture toughness calculations and will be used in this paper.

The Mean

The mean fracture toughness can be calculated as arithmetic mean from a small number of tests, say from two to three valid results, according to E-399-74,[5]. This is then the mean of a (small) sample which has to be reduced to the mean of the population using normal statistical procedures[6] !

In a strength of materials problem one always has to make the conservative assumption that the mean of the population is lower than the mean of the sample. For this calculation the coefficient of variation is necessary. Its numerical value should not be the one determined from the sample (even if it were large enough), rather it should be a "typical" or even an "upper limit" coefficient of variation, see below, and Section 3 and 4.

The Coefficient of Variation

If more than four fracture toughness tests are carried out on one heat of a material for one specimen orientation, a statistical evaluation is possible and should be done according to the formula

$$P_s = \frac{3m - 1}{3n + 1} \cdot 100 \text{ (per cent)},$$

where P_s : probability of survival

m : order number, where

$m = 1$ ≙ highest fracture toughness of the series
$m = n$ ≙ lowest fracture toughness of the series

n : number of tests.

Plotting this on Normal probability paper will result in a more or less straight line. From this the standard deviation σ can be taken and the coefficient of variation v calculated as

$$v = \frac{\sigma}{\bar{x}}$$

where $\bar{x}$ = arithmetic mean fracture toughness.
(P_s = 50 per cent).

This then is a measure of the scatter of the one heat of material tested, ie of the sample. There is another kind of scatter between different heats of a nominally identical material. If all the fracture toughness tests on different heats of a nominally identical material in one specimen orientation are evaluated together there is an implicit assumption that they belong to one population. There are statistical procedures to test this assumption[6, 7].

Finally it must be recognized that the ASTM-standard method itself may have an inherent scatter, probably due to its many requirements which will be met in varying degrees in one test series. That is, even if a number of specimens of one sample actually had identical fracture toughness, the results would certainly still show some scatter due to the inherent weaknesses of the ASTM standard.

3 NUMERICAL DATA FOR THE COEFFICIENT OF VARIATION OF FRACTURE TOUGHNESS AND CRACK PROPAGATION

3.1 Procedure and Data for K_{Ic}

The literature known to the author (2, 8-22) was screened for test series with five or more nominally identical specimens in one specimen orientation resulting in valid ASTM-standard tests. Most data were obtained from the Damage Tolerant Design Handbook, Part 1,[9], some test series with British alloys from[9a]; a larger number of suitable test series was also obtained from IABG reports (8, 12-14, 20-22). Each series was evaluated by computer, using the formula given above in Section 2.2 and the coefficient of variation was obtained. Some examples of these evaluations are given in Figures 1 and 2,

which were taken from IABG tests, Figure 1 from[3], Figure 2 from[14]. Forgings have been excluded from the present analysis. Data on forgings will be found in the relevant chapter in this volume.

The coefficients of variation (65 for aluminium alloys, 46 for titanium alloys and 64 for steels) were plotted against σ_y specifying the following parameters:

- type of alloy (Ti 6-4, Ti 8-1-1 etc.)
- type of product (plate, sheet, extrusions)
- specimen orientation
- miscellaneous (temperature, corrosion etc.)

One example of such a plot is shown in Figure 3 for Ti-alloys.

It became apparent that none of these parameters influenced the coefficient of variation within one class of materials, with one (well known) exception: D6AC steel showed a larger-than-normal scatter.

Next the coefficient of variation were evaluated statistically for Al-, Ti- and Fe-alloys according to the formula in Section 2.2, see Figures 4 - 6. However, the 23 test series for D6AC steel were evaluated separately, see Figure 7. In these statistical evaluations the distribution developed by the IABG[4] and mentioned above was used in lieu of the Normal distribution:

- because it results in a probability $P_s = 0$ at a coefficient of variation $v > 0$; this is obviously a necessary requirement, because zero scatter of fracture toughness is physically impossible and
- because it gives a probability $P_s = 100$ per cent at a sensible coefficient of variation.

In the following Table 1 the results of Figures 4 - 7 are condensed.

TABLE 1

Material	Al-alloys	Ti-alloys	Steels except D6AC	D6AC
Coefficient of variation v				
at 50	0.03	0.05	0.05	0.1
90	0.06	0.12	0.10	0.22
100 per cent probability	0.14	0.27	0.22	0.4

$v = 0.14$ at 100 per cent probability for Al-alloys means that using the assumed distribution[4] 100 per cent of the test series had a lower coefficient of variation than 0.14; 0.05 at 50 per cent probability for steels means that the fracture toughness of half of the steel test series had a lower coefficient of variation than 0.05.

As can be seen from Table 1 the scatter of fracture toughness K_{Ic} is lower for Al-alloys than for Ti-alloys and steels. Table 1 also shows numerical values of the coefficient of variation to be expected for the different classes of material and at different probabilities.

Another important numerical value is the mean fracture toughness $\bar{K}_{Ic}$ of different heats of a certain alloy in a certain specimen orientation and its scatter. This was obtained in two ways:

- All test series with five or more valid ASTM tests of one specific alloy and specimen orientation were extracted from the literature and their arithmetic mean fracture toughness $\bar{K}_{Ic}$ determined. These values were then evaluated statistically using the formula given in Section 2.2. Some examples are shown in Figures 8 - 11.
- All the valid test results in[9] for one specific alloy and specimen orientation were evaluated together, even if only one or two valid tests per heat were available. The result is given in Figure 12 for 7050-T73651,[9] in the L-T-direction.

Figures 8 - 12 show the mean fracture toughness to be expected from several heats of one material, that is (at 50 per cent probability) its "typical" fracture toughness. They also show the coefficient of variation is again lower for the Al-alloy than for Ti-alloy, while D6AC is highest.

3.2 Procedure and Data for K_c

As there is no universally agreed method to determine K_c, it is not intended to give numerical data here. However, should such a method be available some day, the procedures presented in Section 3.1 can also be used. It might even be possible to use the numerical data shown in Section 3.1 for the coefficient of variation of fracture toughness K_{Ic} also for K_c because in the author's opinion there is no valid reason why the scatter should be different.

4 RECOMMENDED VALUES OF FRACTURE TOUGHNESS PROPERTIES FOR DESIGN PURPOSES

4.1 General Remarks

When using the data described in Section 3.1 (or similar specimen data) for the derivation of numerical fracture toughness values for the purpose of designing components, one implicitly assumes that the scatter of specimens fracture toughness is identical with the scatter of the component fracture toughness.

This assumption is not always correct as was shown by the author in[23] (see also Chapter 6). Whereas the scatter of fracture toughness of standard ASTM specimens taken from a forged component was quite normal, the scatter of the component fracture toughness was much higher. Nevertheless the above assumption must be made, otherwise one could not use specimen data for the design of components.

For designing a component using probabilistic fracture mechanics the necessary probability of survival must be selected according to engineering judgement. In strength of materials problems often the "mean minus three sigma" value is used (a P_s = 99.8 per cent); in certain standards for fatigue of welded bridges the "mean minus two sigma" value is employed corresponding to 97.7 per cent probability of survival assuming a Normal distribution. The author is aware of only one suggestion of a similar nature for fracture mechanics: Ordorico showed in an AGARD paper[11] that the Aerospatiale Company of France uses the "mean minus two sigma" fracture toughness for calculating critical crack length etc. The other numerical values necessary, the mean fracture toughness $\overline{K}_{Ic}$ and the standard deviation σ are obtained in the following way according to[7]. All the available ASTM tests on one material in one condition and one specimen orientation that is from several heats, are statistically evaluated together. As the various Al-alloys have different scatter, different standard deviations are used.

4.2 Procedure and Numerical Data for K_{Ic}

In the present paper a slightly different procedure is proposed:

- the coefficient of variation is equal within one class of material (but excluding all forgings), namely:
  - 0.06 for Al-alloys
  - 0.12 for Ti-alloys — for normal applications
  - 0.10 for steels
- and
  - 0.14 for Al-alloys
  - 0.27 for Ti-alloys — for critical applications
  - 0.22 for steels

These numbers correspond to probabilities of 90 per cent for normal and 100 per cent for critical applications according to Table 1.

The above coefficients of variation are applicable in principle to all semi-finished products, that are plates, bars and extrusions.

For mean fracture toughness $\overline{K}_{Ic}$ either the actual test results available for the specific problem can be used; if such data are not available $\overline{K}_{Ic}$ can be taken from the literature (for example from[2,8,9-14]) using all valid test results available ie from many different heats. It must be understood that this $\overline{K}_{Ic}$ is in both cases the mean of a sample, which must be reduced to the mean of the population, using the coefficients of variation given above.

5 REFERENCES

1 N.N., "Military Standardization Handbook. Metallic Materials and Elements for Aerospace Vehicle Structures".
MIL-HDBK-5B (1974).

2 N.N., "Werkstoffhandbuch der Deutschen Luftfahrt".
Beuth-Vertrieb, Koln.

3 Dengel, D., "Die arc sin $\sqrt{P}$ - Transformation - ein einfaches Verfahren zur grafischen und rechnerischen Auswertung geplanter Wöhlerversuche".
Zeitschrift für Werkstofftechnik, Heft 8 (1975).

4 Huck, M., "Ansatz und Auswertung von Treppenstufenversuchen im Dauerfestigkeitsbereich".
IABG-Report B-TF-742 B.

5 N.N., "Standard Method of Test for Plan-Strain Fracture Toughness of Metallic Materials".
ASTM Designations E-399-74. Annual Book of ASTM Standards, Part 31 (1974).

6 Little, R.E., "Manual of Statistical Planning and Analysis".
ASTM STP 588 (1975).

7 N.N., "Comparison of Samples".
ESDU ITEM No. 68016, Engineering Sciences Data Unit, London (1968).

8 Oberparleiter, W., Kratzer, H., Schütz W., "Zusammenstellung bruchmechanischer Kennwerte". IABG-Report TF-645 (1977).

9 N.N., "Damage Tolerant Design Handbook. A Compilation of Fracture and Crack-Growth Data for High-Strength Alloys. Part 1". MCIC-HB 01.

9a Kirkby, W., "Fracture Toughness Test Results", in: Fracture Mechanics of Aircraft Structures. AGARD-AG-176 (1975) ed. by H Liebowitz.

10 N.N., "Statistische Auswertung der 1975/76 and ungeknickten Trägerplatten ermittelten Bruchzähigkeitswerte". Krupp Metall- und Schmiedewerke, Essen (1977)

11 Odorico, J., "Application de la Mechanique de la Rupture à la Selection des Alliages d'Aluminium". AGARD-CP-221 (1977).

12 Oberparleiter, W., "Bauteilspezifische Werkstoffuntersuchungen. Untersuchungen am Halbzeug Ti6Al4V-Platte". IABG-Report TF-675.3 (1977).

13 Zenner, H., "Bauteilspezifische Werkstoffuntersuchungen. Untersuchungen am Halbzeug 6060-T73651". IABG-Report TF-621.3 (1976).

14 Zenner, H., "Bauteilspezifische Werkstoffuntersuchungen. Untersuchungen am Halbzeug Ti6Al4V-Schreiben". IABG-Report TF-676.3 (1978).

15 Schütz, W., "Fatigue Life Prediction of Aircraft Structures - Past, Present and Future". Eng. Fracture Mechanics, Vol 6, No 3 (1976) pp 671-699.

16 Witzke, W.R., Stephens, J.R., "Comparison of Equivalent Energy and Energy Per Unit Area Data with Valid Fracture Toughness Data for Iron, Aluminium, and Titanium Alloys". JTEVA, Vol 6, No 1 (1978) pp 75-79.

17 May, J.M., "British Experience with Plane Strain Fracture Toughness (K_{Ic}) Testing". ASTM STP 463 (1970) pp 41-62.

18 Heyer, R.H., and McCabe, D.E., "Evaluation of a Method of Test for Plane Strain Fracture Toughness Using a Bend Specimen". ASTM STP 463 (1970) pp 22-41.

19 Brown, W.F., Jr., "Review of Developments in Plane Strain Fracture Toughness Testing". ASTM STP 463 (1970).

20 Kratzer, H., Oberparleiter, W., and Schütz, W., "Ergänzende bruchmechanische Untersuchungen an Flugzeugbauwerkstoffen". IABG-Report TF-560 (1976).

21 Oberparleiter, W., Kratzer, H., and Schütz, W., "Bruchzähigkeit verschiedener Luftfahrtwerkstoffe bei - 50° C".

22 Kratzer, H., Oberparleiter, W., and Schütz, W., "Bestimmung der Bruchzähigkeit verschiedener Luftfahrtwerkstoffe". IABG-Report TF-492 (1975).

23 Schütz, W., "Crack Propagation and Residual Static Strength of Typical Aircraft Forgings". AGARD-CP-211 (1977).

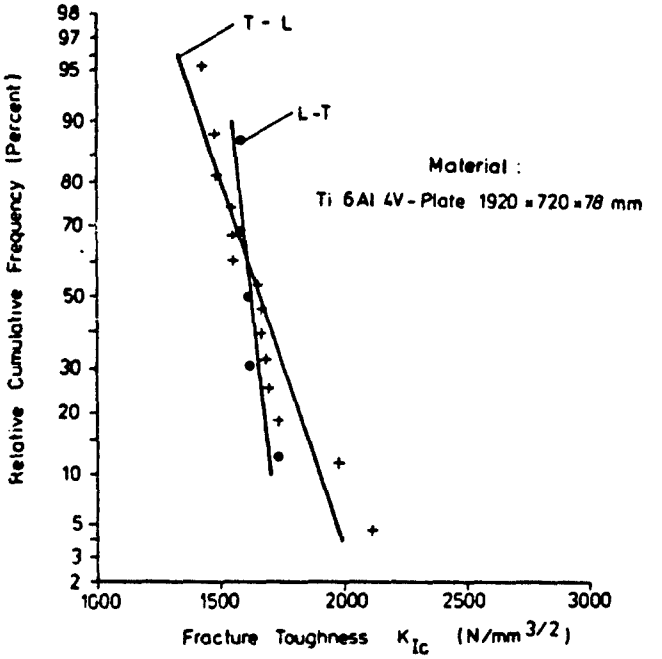

o $\overline{K_{Ic}}$ (50 Percent) = 1623 N/mm$^{3/2}$ v = 0.037
+ $\overline{K_{Ic}}$ (50 Percent) = 1660 N/mm$^{3/2}$ v = 0.12

FIGURE 1. STATISTICAL EVALUATION OF FRACTURE TOUGHNESS

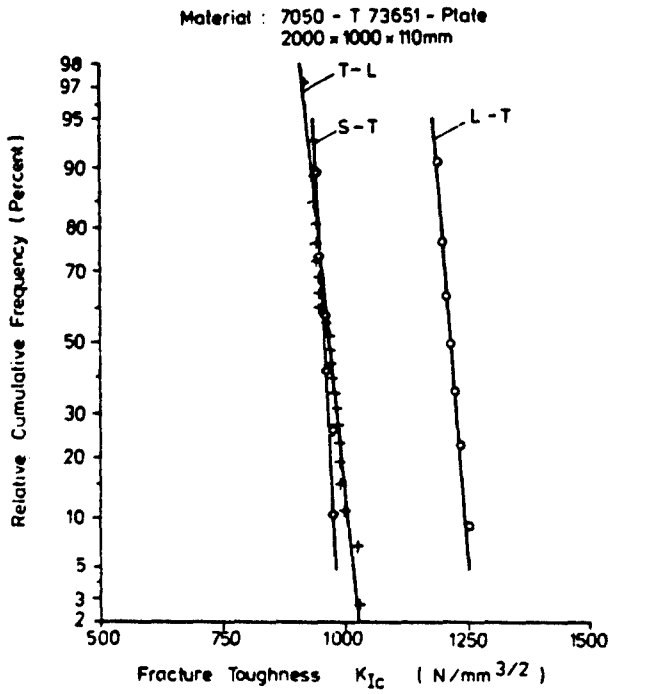

• $\overline{K_{Ic}}$ (50 Percent) = 1214 N/mm$^{3/2}$ v = 0.019
• $\overline{K_{Ic}}$ (50 Percent) = 966 N/mm$^{3/2}$ v = 0.03
◊ $\overline{K_{Ic}}$ (50 Percent) = 957 N/mm$^{3/2}$ v = 0.015

FIGURE 2. STATISTICAL EVALUATION OF FRACTURE TOUGHNESS

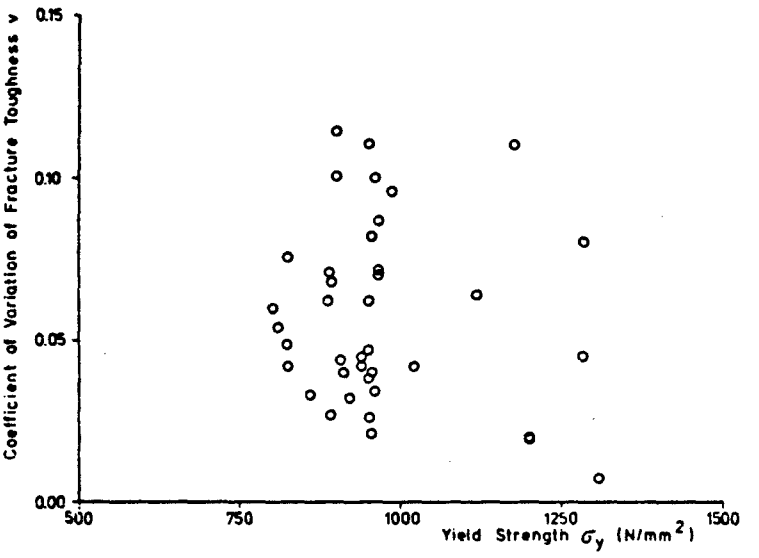

FIGURE 3. COEFFICIENT OF VARIATION v VERSUS YIELD STRENGTH σ_y FOR TI-ALLOYS

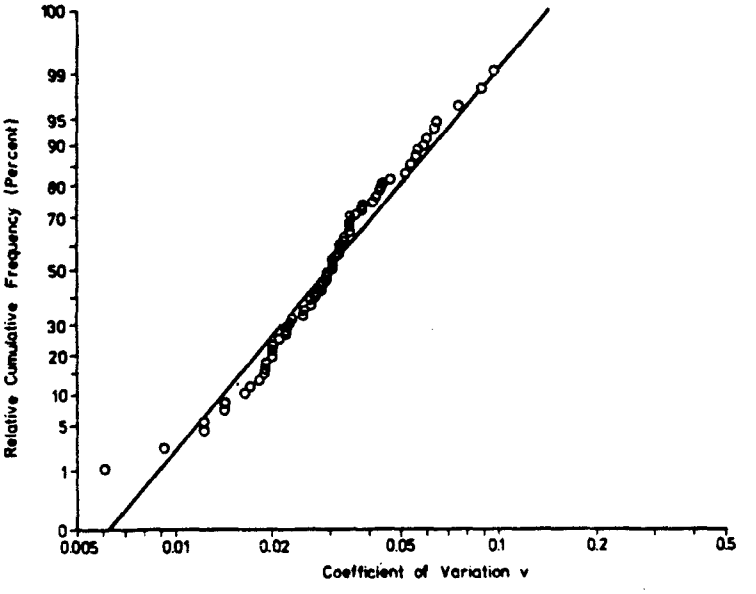

FIGURE 4. STATISTICAL EVALUATION OF THE COEFFICIENT OF VARIATION OF AL-ALLOYS

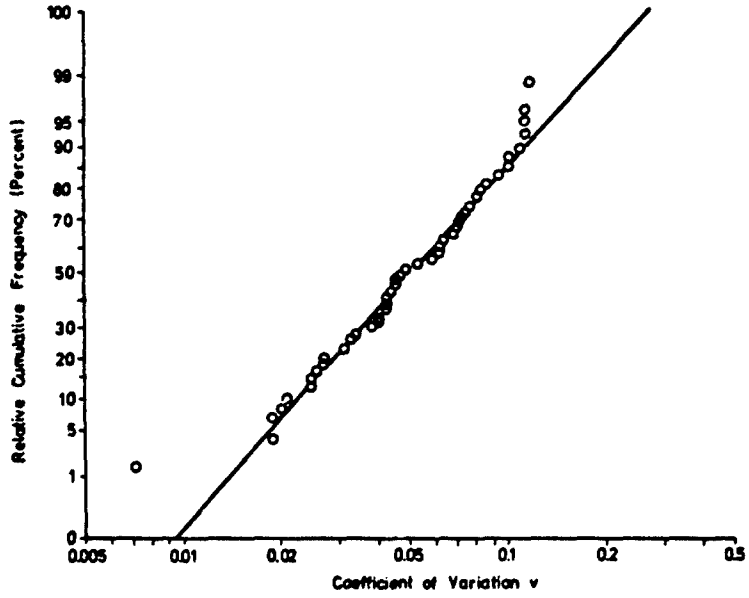

FIGURE 5. STATISTICAL EVALUATION OF THE COEFFICIENT OF VARIATION OF TI-ALLOYS

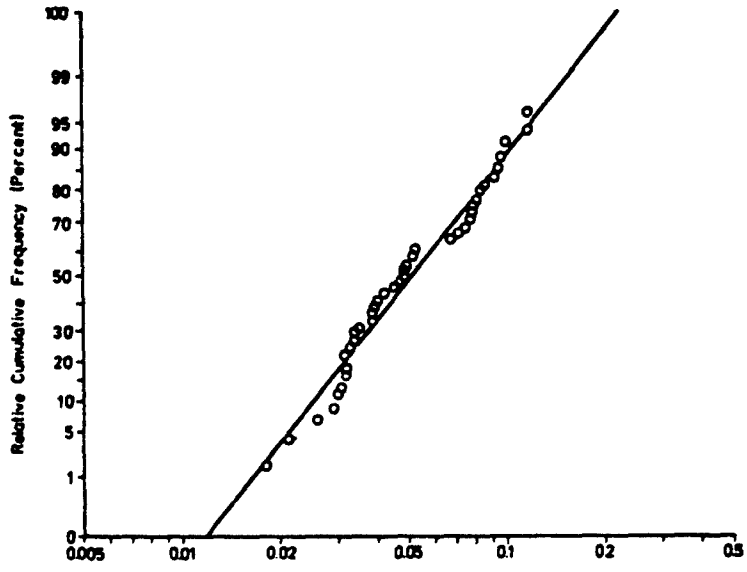

FIGURE 6. STATISTICAL EVALUATION OF THE COEFFICIENT OF VARIATION OF STEELS, EXCEPT D6AL

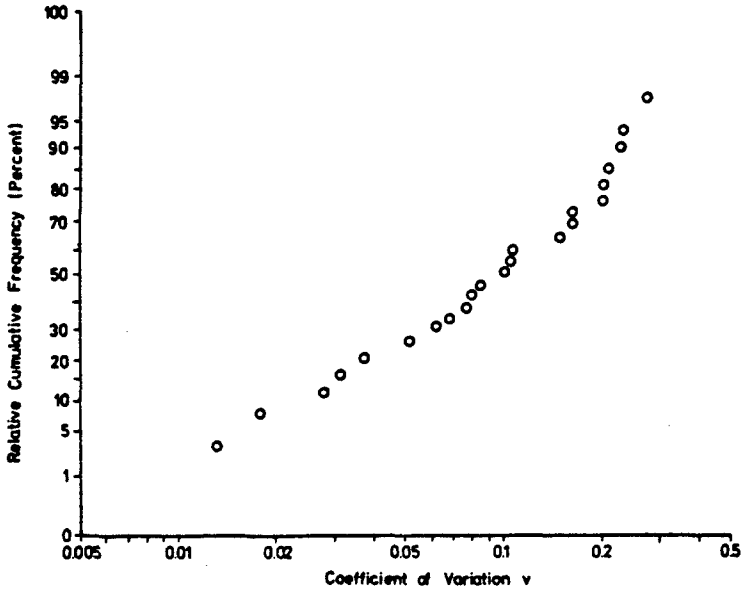

FIGURE 7. STATISTICAL EVALUATION OF THE COEFFICIENT OF VARIATION OF D6AC-STEEL

Spec. Orientation : L - T

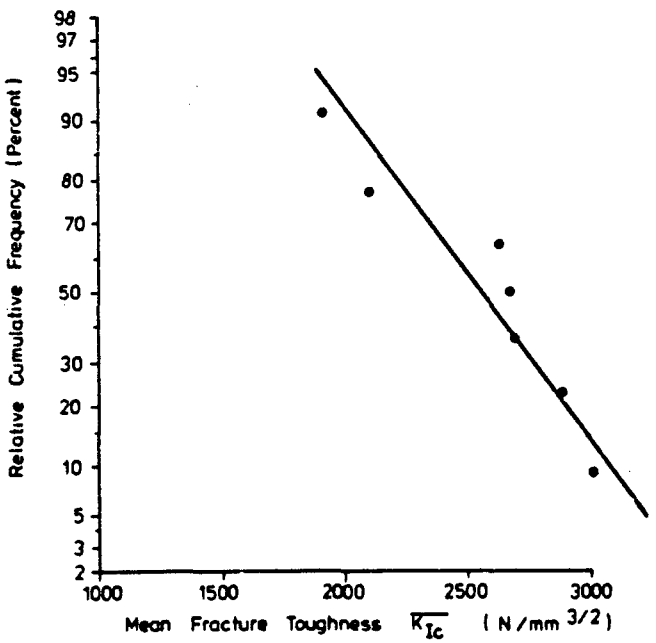

$\overline{K_{Ic}}$ (50 Percent) = 2560 N/mm$^{3/2}$ v = 0.16

FIGURE 8. STATISTICAL EVALUATION OF MEAN FRACTURE TOUGHNESS OF 7 DIFFERENT HEATS OF TI6AL4V

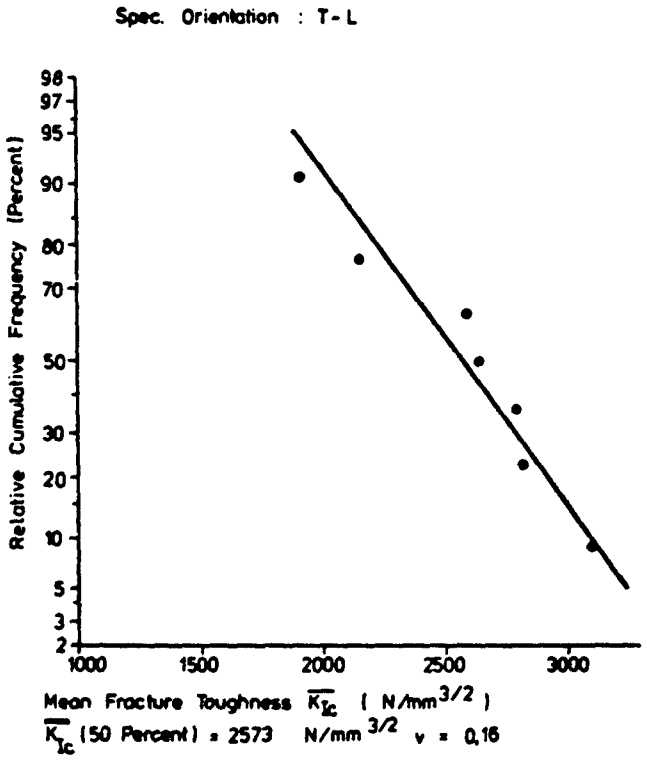

FIGURE 9. STATISTICAL EVALUATION OF MEAN FRACTURE TOUGHNESS OF 7 DIFFERENT HEATS OF TI6AL4V

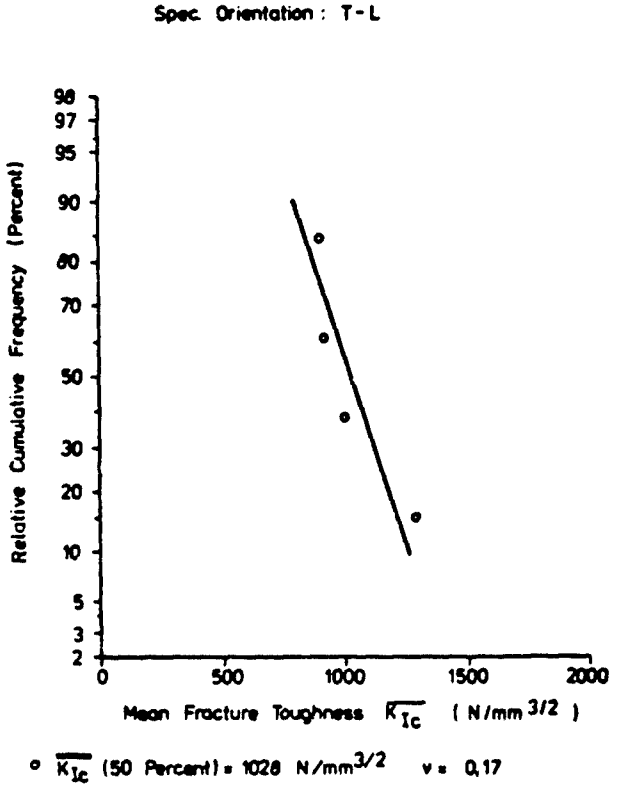

FIGURE 10. STATISTICAL EVALUATION OF MEAN FRACTURE TOUGHNESS OF 4 DIFFERENT HEATS OF 7050-T73651

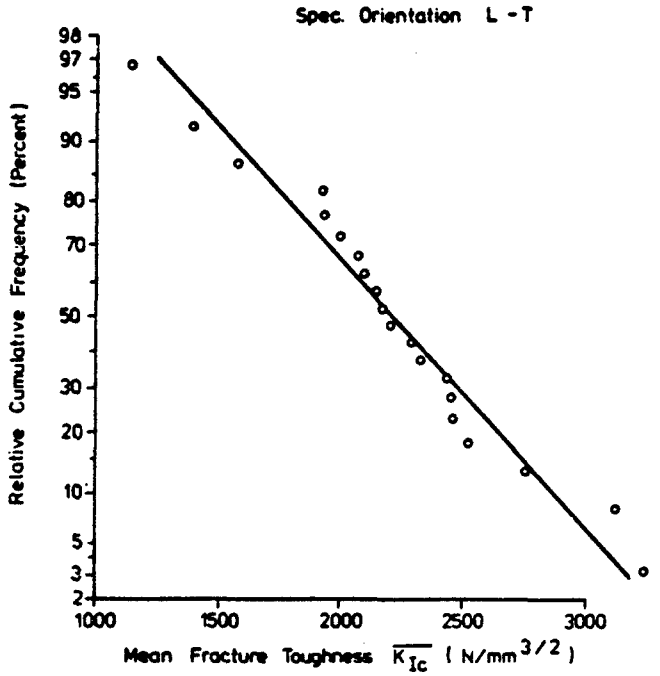

FIGURE 11. STATISTICAL EVALUATION OF MEAN FRACTURE TOUGHNESS OF 20 DIFFERENT HEATS OF D6AC

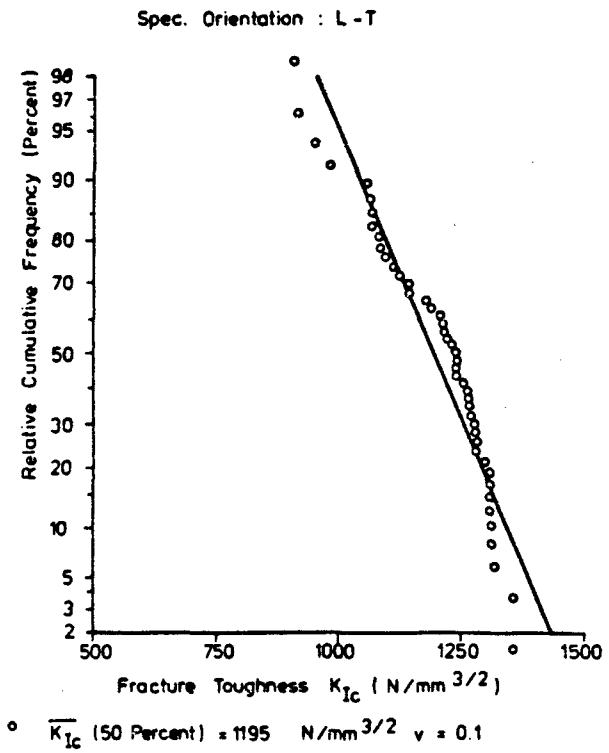

FIGURE 12. STATISTICAL EVALUATION OF FRACTURE TOUGHNESS OF 17 DIFFERENT HEATS OF 7050-T73561 PLATE

8B. ALLOWANCE FOR VARIABILITY IN CRACK PROPAGATION DATA (Anstee)

1. INTRODUCTION 8-15

2. THE NEED FOR VARIABILITY ALLOWANCES. 8-15

3. SOURCES OF VARIABILITY 8-15

4. CHARACTERISATION OF VARIABILITY. 8-16

   4.1 Distribution. 8-16

   4.2 Standard Deviation or Coefficient of Variations 8-16

5. EXPERIMENTAL EVIDENCE OF VARIABILITY IN CRACK GROWTH PERFORMANCE .8-16

   5.1 Aluminium Alloys. 8-17

      5.1.1 2024-T3. 8-17

      5.1.2 Other Aluminium Alloys 8-17

   5.2 Titanium Alloys 8-17

   5.3 Steels. 8-18

   5.4 Comparison of Variability under Constant Amplitude and Variable Amplitude Loading. 8-18

   5.5 Effect of Environment on Variability. 8-18

   5.6 Variability of Structural Components. 8-19

6. DISCUSSION 8-19

7. CONCLUSIONS. 8-19

8. REFERENCES 8-20

CHAPTER 8B

ALLOWANCE FOR VARIABILITY IN CRACK PROPAGATION DATA

by

R F W Anstee

Royal Aircraft Establishment
Farnborough, Hants, England

1. INTRODUCTION

Information on the measured variability in crack propagation rate (or life) of aircraft materials has been available for some considerable time[1-6]. In addition there have been several more recent experimental programmes in which variability has been measured either under constant amplitude loading[7-15], variable amplitude loading[16-20] or in which a quantity of results under both forms of loading has been obtained[21-28]. Further data are available from reports in which variability has not been examined directly but from which, by re-analysing the data, conclusions on variability can be drawn[29-37].

In view of the available data it is perhaps surprising that many workers in fatigue hold the view that variability is not a consideration in crack propagation calculations, but is only important during initiation of damage. The published design requirements are not consistent in allowance for variability in crack propagation. Mil Spec 83444[38] makes no mention of variability in crack propagation, although a factor of 2 is included to safeguard against imperfect inspection[39]. In contrast the British Design Requirements for Military Aeroplanes (AvP 970)[40] specify a factor of 3 to allow for variability in crack growth rate in 'fail safe' structures.

In this Chapter the available information on variability is presented to provide a basis for a decision on whether an allowance for variability should be included in design.

2. THE NEED FOR VARIABILITY ALLOWANCES

For safe life structures it is established practice to use scatter factors on fatigue life (both from test and calculation) to ensure aircraft safety. There is as yet no established practice for damage tolerant structures. However similar arguments to those applied to safe life structures apply equally well to damage tolerant design, in that variability in design data which can be shown to exist should be taken into account in the design process. It may be argued that a variability allowance should also account for the likelihood of a crack occurring in a critical location and also the possibility of the crack remaining undetected. While these considerations may modify the factor to be applied they do not negate the need to recognise that variability must be accounted for. Failure to account for variability must mean that in the presence of an undetected crack 50% of the structures will fail to reach the desired life at a limiting crack length.

Traditionally demonstration of safety has been by a fatigue test. In damage tolerant design this has its counterpart in the crack propagation test. The service life or inspection period being based on the crack growth life between limiting crack lengths with some allowance for variability. A difficulty arises however in the design process. Crack propagation rate data is required for design, not crack growth life information. Crack propagation rate data is obtained by manipulation of the crack growth curve. This additional operation results in increased variability in crack growth rate data over that obtained in crack growth life data[7], as will be shown later. Thus the designer will need to include a greater allowance for variability during design calculations to ensure the required life is obtained on test.

Demonstration of damage tolerance by test of a complete airframe or component may be made difficult by generation of representative flaws, choice of representative damage locations, and possible interactions if more than one location is tested at once. To limit the test work resort may possibly be made to demonstration by calculation for some damage locations. It is accepted practice for safe life design to employ larger factors for demonstration by calculation[41]. It would be prudent to carry this practice through into damage tolerant design. The reasons for an augmented safe life factor apply equally to calculations of damage growth, perhaps more so since there is generally a more severe power law dependence, and additionally greater variability in design data (ie growth rate data) than in life demonstration on test.

3. SOURCES OF VARIABILITY

Variability in crack propagation characteristics can be considered to arise from two sources: experimental procedures, including analysis techniques, and variation within the material itself. The influence of analysis techniques has been discussed elsewhere[7,8]. Accuracy of loading and load distribution (ie elimination of unintentional offsets) are important, since the crack growth rate is a power function of stress. A stable laboratory environment can be seen to be important[24,31].

Material sources of variability can be considered as due to production of the basic material and production of the test specimen. Many investigations have been made into the influence of variations

---

The Author wishes to acknowledge the generosity of Professor A Salvetti of the Institute of Aeronautics, University of Pisa, Mr J I M Forsyth of Structures Department, RAE Farnborough and of Mr F E Kiddle (formerly) of Structures Department, RAE Farnborough, who have all made information on their investigations available prior to publication by themselves.

within the chemical specification and production processes (typical examples[42,43]). Additional variability can arise from position of the test specimen from within the sheet or plate of material[44]. Fig 1 reproduced from Ref 6 shows the difference in crack growth life due to selection of specimens from different positions along the length of a plate and through the thickness of the plate. The effects of residual stresses have been examined (among others by Forsyth[45] and Heath-Smith[46]) and surface treatment and tempering are also important influences[47]. Other results from Kiddle's work[16] are reproduced in Figs 2-6. Each figure shows results for five specimens at each of five different temperatures under programmed load conditions. The results are for crack growth from the edge of a hole and show very high scatter at short crack lengths due to residual stresses resulting from the drilling operation. Figs 2 and 3 are for clad sheet and show large variation to 5 mm crack length. Figs 4 and 5 are for unclad sheet and there is a tendency for the variation to be smaller as crack length increases. Fig 6 for plate material also shows large variations at very short crack lengths which quickly reduce as crack length increases.

4. CHARACTERISATION OF VARIABILITY

Before account of variability can be made it is necessary to establish a method of characterisation. This requires the determination of the typical distribution function and a decision as to whether the standard deviation or the coefficient of variation is the most useful design parameter.

4.1 Distribution

Virkler et al[7] tested 68 identical specimens of 2024-T3 material under identical conditions. Their experimental results are shown in Fig 7. They investigated the methods of obtaining crack growth rates from the data and the best distribution to characterise the lives and rates obtained. Six different distributions were fitted to the experimental data. It was found that at a given ΔK value the best fit to the count of cycles to a given crack length (crack growth life) and to the crack growth rate data $\left(\frac{da}{dn}\right)$ were provided by different distributions. Typical results (reproduced from Virkler's report) are shown in Figs 8a, b, c for cycle count data and Figs 9a, b, c for crack growth rate data.

For cycle count data the three parameter log normal distribution provided the best fit most often. The two parameter distribution did not provide the best fit very often due to the lack of a location parameter. The three parameter Weibull was deficient in that the shape of the density function did not match the data well.

The distribution which best fitted crack growth rate data depended upon whether the data was skewed right or left. With a left skew or symmetric distribution the normal distribution provided the best fit. With a right skew, which was the usual condition, the other distributions fitted better, with the two parameter log normal distribution providing the best fit most frequently overall.

A separate but less comprehensive investigation has been made by the present author. Rooke[5] reported crack propagation tests on DTD 5070A sheet material. The raw data has been reprocessed to investigate crack growth rate distribution at a range of ΔK values with up to 91 specimens at each ΔK value. In this case the material was drawn from 14 different sheets from two different casts. The fit to both the normal distribution and the log normal distribution are shown on Figs 10 and 11 for three different ΔK values. The fit becomes increasingly poor as the ΔK value is increased, but with the log normal distribution providing the best fit.

Clark and Hudak[8] in analysis of a round robin test programme on 10 Ni-8 Co-1 Mo steel commented that the log normal distribution characterised the crack growth process more accurately than the normal distribution.

While the two parameter log normal distribution is not consistently the best fit, it is overall superior to the normal distribution and provides a reasonable compromise for both life and rate distributions. In addition it is consistent with existing practice on safe life distribution. In the absence of further information it is intended to use the log normal distribution.

4.2 Standard Deviation or Coefficient of Variation

If variability is allowed for in the usual way by a scatter factor applicable to all conditions the factor should be based upon a constant value of either standard deviation (σ) or coefficient of variation (C_v). Considering the usual $\frac{da}{dn}$, ΔK curve a constant standard deviation implies that the confidence limits are at a constant displacement from the mean value curve. A constant coefficient of variation corresponds to confidence limits which diverge as the ΔK value increases. Reference to the literature shows confidence limits, where drawn, are usually at (near) constant displacement[10,13,37].

The data obtained from re-analysis of Rooke's experiments[5] have been used to derive the variations of σ and C_v with ΔK. The results are shown on Fig 12 and are inconclusive. It will be seen that neither σ nor C_v are constant. There is an approximate 2:1 variation between the extreme values of σ and similar variations in C_v but with a particularly high value at low ΔK. At high ΔK the value of σ has probably reached a maximum value while C_v continues to decrease. Thus an assumption of constant σ in order to determine a scatter factor is expedient although not well supported by the test evidence. Such an assumption is consistent with safe life practice.

5. EXPERIMENTAL EVIDENCE OF VARIABILITY IN CRACK GROWTH PERFORMANCE

Data collected from the listed references fall into four main groups; those for 2024-T3, for all other aluminium alloys, for steels and for titaniums. Within these groups it is possible to contrast tests to obtain life to a given crack length and tests to obtain crack growth rate at given values of

ΔK . There is also sufficient evidence to comment upon the differences between constant amplitude and random/programmed amplitude tests, the effects of environment on variability and experience from service aeroplanes.

Some of the rate data have been obtained from specimens at different stress levels but at the same ΔK values, corresponding to the application of data in design. Other values have been obtained from striation counting as well as measurement of local slope of the crack growth curve. Finally some of the standard deviations on rate have been derived from confidence limits presented on graphs, the ESDU[37] results in particular being a distillation from several different references.

While there are sufficient results to demonstrate variability in crack growth performance the collected data relates to a range of different conditions. Some results are for specimens taken from a single piece of material while others are for specimens from many pieces and from more than one melt. To represent design information the variability must relate to the range of crack growth performance which could be expected from material used during the construction run of a number of aircraft. Thus the variability should relate to material drawn from a number of different melts and positions in the plate or sheet together with representative thicknesses and environments. Many of the reported data are related to investigations where causes of variability have been reduced to a minimum to meet the original purposes of the test. For this reason the data cannot be considered as belonging to a single population representative of design conditions and no attempt has been made to evolve a typical measure of variability.

5.1 Aluminium Alloys

There is considerably more data available on aluminium alloys than on steel or titanium. In this group of materials 2024-T3 has been used for more experimental programmes than any other material. Sufficient information has been gathered on variability of 2024-T3 specimens for these results to be presented separately.

5.1.1 2024-T3

The data on 2024-T3 is presented in Figs 14a and 14b for standard deviation on log crack growth life and standard deviation log crack growth rate respectively. The reference source, number of specimens and derivation (ie direct quote, measurement of published data, re-analysis) is shown together with any comments. Different symbols have been used for constant amplitude loading, programmed block loading and random amplitude loading.

Much of the data which show low variability are derived from tests where specimens have been taken from a restricted source of material (perhaps one panel). In this case typical values of σ would appear to be around 0.07. Schijve[6] tested seven different batches of material and obtained values of σ on crack life of 0.07 to 0.12 at various loading conditions. Re-analysis of Schijve's data to obtain crack growth rates results in σ values up to 0.15. Ellis[9] tested a number of large panels to obtain crack growth data. Most of these tests were at different load levels and comparison can therefore only be made at constant ΔK values to obtain rates. Furthermore only 'spot' values of ΔK are given. Confining attention to only seven of a possible 18 results rates can be compared over a small range of ΔK ($17.33 - 18.4$ MN $m^{-3/2}$) resulting in a value $\sigma = 0.29$. Attention is also drawn to the values obtained from confidence limits aligned to the design data in the ESDU data items[37]. Here data has been collected from a number of different sources and design curves have been derived. Significantly when design information is derived in this way; arguably most representative of material variations during a long production run; variability is considerably increased to give values of σ equal 0.2 to 0.4.

Comparatively little 'life' information is available compared to 'rate' information. Where comparison can be made (ie Schijve[6]) it will be seen that the variability in rate is greater.

5.1.2 Other Aluminium Alloys

The collected information on all aluminium alloys other than 2024-T3 is presented on Figs 15a and 15b for crack growth life and rate respectively.

Rather more information on crack growth life is available for comparison than was the case for 2024-T3. O'Neill[32] tested a number of specimens under constant strain amplitude, with between five and 16 specimens at each of eight load levels. Standard deviation values of between 0.06 and 0.08 were obtained at six load levels, the other two values being 0.10 and 0.125. Comparison can be made with tests by van Dijk and Nederveen[20] under 11 different flight simulation programmes. Standard deviation values for five or six specimens at each load condition range from 0.05 to 0.11.

The variability found during O'Neill's tests[32] is presented on both Figs 15a and 15b for crack growth life and crack growth rate. As for the example for 2024-T3, the variability in rate is greater than in life; in the case of O'Neill's L73 data by a factor of almost two.

5.2 Titanium Alloys

Data for titanium alloys are presented in Figs 17a and 17b. There is much less information than for aluminium alloys. The variability in crack growth life was generally found to be small, particularly for sheet material[18]. However the results for crack growth rate variability show both high and low values of standard deviation. Some of these values were obtained from confidence limits. Impellizzeri's results[19] have been analysed to obtain the standard deviation for both rate and life and show greater variability in rate. The general level of variability is not subjectively different from aluminium alloys.

5.3 Steels

Data for steels are shown in Figs 18a and 18b, again following the presentation style previously adopted. As with titanium there is comparatively little information. With the exception of the data for mild steel the results show variability which does not exceed that of aluminium alloys. In the absence of more experimental results an assumed variability based upon the aluminium alloy data would be justified.

5.4 Comparison of Variability under Constant Amplitude and Variable Amplitude Loading

Attention has previously been directed to comparison of the results from re-analysis of O'Neill's[32] experiments and the standard deviations quoted by van Dijk and Nederveen[20]. In numbers of specimens and test conditions these sets of experiments are comparable, and it will be seen from Fig 15a that the standard deviations obtained under constant amplitude and random amplitude loadings are very similar.

Strictly, comparison should be made between sets of results obtained using the same standard of technology for all loading conditions. This is extremely difficult to ensure without a background of direct involvement in the test programme. Comparisons restricted to results under both load waveforms which come from the same source, preferably in the same report, should provide valid indications.

Schijve[6] included in his experiments some programme load tests. The standard deviations for his constant amplitude tests vary from 0.07 to 0.12. The single group of programme load tests gave a value of $\sigma = 0.06$.

Salvetti[11] as a prelude to crack propagation tests on stiffened panels tested four panels of 2024-T3. Typical standard deviations for these tests are around 0.005. Later tests[23] under FALSTAFF loading on flat panels of the same material resulted in σ values of 0.02 to 0.045.

Oberparleiter[26] in a series of experiments on Titanium 6 Al-4 Vn plate provides data for a number of comparisons of the effects of load waveform. Under constant amplitude standard deviations for two different groups of experiments were 0.06 and 0.075. The corresponding values under FALSTAFF and an operational spectrum were 0.11 and 0.08. Tests were also made on a modified alloy which was found to be sensitive to frequency effects. At the same frequency the constant amplitude test variability gave $\sigma = 0.016$ and under an operational spectrum $\sigma = 0.096$.

Oberparleiter and Schutz[27] tested several different materials under both constant amplitude loading and FALSTAFF loading. The standard deviations derived from these results are tabulated below:

STANDARD DEVIATIONS (Data of Ref 27)

Material	Constant Amplitude	FALSTAFF
7075-T7351	0.0228	0.0273 and 0.0171
HP 9-4-30	0.0670	0.0349
Titanium 6 Al-4 Vn	0.0608	0.0259

The effects of environment on crack propagation data have been studied at NLR and the experimental results have been reported[24]. These also give further comparisons between constant amplitude and random amplitude tests for 7075-T6 material. The values of standard deviation for tests under constant amplitude loads in normal air and salt water were 0.008 and 0.011 respectively. Corresponding standard deviation values under random amplitude loads were 0.08 and 0.016.

The results above give no support to the sometimes proposed suggestion that there is less variability in crack propagation tests under random amplitude loading than under constant amplitude loads. Possibly the reverse could be true, but on the evidence available at present it would be prudent to assume that load waveform has no substantial influence on variability.

5.5 Effect of Environment on Variability

Studies by the NLR[24] provide the only data on this topic known to the author. The results of this work are tabulated below:

Material	Environment	Load Waveform	Thickness (mm)	Standard Deviation
2024-T3	Dry air	Random amplitude	2	0.058
	Normal air			0.028
	Salt water			0.055
7075-T6	Dry air	Random amplitude	2	0.060
	Normal air			0.077
	Salt water			0.016
7075-T6	Normal air	Constant amplitude	2	0.008
	Salt water			0.011
7075-T6	Normal air	Constant amplitude	10	0.015
	Salt water			0.057

There is no evidence of any systematic influence of environment on variability.

5.6 Variability of Structural Components

Most of the results discussed are for simple specimens. A few are for component items. These include lugs, rotor blades and stiffened panels, the latter being both integral and built up, with some information from service use.

The standard deviations for crack propagation life tests on lugs[19] were 0.055 and 0.06 for male and female lugs tested in the laboratory. Forsyth[15] has analysed 31 cases of cracking of an aircraft lug in service. Of these 18 occurred at one location and the remaining 13 at another. The lug was an undercarriage operating jack attachment point, loaded once per jack operation corresponding to constant amplitude loading. Measurements of crack length must be considered crude. For 18 cracks the standard deviation on crack growth life was 0.10 and for 13 cracks 0.15.

Stiffened panels have been tested by Salvetti[11,23] and by the present author[14] and Forsyth[15] has also provided information from service aircraft. In his earlier work[11] Salvetti included two separate groups of three specimens tested identically under constant amplitude loads. These gave standard deviation values on crack growth life of 0.15 and 0.02. In his more recent work Salvetti[23] tested six stiffened panels under FALSTAFF loading and obtained standard deviations of around 0.04. Anstee and Morrow[14] reported tests on integrally stiffened fuselage panels which gave a standard deviation of 0.15. Experience from five incidents of closely monitored wing skin cracking which occurred on a jet trainer aircraft gave a standard deviation of 0.03 under service flying loads.

Crack propagation tests are regularly made on helicopter rotor blades by some sections of the Industry. Two manufacturers have reported tests under block loading sequences[25,28]. Eight samples of one blade type were tested. Five to an anti-submarine spectrum and three to a search and rescue spectrum. The standard deviations on crack propagation life were 0.12 and 0.03 respectively. Ten samples of a different blade were tested to a general flying spectrum and standard deviations of 0.07 to 0.12 were obtained, depending upon final crack length.

From these data a wide range of standard deviations have been obtained but showing no significant differences to the range of values found for the simple specimens.

6 DISCUSSION

The variability found from the referenced papers can be seen to be greater for crack growth rate than for crack growth life. There is no evidence of load waveform or environment having a strong influence on variability. There is evidence that overall variability is influenced by selection of specimens from within a section of material and by the inclusion of additional melts in the test material stock pile. For this reason results which show small variability where material has been carefully selected should not be used to produce design guidelines.

Much of the material presented is far from ideal as a base for design rules. Even so the standard deviations found for crack growth life can be said to be quite similar to those found in safe life testing. This conclusion has been reached independently by van Dijk and Nederveen[20] who compared their results with a survey of safe life test experience by Hooke[49]. The range of standard deviations are reasonably bounded by a value $\sigma = 0.176$ as used for life prediction in the UK. It seems reasonable then to assume that the same variability occurs in crack growth life as in safe life testing. This may not mean use of the same scatter factors since, as discussed previously, the probabilities of cracks occurring and of them being detected (or not detected) may need to be considered.

Development of crack growth rate curves for design purposes poses a particular problem due to the demonstrated greater variability in rate than in life. One solution would be the development of 'A' and 'B' design curves in the same manner as used to define 'A' and 'B' static strength design data. The procedures are set out in MIL Handbook 5[48]. The crack growth rate at a given stress intensity factor range is then given by:

$$\frac{da}{dn} = \text{antilog}\left[\log_{10}\left(\frac{da}{dn}\right) + K\ SD\ \log_{10}\left(\frac{da}{dn}\right)\right]$$

where K is obtained from the Handbook. The A and B design curves have been developed for the Rooke[5] data and are shown on Fig 18. The factor on crack growth rate ranges from 2 to 4 and is strongly dependant upon the standard deviation and less so on the number of tests at each level.

7 CONCLUSIONS

7.1 There is considerable evidence of variability in crack growth performance.

7.2 Due to the extra manipulation of test measurements there is more variability in crack growth rate data than in crack growth life data.

7.3 No single distribution fits the data. A three parameter log normal distribution has been found to provide the best fit most often. A two parameter log normal has been used in this paper to conform with existing practice.

7.4 Load waveform and environment have little effect upon variability.

7.5 Variability can be minimised by careful selection of specimens. This may result in insufficient account of variability in design.

7.6 All groups of materials discussed have much the same variability.

7.7 Variability in crack growth life is similar in magnitude to the variability which occurs in safe life tests.

7.8 Crack growth rate design curves which include factors for variability can be developed from relatively few tests using established procedure.

8. REFERENCES

1. BARROIS W Critical Study on Fatigue Crack Propagation.
AGARD Report 412 (June 1962).

2. DONALDSON D R and ANDERSON W E Crack Propagation Behaviour of Some Airframe Materials in Proceeding of the Crack Propagation Symposium, Cranfield 1961.

3. PARRY-JONES G Fatigue Crack Propagation in Mustang Wings.
ARL Report SM 289 (June 1962).

4. JOST G S The Fatigue of 24 S-T Aluminium Alloy Wings under Asymmetric Spectrum Loading.
ARL Report SM 295 (February 1964).

5. ROOKE D P, GUHN N J F, BALLETT J T, BRADSHAW F J Crack Propagation in Fatigue. Some Experiments with DTD 5070A Aluminium Alloy Sheet.
RAE TR 64025 (October 1964).

6. SCHIJVE J and de RIJK P The Fatigue Crack Propagation in 2024-T3 Alclad Sheet Materials from Seven Different Manufacturers.
NLR TR M.2162 (May 1966).

7. VIRKLER D A, HILLBERRY B M, GOEL P K The Statistical Nature of Fatigue Crack Propagation.
AFFDL TR 78-43 (April 1978).

8. CLARK W G, HUDAK S J Variability in Fatigue Crack Growth Rate Testing.
Journal of Testing and Evaluation, TJEVA, Vol 3, No 6 (1975).

9. ELLIS R Fracture Mechanics Studies of Fatigue Crack Propagation in 2024 Aluminium Alloy Panels Containing Transverse Slits.
ARL SM 379 (August 1972).

10. POE C C Fatigue Crack Propagation in Stiffened Panels, in Damage Tolerance of Aircraft Structures.
ASTM STP 486 (1971).

11. SALVETTI A Dati Sperimentali e Risultati Della Elaborazione Di 50 Prove Di Propagazioni Della Fessura per Fatica in Pannelli Con e Senza Irrigidimenti.
Documenti Dell Instituto Di Aeronautica Dell 'Universita' Di Pisa (1977).

12. BARROIS W Private Communication to ICAF Members, London ICAF Conference (1973).

13. FROST N E, POOK L P, DENTON K A Fracture Mechanics Analysis of Fatigue Crack Growth Data for Various Materials.
Engineering Fracture Mechanics, Vol 3, No 2 (1971).

14. ANSTEE R F W, MORROW Sarah M The Effects of Biaxial Loading on the Propagation of Cracks in Integrally Stiffened Panels.
10th ICAF Symposium, Brussels (1979).

15. FORSYTH J I M Unpublished Investigations.
RAE 1978/79.

16. KIDDLE F E Unpublished Research.
RAE.

17. OBERPARLEITER W, SCHUTZ W Ribfortschritt an 7075-T7351 Platten unter Einzelflugbelastung.
IABG-Report TF-482 (1975).

18. ZENNER H, SCHUTZ W Ribfortschritt an Titanblenchen im Einzelflugversuch.
IABG-Report TF-224 (1972).

19. IMPELLIZZERI L F, RICH D L Spectrum Fatigue Crack Growth in Lugs in Fatigue Crack Growth under Spectrum Loads.
ASTM STP 595 (1976).

20. van DIJK G M, NEDERVEEN A F104G Related Flight Simulation Fatigue Tests on 7075-T6 Notched Specimens.
NLR TR 75071 U (1975).

21. SWANSON S R, CICCI F, HOPPE W Crack Propagation in Clad 7079-T6 Aluminium Alloy Sheet under Constant and Random Amplitude Fatigue Loading.
ASTM STP 415 (1967).

22. von EUW E F J, HERTZBERG R W, ROBERTS R Delay Effects in Fatigue Crack Propagation.
ASTM STP 513 (1972).

23. SALVETTI A Research Results to be Published (1979).

24. N N Compilation of Test Data from an Investigation on the Effect of Environment on Crack Growth under Flight Simulation Loading.
NLR TR 76096 U (1976).

25. Private Communication. Helicopter Industry (Manufacturer A).

26. OBERPARLEITER W Bauteilspezifische Werkstoffuntersuchungen. Untersuchungen am Halbzeug Ti6Al4V-Platte.
IABG-Report TF-675.3 (1977).

27. OBERPARLEITER W, SCHUTZ W Ribfortschrittsverhalten von 7075-T7351, HP 9-4-30, 300 M und Ti6Al4V unter Einzelflug- und Einstufenbelastung.
IABG-Report TF-549 (1975).

28. Private Communication. Helicopter Industry (Manufacturer B).

29. HUDSON C M Effect of Stress Ratio on Fatigue Crack Growth in 7075-T6 and 2024-T3 Aluminium Alloy Specimens.
NASA TND-5390 (1969).

30. HUDSON C M, NEWMAN J C Effect of Specimen Thickness on Fatigue Crack Growth Behaviour and Fracture Toughness of 7075-T6 and 7178-T6 Aluminium Alloys.
NASA TN-D-7173 (1973).

31. FERGUSON R R, BERRYMAN R C Fracture Mechanics Evaluation of B1 Materials (Vol II).
AFML-TR-76-137, Vol II (1976).

32. O'NEILL P H Fatigue Crack Propagation in Thin Sheets of L73 Under Constant Strain Amplitude.
RAE TR 74042 (1974).

33. GUNN N J F, BALLETT J T, ROOKE D P, BRADSHAW F J Fatigue Crack Propagation at High Rates in Clad RR 58 Sheet to DTD 5070A and in Machined RR 58 Plate to BAC M76A-4.
RAE TM Mat 103.

34. GUNN N J F, BALLETT J T Fatigue Crack Propagation and Residual Strength Tests on 5 inch Wide Panels Cut from CM 003D-4 and BAC M76A-4 Integrally Stiffened Panels.
RAE TM Mat 91 (1970).

35. ANCTIL A A, KULA E B Effect of Tempering Temperature on Fatigue Crack Propagation in 4340 Steel.
ASTM STP 462 (1970).

36. WALKER E K An Effective Strain Concept for Crack Propagation and Fatigue Life with Specific Applications to Biaxial Stress Fatigue.
AFFML TR 70-144 (1970).

37. Engineering Sciences Data Unit (ESDU). Fatigue Sub-Series, Vol 4. Crack Propagation.

38. N N Airplane Damage Tolerance Requirements.
Military Specification MIL-A-83444 (USAF) (July 1974).

39. McCARTHY J F, TIFFANY C J, ORRINGER O The Application of Fracture Mechanics to Decisions on Structural Modifications of Existing Aircraft Fleets.
AMMRC M577-5 (Case Studies in Fracture Mechanics. Editors RICH T P and CARTWRIGHT D J.)

40. N N AvP 970 Design Requirements for Service Aircraft.

41. MAXWELL R D J The Practical Implementation of Fatigue Requirements to Military Aircraft and Helicopters in the United Kingdom.
6th ICAF Symposium, Florida (1971).

42. GUNN N J F, BALLETT J T, BINNING M S Fatigue Crack Propagation and Residual Strength Tests on 5 inch Wide x 0.06 inch Thick Panels Cut from a 'Dilute RR 58' Plate.
RAE TM Mat 134 (1972).

43. AMATEAU M F, HANNA W D, KENDALL E G The Effect of Microstructure on Fatigue Crack Propagation in Ti-6Al-6V-2Sn Alloy.
SAMSO TR 71-268.

44. WANHILL R J H The Effect of Sheet Thickness on Flight Simulation Fatigue Crack Propagation in 2024-T3, 7475-T761 and Mill Annealed Ti-6Al-4V.
NLR MP 77024 U (1977).

45. FORSYTH P J E, BOWEN A W The Relationship between Fatigue Crack Behaviour and Microstructure in 7178 Aluminium Alloy.
RAE TR 78006 (1978).

46. HEATH-SMITH J R, APLIN JUDY E The Effect of an Application of Heat on the Fatigue Performance under Random Loading of a Notched Specimen of DTD 5014 (RR 58).
RAE TR 71209 (1971).

47. FORSYTH P J E The Microstructural Changes that Drilling and Reaming can Cause in the Bore of Holes in DTD 5014 (RR 58 Extrusions) and the Effects of Subsequent Heating.
Aircraft Engineering (November 1972).

48. N N Military Standardization Handbook. Metallic Materials and Elements for Aerospace Vehicle Structures.
MIL-HDBK-5B (1974).

49. HOOKE F H The Fatigue Life of Safe Life and Fail Safe Structures, a State of the Art Review.
ARL-SM Report 334 (1971).

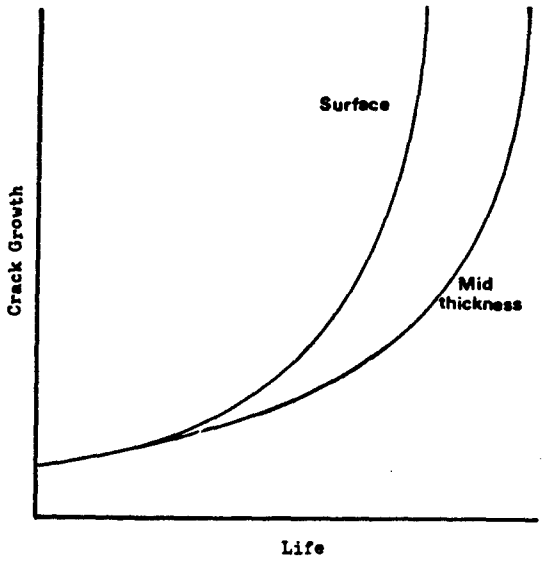

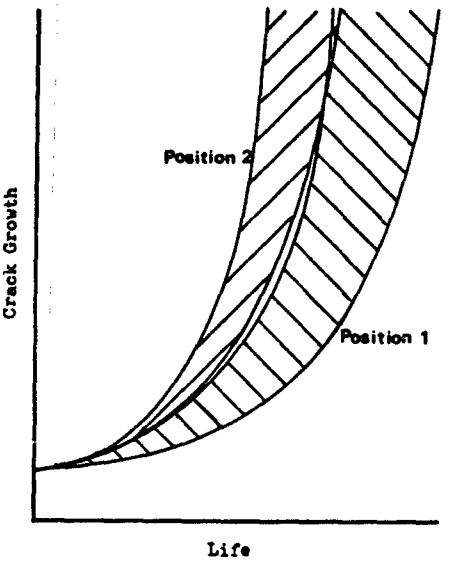

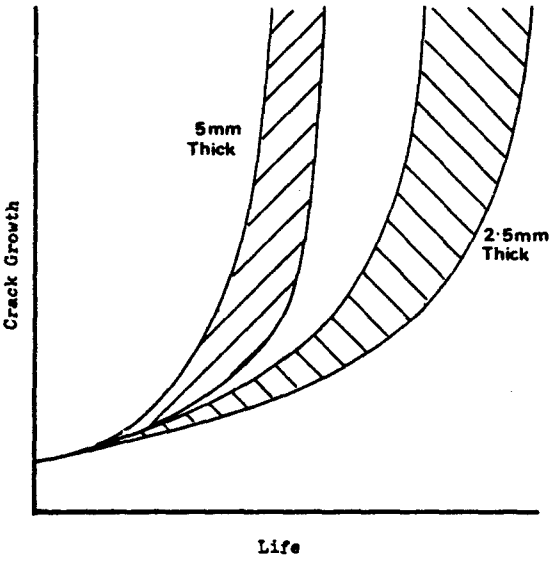

FIGURE 1
Effect of
a) surface & mid. thickness
b) location in plate length
c) specimen thickness

Data from Ref. 26

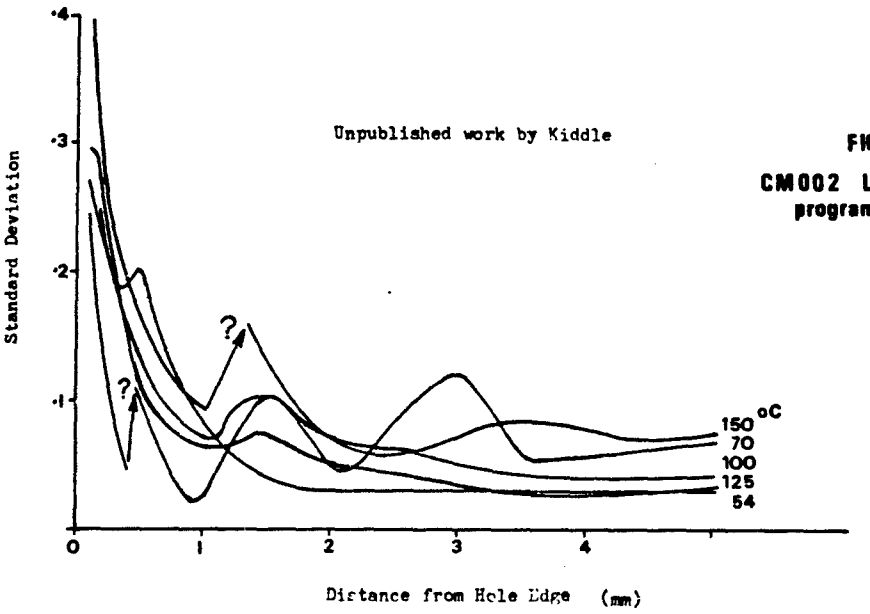

Unpublished work by Kiddle

FIGURE 2

CM002 Loaded to programme 1

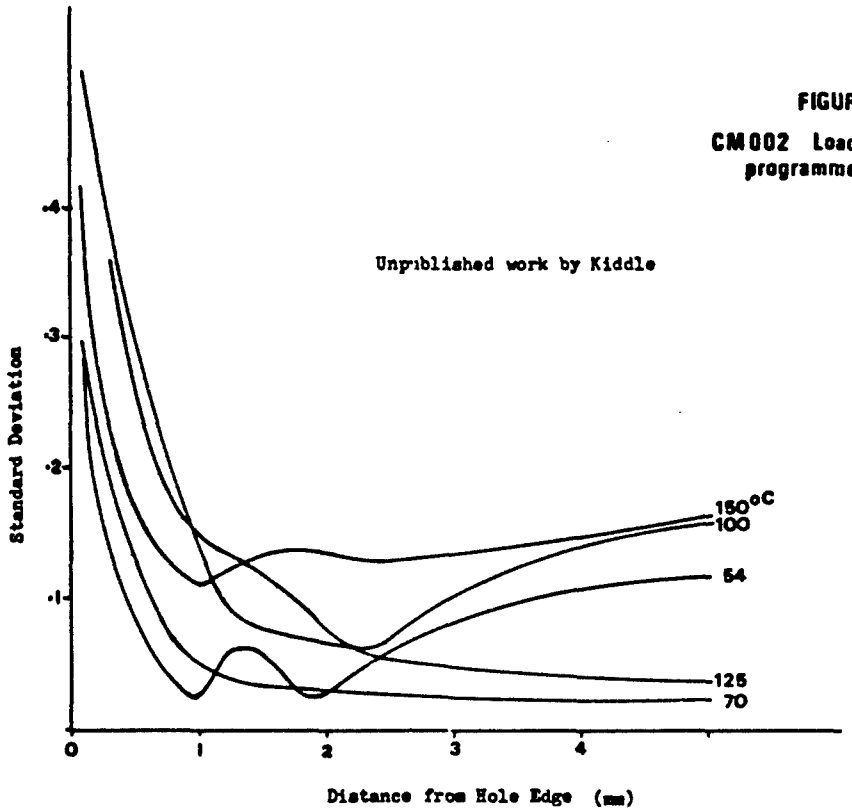

FIGURE 3

CM002 Loaded to programme 2

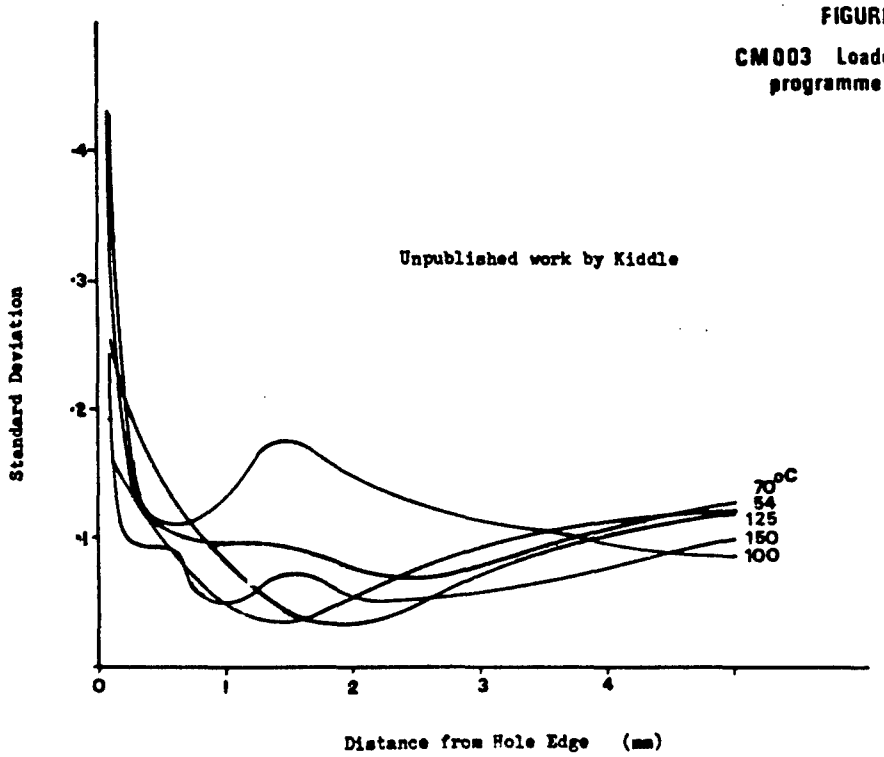

FIGURE 4

CM003 Loaded to programme 1

FIGURE 5

CM001 Loaded to programme 1

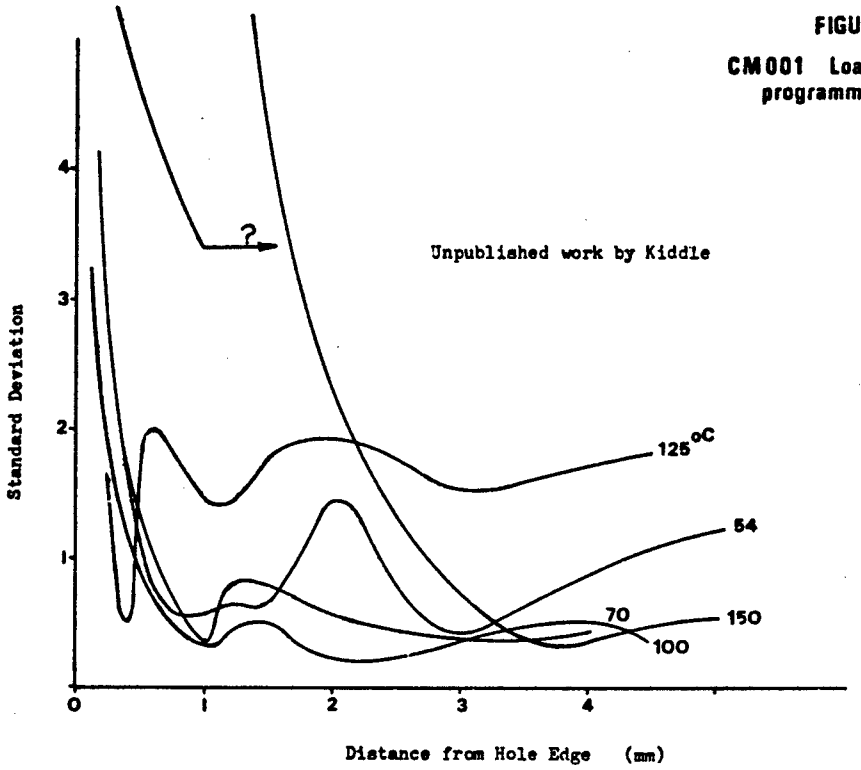

FIGURE 6

CM001 Loaded to programme 2

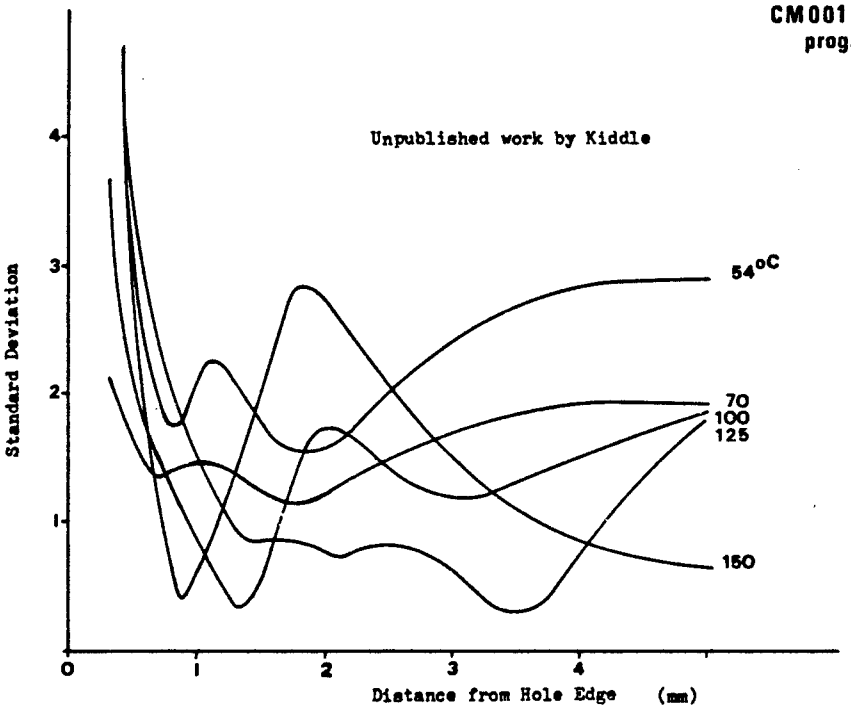

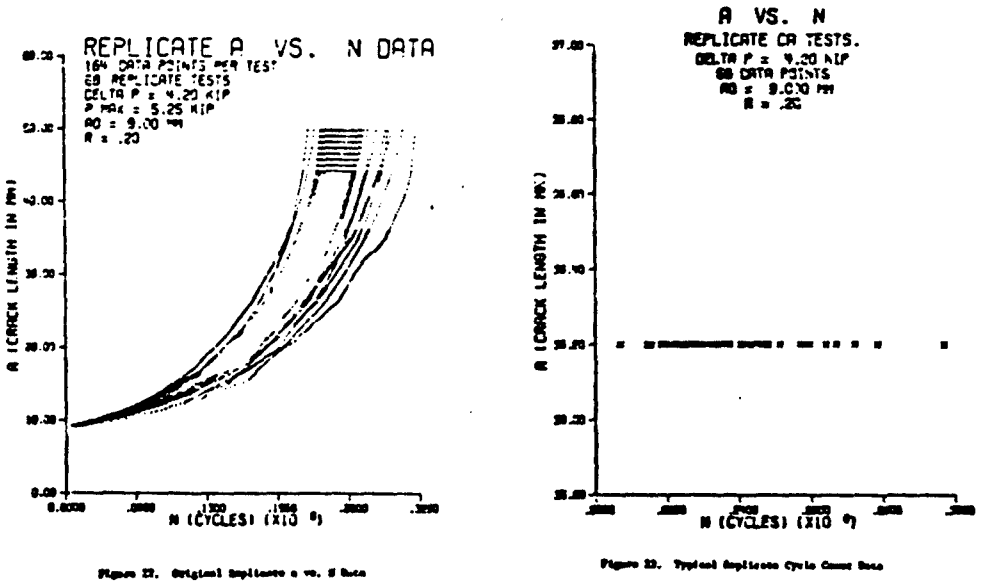

Figure 32. Original Replicate a vs. N Data

Figure 33. Typical Replicate Cycle Count Data

FIGURE 7 Data from 68 identical crack growth tests

Figs from Ref 7 (Virkler et al)

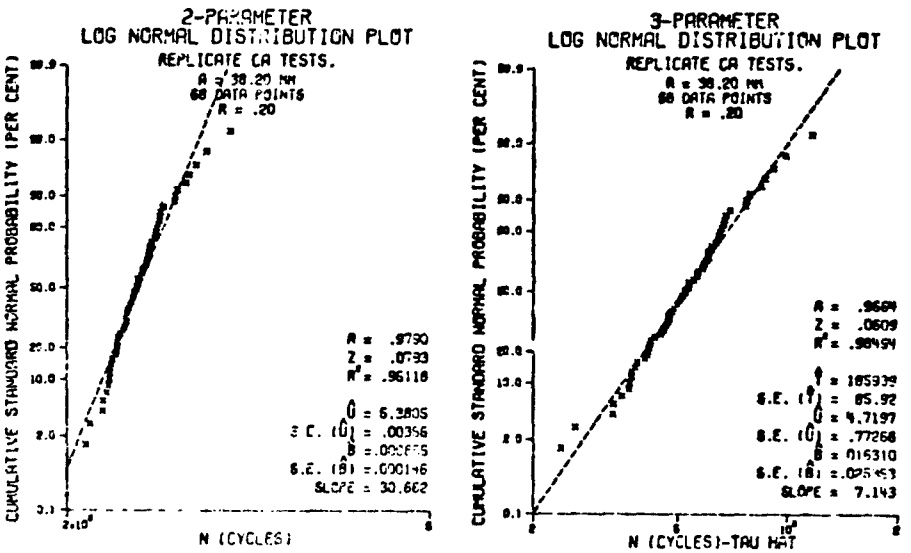

Figure 69. Typical Fit of the Cycle Count Data to the 2-Parameter Log Normal Distribution

Figure 70. Typical Fit of the Cycle Count Data to the 3-Parameter Log Normal Distribution

FIGURE 8 Fit of distributions to crack growth life data

Figs from Ref 7 (Virkler et al)

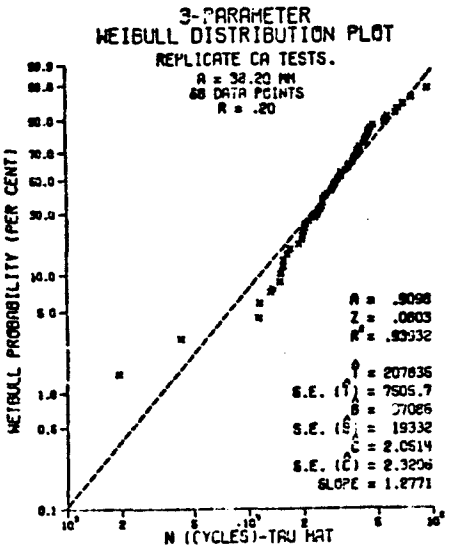

Figure 71. Typical Fit of the Cycle Count Data to the 3-Parameter Weibull Distribution

FIGURE 8 continued

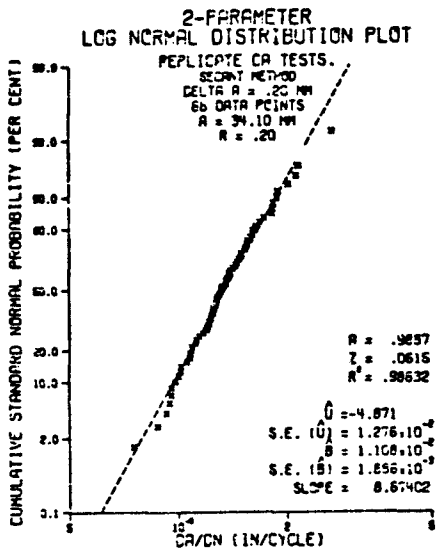

Figure 78. Typical Fit of Skewed Right da/dN Data to the 2-Parameter Log Normal Distribution

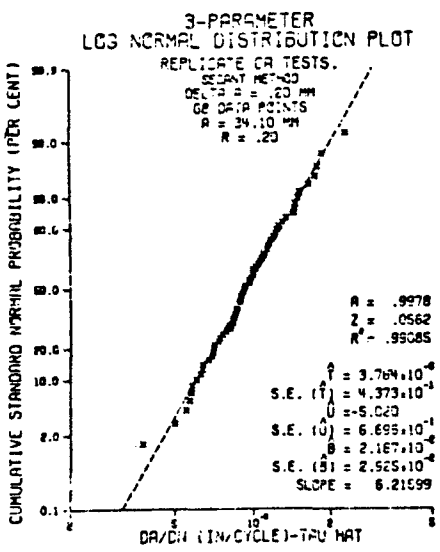

Figure 79. Typical Fit of Skewed Right da/dN Data to the 3-Parameter Log Normal Distribution

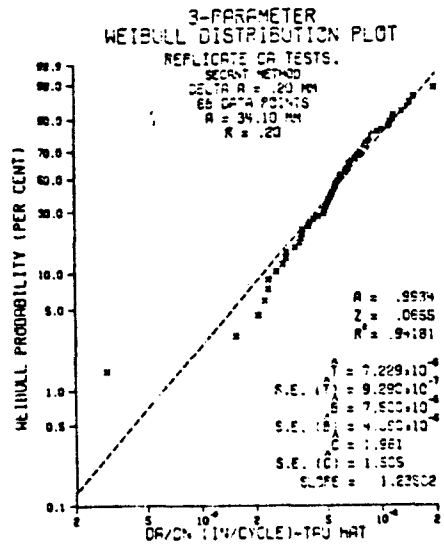

Figure 80. Typical Fit of Skewed Right da/dN Data to the 3-Parameter Weibull Distribution

FIGURE 9 Fit of distributions to crack growth rate data

Figs from Ref 7 (Virkler et al)

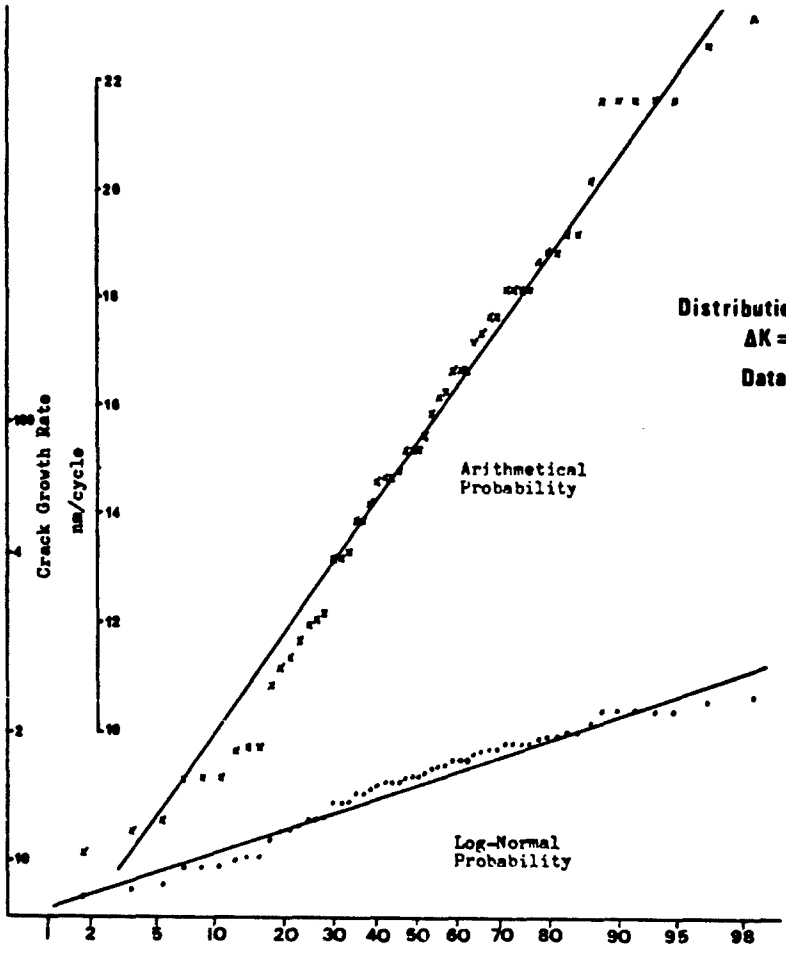

FIGURE 10

Distribution of crack growth rate values
$\Delta K = 4{\cdot}4\ MNm^{-3/2}$
Data from Ref 5

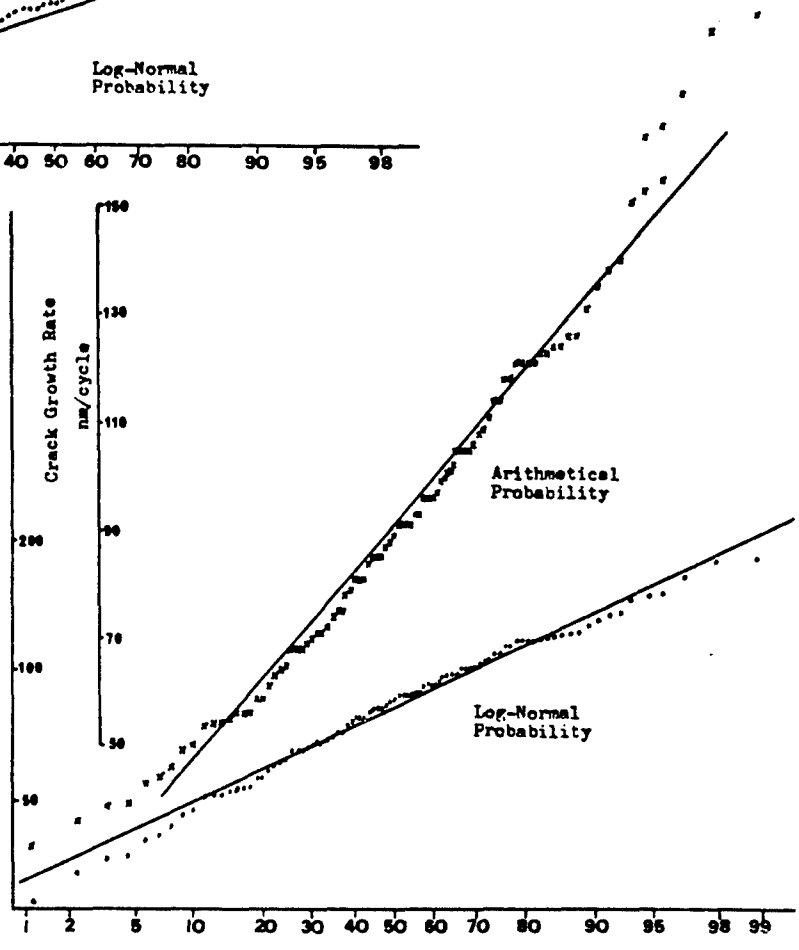

FIGURE 11

Distribution of crack growth rate values
$\Delta K = 6{\cdot}6\ MNm^{-3/2}$
Data from Ref 5

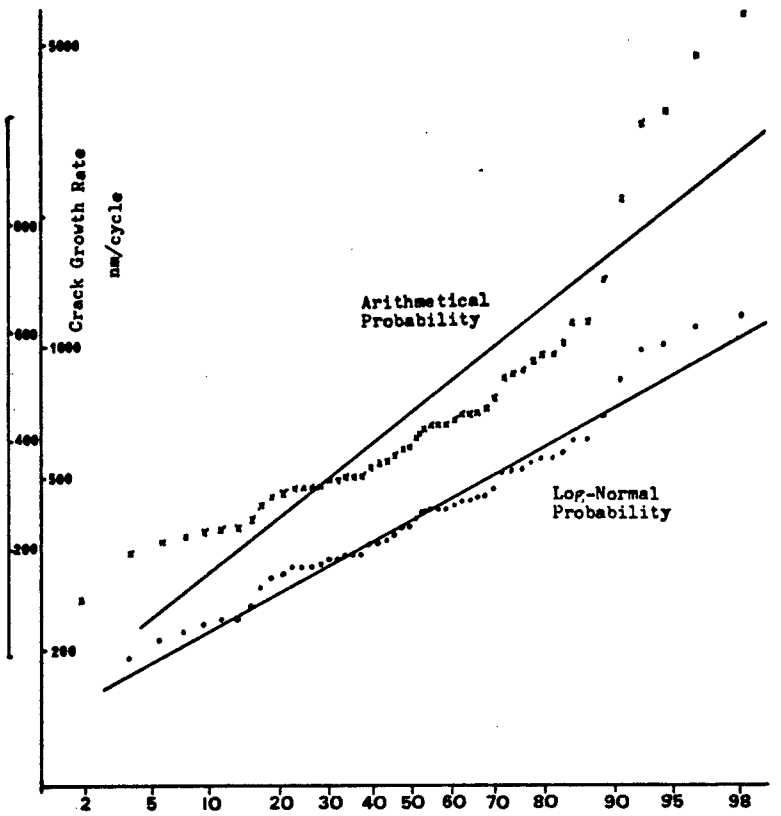

FIGURE 12 Distribution of crack growth rate values
$\Delta K = 8{\cdot}8\ MNm^{-3/2}$
Data from Ref 5

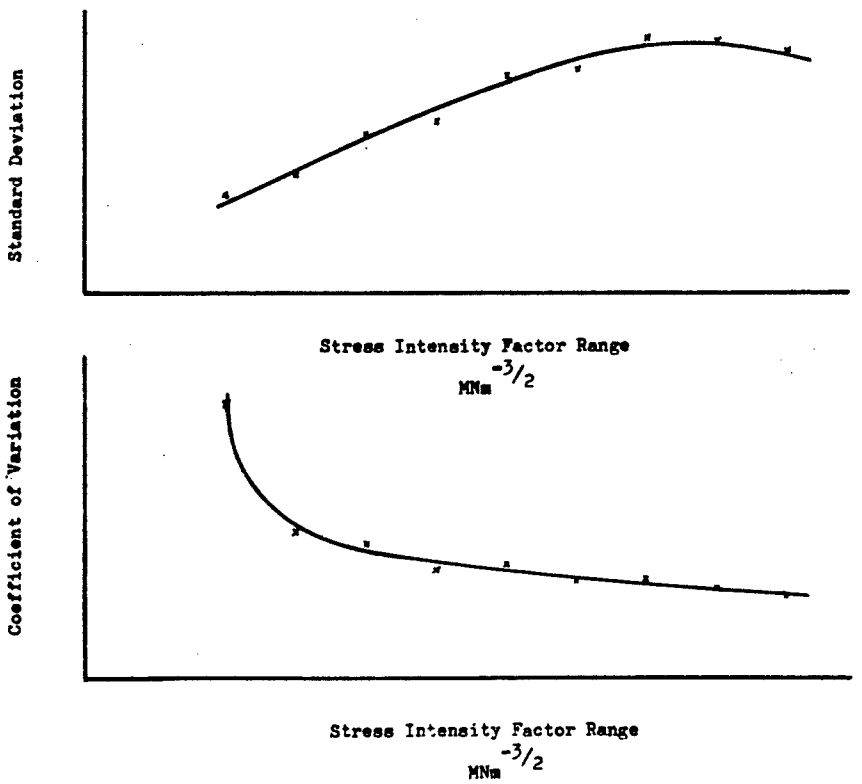

FIGURE 13 Variation of σ' and C_v with ΔK

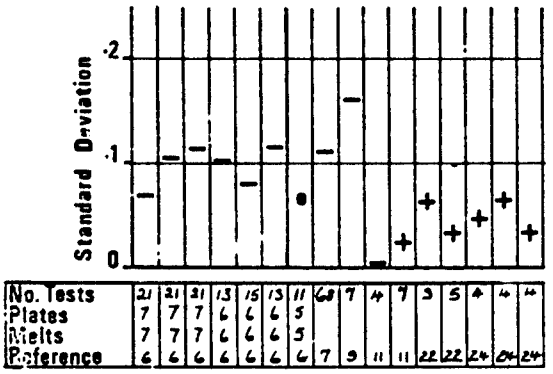

14a Crack Growth Life

- Constant Amplitude
o Block Programme
+ Random

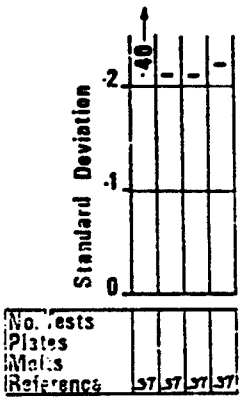

14b Crack Growth Rate

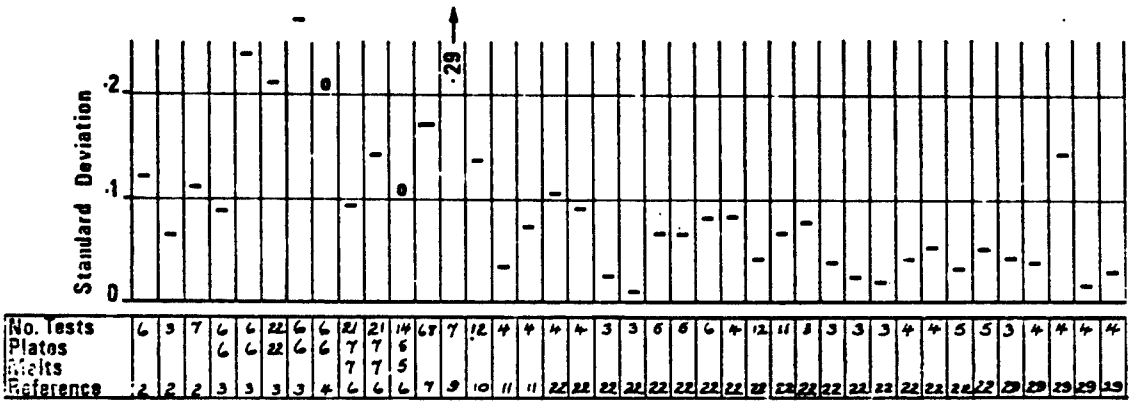

14b Crack Growth Rate

FIGURE 14 Standard Deviations - 2024-T3

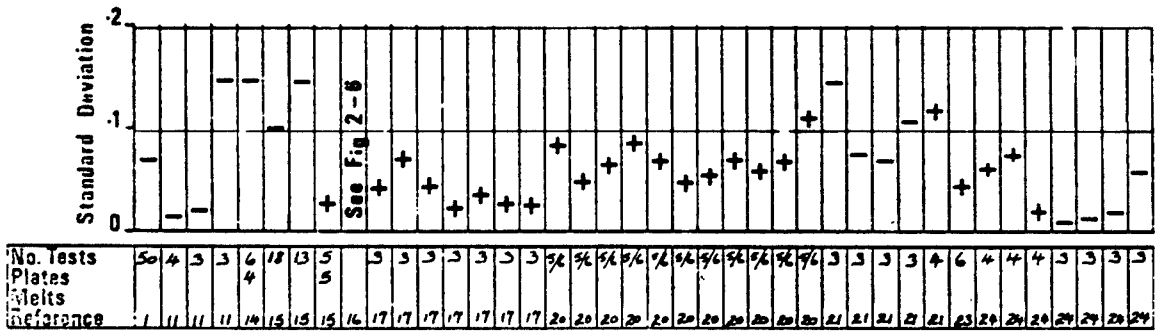

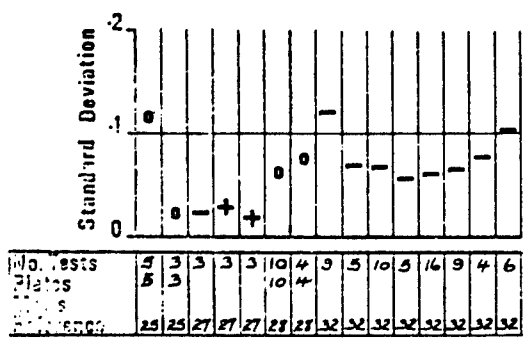

15a Crack Growth Life

- Constant Amplitude
o Block Programme
+ Random

FIGURE 15 Standard Deviations

Aluminium Alloys excluding 2024-T3

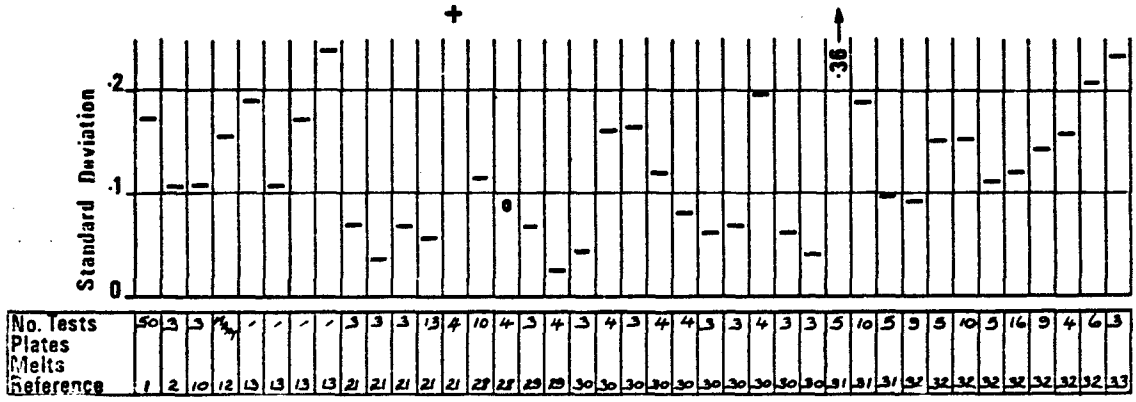

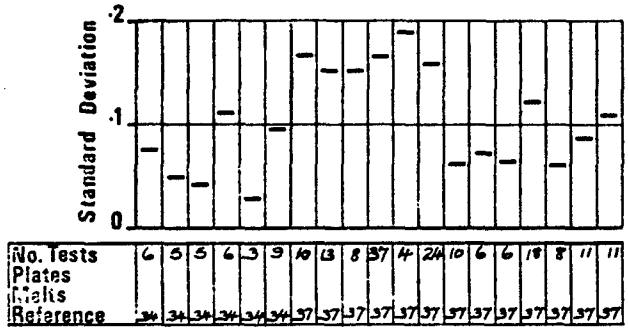

15b Crack Growth Rate

– Constant Amplitude
o Block Programme
+ Random

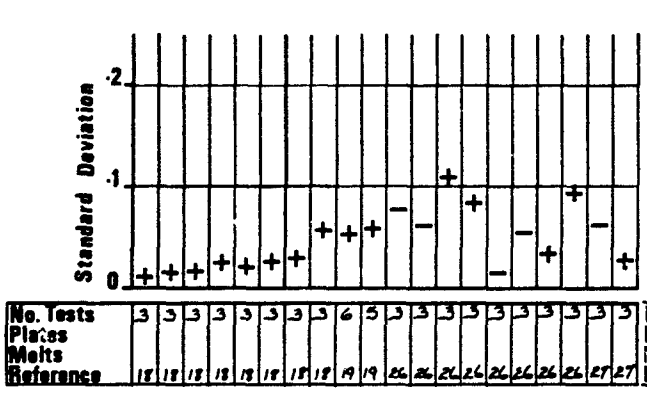

16a Crack Growth Life

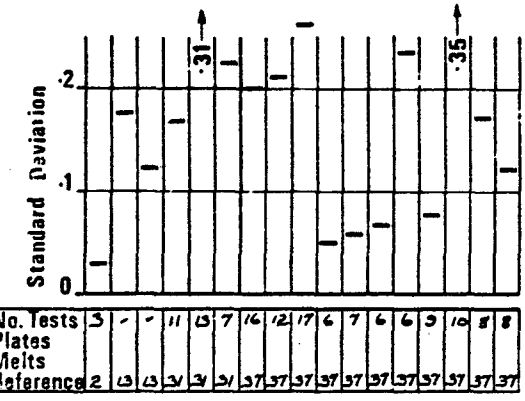

16b Crack Growth Rate

FIGURE 16 Standard Deviations – Titanium Alloys

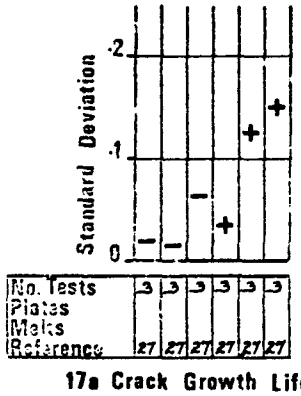

17a Crack Growth Life

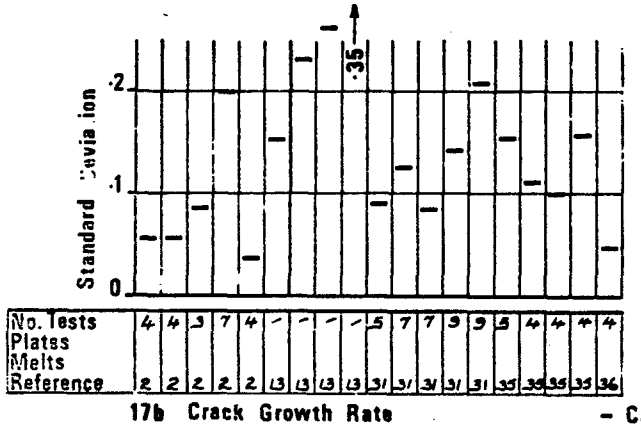

17b Crack Growth Rate

– Constant Amplitude
o Block Programme
+ Random

FIGURE 17 Standard Deviations – Steels

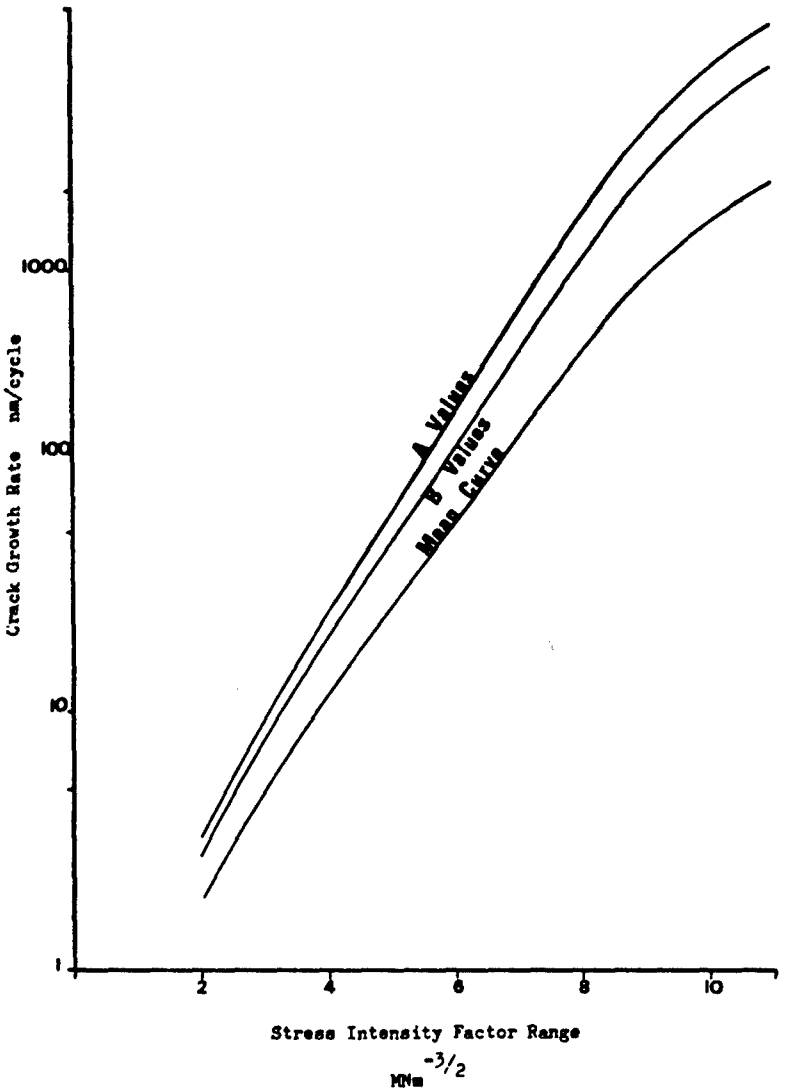

FIGURE 18 A and B design curves DTD 5070A
(16swg; R = 0·1)

APPENDIX A: AN INTRODUCTION TO STATISTICAL TERMS AND METHODS USED IN ANALYSING DATA (Item 68013)

1. NOTATION 8-34
2. DEFINITION OF GENERAL TERMS. 8-34
3. PRESENTATION OF EMPIRICAL DATA 8-35
4. ESTIMATION OF POPULATION PROPERTIES FROM A SAMPLE. 8-35
5. COMPARISON OF SAMPLES. 8-36

A.1 PLOTTING POSITION OF VARIATE ON PROBABILITY SCALE. 8-38

APPENDIX B: THE ANALYSIS OF NORMALLY DISTRIBUTED DATA (Item 68014)

1. NOTATION 8-41
2. INTRODUCTION 8-41
3. ESTIMATES OF PROPERTIES OF POPULATION FROM SAMPLE. 8-42
4. DERIVATION 8-43
5. ADDENDUM 8-51

APPENDIX C: THE ANALYSIS OF DATA CONFORMING TO AN EXTREME-VALUE DISTRIBUTION (Item 68015)

1. NOTATION 8-52
2. INTRODUCTION 8-52
3. ANALYSIS OF DATA USING PROBABILITY PAPER 8-52
4. DERIVATION 8-53

APPENDIX A
AN INTRODUCTION TO STATISTICAL TERMS AND METHODS USED IN ANALYSING DATA
(Item 68013)

1. NOTATION

s	order number
N	fatigue endurance
n	number of observations
$P(x)$	proportion of total population having values less than a given value of x
$p(x)$	relative frequency of occurrence of x
X	random variable
x	variate $F(X)$
$x_{(p)}$	percentile

2. DEFINITIONS OF GENERAL TERMS

In order to illustrate the terms used in statistical analysis, a typical set of fatigue data is shown. The observations are listed in ascending order of magnitude against the corresponding values of s.

Order s	1	2	3	4	5	6	7	8
Endurance N kc	20.6	124.4	168.7	187.2	203.0	213.4	213.4	215.7
$Log_{10}N$	1.31	2.09	2.23	2.27	2.31	2.33	2.33	2.33
Order s	9	10	11	12	13	14	15	
Endurance N kc	219.2	221.0	254.0	274.0	283.8	348.6	391.2	
$Log_{10}N$	2.34	2.34	2.40	2.44	2.45	2.54	2.59	

The random variable is the property which is observed to vary over a number of repetitions of a given process, such as fatigue strength or endurance. In the example, the random variable is $X = N$.

The variate is that function whose distribution of values is considered. In the example the variate may be either N or $\log N$, the latter transformation being made as a result of the convenience of this form for subsequent analysis.

The order number is the number ascribed to each observation corresponding to its position in the data arranged in order of magnitude.

The arithmetic mean of the variate is the sum of all values of the variate divided by the number of data n. In the example, the arithmetic mean of N is 222.4 and of $\log N$ is 2.29.

The geometric (or log) mean of the variate is the n^{th} root of the product of all n values, that is the antilog of the arithmetic mean of $\log X$. In the above example, antilog 2.29 = 195.0.

A percentile is the value of the variate below which a given percentage of the data lies. In the above example, 20 per cent of the observations lie below $N = 187.2$ or $\log N = 2.27$.

The median value is the value corresponding to the middle order of the data, i.e. the fiftieth percentile. In the example the median is $N = 215.7$ or $\log N = 2.33$, corresponding to order number 8. If the number of data is even, the median is given by the average of the two central observations.

The deviation is the difference between any single value and the mean of all the values. In the example, at order number $s = 4$, the deviation of N is $187.2 - 222.4 = -35.2$ and the deviation of $\log N$ is $2.27 - 2.29 = -0.02$.

The variance of the data is the sum of the squares of the deviations divided by n. In this case, the variance of N is 7103 and of $\log N$ 0.079.

The standard deviation of the data is the square root of the variance and is often taken as a measure of the dispersion (scatter) of the results. In this case, the standard deviation of N is 84.3 and of $\log N$ 0.28.

The coefficient of variation is the ratio of the standard deviation to the mean, and is usually expressed as a percentage. In the example, the coefficient of variation of N is (84.3/222.4) x 100 = 37.91 per cent, and of $\log N$ (0.28/2.29) x 100 = 12.23 per cent.

3. PRESENTATION OF EMPIRICAL DATA

3.1 The Histogram

A histogram is a diagram in which the number of observations, or proportion of the total number of observations, falling within each successive class interval is represented by blocks erected on a base subdivided into those intervals.

Figure 1 is the histogram for the above example representing the frequency of occurrence of failure in class intervals of 0.2.

3.2 The Cumulative Frequency Diagram

A cumulative frequency diagram is one in which the number of observations, or proportion of the total number of observations, falling below the upper limit of each successive class interval is represented by blocks erected on a base subdivided into those intervals.

Figure 2 shows the cumulative frequency diagram corresponding to the histogram for the above example.

The same set of results may be presented in a cumulative frequency diagram showing the number or proportion of observations *exceeding* the upper limit of each successive class interval. In the analysis of fatigue endurance, such a diagram would show the number of specimens whose endurances exceeded a given number of cycles.

4. ESTIMATION OF POPULATION PROPERTIES FROM A SAMPLE

4.1 Sample and Population

A batch of test results is of value only in so far as inferences may be drawn as to the probable behaviour of other nominally identical specimens not tested. The specimens tested are described collectively as the sample, and the whole body of specimens from which the sample is drawn is termed the population.

4.2 The Assumption of a Theoretical Frequency Distribution

In the analysis of fatigue test results, the sample is considered to be drawn from an infinitely large population, since the latter will consist of all possible specimens which could be produced. Presentation of the results in the manner suggested in Section 3 will therefore only give a reliable indication of the characteristics of the population if the sample is large.

If it were possible to test an infinitely large sample, a histogram of infinitely narrow class intervals could be constructed, the profile of which would be a continuous function. Clearly this will represent exactly the frequency distribution of the population, since the complete population has been tested. This distribution cannot, of course, be determined in practice. However, by assuming that it is of some standard form, the test results may be analysed from predetermined data relating to that particular form.

Selection of a theoretical distribution should be effected with consideration of the expected boundary conditions of the population. The use of an inappropriate distribution could lead to errors particularly at its extremities.

The relevance of two theoretical distributions to the analysis of fatigue data is discussed in Item Nos. 68014 and 68015.

Figure 3 shows a Normal or Gaussian frequency distribution. The slope and relative height of the curve depend upon the dispersion of the variate.

The area enclosed by the curve to the left of the ordinate at $x_{(p)}$, i.e. $\int_{-\infty}^{x_{(p)}} p(x)dx$, is the proportion $P(x)$ having values not greater than $x_{(p)}$. The area under the complete curve is 1, and therefore the probability of a result being greater than $x_{(p)}$ is $1 - P(x)$, that is the area to the right of $x_{(p)}$, i.e. $\int_{x_{(p)}}^{\infty} p(x)dx$.

4.3 Probability Curves

Figure 4 shows the probability curve $1 - P(x)$ against x for the Normal distribution.

By suitably modifying the scale of the ordinate, the probability curve may be represented by a straight line. The parameters of the distribution are then given by the slope and intercept of the line.

Plotting a sample of results on this grid in the manner proposed in Appendix A1 facilitates the determination of point estimates of the properties of the parent population.

4.4 Accuracy of Estimations

The analysis of only one sample gives point estimates of the properties of the population and as such it is not possible to specify the probability that they are exact. If all possible samples of a given size within the population were analysed and point estimates of the population parameters obtained from each sample in the manner outlined above, then there would be a population of values for each parameter. These populations themselves have some forms of distribution referred to as sampling distributions. These provide a means of specifying the precision of a particular estimate from a single sample in terms of the limits within which the population parameter will lie with a given probability.

4.5 Terms Associated with the Specification of Precision

The confidence interval is the range within which it is forecast that the property of the population will lie.

The confidence limits are the two boundary values enclosing the confidence interval.

The confidence level is the probability that the forecast is correct. For example a 90 per cent confidence level indicates that the property has a 90 per cent chance of lying in the specified interval.

5. COMPARISON OF SAMPLES

5.1 Purpose of Such Analysis

Section 4 considers the analysis of only one sample. However it is sometimes required to determine whether two or more samples are drawn from the same population. This may arise for example if it is required to determine the effect of a change in detail design or manufacture on the strength of a component, or to see if it is permissible to pool the results from various stress levels in a set of fatigue results and so increase the sample size.

5.2 Terms Associated with the Comparison of Samples

A statistical hypothesis is an initial postulate of the actual situation. For example the hypothesis might be that two samples are from the same population.

A significance test is one by which the acceptance or rejection of the hypothesis is justified.

The difference between two values is judged *significant* when the chance of occurrence of such a difference is, under the hypothesis of a common parent population, below an assigned value. The possibility of this relationship is consequently dismissed.

The chance of the occurrence of a difference below which it is decided that a common parent population may be discounted is termed the *level of significance*. For example, a 5 per cent level of significance implies that the hypothesis of a common parent population will be rejected unless the observed difference has a greater than one chance in twenty of occurring under this hypothesis.

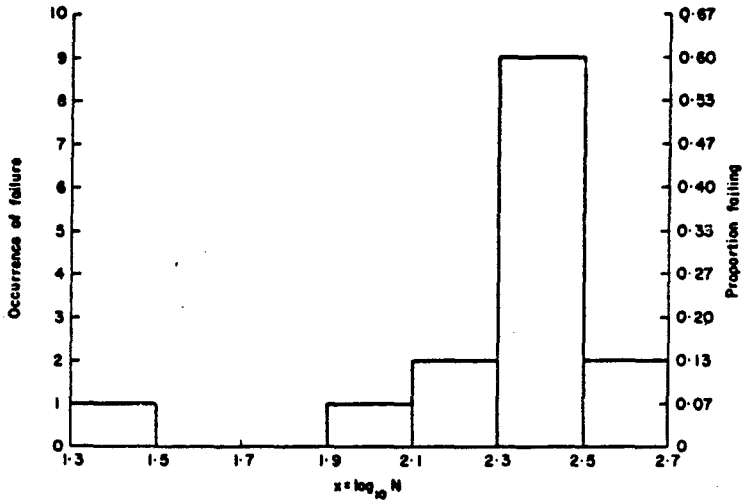

FIGURE 1

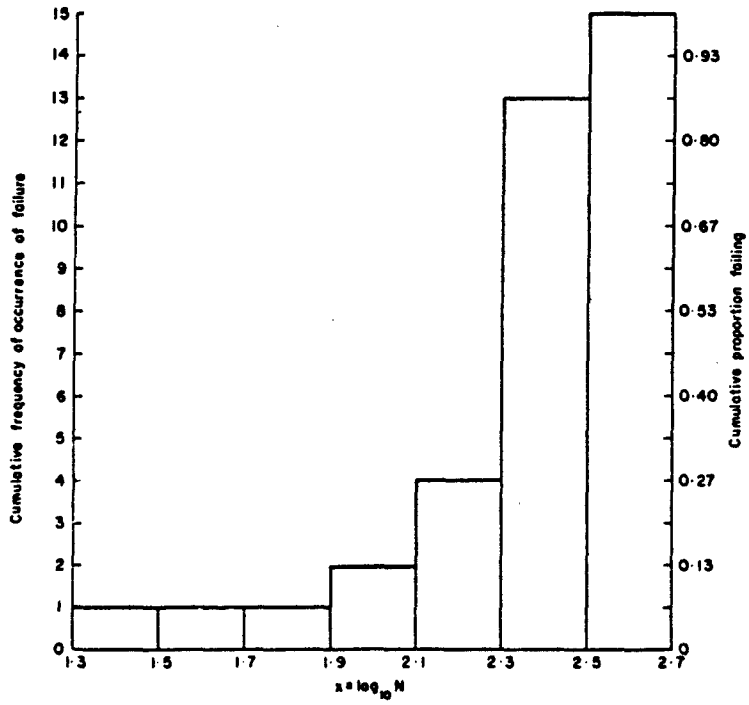

FIGURE 2

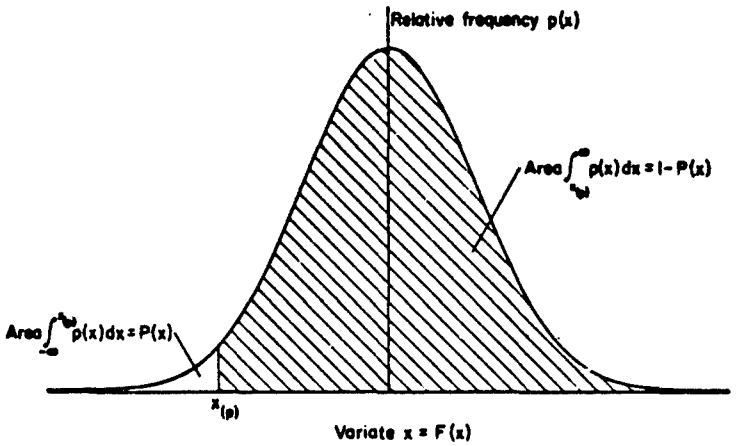

FIGURE 3 NORMAL FREQUENCY DISTRIBUTION

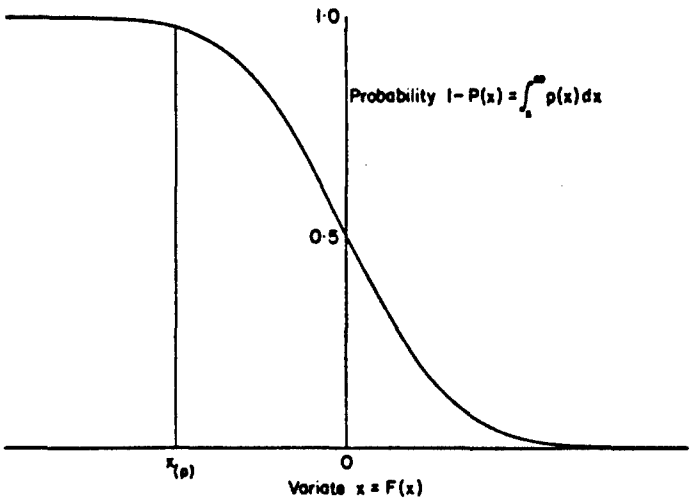

FIGURE 4 NORMAL PROBABILITY CURVE

APPENDIX A.1

PLOTTING POSITION OF VARIATE ON PROBABILITY SCALE

A.1 INTRODUCTION

Table A.1 gives plotting positions of the variate on the probability scale, $(1-P(x)) \times 100$, for samples sizes $10 \leq n \leq 50$.

The values are obtained from the relationship,

$$1 - P(x) = 1 - \frac{n}{n+1},$$

which though not exact is equally appropriate to both Normal and extreme-value distributions.

DERIVATION

1. WEIBULL, W. *Fatigue testing and the analysis of results.* Pergamon Press, Oxford, 1961.

TABLE A1

n	10	11	12	13	14	15	16	17	18	19	20	21	22	23	24	25	26	27	28	29
0																				
1	90.91	91.67	92.31	92.86	93.33	93.75	94.12	94.44	94.74	95.00	95.24	95.45	95.65	95.83	96.00	96.15	96.30	96.43	96.55	96.67
2	81.82	83.33	84.62	85.71	86.67	87.50	88.24	88.89	89.47	90.00	90.48	90.91	91.30	91.67	92.00	92.31	92.59	92.86	93.10	93.33
3	72.73	75.00	76.92	78.57	80.00	81.25	82.35	83.33	84.21	85.00	85.71	86.36	86.96	87.50	88.00	88.46	88.89	89.28	89.66	90.00
4	63.64	66.67	69.23	71.43	73.33	75.00	76.47	77.78	78.95	80.00	80.95	81.82	82.61	83.33	84.00	84.62	85.19	85.71	86.21	86.67
5	54.55	58.33	61.54	64.29	66.67	68.75	70.59	72.22	73.68	75.00	76.19	77.27	78.26	79.17	80.00	80.77	81.48	82.14	82.76	83.33
6	45.45	50.00	53.85	57.14	60.00	62.50	64.71	66.67	68.42	70.00	71.43	72.73	73.91	75.00	76.00	76.92	77.78	78.57	79.31	80.00
7	36.36	41.67	46.15	50.00	53.33	56.25	58.82	61.11	63.16	65.00	66.67	68.18	69.57	70.83	72.00	73.08	74.07	75.00	75.86	76.67
8	27.27	33.33	38.46	42.86	46.67	50.00	52.94	55.56	57.89	60.00	61.90	63.64	65.22	66.67	68.00	69.23	70.37	71.42	72.41	73.33
9	18.18	25.00	30.77	35.71	40.00	43.75	47.06	50.00	52.63	55.00	57.14	59.09	60.87	62.50	64.00	65.38	66.67	67.86	68.97	70.00
10	9.09	16.67	23.08	28.57	33.33	37.50	41.18	44.44	47.37	50.00	52.38	54.55	56.52	58.33	60.00	61.54	62.96	64.29	65.52	66.67
11		8.33	15.38	21.43	26.67	31.25	35.29	38.89	42.11	45.00	47.62	50.00	52.17	54.17	56.00	57.69	59.26	60.71	62.07	63.33
12			7.69	14.29	20.00	25.00	29.41	33.33	36.84	40.00	42.86	45.45	47.83	50.00	52.00	53.85	55.56	57.14	58.62	60.00
13				7.14	13.33	18.75	23.53	27.78	31.58	35.00	38.10	40.91	43.48	45.83	48.00	50.00	51.85	53.57	55.17	56.67
14					6.67	12.50	17.65	22.22	26.32	30.00	33.33	36.36	39.13	41.67	44.00	46.15	48.15	50.00	51.72	53.33
15						6.25	11.76	16.67	21.05	25.00	28.57	31.82	34.78	37.50	40.00	42.31	44.44	46.43	48.28	50.00
16							5.88	11.11	15.79	20.00	23.81	27.27	30.43	33.33	36.00	38.46	40.74	42.86	44.83	46.67
17								5.56	10.53	15.00	19.05	22.73	26.09	29.17	32.00	34.62	37.04	39.29	41.38	43.33
18									5.26	10.00	14.29	18.18	21.74	25.00	28.00	30.77	33.33	35.71	37.93	40.00
19										5.00	9.52	13.64	17.39	20.83	24.00	26.92	29.63	32.14	34.48	36.67
20											4.76	9.09	13.04	16.67	20.00	23.08	25.93	28.57	31.03	33.33
21												4.55	8.70	12.50	16.00	19.23	22.22	25.00	27.59	30.00
22													4.35	8.33	12.00	15.38	18.52	21.43	24.14	26.67
23														8.17	8.00	11.54	14.81	17.86	20.69	23.33
24															4.00	7.69	11.11	14.29	17.24	20.00
25																3.85	7.41	10.71	13.79	16.67
26																	3.70	7.14	10.34	13.33
27																		3.57	6.90	10.00
28																			3.45	6.67
29																				3.33
30																				
31																				
32																				
33																				
34																				
35																				
36																				
37																				
38																				
39																				
40																				
41																				
42																				
43																				
44																				
45																				
46																				
47																				
48																				
49																				
50																				

Values tabulated show $\left(1 - \frac{n}{n+1}\right) \times 100$

TABLE A1 (Contd.)

n	30	31	32	33	34	35	36	37	38	39	40	41	42	43	44	45	46	47	48	49	50
r																					
1	96.77	96 88	96 97	97 00	97 14	97 23	97 30	97 37	97 44	97 50	97 56	97 62	97 67	97 73	97 78	97 82	97 87	97 92	97 96	98 00	98 04
2	92.56	93.75	93 94	94 12	94 40	94 46	94 59	95 04	95 09	95 13	95 17	95 21	95 25	95 29	95 33	95 36	95 39	95 42	95 45	95 48	95 51
3	90.32	90 62	90 91	91 18	91 43	91 67	91 90	92 11	92 31	92.50	92 68	92 86	93 02	93 18	93 33	93 48	93 62	93 75	93 88	94 00	94 13
4	87.10	87 50	87 88	88 24	88 57	88 89	89 19	89 47	89 74	90 00	90 24	90 46	90 70	90 91	91 11	91 30	91 48	91 67	91 84	92 00	92 16
5	83 87	84 38	84 88	85 35	85 71	86 11	86 48	86 84	87 18	87 50	87 80	88 10	88 37	88 64	88 89	89 13	89 36	89 58	89 80	90 00	90 20
6	80 65	81 25	81 82	82 35	82 86	83 33	83 78	84 21	84 62	85 00	85 37	85 71	86 05	86 38	86 68	86 97	87 25	87 50	87 75	88 00	88 24
7	77 42	78 12	78 78	79 41	80 00	80 56	81 09	81 59	82 06	82 50	82 93	83 33	83 72	84 08	84 44	84 78	85 11	85 42	85 71	86 00	86 27
8	74.19	75 00	75 76	76 47	77 14	77 78	78 38	78 95	79 49	80 00	80 49	80 96	81 40	81.82	82 22	82 61	82 98	83 33	83 67	84 00	84 31
9	70 97	71 88	72 72	73 53	74 28	75 00	75 68	76 32	76 92	77 50	78 05	78 57	79 07	79 56	80 00	80 43	80.85	81 25	81 63	82 00	82 35
10	67 74	68 75	69.70	70 59	71 43	72 22	72 97	73 68	74 36	75 00	75 61	76 19	76 74	77 27	77 78	78 26	78 72	79 17	79.59	80 00	80 39
11	64.52	65 62	66 67	67 65	68.57	69 44	70 27	71 06	71 79	72 50	73 17	73 81	74 42	75.00	75 56	76.09	76 60	77 08	77 55	78 00	78 43
12	61 29	62 50	63 64	64 71	65 71	66 67	67 57	68 42	69 23	70 00	70 73	71 43	72 09	72 73	73 33	73 91	74.47	75 00	75 51	76 00	76 47
13	58 06	59 38	60 61	61 76	62 86	63 89	64 86	65 79	66 67	67 50	68 29	69 05	69 77	70 45	71 11	71 74	72 34	72 92	73 47	74 00	74.51
14	54.84	56 25	57 58	58 82	60 00	61 11	62 16	63 16	64 10	65 00	65 85	66 67	67 44	68 18	68 89	69 57	70 21	70 83	71 43	72 00	72 56
15	51 61	53 12	54 55	55 88	57 14	58 33	59 46	60 53	61 54	62 50	63 41	64 29	65 12	65 91	66 67	67 39	68 08	68 75	69 39	70 00	70 59
16	48 39	50 00	51 52	52 94	54 29	55 56	56 76	57 89	58 97	60 00	60 98	61 90	62 79	63 64	64 44	65 22	65 96	66 67	67 35	68 00	68 63
17	45.16	46 88	48 48	50 00	51 43	52 78	54 06	55 26	56 41	57 50	58 54	59 52	60 45	61 36	62 22	63 04	63 83	64 58	65 31	66 00	66 67
18	41 94	43 75	45 45	47 06	48 57	50 00	51 35	52 63	53 85	55 00	56 10	57 14	58 14	59 09	60 00	60 87	61 70	62 50	63 27	64.00	64 71
19	38 71	40 62	42 42	44 12	45 71	47 22	48 65	50 00	51 28	52 50	53 66	54 76	55 81	56 82	57 78	58 70	59 57	60 42	61.22	62 00	62 75
20	35 48	37 50	39 39	41 18	42 86	44 44	45 90	47 37	48 72	50 00	51 22	52 38	53 49	54 54	55 56	56 52	57 45	58 33	59 18	60 00	60 78
21	32 26	34 38	36 36	38 24	40 00	41 67	43 24	44 74	46 15	47 50	48 78	50 00	51 16	52 27	53 33	54 36	55 32	56 25	57 14	58 00	58 82
22	29 00	31 25	33 33	35 29	37 14	38 89	40 54	42 11	43 59	45 00	46 34	47 62	48 84	50 00	51 11	52 17	53 19	54 17	55 10	56 00	56 86
23	25 81	28 12	30 30	32 35	34 29	36 11	37 84	39 47	41 03	42 50	43 90	45 24	46 51	47 73	48 89	50 00	51 06	52 08	53 06	54 00	54 90
24	22 58	25 00	27 27	29 41	31 43	33 33	35 14	36 84	38 46	40 00	41 48	42 86	44 19	45 45	46 67	47 83	48 94	50 00	51 02	52 00	52 94
25	19 35	21 88	24 24	26 47	28 57	30 56	32 43	34 21	35 90	37 50	39 02	40 48	41 88	43 18	44 44	45 65	46 81	47 92	48 98	50 00	50 98
26	16 13	18 75	21 21	23 53	25.71	27 78	29 73	31 58	33 33	35 00	36 59	38 10	39 53	40 91	42 22	43 48	44 68	45 83	46 94	48 00	49 02
27	12 90	15 62	18 18	20.59	22 86	25 00	27 03	28 95	30 77	32.50	34 15	35 71	37 21	38 64	40 00	41 30	42 56	43 75	44 90	46 00	47 06
28	9 68	12.50	15 15	17 65	20 00	22.22	24 32	26 32	28 21	30 00	31 71	33 33	34 88	36 36	37 78	39.13	40 43	41 67	42.86	44 00	45 10
29	6.45	9 38	12 12	14 71	17 14	19 44	21 62	23 68	25 64	27 50	29 27	30 95	32 56	34 09	35 56	36.96	38 30	39 58	40.82	42.00	43 14
30	3.23	6 25	9 09	11 76	14 29	16 67	18 92	21 05	23 08	25 00	26 83	28 57	30.23	31 82	33 33	34 78	36 17	37 50	38 78	40 00	41 18
31		3 12	6 06	8.82	11.43	13.89	16 22	18.42	20 51	22 50	24 39	26 19	27 91	29 55	31 11	32 61	34 04	35 42	36 73	38 00	39 22
32			3.03	5 88	8 57	11 11	13 51	15 79	17 98	20 00	21 90	23 81	25 58	27 27	28 89	30 43	31 91	33 33	34 69	36 00	37 25
33				2 94	5 71	8 33	10 81	13 16	15 38	17 50	19 51	21 43	23 28	25 00	26 67	28 20	29 70	31 25	32 69	34 00	35 29
34					2 86	5 56	8 11	10 53	12 82	15 00	17 07	19 05	20 93	22 73	24 44	26 09	27 66	29 17	30 61	32 00	33 33
35						2 78	5 41	7 89	10 26	12 50	14 63	16 67	18 60	20 45	22 22	23 91	25 53	27 08	28 57	30 00	31 37
36							2 70	5 26	7 69	10 00	12 20	14 29	16 28	18 18	20 00	21 74	23 40	25 00	26 53	28 00	29 41
37								2 63	5 13	7 50	9 76	11 90	13 96	15 91	17 78	19 57	21 28	22 92	24 49	26 00	27 45
38									2 56	5 00	7 32	9 52	11 63	13 64	15 56	17 39	19 15	20 83	22 45	24 00	25 49
39										2 50	4 88	7 14	9 30	11 36	13 33	15.22	17 02	18 75	20 41	22 00	23 53
40											2 44	4 76	6 98	9 09	11 11	13 04	14 89	16 67	18 37	20 00	21 57
41												2 38	4 65	6 82	8 89	10.87	12 77	14 58	16 33	18 00	19 61
42													2 33	4 55	6 67	8 70	10 64	12 50	14 29	16 00	17 65
43														2 27	4 44	6 52	8 51	10 42	12 24	14 00	15 69
44															2 22	4 35	6 38	8 33	10 20	12 00	13 73
45																2 17	4 26	6 25	8 16	10 00	11 76
46																	2 13	4 17	6 12	8 00	9 80
47																		2 08	4 08	6 00	7 84
48																			2 04	4 00	5 88
49																				2 00	3 92
50																					1 96

Values tabulated show $\left(1 - \frac{n}{n+1}\right) \times 100$

APPENDIX B
THE ANALYSIS OF NORMALLY DISTRIBUTED DATA
(Item 68014)

1. NOTATION

c	correction factor for bias of estimated variance of population
K	$\frac{1}{c}\left\{\frac{n}{n-1}\right\}^{1/2}$
$k_{(\alpha)}$	number of standard deviations (σ_e) between sample mean and a percentile of population corresponding to a confidence level α
m	order number
n	number of observations
$P(x)$	proportion of total population having values less than a given value of x
$p(x)$	relative frequency of occurrence of x
q_1	$(100 + \alpha)/2$
q_2	$(100 - \alpha)/2$
s	standard deviation of sample
$t_{(\alpha)}$	number of standard deviations (σ_m) between sample mean and mean of population corresponding to a confidence level α
$u_{(p)}$	number of standard deviations (σ_e) between percentile and estimated mean of population
$u_{(\alpha)}$	factor proportional to deviation of sample percentile from population percentile corresponding to a confidence level α
X	random variable
X_0	lower limit of X
x	variate $F(X)$
$\bar{x}$	mean of sample
$x_{(p)}$	percentile
α	confidence level
μ	mean of population
μ_e	estimate of mean of population from sample
σ	standard deviation of population
σ_e	unbiased estimate of standard deviation of population
σ_m	standard deviation of sampling distribution of means $\sigma/\sqrt{n}$

2. INTRODUCTION

This Data Sheet gives information on the use of the Normal or Gaussian distribution, with particular reference to the analysis of fatigue results. Methods of estimating the mean, the standard deviation and percentile values of a population from a sample of that population are presented on the assumption that the distribution of the population is Normal.

Figure 1 shows the relative frequency of occurrence and the cumulative probability of x, where x has a Normal distribution. Data which do not initially conform to a Normal distribution may reduce to that character upon suitable transformation e.g. $x = F(X) = \log X$ or $x = F(X) = \log \log X$ or $x = F(X) = X^n$. In the analysis of fatigue data logarithmic transformations are often used to normalise the results.

A further transformation, $x = \log (X - X_0)$, is applicable when the distribution of the variate $\log X$ has a finite lower limit. However, estimation of X_0 in the manner described in Item No.68015 for the Weibull distribution does not give satisfactory results for the Normal form and at present no alternative method is available. Therefore in the analysis of high or low probabilities when a finite lower limit is suspected, other distributions (see Item No.68015) may be more appropriate.

3. ESTIMATES OF PROPERTIES OF POPULATION FROM SAMPLE

3.1 Point Estimates

3.1.1 Numerical analysis of data

Mean

The mean of the observations $\bar{x}$ may be obtained by the general numerical method given in Item No. 68013.

A point estimate of the mean of the population is then given by the relationship:

$$\mu_e = \bar{x} \ .$$

Standard deviation

The variance of the observations s^2 may be obtained by the method given in Item No. 68013. A point estimate of the variance of the population is then given by $s^2\left\{\frac{n}{n-1}\right\}$.

However, the square root of this equation gives a biased estimate of the standard deviation of the population and in order to eliminate this bias, it is necessary to apply a correction factor as follows:

$$\sigma_e = \frac{s}{c}\left\{\frac{n}{n-1}\right\}^{1/2} = Ks \ .$$

Figure 2 gives K for sample sizes $2 \leq n \leq 101$. When $n > 101$ K may be taken as unity.

Percentiles

An estimate of a percentile of a normally distributed population is given by:

$$x_{(p)} = \mu_e + u_{(p)}\sigma_e$$

where values of $u_{(p)}$ may be obtained from Figure 3 for the required percentage $(1-P(x)) \times 100$.

3.1.2 Analysis of data using probability paper

Normal probability paper master grids (Figures 6 and 7) are provided with both linear and logarithmic abscissae. The ordinate, $1 - P(x)$, represents the probability of survival in the analysis of fatigue data.

The data, listed in ascending order of magnitude, are plotted with co-ordinates X, $(1 - a/(n + 1)) \times 100$ where the plotting positions $(1 - a/(n + 1)) \times 100$ are given in Table AI, Item No. 68013, for sample sizes $10 \leq n \leq 50$. If the points lie in an approximately straight line, then they may have been drawn from a normally distributed population. If however the points exhibit some definite non-linearity, transformation of the data may be tried or some other standard distribution considered.

Assuming that the distribution of values of some function of X, $F(X) = x$, implies a Normal population, then the properties of that population may be obtained from the best fitted straight line through the data in the manner described below.

Mean

An estimate of the mean of the population is given by the median value of the observations or the fiftieth percentile $x_{(50)}$, i.e. the value of x corresponding to $(1-P(x)) \times 100 = 50$.

Standard deviation

An unbiased estimate of the standard deviation of the population is given by the difference between the mean and the percentile $x_{(15.9)}$ (or $x_{(84.1)}$ since the distribution is symmetrical),

$$\text{i.e.} \quad \sigma_e = \mu_e - x_{(15.9)} \ .$$

Percentiles

An estimate of the percentile $x_{(p)}$ of the population is the value of x corresponding to the desired percentage on the $1 - P(x)$ axis.

3.2 Estimates with Specified Confidence

Mean

It can be shown that with a given confidence level α, the value of μ will lie in the interval bounded by the limits,

$$\mu = \bar{x} \pm \left(\frac{t_{(\alpha)}}{\sqrt{n}}\right)\sigma_e$$

Figure 4 gives $(t_{(\alpha)}/\sqrt{n})$ plotted against $n - 1$ for various values of α.

Standard deviation

The limits within which the ratio σ/σ_e can be expected to lie with a given confidence level α are:

$$\left(\frac{\sigma}{\sigma_e}\right)_{\eta_2} > \frac{\sigma}{\sigma_e} > \left(\frac{\sigma}{\sigma_e}\right)_{\eta_1}$$

where $\eta_1 = \dfrac{100 + \alpha}{2}$, and $\eta_2 = \dfrac{100 - \alpha}{2}$.

Figure 5 gives $(\sigma/\sigma_e)_{\eta_1}$ and $(\sigma/\sigma_e)_{\eta_2}$ plotted against $n - 1$.

Percentiles

It is often of particular interest in the analysis of fatigue results to estimate the percentile life or endurance for extremely low proportions of specimen failure, that is, for a high probability of survival, with a given level of confidence.

Accordingly the value of $x_{(p)}$, above which there is a confidence level α that $[(1 - P(x)) \times 100]$ percent of the population will survive, is given by

$$x_{(p)} = \mu_e + k_{(\alpha)}\sigma_e .$$

where
$$k_{(\alpha)} = \frac{u_{(p)} + u_{(\alpha)}\left\{\frac{1}{n}\left[1 - u^2_{(\alpha)}/2(n-1)\right] + u^2_{(p)}/2(n-1)\right\}^{1/2}}{1 - u^2_{(\alpha)}/2(n-1)} .$$

The factors $u_{(p)}$ and $u_{(\alpha)}$ may be read directly from Figure 3 for the appropriate values of $1 - P(x)$ and α.

4. DERIVATION

The expressions:

$$p(x) = \frac{1}{\sigma\sqrt{2\pi}} \exp\left[-\frac{1}{2}\left\{\frac{x - \mu}{\sigma}\right\}^2\right],$$

$$P(x) = \frac{1}{\sigma\sqrt{2\pi}} \int_{-\infty}^{x} \exp\left[-\frac{1}{2}\left\{\frac{x - \mu}{\sigma}\right\}^2\right] dx .$$

1. HALD, A. — *Statistical theory with engineering applications.* J. Wiley, New York, 1952.

2. DIXON, W.J. MASSEY, F.J. — *Introduction to statistical analysis.* McGraw-Hill, New York, Third edition, 1969.

3. PEARSON, E.S. HARTLEY, H.O. — *Biometrika tables for statisticians.* Vol. 1. Cambridge University Press, 1962.

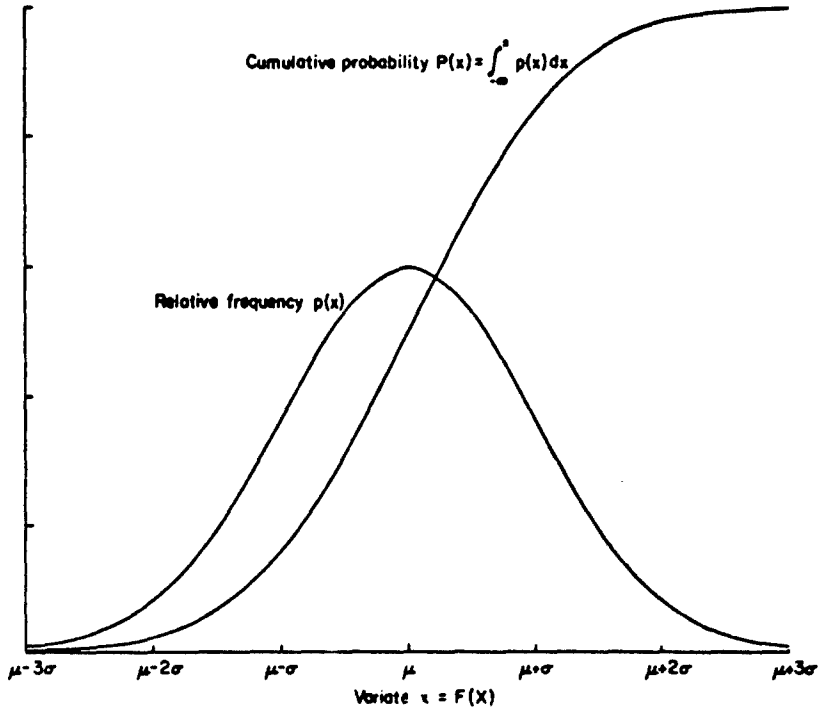

FIGURE I. NORMAL DISTRIBUTION

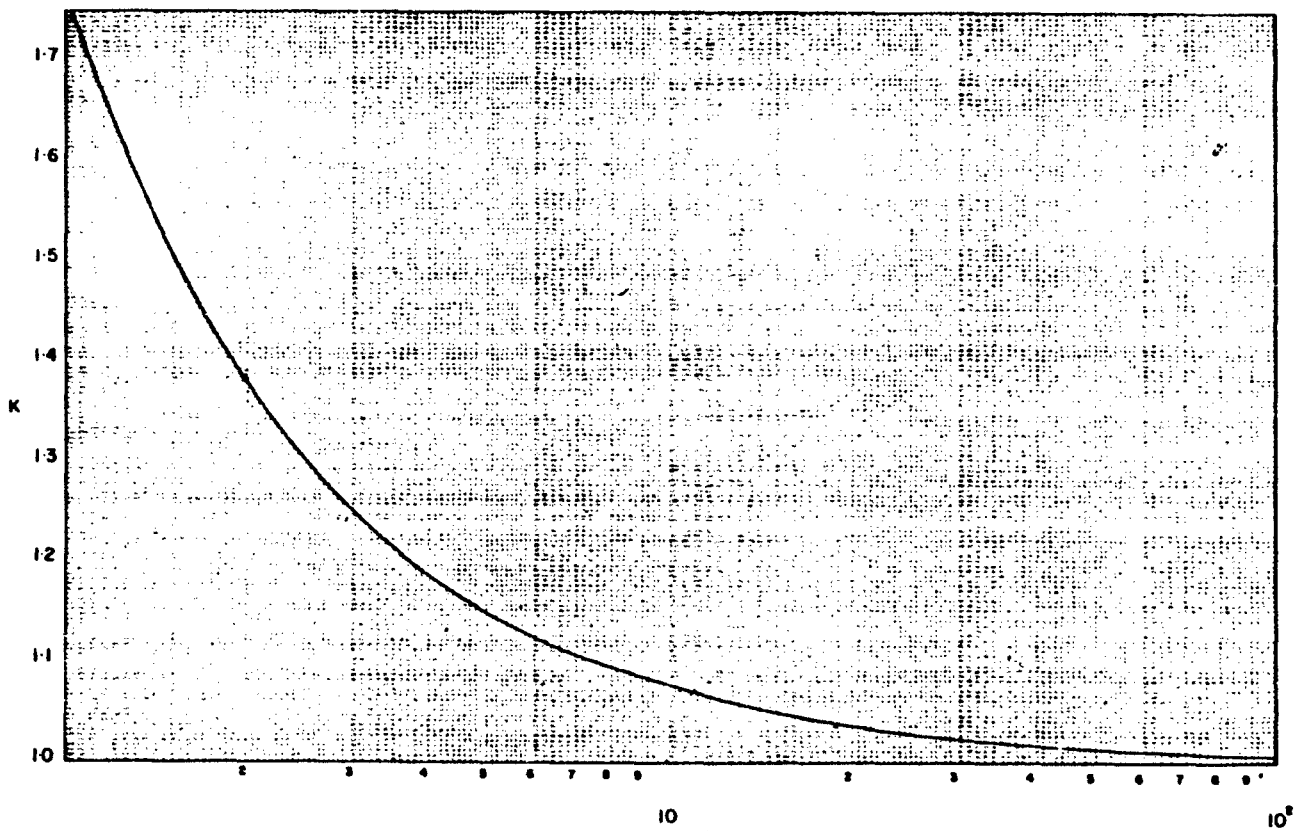

FIGURE 2

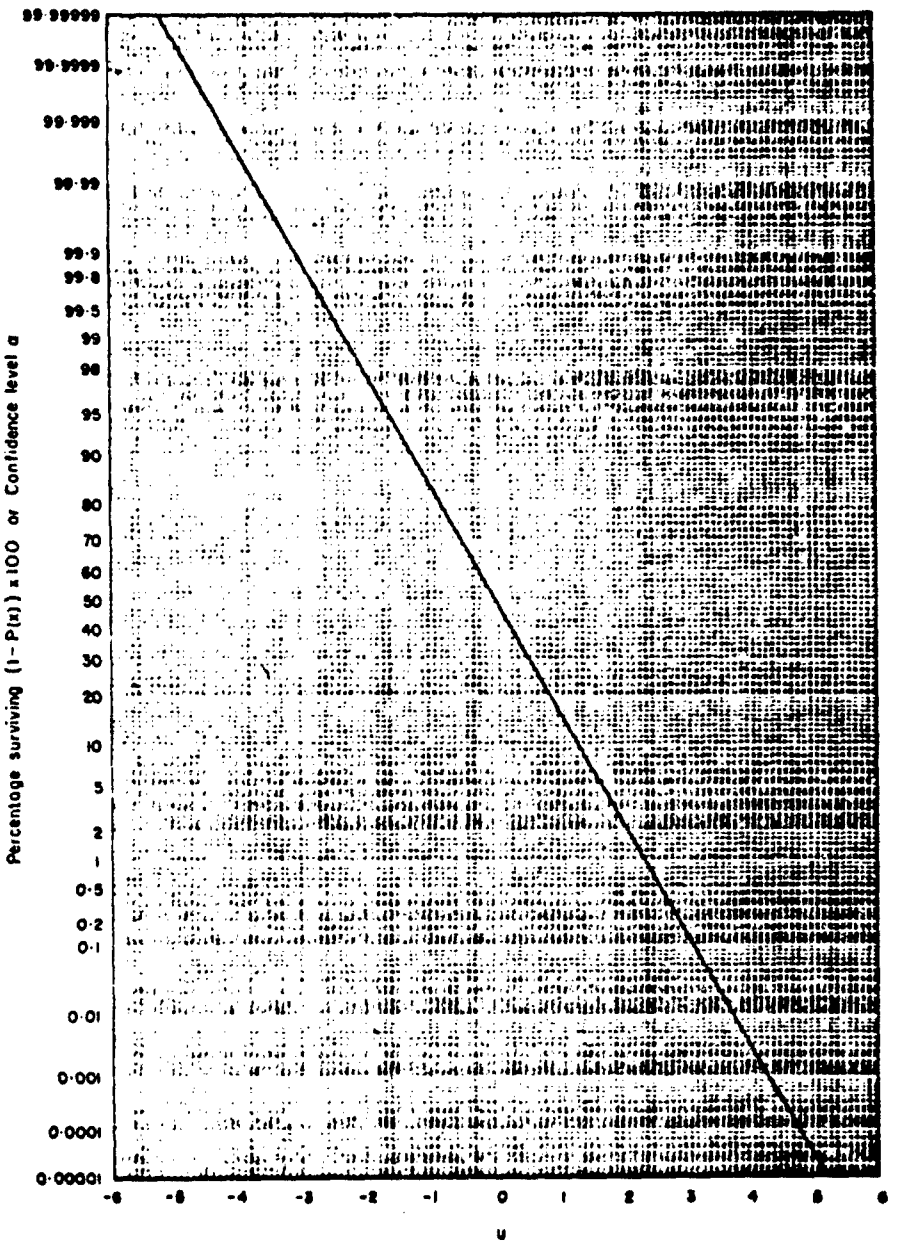
Percentage surviving (1 – P(x)) x 100 or Confidence level α
99·99999
99·9999
99·999
99·99
99·9
99·8
99·5
99
98
95
90
80
70
60
50
40
30
20
10
5
2
1
0·5
0·2
0·1
0·01
0·001
0·0001
0·00001
-6
-5
-4
-3
-2
-1
0
1
2
3
4
5
6
u

FIGURE 3

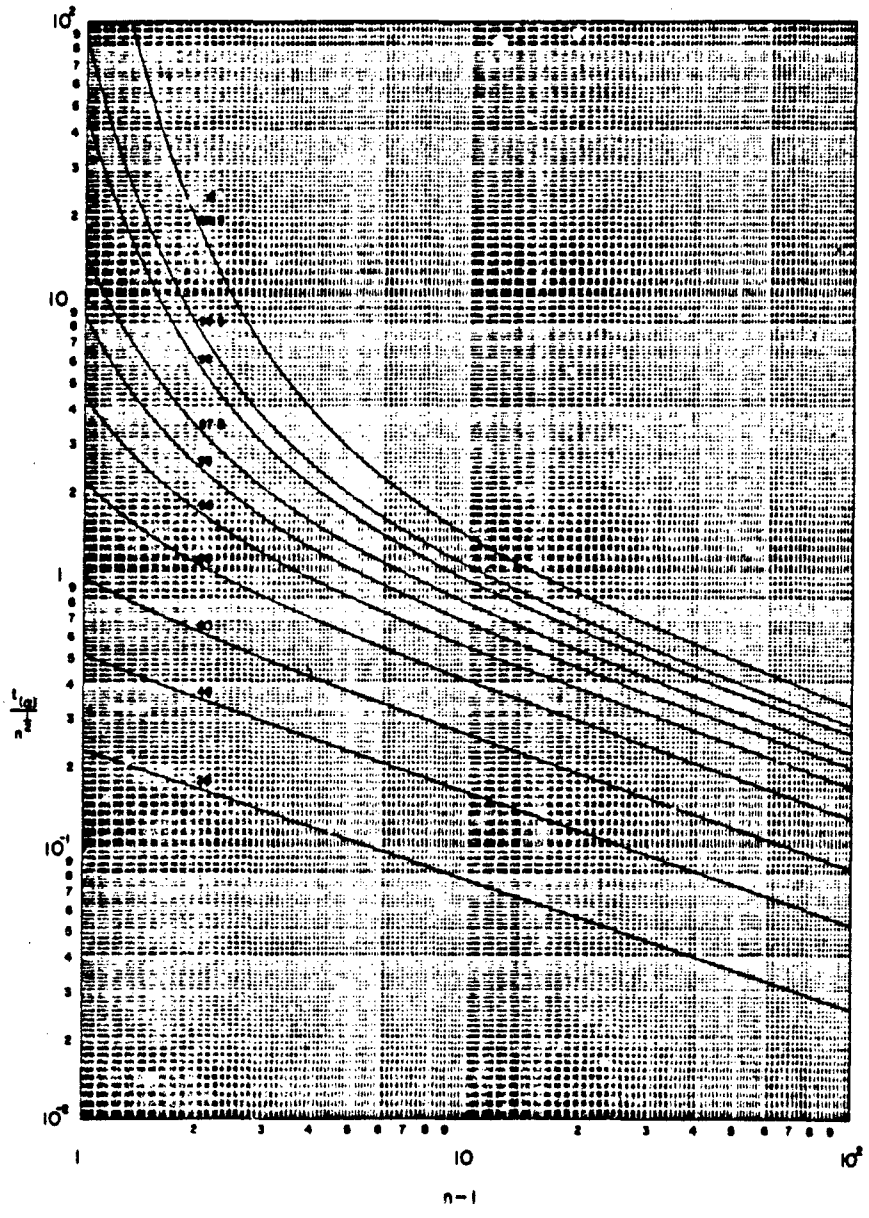

FIGURE 4

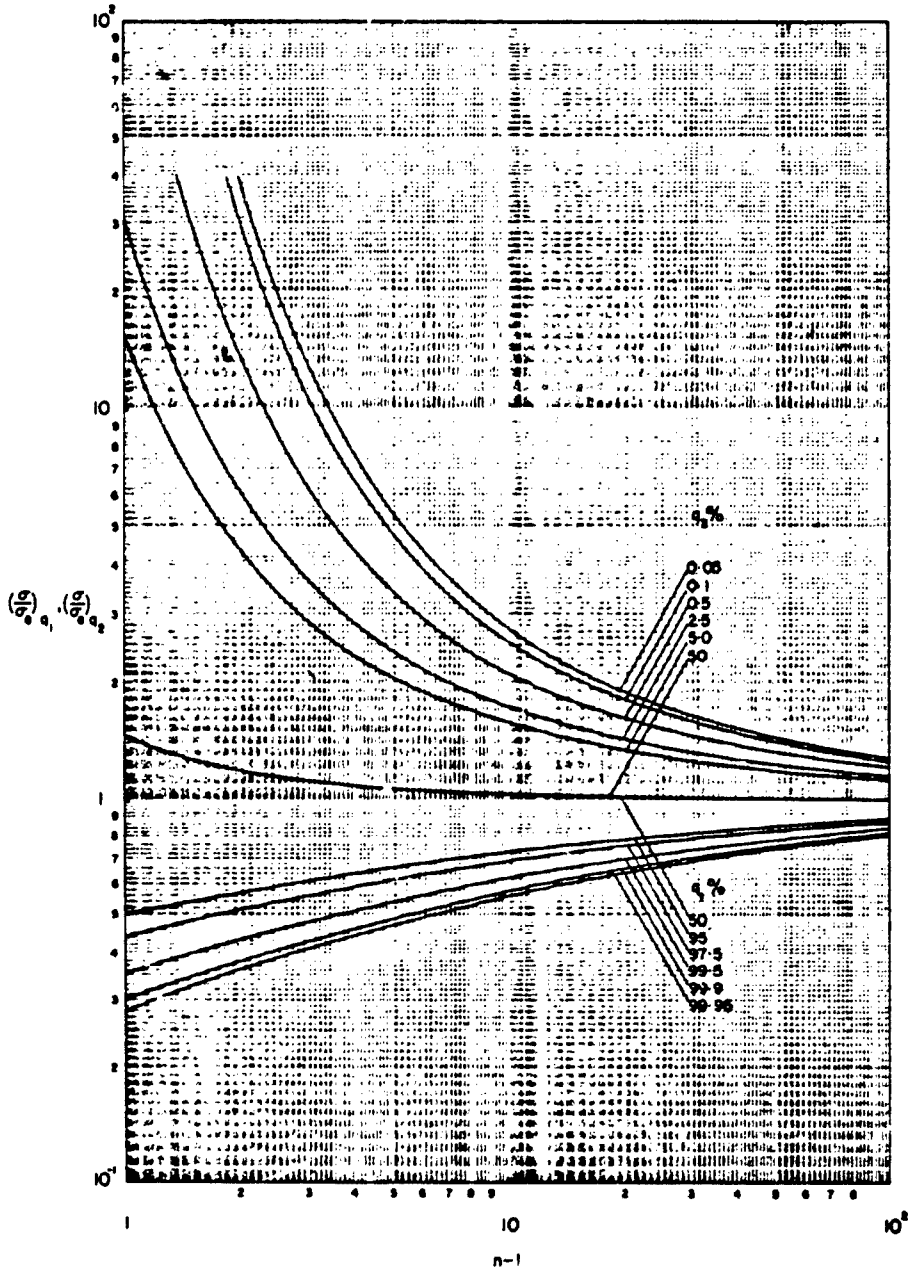
10^2
10
1
10^{-1}
$(\frac{\sigma}{\sigma})_{q_1}, (\frac{\sigma}{\sigma})_{q_2}$
q_2%
0·08
0·1
0·5
2·5
5·0
50
q_1%
50
95
97·5
99·5
99·9
99·96
1
10
10^2
n-1

FIGURE 5

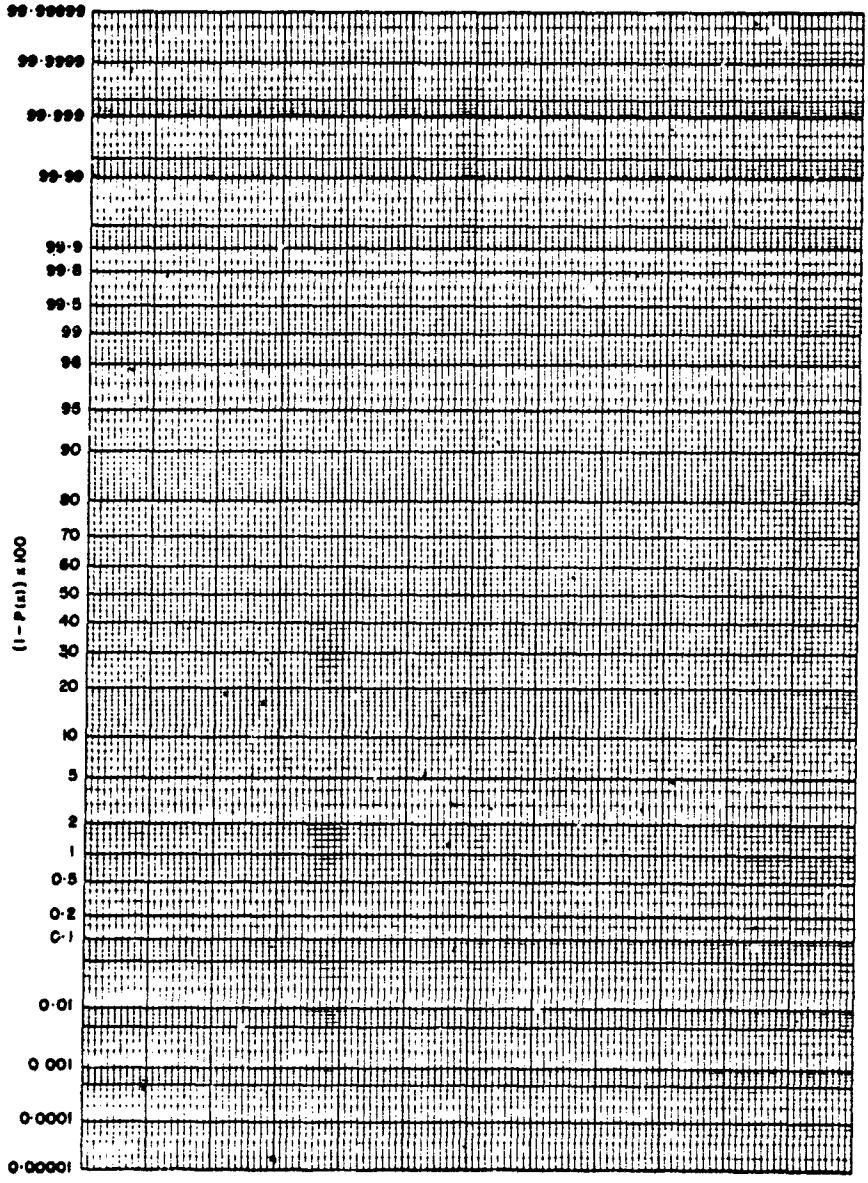

FIGURE 6. NORMAL PROBABILITY X LINEAR MASTER GRID

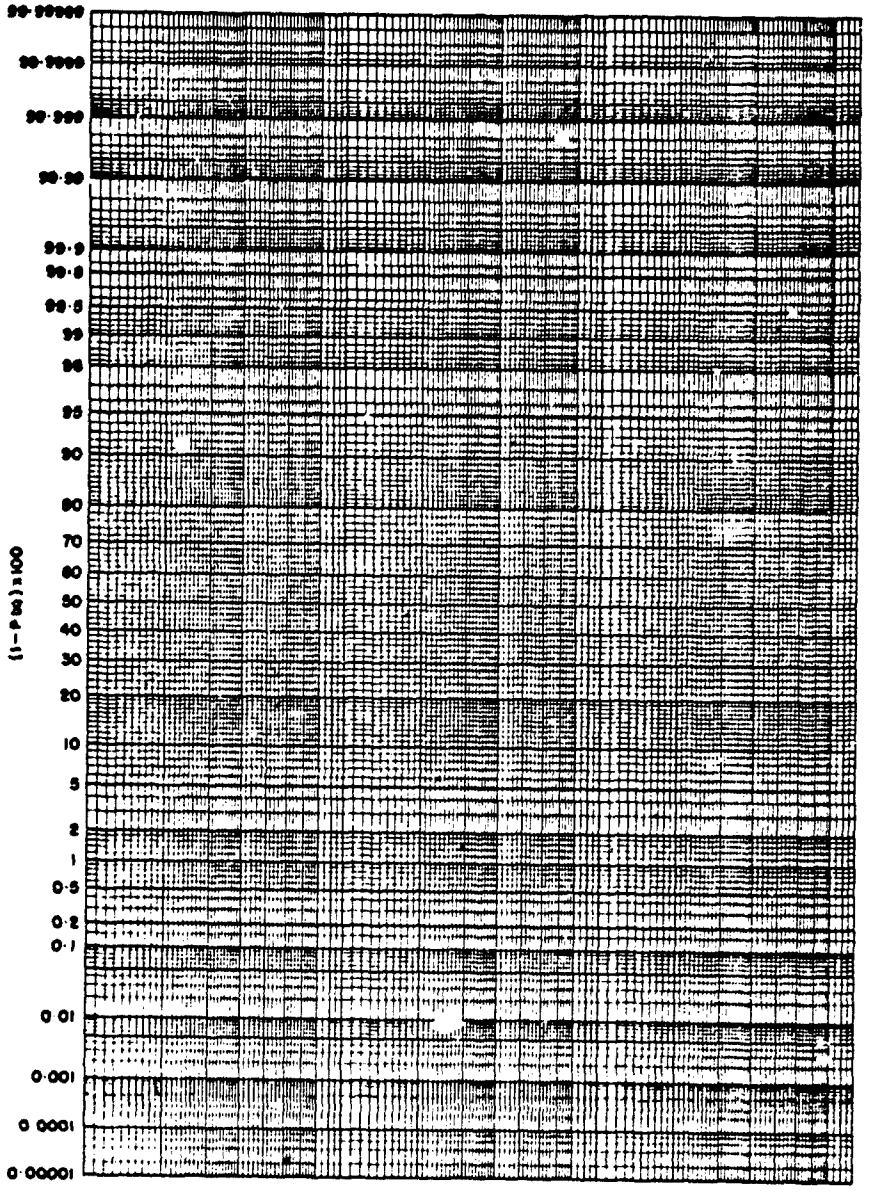

FIGURE 7. NORMAL PROBABILITY X LOGARITHMIC MASTER GRID

5. ADDENDUM

Section 2 of this Item notes that in some cases distributions other than the normal distribution may be more appropriate. Item No. 68015 deals with the analysis of data that conform to an extreme-value distribution and provides master grids (Figures 2 and 3 of that Item) parallel to the Figures 6 and 7 of this Item. If Figure 6 or 7 of this Item is used to analyse data that in reality conform to an extreme-value distribution a curve such as that shown on the accompanying Figure A.1 will result. Such a curve should therefore be taken to indicate that the extreme-value distribution is more appropriate.

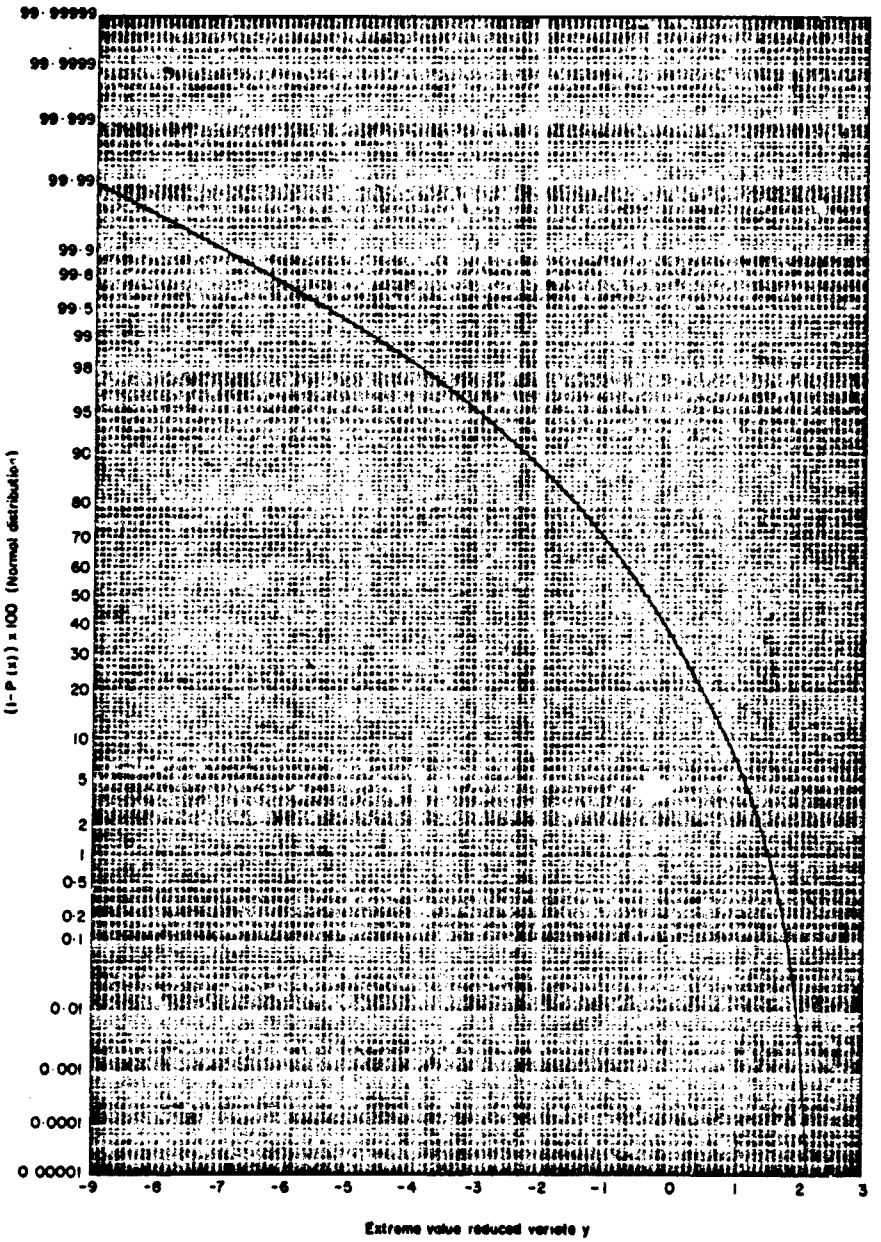

FIGURE A.1

APPENDIX C

THE ANALYSIS OF DATA CONFORMING TO AN EXTREME-VALUE DISTRIBUTION

(Item 68015)

1. NOTATION

b	parameter of distribution defining dispersion
s	order number
n	number of observations
$P(x)$	proportion of total population having values less than a given value of x
$p(x)$	relative frequency of occurrence of x
X	random variable
X_0	lower limit of X
x	variate $F(X)$
x_a	characteristic value of x
$x_{(p)}$	percentile
y	reduced variate

2. INTRODUCTION

This Data Sheet gives information on the use of extreme-value distributions with particular reference to the analysis of fatigue endurance. Estimates of b, x_a, X_0 and $x_{(p)}$ of a population are made from a graphical analysis of a sample drawn from that population on the assumption that the population has an extreme-value distribution.

Figure 1 shows the relative frequency of occurrence and the cumulative probability of x, where x has an extreme-value distribution. Data which do not initially conform to an extreme-value distribution may reduce to that character upon suitable transformation e.g. $x = F(X) = \log X$ or $x = F(X) = \log \log X$ or $x = F(X) = X^n$. In the analysis of fatigue data, log transformations are often used.

The Weibull distribution is a derivative of the basic extreme-value distribution satisfying the condition that $X_0 \geq 0$. In the event that $X_0 = 0$ the Weibull distribution function reduces to that of the basic extreme-value function of $\log_e X$.

It is suggested therefore that the Weibull distribution gives a closer approximation to the probable behaviour of fatigue specimens than do other standard distributions, and this theory admits the possible existence of minimum lives and fatigue limits.

3. ANALYSIS OF DATA USING PROBABILITY PAPER

Extreme-value probability paper master grids (Figures 2 and 3) are provided with both linear and logarithmic abscissae. In the analysis of fatigue data, the ordinate $(1 - P(x)) \times 100$ is the probability of survival.

The data, listed in ascending order of magnitude, are plotted with co-ordinates X, $(1 - s/(n + 1)) \times 100$ where the plotting positions $(1 - s/(n + 1)) \times 100$ for sample sizes $10 \leq n \leq 50$ are given in Table A1, Item No. 68013. If the points lie in an approximately straight line, they may have been drawn from a population having an extreme-value distribution. The lower limit of this distribution will be either $X_0 = -\infty$ if the variate is X, or $X_0 = 0$ if the variate is $\log X$. The two parameters x_a and b defining the distribution may be obtained from the best fitted straight line through the data.

A point estimate of b is given by the rate of change of the reduced variate y (obtainable from the Figure) with x.

A point estimate of the characteristic value of the population x_a is the value of x corresponding to the percentage $(1 - P(x)) \times 100 = 36.8$.

The percentiles of the distribution may be read as the value of x corresponding to the required percentage $(1 - P(x)) \times 100$. When percentages greater than 99.9 are of interest, the use of Table I facilitates the necessary extrapolation. Other values not tabulated may be obtained by the use of the equation for $1 - P(x)$ given in Section 4 of this Item.

If the plotted data exhibit a definite non-linearity, transformation of the data may be tried or some other standard distribution considered. In particular, if the variate is $x = \log X$ and the points lie in a curve concave upwards and asymptotic to some value of the abscissa then the implication is that the parent population conforms to the Weibull distribution having a lower limit of X equal to the value of X at $(1 - P(x)) \times 100 = 100$. A point estimate of X_0 may therefore be made by inspection.

It will then be necessary to replot the data with a revised variate $\log (X - X_0)$. If a straight line is obtained, the estimate of X_0 is approximately correct. If not, successive estimates of X_0 may be made until a linear plot is obtained. The remaining parameters of the distribution x_a and b may be determined in exactly the same way as for the basic extreme-value distribution.

4. DERIVATION

For the basic (1st smallest) extreme-value distribution;

$$1 - p(x) = b \exp(y - e^y) ,$$

and

$$1 - P(x) = \exp(-e^y) ,$$

where

$$y = -b(x - x_n) .$$

For the Weibull (3rd smallest extreme-value) distribution;

$$1 - p(x) = \frac{b}{X - X_n}\left\{\frac{X - X_0}{X_n - X_0}\right\}^{b-1} \exp\left[-\left\{\frac{X - X_0}{X_n - X_0}\right\}^b\right] ,$$

and

$$1 - P(x) = \exp(-e^y) ,$$

where

$$y = -b\left\{\log_e (X - X_0) - \log_e (X_n - X_0)\right\} .$$

1. – Probability tables for the analysis of extreme-value data. U.S. Department of Commerce. National Bureau of Standards Applied Mathematics Series 22, 1953.

2. WEIBULL, W. *Fatigue testing and the analysis of results.* Pergamon Press, Oxford, 1961.

3. – A guide for fatigue testing and the statistical analysis of fatigue data. *Spec. tech. Publs Am. Soc. Test. Mater.*, No.91 – A (Second Edition), 1963.

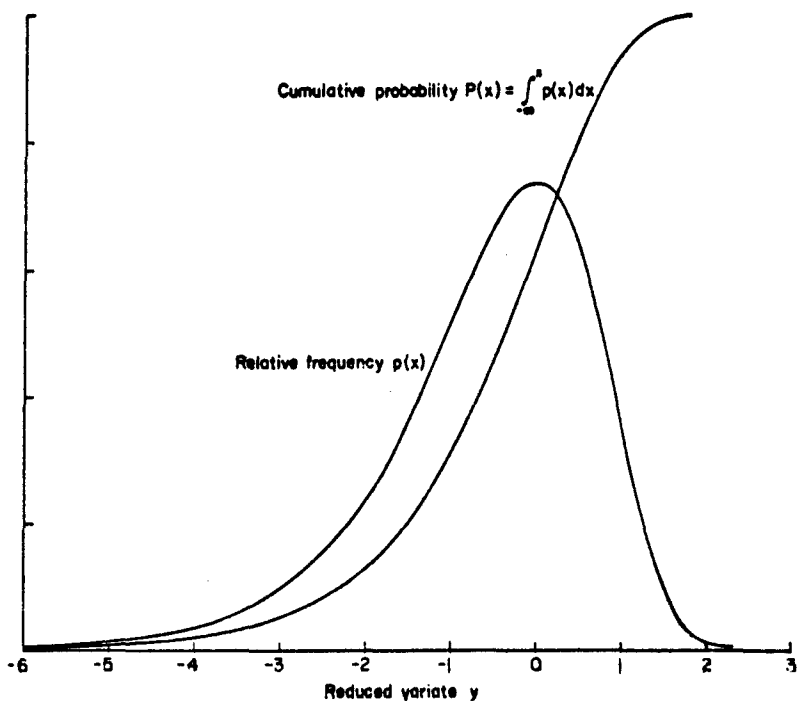

FIGURE 1. First Smallest Extreme-Value Distribution

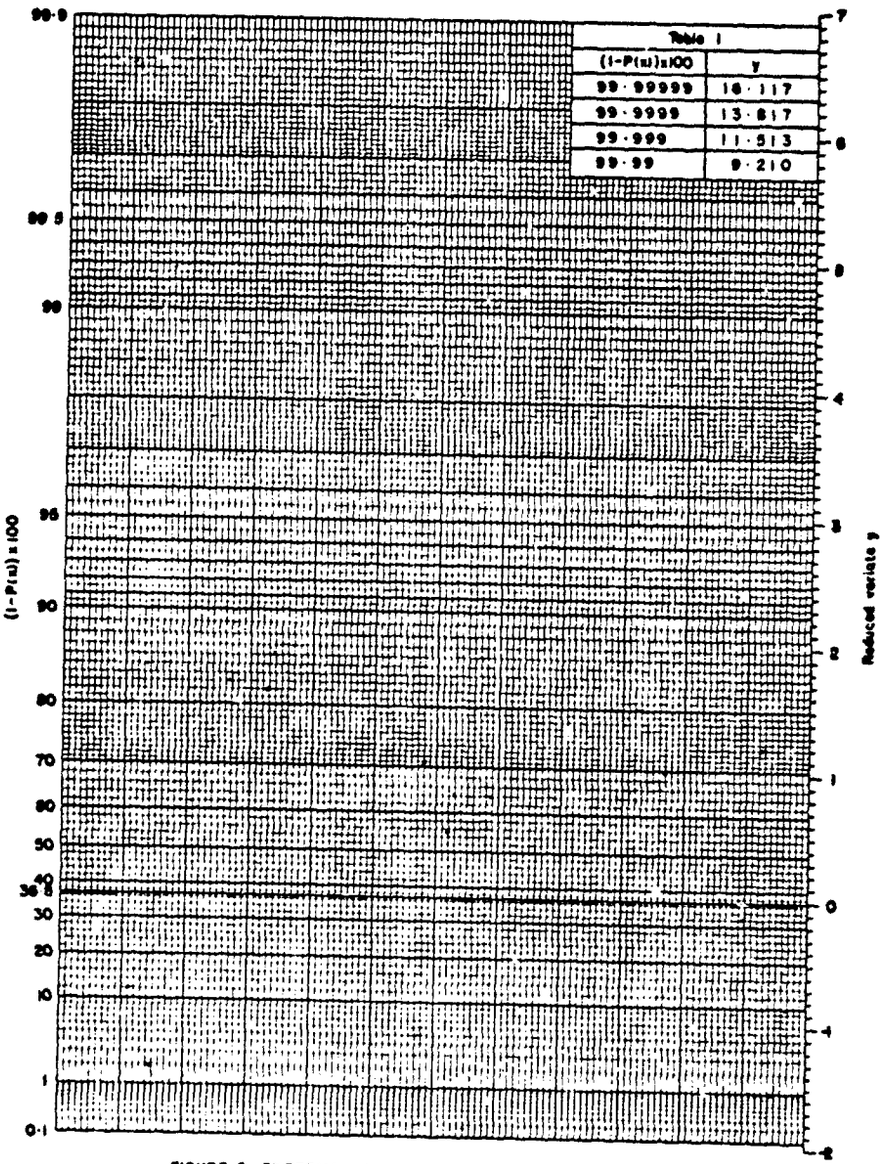

FIGURE 2. EXTREMAL PROBABILITY X LINEAR MASTER GRID

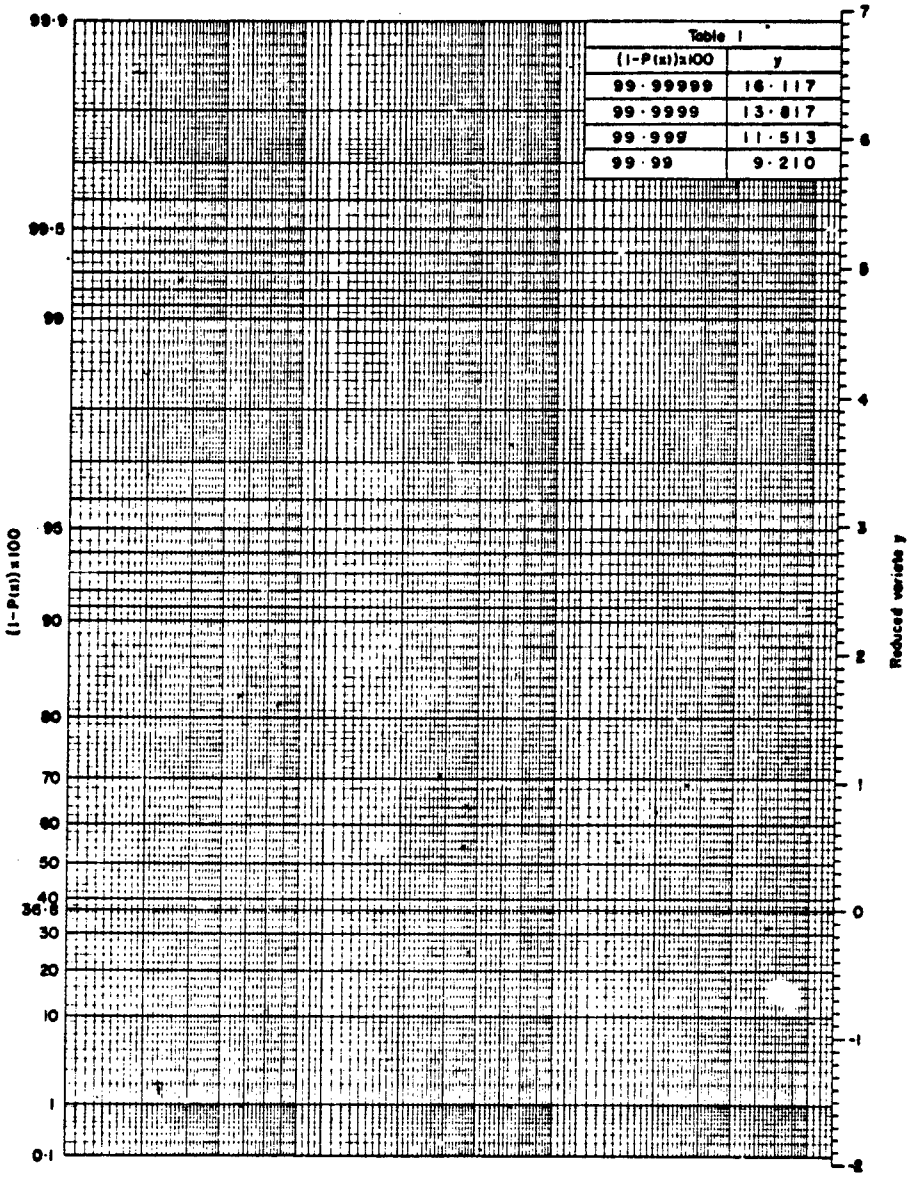

FIGURE 3. EXTREMAL PROBABILITY X LOGARITHMIC MASTER GRID

9. APPLICATION OF FRACTURE MECHANICS TO STRESS CORROSION CRACKING

BY

C. S. CARTER
Boeing Commercial Airplane Company
Seattle, Washington
USA

SUMMARY

9.1 INTRODUCTION 9-3

9.2 SERVICE FAILURES 9-3

9.3 SCC TESTING. 9-4

9.3.1 Smooth Specimen Tests. 9-4
9.3.2 Fracture Mechanics Tests 9-4
9.3.3 Test Environment 9-5

9.4 SCC DATA 9-5

9.5 DESIGN APPLICATION 9-6

9.5.1 Combination of Smooth Specimen and Fracture Mechanics Data 9-6
9.5.2 Relevance to Specification MIL-A-83444 9-7
9.5.3 Proof Testing 9-8
9.5.4 SCC in Service 9-9

9.6 INFLUENCE OF ENVIRONMENT ON FATIGUE CRACK GROWTH. . . 9-9

ACKNOWLEDGEMENTS. 9-10

REFERENCES... 9-10

9. APPLICATION OF FRACTURE MECHANICS TO STRESS CORROSION CRACKING

by

C. S. Carter
Boeing Commercial Airplane Company
Seattle, Washington
USA

SUMMARY

Evaluation of stress-corrosion cracking behavior is described in terms of stress and stress intensity parameters. Typical values are given for commonly used airframe materials. Incorporation of the data into damage tolerance analysis is discussed.

9.1 INTRODUCTION

Stress-corrosion cracking (SCC) denotes a cracking process caused by the conjoint action of sustained stress and a corrodent. Depending upon the material, SCC can occur in a variety of corrodents including such ubiquitous environments as moist air.

Many airframe components have fractured as a result of SCC; indeed, SCC has been a cause of failures in essentially every branch of industry. Table 1 summarizes the causes of failure in a number of landing gear components from several military airplanes, and highlights the fact that SCC failures are far from being an exception. The purpose of this paper is to describe how SCC susceptibility can be characterized in terms of stress and stress intensity, and to show how these can be incorporated into the damage tolerance analysis of airframe structures.

9.2 SERVICE FAILURES

Cracking of high-strength aluminum alloys has been, by far, the most frequently occurring SCC problem in airframes. The majority of failures have been in 7079-T6 followed by 7075-T6, but cracking has also been encountered with 2014-T6 and 2024-T3. Crack propagation usually occurs in the short transverse direction because of its much greater sensitivity to SCC. High-strength steel (tensile strength exceeding 200 ksi) components have also failed by SCC; approximately 50% of steel landing gear failures have been attributed to this type of cracking (ref. 1). All types of low-alloy steels (4340, 300M, 4340M, 4330V, D6AC, and H11) have fractured in this way. Some fractures have also been experienced with maraging steel and with precipitation-hardening stainless steels (17-7PH, PH15-7Mo, 17-4PH, and PH13-8Mo) heat treated to their maximum strength levels. Magnesium alloys, principally AZ91-T6 and AZ80-AF, have fractured by SCC. All these failures have occurred in the environments normally encountered by airframes. Titanium alloys have not cracked under these conditions, but SCC has been experienced in specific environments such as methanol and liquid N_2O_4, and in contact with solid cadmium (refs. 2-4).

The sources of stresses causing propagation of SCC cracks in aluminum alloys are primarily residual tension stresses, from heat treatment and fabrication, and assembly stresses (fit-up, improper shimming, and bushing installation). Stresses due to sustained applied loads also have caused failures, but to a lesser extent. In the case of high-strength steels, service-induced stresses are the main cause of failure with residual and assembly stresses as smaller factors.

Stress risers (holes, sharp radii) and corrosion pits have been the main initiation sites for SCC in both aluminum and steel alloys. Improper machining, leading to the formation of untempered martensite, is a major cause of SCC in steels, particularly in reworked components. Fatigue cracks also have provided sites for SCC in both types of materials.

A number of remedies have been adopted to minimize the risk of SCC. They include the following:

- Use of alloys with greater resistance to SCC--overaging of 7075 to the T73 condition and the recently developed 7049-T73, 7050-T736, and 7175-T736 alloys provide good SCC resistance. Replacement of 4340 with 300M/4340M also has led to improvements in service behavior (refs. 4 and 5).
- Careful design practice--limiting the stress developed by minimizing assembly and fit-up stresses by control of tolerances and shimming, and by control of grain flow.
- Shot peening to introduce residual surface compressive stresses (SCC does not occur under compressive stress).
- Surface protection by cadmium plating (of steel) and painting.

Most of the above were reviewed in detail in previous AGARD publications (refs. 6 and 7).

PRECEDING PAGE BLANK-NOT FILMED

9.3 SCC TESTING

9.3.1 Smooth Specimen Tests

The term "smooth" specimens refers to test specimens that do not contain any intentionally introduced notches or precracks. Test specimens are loaded (in tension or bending) to a series of stress levels and exposed to the corrosive environment until failure occurs or an arbitrary time limit is reached. Time to failure is plotted as a function of the applied stress, as illustrated in figure 1. A threshold stress can be defined below which no SCC failures occur. This threshold stress depends upon the environment, alloy, heat treatment, grain direction, product form, and testing time. Figure 1 clearly illustrates the influence of grain direction on aluminum alloys (ref. 8). The most widely used testing procedure involves immersion in 3.5% sodium chloride solution; alternate immersion is often used for aluminum alloys. Test times usually extend from about 30 to 180 days in aggressive environments. In less severe corrodents, such as industrial environments, testing times of not less than 3 years are required.

A number of problems are associated with smooth specimen testing. A large number of specimens are required to establish the threshold stress with a high degree of confidence because of the scatter inherent in smooth specimen testing. The data cannot account for SCS susceptibility in the presence of a crack; titanium alloys are resistant to SCC when tested as smooth specimens, but may be very susceptible when precracked. In spite of these shortcomings, such data have been widely used in the airframe industry to reduce the risk of SCC, the aim being to keep the stress level below the threshold.

9.3.2 Fracture Mechanics Tests

In recent years, tests with smooth specimens have been supplemented with tests that were designed to measure stress-corrosion resistance in the presence of a precrack One of the justifications for this is that SCC service failures often originate from stress risers or flaws (e.g., notches, fatigue cracks, localized corrosion). A measure of the resistance to SCC of an alloy (or structure) under stress with a crack present is given by the threshold stress intensity K_{ISCC}, below which SCC does not occur. This can be determined by sustained loading of fatigue precracked specimens at different stress intensity levels in the corrodent. Specimens should be exposed to the corrodent prior to loading; otherwise oxidation at the crack tip can give misleading results. In specimens loaded above K_{ISCC}, the stress-corrosion crack grows until the stress intensity reaches K_{IC} (or K_C) and the specimen breaks. Below K_{ISCC}, no stress-corrosion cracking occurs. By plotting the initial stress intensity level against time to failure, the threshold K_{ISCC} can be established (fig. 2).

The growth rate of stress-corrosion cracks (above K_{ISCC}) is controlled by the stress intensity factor. Accordingly, the SCC behavior can be described by a curve of crack growth rate versus K, as illustrated schematically in figure 3. This type of curve is found with many material/environment combinations (refs. 5, 8, 9, and 10) and generally exhibits three regions. In region I, at stress intensities close to K_{ISCC}, the crack growth rate is strongly K dependent. At intermediate stress intensities, region II, the crack growth rate is independent of the applied stress intensity, i.e., the curve exhibits a plateau. At relatively high stress intensities, the crack growth rate may again be K dependent, region III. All three regions have been observed in high-strength steels, but in commercial high-strength aluminum alloys, generally only regions I and II have been reported. Region I is essentially absent in titanium alloys.

Typical curves are shown in figure 4 for two high-strength aluminum alloys. These data represent the results of many tests with specimens from several different plates of the alloys. The data are in good agreement with test results for different conditions of loading, net section stress, crack length, and specimen shapes, thus indicating that the SCC growth rate correlates well with the crack tip stress intensity if the metallurgical and environmental parameters are kept constant. The scatter indicated in figure 4 is reduced if specimens from only one plate are used. The shape of the curves is characteristic of most aluminum alloys.

A variety of types of precracked specimen can be used to determine the growth rate and/or K_{ISCC}. These are illustrated in figure 5 and are classified with respect to the relationship between the stress intensity factor K_I and crack extension (ref. 11). Depending on the method of loading and/or the geometry of the test specimen, the stress intensity factor can be made to increase, decrease, or remain constant as the crack length increases. Details of testing procedures are given in refs. 11 and 12.

Although the fracture mechanics approach overcomes many of the disadvantages associated with smooth specimen (threshold stress) tests, it is not devoid of problems. In particular, the testing time required to establish a true threshold K_{ISCC} can be very long and still have an element of uncertainty (i.e., would longer times lower the value?). There are two reasons for this. First, the crack growth may be very slow, particularly in region I of the crack growth-K curve (fig. 3), so that long testing times can be required to break a specimen or to define region I. This is observed with aluminum alloys and some steels. One approach is to define the threshold at a selected growth rate; for example, 1×10^{-5} in./hour has been used for aluminum alloys (ref. 8). Secondly, some steels exhibit an extensive incubation period before SCC growth initiates from the precrack. The incubation period increases with decreasing initial stress intensity level, usually with a reduction in strength level (refs. 13 and 14). Titanium

alloys do not present a problem, as the incubation period is negligible (as with aluminum alloys) and the SCC crack grows rapidly or not at all.

9.3.3 Test Environment

Ideally, the test environment should be fully representative of the service conditions. Both chemical composition and temperature should be accounted for. In the case of pressure vessels containing gases, the pressure should be duplicated since this can have a significant effect on K_{ISCC}. Furthermore, the possibility of transients in these variables needs to be considered; the effect of locally high concentration buildup due to evaporation or other physio-chemical effects should not be ignored. In addition, the effect of fluids used during processing (e.g., cutting, degreasing) and NDI should be evaluated.

Selection of test environment(s) that adequately simulate all the conditions experienced by the airframe presents some difficulties because of the wide variety of conditions that can be encountered. Internal environments include jet fuel, hydraulic fluid, and water containing various chemicals (chlorides, chromates) of varying concentrations. External environments include the whole gamut of normal atmospheres, including rural marine and industrial, humidities from 0 to 100%, and a wide regime of temperature (approximately -50 to 100°C).

The importance of accurately simulating these environments has been recognized and data are now being reported for some of the above, including sump tank water, cleaning fluids, and JP4 fuel. Sump tank water, having the composition shown in table 2, is representative of the fluids found in airplane sumps. This was used as the test environment for the determination of K_{ISCC} values used in the damage tolerance analysis of the B1 and F16 airplanes. Available data (ref. 15) indicate that the K_{ISCC} values measured in sump tank water are generally comparable to those in 3.5% sodium chloride solution for aluminum and steel alloys, but can be higher in the case of titanium alloys.

Very long testing times are required to establish a threshold stress intensity in air. Fortunately, a number of tests have shown that K_{ISCC} measured in 3.5% sodium chloride solution, which can be determined faster, usually provides a reasonable correlation with the threshold measured in a marine atmosphere for most airframe materials (refs. 16 and 17). Precipitation-hardening stainless steels are an exception in that a 20% sodium chloride solution is required to provide the correlation, probably because of the corrosion resistance of these alloys.

This correlation does not hold for SCC growth rates. Table 3 shows that the plateau growth rate for aluminum alloys in 3.5% sodium chloride solution is 5-10 times faster than in corrosive air environments; for precipitation-hardening steels and titanium alloys, there can be a 10-100 times difference in rates (refs. 17 and 18). Furthermore, the growth rate is sensitive to the type of air environment (table 3). This is due, in part, to differences in the relative humidity; as shown in figure 6, the growth rate can be quite dependent on RH. The presence of chlorides accelerates the growth rate in aluminum alloys, the extent depending upon the specific alloy. On the other hand, in some high-strength steels the cracking rate is faster in the absence of chlorides (refs. 13 and 19).

Based upon the above considerations it appears that, in general, 3.5% sodium chloride solution or sump tank water provide a realistic aqueous environment for the determination of K_{ISCC} for airframe materials. For crack growth rate measurement, sump tank water is probably more representative of severe service conditions than the more aggressive 3.5% sodium chloride solution.

9.4 SCC DATA

Threshold stress and K_{ISCC} data for high-strength aluminum alloys are given in table 4; plateau crack growth rates are presented in table 5. The alloys that have exhibited SCC in service (i.e., 2014-T6, 2024-T3, 7075-T6, and 7079-T6) are characterized by low threshold stress and K_{ISCC} values. Much higher values are recorded by the highly resistant alloys, such as 7075-T73, that also exhibit considerably slower growth rates.

Similar data for high-strength steels are given in tables 6-8. The main factor controlling K_{ISCC} in steels is the strength level. Above 220 ksi tensile strength, most alloys have low K_{ISCC} values. Even the recently developed AF1410 alloy, which has particularly high fracture toughness, is little better with respect to K_{ISCC}, although the growth rate is slower than in competitive steels. Lowering the strength level below 200 ksi produces significant improvements in SCC resistance. It should be noted that contact with a dissimilar metal (e.g., aluminum) can markedly reduce the K_{ISCC} value, particularly for the precipitation-hardening stainless steels (ref. 4).

Stress corrosion is difficult to induce in smooth specimens of titanium alloys. However, as indicated in table 8, some alloys are quite susceptible to SCC in the presence of a precrack. Table 8 illustrates the wide range of K_{ISCC} values that can be obtained with titanium alloys according to their chemical composition and heat treatment. Plateau crack growth rates are usually within the range of 1-10 in./hour (ref. 10).

High-strength magnesium alloys typically have K_{ISCC} values of 7 ksi $in.^{1/2}$ in sodium chloride solution (ref. 9). The nickel-base alloy INCO 718 has high resistance to SCC in

sump tank water, K_{ISCC} being approximately equal to K_{IC} (ref. 15). Some other precipitation-hardening nickel-base alloys, however, have shown much greater susceptibility in water (ref. 20).

Little information is available on the influence of thickness constraint on the threshold stress intensity. Table 8 shows that the effect can be considerable, the threshold for 0.05/0.06-inch sheets of either Ti-6Al-4V or Ti-8Al-1Mo-1V being much greater than at 0.5 inch thickness. However, SCC problems are usually confined to heavy section components (forgings, extrusions) and thus are generally limited to cases where plane-strain conditions prevail.

The reader is cautioned that the typical data given in tables 3-8 are based upon very limited information for most materials. For critical applications, further testing should be considered.

9.5 DESIGN APPLICATION

9.5.1 Combination of Smooth Specimen and Fracture Mechanics Data

While the designer would obviously prefer to use an alloy that is fully resistant to SCC in the service environment, other constraints on material selection such as strength, availability, and cost can dictate the use of a material that is susceptible to SCC. Therefore, we need to consider how the SCC data given in section 9.4 can be used to avoid failure.

A prime requirement is to check that the sustained stress (applied stress + residual and assembly stress) does not exceed the smooth threshold stress for the relevant environment(s). The magnitude of the residual stresses present can be experimentally determined by X-ray or strain-gage techniques, or based upon judgment with respect to the component configuration, and heat treatment. Assembly stresses can be estimated from the build-up of tolerances, or the interference fit, in a joint.

The parameter K_{ISCC} defines the minimum conditions of stress (σ) and crack size (a) that will cause SCC according to the following relationship:

$$K_{ISCC} = \sigma (\pi a)^{1/2} Y \qquad (1)$$

where Y depends upon the crack geometry and boundary conditions. A typical relationship, for a long, thin surface flaw in 7079-T6 plate, is shown in figure 7. This indicates, for example, that inthe presence of a 0.001-inch-deep crack, a tension stress of 20 ksi can be sustained indefinitely. However, smooth specimens loaded to this stress level fail within a short time, the threshold stress being 8 ksi. This is because the fracture mechanics analysis does not take into account the fact that cracks can initiate in the absence of defects, for example, at metallurgical discontinuities. Thus, it is desirable to combine the threshold stress and K_{ISCC} data into a single diagram that describes the SCC resistance in the presence or absence of a precrack. Figure 8 illustrates a composite diagram that combines these data for 7079-T6 and defines a "safe" region for the prevention of SCC. Composite diagrams can be constructed for any material provided K_{ISCC} and the threshold stress are known, and for the desired crack configuration using the appropriate Y factor.

Composite diagrams for several aluminum alloys were developed in reference 17 and are given in figure 9. These point out the superiority of the highly SCC resistant alloys that have become available in recent years. Moreover, figure 9 shows that the transition from stress-controlled SCC to stress-intensity-controlled SCC occurs at quite large flaw sizes for these resistant alloys. In other words, for small flaw sizes the SCC resistance is determined by the threshold stress and not K_{ISCC}; the use of K_{ISCC} alone could lead to an unrealistic expectation of SCC resistance.

Steel and titanium alloys have somewhat different characteristics. These alloys have, in general, quite high threshold stresses, but can have low K_{ISCC} values. Consequently, except at very small flaw sizes, the SCC behavior is controlled by K_{ISCC} rather than the threshold stress (fig. 10).

This approach was used to assess the structural integrity of a primary component of the Saturn 1B space vehicle (ref. 21). This was an E-beam, forged from 7178-T6, located in the thrust support structure. Stress-corrosion cracking had been encountered in some forgings due to residual stresses, and it was necessary to determine the possible extent of cracking and resulting structural behavior in the members intended for service.

The method for predicting the potential crack size is shown schematically in figure 11. The solid line was constructed from threshold stress and K_{ISCC} data for 7178-T6, as described above, and defines the stress-crack length conditions for SCC. The dotted line depicts a typical sustained stress profile (assembly and residual stresses plotted against E beam location). The intersection of the two lines defines the maximum possible extent of crack growth, since at longer crack lengths the sustained stress is insufficient to maintain crack growth (i.e., the stress intensity is less than K_{ISCC}). This crack length was then compared to the critical crack length that would cause failure at the design stress level. Each potential cracking site was analyzed in this way and an assessment made of the resulting load-carrying capability. Based upon this, certain restrictions were placed on the conditions for vehicle launch, and the parts were used successfully.

9.5.2 Relevance to Specification MIL-A-83444

The USAF specification MIL-A-83444 (ref. 22) recognizes that due to the limitations of NDI procedures, components entering service can contain defects or crack-like flaws. This specification defines the sizes of the initial flaws to be considered in the damage tolerance analysis according to the method of qualification (i.e., fail-safe or slow crack growth--for definitions see MIL-A-83444), and assumes 100% inspection of the component using conventional NDI procedures. These initial flaw sizes are shown in figure 12.

To avoid SCC crack growth from these flaws, the components must be designed to operate at a sustained stress level (applied stress + residual stress and assembly stresses) lower than σ_{SCC}, which is given by:

$$\sigma_{SCC} = \frac{K_{ISCC}}{Y(\pi a_i)^{1/2}} \tag{2}$$

where a_i is defined in figure 12, and provided of course that σ_{SCC} is less than the smooth specimen threshold stress. A composite diagram (sec. 9.5.1, constructed for the appropriate flaw configuration and material, can be conveniently used for this purpose. An example is shown in figure 10 for titanium 6Al-4V (STA) and indicates that the sustained stress level should not exceed 90 ksi for safe life structure containing a 0.05-inch-deep surface flaw. The minimum level of K_{ISCC} that would be required at a given stress level also can be established from equation (2).

In principle, one could allow the stress level to exceed σ_{SCC} for inspectable structure, provided that integration of the crack growth-K curve demonstrates that the time to grow from the initial flaw size to the critical flaw size sufficiently exceeds the inspection interval. However, this approach cannot be recommended because of the uncertainties involved. These include the limited amount of growth rate data available, and accurate definition of the service environment and the residual stresses present. Furthermore, tables 5 and 8 show that the growth rate in many high-strength materials exceeds 10^{-3} in./hour in sodium chloride solution. This corresponds to 1 inch of growth in about 6 weeks and would require an impractically high frequency of inspection.

As noted in section 9.2, stress-corrosion crack growth initiated from fatigue cracks has been found in service. In other words, crack extension to the critical crack length is accelerated by SCC. Consequently, a damage tolerance analysis based solely upon fatigue crack growth may significantly overestimate the component life. To avoid such an event, it is necessary to recognize in the damage tolerance analysis that SCC occurs under a steady stress and that for in-flight conditions this corresponds to the 1g stress level together with any residual/assembly stresses. While the rate of fatigue crack growth, da/dN, can be accelerated by the environment, this should be separately accounted for as part of the fatigue crack growth analysis (sec. 9.6). The maximum size of crack a_c that cannot be exceeded during the required life (or inspection interval) is given by:

$$K_{IC} = \sigma_{xx} (\pi a_c)^{1/2} Y \tag{3}$$

where σ_{xx} is the maximum stress the structure must be capable of tolerating and depends upon the inspectability level. This is a basic requirement of damage tolerance analysis to avoid failure. Thus, to prevent SCC at any crack size below a_c, the 1g stress (σ_{1g}), including the residual and assembly stresses, should be less than:

$$K_{ISCC} = \sigma_{1g} (\pi a_c)^{1/2} Y \tag{4}$$

It follows from equations (3) and (4) that SCC can be prevented when the following requirement is met:

$$\frac{K_{ISCC}}{K_{IC}} > \frac{\sigma_{1g}}{\sigma_{xx}} \tag{5}$$

For noninspectable safe life structure, σ_{xx} is equal to the limit load (σ_{LL}) so that equation (5) can be written as:

$$\frac{K_{ISCC}}{K_{IC}} > \frac{\sigma_{1g}}{\sigma_{LL}} \tag{6}$$

Such an analysis was conducted as part of the damage tolerance analysis for the F111 recovery program (ref. 23). For the wing pivot fitting lower plate fitting, fabricated from D6AC steel (220-240 ksi), the following was shown:

$$\frac{K_{ISCC} = 16 \text{ ksi in.}^{1/2} \text{ (in water)}}{K_{IC} = 42.5 \text{ ksi in.}^{1/2} \text{ (at +10°F)}} > \frac{\text{max. } \sigma_{1g} = 23 \text{ ksi}}{\text{max. } \sigma_{LL} = 96.1 \text{ ksi}}$$

i.e., 0.276 > 0.239

Hence, SCC was not expected to be an in-service problem with this component.

It is important to emphasize that the magnitude of σ_{xx} (as defined in MIL-A-83444) depends upon the inspectability level. For example, for damage that can be detected by walkaround visual inspection, the structure is required to be able to withstand the maximum stress that occurs once in 1000 flights, or in the case of flight-evident damage, this is reduced to once in 100 flights. These σ_{xx} stress levels are considerably less than the limit load stress (σ_{LL}). Consequently, for these stress levels the σ_{1g}/σ_{xx} ratio will be greater than σ_{1g}/σ_{LL}, and to avoid SCC, the K_{ISCC}/K_{IC} ratio will have to be correspondingly larger than for limit load capability.

The MIL-A-83444 specification also requires that when the primary crack terminates due to structural discontinuities, or element failure in fail-safe structure, damage must be assumed to exist in the remaining structure. The degree of damage to be assumed depends upon the design concept that is being qualified. Equation (5) can be used to assure that SCC does not occur during crack growth from this damage in the remaining structure. An important consideration here is that the $_{1g}$ stress may be considerably increased when the primary crack terminates, because of the reduced load-carrying area. Accordingly, the required level of K_{ISCC}/K_{IC} will be higher than prior to primary crack termination.

While the military specification has been used above to illustrate the use of fracture mechanics in preventing SCC, the general approach should be applicable to other damage tolerance criteria. For example, in commercial airplanes, the limit load condition can usually be expressed as 2.5g. Therefore, the minimum K_{ISCC}/K_{IC} ratio required to be met in the damage tolerance analysis is given by:

$$\frac{K_{ISCC}}{K_{IC}} > \frac{\sigma_{1g}}{\sigma_{2.5g}} \qquad (7)$$

$$\text{i.e., } \frac{1}{2.5} = 0.4$$

However, in the event of element failure in the fail-safe structure, a higher K_{ISCC}/K_{IC} could be required to prevent SCC from continuing damage in the remaining structure.

9.5.3 Proof Testing

Proof testing can be used to establish the maximum size of flaw that may exist in the structure. At the completion of a successful proof test, the maximum flaw size a_p that can be present is given by:

$$a_p = \frac{K_{IC}^2}{\sigma_p^2 y^2} \qquad (8)$$

where σ_p is the proof stress level.

The environment in which the proof test is conducted may be conducive to SCC of the structural material. Crack growth may then occur during the proof test and can result in failure during the proof test. This actually occurred when methanol was used for the proof testing of Ti-6Al-4V vessels (ref. 2). If SCC can occur, then two additional possibilities must be considered. First, a crack that was not of critical size at the proof stress level might continue to grow to a size larger than a_p during the unloading period. The magnitude of the growth that could occur can be estimated from the relevant crack growth-K curve, or experimentally determined from precracked specimens that are loaded in the test environment to simulate the proof load cycle. A second consideration is that remnants of the test fluid may cause SCC in service. This was a factor in the failure of a large pressure vessel fabricated from a low-alloy steel (100 ksi yield strength). Cracking initially occurred during processing in a weld of high hardness, probably as a result of the stress relief heat treatment. This crack subsequently extended to critical size by SCC as a result of residual stresses (the stress relief was only partially effective) and the moisture that remained from hydrotesting (ref. 24). This failure illustrates the importance of considering all the metallurgical variables and environments that can be encountered during fabrication and service.

One further item to be considered is the possibility of SCC occurring prior to the proof test, due to the combined action of residual stresses and the presence of processing fluids or water. If the proof test is conducted immediately after fabrication, such flaws may not have grown to sufficient size to be detected, but could extend to a size greater than a_p subsequent to the proof test.

This problem was encountered during the F111 recovery program, which included proof testing of the wing structure (ref. 23). Interference fit bolts were used in certain areas of the D6AC steel (220-240 ksi) structure for fatigue life improvement. Tensile residual stresses were developed by these bolts, and the introduction of aggressive environments such as water, drilling coolants, and cleaning agents was possible during installation. Stress corrosion could occur if these environments were present. Calculations were made to determine the maximum time required for a stress-corrosion crack to grow to a size that would be detected during proof test. Plateau crack growth rates (lower bound of the scatter band) and maximum incubation times for the initiation of cracking for all

environments were used for the analysis. A time delay of 115 days was established and incorporated into the proof test program.

There is evidence to show that proof loading may increase the K_{ISCC} for cracks present during the test (ref.25). However, this crack blunting effect would be destroyed by subsequent fatigue growth.

9.5.4 SCC in Service

It is conceivable that in spite of all the precautions taken, SCC may be experienced in service. Unexpected residual or assembly stresses are a possible cause. Under these circumstances, it may be necessary to institute periodic inspection, rather than to immediately replace the component.

To determine the required inspection interval, the most straightforward method is to assume that the SCC growth rate corresponds to the plateau value (da/dt) for the material in the most severe environment anticipated. The inspection interval t_1, which will be in real time, then is given by:

$$t_1 = \frac{(a_{cr} - a_i)}{n} \cdot \frac{da}{dt} \qquad (9)$$

where a_i is the maximum size of crack likely to be missed by the NDI method used and a_{cr} is the critical flaw size that would cause unstable fracture at the maximum stress level that could occur between inspections. The factor n (>2) is used to ensure that the crack is found prior to reaching a_{cr} and to account for variability in da/dt.

This method was used to estimate the extent of SCC that could occur in a 7079-T6 component used in the Saturn 1B space vehicle (ref. 21). Fracture mechanics analysis showed that the stress intensity level in service could significantly exceed K_{ISCC}. Although the part was fully loaded for only a few hours, the potential SCC growth (at the plateau growth rate) was such that structural modifications were required.

9.6 INFLUENCE OF ENVIRONMENT ON FATIGUE CRACK GROWTH

The rate of fatigue crack growth can be related to stress intensity by the expression:

$$da/dN = C\Delta K^n \qquad (10)$$

where C and n are parameters that depend upon the material and the environment. The values of C and n do not vary markedly for a given alloy family (e.g., high-strength steels, 7XXX aluminum alloys) when tested in a nonaggressive environment. In a corrosive environment, there can be significant differences between individual alloys, or even heat treatment conditions for a single alloy. The influence of environment on fatigue crack growth was discussed at a recent AGARD conference, where much of the available data was reviewed (ref. 26). While it is redundant to reiterate this information, it is important to emphasize that the influence of several variables on fatigue growth rate in the corrodent can be considerably different from their effect in air. These include the following:

- cyclic frequency
- wave form (e.g., hold period at K_{max})
- stress ratio
- material thickness
- spectrum loading
- metallurgical variables (e.g., heat treatment condition, composition, grain direction, galvanic contact)

Furthermore, altering one variable can modify the response to changes in another. Unless these factors are adequately accounted for, the damage tolerance analysis may lead to an overly optimistic estimate of service life.

If the maximum cyclic stress intensity exceeds K_{ISCC}, the crack growth in each cycle can occur by a combination of fatigue and SCC. The contribution from SCC increases with decreasing cyclic frequency since a longer time is available for SCC growth. Figure 13 illustrates this effect in 4340M steel exposed to water. The marked effect of frequency at stress intensity levels exceeding 13 ksi $in.^{1/2}$, which is approximately equal to K_{ISCC}, is due to the dominance of SCC in the cracking process. For materials that exhibit much slower rates of SCC growth than 4340M, significant acceleration in fatigue crack growth rates only occur at low cyclic frequencies.

Thus, calculation of the fatigue crack propagation life, using the da/dN-ΔK curve appropriate to the service condition, such as figure 13, adequately accounts for environmental damage during fatigue cycling. Crack growth by SCC at the sustained lg stress level can be avoided by the procedures outlined in section 9.5.2.

It should be noted that substantial accelerations in fatigue crack growth rate may be produced by the aggressive environment when K_{ISCC} is not exceeded by the cyclic stress intensity. Further information is given in reference 26.

ACKNOWLEDGMENTS

The author is grateful to Dr. H. P. van Leeuwen for his assistance, and to M. V. Hyatt, W. E. Quist, and U. G. Goranson for review of the paper.

REFERENCES

1. I. Perlmutter and C. S. Carter, "Material Factors and Reliability in the Design of Landing Gear," Symposium on the Relevance of Fracture Toughness, Cambridge, England, 1973.

2. B. F. Brown, "Stress Corrosion Cracking Control Measures," Natl. Bureau of Stds. Monograph 156, 1977.

3. M. O. Speidel, "Practical Problems of Stress Corrosion Cracking in High Strength Metallic Materials," ARPA Conference on Environmental Degradation of Stressed Materials, Vol. II, U.S. Govt. Report No. AD744205, 1971.

4. C. S. Carter, "Stress Corrosion and Corrosion Fatigue of Medium Strength and High Strength Steels," Handbook on Stress Corrosion and Corrosion Fatigue, to be published 1979.

5. L. D. Griffin and D. Latterman, "C141A Service Experience--Materials and Processes," Materials and Processes in Service Performance, SAMPE, 1977.

6. "The Theory and Preventional of Corrosion in Aircraft Structures," AGARD Lecture Series No. 54, 1976.

7. "Engineering Practice to Avoid Stress Corrosion Cracking," AGARD Conference Proceedings No. 53, 1970.

8. M. O. Speidel and M. V. Hyatt, "Stress Corrosion of High Strength Aluminum Alloys," Advances in Corrosion Science and Technology, Vol. 2, ed. M. G. Fontana and R. W. Staehle, Plenum Press, 1972.

9. M. O. Speidel, "Stress Corrosion of Magnesium Alloys," Handbook on Stress Corrosion and Corrosion Fatigue, to be published 1979.

10. M. S. Blackburn, W. H. Smyrl, and J. A. Feeney, "Titanium Alloys," Stress Corrosion Cracking in High Strength Steels and in Titanium and Aluminum Alloys," ed. B. F. Brown, Naval Research Laboratory, 1972.

11. H. R. Smith and D. E. Piper, "Stress Corrosion Testing with Precracked Specimens," Stress Corrosion Cracking in High Strength Steels and in Titanium and Aluminum Alloys," ed. B. F. Brown, Naval Research Laboratory, 1972.

12. S. R. Novak and S. T. Rolfe, "Modified WOL Specimen for K_{ISCC} Environmental Testing," J. Materials, Vol. 4, 1969, p. 701.

13. W. D. Benjamin and E. A. Steigerwald, "Environmentally Induced Failures in Martensitic High Strength Steels," Air Force Materials Laboratory, WPAFB, Report No. AFML-TR-68-80, 1968.

14. R. P. Wei, S. R. Novak, and D. P. Williams, "Some Important Considerations in the Development of Stress Corrosion Cracking Test Methods," Matls. Res. and Stds., ASTM, 12, 1972, p. 25.

15. R. R. Ferguson and R. C. Berryman, "Fracture Mechanics Evaluation of B1 Materials," WPAFB, Report No. AFML-TR-76-137, Vol. 1, 1976.

16. A. H. Freedman, "An Accelerated Stress Corrosion Test for High Strength Ferrous Alloys," J. Materials, 5(2), 1970, p. 431.

17. D. O. Sprowls et al., "Evaluation of Stress Corrosion Cracking Susceptibility Using Fracture Mechanics Techniques," Final Report, NASA Contract No. NAS8-21487, 1973.

18. D. O. Sprowls, J. W. Coursen, and J. D. Walsh, "Evaluating Stress Corrosion Crack Propagation Rates in High Strength Aluminum Alloys," Proc. of the 1974 Triserve Corrosion of Military Equipment Conference, WPAFB, Report No. AFML-TR-75-42, Vol. II, 1975, p. 1.

19. J. C. Charbonnen, "Study of Several Physio-Chemical and Metallurgical Factors on the Propagation of Stress Corrosion Cracks in 35NCD16 Steel," Mem. Sci. Rev. Metal., 72, 1975, p. 795.

20. M. O. Speidel, "Stress Corrosion of Nickel Alloys," Handbook on Stress Corrosion and Corrosion Fatigue, to be published 1979.

21. P. F. Munafo and T. O. Knight, "Saturn 1B/Skylab IV Stress Corrosion Problems," Proc. of the 1974 Triservice Corrosion of Military Equipment Conference, WPAFB, Report No. AFML-TR-75-42, Vol. I, 1975, p. 103.

22. Military Specification MIL-A-83444, Airplane Damage Tolerance Requirements, 1974.

23. W. D. Bunlin, "Concept and Conduct of Proof Test of F111 Production Aircraft," Aeronautical J., Oct. 1972, p. 587.

24. T. Moisio, "Brittle Fracture in Failed Ammonia Plant," Met. Constr., and Brit. Weld J., 4, 1972, p. 3.

25. C. S. Carter, "Effect of Prestressing on the Stress Corrosion Resistance of Two High Strength Steels," Met. Trans., 3, 1972, p. 584.

26. "Corrosion Fatigue of Aircraft Materials," AGARD Report No. 659, 1977.

27. W. E. Routh, "Lower Cost by Substituting Steel for Titanium," WPAFB, Report No. AFFDL-TR-77-77-3, 1977.

TABLE 1

SUMMARY OF LANDING GEAR COMPONENT FAILURES REPORTED IN REFERENCE 1

A/P Model	Material	No. of Failures	Type of Failure	Failure Origin	Influencing Factors
A	4340	6	Fatigue	Hole	Corrosion
B	7075-T6	4	Fatigue	Tool scratch	---
	98BV40	50	Fatigue	Wear scratches	Corrosion
C	7075-T6	7	Fatigue	Hole	Residual stress
	7075-T6	1	Stress corrosion	Forging parting plane	Corrosion
	2014-T6	1	Fatigue	Sharp corner	Corrosion
	4340	2	Stress corrosion	Hole	---
	4340	4	Stress corrosion	Corrosion pit	Residual stress
	4340	4	Overstress	Sharp corner	Corrosion
	4340	4	Stress corrosion	Surface flaw	Residual stress
D	4340	2	Fatigue	Surface flaw	Corrosion
	4340	3	Stress corrosion	Surface flaw	Surface imperfections
	4340	2	Fatigue	Surface flaw	---
	4340	1	Fatigue	Corrosion pit	Corrosion
	4340	2	Stress corrosion	Tool scratch	---
	4340	1	Stress corrosion	Unknown	Corrosion
	4340	2	Fatigue	Sharp corner	Corrosion
E	4340	16	Impact load	Sharp corner	Corrosion
	4340	1	Fatigue	Corrosion pit	Corrosion
	4340	1	Unknown	Unknown	Surface imperfections
	4340	1	Fatigue	Forging flaw	---
F	7075-T6	27	Stress corrosion	Unknown	Residual stress
	7075-T6	5	Stress corrosion	Hole	Fitup stress
	4340	2	Stress corrosion	Hole	Untempered martensite
	4340	2	Stress corrosion	Hole	Fitup stress
G	7075-T6 (extrusion)	1	Stress corrosion	Sharp corner	Fitup stress
H	7079-T6	39	Fatigue	Wear scratches	---
	7079-T6	3	Stress corrosion	Forging parting plane	Fitup stress
	7079-T6	15	Stress corrosion	Forging parting plane	---
	7079-T6	1	Stress corrosion	Hole	Corrosion

NOTES:

1. Each line entry represents a specific component.
2. All parts fabricated from forgings except where indicated.

TABLE 2

CHEMICAL CONTENT OF SIMULATED SUMP TANK RESIDUE WATER

Constituent	Concentration (ppm)
$CaCl_2$	50
$CdCl_2$	1000
$MgCl_2$	50
NaCl	100
$ZnCl_2$	10
$PbCl_2$	1
$CuCl_3$ $2H_2O$	1
$CrCl_3$ $6H_2O$	1
$FeCl_3$	5
$MnCl_2$ $4H_2O$	5
$NiCl_2$ $6H_2O$	1
Distilled water	balance

TABLE 3

COMPARISON OF SCC PROPAGATION RATES IN THE 3.5% NaCl ACCELERATED TEST AND IN OUTDOOR ATMOSPHERES (REF. 18)

Alloy and Temper	Average Plateau Velocity, in./hr x 10^{-5}		
	3.5% NaCl	Seacoast	Industrial
7079-T651	320	35	25
7079-T6351	220	30	25
5456-Sens.	210	40	2
2219-T37	210	35	20.
2014-T65	120	15	10
2024-T351	100	20	10
7075-T651	100	20	10

TABLE 4

SHORT TRANSVERSE STRESS-CORROSION AND FRACTURE TOUGHNESS PROPERTIES OF HIGH-STRENGTH ALUMINUM ALLOYS (REF. 8)

Alloy	Smooth Specimen Stress Corrosion Threshold Stress ksi	Threshold Stress Intensity K_{ISCC} ksi $\sqrt{in.}$	Fracture Toughness K_{IC} ksi $\sqrt{in.}$
2014-T451	7	5	21
2014-T651	6	6	18
2024-T351	6	7	22
2048-T851	-	17	38
2124-T851	>30	11	22
2219-T37	<10	6	33
2219-T87	38	>22	28
6061-T651	>36	<20	34
7049-T73	>25	< 8	21
7050-T736	>25	9	23
7050-T73651	>45	9	25
7075-T651	7	5	18
7075-T7651	25	<14	19
7075-T7351	40	15	20
7079-T651	7	4	20
7175-T66	7	5	21
7178-T651	7	6	17

TABLE 5

PLATEAU CRACK GROWTH RATES IN THE SHORT TRANSVERSE DIRECTION FOR HIGH-STRENGTH ALUMINUM ALLOYS (REF. 8)

Alloy	Plateau Crack Growth Rate in 3.5% NaCl Solution (in./hr)	Plateau Crack Growth Rate in Distilled Water (in./hr)
2014-T451	3×10^{-3}	---
2014-T651	8×10^{-4}	---
2024-T351	9×10^{-4}	3×10^{-4}
2048-T851	6×10^{-4}	2×10^{-5}
2124-T851	6×10^{-4}	---
2219-T37	2×10^{-3}	---
7049-T73	9×10^{-5}	9×10^{-5}
7050-T736	8×10^{-5}	8×10^{-5}
7050-T73651	2×10^{-4}	---
7075-T651	2×10^{-3}	5×10^{-4}
7075-T7651	3×10^{-5}	3×10^{-5}
7075-T7351	5×10^{-6}	---
7079-T651	2	6×10^{-3}
7175-T66	2×10^{-2}	5×10^{-4}
7175-T736	1×10^{-4}	---
7178-T651	2×10^{-3}	5×10^{-4}
7475-T651	2×10^{-3}	6×10^{-4}

TABLE 6

THRESHOLD STRESSES FOR HIGH-STRENGTH STEELS
IN 3.5% SODIUM CHLORIDE SOLUTION (REF. 4)

Alloy and Tensile Strength or Heat Treatment	Threshold Stress, ksi
300M (280-300 ksi)	170 (L) 136 (T) 115 (ST)
4330M (220-240 ksi)	150 (L) 115 (T) 100 (ST)
9Ni-4Co-0.3C (220-240 ksi)	150 (L) 130 (T) 110 (ST)
17-4PH (H900)	>75% YS*
17-4PH (H1000)	> 80% YS
15-5PH (H900)	> 100% YS*
15-5PH (H1000)	>100% YS
PH13-8Mo (H950)	>100% YS*
PH13-8Mo (H1050)	> 75% YS
17-7PH (RH950)	<25% YS
17-7PH (TH1050)	<27% YS
PH15-7Mo (RH950)	<25% YS

*Threshold stress is <75% YS in a marine environment.

TABLE 7

TYPICAL STRESS-CORROSION AND FRACTURE TOUGHNESS PROPERTIES FOR HIGH-STRENGTH STEELS (REF. 4)

Alloy and Tensile Strength or Heat Treatment	Threshold Stress Intensity, K_{ISCC} ksi $in.^{1/2}$	Fracture Toughness K_{IC} at 70°F ksi $in.^{1/2}$
300M (280-300 ksi)	15	55
4340 (260-280 ksi)	10	53
4340 (200-220 ksi)	10	80
4340 (180-200 ksi)	27	105
4330M (220-240 ksi)	20	80
H11 (280-300 ksi)	8	25
H11 (220-240 ksi)	23	50
D6AC (220-240 ksi)	16	80
9Ni-4Co-0.2C	80	140
9Ni-4Co-0.3C	27	90
AF1410	<30	140
Maraging 300	10	65
Maraging 250	15	80
Maraging 200 (220 ksi yield)	25	120
Maraging 200 (200 ksi yield)	50	110
17-4PH (H900)	37*	50
17-4PH (H1000)	120	120
15-5PH (H900)	33*	70
15-5PH (H1000)	120	120
PH13-8Mo (H950)	<31**	62
PH13-8Mo (H1050)	<44**	87
17-7PH (RH950)	<20	32
17-7PH (TH1050)	14	47
PH15-7Mo (RH950)	<10*	30
PH15-7Mo (TH1050)	16	33

All test data in 3.5% NaCl solution except as noted.

*Tested in 20% NaCl; comparable values were obtained at a marine coast.

**Marine coast.

TABLE 8

PLATEAU CRACK GROWTH RATES FOR HIGH-STRENGTH STEELS (REF. 4)

Alloy and Tensile Strength or Heat Treatment	Plateau Crack Growth Rate, in./hr
300M (280-300 ksi)	8 x 10-1 (1)
4340 (260-280 ksi)	6.0 (1)
4340 (220-240 ksi)	5 x 10-1 (1)
4340 (200-220 ksi)	9 x 10-3 (1)
4130 (220-240 ksi)	7 x 10-1 (1)
4130 (180-200 ksi)	4 x 10-2 (1)
D6AC (220-240 ksi)	8 x 10-3 (1)
H11 (220-240 ksi)	2 x 10-2 (1)
AF1410 (235 ksi min.)	3 x 10-4 (2)*
Maraging 300	3 x 10-2 (2)
Maraging 250	3 x 10-3 (2)
15-5PH (H900)	2 x 10-3 (3)
PH13-8Mo (H950)	2 x 10-2 (3)
PH13-8Mo (H1050)	3 x 10-2 (3)
17-7PH (RH1050)	4 x 10-1 (3)
PH15-7Mo (RH1050)	4 x 10-2 (3)

(1) Distilled water
(2) 3.5% NaCl solution
(3) 20% NaCl solution

*Estimated from data in reference 27

TABLE 9

TYPICAL STRESS CORROSION AND FRACTURE TOUGHNESS PROPERTIES
OF COMMERCIAL TITANIUM ALLOYS (REF. 10)

Alloy	Thickness, inch	Heat Treatment	K_{IC} or K_C, ksi $in.^{1/2}$	K_{ISCC} or K_{SCC}, ksi $in.^{1/2}$
α Alloys				
Ti-70A	0.50	A-AC	123	33
Ti-5Al-2.5Sn	0.50	A-AC	88	30
α+β Alloys				
Ti-8Al-1Mo-1V	0.05	MA	75	30
	0.05	DA	160	50
	0.5	MA	48	20
	0.5	DA	100	32
Ti-6Al-4V	0.06	MA	150	110
	0.06	DA	150	110
	0.06	STA	95	65
	0.06	β-STA	95	65
	0.5	MA	60	35
	0.5	DA	70	52
	0.5	STA	47	25
	0.5	β-STA	70	45
Ti-6Al-6V-2Sn	0.50	MA	60	20
	0.50	STA	45	30
	0.50	β-STA	70	45
Ti-6Al-2Sn-4Zr-6Mo	0.50	MA	55	20
	0.50	DA	80	45
β+α Alloys				
Ti-13V-11Cr-3Al	0.50	β-STA	70	30
Ti-11.5Mo-6Zr-4.5Sn	0.50	β-STA	65	25
Ti-8Mo-8V-3Al-2Fe	0.50	β-STA	50	31
Ti-3Al-8V-6Cr-4Mo-4Zr	0.50	β-STA	50	37

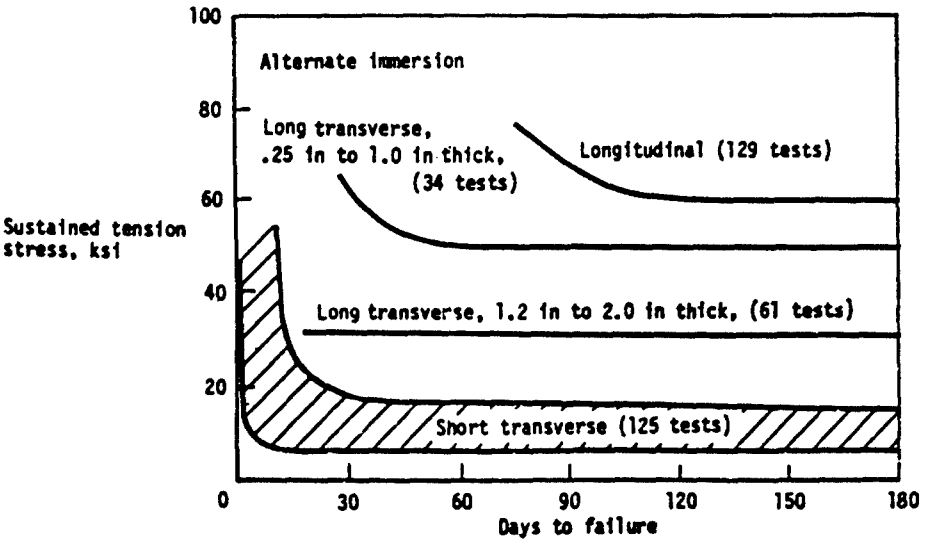

Figure 1 - Smooth-specimen stress corrosion test results for 7075-T6 extruded sections in 3.5% Sodium Chloride solution (Ref 8)

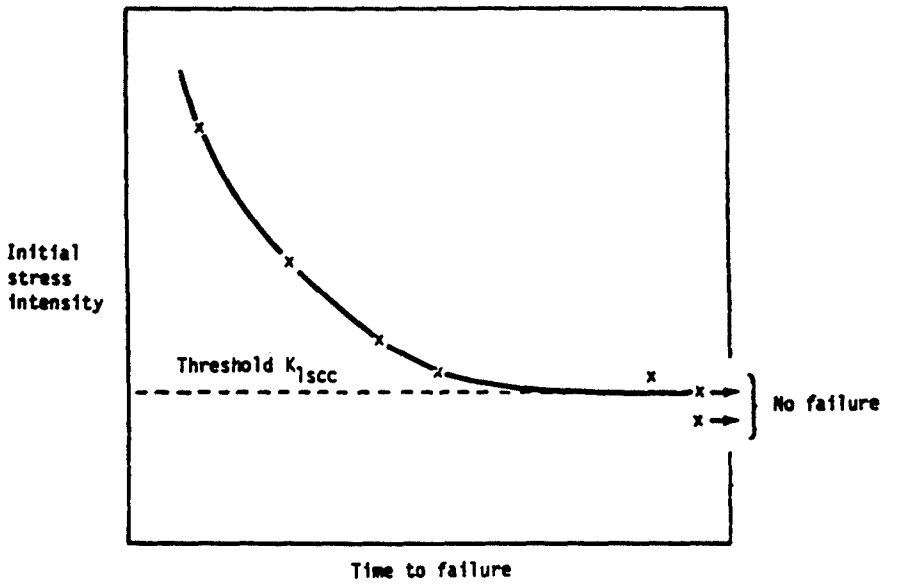

Figure 2 - Schematic representation of initial stress intensity-time to failure plot

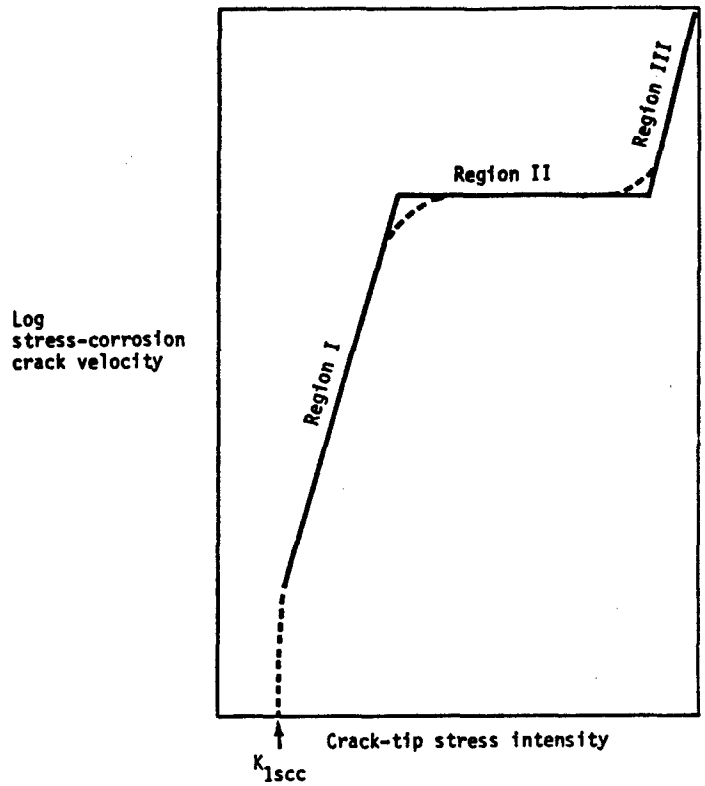

Figure 3 - Schematic representation of the effect of stress intensity on the growth rate of stress corrosion cracks

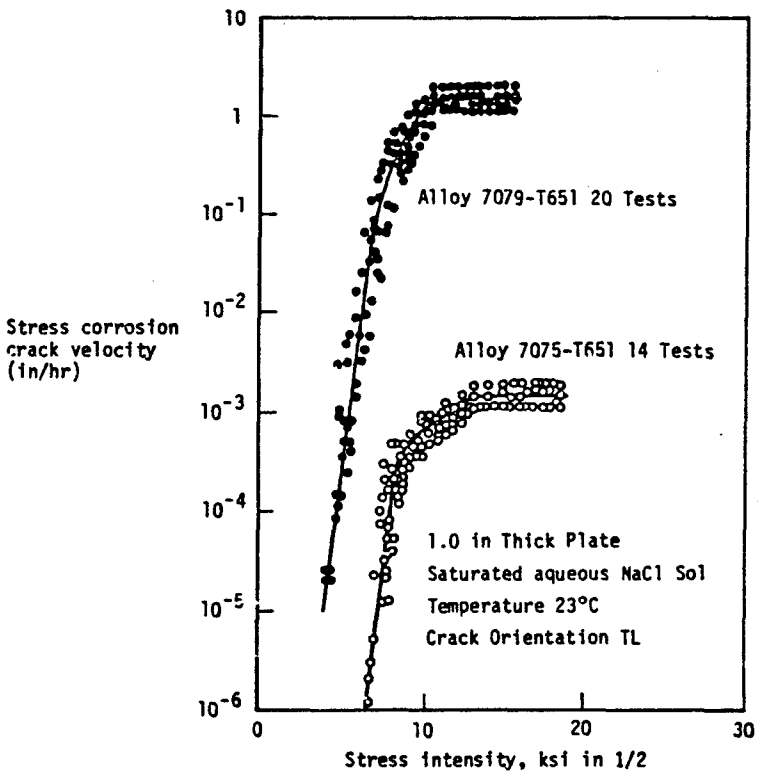

Figure 4 - Typical effect of stress intensity on stress corrosion crack velocity in two high strength aluminum alloys in NaCl solution (Ref 8)

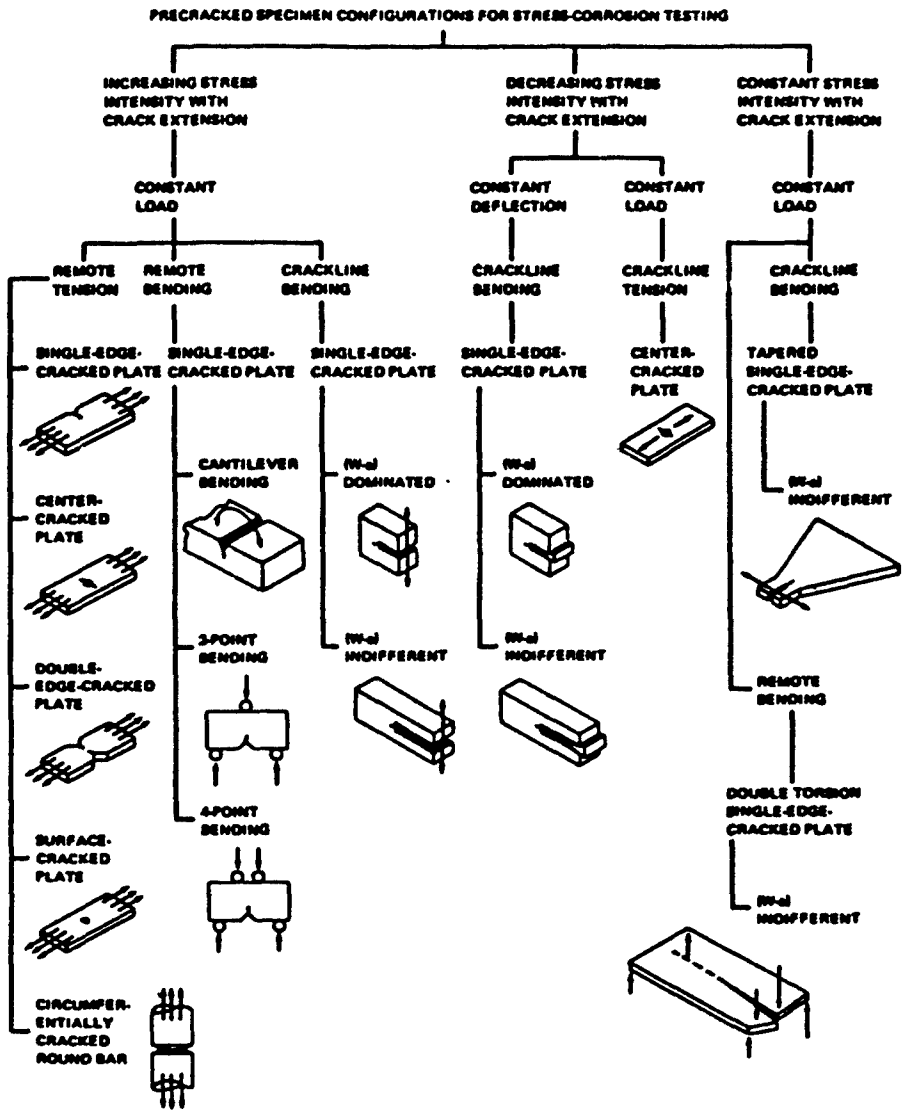

Figure 5 - Precracked specimens used for stress corrosion testing (Ref 11)

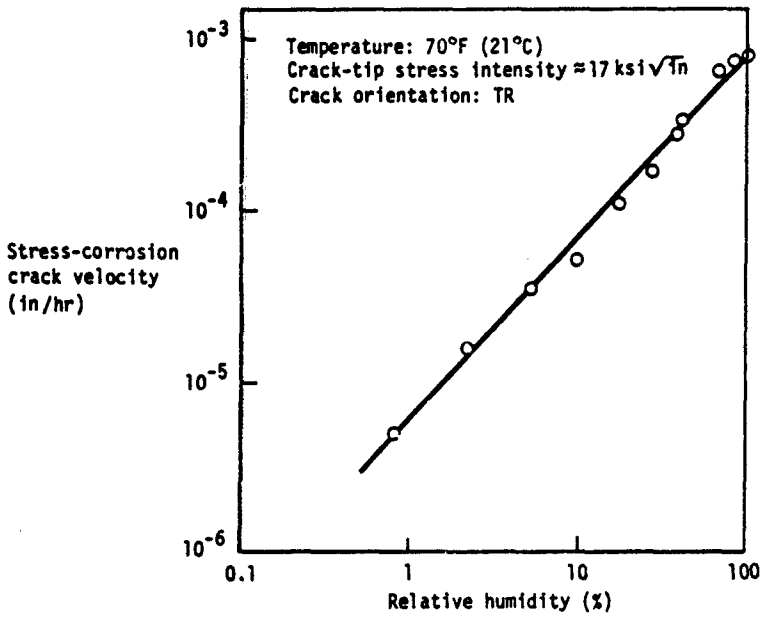

Figure 6 - Effect of humidity of air on stress-independent stress-corrosion crack velocity of 7075 - T651 (Ref 8)

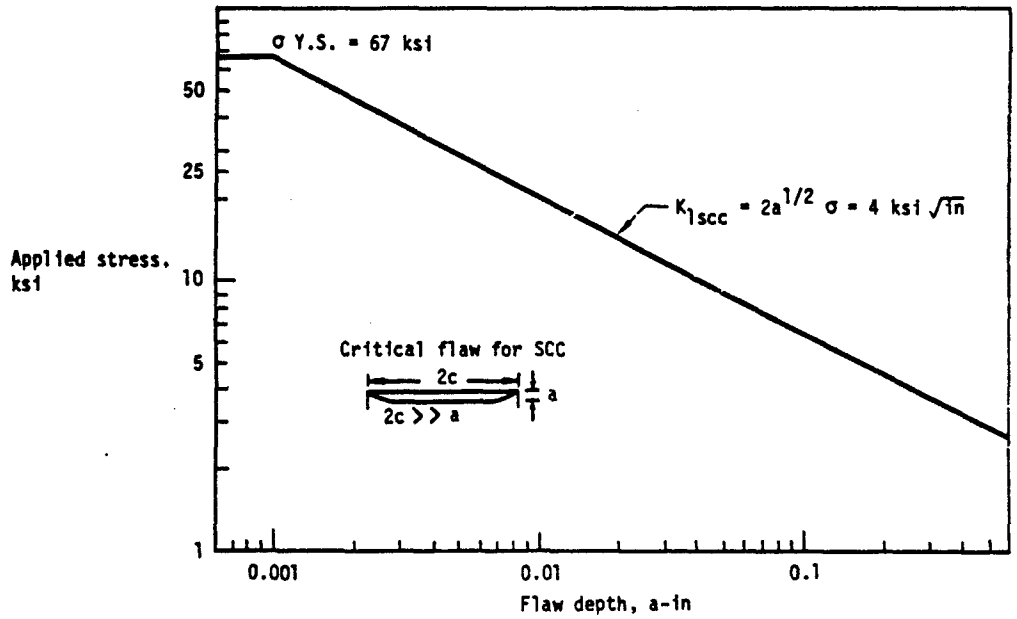

Figure 7 - Relationship between applied stress and crack length for SCC in 7079-T6 plate, short transverse direction (Ref 17)

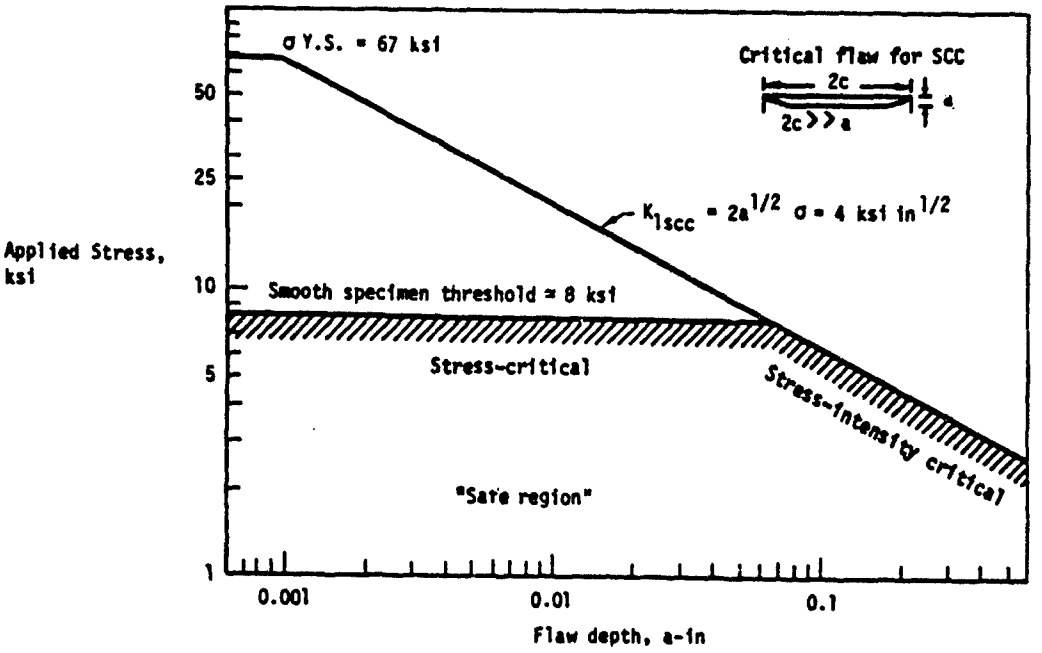

Figure 8 - Composite threshold stress-K_{1scc} diagram for 7079-T651 plate, short transverse direction (Ref 17)

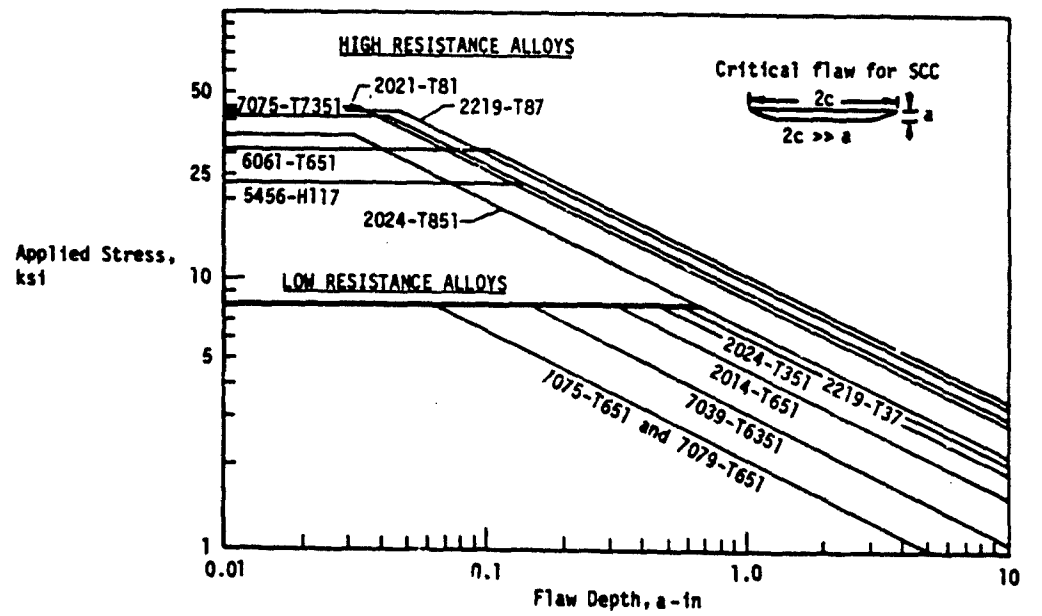

Figure 9 - Composite threshold stress - K_{1scc} characterization of aluminum alloy plate - short transverse stress (Ref 17)

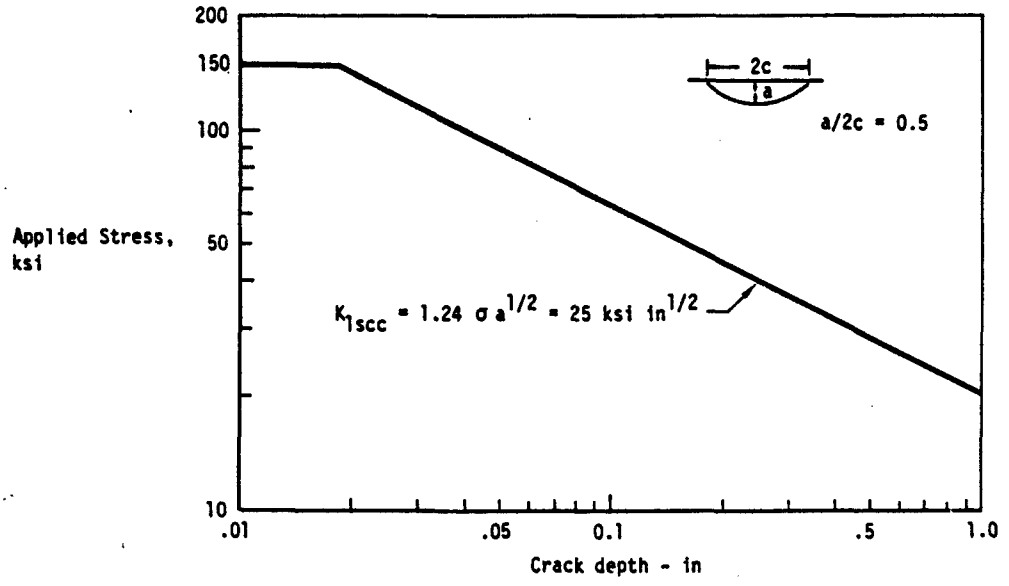

Figure 10 - Composite diagram for titanium 6Al-4V alloy, STA condition, containing a semi circular crack

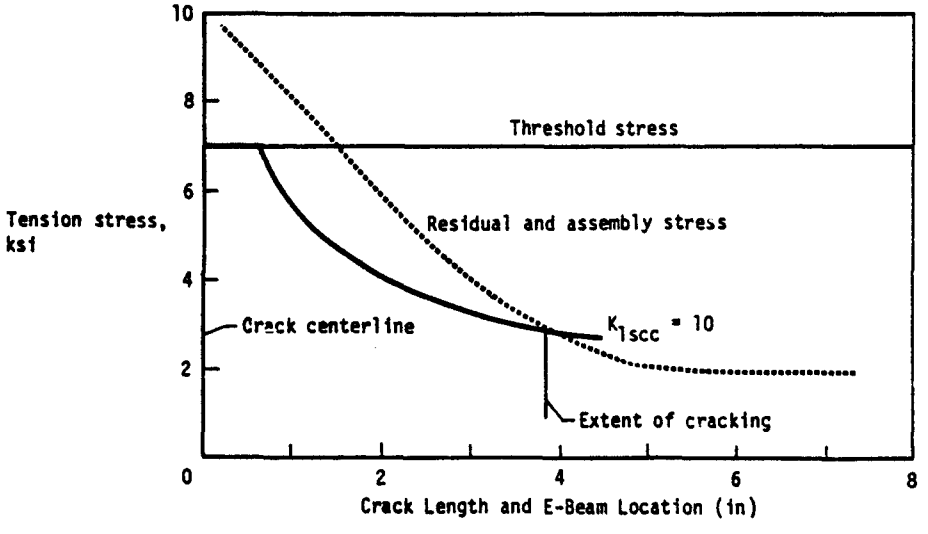

Figure 11 - Crack initiation and growth-sustained stress conditions (Ref 21)

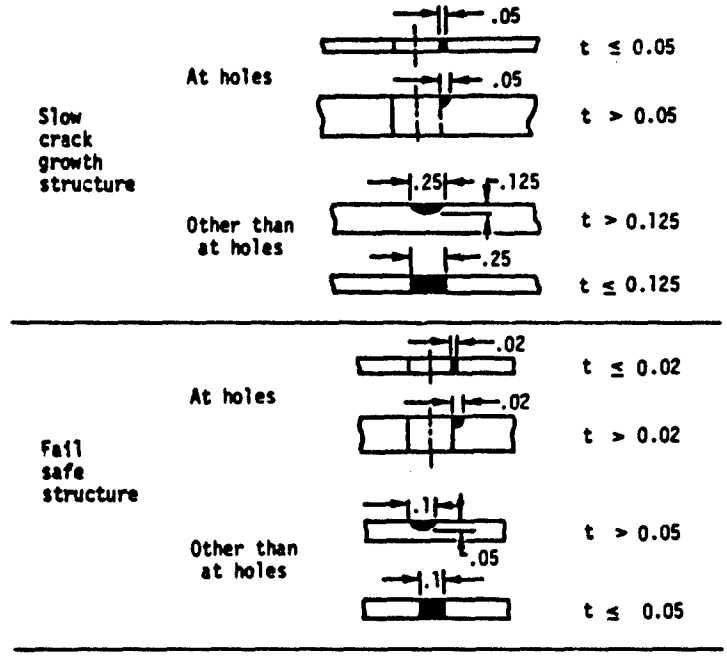

Figure 12 - Initial flaw sizes defined in MIL-A-83444

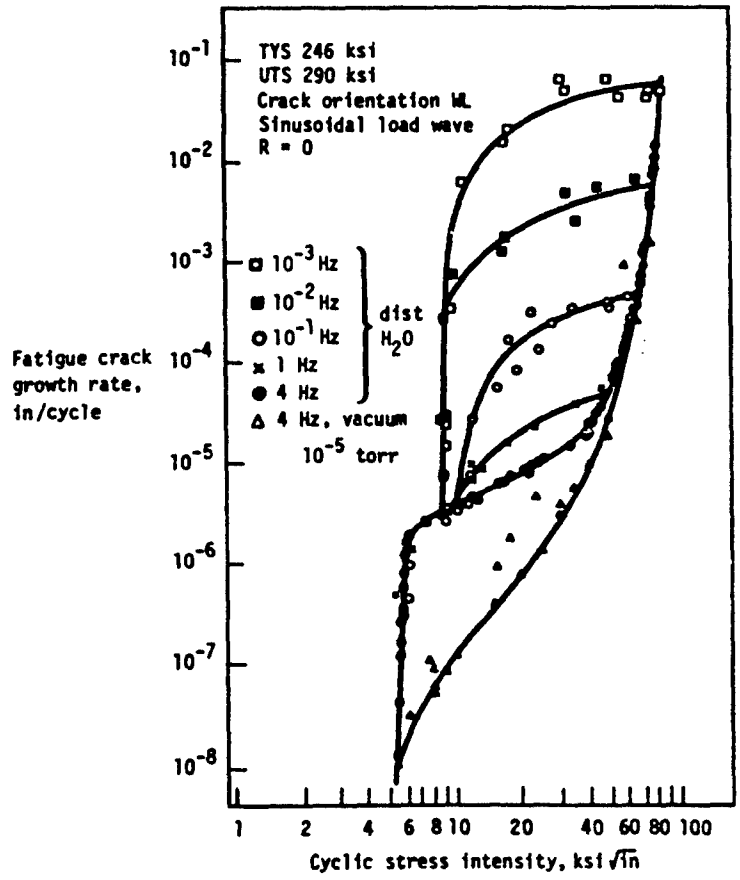

Figure 13 - Effect of cyclic frequency on fatigue crack growth rate of 4340M steel in distilled water (Ref 4)

10. SIMPLE METHODS OF DETERMINING STRESS INTENSITY FACTORS

D. P. ROOKE
Royal Aircraft Establishment
Farnborough, Hampshire
United Kingdom

FRANCIS L. BARATTA
Department of the Army
Army Materials and Research Center
Watertown, Massachusetts 02172

D. J. CARTWRIGHT
Department of Mechanical Engineering
The University of Southampton
Southampton, United Kingdom

CONTENTS

SUMMARY 10-1

SYMBOLS 10-2

10.1 INTRODUCTION. 10-3

10.2 REVIEW OF METHODS 10-3

10.2.1 Superposition 10-5
10.2.2 Stress Concentrations 10-8
10.2.3 Stress Distributions. 10-8
10.2.4 Green's Functions 10-9
10.2.5 Weight Functions. 10-12

10.3 METHODS FOR SIMPLE GEOMETRIES 10-13

10.3.1 Stress *Concentration* Factors. 10-13
10.3.2 Stress Distributions. 10-16

10.4 STRESS INTENSITY FACTORS FOR COMPLEX GEOMETRIES . . 10-19

10.4.1 Compounding Technique 10-19
10.4.2 Load Relief Factors 10-25

10.5 DISCUSSION AND CONCLUSIONS. 10-27

REFERENCES. 10-27

SUMMARY

A prerequisite for any fracture mechanics analysis of a cracked structure, is a knowledge of the stress intensity factor at the tip of the crack. Many methods are available for evaluating stress intensity factors, but if the structural configuration is complex, they are usually costly in time and money. This chapter describes some simpler approximate methods which are both quick and cheap. Their use is illustrated by examples typical of aerospace applications, *eg* cracks at holes and cracks in stiffened sheets. The errors introduced into calculations of residual static strength and fatigue lifetimes by the use of such approximations are acceptable for many practical cases: they are usually no greater and often smaller than those due to uncertainties in other parameters such as service loads, material toughness, etc.

LIST OF SYMBOLS

a, a', a_n, a'_n	crack lengths
A_s	cross-sectional area of stiffener
b, b_n, b'_n	distance between boundaries
c	notch depth
d	width of pressure band
E	Young's modulus of sheet
E_s	Young's modulus of stiffener
F	load relief factor
$g(x)$	Green's function
G	shear modulus
h	weight function
K, K_I, K_{II}, K_{III}	stress intensity factors (sif)
$\bar{K}$	sif in the absence of boundaries
K_n, K'_n	sif in the presence of nth boundary
K_e	sif due to boundary interaction
K_p	sif in periodically stiffened sheet
K_r	resultant stress intensity factor
$K_{m,f}$	sif for multiple cracks in a finite body
$K_{s,f}$	sif for a single crack in a finite body
$K_{m,\infty}$	sif for multiple cracks in an infinite body
$K_{s,\infty}$	sif for a single crack in an infinite body
K_t	stress *concentration* factor
ℓ	crack length from edge
L	total crack length (= 2a)
M, m	constants - equation (48)
M_f	free surface correction
p	pressure or stress
$p(x), p_o$	internal pressure in crack
P	localized force
Q	constant - equation (48)
Q_e, Q_n, Q'_n, Q_r	normalized stress intensity factors
$R; R_i, R_o$	radius; inner and outer radius
s	stiffness parameter, $E_s A_s/(Ebt)$
t	sheet thickness
v	displacement of crack surfaces
x, y	cartesian coordinates
κ	$3-4\nu$ or $(3 - \nu)(1 + \nu)$
ν	Poisson's ratio
ρ	notch root-radius
σ, σ_o	applied stress
σ_{mean}, σ_m	mean stress over crack-site
σ_{max}	maximum stress on crack-site
σ_{tip}	stress at tip of crack-site
$\sigma_x, \sigma_y, \tau_{xy}$	cartesian components of stress
τ_{max}	maximum shear stress

10.1 INTRODUCTION

Highly stressed aircraft structures may contain crack-like flaws, or they may develop cracks during their service life. The existence of such cracks and their subsequent growth can cause a loss of strength and a reduction in the service life of a structure. Fracture mechanics provides a means of quantitatively assessing the behaviour of cracks. A knowledge of this behaviour means that the safety of a structure during its service life can be assured and that the most economic inspection and maintenance schedules can be adopted. The application of the principles of fracture mechanics to a practical problem requires a knowledge of the crack size, the service stresses, the stress intensity factor and the appropriate properties of the material. This chapter illustrates some of the methods available for evaluating stress intensity factors, with particular emphasis on simple methods which do not require a large investment in either computing or experimental equipment.

Stress intensity factor solutions are now available for a wide range of geometrical configurations, both two and three dimensional; many solutions have been collected together [1-3]. Many other solutions are available, for instance, in the series of Special Technical Publications published by the American Society for Testing Materials (ASTM), in the series entitled 'Fracture' edited by H. Liebowitz [4] and in the series entitled 'Mechanics of Fracture' edited by G.C. Sih [5]. The methods, both theoretical and experimental, of obtaining these solutions have been reviewed by Cartwright and Rooke [6], Liebowitz (Vol II of Ref[4]), Sih (Vol I of Ref[5]) and Kobayashi [7]. Numerical methods have also been reported recently [8].

In practical problems, structural geometries and loadings are often so complex that the available stress intensity factor solutions are inadequate. Evaluation of the stress intensity factor for the actual problem using standard methods may be prohibitively expensive in both time and money. Thus there is a need to develop simpler methods which will be cheap and easy-to-use even if less accurate than most standard methods. Many simple methods have been suggested and their relative merits are discussed in section 10.2.

Some of the simple methods are more generally applicable than others, and these are dealt with in detail in sections 10.3 and 10.4. In section 10.3, methods are described by which the stress intensity factor is derived from the stress *concentration* factor. These methods are important since cracks frequently occur at the site of stress concentrations and the appropriate stress *concentration* factors are often already known [9]. Also in section 10.3 there is a method of evaluating the stress intensity factor from a knowledge of the stress distribution in the uncracked configuration; such a stress distribution may already be known or, if not, will be easier to obtain than the solution to the crack problem. The compounding technique [10], with the special case of 'load relief factors' [11], is widely applicable and is described in section 10.4. This technique makes use of the solutions for simple configurations which are already available [1-3].

The accuracy of these simple methods of evaluating the stress intensity factor and the consequent accuracy of fracture mechanics calculations is discussed in section 10.5. A comparison is made of the likely errors due to inaccurate stress intensity factors with the likely errors due to other uncertainties in the parameters used in a fracture mechanics calculation. This information is required so that a sound decision can be made between a cheap and simple method or a costly and probably lengthy method for a given fracture mechanics application. Some guidelines on the use of these methods in practical applications is given in the final section.

10.2 REVIEW OF METHODS

The usefulness of stress intensity factors (K-solutions) is now well established. They are used to calculate the static strength of a cracked structural component (the 'residual' strength), the lengths of critical cracks and the rates of crack growth in fatigue (see for example Ref[12]). The basis of the stress intensity factor approach lies in the assumption that the growth of a sharp crack is determined by the stress field at the crack tip. This greatly reduces the necessary stress analysis, particularly when the cracked configuration is complex, since it is necessary to determine only the stress near the crack tip rather than the whole stress field.

Over the last thirty years many methods of obtaining K-solutions have been developed. Several hundred solutions, mostly for two-dimensional configurations, are now available. The common methods are set out in Fig 1; the methods are divided into three groups depending on the time required to obtain a solution. The choice of a method to determine an unknown stress intensity factor will depend on the following:

(i) the time available;

(ii) the required accuracy;

(iii) the cost;

(iv) the use (once or many times);

(v) how simply the real structure can be modelled.

For simple geometrical situations, or where a complex structure can be simply modelled, it may be possible to use one of the reference books [1-3]. This should

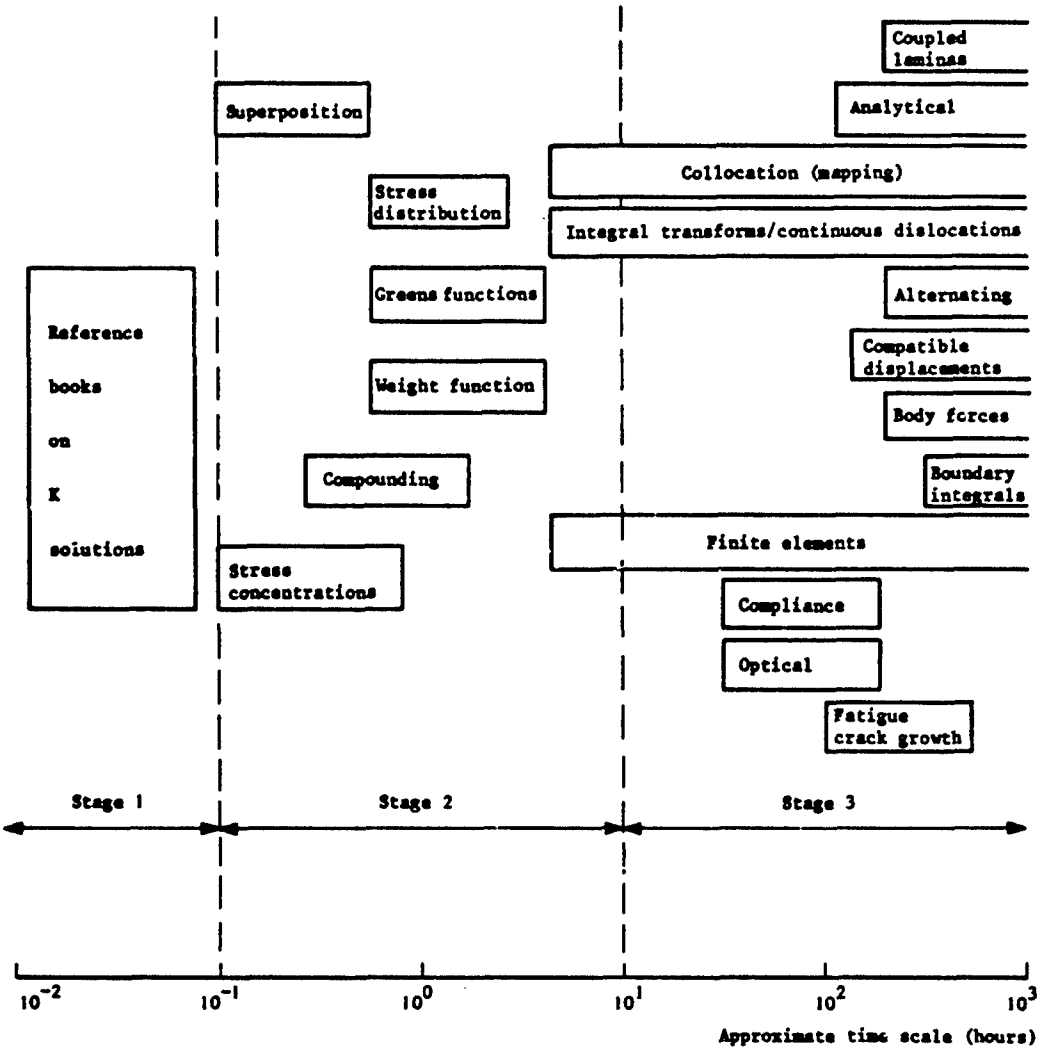

Fig 1 Methods of determining stress intensity factors

always be attempted first, since if the stress intensity factor can be found, it will usually involve no more than a few man-minutes (see Fig 1). Where a solution cannot be obtained directly from a reference book then one of the relatively simple methods in stage 2 may often be adequate [13] and will seldom require more than a few man-hours.

In applications where a particular stress intensity factor is required repeatedly - that for a standard test-piece, say, - it would probably be worth obtaining a more accurate solution by using a numerical technique from stage 3. Such methods will also be needed when the structure cannot be modelled simply, and in these cases the methods based on finite element techniques are often appropriate. The type of application will have an influence on the choice of method; for instance, estimates of the rate of growth of fatigue cracks are more sensitive to errors in the stress intensity factor than estimates of the residual strength. Methods of solving crack problems in three dimensions are limited if no adequate two-dimensional analogue is available. Methods which use finite elements or boundary integral equations or distributions of point forces are usually required. In addition to these there are experimental methods based on photoelasticity and on the growth rates of fatigue cracks. They have the advantage that components closely resembling the actual structure can be tested.

The numerical methods in stage 3 usually have an accuracy of about 2%. However alternating methods and those based on finite elements often have errors as large as 6%. In general the experimental methods are less accurate; but errors can be kept within 2-5% using the compliance method provided that sufficient care is exercised. Photoelastic methods may result in errors of about 10%.

Unless computer programs or suitable experimental facilities are readily available then these stage 3 methods can involve substantial effort (tens of man-days). It is for this reason that many of the simple methods have been proposed and developed. Several of the methods are concerned with the calculation of stress intensity factors for the

important problem of a crack at or near stress concentrations. The usual approach is to construct an approximate solution which fits known constraints and then test it against a solution of known accuracy. Any application to general problems must be carried out with care in order to ensure that restrictions inherent in the original approximation are not violated. Methods of more general application, such as the compounding method and its special cases, are described in section 10.4 together with illustrations of their use in aerospace applications.

Other methods have been developed to solve three-dimensional problems approximately [14-16] by making use of the known solutions for two-dimensional configurations. At present, these methods are not sufficiently well developed to be simple to apply but they can be extremely useful in solving problems involving corner cracks and surface cracks which occur frequently in aerospace structures [17].

Some of the more common methods and their uses are outlined below.

10.2.1 Superposition

Superposition is probably the most common and simplest technique in use for obtaining stress intensity factors. Complex configurations are considered to be a combination of a number of separate simpler configurations with separate boundary conditions and which have known stress intensity factors. The stress intensity factors for the simple configurations are then added together to obtain the required solution. Errors from using superposition can arise when the complex configuration being analysed cannot be precisely built up from configurations with known stress intensity factors.

An illustration of the use of this technique is shown in Fig 2. The stress intensity factor for the configuration shown in Fig 2a is the sum of the stress intensity factors for the two simpler configurations shown in Fig 2b&c. Another important application of superposition, the analysis of pin-loaded lugs in aerospace applications, is shown Fig 3. By using the procedure shown, opening mode stress intensity factors for non-symmetrical loadings can be found by adding the more easily obtainable results for simpler symmetrical loadings. Application of the principle of superposition leads to an important result about the equivalence of stress intensity factors resulting from external loading on a body and those resulting from internal tractions on the crack surface. The stress intensity factor for a crack in a loaded body may be determined by considering the crack to be in an unloaded body with applied tractions on the crack surface only (see Fig 4). These surface tractions are equal in magnitude but opposite in sign to those evaluated along the line of the crack site in the uncracked configuration. This method of determining stress intensity factors is important in the use of the Green's function and the weight function methods discussed in sections 10.2.4 and 10.2.5.

The superposition of stress intensity factors is subject to the same restrictions as the more usual superposition of stresses and displacements. In addition, the crack surfaces in the final configuration must always be separated along their entire length although there may be some overlap of the crack surfaces, or K_I (the opening mode stress intensity factor) may be negative in some of the ancillary configurations. If overlap does occur in an ancillary configuration it must be ignored in evaluating the ancillary stress intensity factors, otherwise the results of the superposition will be invalid. Superposition of the stress intensity factors with particular reference to the limitations in solving crack problems, has been considered by Aamodt and Bergan [18].

Certain solutions for partially loaded cracks may be superimposed to obtain approximate solutions for cracks in arbitrary stress fields. Consider the determination of the stress intensity factor for an edge-cracked strip subjected to in-plane bending stresses, as shown in Fig 5a, with a crack length of one half of the strip width b. As previously stated the problem can be reduced to determining the stress intensity factor for the crack subjected to a linear distribution of pressure over the crack surfaces as shown in Fig 5, that is

$$(K_I)_{5(a)} = (K_I)_{5(b)}. \qquad (1)$$

An approximate solution to the linear distribution of pressure can be obtained by superimposing results given by Emery [19,20], for a band of pressure of variable width acting over part of the crack surface. The solution is shown, for $a/b = 0.5$, in Fig 6a. The linear distribution of pressure is represented by a finite number of incremental steps (in this case three) as shown in Fig 6b which in turn can be represented as the summation of bands of pressure over the crack surface as shown in Fig 6c.

The stress intensity factor of the crack subjected to the stepped pressure distribution, for $a/b = 0.5$, is given by the superposition of three terms which are a consequence of the three stress bands shown in Fig 6c; thus

$$(K_I)_{total} = K_I\Big|_{\substack{d/a=1.0 \\ p=\sigma/6}} + K_I\Big|_{\substack{d/a=2/3 \\ p=\sigma/3}} + K_I\Big|_{\substack{d/a=1/3 \\ p=\sigma/3}}, \qquad (2)$$

which using Fig 6a becomes

$$(K_I)_{total} = \sqrt{\pi a}\left\{\frac{\sigma}{6} \times 2.74 + \frac{\sigma}{3} \times 1.86 + \frac{\sigma}{3} \times 0.94\right\}, \qquad (3)$$

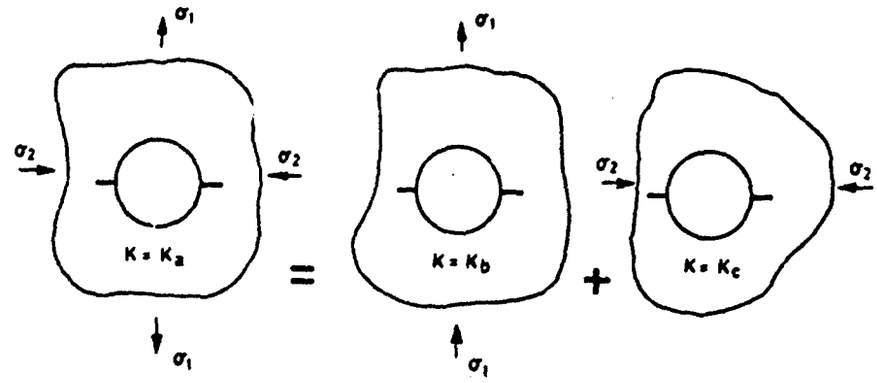

Fig 2 Superposition of stress intensity factors

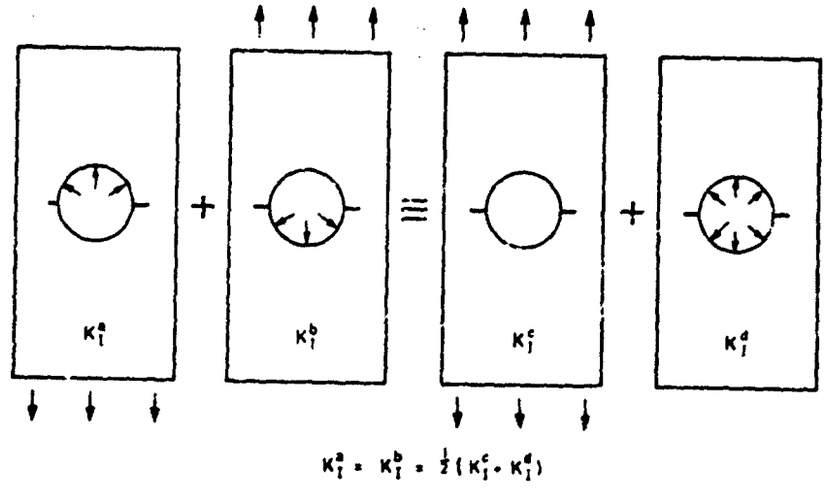

Fig 3 Superposition for a pin-loaded hole with radial cracks

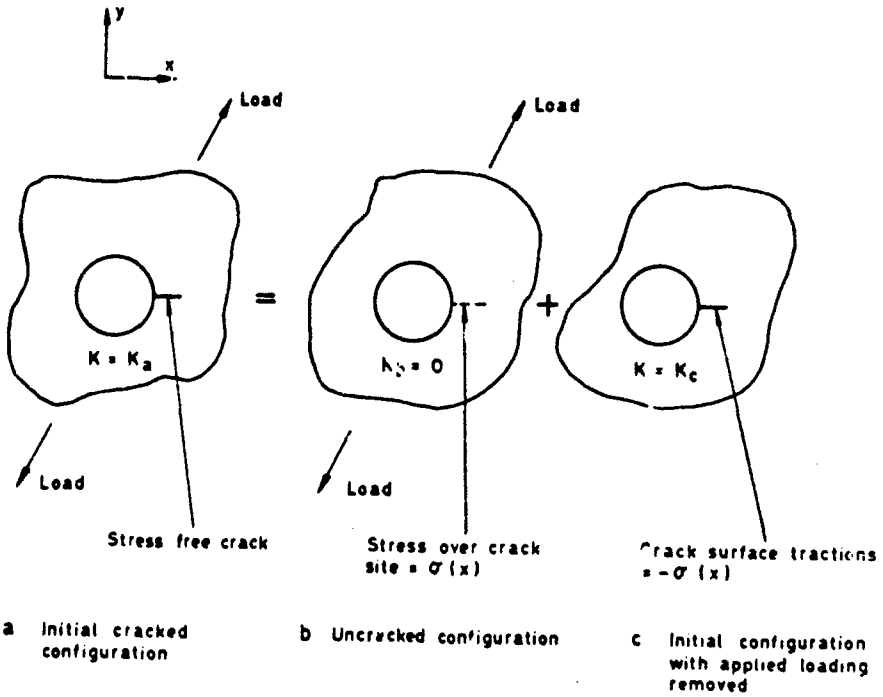

Fig 4 Superposition showing the equivalence of $K(K_a = K_c)$ for general loading and crack surface tractions

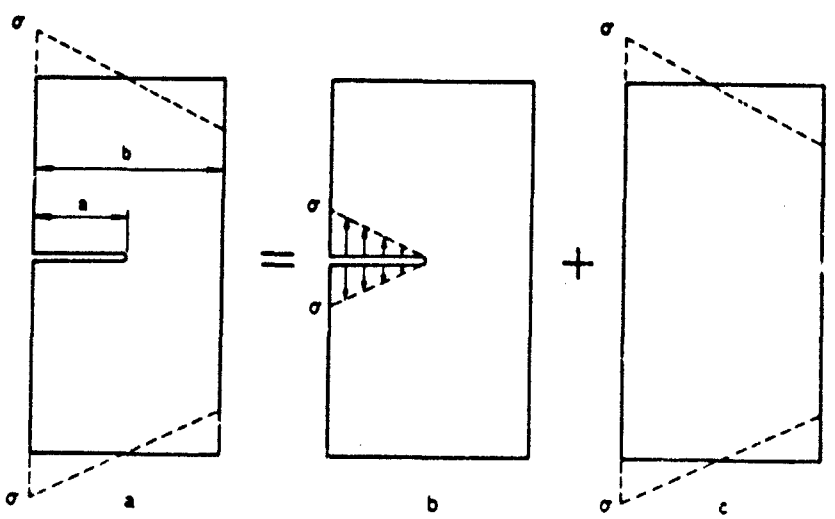

Fig 5 Superposition for an edge-cracked strip in bending

that is,

$$(K_I)_{total} = 1.39\sigma\sqrt{\pi a}\ , \tag{4}$$

which is 7% less than the accurate result for this linear distribution of stress. It is possible to improve the accuracy by increasing the number of steps used in approximating the actual distribution. This method can be used for any arbitrary distribution of stress (see for example Ref 20), providing that the stress intensity factor for the band of pressure in the configuration is known. The method is a special form of the Green's function technique outlined in section 10.2.4. Lachenbruch [21] has obtained a step function loading on the crack surface for a/b = 0.0 which has been expressed in algebraic form by Emery [22] and applied to the solution of crack problems in thermally stressed cylinders. Similar results can be obtained by the approach described in section 10.2.4 using the Green's function of Hartrauft and Sih [23].

10.2.2 Stress concentrations

Irwin [24] proposed that Neuber's [25] stress concentration results for notches of very small flank angle and very small root radius may be used to obtain theoretical expressions for stress intensity factors.

Consider a notch which, in the limit of zero root radius (ρ), tends to a crack along the $y = 0$ axis: if σ_{max} is the maximum value of σ_y at the tip we have

$$K_I = \frac{\sqrt{\pi}}{2} \lim_{\rho \to 0} \left\{\sigma_{max}\sqrt{\rho}\right\}; \tag{5}$$

if τ_{max} is the maximum value of τ_{xy} near the tip along the line $y = 0$ (the position of the maximum tends to the tip as $\rho \to 0$) we have

$$K_{II} = \sqrt{\pi} \lim_{\rho \to 0} \left\{\tau_{max}\sqrt{\rho}\right\}; \tag{6}$$

and similarly if τ_{max} is the maximum value of τ_{zy} at the tip we have

$$K_{III} = \sqrt{\pi} \lim_{\rho \to 0} \left\{\tau_{max}\sqrt{\rho}\right\}. \tag{7}$$

Although the relationship between K and σ_{max} (or τ_{max}) is exact, the actual expression for the maximum stresses may be known only approximately. Harris [26] has made considerable use of equations (5) to (7) and Neuber's work on stress *concentration* factors K_t (ratio of maximum stress to applied stress) in deriving expressions for K_I, K_{II} and K_{III} in circumferentially cracked round bars subjected to bending, transverse shear, torsion and longitudinal tension. Pook and Dixon [27] have analysed a finite rectangular sheet with an edge crack loaded such that there is combined tension and bending at the crack tip.

Hasebe and Katanda [28] have suggested a systematic method of determining stress intensity factors which involves expressing the stress *concentration* factor in series form. The unknown coefficients in the series are determined by fitting the expression to available data for the stress *concentration* factor at various values of the root radius ρ. In this way it is possible to make better use of stress *concentration* factors determined for values of ρ too large for equations (5) to (7) to be applied directly. The stress *concentration* factor used can be determined analytically, numerically or experimentally. More detailed consideration of the method together with some examples is given in section 10.3.

10.2.3 Stress distributions

Some simple methods have been proposed for determining stress intensity factors from stress distributions. The methods are all based on using the stress intensity factor for an edge crack, subjected to a uniform internal pressure p, in a semi-infinite plane. This is given, for a crack of length ℓ, by

$$K_I = 1.12p\sqrt{\pi\ell}\ ; \tag{8}$$

the factor 1.12 is often called the 'free surface correction'.

Equation (8) can be used to provide approximate stress intensity factors for cracks at a hole providing that the crack length ℓ is small compared to the radius of the hole R. In the application to short cracks at holes or notches the pressure p is replaced by a stress characteristic of that over the crack site in the uncracked solid $\sigma(x)$. In the maximum stress method

$$p = \sigma_{max} = \sigma(0)\ ; \tag{9}$$

in the mean stress method

$$p = \sigma_{mean} = \frac{1}{\ell}\int_0^{\ell} \sigma(x)dx\ ; \tag{10}$$

and in the tip stress method

$$p = \sigma_{tip} = \sigma(\ell) . \tag{11}$$

Results using the maximum stress method equation (9) are shown in Fig 7 for a crack at both a circular and an elliptical cut-out in a uniform stress field. It can be seen that for short crack lengths equation (9) gives a reasonable approximation to the accurate (dotted line) solution [29]. The crack length over which equation (9) remains a reasonable estimate of K_I depends on the tip radius of the notch, the blunter the notch the better the approximation. At long crack lengths, *ie* $\ell \gg R$, the stress intensity factor for two equal length cracks approaches that for an isolated crack of length $2(R + \ell)$ in a uniform stress field as given by

$$K_I = \sigma\sqrt{\pi(R + \ell)}. \tag{12}$$

For a single crack of length ℓ it approaches the stress intensity factor for an isolated crack of length $2R + \ell$ given by

$$K_I = \sigma\sqrt{\pi(2R + \ell)/2} \tag{13}$$

Hence an approximation can be obtained over the whole range of crack lengths and is shown by the solid line in Fig 7.

The short crack approximation in Fig 7 can be replaced by equations (10) or (11). This will involve more calculations since the distribution of stress over the whole crack site in the uncracked solid must be known rather than just the maximum stress (*ie* K_t for the notch or hole). The maximum stress method has been compared to other simple approximations [30] for an edge crack in a thermally stressed plate. Williams and Isherwood [31] have proposed a method based on the mean stress and have suggested an empirical way of making corrections for finite width effects. This method has been used for determining stress intensity factors for a central radial crack in a rotating disc [32] and an edge crack in a circular bar subjected to pure bending [33]. Smith [34] has stated that for an edge with a length ℓ in a monotonically decreasing stress field the stress intensity factor K_I will lie between the bounds given by

$$[0.29\sigma(\ell) + 0.83\sigma_{mean}]\sqrt{\pi\ell} < K_I < 1.12\sigma_{mean}\sqrt{\pi\ell} . \tag{14}$$

This result applies strictly to an edge crack in a half-plane, but should be applicable to short cracks ($\ell \ll R$) at holes providing that $\sigma(x)$ is monotonically decreasing. This will be so for many stress distributions near holes unless there are significant residual compressive stresses such as occur near holes which have been subjected to cold-working. The mean stress method and the tip stress method are considered in section 10.3 where some particular applications are described in detail.

10.2.4 Green's functions

The Green's function method of determining stress intensity factors is applicable to a wide variety of aerospace problems, for example cracks at pin-loaded holes and at fastener holes, and cracks in the residual stress fields at the edge of cold-worked holes. In order to apply the method it is necessary to know

(i) the appropriate Green's function, and

(ii) the distribution of stress along the crack site in the uncracked solid.

Once these are known, obtaining a stress intensity factor is reduced to a simple summation procedure which can be done numerically or graphically or analytically depending on the form of the Green's function. The technique will give exact results providing that the exact Green's function is used. Often this may not be available and it is then necessary to make approximations. For cracks in residual stress fields care must be taken to ensure that the crack surfaces are separated along their entire length. If they are not, crack surface contact conditions must be included in the Green's function.

The opening mode stress intensity factor K_I for a crack which lies along the x axis between $x = +a$ and $x = -a$, can be written in terms of the Green's function $g(x)$ and $\sigma_y(x)$, the stress along the crack site in the uncracked body, as

$$K_I = \frac{1}{\sqrt{\pi a}} \int_{-a}^{a} \sigma_y(x)g(x)dx . \tag{15}$$

The stress $\sigma_y(x)$ may be measured experimentally in the uncracked solid or determined theoretically and then used in equation (15) to give the stress intensity factor. Equivalent forms can be written for K_{II} and K_{III}, the sliding and tearing mode stress intensity factors.

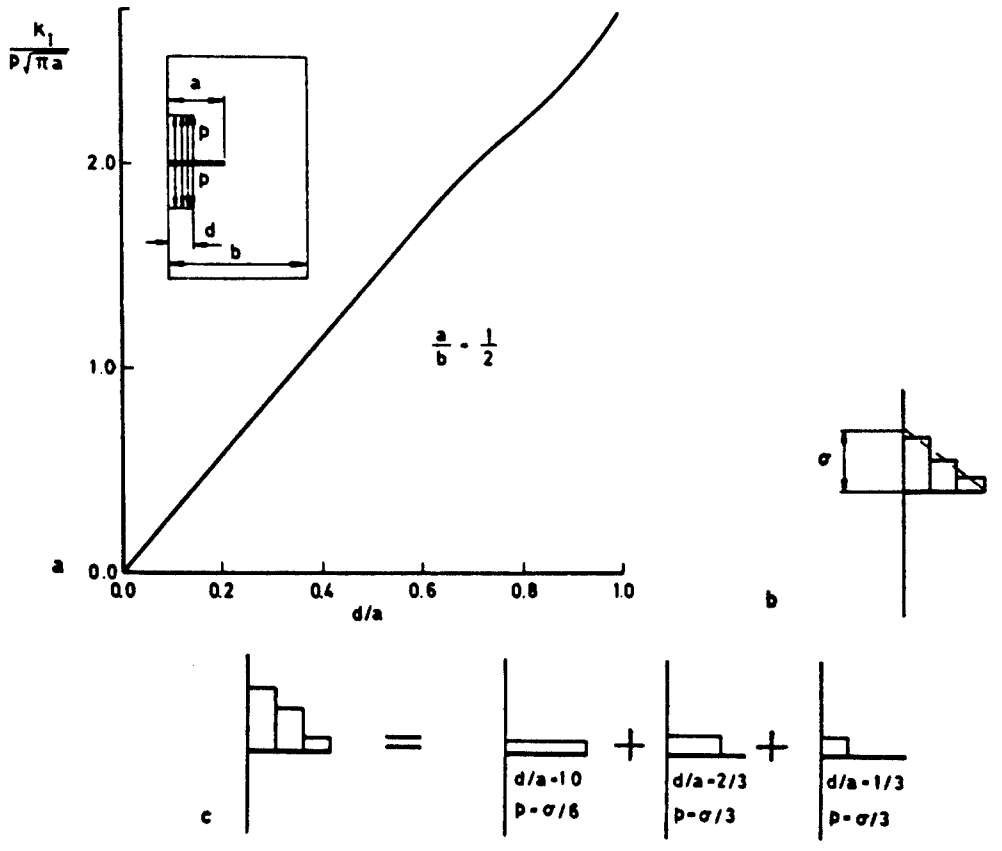

Fig 6 Superposition for edge-cracked strip in bending

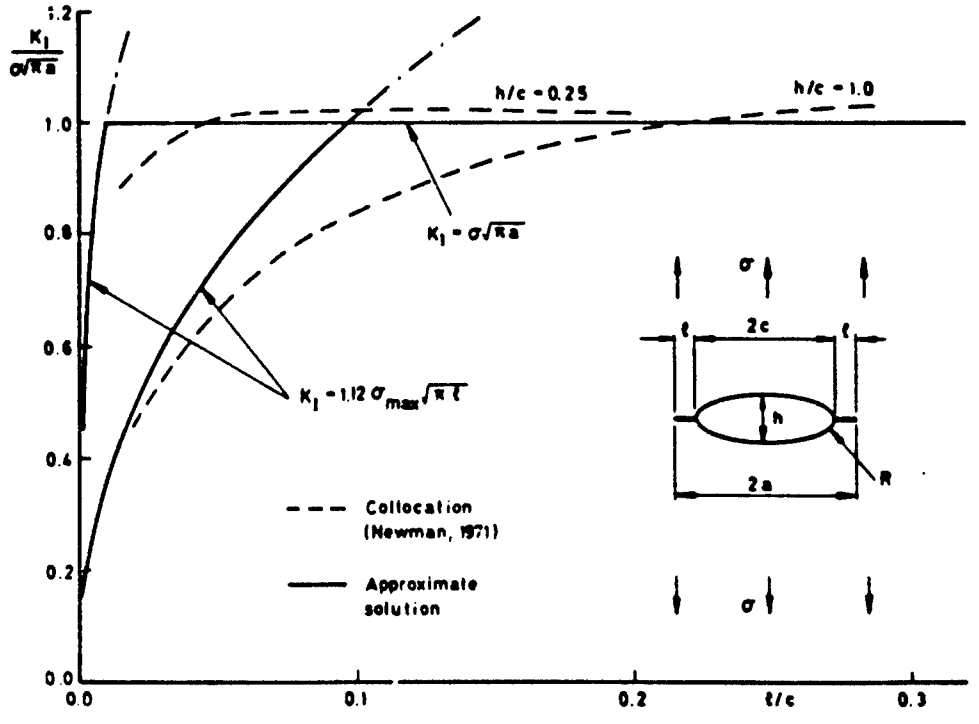

Fig 7 Comparison of stress intensity factors for cracks at elliptical and circular cut-outs

Green's functions which give the stress intensity factor for an isolated force on the crack surface have been determined for embedded cracks [35-37] and for edge cracks [23,38]. Other sources of Green's functions are given in Refs [1-3].

Shah [39,40] has used the Green's function $g_1(x)$ for a crack of length $2a$ subjected to a pair of symmetrical point forces in an infinite sheet under plane stress conditions. This is given by

$$g_1(x) = \left[\frac{a + x}{a - x}\right]^{\frac{1}{2}} . \tag{16}$$

The substitution of equation (16) into equation (15) gives

$$K_I = \frac{1}{\sqrt{\pi a}} \int_{-a}^{a} \sigma_y(x)\left[\frac{a + x}{a - x}\right]^{\frac{1}{2}} dx , \tag{17}$$

where $\sigma_y(x)$ is the stress over the crack site in the uncracked solid. Shah has modified equation (17) to determine approximate stress intensity factors for cracks at holes subjected to a variety of loadings. The approximation involves interpreting equation (17) as giving the stress intensity factor for two equal length (ℓ), diametrically opposed cracks at a hole of radius R where x is measured from the hole boundary along the crack line. Shah modifies equation (17) to give the stress intensity factor for both tips as

$$K_I = \frac{M_f}{\sqrt{\pi \ell}} \int_{-\ell}^{+\ell} \sigma_y(x)\left[\frac{\ell + x}{\ell - x}\right]^{\frac{1}{2}} dx \tag{18}$$

where M_f is a free surface correction given by

$$M_f = 1.0 + 0.12\left(\frac{0.3 - \ell/R}{0.3}\right) , \qquad \text{for } 0 \leq \frac{\ell}{R} \leq 0.3 \tag{19}$$

and

$$M_f = 1.0 , \qquad \text{for } \frac{\ell}{R} > 0.3 . \tag{20}$$

The stress intensity factor for one crack is given by Shah as

$$(K_I)_{\text{one crack}} = \sqrt{\frac{2R + \ell}{2R + 2\ell}}\ (K_I)_{\text{two cracks}} \tag{21}$$

which has the correct limiting values, that is

$$\text{for } \ell \gg R \qquad (K_I)_{\text{one crack}} = \frac{1}{\sqrt{2}}(K_I)_{\text{two cracks}} , \tag{22}$$

$$\text{and for } \ell \to 0 \qquad (K_I)_{\text{one crack}} = (K_I)_{\text{two cracks}} . \tag{23}$$

Equations (18) to (23) are based on the solution for an arbitrarily loaded through thickness crack remote from other boundaries. The effect of the hole is only allowed for by using $\sigma_y(x)$ appropriate to the distribution at the hole. The approximate Green's functions used by Shah will be least accurate at short crack lengths. In order to improve the accuracy at short crack lengths ($\ell/R \leq 0.3$), he introduces a free surface correction M_f to account for the stress free edge of the hole. This approach of interpolating between known solutions for short and long cracks is discussed in more detail in section 10.3. The approximate stress intensity factor obtained by using Shah's method will be more inaccurate for cracks at holes near other boundaries as these cause changes in both $\sigma_y(x)$ and the Green's function. In Shah's method the Green's function always remains the same and other finite boundaries are only allowed for in so far as $\sigma_y(x)$ is affected. The method has been extended [41] to consider part-circular cracks at holes. Shah [39] has shown that using equations (18) to (23), stress intensity factors can be determined to an accuracy of a few per cent for several configurations.

Hsu and Rudd [42] have constructed a Green's function for two equal length diametrically-opposed radial cracks at a circular hole in a strip of finite width. Each crack is subjected to a symmetrical pair of concentrated forces and the Green's function is determined by finite element methods. The Green's function is not given explicitly, but is used to solve several problems with different ratios of hole diameter to strip width. Problems involving residual stress fields or the stress fields which result from the use of interference-fit fasteners are also analysed. Recent work [43] indicates that results using the Green's functions [39,42] are in agreement for cracked holes remote from other boundaries. Tada and Paris [44] have used the Green's function technique to provide upper and lower bounds on the stress intensity factor for an edge crack in a residual stress field. Chell [45-48] has produced a series of results for cracks in arbitrary stress fields; they are directly applicable to edge and centre cracks under arbitrary loadings.

10.2.5 Weight functions

The method of determining stress intensity factors using weight functions was proposed by Bueckner [49] and considered further by Rice [50]. More recently these results have been given a rather more direct derivation by Paris, McMeeking and Tada [51]. Two-dimensional plane stress or plane strain problems of a crack of length L in an infinite body subjected to an arbitrary symmetrical loading can be solved provided that certain results are known for one symmetrical loading. The results required are $v^{(1)}(L,x)$, the displacement of the crack faces, and $K_I^{(1)}$, the stress intensity factor. The stress intensity factor for any other symmetrical loading $K_I^{(2)}$, at the crack tip $x = L$, is given by

$$K_I^{(2)} = \int_0^L \sigma(x)h(L,x)dx \ , \tag{24}$$

where $h(L,x)$ is the weight function and is independent of $\sigma(x)$, the stress over the crack site in the uncracked solid. The weight function is defined as

$$h(L,x) = \frac{8G}{1+\kappa} \frac{1}{K_I^{(1)}} \frac{\partial v^{(1)}}{\partial L} \ , \tag{25}$$

where $\kappa = 3 - 4\nu$ for plane strain,

$\kappa = \frac{3-\nu}{1+\nu}$ for plane stress

and G is the shear modulus.

The weight function method is exact providing that the correct weight function is used. However it is often possible to construct approximate weight functions so avoiding the need to use more time-consuming and costly stage 3 methods (see Fig 1).

As an example of the method, consider the problem of determining the stress intensity factor for a crack subjected to a distribution of internal pressure $p(x)$. The crack face displacement $v^{(1)}(L,x)$ is taken to be that for a crack subjected to a uniform pressure p_0, *ie*

$$v^{(1)}(L,x) = \frac{p_0(1+\kappa)}{4G} \sqrt{x(L-x)} \ , \tag{26}$$

where the crack tips are at $x = 0$ and $x = L$. The stress intensity factor $K_I^{(1)}$ is given by

$$K_I^{(1)} = \frac{p_0\sqrt{\pi L}}{\sqrt{2}} \ . \tag{27}$$

The weight function given in equation (25) becomes

$$h(L,x) = \frac{2\sqrt{2}}{\sqrt{\pi L}} \frac{\partial}{\partial L} \sqrt{x(L-x)} \tag{28}$$

$$= \frac{\sqrt{2}}{\sqrt{\pi L}} \left[\frac{x}{L-x}\right]^{\frac{1}{2}} \ . \tag{29}$$

With $\sigma(x) = p(x)$, equation (24) becomes

$$K_I^{(2)} = \left(\frac{2}{\pi L}\right)^{\frac{1}{2}} \int_0^L p(x)\left[\frac{x}{L-x}\right]^{\frac{1}{2}} dx \ . \tag{30}$$

By moving the origin of coordinates to the centre of the crack and by putting

$$L = 2a \quad \text{and} \quad X = x - a \tag{31}$$

where a is the semi-crack length, equation (30) becomes

$$K_I = \frac{1}{\sqrt{\pi a}} \int_{-a}^{a} p(x)\sqrt{\frac{a+x}{a-x}}\, dx \ . \tag{32}$$

This result is identical to the known expression [35] given in equation (17).

Equations (24) and (25) have been used extensively, see for example [52,54], to determine stress intensity factors for cracks at regions of stress concentration in two-dimensional solids. Grandt [52] has determined the weight function for two symmetrical radial cracks at a hole in a sheet subjected to a uniform tensile stress. He used finite element results for $v^{(1)}(L,x)$ and Bowie's results [53] for $K_I^{(1)}$. Using this weight function Grandt determined stress intensity factors for a variety of loadings. These included the important cases of cracks in a residual stress field either due to cold work at the hole boundary or due to interference fit fasteners. Impellizzeri and Rich [54] have analysed similar problems in pin-loaded lugs. They used an approximate weight function which Bueckner [55] obtained for a strip with an edge crack. They corrected for the effects of having either single or double cracks at the hole and for the finite dimensions of the lug. These corrections give an advantage over the weight function used by Grandt, particularly since holes in lugs are usually close to boundaries whereas fastener holes are not. Impellizzeri and Rich have used their weight function to predict crack growth rates for cracks in lugs which have residual compressive stresses around the hole. A comparative study [43] indicates that results of Grandt [52] and Impellizzeri and Rich [54] are in agreement for several configurations. They also agree with those of Shah [39] and Hsu and Rudd [42] which were based on Green's function techniques (see section 10.2.4.)

A useful contribution has been made by Petroski and Achenbach [56] who have proposed a versatile method for determining approximate weight functions. The method involves choosing a configuration for which $K_I^{(1)}$ is known and specifying the crack surface displacement $v^{(1)}(L,x)$ in an approximate form which satisfies certain conditions. The particular form of $v^{(1)}(L,x)$ includes a single arbitrary constant which is determined from equations (24) and (25) with $K_I^{(2)} = K_I^{(1)}$. Hence the now known displacement $v^{(1)}(L,x)$ can be used to evaluate the weight function $h(L,x)$ from equation (25). This method makes it unnecessary to determine the actual displacements $v^{(1)}(L,x)$ of the crack surfaces; thus only the stress intensity factor $K_I^{(1)}$ is required. Since the displacements of the crack surface are often not available or are difficult to obtain, this method provides a simple means of obtaining approximate stress intensity factors.

Other configurations that have been analysed using weight function techniques include cracks with narrow plastic zones at the tip; these were studied by Bowie and Tracy [57].

10.3 METHODS FOR SIMPLE CONFIGURATIONS

In section 10.2 many simple methods of obtaining stress intensity factors were reviewed. In this section two of the simplest methods based on stress *concentration* factors (section 10.2.2) and stress distributions (section 10.2.3) are applied to simple configurations (few boundaries interacting with the crack). The approximations, inherent in these two methods, are shown to be acceptable for engineering purposes by comparison with known accurate solutions.

10.3.1 Stress *concentration* factors

The expressions given in equations (5) to (7) provide powerful, but simple, tools to obtain stress intensity factors from stress *concentration* factors, many of which are readily available. Peterson [9], Neuber [25], Heywood [58] and others provide experimental K_t data and theoretical expressions for many configurations. As an example of this approach consider a semi-elliptical edge notch of depth c in a semi-infinite sheet subjected to a remote uniaxial tensile stress σ_0 (see Fig 8). Equation (5) can be written in terms of K_t, the stress *concentration* factor, as follows:

$$\frac{K_I}{\sigma_0\sqrt{\pi \ell}} = \lim_{\rho \to 0} \left(\tfrac{1}{2} K_t \sqrt{\frac{\rho}{c}} \right), \tag{33}$$

where ℓ is the crack length ($c = \ell$ at $\rho = 0$). The stress *concentration* factor has been been obtained for this configuration as a function of ρ/c by Bowie [59] and is given in Table 1, together with the values of the expression in parenthesis in equation (33). By plotting the final column in Table 1 as a function of ρ/c, as shown in Fig 8, we can determine the limit for $\rho \to 0$ and $c \to \ell$, as

$$\frac{K_I}{\sigma_0\sqrt{\pi \ell}} = 1.13 . \tag{34}$$

The most accurate value for this function, obtained by Koiter [60], is 1.1215; thus the error is less than +1%. If the stress *concentration* factor is known for extremely sharp notches, the methods of Ref [28] can be used and extrapolation eliminated; this procedure would reduce the errors to much less than 1%.

Experimental data can be used in a similar way. Consider the data of Frocht [61] shown in Fig 9 for two symmetrical U-notches in an infinite strip subjected to a uniform uniaxial tensile stress σ_0, remote from the notches. The depth of each notch L is

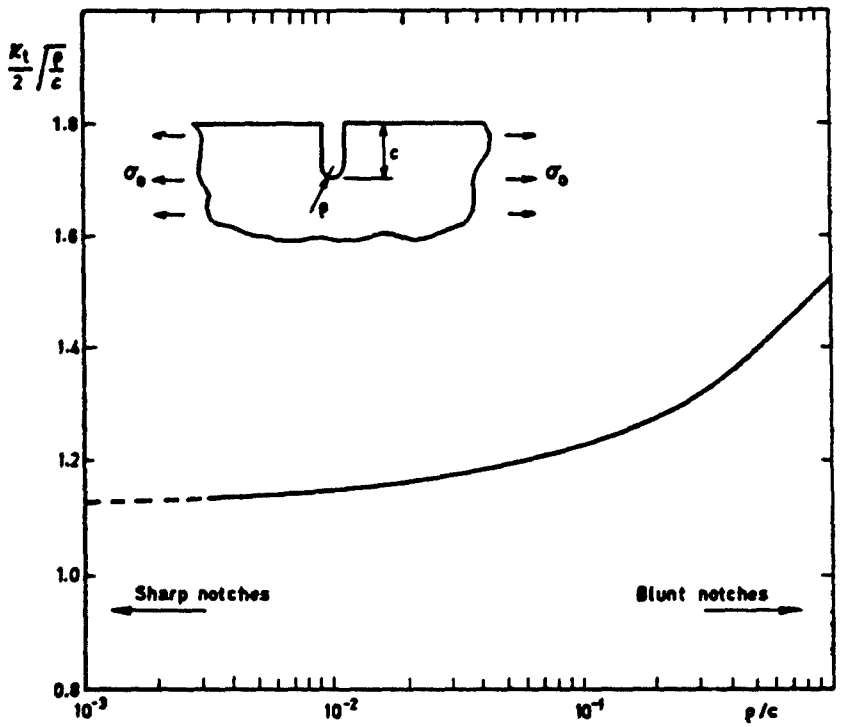

Fig 8 Stress concentration factor as a function of notch radius: single edge notches

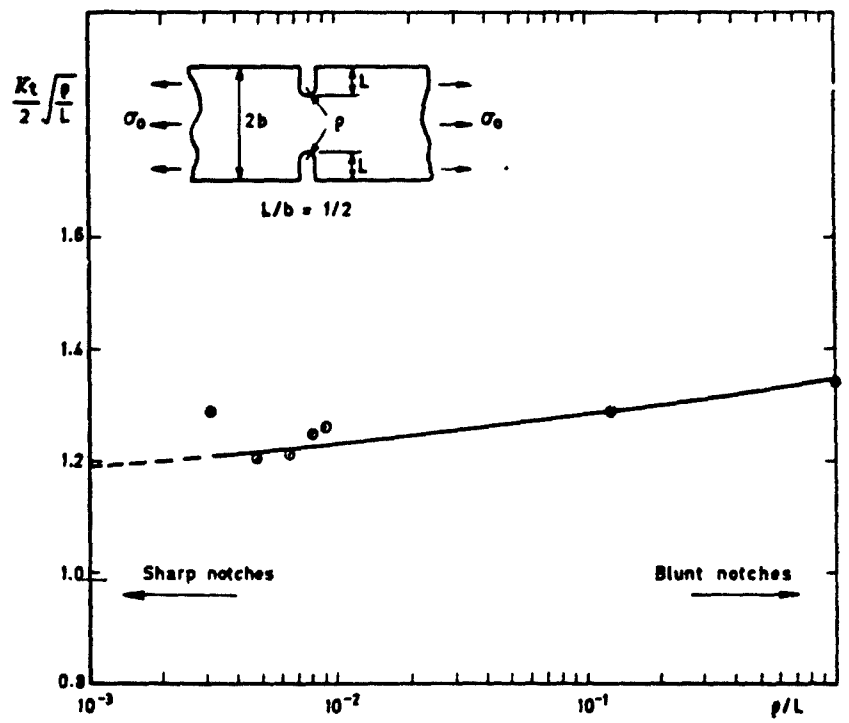

Fig 9 Stress concentration factor as a function of notch radius: double edge notches

Table 1

Stress *concentration* factor as a function of notch radius

$\frac{\rho}{c}$	K_t	$\frac{1}{2}K_t\sqrt{\frac{\rho}{c}}$
1.0	3.065	1.53
0.50	3.96	1.40
0.333	4.63	1.34
0.250	5.20	1.30
0.167	6.16	1.26
0.111	7.41	1.23
0.063	9.62	1.20
0.031	13.32	1.18
0.012	20.77	1.16
0.0028	43.2	1.14

$b/2$ where $2b$ is the width of the strip. The data are presented in Fig 9 as a plot of $\sqrt{\rho/L}K_t/2$ vs ρ/L on a semi-log scale. The data point at $\rho/L = 0.03$ may not be reliable since the notch radius is small, and this can result in large experimental errors in the stress *concentration* factor obtained using photoelastic methods. Therefore, this data point was ignored. By extrapolating the curve drawn through the remaining data and by using equation (33) we obtain

$$\frac{K_I}{\sigma_0\sqrt{\pi \ell}} = 1.19 , \tag{35}$$

where $L \to \ell$ as $\rho \to 0$. A more accurate value obtained by Bowie [62] is 1.15, so the error is approximately +3.5%. If all the data in Fig 9 had been used to determine K_I by extrapolation then a larger error would have resulted; thus it is seen that care must be taken to eliminate unreliable data if a reasonable approximation to K_I is to be obtained.

Finally, as an illustration of how equation (33) can be applied to a closed-form expression, consider the formula derived by Baratta and Neal [63] for the configuration shown in Fig 9, namely

$$K_t = \left[0.780 + 2.243\sqrt{\frac{L}{\rho}}\right]\left[0.993 + 0.180\left(\frac{L}{b}\right) - 1.060\left(\frac{L}{b}\right)^2 + 1.710\left(\frac{L}{b}\right)^3\right] \tag{36}$$

for $1.0 \leq L/\rho \leq 361$ and $0 \leq L/b \leq 0.723$. Substitution of equation (36) into equation (33) gives

$$\frac{K_I}{\sigma_0\sqrt{\pi \ell}} = 1.122\left[0.993 + 0.180\left(\frac{\ell}{b}\right) - 1.060\left(\frac{\ell}{b}\right)^2 + 1.710\left(\frac{\ell}{b}\right)^3\right]. \tag{37}$$

A comparison of the results given by equation (37) with the more accurate data given in Ref [62] is shown in Table 2; it is seen that the differences are less than 1%.

Table 2

Stress intensity factors for a strip with two collinear edge cracks

$\frac{a}{b}$	Ref [62]	Equation (37)	% Difference
0.1112	1.12	1.12	0
0.1667	1.12	1.12	0
0.2222	1.13	1.12	- 1
0.3333	1.13	1.12	- 1
0.3889	1.14	1.13	- 1
0.5001	1.15	1.16	+ 1
0.7230	1.37	1.36	- 1

It is concluded that the method of obtaining stress intensity factors from stress *concentration* data is simple to use, but the accuracy depends upon the accurate determination of the stress *concentration* factor as a function of the notch radius (see also section 2.2, Refs [26] and [28]).

10.3.2 Stress distributions

The methods of obtaining stress intensity factors from stress distributions which were described in section 2 are demonstrated in this section by solving several problems and comparing these results to more exact analysis.

The approach of Williams and Isherwood[31] is illustrated by considering two radial cracks of length ℓ at the boundary of a circular hole in an infinite plate subjected to a uniaxial tensile stress σ_0 remote from the hole (see Fig 10a). The mean stress for this configuration is given by equation (10) with $\sigma(x)$ given[64] by

$$\sigma(x) = \sigma_0\left[1 + \frac{1}{2}\left(\frac{R}{R+x}\right)^2 + \frac{3}{2}\left(\frac{R}{R+x}\right)^4\right] . \tag{38}$$

Rewriting equations (8) and (10) it follows that for an edge crack

$$\frac{K_I}{\sigma_0\sqrt{\pi\ell}} = 1.12\,\frac{\sigma_m}{\sigma_0} \tag{39}$$

where σ_m replaces σ_{mean}. After performing the integration in equation (10) with $\sigma(x)$ given by equation (38) and substituting into equation (39) we have

$$\frac{K_I}{\sigma_0\sqrt{\pi\ell}} = 1.12\,\frac{R}{\ell}\left\{1 + \frac{\ell}{R} - \frac{1}{2}\left(\frac{R}{R+\ell}\right)\left[1 + \left(\frac{R}{R+\ell}\right)^2\right]\right\} . \tag{40}$$

Williams and Isherwood[31] also examined the biaxially-stressed infinite plate with two cracks located at the hole boundary (see Fig 10b). In this case $\sigma(x)$ is given[64] by

$$\sigma(x) = \sigma_0\left[1 + \left(\frac{R}{R+x}\right)^2\right] , \tag{41}$$

and as before, using equation (10) and (39), we have

$$\frac{K_I}{\sigma_0\sqrt{\pi\ell}} = 1.12\left(\frac{\ell + 2R}{\ell + R}\right) . \tag{42}$$

In order to determine the errors in the approximate stress intensity factors for short cracks ($\ell/R \leq 1$) calculated from equations (40) and (42) the results are compared, in Table 3, with the accurate calculations of Tweed and Rooke[65].

Table 3

Stress intensity factors for two cracks at the edge of a hole ($\ell/R \leq 1$)

	Uniaxial stress			Biaxial stress		
ℓ/R	Ref[65]	Equation (40)	% Difference	Ref [65]	Equation (42)	% Difference
0.00	3.36	3.36	0	2.24	2.24	0
0.01	3.29	3.32	+1	2.21	2.23	+1
0.05	3.04	3.18	+5	2.11	2.19	+4
0.10	2.79	3.02	+8	2.00	2.14	+7
0.15	2.58	2.88	+12	1.91	2.09	+9
0.20	2.41	2.77	+15	1.84	2.05	+11
0.30	2.16	2.56	+18	1.72	1.98	+15
0.50	1.83	2.28	+24	1.56	1.87	+20
1.00	1.47	1.89	+27	1.37	1.68	+23

It can be seen from Table 3 that the mean stress method gives a reasonable approximation for very short cracks; for uniaxial stresses the errors are less than 8% for $\ell/R \leq 0.1$ and less than 15% for $\ell/R \leq 0.2$; the errors for biaxial stresses are slightly smaller. However for longer cracks the errors exceed 20%. This method will always over-estimate the stress intensity factor when the stress field decreases monotonically away from the stress concentration, and hence will lead to conservative estimates of residual strength and fatigue lifetime.

There is a very simple approximation available[13] for long cracks which assumes that the effect of the hole on the stress field is negligible and that the crack behaves as if it were of length $2(\ell + R)$, *i.e.* the tip-to-tip distance, in a uniform stress field of σ_0 . The stress intensity factor would therefore be $\sigma_0\sqrt{\pi(R+\ell)}$, thus

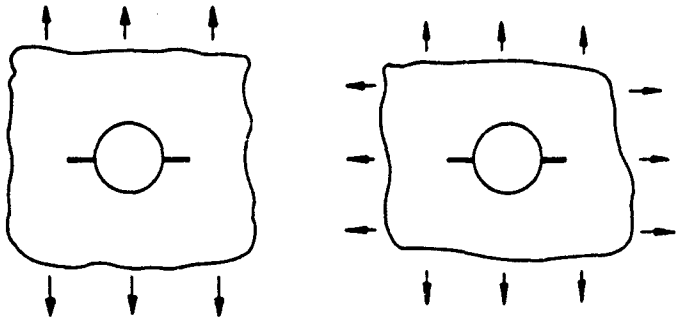

a Unixial stress b Biaxial stress

Fig 10 Radially cracked hole in an infinite sheet

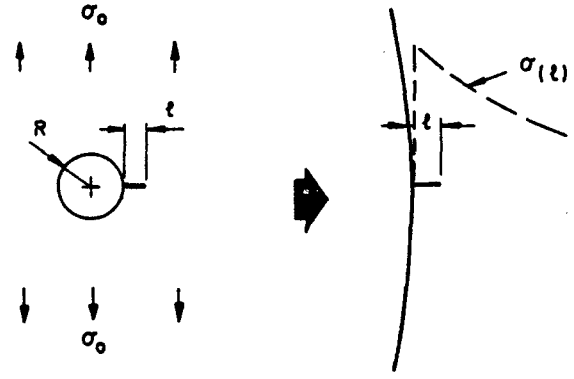

a Cracked circular hole b Equivalent edge crack

Fig 11 Circular hole with a single radial crack

$$\frac{K_I}{\sigma_0\sqrt{\pi\ell}} = \sqrt{\frac{R + \ell}{\ell}} \qquad (43)$$

This approximation is suitable for both uniaxial and biaxial applied stresses because the stress intensity factor tends to the same limit for long cracks. Results using the approximation given in equation (43) are compared with the accurate results in Table 4.

Table 4

Stress intensity factors for two cracks at the edge of a hole ($\ell/R \geq 0.15$)

	Uniaxial stress			Biaxial stress		
ℓ/R	Ref [65]	Equation (43)	% Difference	Ref [65]	Equation (43)	% Difference
0.15	2.58	2.77	+ 7	1.91	2.77	+ 45
0.2	2.41	2.45	+ 2	1.84	2.45	+ 33
0.3	2.16	2.08	- 4	1.72	2.08	+ 21
0.5	1.83	1.73	- 5	1.56	1.73	+ 11
1.0	1.47	1.41	- 4	1.37	1.41	+ 3
2.0	1.24	1.22	- 2	1.22	1.22	0
4.0	1.12	1.12	0	1.12	1.12	0
9.0	1.05	1.05	0	1.05	1.05	0

From Tables 3 and 4 it can be seen that the errors can be minimised by a suitable combination of the 'mean stress' and the 'uniform stress' approximation. For example, under uniaxial stresses the maximum error is of the order of 10% if the changeover from the 'mean stress' to the 'uniform stress' approximation occurs between $\ell/R = 0.10$ and 0.15 and under biaxial stresses the maximum error is of the order of 15% if the changeover occurs between $\ell/R = 0.3$ and 0.5 . These approximations will thus be adequate for many engineering applications. The combination of the 'maximum stress' and 'uniform stress' approximations has been studied [13], and is briefly discussed in section 11.2.

The 'tip stress' approach suggested by Cartwright [66] for short cracks at holes and notches (see equation (11) of section 11.2.3) has been extended to long cracks by Baratta [67] by using an interpolation procedure for linking the two known limits ($\ell = 0$ and ∞) for the stress intensity factor. In order to demonstrate the procedure and to evaluate the accuracy of the approximation, it will be applied to a crack configuration for which an accurate solution exists. The configuration consists of a single radial crack at the edge of a circular hole in an infinite plate subjected to a uniform uniaxial tensile stress σ_0 remote from the hole (see Fig 11). When the crack length is small ($\ell/R \ll 1$) the stress intensity factor is given by equations (8) and (11) therefore

$$\frac{K_I}{\sigma_0\sqrt{\pi\ell}} = 1.12\,\frac{\sigma(\ell)}{\sigma_0} \quad . \qquad (44)$$

For very long cracks ($\ell/R \gg 1$) we have

$$\frac{K_I}{\sigma_0\sqrt{\pi\ell}} = \frac{1}{\sqrt{2}} \qquad (45)$$

since as $\ell/R \to \infty$ the crack-tip stress field will approach that of a crack of total length ℓ in a uniformly stressed sheet. Since $\sigma(\ell) \to \sigma_0$ as $\ell \to \infty$ we can combine equations (44) and (45) to give

$$\frac{K_I}{\sigma_0\sqrt{\pi\ell}} = f(\ell/R) \qquad \text{for all } \ell/R \ , \qquad (46)$$

where $f(\ell/R)$ is an unknown function with the limiting values $f(0) = 1.12$ and $f(\infty) = 0.707$. The approximation consists of choosing a suitable well-behaved function, which lies between these limits. The function arbitrarily chosen [67] for this problem, as well as for others, is

$$f(\ell/R) = Q - M\left[\tan^{-1}\left(\frac{\ell}{R}\right)\right]^m \ , \qquad (47)$$

where Q, M and m are constants to be determined. By combining equations (46) and (47) with the expression for $\sigma(\ell)$, given in equation (38) with ℓ replacing x , we obtain

$$\frac{K_I}{\sigma_0\sqrt{\pi\ell}} = \left[Q - M\left[\tan^{-1}\left(\frac{\ell}{R}\right)\right]^m\right]\left[1 + \frac{1}{2}\left(\frac{R}{\ell + R}\right)^2 + \frac{3}{2}\left(\frac{R}{\ell + R}\right)^4\right] \ . \qquad (48)$$

The constants Q, M and m were obtained [57] by fitting the expression at the two limiting values and at an intermediate value chosen to minimise the errors; they are Q = 1.12, M = 0.119 and m = 2.748 . Results obtained from equation (48) are compared with the accurate results of Tweed and Rooke [68] in Table 5, where it can be seen that for the above two-dimensional configuration the errors are small.

Table 5

Stress intensity factors for a single crack at the edge of a hole

t/R	Ref [68]	Equation (48)	% Difference
0.0	3.36	3.36	0
0.1	2.77	2.73	- 1
0.2	2.37	2.32	- 2
0.5	1.73	1.69	- 2
1.0	1.31	1.29	- 2
1.5	1.13	1.13	0
2.0	1.03	1.03	0
3.0	0.93	0.94	+ 1
5.0	0.88	0.86	- 2
10.0	0.78	0.78	0

This method has been applied to two three-dimensional problems (see Ref [67]) where it was assumed that the errors would still be within acceptable engineering accuracies. The problems studied were (i) a spherical void with a circumferential crack in a uniformly stressed body and (ii) a hemispherical pit with a circumferential crack at the surface of a semi-infinite body subjected to uniaxial tensile stresses. In both cases only the two limiting values of the function f(t/R) are known and it was therefore assumed that m = 2.748 , as in the two-dimensional problem, and Q and M were calculated to satisfy the limits. A knowledge of these constants enables the stress intensity factor to be calculated from equations (46) and (47). Since there are no alternative solutions available for these three-dimensional problems the accuracy of the approximation cannot be ascertained; however the author [67] claimed that the errors would be within normal engineering limits.

10.4 STRESS INTENSITY FACTORS FOR COMPLEX CONFIGURATIONS

Stress intensity factors for many simple configurations are available [1-5] but they are not directly applicable to the more complex configurations of typical engineering components. The compounding method described here is a versatile and quick way of extending these solutions to other, more complex, configurations for which the stress intensity factors are not known. Empirical methods which were used by Figge and Newman [69], Smith [70], Liu [71] and Paratta [11] can be shown to be special cases of compounding.

In this chapter only two-dimensional configurations are considered but solutions for three-dimensional configurations may also be obtained. The compounding method is described and shown, by comparison with some known results, to give approximate stress intensity factors which contain errors of only a few per cent. The method is applied to two common aircraft problems - cracks in stiffened sheets and a cracked hole in a row of holes.

10.4.1 Compounding technique

A cracked structural component has several boundaries, *eg* holes, other cracks or sheet edges; all these will influence the stress intensity factor at the tip of the crack. The main principle of the compounding method is to obtain a solution by separating the complex configuration into a number of simpler ancillary configurations which have known solutions. Each ancillary configuration will, usually, contain only one boundary which interacts with the crack. The contributions from each ancillary configuration are compounded [10] according to the following formula:

$$K_r = \bar{K} + \sum_{\text{all } n} (K_n - \bar{K}) + K_e \,, \qquad (49)$$

where K_r is the resultant stress intensity factor with all the boundaries present, K_n is the stress intensity factor with only the nth boundary present, $\bar{K}$ is the stress intensity factor in the absence of all boundaries and K_e is the contribution which may be present due to boundary-boundary interaction. It is convenient to express the compounding formula in terms of normalized stress intensity factors $Q(= K/\bar{K})$ since many of the known ancillary solutions (in particular Ref [1]) are given in this form. Equation (49) becomes

$$Q_r = 1 + \sum_{\text{all } n} (Q_n - 1) + Q_e \,, \qquad (50)$$

where $Q_r = K_r/K$, $Q_n = K_n/K$ and $Q_e = K_e/K$. The compounding procedure is applicable to all three modes of cracking (K_I, K_{II} and K_{III}).

The resultant stress intensity factor calculated from some of the empirical methods [11, 69-71] which have been used in the past, can be compared with that obtained by compounding. In the case of two boundaries, the empirical methods give

$$Q_r = Q_1 Q_2 , \tag{51}$$

while the compounding method reduces to

$$Q_r = Q_1 + Q_2 - 1 + Q_e . \tag{52}$$

If $Q_1 = 1 + \alpha$ and $Q_2 = 1 + \beta$, then equations (51) and (52) become

$$\left.\begin{aligned} Q_r &= 1 + \alpha + \beta + \alpha\beta \\ \text{and} \quad Q_r &= 1 + \alpha + \beta + Q_e \end{aligned}\right\} . \tag{53}$$

If $\alpha, \beta \ll 1$ the two expressions for Q_r are the same except for the very small correction terms $\alpha\beta$ or Q_e. However if α and β are not small compared to unity then boundary-boundary interactions must be considered. Such effects are not included in the empirical methods, but are the source of the term Q_e in the compounding method. Thus the empirical methods are a special case of compounding when boundary-boundary interaction effects are negligible.

The evaluation of Q_e will often be difficult; it can be formally expressed [10] in terms of the residual stress fields at the boundaries by using the Schwarz alternating technique. The residual stresses were originally ignored in the derivation of equation (49) which is based on the principle of superposition. For many plane-sheet problems Q_e is small (a few per cent) and can be ignored; for problems where it is important approximate methods have been developed [72] for evaluating it.

The magnitude of the boundary-boundary interactions have been estimated by calculating stress intensity factors from equation (50) without Q_e, for crack problems for which alternative solutions were available [10]. The magnitude of Q_e was found to depend on the number and type of boundary; it increased as the number of boundaries increased and as the crack approached a boundary. Straight boundaries had more effect than curved boundaries such as holes, and other cracks had a smaller effect than holes. The magnitude of Q_e was less than 10% for the range of crack lengths considered.

The simple compounding procedure of adding together the effects of the individual boundaries needs to be modified if the crack crosses one of the boundaries, eg a crack at the edge of a hole, or a crack beneath a stiffener (which is treated as a boundary). Before the effect of the other boundaries can be considered, the crack plus the boundary it crosses must be replaced by an equivalent crack [72,73] which then interacts with the other boundaries. If the stress intensity factor is K_0 when only the boundary the crack crosses is present, then the equivalent crack length a' is given [72,73] by

$$a' = (K_0/K)^2 a = Q_0^2 a . \tag{54}$$

The effects of the other boundaries on the original crack plus boundary is now considered to be the same as the effects on the equivalent crack. In order to calculate these effects the distances of the other boundaries from the equivalent crack must be determined. These distances are determined subject to the condition that each boundary must be the same distance from the nearer tip of the equivalent crack in each ancillary configuration as it was in the original configuration. The compounding formula (49) is then modified to

$$K_r = K_0 + \sum_{n \neq 0}' (K_n' - K_0) + K_e \tag{55}$$

where K_n' is the stress intensity factor for the equivalent crack in the presence of the nth boundary only. Equation (55) can be written in terms of the normalized stress intensity factors, and becomes

$$Q_r = Q_0 \left[1 + \sum_{n \neq 0}' (Q_n' - 1) \right] + Q_e \tag{56}$$

where $Q_n' = K_n'/K_0$. With these modified formulae the stress intensity factor has been calculated for a crack in a sheet with a periodic array of stiffeners and compared with the work of Poe [74,75]; the compounded results were within 5% of the numerical calculations of Poe indicating that boundary-boundary interactions were small.

In some configurations boundary-boundary interactions cannot be neglected, for instance a crack at the edge of a hole that is near another boundary. A measure of the interaction may be obtained from the difference in the stress *concentration* factor K_t at the edge of the hole in the uncracked configuration, with and without other boundaries. If the change in K_t is significant then the boundary-boundary interaction Q_e in the cracked configuration will also be significant particularly for short cracks when the limiting value of the stress intensity factor is proportional to K_t (see section 10.2 and Ref[72]).

In the original derivation[10]of the compounding method Q_e was shown to arise because the stresses induced on any one boundary site by the presence of the other boundaries, were not allowed for. An approximate technique for allowing for these stresses has been developed[72]and used in the evaluation of the stress intensity factor for a hole with two equal-length cracks located symmetrically in a finite-width strip. The distribution of stresses around the hole boundary is replaced by two equal and opposite localized forces P acting, on the hole perimeter, perpendicular to the crack line. The magnitude of P is chosen so that the maximum tensile stress (σ_{max}) at the edge of the uncracked hole due both to the remote loading and to the forces P, in the absence of other boundaries, is equal to that in the real configuration. For example, for a circular hole of radius R in a finite-width strip with a uniform stress σ, the force P would be obtained from

$$\sigma_{max} = 3\sigma + \frac{2P}{\pi R} = K_t\sigma \ , \qquad (57)$$

where σ_{max} is the maximum stress at the edge of a circular hole in a uniformly stressed sheet, $2P/(\pi R)$ is the stress, at the same position, due to the forces P acting on a hole in an infinite sheet[64]and K_t is the stress *concentration* factor for a hole in a strip. Stress *concentration* factors for this configuration, and many others, have been collected by Peterson[ ]. Q_e is thus obtained from the solution of Tweed and Rooke[65] for cracks at the edge of a hole subjected to localized loads and added to the other terms in equation (50). The resultant stress intensity factor will thus be a good approximation since, for a crack of length ℓ, the limiting value will be

$$\lim_{\ell/R \to 0} |K_r| = 1.12\sigma_{max}\sqrt{\pi\ell} = 1.12K_t\sigma\sqrt{\pi\ell} \ . \qquad (58)$$

The compounded results for a central hole with two equal-length cracks in a uniformly stressed strip have been compared[72]with the stress intensity factors calculated by Newman[76]using the boundary collocation technique. For a hole-radius equal to one quarter of the strip-width the maximum difference was 4%, for a hole-radius of one half of the strip-width the maximum difference is 9%; in both cases the differences were less than 1% for short cracks. The interaction term Q_e contributed as much as 30% to Q_r - the maximum being for the largest hole with the shortest crack.

In the following the principles of compounding are applied to calculate the stress intensity factor in two configurations which typify structural components of an airframe. The first configuration is a periodically spaced row of holes in a loaded sheet with either one or two cracks at the edge of one of the holes; this configuration plus the required ancillary configurations are shown in Fig 12. The second configuration is a periodically stiffened, loaded sheet with a series of collinear, equal-length cracks centred on each of the stiffeners; this plus the ancillary configurations are shown in Fig 13.

In the first configuration the crack(s) is along the line joining the hole centres, a distance b apart, and is perpendicular to the applied tensile stress σ. The ancillary configurations required for this problem are (i) a cracked hole in an infinite sheet (case 1.3.3. in Ref[1]) and (ii) a crack near a circular hole (case 1.3.5 in Ref[1]). If tip A in Fig 12 is the tip under consideration and holes to the right of A are labelled with positive integers and holes to the left with negative integers, then equation (56) becomes

$$Q_r = Q_0\left[1 + \sum_{n=-\infty,\, n\neq 0}^{n=\infty} (Q'_n - 1)\right] + Q_e \ , \qquad (59)$$

For the configurations considered ($b/R \geq 3$) contributions to Q_r were negligible for holes with $|n| > 2$. To ensure that the distances from crack tip A to the various boundaries remain the same as in the original configuration it follows that (see Fig 12) for $n > 0$

$$b'_n - a' = b_n - a = nb - a \ , \qquad [b'_n = b'_{+1} + (n-1)b] \qquad (60)$$

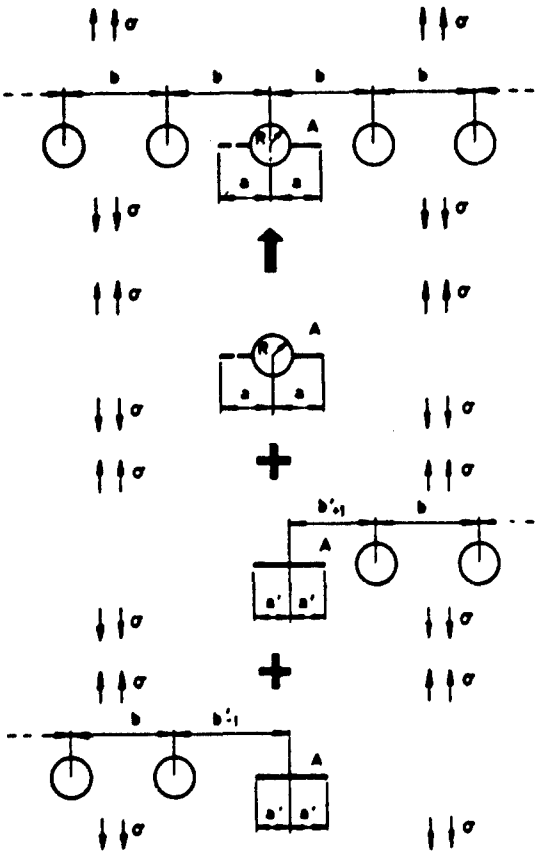

Crown copyright

Fig 12 Ancillary configurations for a cracked hole in a periodic array

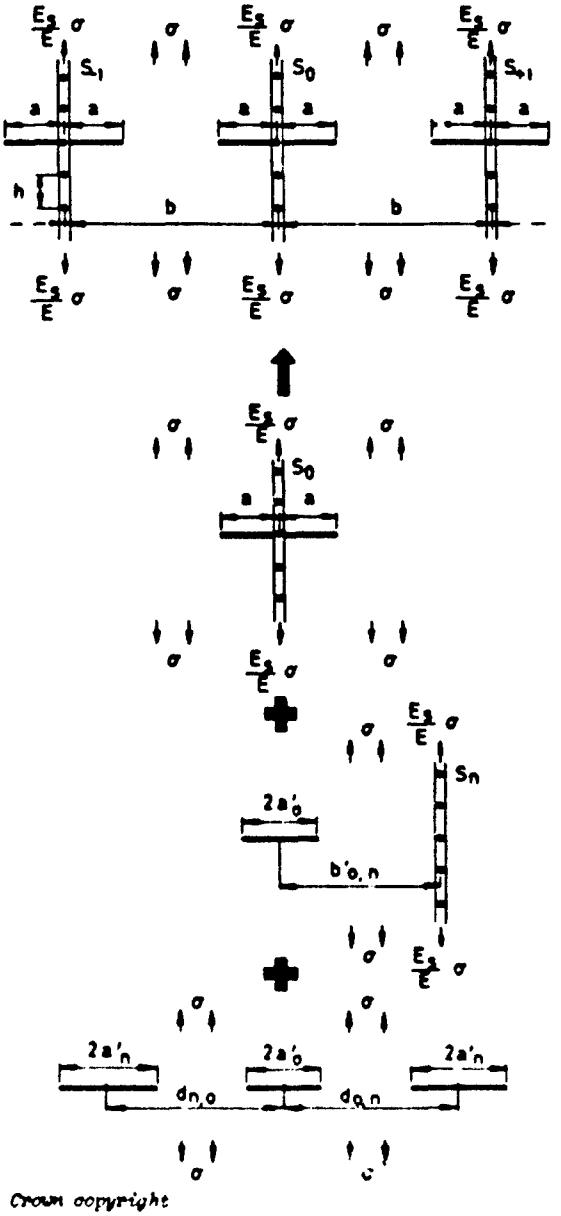

Crown copyright

Fig 13 Ancillary configurations for collinear cracks in a periodically stiffened sheet

for both one and two cracks; for $n < 0$* it follows that

$$\left.\begin{aligned} b'_n - a' &= b_n - R = |n|b - R , && \text{for one crack} \\ \text{and} \quad b'_n - a' &= b_n - a = |n|b - a , && \text{for two cracks .} \end{aligned}\right\} \qquad (61)$$

The boundary-boundary interaction term Q_e is small, less than 3% of Q_r, the biggest values were obtained for very short cracks for $b/R = 3$.

The results are plotted as $K_r/(\sigma\sqrt{\pi(a - R)})$ vs a/R, for both one and two cracks, in Fig 14. Values of K_r for $b/R = 10$ differ by less than 1% from those for $b/R = \infty$ (an isolated cracked hole). For values of a/R greater than those shown, a good approximation may be obtained by replacing the cracked hole by a crack of length $2a$ and compounding the solution from that of a crack located centrally between two holes (case 1.3.7 in Ref[1]).

The second configuration considered contains an infinite series of cracks, of length $2a$, centred on and perpendicular to stiffeners that are a distance b apart. The sheet is subjected to a uniform stress σ remote from the crack; the stress in the stiffeners, in order to maintain strain compatibility, is $(E_s/E)\sigma$ where E and E_s are the Young's modulus of the sheet and stiffener respectively. The ancillary configurations required, in general, are (i) a crack centred about a stiffener which may be broken or unbroken (case 2.2.1 in Ref[1]), (ii) a crack near to an unbroken stiffener (case 2.2.2 in Ref[1]), and (iii) three collinear cracks in a uniformly stressed sheet (case 1.2.7 in Ref[1]). If tip A of the crack at stiffener S_0, in Fig 13, is the tip under consideration and stiffeners to the right of A are labelled with positive integers and stiffeners to the left with negative integers, then equation (55) has been shown[77] to become

$$K_r = K_0 + \sum_{n\neq 0} (K'_{s,n} - K_0) + \sum_{n>0} (K'_{c,\pm n} - K_0) . \qquad (62)$$

The stress intensity factors K_0, $K'_{s,n}$ and $K'_{c,\pm n}$ are defined as follows: K_0 is for a crack of length $2a$ in ancillary configuration (i); $K'_{s,n}$ is for a crack of length $2a'_0 (= 2Q_0^2 a)$ whose centre is a distance $b'_{0,n}$ from the nth stiffener as in ancillary configuration (ii); and $K'_{c,\pm n}$ is for a crack of length $2a'_0$ located symmetrically between two cracks of length $2a'_n (= 2Q_n^2 a)$ as in ancillary configuration (iii). The equivalent cracks of length $2a'_n$ are obtained by replacing each crack/stiffener pair by a crack with the same stress intensity factor; the length a'_n is given in terms of a_n by equation (54) with Q_n replacing Q_0 and the distance between crack centres $d_{0,n}$ is given by

$$d_{0,n} - a'_0 - a'_n = b - 2a . \qquad (63)$$

Q_n is the normalized stress intensity factor for a crack of length $2a_n$ centred on stiffener S_n in a sheet with no other stiffeners or cracks present (case 2.2.1 in Ref[1]). In this periodic configuration $a_n = a$ for all n. If all the stiffeners are unbroken then $Q_n = Q_0$ for all n, but if S_0 is broken then all the Q_ns are equal for $n \neq 0$ and $Q_0 > Q_n$.

Because of the periodicity of the stiffeners equation (62) can be simplified since

$$K_0 + \sum_{n\neq 0} (K'_{s,n} - K_0) = K_p , \qquad (64)$$

where K_p, the stress intensity factor for a crack centred about one of the stiffeners in a periodic set, has been calculated by Poe[74,75]. Results for a periodic set of riveted stiffeners are shown in Fig 15; the particular configuration is defined by $h/b = \frac{1}{12}$ where h is the rivet pitch and $s = 1$ where s is the ratio of the stiffness of the stiffener to that of a sheet of width b and thickness t, *ie* $s = E_s A_s/(Ebt)$, where A_s is the cross-sectional area of a stiffener. Results for the stress intensity factor for S_0 both broken and unbroken are shown and compared with those for a single crack in a periodic array of stiffeners (*ie* K_p).

---

* This is a modified form of equations (19) and (20) in Ref[72] which enables a consistent extension of the method to be made for cracks near broken stiffeners: results for the present problem are virtually unaffected.

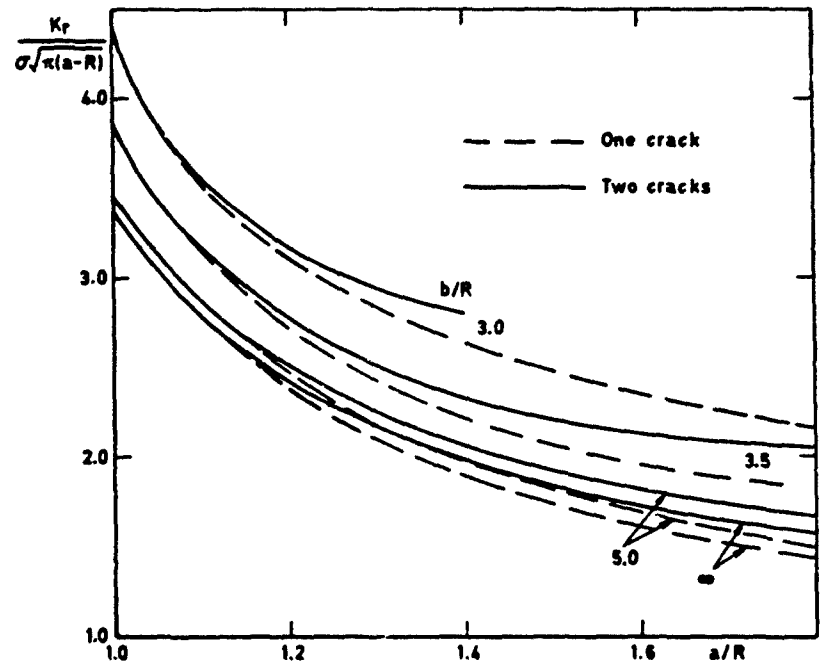

Crown copyright

Fig 14 Resultant stress intensity factor for a cracked hole in a periodic array

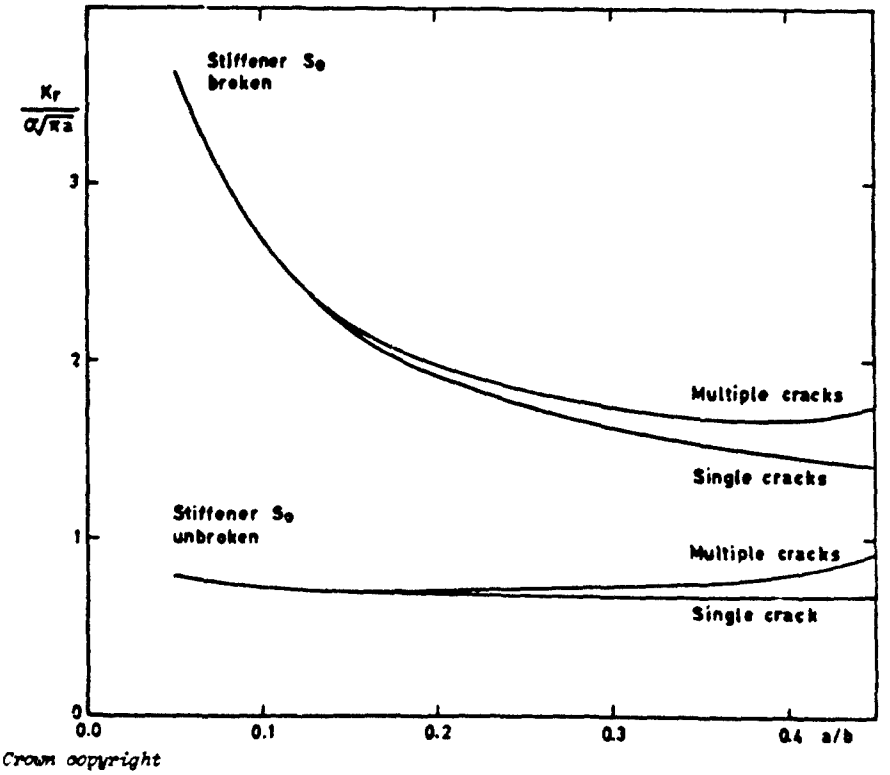

Crown copyright

Fig 15 Stress intensity factors for single and multiple cracks in a periodically stiffened sheet

10.4.2 Load relief factors

There are a number of situations where multiple cracks occur, they include cracks arising at fastener holes in stiffened structures or cracks caused by surface finishing processes etc. Only a few solutions are available for stress intensity factors for multiply-cracked finite bodies. Accurate mathematical analyses are complex and time-consuming to apply to such cases. However, if high accuracy is not required for a given application, a simple approach based on the concept of 'load relief' may be adequate.

It is known that under certain loading conditions the stress concentration effect of multiple parallel notches is less than that of a single notch. In fact, a design procedure [78] in which additional notches are provided primarily to effect a redistribution of the stresses is called 'load-relieving notches'. Neuber [25] investigated this effect and suggested a concept that he referred to as the 'coefficient of load relief' for notches. A similar concept to be called the 'load relief factor' may be appropriate to opening mode stress intensity factors for multiple cracks in stressed bodies [11].

The load relief factor F can generally be defined as the stress intensity factor of a multiply-cracked, infinite body $(K_I)_{m,\infty}$ divided by the stress intensity factor of a single cracked body $(K_I)_{s,\infty}$ of the same geometry and loading conditions. Hence for the mode I stress intensity factors the load relief factor is given by

$$F = (K_I)_{m,\infty} / (K_I)_{s,\infty} \quad . \tag{65}$$

When F is known for an infinite (or semi-infinite) body it is then assumed that the same value of F applies to a finite cracked body with similar geometry and loading conditions, *ie*

$$(K_I)_{m,f} = F_x (K_I)_{s,f} \tag{66}$$

where $(K_I)_{s,f}$ is the stress intensity factor for a single-cracked finite body of the same loading conditions as that included in the determination of F, and $(K_I)_{m,f}$ is the required solution for the same finite body with multiple cracks.

The first configuration to be considered is that of an infinite row of parallel cracks of length $2a$ and separated by a distance $2h$; the cracks, which are internally pressurized with a uniform pressure p, are located centrally in an infinitely long strip of width $2b$ (see Fig 16). Watanabe and Atsumi [79] have obtained the stress intensity factor for this configuration and the results from this method will be compared with their more accurate ones. The load relief factor for this particular case can be obtained from the stress intensity factor for an infinitely wide strip of height $2h$ containing a central crack of length $2a$ midway between and parallel to the edges (see case 1.1.6 in Ref [1]). The crack is opened by uniform pressure p, and the particular boundary conditions on the two edges of zero normal displacement and zero shear stress are identical with those that occur midway between parallel cracks in an infinite periodic array. The resulting load relief factor which is a function of a/h is given in Fig 8 of Ref [1]. The second solution needed is that of a pressurized central crack in a finite-width strip. The solution to this is identical to that of a central crack in a uniformly stressed strip and is known (see case 1.1.1 in Ref [1]).

The substitution of equation (65) into equation (66) gives

$$(K_I)_{m,f} = \frac{(K_I)_{m,\infty}}{(K_I)_{s,\infty}} \times (K_I)_{s,f} \quad . \tag{67}$$

This relationship is illustrated schematically in Fig 16 and demonstrates the way in which Watanabe and Atsumi's results can be approximated from two other known solutions. The two sets of results are given in Fig 17, where it can be seen that for values of $a/b \leq 0.5$ and $h/a \geq 0.5$ the differences $\leq 20\%$; the approximate results are always conservative for this configuration.

Another problem that has been solved [11] is the determination of the stress intensity factors for multiple cracks, each of length ℓ, in a thick-walled cylinder subjected to internal pressure p (see Fig 18). The procedure is similar to that used before, namely it is assumed that the load relief factor for an infinitely thick cylinder, which can be derived from the work of Tweed and Rooke [80] is the same as that for a finite thickness cylinder. The solution for two cracks of length ℓ in a finite thickness cylinder, which is also required, is available (see case 3.2.4 of Ref [1]). Results are given in Table 6 for a cylinder with a ratio of outer radius R_o to inner radius R_i of 1.5; the results are given for different values of the ratio of the crack length ℓ to the wall thickness $(R_o - R_i)$ and for different numbers of cracks n. Also shown, for comparison are the more accurate finite element results of Pu and Hussain [81] and the percentage differences between the two.

It can be seen from Table 6 that for $\ell/(R_o - R_i) \leq 0.2$ the differences are acceptable for many engineering applications; similar results were obtained for $R_o/R_i = 2$. The fact that the differences increase as $\ell/(R_o - R_i)$ increases reflects the fact that

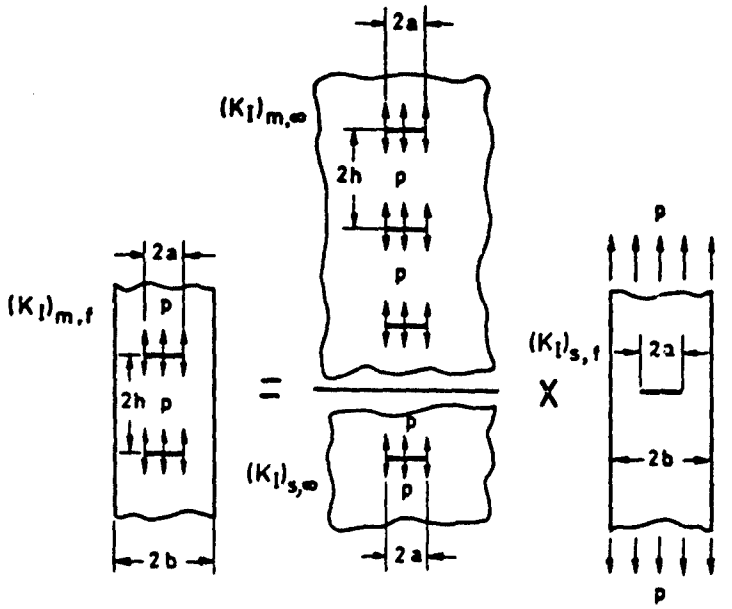

Fig 16 Schematic showing method of obtaining stress intensity factor for an infinite array of internally-pressurized central parallel cracks in an infinitely long strip of finite width

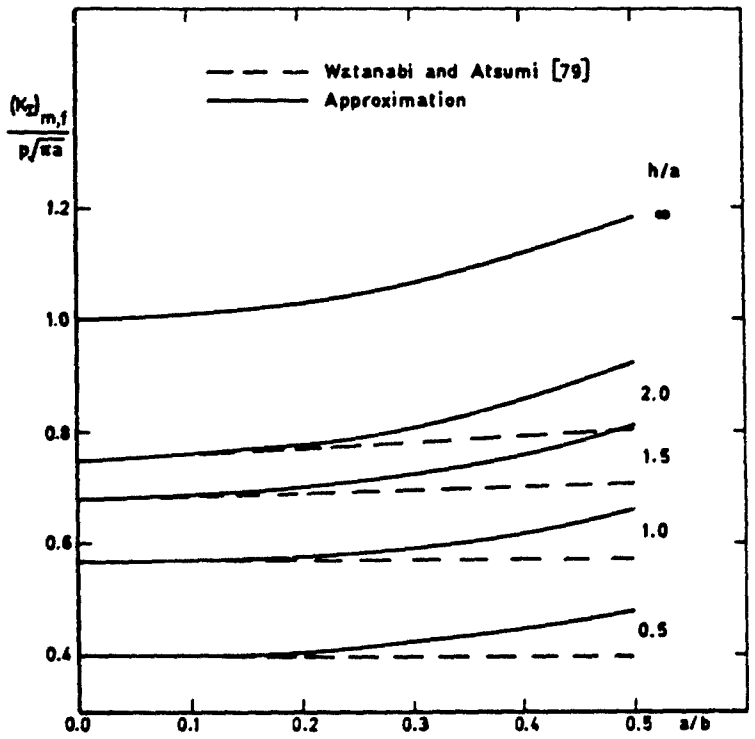

Fig 17 Comparison of stress intensity factors

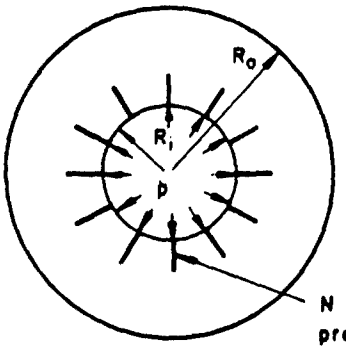

N equally spaced pressurised cracks length ℓ

Fig 18 Internally pressurised tube with multiple radial cracks

Table 6

Values of $(K_I)_{m,f}/(p\sqrt{\pi\ell})$ for a multiply-cracked cylinder with $R_o/R_i = 1.5$

$\frac{\ell}{R_o - R_i}$	0.1			0.2			0.3			0.4		
n	Eq. (67)	Ref [81]	% Diff.	Eq. (67)	Ref [81]	% Diff.	Eq. (67)	Ref [81]	% Diff.	Eq. (67)	Ref [81]	% Diff.
3	3.99	3.99	0	4.36	4.33	+1	4.96	4.72	+5	5.73	5.33	+8
4	3.98	3.95	+1	4.36	4.23	+3	4.94	4.50	+10	5.68	4.96	+14
5	3.98	3.93	+1	4.32	4.12	+5	4.86	4.32	+12	5.65	4.64	+22
6	3.98	3.93	+1	4.28	4.02	+6	4.78	4.07	+17	5.38	4.33	+24
8	3.94	3.82	+3	4.16	3.78	+10	4.53	3.66	+24	4.98	3.79	+31
10	3.90	3.77	+3	4.00	3.63	+10	4.24	3.42	+24	4.57	3.47	+32
15	3.73	3.63	+3	3.56	3.27	+9	3.58	2.96	+21	3.78	2.91	+29
20	3.53	3.46	+2	3.15	2.93	+7	3.11	2.61	+19	3.31	2.57	+29
30	3.08	3.05	+1	2.57	2.42	+6	2.57	2.18	+18	2.74	2.17	+26
40	2.75	2.71	+1	2.30	2.13	+8	2.29	1.93	+19	2.44	1.94	+26

boundary-boundary interactions are becoming important. The assumption that the load relief factor for a finite body is the same as for an infinite body explicitly excludes such interactions. This problem of boundary-boundary interactions has been previously discussed in section 10.4.1 where the more general method of compounding contains a procedure for incorporating the effects of such interactions into the calculation of stress intensity factors.

10.5 DISCUSSION AND CONCLUSIONS

The various simple methods of calculating stress intensity factors described in this chapter all involve approximations and hence their use in a fracture mechanics analysis will introduce errors. It has been shown that for many cases the magnitude of the errors is within acceptable engineering limits. The errors due to the approximations in determining K are not the only source of uncertainty. There will be uncertainties in the crack length measurements, in the applied loads and in the material properties. All of these need to be considered in forming a judgement on the use, or otherwise, of approximations for the stress intensity factor. A comparison of these sources of uncertainty and the consequences for the residual strength and fatigue crack growth-rate have been examined in detail for one simple approximation [13]. The approximation was a combination of the 'maximum stress' method for short cracks and the 'uniform stress' method for long cracks (see sections 10.2 and 10.3). Since the maximum stress approximation overestimates the stress intensity factor, conservative values were obtained for the residual strength and the lifetime of fatigue cracks; the errors were no more and often less than those due to uncertainties in crack length, stress level and material properties and would therefore be acceptable for many engineering applications.

The use of simple methods may often be dictated by economic considerations. The use of alternative methods can be very costly in both time and money (see section 10.2, Fig 1) if such methods are available at all.

Since safety is always of paramount importance in aerospace applications care must be exercised in choosing a simple method which will result in conservative estimates of strength and lifetime. As much of the lifetime of a fatigue crack is spent while the crack is short, this usually means ensuring that the chosen method overestimates the stress intensity factor for short cracks. It is however important to choose a method which minimizes the overestimate at short crack lengths; over-conservative estimations can result in designs which would have a severe weight penalty.

Methods suitable for simple configurations and methods suitable for complex configurations with multiple boundaries have been described. In many applications it will be necessary to combine these methods. For instance the ancillary configurations which result from the use of the compounding technique may not have known solutions; but some of the simpler techniques may be used to obtain the ancillary solutions.

REFERENCES

[1] D.P. Rooke, D.J. Cartwright — *Compendium of Stress Intensity Factors.* London, HMSO (1976)

[2] H. Tada, P. Paris, G. Irwin — *The Stress Analysis of Cracks Handbook.* Hellertown, Pa., Del Research Corp. (1973)

[3] G.C. Sih — *Handbook of Stress Intensity Factors.* Bethlehem, Pa., Lehigh University (1973)

[4] H. Liebowitz (Ed) — *Fracture* (in 7 volumes). New York, Academic Press, (1968-70)

[5] G.C. Sih (Ed) — *Mechanics of Fracture* (6 volumes announced to date). Leyden, Noordhoff, (1973-)

[6] D.J. Cartwright, D.P. Rooke — Evaluation of stress intensity factors. *J. Strain Analysis*, 10, 217-224 (1975)

[7] A.S. Kobayashi — *Experimental Techniques in Fracture Mechanics*. Connecticut, SESA (1973)

[8] A.R. Luxmore, D.R.J. Owen (Eds) — *Numerical Methods in Fracture Mechanics*. Swansea, University College (1978)

[9] R.E. Peterson — *Stress Concentration Factors*. 2nd Edition, New York, Wiley (1974)

[10] D.J. Cartwright, D.P. Rooke — Approximate stress intensity factors compounded from known solutions. *Engng Fracture Mech.*, 6, 563-571 (1974)

[11] F.I. Baratta — Stress intensity factors for internal multiple cracks in thick walled cylinders stressed by internal pressure using load relief factors. AMMRC TN 77-3 (1977)

[12] H. Liebowitz (Ed) — *Fracture Mechanics of Aircraft Structures*. AGARDograph No.176, London (1974)

[13] D.P. Rooke — Evaluation of asymptotic stress analysis for fracture mechanics applications. RAE Technical Report 78074 (1978)

[14] J.R. Dixon — A photoelastic investigation of the stress distribution in uniaxially loaded thick plates containing slits. N.E.L. Report No. 288 (1967)

[15] J.R. Rice, N. Levy — The part-through surface crack in an elastic plate. *J. Appl. Mech.*, 39, 185-194 (1972)

[16] D.O. Harris — Slicing procedure for approximate three-dimensional Green's functions for cracks in plates of finite thickness. *Int. J. Fracture*, 9, 21-32 (1973)

[17] W.T. Fujimoto — Determination of crack growth and fracture toughness parameters for surface flaws emanating from fastener holes. Proc. AIAA/ASME/SEA 17th SDM Meeting, Valley Forge, Pa., May (1976)

[18] B. Aamodt, P.G. Bergan — On the principle of superposition for stress intensity factors, *Engng. Fracture Mech.*, 8, 437-440 (1976)

[19] A.F. Emery, G.E. Walker — Stress intensity factors for edge cracks in rectangular plates with arbitrary loadings. Sandia Corporation, Livermore, Ca., Report SCL-DC-67-105 (1968)

[20] A.F. Emery, G.E. Walker, J.A. Williams — A Green's function for the stress intensity factors of edge cracks and its application to thermal stresses. *J. Bas. Engng.*, 91, 618-624 (1970)

[21] A.H. Lachenbruch — Depth and spacing of tension cracks. *J. Geophysical Research*, 66, 4273-4291 (1961)

[22] A.F. Emery — Stress intensity factors for thermal stresses in thick hollow cylinders. *J. Bas. Engng.*, 88, 45-52 (1966)

[23] R.J. Hartranft, G.C. Sih — Alternating method applied to edge and surface crack problems. In *Methods of analysis and solutions of crack problems*, edited by G.C. Sih, Chap. 4, pp 179-238. Leyden, Noordhoff International Publishing (1973)

[24] G.R. Irwin — Fracture. In Handbuch der Physik VI, pp 551-590, Springer-Verlag, Berlin (1958)

[25] H. Neuber — Theory of Notch Stresses. Springer, Berlin (1958). Translation series AEC-tr-4547, US Atomic Energy Commission

[26] D.O. Harris — Stress intensity factors for hollow circumferentially notched round bars. *J. Bas. Engng.*, 89, 49-54 (1967)

[27] L.P. Pook, J.R. Dixon — Fracture Toughness of High Strength Materials: Theory and Practice, ISI Publication 120, pp 45-50 (1970)

[28] N. Hasebe, Y. Kutanda — Calculation of stress intensity factor from stress concentration factor. *Engng. Fracture Mech.*, 10, 215-221 (1978)

[29] J.C. Newman — An improved method of collocation for the stress analysis of cracked plates with various shaped boundaries. NASA TND-6376 (1971)

[30] J.M. Bloom, W.A. Van Der Sluys — Determination of stress intensity factors for gradient stress fields. *J. Pressure Vessel Technology*, 99, 477-484 (1977)

[31] J.G. Williams, D.P. Isherwood — Calculation of the strain energy release rates of cracked plates by an approximate method. *J. Strain Anal.*, 3, 17-22 (1968)

[32] S.K. Chan, I.S. Tuba, W.K. Wilson — On the finite element method in linear fracture mechanics. Westinghouse Research Laboratories Report 68-1D7-FMPWR-P1 Pittsburgh, Pa. (1968)

[33] D.F. Cannon, R.J. Allen — Application of fracture mechanics to railway failures. *Railway Engng. Journal*, 3, 6-17 (1974)

[34] E. Smith — Simple approximate methods for determining the stress intensification at the tip of a crack. *Int. J. Fracture*, 13, 515-518 (1977)

[35] F. Erdogan — On the stress distribution in plates with collinear cuts under arbitrary loads. Proc. 4th US National Congress of Applied Mechanics, 1, 547-553 (1962)

[36] G.R. Irwin — Analysis of stresses and strains near the end of a crack traversing a plate. *J. Appl. Mech.*, 24, 361-364 (1957)

[37] G.I. Barenblatt — Mathematical theory of equilibrium cracks in brittle fracture. In *Advances in Applied Mechanics*, Vol 7, pp 55-111, Academic Press (1962)

[38] D.P. Rooke, D.A. Jones — Stress intensity factors in fretting fatigue. RAE Technical Report 77181 (1977)

[39] R.C. Shah — Stress intensity factors for through and part-through cracks originating at fastener holes. In *Mechanics of Crack Growth*, STP 590, pp 429-459, ASTM (1976)

[40] R.C. Shah — On through cracks at interference fit fasteners. *J. Pressure Vessel Technology*, 99, 75-82 (1977)

[41] R.C. Shah — Quarter or semi-circular cracks originating at interference fit fasteners. Proc. 17th AIAA/ASME/SAE Structures, Structural Dynamics and Materials Conference, King of Prussia, Pa. (1976)

[42] T.M. Hsu, J.L. Rudd — Green's function for thru-crack emanating from fastener holes. In *Fracture* 1977, Vol 3, ICF4, edited by D.M.R. Taplin, pp 139-148, Ontario, University of Waterloo Press (1977)

[43] R.S. Whitehead — BAe Warton (private communication)

[44] H. Tada, P.C. Paris — Stress intensity factor bounds for certain residual stresses with long surface cracks. Consulting Report to the Nuclear Regulatory Commission, Washington University, Materials Research Laboratory (1977)

[45] G.G. Chell — The stress intensity factors for cracks in stress gradients. *Int. J. Fracture Mech.*, 9, 338-341 (1973)

[46] G.G. Chell — The stress intensity factors for centre and edge cracked sheets subjected to an arbitrary loading. *Engng. Fracture Mech.*, 7, 137-152 (1975)

[47] G.G. Chell — The stress intensity factors for part through thickness embedded and surface flaws subject to a stress gradient. *Engng. Fracture Mech.*, 8, 331-340 (1976)

[48] G.G. Chell — The stress intensity factors and crack profiles for centre and edge cracks in plates subject to arbitrary stresses. *Int. J. Fracture Mech.*, 12, 33-46 (1976)

[49] H.F. Bueckner — A novel principle for the computation of stress intensity factors. *Z. Angew. Math. Mech.*, 50, 529-546 (1970)

[50] J.R. Rice — Some remarks on elastic crack-tip stress fields. *Int. J. Solids Structures*, 8, 751-758 (1972)

[51] P.C. Paris, R.M. McMeeking, H. Tada — The weight function method for determining stress intensity factors. In *Cracks and Fracture* STP 601, pp 471-489, ASTM (1976)

[52] A.F. Grandt — Stress intensity factors for some through-cracked fastener holes. *Int. J. Fracture*, 11, 283-294 (1975)

[53] O.L. Bowie — Analysis of an infinite plate containing radial cracks originating at the boundary of an internal circular hole. *J. Math. Phys.*, 35, 60-71 (1956)

[54] L.F. Impellizzeri, D.L. Rich — Spectrum fatigue crack growth in lugs. In *Fatigue crack growth under spectrum loads*, STP 595, pp 320-336, ASTM (1976)

[55] H.F. Bueckner — Weight functions for the notched bar. *Z. Angew Math. Mech.*, 51, 97-109 (1971)

[56] H.J. Petroski, J.D. Achenbach — Computation of the weight function from a stress intensity factor. *Engng. Fracture Mech.*, 10, 257-266 (1978)

[57] O.L. Bowie, P. Tracy — On the solution of the Dugdale model. *Engng. Fracture Mech.*, 10, 249-256 (1978)

[58] R.B. Heywood — *Designing by Photoelasticity*, London, Chapman and Hall (1952)

[59] O.L. Bowie — Analysis of edge notches in a seni-infinite region. *J. Math. and Phys.*, 45, 356-366 (1966)

[60] W.T. Koiter — Discussion on rectangular tensile sheet with symmetric edge cracks (see Ref [62]). *J. Appl. Mech.*, 32, 237 (1965)

[61] M.M. Frocht — A photoelastic investigation of stress concentrations due to small fillets and grooves in tension. Nat. Advis. Comm. Aeronaut., Report No.2442, Washington (1951)

[62] O.L. Bowie — Rectangular tensile sheet with symmetric edge cracks. *J. Appl. Mech.*, 31, 208-212 (1964)

[63] F.I. Baratta — Stress concentration factors in U-shaped and semi-elliptical edge notches. *J. Strain Analysis*, 5, 121-127 (1970)

[64] S. Timoshenko, J.N. Goodier — *Theory of Elasticity*, 2nd Ed., New York, McGraw-Hill (1951)

[65] J. Tweed, D.P. Rooke — The elastic problem for an infinite solid containing a circular hole with a pair of radial edge cracks of different lengths. *Int. J. Engng. Sci.*, 14, 925-933 (1976)

[66] D.J. Cartwright — Stress intensity factors and residual static strength in certain structural elements. Ph.D. Thesis, Mech. Engng. Dept., University of Southampton (1971)

[67] F.I. Baratta — Stress intensity factor estimates of a peripherally-cracked spherical void and a hemispherical surface pit. *J. Amer. Ceramic Soc.*, (to be published)

[68] J. Tweed, D.P. Rooke — The distribution of stress near the tip of a radial crack at the edge of a circular hole. *Int. J. Engng. Sci.*, 11, 1185-1195 (1973)

[69] I.E. Figge, J.C. Newman Jr — Fatigue crack propagation in structures with simulated rivet forces. *Fatigue Crack Propagation*, edited by J.C. Grosskreutz, pp 71-93, STP 415, ASTM (1967)

[70] F.W. Smith — Stress intensity factors for a semi-elliptical surface flow. Boeing Co., Structural Development Research Memo 17 (1966)

[71] A.F. Liu — Stress intensity factors for a corner flaw. *Engng. Fracture Mech.*, 4, 175-179 (1972)

[72] D.P. Rooke — Stress intensity factors for cracked holes in the presence of other boundaries. *Fracture Mechanics in Engineering Practice*, edited by P. Stanley, pp 149-163, London, Applied Science (1977)

[73] D.P. Rooke, D.J. Cartwright — The compounding method applied to cracks in stiffened sheets. *Engng. Fracture Mech.*, 8, 567-573 (1976)

[74] C.C. Poe Jr — Stress-intensity factor for a cracked sheet with riveted and uniformly shaped stringers. NASA TR R-358 (1971)

[75] C.C. Poe Jr — The effect of broken stringers on the stress intensity factor for a uniformly stiffened sheet containing a crack. NASA TM X-71947 (1973)

[76] J.C. Newman Jr — An improved method of collocation for the stress analysis of cracked plates with various shaped boundaries. NASA TN D-6376 (1971)

[77] D.P. Rooke, D.J. Cartwright — Stress intensity factors for collinear cracks in a stiffened sheet. RAE Technical Report TR78066 (1978)

[78] A. Thum, H. Oschatz — Increase of the endurance strength in round bars with transverse bores. *Forschg. Ing. -Wes.*, 3, 87 (1932)

[79] K. Watanabe, A. Atsumi — Infinite row of parallel cracks in a strip. *Int. J. Engng. Sci.*, 10, 78-84 (1972)

[80] J. Tweed, D.P. Rooke — The stress intensity factor for a crack in a symmetric array originating at a circular hole in an infinite elastic solid. *Int. J. Engng. Sci.*, 13, 653-660 (1975)

[81] S.L. Pu, M.A. Hussain — Stress intensity factors for a circular ring with uniform array of radial cracks using cubic isoparametric singular elements. 11th Nat. Symp. on Fracture Mechanics, V.P.I., Blacksburg, Va., June (1978)

SUBJECT INDEX

A

Accuracy of the crack propagation calculation, 7-7
Actual failing load, 6-7
Aircraft gas turbine engine component analysis, 2-2
Aircraft structural forgings, 6-3
Airfoil life prediction problems, 2-5
Aluminium alloy AZ74, 6-10
Aluminium alloys, 9-4, 9-5
Aluminium forgings, 6-8, 6-14
Analytical fracture curve, 3-27
Analytical, numerical and experimental procedures available for determining the stress intensity, 7-10
Anisotropy, 4-13
Applied stress, 4-9
Applied stress intensity, 9-4
Arithmetic mean, 8-34
Arrest capability, 4-18
Arrest power of small holes, 4-18
Assembly stresses, 9-3
Assessment of currently-used calculation procedures, 7-22
Associated scatter, 6-8
ASTM E-399, 6-5, 6-8
ASTM thickness, 6-7
Asymmetric crack, 3-7

B

Backfree surface correction, 4-13
Baseline crack-growth, 4-49
Baseline propagation data, 3-77
Bearing stress, 4-35
Bi-axiality, 5-7
Biaxial applied stress, 10-18
Bi-axial efforts, 5-6
Bi-axial loading, 3-25, 5-5
Biaxial stress, 3-25
Bi-axial stresses, 5-7
Bi-axial stress field, 3-86, 5-6, 5-7
Bi-axial stressing, 5-1
Biaxial tension loading, 3-24
Bonded stiffeners, 3-7
Boundary-boundary interactions, 10-20, 10-21, 10-23, 10-27
Bowie analysis, 4-13
Bowie factor, 4-20
Bowie function, 4-5, 4-24, 4-42
Bowie solution, 4-5, 4-9, 4-13
Built-up structures, 3-3, 3-11
Buried defect characterization, 2-3

C

C-shaped specimens, 6-9
Calculated crack propagation rates, 5-5
Calculations of residual static strength, 10-1
Central stiffener failure, 3-18
Centrifugal stresses, 2-6
Circumferential crack, 3-24, 5-6
Circumferential cracks, 5-6
COD, 6-8
Coefficient of load relief, 10-25
Coefficient of variation, 8-5, 8-6, 8-35
Cold working, 4-17
Colinear cracks, 4-17
Collipnest calculation formula, 7-6
Compact tension specimens, 4-36

Comparison between test and calculation for 300M steel, 7-26
Comparison of predicted and experimental crack growth, 7-29
Comparison of stress intensity factors, 10-27
Compliance, 6-5
Component mission simulation analysis, 2-6
Compounding method, 3-7
Compounding technique, 10-19
Compressive stress, 4-9, 4-49
Computer cost of a retardation procedure, 7-30
Constant amplitude, 4-30
Constant amplitude crack propagation tests, 6-9
Constant amplitude cycle loading, 3-27, 3-33
Constant-amplitude loading, 3-29, 4-29, 8-17
Constant amplitude tests, 3-88
Constant load amplitude, 6-8
Constants for the Forman Equation, 4-45
Constant stress intensity, 5-6
Corner cracks, 4-9, 4-13, 4-23, 4-24, 4-35, 4-36, 6-6
Corner flaw, 4-5
Corner flaw type defects, 4-26
Corrosion pits, 9-3
Cost effective fracture mechanics analytical model, 2-5
Crack approaching holes, 4-17
Crack arrest, 3-18, 3-44, 3-58
Crack arrest properties, 3-22
Crack arresting stiffener, 3-38
Crack blunting effect, 9-9
Crack closure concept, 7-19
Crack closure energy, 4-52
Crack configuration and applied stress, 7-20
Crack control techniques, 3-97
Crack depth criteria, 6-7
Crack front, 4-15
Crack growth, 2-5, 3-11, 3-22, 3-82, 3-85, 4-15, 4-23, 4-36, 4-37, 4-52, 5-3, 5-7, 9-8
Crack-growth analysis, 3-26, 3-67, 4-13, 4-46, 4-49, 4-52
Crack-growth analysis with retardation, 4-49
Crack-growth behavior, 4-17, 4-43
Crack-growth calculation, 4-11
Crack-growth curves, 4-15, 8-15
Crack-growth data, 4-29
Crack-growth integration technique, 4-11
Crack-growth life, 3-62, 4-13, 4-15, 4-29, 8-16, 8-19
Crack-growth modeling, 2-4, 2-6
Crack-growth prediction, 2-3
Crack-growth properties, 4-15
Crack-growth rate, 2-3, 2-6, 4-17, 5-5, 6-7, 8-16
Crack-growth resistance, 3-43
Crack-growth simulation, 2-4
Crack increments, 4-25, 4-36
Crack instability, 3-44
Crack initiation, 2-2, 3-3, 4-3
Crack initiation modeling, 2-7
Crack initiation life, 6-10
Crack initiation phase, 2-2
Crack length, 3-20, 3-22
Crack-line loaded specimen, 3-24
Crack opening displacement, 3-24, 4-49, 4-52
Crack opening stress, 7-19
Crack orientation, 4-26
Crack propagation, 2-2, 3-9, 3-70, 3-88, 4-37, 4-44, 5-1, 5-6, 6-3, 6-4, 6-6, 6-7, 6-8, 6-10, 6-12, 8-18, 9-3
Crack propagation acceleration, 7-19
Crack propagation analysis, 3-3, 3-11
Crack propagation behaviour, 3-93, 7-3
Crack propagation calculations, 3-67, 4-44, 4-45
Crack propagation calculation methods, 7-20
Crack propagation calculation models which take account of retardation, 7-11

Crack propagation influenced by environmental conditions, 7-8,
Crack propagation curve, 3-62, 4-17, 4-42, 6-10, 6-12
Crack propagation curves for different load sequences, 7-14
Crack propagation law, 3-88
Crack propagation life, 4-15, 4-45, 6-11, 6-12, 8-19
Crack propagation parameters, 7-5, 7-7
Crack propagation period, 6-10
Crack propagation properties, 3-3, 3-11, 6-3, 6-12
Crack propagation rates, 3-88, 3-93, 3-94, 4-17, 6-4, 7-4, 8-15
Crack propagation rate as a function of stress intensity, 7-8
Crack propagation retardation, 4-44, 4-45, 4-46
Crack propagation tests, 3-77, 3-98, 4-44, 4-45, 5-7, 6-8, 6-9, 6-11, 8-15, 8-18
Crack propagation tests under constant amplitude load, 7-7, 7-8
Crack propagation under constant and multi step amplitude load sequences, 7-3
Crack propagation values, 4-44
Crack resistance curve, 3-18
Crack retardation, 3-82
Crack riveted panels, 3-7
Crack starter notches, 4-44, 6-8
Crack size, 4-5
Crack stopper, 3-33, 3-70
Crack tip element, 4-15
Crack tip plasticity, 3-18
Crack tip stress intensity, 9-4
Crack tip stress intensity factor, 3-39
Crack truncation size, 2-3
Crack wire gauges, 4-44
Cracked stiffened structures, 3-98
Cracked spherical shells, 3-24
Cracking, 9-3
Cracking behavior, 4-9
Creep, 2-5, 2-6
Creep/fatigue interaction, 2-5
Critical crack length, 3-68, 4-45, 6-4, 6-8, 6-15
Critical crack calculations, 6-6
Critical crack size, 4-11, 4-29
Critical flaw size, 9-7
Critical size, 4-15
Critical stress, 3-51, 6-7
Cumulative frequency diagram, 8-35
Curvature, 5-6
Curvature correction factors, 5-6, 5-7
Cyclic crack growth, 2-4
Cyclic stress intensity, 9-9
Cylindrical shells, 3-24

D

Damage configuration, 3-82
Damage development assumptions, 3-67
Damage tolerance, 4-3, 4-11
Damage tolerance analysis, 3-62, 3-71, 4-3, 4-9, 4-11, 4-13, 9-7, 9-8
Damage tolerance analysis of airframe structures, 9-3
Damage tolerance assessment, 4-11, 6-3, 6-4, 6-6, 6-13
Damage tolerance criteria, 9-8
Damage tolerance philosophy, 4-29
Damage tolerance requirements, 5-3, 5-5, 7-3
Damage tolerance structure, 3-3, 3-97, 5-3, 8-15
Damage tolerance tests, 3-47
Davies and Feddersen's calculation formula, 7-6
Deflection measurement, 6-5
Design analysis of crack growth, 2-2
Difficulties in predicting the crack propagation under variable loads, 7-11
Disk fatigue life, 2-2
Disk fractures, 2-3
Disk fracture mechanics model 2-3
Disk low cycle fatigue life prediction problem, 2-2

Displacement compatibility method, 3-38
Doubly riveted stiffener, 3-7
Dugdale plastic zone behaviour, 3-43
Dynamic crack arrest, 4-18
Dynamic stress intensity, 4-17

E

Edge crack problem, 2-5
Effect of multiple stringers, 3-5
Effects of rivet type and material, 3-99
Effective crack length, 3-51
Eidinoff and Bell method, 7-21
Elastic analysis, 3-51, 3-58, 3-77
Elastic energy, 3-20
Elastic energy release rates, 3-20, 4-18
Elastic finite element analysis, 3-38
Elastic finite element methods, 3-34, 3-38
Elastic finite element techniques, 3-28
Elastic fracture, 4-23
Elastic fracture mechanics, 3-3
Elastic fracture mechanics analysis, 2-3
Elastic fracture mechanics models, 2-4
Elastic K-an..lysis, 3-62
Elastic-plastic analysis, 3-24, 3-25, 3-43
Elastic-plastic computer program, 3-38
Elastic-plastic load displacement, 3-38
Flastic stress field, 2-4, 3-9, 3-20
Elliptical crack solutions, 4-5
Elliptical cracks, 3-67, 4-9, 4-13
Elliptical flaws, 4-15
Elliptical integral, 4-5
Elliptical internal flaw, 6-6
Energy balance concept, 3-20
Energy release rate, 3-22
Engine disk structure, 2-2

F

Failed stiffener, 5-4
Failing loads, 6-15
Fail-safe approach, 4-28
Fail-safe design, 5-5
Fail-safe strength, 4-18
Fail-safe stress, 3-18
Fail-safe structure, 6-12
Failure load, 6-12
Failure stress, 4-20, 4-23, 4-26
"Falstaff" load sequence, 6-11
Falstaff methods, 7-29
Fast fracture, 3-11, 3-27, 3-28, 3-33
Fastener, 4-9
Fastener connection flexibility, 3-97
Fastener holes, 4-9
Fastener loads, 3-17
Fastener plasticity, 3-62
Fastening system, 3-18
Fatigue calculations, 3-85
Fatigue crack, 3-11, 5-3
Fatigue crack growth analysis, 9-7
Fatigue-crack growth, 3-62, 4-15, 4-29
Fatigue crack growth-rate, 10-??
Fatigue-crack-growth retardation, 4-46
Fatigue-crack propagation, 3-62, 3-97, 3-100, 4-13, 4-15, 4-23, 6-8
Fatigue crack propagation life, 9-9
Fatigue crack propagation test, 3-97
Fatigue cracks, 6-8, 9-7

Fatigue growth rate, 9-9
Fatigue life, 6-10, 6-11,
Fatigue life calculations, 2-2
Fatigue life improvement, 9-8
Fatigue lifetimes, 10-1
Fatigue life prediction, 2-2, 2-3
Fatigue resistance, 4-9
Fatigue spectrum, 5-5
Fatigue test results, 8-35
Fatigue test specimens, 2-2
Fatigue stress, 4-45
Finite difference thermal analysis computer program, 2-6
Finite-element analysis, 3-33, 3-43, 4-11, 4-13, 4-52
Finite-element method, 3-11, 3-24
Finite-element modeling, 3-43
Finite-element models, 3-9, 3-39, 3-70, 4-52
Finite-element-stress analysis, 4-49
Finite element submodeling, 4-49
Finite element techniques, 10-4
Finite stiffness, 3-70
Finite width correction, 3-77, 4-24
Flat panels, 5-5
Flaw shape parameter, 4-13
Flight-by-flight crack propagation tests, 4-45
Forecasts of crack propagation life, 7-3
Forgings, 6-3
Forman calculation, 7-7
Forman's calculation formula, 7-5
Forman equation, 7-3
Fractographic analysis, 6-12
Fracture behaviour, 6-15
Fracture instability, 3-17
Fracture mechanics in aircraft construction, 7-3
Fracture-mechanics analysis, 3-86, 4-3, 9-9
Fracture mechanics analysis of a crack structure, 10-1
Fracture mechanics application, 2-2
Fracture mechanics assessment, 6-7
Fracture mechanics calculations, 8-3, 10-3
Fracture mechanics criteria, 6-14, 6-16
Fracture mechanics methodology, 2-2
Fracture mechanics modeling, 2-2, 2-5, 2-6
Fracture mechanics principles, 4-9
Fracture mechanics procedures, 6-3
Fracture mechanics tests, 9-4
Fracture stresses, 4-13
Fracture surface, 4-29, 6-4, 6-10, 6-12
Fracture toughness, 2-2, 3-13, 3-18, 4-11, 4-13, 4-15, 6-3, 6-4, 6-6, 6-7, 6-9, 6-10, 6-11, 6-12, 6-13, 6-14, 6-15, 8-3, 8-4, 8-5, 9-5
Fracture toughness behaviour, 6-4
Fracture toughness dependent on the component, 7-8
Fracture toughness properties, 6-8
Fracture toughness tests, 6-14
Fracture toughness values, 6-7
Free surface correction, 4-5, 10-8
Free-surface correction factors, 4-9
Fretting as crack initiator, 6-7
Friction forces, 3-97
Führing and Seeger method, 7-21

G

Geometric (or log) mean, 8-34
Grain flow, 6-14
Grain flow patterns, 6-4, 6-12
Green's function, 10-5, 10-11, 10-9, 10-11
Green's function technique, 10-8
Griffith's criterion, 3-20
Growth rate of stress-corrosion cracks, 9-4

H

Helicopter rotor heads, 6-3
Histogram, 8-35
Hydrotesting, 9-8

I

Identical forgings, 6-15
Improvement of calculations of crack propagation life in aircraft components, 7-30
Influence of additional factors on the prediction of crack propagation life, 7-7
Influence on crack propagation behaviour, 7-10
Influence of environment on fatigue crack growth, 9-9
Influence of initial crack length on retardation, 7-13
Initial flaw sizes defined in MIL-A-83444, 9-24
Initial flaw shapes, 4-15
Inspection crack size, 4-20
Interference, 4-17
Interference fastener, 4-9
Interference fit, 4-9
Integral stiffener, 3-70
Integral structures, 5-1
Integrally stiffened panels, 3-70, 5-4, 5-5, 5-7
Integrally stiffened structures, 5-3
Internal cracks, 2-2

J

J-integral values, 3-24

K

Kinetic energy, 4-18
K-solution, 4-13

L

Landing gear spectrum, 6-9, 6-10
Lateral stiffening, 3-33
Life prediction calculation, 2-5
Life endurance tests, 4-44
Limit load stress, 9-8
Linear analysis, 4-46
Linear elastic fracture mechanics (L.E.F.M.), 2-3, 5-1, 5-5
Linear integration, 4-46, 4-52
Load bearing splices, 4-11
Load carrying elements, 3-3
Load concentration factors, 3-58
Load interaction, 4-15, 4-29
Load interaction (retardation), 4-42
Load path, 6-3
Load-relieving notches', 10-25
Load relief factors, 10-3
Loading spectrum, 3-82
Load spectrum, 4-20, 4-36
Load sequence at different mean stress, 7-24
Load transfer, 3-3, 4-3, 4-11, 4-17, 4-52
Log normal distribution, 8-4, 8-16
Longitudinal cracks, 3-24
Low cycle fatigue, 2-6
Low fracture toughness K_c, 6-7
Low oxygen content, 6-14

M

Magnesium alloys, 9-5
Mandrelizing, 4-9
Maraging steel, 6-10, 9-3
Material sources of variability, 8-15

Maximum size of flaw, 9-8
Mean fracture toughness, 8-4, 8-5, 8-6
Measured variability, 8-15
Mechanics of linear elastic fracture, 7-4
Metallurgical dissipation processes, 2-2
Methods of calculating the crack propagation under variable load sequence, 7-14
Methods of determining stress intensity factors, 10-4
Method for predicting the potential crack size, 9-6
Microcrack initiation, 2-4
MIL-A-83444 Specification, 9-8
MIL-83444 of the U.S.A.F., 7-3
MIL-standard 1587 of the U.S.A.F., 6-3
Mill annealing, 6-14
Mission analysis, 2-5
Modelling of the rivet connection, 3-7
Monte Carlo simulation techniques, 2-3
Multiple colinear cracks, 4-17
Multiple cracks, 4-17, 4-52
Multiple parallel cracks, 4-1

N

Normal distribution, 8-3, 8-4, 8-5
NDI, 9-5, 9-7
NDI method, 2-3, 6-3, 7-3, 7-31, 9-9
NDI techniques, 6-11
Newman method, 7-21
Newman's solution, 4-42, 4-46
Nickel-base alloy, 9-6
Nondestructive inspection, 4-42
Nonlinear crack growth equation, 2-3
Nonlinear shear displacement, 3-83
Notch strength analysis, 3-47
Numerical analysis techniques, 3-11
Natural metallurgical crack initiation, 2-4

O

Opening mode stress intensity factor, 10-5, 10-9
Order number, 8-34

P

Paris's calculation formula, 7-5
Parametric analysis, 4-37, 4-43, 4-49
Parametric studies, 3-7, 3-9
Peak stress intensity, 4-9
Plane strain, 6-3, 10-12
Plane strain conditions, 6-4, 6-5
Plane stress, 4-11, 4-45, 10-12
Plane stress conditions, 3-18, 6-4
Plane stress fracture toughness, 3-17, 3-26
Plastic deformation, 3-9
Plastic zone correction factors, 3-51
Plateau crack growth rates, 9-8
Plateau crack growth rates for high-strength steels, 9-16
Precision forgings, 6-3
Precracked specimen configurations for stress-corrosion testing, 9-20
Predicted failing load, 6-7
Premature fatigue cracks, 6-7
Pressurized elliptical crack, 4-5
Probabilistic approach, 8-3
Probabilistic fracture mechanics, 8-6
Production process, 7-10
Programmed block loading, 8-17
Proof load cycle, 9-8
Proof stress level, 9-8
Proof testing, 9-8

Propagation curves, 4-36
Propagation and failure of the crack, 4-36
Propagation of macrocracks, 2-2
Propagation predictions, 3-82

Q

Quarter circular corner crack, 4-26

R

Radial stiffener, 3-85
Random loading, 4-29, 8-17
Random variable, 8-34
Rapid fatigue crack propagation, 6-7
Rate of crack propagation, 7-5
Rate of fatigue crack growth, 9-9
Rate of growth of fatigue crack, 10-4
R-curve approach, 3-48
R-curve determination, 3-22, 3-24
Recrystallisation annealing, 6-14
Relationship between applied stress and displacement, 7-19
Remote loading, 4-35
Residual/assembly stresses, 9-7
Residual compressive stresses, 4-17
Residual static strength, 6-3, 6-4, 6-7, 6-8. 6-9. 6-11
Residual static strengths, 6-7
Residual strength, 3-3, 3-9, 3-11, 3-25, 3-26, 3-33, 3-34, 4-13, 4-20, 4-24, 4-52, 5-3, 5-5, 5-6, 6-13, 7-10, 10-27
Residual-strength analysis, 3-62, 4-11, 4-13, 4-49
Residual-strength calculation, 3-58, 3-85, 4-11
Residual strength characteristics, 3-26
Residual strength curve, 3-18
Residual strength diagram, 3-17, 3-39, 3-43
Residual strength predictions, 3-24, 3-45, 3-58, 3-82, 4-26
Residual strength requirements, 3-82
Residual strength of a riveted structure, 3-38
Residual strength specimens, 4-26
Residual strength for stiffened panels, 3-28
Residual strength tests, 3-13, 3-51, 5-1, 5-5, 5-6
Residual stresses, 4-15, 4-17, 8-16, 9-6
Residual tension stress, 9-3
Resistance curve approach, 3-24, 3-45
Retardation, 3-62, 4-15, 4-36, 4-46, 4-49, 7-18
Retardation effect, 4-45, 5-6, 6-6, 7-13, 7-15
Retardation effects of different materials as a function of the relative load, 7-13
Retardation effects of various materials, 7-12
Retardation factors, 7-13
Retardation model, 4-29, 4-30
Retardation modeling, 4-11
Retardation relative to the crack propagation, 7-11
Retardation relative to the load cycle number, 7-11
Retarded integration, 4-52
Richards and Lindley's calculation formula, 7-5
Rivet flexibility, 5-4
Rivet forces, 3-7
Riveted stiffener, 5-3
Rotating disk structure, 2-2

S

Safe-life philosophy, 4-29, 6-3, 6-6, 8-19
Safe life of rotating engine structures, 2-7
Safe life structures, 8-15
Safety coefficients, 6-11
Safety factor, 8-3
Scatter, 6-12, 9-4
Scatter band, 3-99
Scatter of the fatigue life to failure, 6-13

Scatter of fracture toughness, 6-10
SCC DATA, 9-5
Semielliptical surface notch, 6-7
Service-induced stresses, 9-3
Service life, 8-15
Service loading, 4-36
Service loads, 6-3
Shear coupling, 4-9
Shear loads, 4-11
Shear modulus, 10-12
Shear stresses, 4-5
Sheet-stiffened interaction, 3-5, 3-7, 3-17, 3-51
Skin fracture toughness, 3-33, 3-38
Skin material fracture toughness, 3-38
Skin-stringer combinations, 3-62
Simultaneous crack growth, 3-7
Slow crack growth, 6-3
Slow stable crack growth, 3-11, 3-20, 3-22
Smooth specimen tests, 9-4
Smooth threshold stress, 9-6
Spectrum of fatigue loading, 5-7
Spectrum loading, 5-6
Spectrum of plane stress, 7-17
Stable crack growth, 3-18, 3-52
Standard elliptical flaw solution, 4-5
Standard oxygen content, 6-14
Static loading, 3-27, 3-33
Static notch strength factor, 3-47
Static structures in engines, 2-7
Statistical hypothesis, 8-36
Steady stress, 9-7
Steel, 9-6
Stiffened panel load, 3-18
Stiffened panels, 3-28, 3-70, 4-11
Stiffened-sheet curve, 3-52, 3-58
Stiffener effectiveness, 3-17
Stiffener failure curve, 3-18, 3-58
Stiffener geometry effect, 3-99
Stiffener load concentration factor, 3-5, 3-17
Stiffener parameter, 5-5
Stiffener-skin combination, 3-77
Stiffener strength, 3-18
Stiffener strength curve, 3-27
Stiffener stresses, 3-26
Stiffening elements, 3-3, 3-11
Stiffening ratio, 3-68
Strain energy, 5-6
Strain gauge measuring, 3-98
Strength of materials, 8-3
Stress, 9-3
Stress analysis, 3-9, 4-11
Stress concentration, 2-6, 4-3, 4-17, 5-3
Stress concentration factor, 3-33, 10-3, 10-8, 10-21
Stress concentration as a function of notch radius, 10-15
Stress concentration magnification effect, 6-7
Stress condition, 3-3
Stress corrosion, 6-7, 9-5, 9-8
Stress corrosion crack growth, 9-7
Stress corrosion cracking, 9-3, 9-6
Stress corrosion cracks, 6-8, 6-13
Stress corrosion resistance, 9-4
Stress displacement relation, 3-5
Stress distribution, 3-17, 3-82, 4-5, 4-9, 4-44, 5-5, 10-3, 10-13, 10-16
Stress excursion, 2-3
Stress field, 7-4
Stress history, 4-11
Stress intensity, 3-5, 3-22, 3-62, 3-68, 3-77, 4-5, 4-9, 4-11, 4-13, 4-15, 4-17, 4-24, 4-28, 4-45, 4-52, 7-4, 7-10, 9-3, 9-4, 9-9

Stress intensity approach, 3-48
Stress-intensity analysis, 3-62, 4-3
Stress intensity correction factor, 3-5, 3-17
Stress-intensity distribution, 4-45
Stress intensity factor, 2-2, 2-3, 3-3, 3-5, 3-6, 3-7, 3-9, 3-11, 3-17, 3-20, 3-22, 3-24, 3-25, 3-51, 3-52, 3-62, 3-70, 3-85, 3-86, 3-97, 4-3, 4-9, 4-11, 4-13, 4-17, 4-20, 4-21, 4-42, 10-1, 10-5, 10-9, 10-11, 10-12, 10-13, 10-18, 10-20, 10-25
Stress intensity factor approach, 3-58
Stress intensity factor solution, 6-5, 7-10
Stress intensity factors for complex configurations, 10-19
Stress intensity factors for a single crack at the edge of a hole, 10-19
Stress intensity factors for a strip with two collinear edge crack, 10-15
Stress intensity factors for two cracks at the edge of a hole, 10-16
Stress intensity solutions, 3-7, 3-77, 3-85, 4-3, 4-24, 4-26, 4-36, 4-52, 10-3
Stress ratio, 2-2, 7-6
Stress risers, 9-3
Stress spectrum, 4-11, 4-45, 4-49, 6-6
Stringer critical stress, 3-43
Stringer failure, 3-9, 3-17
Stringer plasticity, 3-62
Structural life prediction, 2-5
Sub-modeling, 4-11, 4-49, 4-52
Superposition, 10-5
Superposition for an edge-cracked strip in bending, 10-5, 10-10
Superposition for a pin-load hole with radial cracks, 10-5
Superposition of stress intensity factors, 10-5
Surface crack growth, 2-4
Surface crack initiation, 2-4
Surface cracks, 2-2
Surface flaws, 4-15, 4-26
Surface residual stress and hardness, 2-4
Surface retardation, 2-2
Surface stress initiated cracks, 2-2
Sustained loading of fatigue precracked specimens, 9-4
Sustained stress, 9-6
Sustained stress profile, 9-6
Symmetrical grain flow pattern, 6-15

T

Temperature increases and crack propagation, 7-8
Tensile residual stresses, 9-8
Tension stress, 3-11, 9-6
Thermal stresses, 2-6
Threshold stress, 9-4
Threshold stress intensity, 9-5
Threshold stresses for high-strength steel, 9-15
Threshold value, 7-6
Through crack at a hole, 6-6
Through crack at a pin loaded hole, 6-6
Through-the-thickness crack, 4-26, 4-28
Titanium alloys, 9-4, 9-5, 9-6
Titanium crack stopper straps, 3-33, 3-34
Titanium forging, 6-8
Tornado methods, 7-29
Torsional eigenfrequency, 6-5
Total fracture, 3-11
Toughness tests, 4-28
Turbine airfoil, 2-2
Turbine airfoil durability, 2-4
Turbine disks, 6-3
Typical crack in a forging, 6-4 .

U

Uniaxial, 5-6, 10-18
Uniaxial cyclic loading, 3-27
Uniaxial loading, 5-7
Uniaxial loads, 3-27, 3-33

Uniaxial stress, 3-5, 6-7
Uniaxial tensile, 5-3
Uniaxial tension, 3-11, 3-44
Unstable crack growth, 3-17, 3-18, 3-22, 3-58, 3-62
Unstable fracture, 9-9
Unstiffened pressure vessels, 3-24
USAF retardation model, 6-9
USAF specification MIL-A-83444, 9-7

V

Variable stress field, 2-4
Variability, 8-15
Variate, 8-34
Vibration stresses, 2-2

W

Walker's calculation, 7-5
Walker's formula, 7-6
Wanhill and Lof's solution, 4-42
Weibull distribution, 8-4, 8-41, 8-52
Weight function method, 2-4
Weight functions, 10-12
Westergaard complex stress function, 3-38
Wheeler model, 7-3
Wheeler retardation model, 3-70
Willenborg model, 7-17
Willenborg retardation model, 4-49, 6-10

Y

Yield strength, 4-23
Young modulus, 10-23

Z

Zero length rivet pitch, 5-4

AUTHOR INDEX

Aamodt, B., 10-5, 10-28
Achenbach, J.D., 10-13, 10-30
Adams, N.J., 3-112
Adams, N.J.I., 5-6, 5-8
Ahrensdorf, K., 6-17
Aicher, W., 6-19
Allen, R.J., 10-29
Alver, A.S., 2-7
Amateau, M.F., 8-21
Anctil, A.A., 8-21
Anderson, B.E., 6-18
Anderson, J.M., 3-9, 3-109, 3-113
Anderson, R.B., 3-111
Anderson, W.E., 8-20
Annis, C., 2-7
Anstee, R.F.W., 5-6, 5-7, 5-8, 8-1, 8-20
Aplin, J.E., 8-21
Arin, K., 3-9, 3-109
Arkema, W.I., 7-22, 7-33
Atanmo, P., 7-32
Atsumi, A., 10-25, 10-31

Bachmann, V., 7-22, 7-33
Ballet, J.J., 8-20, 8-21
Baratta, F.I., 10-1, 10-15, 10-18, 10-19, 10-28, 10-30
Barenblatt, G.I., 10-29
Barrois, W., 3-113, 8-20
Barson, J.M., 3-113
Bauer, J., 3-113
Beck, E.J., 3-112
Beevers, C.J., 7-33
Bell, P.D., 3-113, 7-21, 7-33
Benjamin, W.D., 9-10
Bergan, P.G., 10-5, 10-28
Berryman, R.C., 8-21, 9-10
Besuner, P.M., 2-7
Billmann, F.R., 6-18
Binning, M.S., 8-21
Blackburn, M.S., 9-10
Bloom, J.M., 3-5, 3-7, 3-108, 10-29
Bowie, O.L., 4-3, 4-9, 4-18, 4-20, 4-21, 4-24, 4-28, 10-13, 10-15, 10-30
Bowen, A.W., 8-21
Bowles, C.Q., 7-32
Boyle, R.M., 3-24, 3-111
Bradley, M., 3-77, 4-20, 4-24, 4-35
Bradshaw, F.J., 3-86, 3-111, 8-20
Branger, J., 6-19
Broek, D., 3-5, 3-62, 3-108, 3-109, 3-110, 3-111, 4-3, 4-18, 4-19, 4-21, 4-26, 7-29, 7-30, 7-32, 7-33
Brown, B.F., 9-10
Brown, W.F., Jr., 6-18, 8-7
Brussat, J.R., 3-112
Bueckner, H.F., 2-7, 10-12, 10-30
Bunlin, W.D., 9-11
Burck, L.H., 4-13, 4-17, 4-18, 4-19
Burns, D.J., 4-15, 4-18

Cannon, D.F., 10-29
Carter, C.S., 9-3, 9-10, 9-11
Cartwright, D.J., 3-7, 3-9, 3-108, 3-109, 4-5, 4-18, 4-28, 4-35, 4-36, 5-4, 5-8, 10-3, 10-18, 10-27, 10-28, 10-31
Casalegno, L., 3-68, 3-113, 4-42

Chan, S.K., 10-29
Charbonnen, J.C., 9-10
Chell, G.G., 10-11, 10-29
Chu, C.S., 3-113
Clark, F., 8-20
Clark, H.McJ., 7-32
Clark, W.G., 8-20
Collipriest, J.E., 7-6, 7-32
Conley, F.M., 3-113
Copley, L.G., 3-111
Corn, D.L., 4-19
Coursen, J.W., 9-10
Creager, M., 3-24, 3-111, 3-112
Crews, J.H., 4-13, 4-18
Crichlow, W.J., 3-111, 3-112
Cruse, T.A., 2-1, 2-7

Dainty, R.V., 6-17
Davenport, O.B., 3-113
Davies, K.B., 7-6, 7-32
de Graaf, E.A.B., 6-18
de Jonge, J.B., 6-19
Del Puglia, A., 3-109
Dengel, D., 8-6
Denke, P.H., 3-28, 3-112
Denton, K., 8-20
De Rijk, P., 4-19, 7-32, 8-20
de Waal, J.F., 6-17
Dixon, J.R., 10-8, 10-28
Donahue, R.J., 7-32
Donaldson, D.R., 8-20
Dowrick, G., 3-7, 3-109
Duffy, A.R., 3-111
Dugdale, D.S., 3-9, 3-18, 3-20, 3-24, 3-51, 3-52, 3-58, 3-109
Duncan, M.E., 3-112, 5-6, 5-8
Dunsby, J.A., 6-17

Ettis, J., 5-6, 5-8
Eide, G.R., 3-112
Eidinoff, H.L., 7-21, 7-33
Ekvall, J.C., 3-112
Elder, W., 7-19, 7-20, 7-21, 7-32, 7-33
Ellis, R., 6-18, 8-20
Emery, A.F., 2-7, 10-5, 10-8, 10-28
Engle, R.M., 5-5, 5-8, 6-19, 7-28 7-32, 7-33
Engstrom, W.L., 3-112, 4-5, 4-7, 4-9, 4-13, 4-18
Erdogan, F., 3-9, 3-25, 3-109, 3-112, 7-20, 10-29
Ertelt, J., 6-19

Feddersen, C.E., 3-11, 3-13, 3-110, 4-5, 4-28, 4-31, 4-46. 7-6, 7-32
Feeney, J.A., 9-10
Ferguson, R.R., 8-21, 9-10
Figge, I.E., 3-48, 10-19, 10-30
Finger, R.W., 4-5, 4-18, 4-20, 4-21, 4-24, 4-26, 4-28, 4-35, 4-36
Fitzgerald, J.H., 3-9, 3-109
Folias, E.S., 3-24, 3-111, 3-112, 5-6, 5-8
Forman, R.G., 3-70, 3-88, 3-89, 3-93, 4-45, 4-49, 4-52 5-5, 5-8, 7-5, 7-6. 7-7, 7-13, 7-15, 7-16, 7-19, 7-22, 7-24, 7-25, 7-28, 7-30, 7-32
Forte, T.P., 4-49

Forsyth, P.J.E., 8-20, 8-21, 8-22
Frasier, J.T., 3-5, 3-108
Frediani, A., 3-109
Freedman, A.H., 9-10
Frocht, M.M., 10-13, 10-30
Frost, N.E., 8-20
Führing, H., 7-20, 7-21, 7-31, 7-33
Fujimoto, W.T., 4-9, 4-18, 10-28

Gallagher, J.P., 7-28, 7-33
Geier, W., 4-42, 4-46, 7-3, 7-32
Gemma, A.E., 2-7, 2-8
Gerharz, J.J., 3-110
Ghadiali, N.D., 4-49
Gierke, H., 6-17
Goel, P.K., 8-20
Gökgöl, A., 3-113
Goodier, J.N., 10-30
Goodlet, I., 6-17
Gran, R.J., 4-18
Grandt, A.F., Jr., 4-3, 4-5, 4-9, 4-18, 6-18, 10-13, 10-30
Grange, D., 4-24, 4-26, 4-28
Grassi, E., 3-109
Green, A.E., 2-7, 6-18
Greif, R., 3-5, 3-7, 3-108, 5-4, 5-8
Griese, F.W., 6-18
Griffin, L.D., 9-10
Griffiths, J.R., 4-18
Gunn, N.J.F., 8-20, 8-21

Habibies, B.J., 7-19, 7-22, 7-33
Hahn, G.T., 3-94, 3-112
Hall, L.R., 4-5, 4-7, 4-9, 4-13, 4-18, 4-20, 4-21, 4-24, 4-26, 4-28, 4-35, 4-36
Hanna, W.D., 8-21
Hardrath, M.F., 7-32
Harris, D.D., 10-8, 10-28
Hart, W.G.J., 3-110
Hartrauft, R.J., 10-8, 10-28
Hart Smith, L.J., 3-9, 3-109
Hasebe, N., 10-8, 10-29
Hayes, D.J., 3-24, 3-111
Heath, W.G., 3-112
Heath-Smith, J.R., 8-2
Hedrick, I.G., 3-113
Heidenreich, R., 6-17
Heller, R.A., 3-113
Hensley, E.K., 3-113
Hertzberg, R.W., 4-18, 8-21
Heyer, R.H., 3-22, 3-24, 3-111, 8-7
Heywood, R.B., 10-13, 10-30
Hilton, P.D., 3-25, 3-112
Hill, J.T., 2-8
Hillberry, B.M., 8-20
Hinnerichs, T.D., 4-18
Hooke, F.H., 8-22
Hoppe, W., 8-20
Hsu, T.M., 3-109, 10-11, 10-13, 10-29
Hück, M., 6-18, 6-19, 8-6
Hudak, S.J., 8-20
Hudson, C.M., 7-32, 8-21
Hunt, R.T., 3-112
Hussain, M.A., 10-25, 10-31
Huth, H., 3-11, 3-110
Hyatt, M.V., 6-17, 9-10
Hyler, W.S., 4-46, 7-32

Iida, S., 3-108
Impellizzeri, L.F., 3-113, 8-20, 10-13, 10-30
Irving, P.E., 7-32
Irwin, G.R., 3-5, 3-7, 3-18, 3-51, 3-52, 3-58, 3-108, 3-109, 3-111, 4-18, 6-5, 6-8, 6-18, 7-32, 10-9, 10-27, 10-29
Isherwood, D.P., 10-9, 10-16, 10-29
Isida, M., 3-5, 3-7, 3-108, 4-5, 4-17, 5-4, 5-8
Itagaki, Y., 3-108

Jacobs, F.A., 4-46, 6-17, 7-32
Jefferson, A., 5-1
Jones, D.A., 10-29
Joshi, S.R., 3-112
Jost, G.S., 8-20

Kanazawa, T., 3-9, 3-109
Kaplan, M.P., 3-113
Katanda, Y., 10-8, 10-29
Kaufmann, J.G., 6-17
Kearney, V.E., 5-5, 5-8, 7-32
Keer, L.M., 3-9, 3-109
Keerl, P., 4-46, 6-19
Kendall, D.P., 6-18
Kendall, E.G., 8-21
Kfouri, A.P., 3-112
Kibler, J.J., 3-25, 3-112
Kiddle, F.E., 8-20
Kies, J.A., 3-111
Kirkby, W.T., 3-112, 4-26
Knight, T.O. 9-11
Knott, J.F., 3-108
Kobayashi, A.S., 2-7, 4-18, 4-19, 4-42, 4-43, 10-3, 10-28
Koiter, W.T., 10-13, 10-30
Krafft, J.M., 3-24, 3-111
Kratzer, H., 8-7
Krimmel, W., 7-32
Kuhlmann, G.W., 6-18
Kuhn, P., 3-47, 3-48, 3-85, 3-86, 3-111
Kula, E.B., 8-21
Kumble, R., 7-32
Kutanada, Y., 10-29

Lacey, D., 3-111
Lachenbruch, A.H., 10-8, 10-28
Lacroix, 2-7
Lalli, D., 3-113
Landes, J.D., 3-24, 3-111
Langer, B.S., 2-8
Larsson, S.E., 6-17
Latterman, D., 9-10
Lazzarino, L., 3-108
Lehmann, H., 3-113
Lehrke, H.P., 3-11, 3-110
Lemaitre, J., 3-112
Leverant, G.R., 2-8
Levy, N., 10-28
Liebowitz, H., 1-1, 4-18, 4-35, 5-8, 10-3, 10-28
Lin, A.F., 4-43
Lin, C.T., 3-109
Lindley, T.C., 7-5, 7-22, 7-32, 7-33
Little, R.E., 8-6
Liu, A.F., 3-24, 3-68, 3-111, 3-112
Liu, C.T., 3-113
Lof, C.J., 4-42, 4-43
Loferski, M.T., 2-7

Loubet, R., 3-112
Love, W.J., 2-7
Lowack, H., 6-19
Luxmore, A.R., 10-28

McCabe, D.E., 3-22, 3-24, 3-111, 8-7
McClintock, F.A., 3-111
McCarthy, J.F., 6-18, 8-21
McEvily, A.J., 7-32
McGee, W.M., 3-109, 3-113
McGowan, J.J., 4-18
McHenry, H.I., 3-113
McMeeking, R.M., 10-12, 10-30
McStay, J., 3-113
Machida, S., 3-109
Maiden, D.E., 4-19
Malik, H.J., 4-49
Malluck, J.F., 3-113
Martin, C.I.P., 5-1
Maxwell, R.D.J., 8-21
May, J.M., 8-7
Melcon, M.A., 3-113
Meyer, T.G., 2-7, 2-8
Meyers, G.J., 2-7
Miller, K.J., 3-112
Miller, M., 3-9, 3-109
Moisio, T., 9-11
Moore, R.L., 6-17
Moore, T.K., 4-19
Morrow, Sarah M., 5-6, 5-7, 5-8, 8-20
Moss, 4-42, 4-43
Munafo, P.F., 9-11
Munz, D., 7-22, 7-33
Murherjee, B., 4-15, 4-18
Murnane, S.R., 3-113
Muskhelishvili, N.I., 3-5, 3-38, 3-108

Nanduri, V.G., 3-47, 3-112
Nederveen, A., 3-110, 8-20
Nelson, L.W., 3-113
Newman, J.C., 2-7, 4-9, 4-18, 4-42, 4-43, 4-46, 7-21, 7-33, 8-21, 10-19, 10-21, 10-29, 10-30, 10-31
Neuber, H., 10-8, 10-13, 10-25, 10-28
Nicholls, L.F., 3-112, 5-1
Nordmark, G.E., 6-17
Novak, S.R., 9-10

Oberparleiter, W., 6-17, 6-18, 6-19, 8-7, 8-20, 8-21
Odorico, J., 8-7
Ogura, Keiji, 3-112
Ohji Kiyolsugu, 3-112
Ohyagi, M., 3-112
Okhubo Yoshiji, 3-112
Oneill, P.H., 8-21
Orario, F.D., 4-18
Orringer, O., 8-21
Oschatz, H., 10-31
Otter, A.A.M., 4-19
Owen, D.R.J., 4-18, 10-28

Paris, P.C., 3-7, 3-39, 3-108, 4-18, 6-18, 7-5, 7-6, 7-31, 7-32, 10-11, 10-27, 10-29, 10-30
Parry-Jones, G., 8-20
Pasley, H.D., 6-17
Perlmutter, I., 9-10
Peters, R.W., 3-111
Peterson, R.E., 10-13, 10-21, 10-28
Petroski, H.J., 10-13, 10-30
Pettit, D.E., 3-113
Phillips, J.S., 2-8
Pickard, J., 3-28
Piper, D.E., 9-10
Poe, C.C., 3-5, 3-6, 3-7, 3-68, 3-77, 3-78, 3-82, 3-85, 3-86, 3-89, 3-94, 3-108, 3-109, 5-4, 5-7, 5-8, 10-20, 10-23, 10-31
Polvanick, N., 2-7
Pook, L.P., 8-20, 10-8, 10-28
Porter, T.R., 3-112
Pu, S.L., 10-25, 10-31

Radzins, K., 3-112
Raju, I.S., 2-7, 4-9, 4-18
Ratcliffe, G.A., 4-5, 4-18, 4-35, 4-36
Ratwani, M.M., 3-7, 3-9, 3-24, 3-25, 3-43, 3-109, 3-110, 3-111, 3-112,
Rau, C.A., 2-7, 2-8
Rau, C.A., Jr., 4-11, 4-17, 4-18, 4-19
Reiman, J.A., 3-113
Rhomberg, H., 6-19
Rice, J.R., 3-24, 3-111, 10-12, 10-28
Rich, D.L., 8-20, 10-13, 10-30
Rich, T.P., 3-109
Richards, C.E., 7-5, 7-22, 7-32, 7-33
Roberts, R., 3-112, 8-21
Robinson, J.L., 7-33
Rolfe, S.T., 3-113, 9-10
Romualdi, J.F., 3-5, 3-108, 5-3, 5-8
Romualdi, J.P., 3-108
Rooke, D.P., 3-7, 3-78, 3-108, 4-28, 5-8, 6-18, 7-32, 8-20, 8-21, 10-1, 10-3, 10-16, 10-19, 10-21, 10-25, 10-27, 10-28, 10-30, 10-31
Rosenfield, A.R., 3-112
Routh, W.E., 9-11
Rudd, J.L., 7-28, 7-32, 10-11, 10-13, 10-29

Salvetti, A., 3-7, 3-97, 3-108, 3-109, 8-20, 8-21
Sanderse, A., 3-110
Sanders, J.L., 3-5, 3-7, 3-108, 3-112, 5-3, 5-4, 5-6, 5-8
Sanders, P.H., 3-108
Sarrate, M., 3-112
Sattar, S.A., 2-7
Sayer, R.B., 3-113
Scanlon, R.D., 6-18
Scharfenberger, W., 6-18
Schewchuk, J., 3-112
Schijve, F.A., 6-17
Schijve, J., 4-46, 7-22, 7-32, 7-33, 8-20
Schimmelbusch, H.W., 6-17
Schöne, W., 6-18
Schra, L., 4-19, 6-17
Schütz, D., 3-110, 6-19
Schütz, R., 6-17
Schütz, W., 6-3, 6-17, 6-18, 6-19, 7-28, 7-29, 7-30, 7-33, 8-1, 8-7, 8-20, 8-21
Schwarmann, L., 3-11, 3-88, 3-89, 3-93, 3-94, 3-110, 3-113
Schwarz, 10-20
Seeger, T., 7-21, 7-31, 7-33
Sergio, G., 3-113
Shah, R.C., 3-112, 4-9, 4-18, 10-11, 10-13, 10-29
Shaver, B., 6-17
Shih, T.T., 7-21, 7-33
Sih, G.C., 3-7, 3-108, 4-35, 6-18, 10-3, 10-8, 10-27, 10-28
Simonen, F.A., 4-52
Simons, H., 3-113

Sinclair, G.M., 6-18
Sippel, K.O., 4-44, 4-46, 6-19, 7-3, 7-30, 7-32
Smith, C.W., 4-18
Smith, E., 10-9, 10-29
Smith, F.W., 10-19, 10-30
Smith, H.R., 9-10
Smith, S.H., 3-25, 3-112, 4-49, 4-52
Smyrl, W.H., 9-10
Sneddon, I.N., 2-7
Sneddon, J.N., 6-18
Snow, D.W., 2-7
Snow, J.R., 2-7
Sorensen, A., 3-112
Speidel, M.O., 9-10
Sprowls et al, D.O., 9-10
Srawley, J.E., 6-18, 7-33
Staley, J.T., 6-17
Steigerwald, E.A., 9-10
Stephens, R.J., 4-46, 8-7
Stewart, R.P., 4-19
Stoffels, E., 3-110
Stone, M., 3-110
Stronge, T.D., 3-113
Subramonian, A.N., 5-8
Sullivan, A.M., 3-24, 3-111
Sullivan, T.L., 3-111
Sundt, C.V., 2-7
Swanson, S.R., 8-20
Swfft, G.W., 3-113
Swift, T., 3-7, 3-11, 3-24, 3-25, 3-26, 3-28, 3-33, 3-34, 3-39, 3-48, 3-71, 3-85, 3-86, 3-89, 3-94, 3-109, 3-110

Tada, H., 3-7, 3-108, 6-18, 10-11, 10-12, 10-27, 10-29, 10-30
Tada, M., 7-32
Thomas, J.N., 3-70
Thrall, E.W., Jr., 3-113
Thum, A., 10-31
Tiffany, C.D., 4-19, 6-19, 8-21
Timoshenko, S., 10-30
Toor, P.M., 3-110
Tracy, P., 10-13, 10-30
Tromp, P.J., 3-110, 4-46, 7-32
Troughton. A.J., 3-113
Tuda, I.S., 10-29
Turbat, A., 3-112
Tweed, J., 10-16. 10-19, 10-21, 10-25, 10-30, 10-31

Underwood, J.H., 6-18

Van Der Sluys, W.A., 10-29
Van Dijk, G.M., 6-19, 8-20
Van Oosten Slingeland, G.L., 4-19
Verette, R.M., 3-24, 3-111
Virkler, D.A., 8-20
Vlieger, H., 3-1, 3-5, 3-11, 3-48, 3-51, 3-52, 3-58, 3-59 3-71, 3-108, 3-110, 3-111
Von Euw, E.F.J., 8-21

Wade, B.G., 4-19
Wagner, W., 6-17
Walker, A.C., 6-17, 7-5, 7-6, 7-31
Walker, E.K., 8-21
Walker, G.E., 10-28
Walker, K., 7-32
Walsh, J.D., 9-10
Wang, D.Y., 3-7, 3-112
Wang, Ke-Jen, 3-7, 3-39, 3-109
Wanhill, R.J.H., 4-42, 4-43, 6-17, 7-32, 8-21
Watanaba, K., 10-25, 10-31
Wehle, L.B., 3-113
Wei, R.P., 7-21, 7-33, 9-10
Weissgerber, D., 4-46, 6-10, 6-19, 7-30, 7-32
Wells, R.H., 3-111
Westergaard, H.M., 3-5, 3-108
Wheeler, C., 3-111
Wheeler, O.E., 5-6, 5-7, 5-8, 7-11, 7-19, 7-22, 7-24, 7-28, 7-30, 7-31, 7-32
White, D.J., 3-112
White, N.H., 4-13, 4-18
Whitehead, R.S., 10-29
Wiebe, W., 6-17
Wilhem, D.P., 3-7, 3-9, 3-24, 3-25, 3-43, 3-48, 3-109, 3-111, 3-112, 3-113
Willenborg, J.D., 4-29, 4-30, 4-52, 5-6, 5-8, 6-9, 6-10, 6-19, 7-11, 7-16, 7-17, 7-18, 7-19, 7-22, 7-24, 7-28, 7-30, 7-31, 7-32
Williams, D.P., 9-10
Williams, J.A., 10-9, 10-16, 10-28, 10-29
Williams, J.G., 3-24, 3-111
Wilson, I.H., 3-112
Wilson, R.B., 2-7
Wilson, W.K., 10-29
Winters, D.C., 6-18
Witzke, W.R., 8-7
Woithe, K., 6-17
Wong, J.K., 2-7
Wood, H.A., 3-113, 4-19, 5-8, 6-19, 7-32
Wood, R.A., 3-111

Yohn, C.P., 6-17

Zenner, H., 6-17, 6-18, 8-7, 8-20
Zielsdorff, G.F., 3-111
Zola, J.C., 6-18

REPORT DOCUMENTATION PAGE			
1. Recipient's Reference	2. Originator's Reference AGARD-AG-257	3. Further Reference ISBN 92-835-1359-2	4. Security Classification of Document UNCLASSIFIED

5. Originator: Advisory Group for Aerospace Research and Development
North Atlantic Treaty Organization
7 rue Ancelle, 92200 Neuilly sur Seine, France

6. Title

PRACTICAL APPLICATIONS OF FRACTURE MECHANICS

7. Presented at

8. Author(s)/Editor(s)

Harold Liebowitz
Dean and Professor of Engineering and Applied Science

9. Date: May 1980

10. Author's/Editor's Address

School of Engineering and Applied Science
George Washington University
Washington DC 20052, USA

11. Pages: 434

12. Distribution Statement: This document is distributed in accordance with AGARD policies and regulations, which are outlined on the Outside Back Covers of all AGARD publications.

13. Keywords/Descriptors

Fracture mechanics
Fracture properties
Fatigue (materials)
Stress corrosion
Aircraft
Aircraft engines
Airframes
Components

14. Abstract

The publication has essentially been oriented to present practical applications of fracture mechanics to all aspects of aircraft design, manufacture and testing. Although theoretical discussions are included to provide an appreciation of the complexity of the problems involved, the emphasis is on practical examples. Applications to engine components; built-up structures; joints, lugs and fasteners; integral structures and forgings are covered. The effects of stress corrosion and problems of scatter affecting determination of stress concentration factors, fatigue crack propagation and residual strength are discussed.

This AGARDograph was sponsored by the Structures and Materials Panel of AGARD.

AGARDograph No.257 Advisory Group for Aerospace Research and Development, NATO PRACTICAL APPLICATIONS OF FRACTURE MECHANICS Edited by H.Liebowitz Published May 1980 434 pages The publication has essentially been oriented to present practical applications of fracture mechanics to all aspects of aircraft design, manufacture and testing. Although theoretical discussions are included to provide an appreciation of the complexity of the problems involved, the emphasis is on practical examples. Applications to engine components; built-up structures; joints, P.T.O.	AGARD-AG-257 Fracture mechanics Fracture properties Fatigue (materials) Stress corrosion Aircraft Aircraft engines Airframes Components	AGARDograph No.257 Advisory Group for Aerospace Research and Development, NATO PRACTICAL APPLICATIONS OF FRACTURE MECHANICS Edited by H.Liebowitz Published May 1980 434 pages The publication has essentially been oriented to present practical applications of fracture mechanics to all aspects of aircraft design, manufacture and testing. Although theoretical discussions are included to provide an appreciation of the complexity of the problems involved, the emphasis is on practical examples. Applications to engine components; built-up structures; joints, P.T.O.	AGARD-AG-257 Fracture mechanics Fracture properties Fatigue (materials) Stress corrosion Aircraft Aircraft engines Airframes Components
AGARDograph No.257 Advisory Group for Aerospace Research and Development, NATO PRACTICAL APPLICATIONS OF FRACTURE MECHANICS Edited by H.Liebowitz Published May 1980 434 pages The publication has essentially been oriented to present practical applications of fracture mechanics to all aspects of aircraft design, manufacture and testing. Although theoretical discussions are included to provide an appreciation of the complexity of the problems involved, the emphasis is on practical examples. Applications to engine components, built-up structures, joints, P.T.O.	AGARD-AG-257 Fracture mechanics Fracture properties Fatigue (materials) Stress corrosion Aircraft Aircraft engines Airframes Components	AGARDograph No.257 Advisory Group for Aerospace Research and Development, NATO PRACTICAL APPLICATIONS OF FRACTURE MECHANICS Edited by H.Liebowitz Published May 1980 434 pages The publication has essentially been oriented to present practical applications of fracture mechanics to all aspects of aircraft design, manufacture and testing. Although theoretical discussions are included to provide an appreciation of the complexity of the problems involved, the emphasis is on practical examples. Applications to engine components; built-up structures, joints, P.T.O.	AGARD-AG-257 Fracture mechanics Fracture properties Fatigue (materials) Stress corrosion Aircraft Aircraft engines Airframes Components

lugs and fasteners; integral structures and forgings are covered. The effects of stress corrosion and problems of scatter affecting determination of stress concentration factors, fatigue crack propagation and residual strength are discussed. This AGARDograph was sponsored by the Structures and Materials Panel of AGARD. ISBN 92-835-1359-2	lugs and fasteners; integral structures and forgings are covered. The effects of stress corrosion and problems of scatter affecting determination of stress concentration factors, fatigue crack propagation and residual strength are discussed. This AGARDograph was sponsored by the Structures and Materials Panel of AGARD. ISBN 92-835-1359-2
lugs and fasteners; integral structures and forgings are covered. The effects of stress corrosion and problems of scatter affecting determination of stress concentration factors, fatigue crack propagation and residual strength are discussed. This AGARDograph was sponsored by the Structures and Materials Panel of AGARD. ISBN 92-835-1359-2	lugs and fasteners; integral structures and forgings are covered. The effects of stress corrosion and problems of scatter affecting determination of stress concentration factors, fatigue crack propagation and residual strength are discussed. This AGARDograph was sponsored by the Structures and Materials Panel of AGARD. ISBN 92-835-1359-2